FORGE

Fate Of Repository Gases

European Commission FP7

Final report on benchmark studies on repository-scale numerical simulations of gas migration Part 1: cell scale benchmark

FORGE Reports D1.4R and D1.6-R pt 1

Keywords.

Benchmark, cell scale, numerical simulation, repository

Bibliographical reference

WENDLING, J (COMPILER). 2013. Final report on benchmark studies on repository-scale numerical simulations of gas migration Part 1: cell scale benchmark .

FORGE Reports D1.4R and D1.6-R pt 1. 168pp.

Euratom 7th Framework Programme Project: FORGE

EURATOM

FORGE Deliverable D1.6-R

Final report on benchmark studies on repository-scale numerical simulations of gas migration Part 1: cell scale benchmark[1]

September 2013

Authored by:

Belgium	Li Yu (SCK-CEN),
France	Eloi Treille & Jacques Wendling (ANDWENDRA)
	Magdalena Dymitrowska & Delphine Pellegrini (IRSN)
	Etienne Ahusborde, Mladen Jurak & Brahim Amaziane (CNRS)
	Florian Caro & Alain Genty (CEA)
Lithuania	Povilas Poskas & Darius Justinavicius (LEI)
Switzerland	Manuel Sentis (ENSI)
United Kingdom	Simon Norris (NDA RWMD)
	Alex Bond (Quintessa)
Canada	Helen Leung (NWMO)
	Nicola J. Calder (Geofirma)

Compiled by:	Jacques Wendling	Date: September 2013
Checked by:	Simon Norris	Date: 28 March 2014
Approved by:	Richard Shaw	Date: 30th April 2014

[1] J. Wendling, L. Yu, E. Treille, M. Dymitrowska, D. Pellegrini, E. Ahusborde, M. Jurak, B. Amaziane, F. Caro, A. Genty, P. Poskas, D. Justinavicius, M. Sentis, S. Norris, A. Bond, H, Leung, N.J. Calder, *Final report on benchmark studies on repository-scale numerical simulations of gas migration, Part 1 : cell scale benchmark*, European Commission FORGE Deliverable D1.6-R, 2013.

Fate **O**f **R**epository **G**as**E**s (FORGE)

The multiple barrier disposal concept is the cornerstone of all proposed schemes for geological disposal of radioactive wastes. The concept is based on a series of passive complementary barriers, both engineered and natural, that act to achieve the required level of safety for radioactive waste disposed in a geological repository.

Demonstrating an appropriate understanding of gas generation and migration is a key component in a safety case for a geological repository for radioactive waste. On the basis of work to date, the overall behaviour of waste-derived gas and its influences on repository system performance require improved understanding. Key issues to be further examined relating to an enhanced understanding of gas-related processes include: dilational versus visco-capillary flow mechanisms; long-term integrity of seals, in particular gas flow along contacts; role of the EDZ as a conduit for preferential flow; and laboratory to field up-scaling. Such issues are the focus of the integrated, multi-disciplinary European Commission FORGE project.

The FORGE project links international radioactive waste management organisations, regulators and academia, and is specifically designed to tackle the key research issues associated with the generation and movement of repository gases associated with waste disposed in a geological repository. Of particular importance are the long-term performance of bentonite buffers, plastic clays, indurated mudrocks and crystalline formations. Further experimental data are required to reduce uncertainty relating to the quantitative treatment of gas in performance assessment.

FORGE will address these issues through a series of laboratory and field-scale experiments, including the development of new methods for up-scaling allowing the optimisation of concepts through detailed scenario analysis. The FORGE partners are committed to training and CPD through a broad portfolio of training opportunities and initiatives which form a significant part of the project.

Further details on the FORGE project and its outcomes can be accessed at www.FORGEproject.org.

Contact details:

EC FORGE Work Package 1 Leader:

Dr Simon Norris

Nuclear Decommissioning Authority – Radioactive Waste Management Directorate

Tel +44 1925 802891

Fax +44 1925 802948

Email simon.norris@nda.gov.uk

Web address: www.nda.gov.uk

Address NDA Harwell
Building 587
Curie Avenue
Harwell Science and Innovation Campus
Didcot
Oxon OX11 0RH
United Kingdom

Table of content

1. Context and introduction 1

2. Definition of the benchmark 2

3. Summary of the work done by the different teams 3

3.1 NDA RWMD contribution 3

3.1.1 Introduction 3
3.1.2 Model Implementation 3
3.1.3 Implementation Issues and Model Stability 6
3.1.4 Base Case Results 6
3.1.5 Prescribed Sensitivity Cases 10
3.1.6 Additional Sensitivities 12
3.1.7 Discussion and Conclusions 14
3.1.8 References 16

3.2 SCK-CEN contribution 17

3.2.1 Introduction 17
3.2.2 Modelisation of the cell module 17
3.2.3 Initial conditions 20
3.2.4 Constitutive models and parameters 20
3.2.5 Results 23
3.2.6 Conclusion and remarks 29
3.2.7 References 29

3.3 Andra contribution 30

3.3.1 Introduction 30
3.3.2 Code 30
3.3.3 Mathematics 31
3.3.4 Boundary Conditions 32
3.3.5 Initial conditions 32
3.3.6 Other deviations from the specifications 32
3.3.7 Base case results 33
3.3.8 Global behavior of the cell 36
3.3.9 Sensitivity cases results 37
3.3.10 Conclusions 47

3.4 CEA contribution 48

3.4.1 Introduction 48
3.4.2 Model Implementation 48
3.4.3 Base Case Results 49
3.4.4 Discussion and Conclusions 51
3.4.5 Issues for further consideration 51
3.4.6 References 51

3.5 CNRS contribution 52

3.5.1 Introduction 52
3.5.2 Model Implementation 52
3.5.3 Base Case Results 54
3.5.4 Prescribed Sensitivity Cases 55
3.5.5 Additional Sensitivities 58
3.5.6 Discussion and Conclusions 58
3.5.7 Lessons Learnt 58

3.5.8 Issues for further consideration 58
3.5.9 References 58
3.6 IRSN contribution 59
3.6.1 Introduction 59
3.6.2 Model Implementation 59
3.6.3 Base Case Results 66
3.6.4 Additional Sensitivities 67
3.6.5 Discussion and Conclusions 70
3.6.6 Lessons Learnt 70
3.6.7 Issues for further consideration 71
3.6.8 References 71
3.7 LEI contribution 73
3.7.1 Introduction 73
3.7.2 Model Implementation 73
3.7.3 Base Case Results 79
3.7.4 Sensitivity Analysis 82
3.7.5 Conclusions 88
3.7.6 References 89
3.8 ENSI/IFSN contribution 90
3.8.1 Introduction 90
3.8.2 Codes Used for the Calculation 91
3.8.3 Numerical Formulation 92
3.8.4 Benchmark Implementation 93
3.8.5 Base Case Results 98
3.8.6 Prescribed Sensitivity Cases 104
3.8.7 Additional Sensitivities 113
3.8.8 Conclusions 114
3.8.9 Issues for further consideration 115
3.8.10 References 115
3.9 NWMO contribution 116
3.9.1 Introduction 116
3.9.2 Model Implementation 116
3.9.3 Base Case Results 119
3.9.4 Prescribed Sensitivity Cases 136
3.9.5 Additional Sensitivities 141
3.9.6 Discussion and Conclusions 144
3.9.7 References 145
4. Global synthesis of the benchmark at cell scale 146
4.1 Base case results 146
4.1.1 Comparison of the available results and main phenomenological results 146
4.1.2 Main conclusions for the base case 150
4.2 Sensitivity analysis results 151
4.3 Main problems encountered 151
4.3.1 Boundary conditions representation 151
4.3.2 Time step management 151
4.3.3 Mesh optimization 152
4.4 Model and code development in the frame work of this cell scale benchmark 153
4.5 Discussion on the representativity of the models used and Interactions with other FORGE WP's 153

5. ANNEX : Full description of the benchmark 155

5.1 CONTEXT AND OBJECTIVES 155

5.2 REFERENCE TEST CASE 155

5.2.1 GEOMETRY 156
5.2.2 PHYSICAL PARAMETERS 157
5.2.3 Initial conditions 159
5.2.4 Boundary conditions 159
5.2.5 Production term for hydrogen 161
5.2.6 Simulation period 161

5.3 SENSITIVITY ANALYSIS 161

5.4 OUTPUT RESULTS 161

5.5 MATHEMATICAL MODEL PROPOSED FOR THE EXERCISE 164

List of figures

Definition of benchmark

Figure 1	Representation of the axisymmetric calculation domain	2
Figure 2	QPAC geometry definition.	3
Figure 3	Gridded geometry for the QPAC runs, coloured by material type. The location of prescribed (non no-flow) boundaries are shown in blue.	5
Figure 4	Plot of gas pressures at points P5 (in the EDZ adjacent to the canister) P7 (drift EDZ) and P9 (radially halfway between the canister and the boundary).	8
Figure 5	Plot of free gas flow into the drift from the EDZ, plug and interfaces (blue) and plot of dissolved gas flux out of the radial boundary (red). Positive fluxes indicate outflow.	8
Figure 6	Log10 Gas Saturation at selected times for the base case	9
Figure 7	Plot of free gas flow into the drift from the EDZ, plug and interfacesfor the different permeabilities of interface – note these are half-model fluxes and should be scaled by x2 to obtain the full model fluxes.	11
Figure 8	Plot of free gas flow into the drift from the EDZ, plug and interfaces for different grid resolutions.	12
Figure 9	3D grid using the 'squared off' grid geometry	12
Figure 10	Plot of gas pressures at points P5 (in the EDZ adjacent to the canister) P7 (drift EDZ) and P9 (radially halfway between the canister and the boundary).	13
Figure 11	Plot of free gas flow into the drift from the EDZ, plug and interfaces (blue) and plot of dissolved gas flux out of the radial boundary (red), no gas generation case. Positive fluxes indicate outflow.	14
Figure 12	Schematic illustration of a possible abstracted model for dilation flow.	16
Figure 13	Problem geometry	18
Figure 14	Mesh of the domain and imposed boundary conditions	19
Figure 15	Time variation condition at the boundary of drift	20
Figure 16	Time evolution of nodal pressure	23
Figure 17	Gas flux vector at t=1,000 years (Unit: kg/s)	24
Figure 18	Liquid saturation contour map at t=10,000 years	24
Figure 19	Comparison of gaseous flux along three boundaries	25
Figure 20	Comparison of the evolution of gas pressure in sensitivity analyses at P2	26
Figure 21	Comparison of the evolution of gas pressure in sensitivity analysis (Unit: MPa)	27
Figure 22	Comparison of the gaseous flux in five sensitivity analyses through (a) interface S_{int1} and (b) EDZ S_{EDZ1}	28
Figure 23	Schematic representation of the points where results are given	34
Figure 24	Base case: evolution with time of liquid pressure (left) and dissolved hydrogen pseudo-pressure (right) for points 1 and 8- 12	34
Figure 25	Base case: evolution with time of gas pressure (left) and liquid saturation (right) for points 2- 7	35
Figure 26	Schematic representation of the surfaces trough which fluxes are calculated	35
Figure 27	Base case: evolution with time of liquid water mass flow (left) and vapor mass flow (right) across different surfaces	36
Figure 28	Base case: evolution with time of gaseous hydrogen mass flow (left) and dissolved hydrogen mass flow (right) across different surfaces	36
Figure 29	Sensitivity case 1: evolution with time of liquid pressure (left) and dissolved hydrogen pseudo-pressure (right) for points 1 and 8- 12	37
Figure 30	Sensitivity case1: evolution with time of gas pressure (left) and liquid saturation (right) for points 2- 7	38
Figure 31	Sensitivity case 1: evolution with time of liquid water mass flow (left) and vapor mass flow (right) across different surfaces	38
Figure 32	Sensitivity case1: evolution with time of gaseous hydrogen mass flow (left) and dissolved hydrogen mass flow (right) across different surfaces	39

Figure 33 Sensitivity case 2: evolution with time of liquid pressure (left) and dissolved hydrogen pseudo-pressure (right) for points 1 and 8- 12 39
Figure 34 Sensitivity case2: evolution with time of gas pressure (left) and liquid saturation (right) for points 2- 7 40
Figure 35 Sensitivity case 2: evolution with time of liquid water mass flow (left) and vapor mass flow (right) across different surfaces 40
Figure 36 Sensitivity case2: evolution with time of gaseous hydrogen mass flow (left) and dissolved hydrogen mass flow (right) across different surfaces 41
Figure 37 Sensitivity case 3: evolution with time of liquid pressure (left) and dissolved hydrogen pseudo-pressure (right) for points 1 and 8- 12 41
Figure 38 Sensitivity case3: evolution with time of gas pressure (left) and liquid saturation (right) for points 2- 7 42
Figure 39 Sensitivity case 3: evolution with time of liquid water mass flow (left) and vapor mass flow (right) across different surfaces 42
Figure 40 Sensitivity case3: evolution with time of gaseous hydrogen mass flow (left) and dissolved hydrogen mass flow (right) across different surfaces 43
Figure 41 Sensitivity case less permeable interfaces 1.e-15 m/s: evolution with time of liquid pressure (left) and dissolved hydrogen pseudo-pressure (right) for points 1 and 8- 12 44
Figure 42 Sensitivity case less permeable interfaces 1.e-15 m/s: evolution with time of gas pressure (left) and liquid saturation (right) for points 2- 7 44
Figure 43 Sensitivity case less permeable interfaces 1.e-15 m/s: evolution with time of liquid water mass flow (left) and vapor mass flow (right) across different surfaces 45
Figure 44 Sensitivity case less permeable interfaces 1.e-15 m/s: evolution with time of gaseous hydrogen mass flow (left) and dissolved hydrogen mass flow (right) across different surfaces 45
Figure 45 Mesh selected for the different simulations 46
Figure 46 Mesh selected for the different simulations (zoom around the access drift) 46
Figure 47 : Mesh used for the benchmark computation. 49
Figure 48: Temporal saturation evolution inside the system 50
Figure 49: Temporal gas pressure evolution inside the system 50
Figure 50 Evolution of the gas pressure with time at given points 55
Figure 51 Evolution of the water saturation with time at given points 56
Figure 52 Evolution of the water pressure with time at given points 56
Figure 53 Evolution of the water fluxes with time through surfaces 57
Figure 54 Evolution of the gas fluxes with time through surfaces 57
Figure 55 : Relative corrections to the standard Henry constant $d_{r,H}$ and the Raoult-Kelvin relation $d_{r,RK}$ taking into account the existence of the capillary pressure in high pressure limit. The curve where P_l=-P corresponds to the situation where the water pressure is negative as a result of strong capillary pressure. At moderate pressures (10MPa) the relative deviations become non-negligible (10%). 60
Figure 56 Phase diagram for a two component system with linear thermodynamic equilibrium relations 61
Figure 57 : Definition of the test case 3b. The general dimensions are: the length 1 m, and the height of 0.1m. 62
Figure 58 : Test 3b - Results at one time = 100 s; pressure of gas (green) and water (red). On the left Diphpom code, on the right ToughII (courtesy of Z.Saadi, IRSN) 62
Figure 59: test 1b - position of the limits of the saturated zone as a function of time. 63
Figure 60 : The mesh used for the cell base case. 64
Figure 61 : Selected results of the base case. Points P2 and P4 are in the interface, P5 in EDZ, P9 and P10 in the sound hostrock. 67
Figure 62 The outer boundary at 40m – results of the sensitivity test case for the point P4. 68
Figure 63 : The drift boundary conditions obtained from the module scale calculations (Quintessa) 68

Figure 64 : Drift BCs from the module scale simulations – results for the cell scale simulations in point P4. 69
Figure 65 Mesh of LEI model coloured by material type 74
Figure 66 Different grids tested in LEI model 75
Figure 67 Schematic representation of boundary conditions: 1 – hydrogen gas injection area; 2 – constant water pressure; 3 – no flow boundary conditions; 4 – time varying boundary conditions 75
Figure 68 Comparison of time varying boundary conditions in benchmark specification and LEI model 76
Figure 69 Relative permeability functions of gas phase for different materials using different expressions 77
Figure 70 Dependence of effective diffusion coefficient on liquid saturation for selected materials in benchmark model using different tortuosity expressions 79
Figure 71 Comparison of gaseous hydrogen (GH2) flux through S_{drift} and dissolved hydrogen (DH2) flux through S_{EDZ} using RP and MQ tortuosity models 79
Figure 72 Base case results: gas saturation (a), liquid pressure (b) and gas pressure (c) evolution with time 80
Figure 73 Base case results: comparison of gaseous hydrogen flow rates through 4 different surfaces 81
Figure 74 Base case results: flow rates of gaseous hydrogen through S_{drift} (a) and dissolved hydrogen through S_{EDZ} (b) 81
Figure 75 Sensitivity 11-12 results: comparison of gas saturation (a) and water pressure (b) evolution with time at selected points 83
Figure 76 Sensitivity 11-12 results: comparison of flow rate for gaseous hydrogen through S_{drift} (a) and dissolved hydrogen through S_{EDZ} (b) 83
Figure 77 Sensitivity 21-24 results: comparison of gas saturation evolution with time in waste interface (a) and EDZ (b) 84
Figure 78 Sensitivity 41-44 results: comparison of gas saturation evolution with time in waste interface (a) and EDZ (b) 85
Figure 79 Comparison of peak pressure in the system for all analysed cases 87
Figure 80 Comparison of gaseous H_2 flux through S_{drift} for all analysed cases 87
Figure 81 Comparison of dissolved H_2 flux through S_{out} for all analysed cases 88
Figure 82 Domain of the model proposed for the first benchmark exercise (cell scale) [1]. 90
Figure 83 Space discretization in the integral finite difference method [3]. 92
Figure 84 Model and dimensions for the first benchmark [1]. 94
Figure 85 ENSI Results for liquid pressure during the first year at different points of the model. 97
Figure 86 Time variable boundary conditions to be used in the drift. 98
Figure 87 Results for the water saturation after 10'000 years for the reference case. 99
Figure 88 Position of the points at which the results of the calculations are shown. 99
Figure 89 Gas pressure at the points where there is a gas phase. 100
Figure 90 Variation of the gas saturation at the prescribed points. 100
Figure 91 Water pressure at different points. 101
Figure 92 Gas Pressure along the line marked as L_{int} on the right part. 101
Figure 93 Gas Pressure along the line marked as LEDZ on the right part. 102
Figure 94 Variation of the water saturation along a perpendicular line L_{cell} to the cell starting in the surface of the waste canister at coordinate y =0.495 m from the axis. 102
Figure 95 Mass flow of water in kg/s through the EDZ. 103
Figure 96 Mass flow rates of water in kg/s through the drift. 103
Figure 97 Hydrogen mass flow rates in kg/a through the EDZ and through the drift. 104
Figure 98 Water pressure at different points. 105
Figure 99 Gas pressure at different points. 105

Figure 100 Mass flow of water through the EDZ and through the drift. In order to compare them with Figure 95 and Figure 96 the same scale was used. 106
Figure 101 Water pressure at different points. 107
Figure 102 Gas pressure at different points. 107
Figure 103 Results of the gas pressure for the sensitivity case 3. 108
Figure 104 Mass flow rates of gas in kg/a through the drift for the reference case and for the sensitivity cases 1 and 3. 108
Figure 105 Water pressure at different points. 109
Figure 106 Water pressure in different points. 109
Figure 107 Mesh used for the numerical simulations with TOUGH2 and TOUGH2-MP, the mesh consists of 6300 nodes. 110
Figure 108 Detail of the mesh (6300 elements) in the common region of the EDZ, bentonite and access drift. The differences in sizes of the nodes for the different materials are noticeable. 111
Figure 109 Detail of the mesh close to the corner in the interface facing canister. 112
Figure 110 Mesh consisting of 2500 nodes used for the calculations shown in this report. 113
Figure 111 Gas und water pressure in point 5 for the sensitivity case 7, in which the permeability of the elements of the source term in the waste canister is Kwaste=10^{-25} m^2. The results are compared with the ones of the reference case.114
Figure 112: Grid discretization 117
Figure 113: Detail of grid discretization around the bentonite plug 117
Figure 114: Comparison of final model grid and simple rectangular model grid gas flows through the access drift for the base case with no diffusion. 118
Figure 115: Relative gas permeability curves for the EDZ/Rock (n=1.5) represented by the benchmark and T2GGM 119
Figure 116: Gas and water pressures for the base case at 1 year 120
Figure 117: Gas and water pressures for the base case at 10 years. 121
Figure 118: Gas and water pressures for the base case at 100 years. 122
Figure 119: Gas and water pressures for the base case at 1000 years. 123
Figure 120: Gas and water pressures for the base case at 10 000 years. 124
Figure 121: Gas and water pressures for the base case at 20 000 years. 125
Figure 122: Gas and water pressures for the base case at 100 000 years. 126
Figure 123: Gas saturations and dissolved gas mass fraction for the base case at 1 year. 127
Figure 124: Gas saturations and dissolved gas mass fraction for the base case at 10 years. 128
Figure 125: Gas saturations and dissolved gas mass fraction for the base case at 100 years. 129
Figure 126: Gas saturations and dissolved gas mass fraction for the base case at 1000 years. 130
Figure 127: Gas saturations and dissolved gas mass fraction for the base case at 10 000 years. 131
Figure 128: Gas saturations and dissolved gas mass fraction for the base case at 20 000 years. 132
Figure 129: Gas saturations and dissolved gas mass fraction for the base case at 100 000 years. 133
Figure 130: Location of pressure and flow time series. Points (point 4, 5 and 9) are circled in red, and the interface for the access drift flow is highlighted in red. 134
Figure 131: Base case water and gas pressures at point 5, located in the middle of the EDZ, half way along the canister. 134
Figure 132: Base case water and gas pressures at point 4, located in the EDZ, at the intersection of the access drift and the bentonite plug. 135
Figure 133: Base case water pressures at point 9, located in the host rock, 5 m away from the center of the cell. 135
Figure 134: Base case gas flux into the access drift, from the EDZ, interface and bentonite plug. 136
Figure 135: Sensitivity case 1 (EDZ K equivalent to rock K) gas flux into the access drift, from the EDZ, interface and bentonite plug. 137
Figure 136: Sensitivity case 2 (Cubic power law relative permeability curve in host rock and EDZ) gas flow into the access drift. 138
Figure 137: Sensitivity case 2 (Cubic power law relative permeability curve in host rock and EDZ) gas flow out of EDZ surface into host rock. 138

Figure 138 : Sensitivity case 3 (increased diffusion coefficient) and base case gas flux into the access drift. 139
Figure 139: Sensitivity case 5 (interface permeability increased to 10^{-15} m^2) gas flux into the access drift, from the EDZ, interface and bentonite plug. 140
Figure 140: Water pressures at point 5 for sensitivity case 5 (interface permeability decreased to 10^{-15} m^2) and base case. Point 5 is located in the middle of the EDZ, half way along the canister. 140
Figure 141: Gas flows to the access drift for the base case, no interface case and upscaled interface case. 142
Figure 142: Gas flows out the EDZ into the host rock for the base case, no interface case and upscaled interface case. 142
Figure 143: Water and gas pressures at point 4 for the base case, no interface case and upscaled interface case. 143
Figure 144: Water and gas pressures at point 5 for the base case, no interface case and upscaled interface case. 144
Figure 145: Water pressures at point 9 for the base, no interface case and upscaled interface case. 144
Figure 146 Evolution with time of water and gas pressures at point 4 147
Figure 147 Evolution of water and gas pressures with time at point 5 148
Figure 148 Evolution of water pressure with time at point 9 148
Figure 149 Evolution with time of the gas flux toward the access drift for all teams except CEN/SCK 149
Figure 150 Evolution with time of the gas flux through the entire EDZ for all teams except CEN/SCK 150
Figure 151 Example of a coarse regular mesh 152
Figure 152 Example of a refined unstructured non conform mesh 153
Figure 153: Representation of the axisymetric calculation domain 156
Figure 154: Dimensions in the calculation domain 156
Figure 155: schematic representation of the boundary conditions 159
Figure 156: Time variable boundary conditions to be used in the drift 160
Figure 157: schematic representation of the surfaces trough which fluxes will be calculated 162
Figure 158: schematic representation of the lines along which results should be given 163
Figure 159: schematic representation of the point where results should be given 164

List of tables

SCK/CEN contribution

Table 1 Material properties used in calculations for the base case 22

IRSN contribution

Table 2 The Initial conditions imposed for the base cell case. The limit values are obtained in the case of saturated materials for the hypothetic gas pressure of 1e+4Pa. The last column illustrates the change in solubility limit when the KK equation (Equation 5) is used instead of Henry law. 65

LEI contribution

Table 3 : Initial conditions set in LEI model 76
Table 4 : Description of variables used in analyses of the results 80
Table 5 : Description of analyzed sensitivity cases 82
Table 6 : Sensitivity 11-12 results: comparison of total transported mass through different surfaces 83
Table 7 : Sensitivity 21-24 results: comparison of total transported mass through different surfaces 84
Table 8 : Sensitivity 31-33 results: comparison of total transported mass through different surfaces 85
Table 9 : Sensitivity 41-44 results: comparison of total transported mass through different surfaces 85
Table 10 : Sensitivity 5 results: comparison of total transported mass through different surfaces 86
Table 11 : Sensitivity 61-62 results: comparison of computation speed 86
Table 12 : Sensitivity 61-62 results: comparison of total transported mass through different surfaces 86

ENSI contribution

Table 13 Dimensions of the model for the first benchmark [1]. 94
Table 14 Physical parameters for the materials [1] in the first benchmark. 94
Table 15 Changes made in the intrinsic permeabilities. 98
Table 16 Calculation cases for the cell scale benchmark 104
Table 17 Different Meshes used for the calculations in the sensitivity analysis 6. 112

Annex

Table 18 : Size of items in the calculation domain 157
Table 19 : Physical characteristics of materials 157

1. Context and introduction

This document is the first part (out of three) of the final report on the work done for FORGE WP1.2 in the context of a benchmark simulation concerning gas generation and migration at repository depth (many hundreds of metres below ground level) and repository scale. The work described has been undertaken during the year 2010 and second semester of 2009.

One of the main problems in dealing with different teams from different countries, who have different disposal concepts, is to find a common representation as a basis for the benchmark. This implies simplifications are necessary to real concepts, in order that they be represented at a basic level that has some degree of consistency to all participants. Another point is to find a common initial benchmark definition that can satisfy any team, so something quite simple is needed at the outset, so that teams can have a first trial and, in comparing the respective results thus obtained, verify that basics are well understood by each team.

At the start of WP1.2 activities, after discussion, there was a general agreement that the reference exercise will be as generic as possible (without targeting precisely on national concepts), with sensitivity analyses making it possible to cover national specificities. The aim here is more to understand the behaviour of the modeled system as underastood by each participant, rather than to undertake an inter-comparison of codes. A second agreement was that, although the final aim of the benchmark studies is to represent repository-scale simulations, the first exercise should be rather simple and at cell scale.

To give some added value to this first exercise, a feature not yet well represented in usual gas simulations was introduced: the explicit representation of the interface between canisters and cell walls.

After a brief description of the benchmark definition (see Section 2), Section 3 of this report collates the results to date of each WP1.2 participant. This is followed (Section 4) by a comparison of the main results produced by each participant. The main problems encountered, and the main conclusions, are also discussed.

N.B. *: there are two other document linked to this one, on module scale (report FORGE D1.6-R part 2: module scale benchmark) and repository scale (report FORGE D1.6 –R part 3: repository scale benchmark) benchmark. The repository scale benchmark has a final conclusion synthethising all the conclusions of the global benchmark work*

2. Definition of the benchmark

N.B. : The complete definition of the benchmark can be found in the Annex

To be able to understand water and gas flow at the repository scale, it is necessary to understand the water and gas flow associated with sub-repository "cell" scale components (e.g. on the scale of a vault or tunnel). Information is needed at an appropriate level of detail in order to upscale from the cell level to the full repository level, via perhaps intermediate modules scales of e.g. several tens of cells.

For this reason, the first benchmark was defined at cell level. The type of cell considered is a somehow generic high level waste cell in a clay host rock. As the scale is quite small, it is possible to represent fine geometric features, and especially the interface between the canister and clay rock as well as interface between bentonite seal and clay rock (considered as a centimetre-thick region). As permeability is increased in the EDZ, this zone is also represented.

To stay as generic as possible, the gas flux rate in this benchmark is represented by a simple step function lasting 10,000 years; the simulation time is limited to 100,000 years. To understand the distinct role of each phenomenon, the reference case is not considering any coupling. This will be done further on in the sensitivity analysis.

As most of the materials in ths benchmark are assigned very low permeability, capillary process will be dominant over gravity. Therefore the mesh can be built as axisymmetric without losing any important phenomenology.

Figure 1 gives a representation of the represent area and the type of material defined.

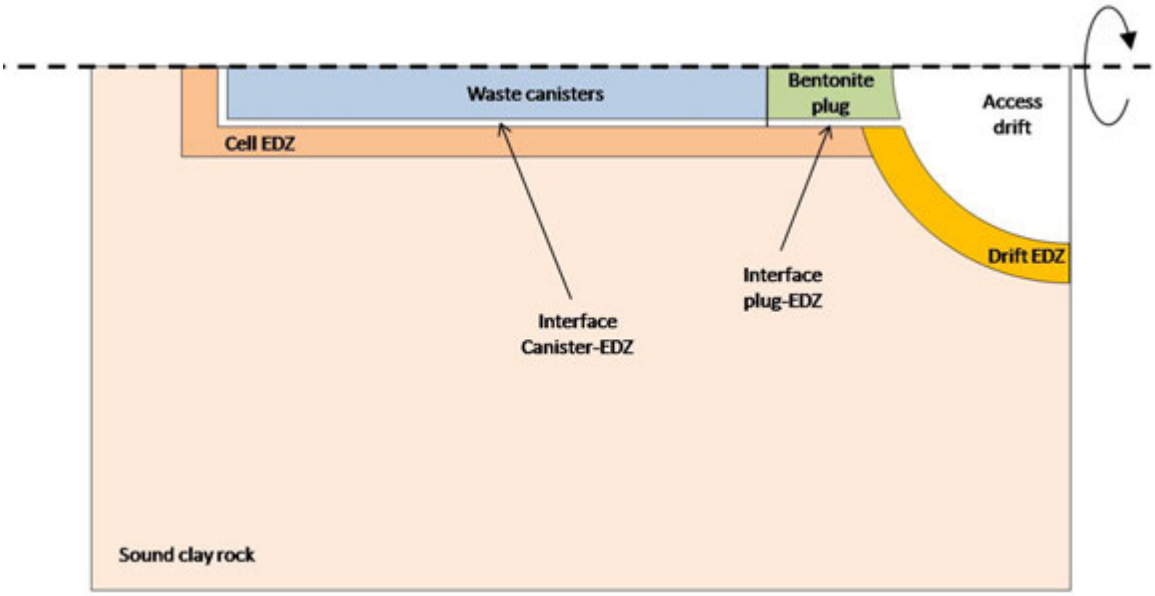

Figure 1 Representation of the axisymmetric calculation domain

More details and the complete benchmark definition can be found in the Annex

3. Summary of the work done by the different teams

3.1 NDA RWMD contribution

3.1.1 Introduction

This document presents the model setup, results, sensitivity cases and key learning points from the first benchmark (see Annex, § 5) produced by the UK Nuclear Decommissioning Authority (NDA) and Quintessa team. It also contains conclusions relevant to the three benchmark studies considered as a whole.

3.1.2 Model Implementation

The model was implemented in the Quintessa multi-physics code "QPAC" using the specification as the only source of input (see Annex, § 5). The standard Multi-Phase-Flow (MPF) QPAC module retains all the process model functionality required by this case [1], and hence the process and geometry could be implemented exactly as described, i.e. multiphase flow of water with a gas phase (hydrogen) together with consideration of dissolved hydrogen and water vapour diffusion. Consistent with the specification there is no distinction between the initially present gas (air) and generated hydrogen.

3.1.2.1 Code and Model Formulation

QPAC is a general purpose modeling tool designed for flexibility and robustness. The 'model as input' approach for the input syntax allows the user to adjust all aspects of the model formulation and to create couplings in internal parameters so that, within certain limitations, any one input parameter can be a function of any other, and such couplings can be expressed naturally through the input language. Problems are solved monolithically and using a time-implicit method supported by automatic time-stepping. Collections of user-input can be compiled to create 'modules'. Such modules (e.g. thermal transport, reactive transport, simple Darcy flow, MPF etc.) can be tested and quality assured much like a conventional code and then used in a modular fashion in new models. The MPF module used in this exercise is one example of such a module.

QPAC does not impose a numerical method on the user, but rather provides a rather generic concept of compartments (volumes) and interfaces (faces between volumes) on which variables (unknowns for the calculation) and properties can be defined (Figure 2). Regions where different process models (sub-systems) are represented are connected via 'joiners'. Grids of compartments and interfaces can be created using the standard QPAC input language on both axi-symmetric (cylindrical) and Cartesian grids. Also abstract geometries of arbitrary or abstract compartment and interface structures can be created, and attached to the more conventional gridded structures.

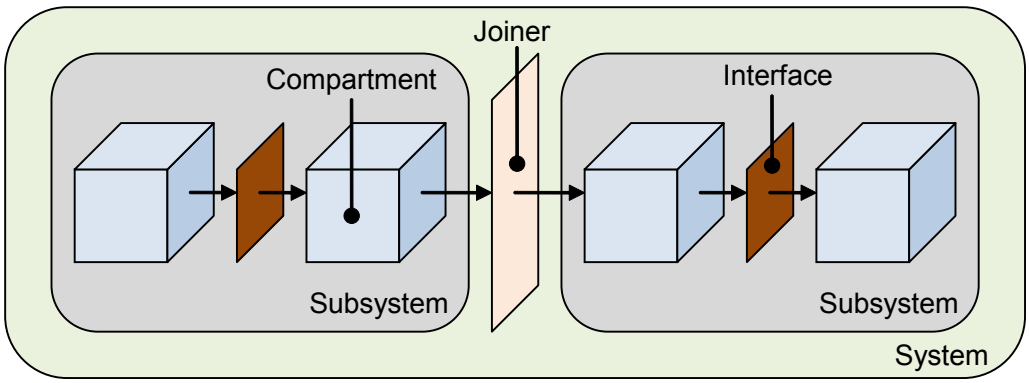

Figure 2 QPAC geometry definition.

Most QPAC models and modules use a Finite Volume formulation, however Mixed Element and Finite Difference schemes can also be adopted. The MPF module uses a conventional Finite Volume formulation. In contrast to some other codes, the MPF module uses a continuous formulation for water and gas; this means that for numerical reasons, when fully water saturated, small amounts of immobile gas are assumed to be present and that this gas is in pressure equilibrium with the water (i.e. capillary pressure is zero).

Dissolution is considered to proceed according to Henry's law:

$$p = k_H . c$$

where

p is the pressure of the gas phase (this is equal to the total pressure of the gas phase when only a single gas is present, or the partial pressure when a mixture of gases are present) (Pa)

c is the concentration of the gas in the solution (mol m^{-3})

k_H is Henry's constant for the gas (Pa m^3 mol^{-1})

In a two-phase (or multi-phase) system, comprising gas and water, as the amount of free gas becomes increasingly small the gas pressure tends to the water pressure. When only very small amounts of free gas are present the gas pressure is equal to the water pressure, but there may not be sufficient gas to satisfy the equilibrium dissolved gas concentration calculated using the equation above. This implies that all the gas will dissolve, there will be no free gas, and the system will transition to a single phase system (water partially saturated with dissolved gas).

Two mathematical approaches are available to model this phase transition:

- Apply different mathematical models for multi-phase and single phase conditions, with discontinuous change between models according to defined criteria.
- Apply a single mathematical model, so there is no discontinuity, but appropriately modify the mathematical model when single phase conditions are implied.

In the QPAC code the latter approach is taken. The amount of gas that can be dissolved is given by:

$$Amount\ dissolved\ gas = \min\left(\frac{p}{k_H} V_w m_g,\ Hf\ A_g\right)$$

Where

V_w is the volume of water (m^3)

m_g is the molar weight of gas (g mol^{-1})

A_g is the total amount of gas either as free gas or dissolved gas (in the given model compartment) (kg)

Hf is the Henry's law scaling factor which defaults to 0.99 (-)

Since QPAC primarily solves for the amount of gas present in any compartment, the above equation is simple to evaluate and restricts the amount of dissolved gas when there is very little gas in a given compartment. When there is a very small amount of gas, 1% (by default) of the total gas is always free gas to maintain the continuous formulation. Under these conditions, QPAC calculates a gas pressure that is equal to the water pressure. The Hf parameter can be adjusted to increase or decrease the strength of this effect, and the user will ensure that the parameterisation of the residual gas phase is effectively immobile once the water becomes under-saturated with respect to dissolved gas.

This approach is similar to some other multi-phase codes (e.g. Eclipse) and is consistent with other physic-chemical mathematical models, for example it is possible to calculate a vapour pressure for a single phase (liquid only) system. It also has a conceptual basis: dissolved gas molecules will have a range of energies,

and some molecules will have sufficient energy to effectively be disassociated from water, even if the number of such molecules is too small for a distinct free gas phase to form.

3.1.2.2 Grid

For the base case the model geometry was implemented using a simple reclined cylindrical grid (see Figure 3), with a single compartment in the angular direction to give a total of 515 active compartments. The specification indicates that the cylindrical section is effectively horizontal (i.e. out of the plane of gravity), so buoyancy effects are ignored.

A 3D half-cylinder representation was also set up, as this allowed the possibility of examining the effect of gravity on the results through the use of additional angular discretisation, without forcing the use of a prohibitive number of compartments.

For convenience, the volume representing the waste was discarded from the model during calculation. The compartments representing the interfaces between the waste and EDZ, and plug and EDZ were specified as being a single compartment thick. The numerical formulation implementation used in QPAC meant this gave no particular problems in representing the high lateral conductivity along the outside of the waste.

The definition of the anisotropy in the system and the effective assumption of horizontality of the 2D modelling section, meant that no anisotropy was present in the 2D model, although of course material variations were present.

A number of gridding options are available for representing the curve of the access drift and associated EDZ. It was decided that a simple step-wise approximation to the curve was the most appropriate as it gave addition resolution around the periphery of the disposal cell and drift, and made discretising a full 3D version of the case relatively easy to implement.

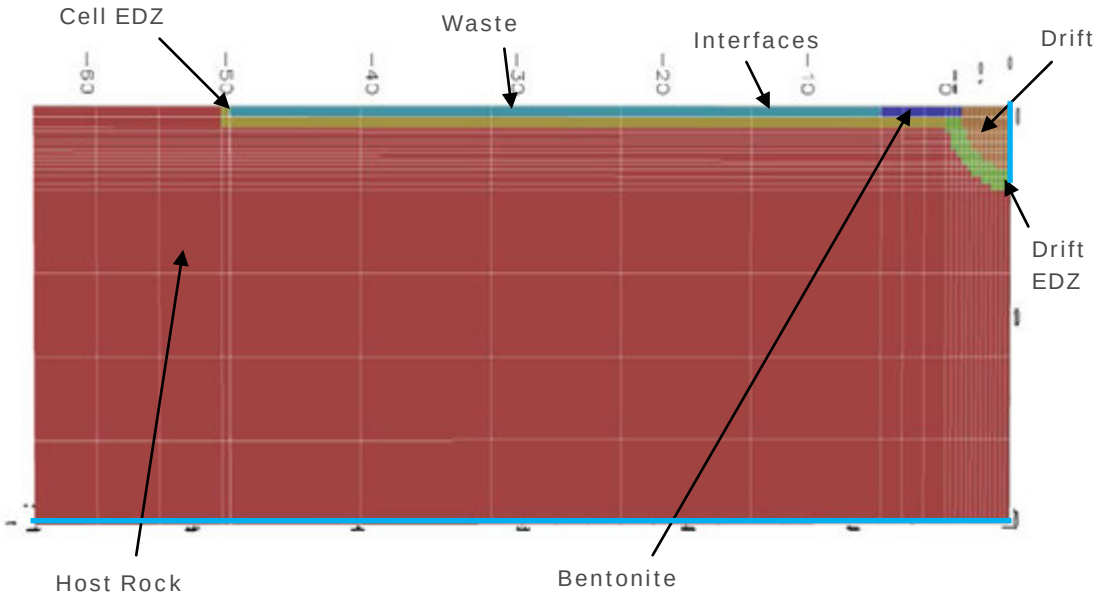

Figure 3 *Gridded geometry for the QPAC runs, coloured by material type. The location of prescribed (non no-flow) boundaries are shown in blue.*

3.1.2.3 Boundary Conditions and Sources

As specified in the benchmark specification, the interface between the waste and EDZ received the H2 gas, generated as a result of corrosion of the disposal canister, at a total rate of 50 mol/y (equivalent to 100 mol/y for the full model) across the surface of the waste canister into both the waste interface and the bentonite plug. This injection pattern was agreed in meetings as a clarification to the definition of the source flux in the specification.

The boundary condition for water (water pressure, gas pressure and fluid saturation) at the access drift was implemented as specified using the tabulated data provided to create linearly interpolated time-dependent lookups for each property.

The outer radial boundary was implemented precisely as described, all other boundaries were designated as no-flow, consistent with the specification.

3.1.2.4 Initial Conditions

Initial conditions used were exactly as in the specification.

Initially the air saturation is 0.3 in the bentonite plug and drift access and 0.95 in the waste and plug interfaces. The remainder of the domain is fully water saturated. Because of the continuous formulation, it is numerically convenient to prevent zero phase saturations, hence the starting saturation of air in the model is 1e-6 in all fully saturated water compartments.

Because the 2D model is a 2D cylindrical representation of the halfspace, the elevation of the 2D section is a constant. Therefore the background saturated water pressure is 5 MPa everywhere in the model, when fully water saturated. Hence, initial fluid pressures are 5 MPa in all water saturated parts of the model (note that with a continuous formulation the gas and water pressures are the same when there is only residual gas present). In other parts of the model that are not initially fully saturated with water, gas pressures are at 1e5 Pa and water pressures in capillary equilibrium with the gas pressure.

3.1.2.5 Deviations from the specification

Aside from the use of a rectangular mesh to approximate the curve of the access drift, the specification was implemented exactly as described in the specification.

3.1.3 Implementation Issues and Model Stability

There were no particular problems implementing the model as prescribed either in terms of geometry or through processes. The model results were examined for signs of significant numerical instability, but no evidence of problematic behaviour was observed that wasn't explainable in terms of the time variant boundary conditions or expected behaviour. Solver information also showed no symptoms of particular problems, noting that the most 'difficult' part of the transient appears to be associated with the sudden cessation of gas generation at 10000 years.

3.1.4 Base Case Results

The fluid saturation, pressure and flux results appear to be generally consistent with the boundary conditions and initial conditions. In terms of water flow, the access drift initially acts as a significant sink to water, generating a large low pressure zone around the disposal cell which draws water towards this area. This low pressure zone disperses as the pressure in the access drift, which controlled by the prescribed boundary condition, rises, and is virtually eliminated after approximately 5000 years. Selected, but representative, pressure responses close to and away from the canister are shown in Figure 4.

The flux results (selected outputs in Figure 5) show that loss of gas from the disposal cell is dominated almost completely by losses of free gas (negative fluxes imply fluxes into the drift) into the access drift during the period while gas is being generated (up until 10000 years). When gas generation ceases the drift flux reverses and losses from the model become dominated by the dissolved flux on the radial outer boundary. The large negative fluxes at early times result from gas in the drift moving into the EDZ as the

water flows towards the low pressure sink at the access drift boundary and displaces gas in the access tunnel.

Free gas saturations only reach significant levels in the waste/EDZ interfaces, access drift and some parts of the EDZ (Figure 6). Saturations of free gas never reach more than 1.0e-3 in the host rock and seem to be largely associated with dissolved H2 coming out of solution after having diffused away from the EDZ.

Nearly all of the remaining gas is lost via diffusion of dissolved gas from the drift and waste EDZs to the host-rock and then on to the outer radial boundary. Overall, the majority of the gas is lost via advection into the drift.

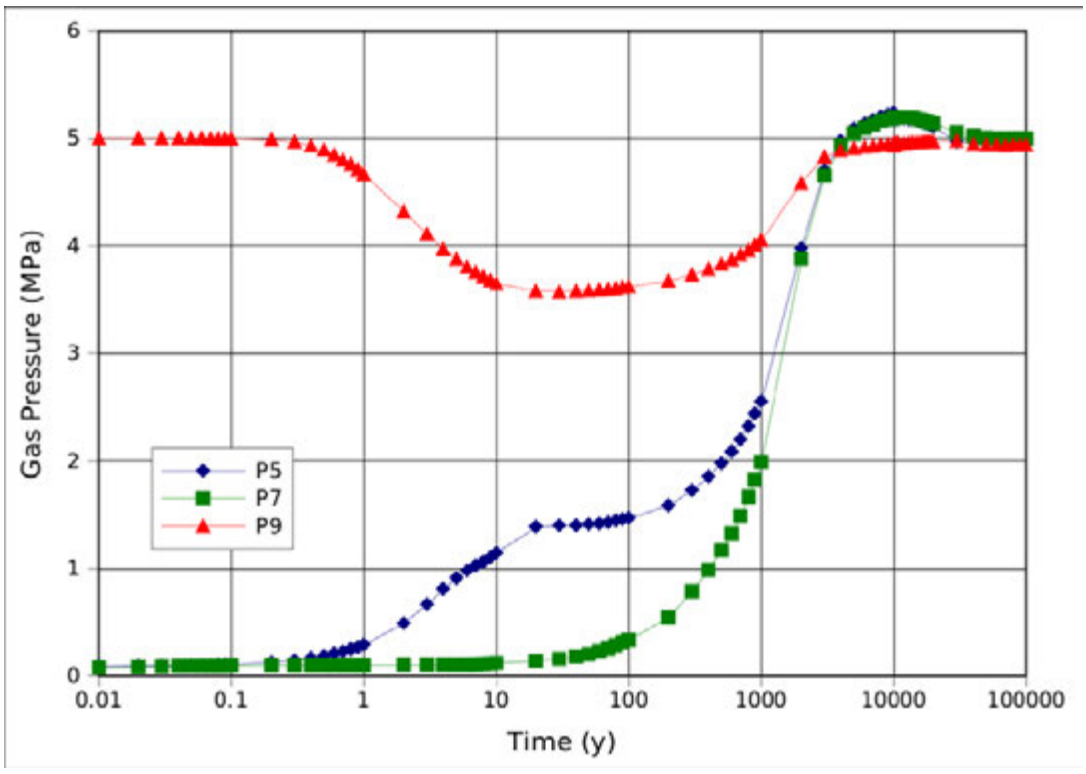

Figure 4 *Plot of gas pressures at points P5 (in the EDZ adjacent to the canister) P7 (drift EDZ) and P9 (radially halfway between the canister and the boundary).*

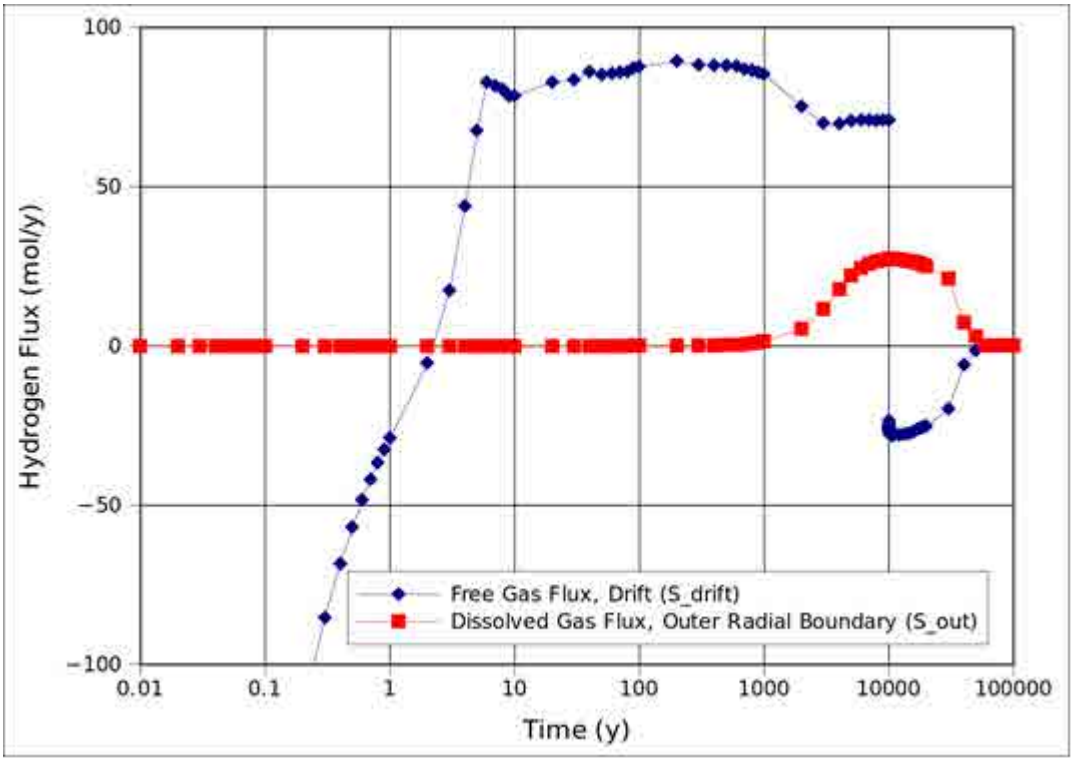

Figure 5 *Plot of free gas flow into the drift from the EDZ, plug and interfaces (blue) and plot of dissolved gas flux out of the radial boundary (red). Positive fluxes indicate outflow.*

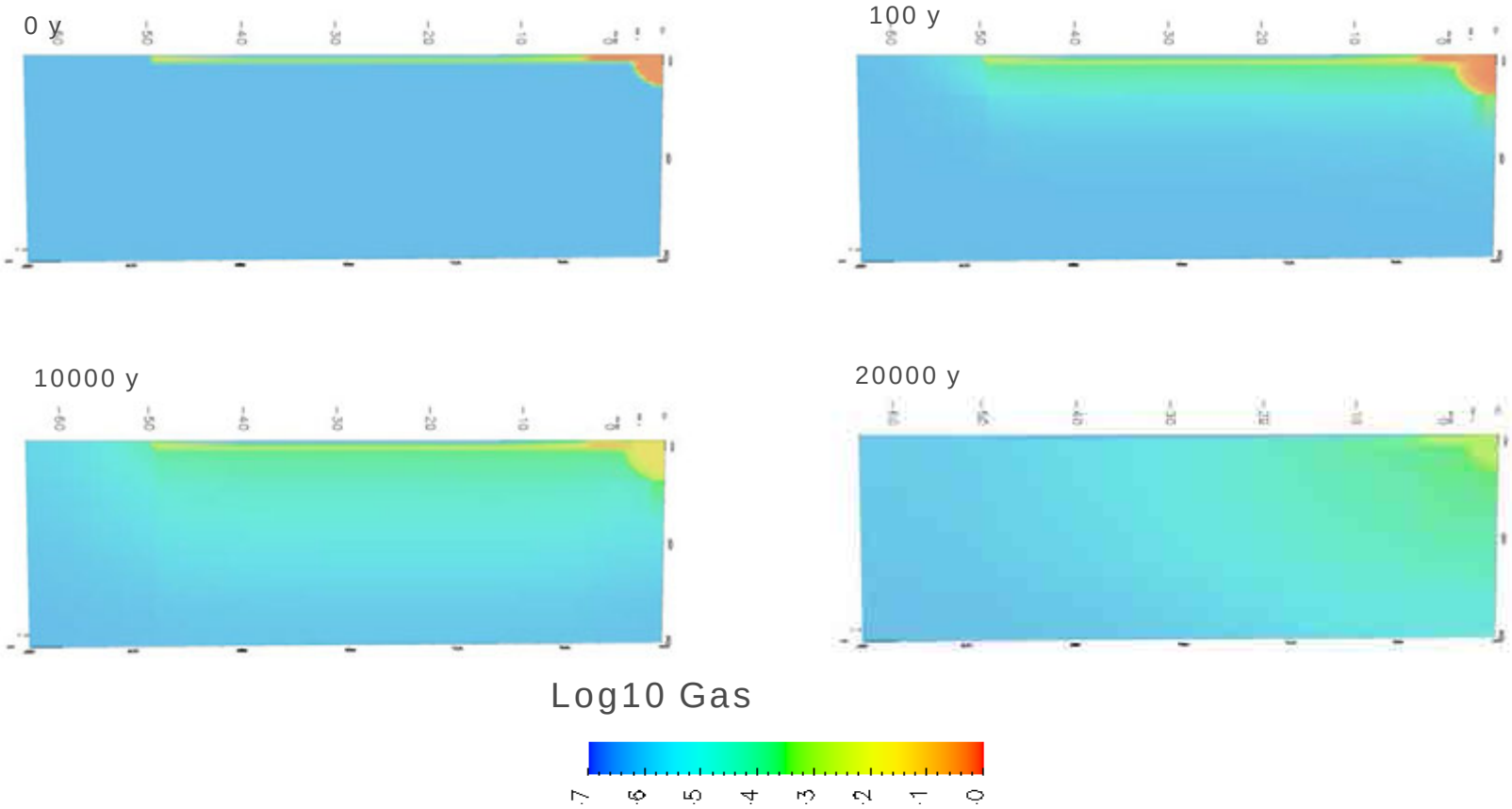

Figure 6 *Log10 Gas Saturation at selected times for the base case*

3.1.5 Prescribed Sensitivity Cases

Six overall sensitivity cases are prescribed in the specification (Cases 1 to 6 below) and a number of additional variants were defined during the course of the model development. The summary results for these cases are given in the following sections.

3.1.5.1 Case 1: Self Healing EDZ

Removal of the EDZs had a significant impact at early times, limiting gas invasion from the access drift and modifying the distribution of water pressure in the host-rock. However it did little to change the general characteristics of gas losses from disposal cell, with losses from the interfaces being even more dominant than in the base case.

3.1.5.2 Case 2: Altered Relative Permeability Curves

The alternative relative permeability curves for selected media had almost no effect on the bulk fluxes and pressures. This is consistent with the interfaces dominating free gas movement in the model, with most other gas transport in the model being via diffusion of dissolved gas.

3.1.5.3 Case 3: Increased Diffusion in Water

The enhancement of gas diffusivity by an order of magnitude had a dramatic effect on the bulk fluxes. It caused loss from the disposal cell due to the radial diffusion of hydrogen to dominate the gas transport processes at later times, and the role of free gas flows via the interfaces to be almost eliminated.

3.1.5.4 Case 4: Gas Generation Delayed

Three sub cases were examined, in which the onset of gas generation was delayed by 1, 2 and 10 years respectively. The impacts were relatively minor timing changes to the free gas fluxes at the drift and minor changes to the propagation of pressure fronts due to the pressurisation around the interfaces. In all cases the changes versus the base case were completely eliminated by 50 years model time.

3.1.5.5 Case 5: Less Permeable Interfaces

Three sub cases were examined, decreasing the waste interface permeability from the base value of 1e-12m^2 to 1e-15 m^2, 1.0e-18 m^2 and having the same properties as the EDZ (no interface). These changes had two important effects. The results clearly showed a build-up of gas pressure around the canister with an associated increase in gas saturation above that seen in the base case. Also gas fluxes to the drift were significantly reduced for the first 500 years due to build of gas as a free phase in the EDZ because of the length of time required to generate enough gas to maintain sufficient gas saturation to establish and maintain an equilibrium pathway to the drift (Figure 7).

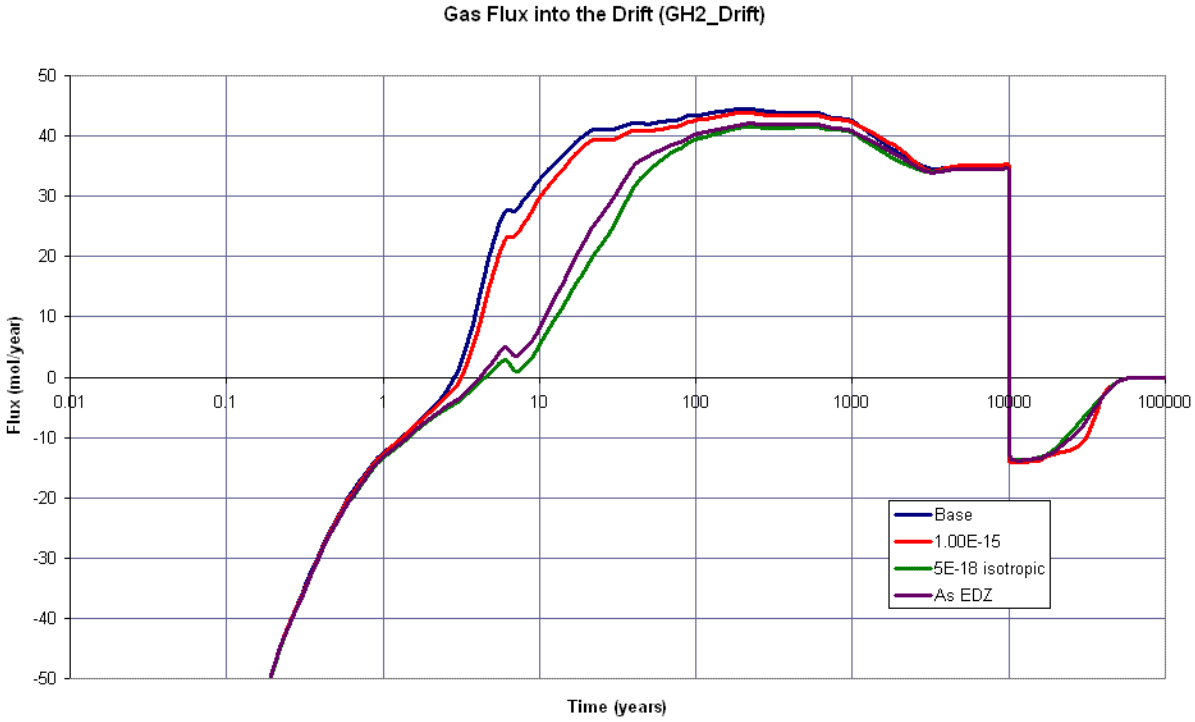

Figure 7 *Plot of free gas flow into the drift from the EDZ, plug and interfacesfor the different permeabilities of interface – note these are half-model fluxes and should be scaled by x2 to obtain the full model fluxes.*

3.1.5.6 Case 6: Mesh sensitivities

Various mesh sensitivity cases were examined using the base parameters. The sensitivities comprised two steps

1. Simplification of the geometry around the drift such that the geometry of the access drift was 'squared off' and a general reduction in resolution around the disposal cell. This results in fewer compartments/unknowns in the problem and hence provides a faster model that can be more effectively used as the basis for sensitivity analysis.

2. The squared-off case was further developed to analyse grid convergence. A series of models, the coarsest using 44 compartments and the finest in excess of 1200 compartments, was run using the gas flux to the drift as the metric for comparison between cases.

Inclusion of a simplified 'squared off' geometry for the drift only impacted on pressures and saturations local to the geometrical change and then only to a relatively minor degree – other differences, including to the bulk fluxes in the model, were relatively minor. The grid convergence testing showed that stable, and extremely similar, results could be obtained even using the coarsest of the grids (see Figure 8) with progressive refinement resulting in only relatively small changes to the timing of flux changes, and not significantly impacting on the magnitudes of fluxes or their variation with time.

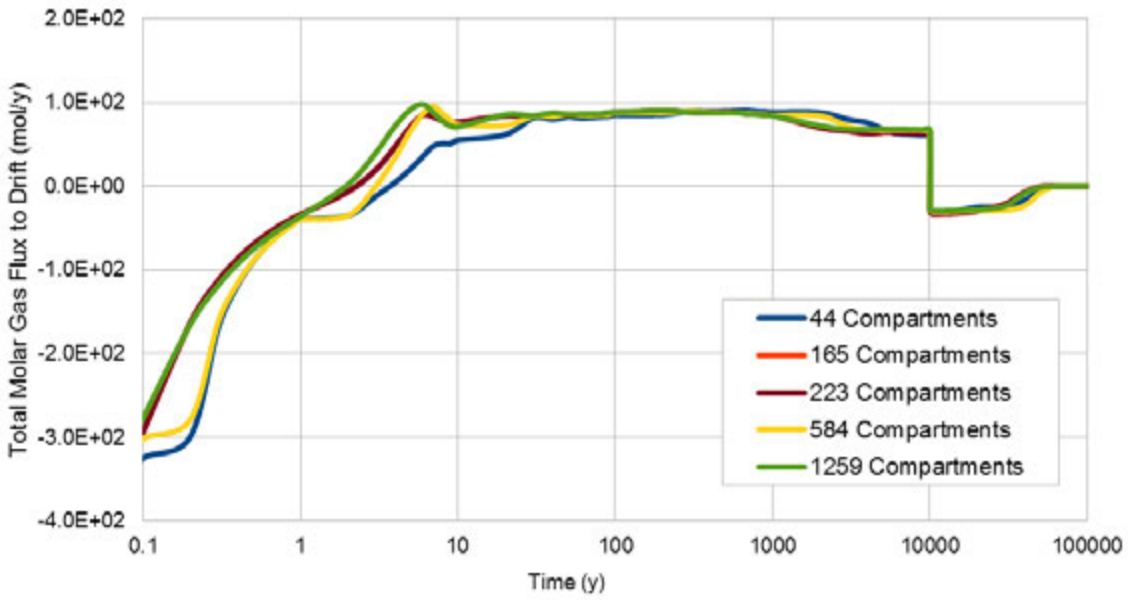

Figure 8 *Plot of free gas flow into the drift from the EDZ, plug and interfaces for different grid resolutions.*

3.1.6 Additional Sensitivities

In addition some further scoping calculations were conducted, the two most instructive of which are presented here. The first was an examination of the impact of the choice of using only a 2D grid and hence neglecting gravitational effects. This involved implementation of a full 3D model using angular discretisation of the "squared off" version of the geometry (Figure 9).

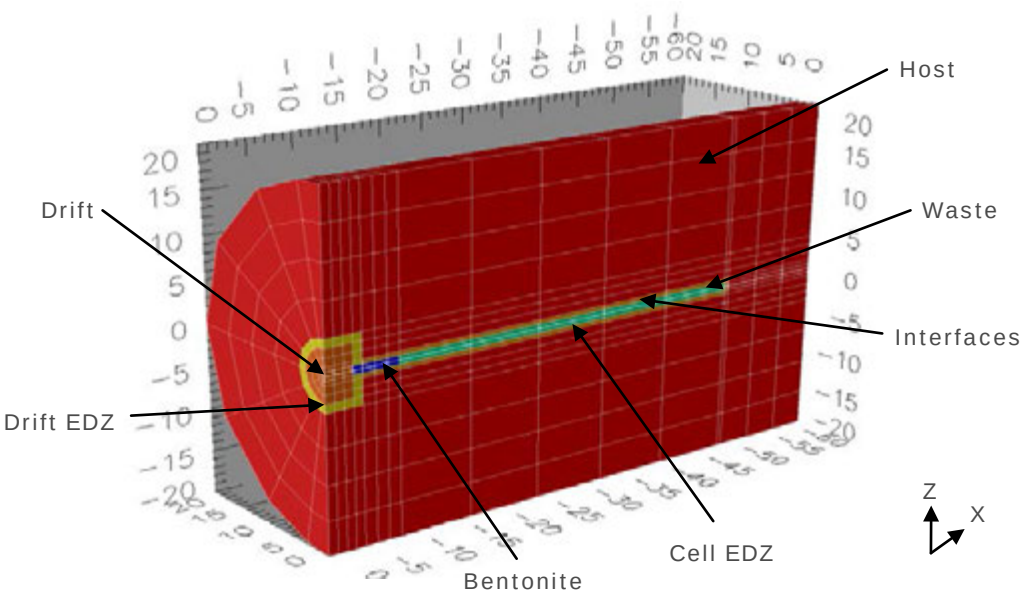

Figure 9 *3D grid using the 'squared off' grid geometry*

The 3D model showed some changes to local pressures and saturations compared with the equivalent 2D case, most notably gas accumulating at the top of the cell EDZ and interfaces. Otherwise the overall patterns and magnitudes fluxes of gas to the host-rock and drift access were largely unchanged. The spatial variations in saturations observed in the 3D case appeared to average out in some manner to produce a result that is very similar to the equivalent 2D case.

The second additional case examined the response of the system when no gas generation occurs. The equivalent plots to Figure 10 and Figure 11 are shown below. The results clearly show that without gas generation there is no significant free gas outflow into the drift. Instead, there is net inflow of gas into the system via the drift which then diffuses out of the model via the radial boundary. The diffusive gas flux results are so similar to the base case that it must be concluded that the diffusive outflows originate mainly from the partial desaturation of the access drift rather than from the gas generation around the canister. In terms of the pressure results one sees a small drop in pressurisation around the canister (P5) otherwise the form is very similar to the base case. Clearly the boundary conditions, especially the condition imposed at the drift, are exhibiting a very strong control on the results.

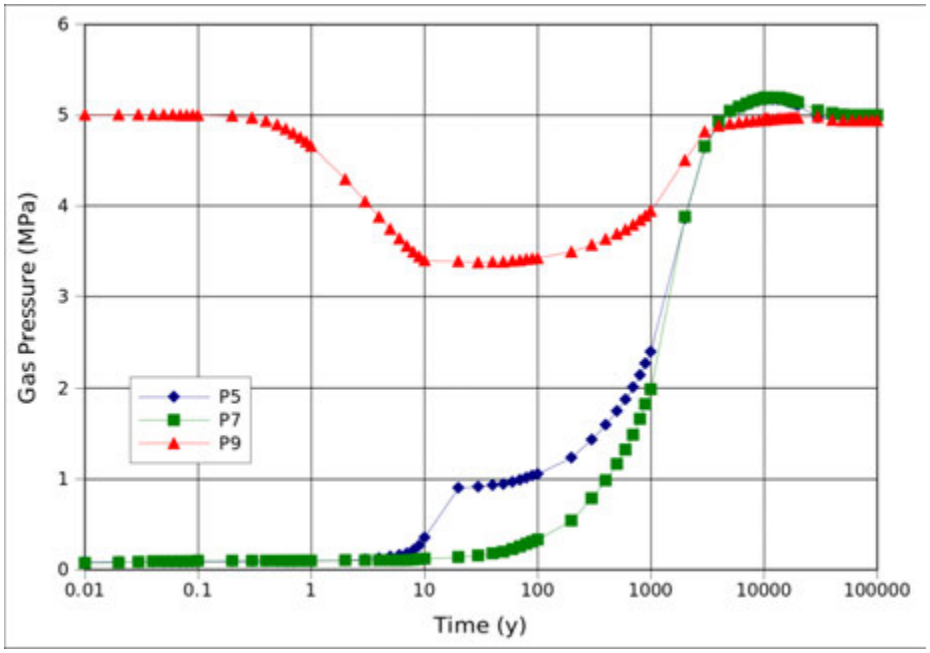

Figure 10 *Plot of gas pressures at points P5 (in the EDZ adjacent to the canister) P7 (drift EDZ) and P9 (radially halfway between the canister and the boundary).*

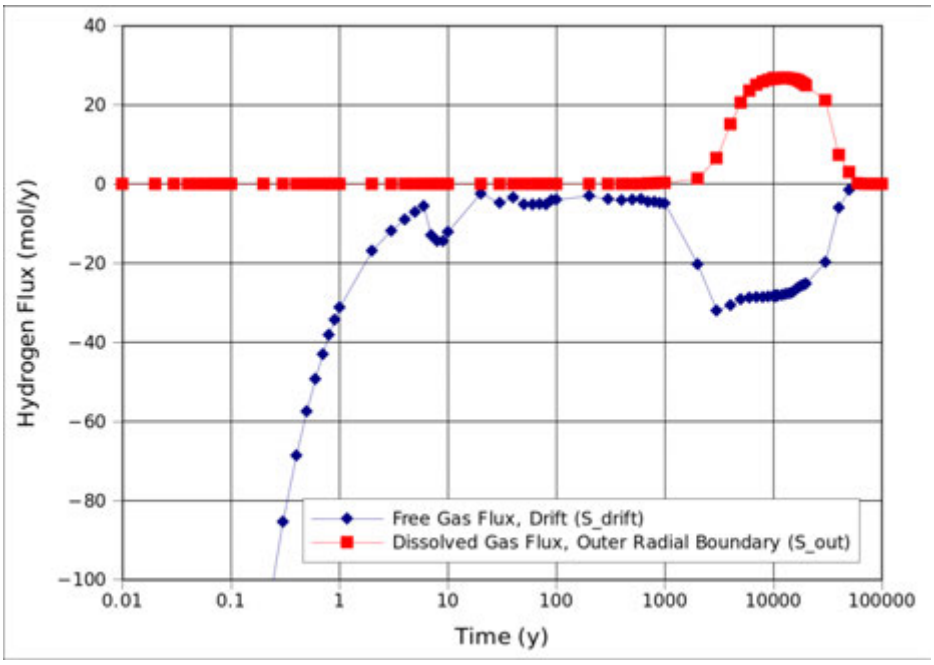

Figure 11 *Plot of free gas flow into the drift from the EDZ, plug and interfaces (blue) and plot of dissolved gas flux out of the radial boundary (red), no gas generation case. Positive fluxes indicate outflow.*

3.1.7 Discussion and Conclusions

3.1.7.1 Lessons Learnt

During the process of constructing the model and clarifying potential ambiguities in the specification a number of potentially significant points were identified.

1. It is possible to construct a full multi-phase flow model at the cell-scale using QPAC, including small scale features such as interfaces. The run times were sufficiently fast and the model sufficiently flexible to allow a large number of sensitivity cases to be run, including investigations into different grid dimensions and resolutions. The ability to run many models, all with mutually consistent behaviour, significantly increases confidence in the results.

2. The presence of the high permeability interfaces presents a significant numerical challenge, and while the code was able to solve the case, solver diagnostics indicated that these areas were of particular concern and controlled the timestepping behaviour.

3. The choice of the representation of storativity in the specification is unusual in that matrix compressibility is accounted for by compressing the water phase rather than by adjusting the porosity. Moreover the pressure term used in the storativity term only uses the water pressure and does not include a gas pressure component, as one would expect from a conventional effective stress type formulation [2]. The impact of adopting such a simple model was seen in early versions of the calculations, carried out before the specification was finalised to precisely define the storativity model. Using the default QPAC storativity model (a simple Bishop effective stress approach) significant changes in fluid pressures were seen during the mid-time part of the simulation. However early and late-time behaviour was almost identical and the calculated fluxes were largely insensitive to this change.

4. The boundary conditions at the access drift exert an extremely strong control on the model behaviour, largely due to their type and proximity to the waste cell. As shown in the other

benchmarks [4, 5], it is clear that these boundaries are not representative of the general behavior of the repository, for the parameterization given in the specification.

5. The grid refinement and 3D results are interesting in that they imply that quite radical simplifications can be made to system representation without impacting significantly on the key features of the results. In particular the grid convergence results imply, as the case is currently specified, that the specification of the case as a 2D section does not compromise the realism of the model in any significant fashion. The results of the squared off geometry case and representation of the case in 3D suggest that a fairly simplified and coarsely discretised representation of the 2D geometry is still appropriate using this numerical formulation. This is of particular interest when modelling at larger scales [4, 5], as it provides the possibility of using large numbers of relatively coarsely-gridded grid sections to represent the facility in whole or part. Such techniques are explored in the larger-scale benchmarks [4, 5].

3.1.7.2 Issues for further consideration

It is clear that the interfaces, as parameterised, have a significant impact on the fate of gas at this small scale. This brings into question whether the selected parameterisation, evolution and associated process models for the interfaces are appropriate, or whether this simplified description is missing key aspects of behaviour.

It has been noted widely (e.g.[3]) that fluids (especially gases) in bentonites can exhibit dilatant flow behaviour at material boundaries, giving rise to flow behaviours that cannot readily be reproduced using the conventional multi-phase flow formulation. The impact of bentonite saturation, bentonite swelling and stress state, together with fluid pressures and saturations could significantly impact on the hydraulic behaviour of these features. Given this potential dependency it is suggested that thought be given to a suitably simplified and upscaled hydro-mechanical model that might be implemented. An example 'proof of principle' model has been proposed and constructed in QPAC to demonstrate that such a process model can be used (Figure 12). This abstracted model estimates a swelling pressure associated with a compartment which is part of the bentonite plug on the basis of fluid saturation in the plug. Using QPAC input it is then possible to use that swell pressure (and hence implied mechanical stress) on the adjacent compartments representing the interfaces. A modified relative permeability curve for gas transport parallel to the interface can then be used to create enhanced flow (including creating net permeabilities greater than the reference intrinsic permeability for gas only) under different effective stress conditions. The major advantage of such an approach is that the mechanical component of the problem (which can be extremely complex for bentonite) is greatly simplified, and hence can be implemented relatively simply in a multi-phase flow model with little computational overhead, while retaining the overall behaviour required.

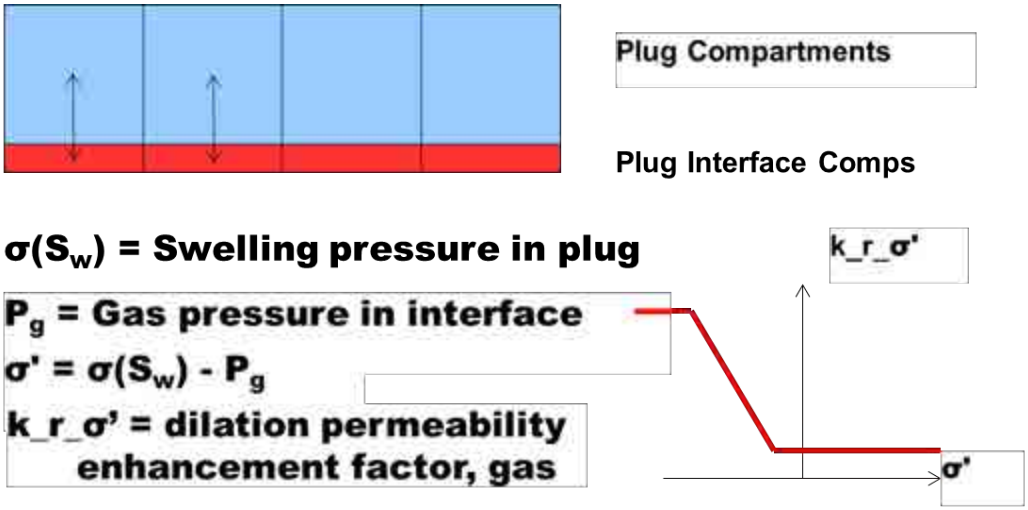

Figure 12 *Schematic illustration of a possible abstracted model for dilation flow.*

Such a model was implemented and tested successfully using estimated parameters for the cell-scale benchmark models discussed here, however, there is currently insufficient information to properly parameterise such a model and develop this simplified model further. Discussions with other programmes examining the physical response of such systems may give an opportunity to better model and help understand the true importance of interfaces in these systems.

3.1.8 References

1 Bond AE. and Benbow SJ. (2009). QPAC Multi-Phase Flow Module Functional Specification and Architectural Design. Quintessa Report QRS-3000C-4 v1.0.

2 Bishop AW. (1959). The principle of effective stress. Tecnisk Ukeblad. 39:859-863.

3 PAMINA (2009). PA approach to gas migration. Deliverable No. 3.2.1.

4 FORGE (2013). Deliverable D1.6 Final report on benchmark studies on repository-scale numerical simulations of gas migration. Part 2 : module scale benchmark

5 FORGE (2013). Deliverable D1.6 Final report on benchmark studies on repository-scale numerical simulations of gas migration. Part 3 : repository scale benchmark

3.2 SCK-CEN contribution

3.2.1 Introduction

The aim of this first benchmark is trying to answer some precise questions in a PA logical (for example, which could be the relative role of the EDZ, interfaces, backfill in the migration of gas). It aims to know better how the systems react and why they can react differently rather than an inter-comparison of codes. Although the final aim of the benchmark studies is to represent repository-scale simulations, the first exercise is at cell scale and as generic as possible.

This benchmark exercise representing gas transport in a repository for radioactive waste is to model simultaneously all gas sources (located in the disposal cells) and the transport pathways constituted by the network of interfaces, plugs and underground drift.

Compared to the results of SCK in delivery D1.3 [1], parameter differences from the benchmark definition were minimized after solving several numerical convergence difficulties. The role of interface in gas migration and more sensitivity analyses were analysed in this report.

3.2.2 Modelisation of the cell module

Software GID 8.0 developed by International Centre for Numerical Methods in Engineering (CIMNE) was used for the mesh generation and CODE_BRIGHT 3.0 by Technical University of Catalunya (UPC) was used for the calculation. In absence of validation data for the complex problem of gas generation and transport in geological repositories, the confidence of the validity of the numerical tool in solving THG (thermo-hydro-gas) coupling problems was achieved by comparing benchmark results between CODE_BRIGHT and TOUGH [2].

3.2.2.1 Geometry and boundary conditions

The benchmark is to simulate the gas production and migration in a disposal cell and a portion of the drift (Figure 13).

The benchmark exercise is an axisymetric two-dimensional problem with isothermal hypothesis at 20°C. In the direction of the disposal cell axis, the extension is assumed to be 50 m which takes into account the length of the cell, the distance between two adjacent cells and a portion of the access drift. The radius of the axisymetric domain is assumed to be 20 m which is a compromise between the inter-cell distance along the access drift and the thickness of the geological layer. For the detailed dimensions of the problem, please refer to the definition of the benchmark exercise [3].

A gas production term is provided by the disposal cell. It is imposed on the external surface of the cylinder which represents schematically the waste canisters. The disposal cell is constituted as a material impermeable to both water and gas. The materials to be taken into account in the simulation include the EDZ of both the cell and the access drift, the cell plug, the backfill of the drift, interface and geological medium.

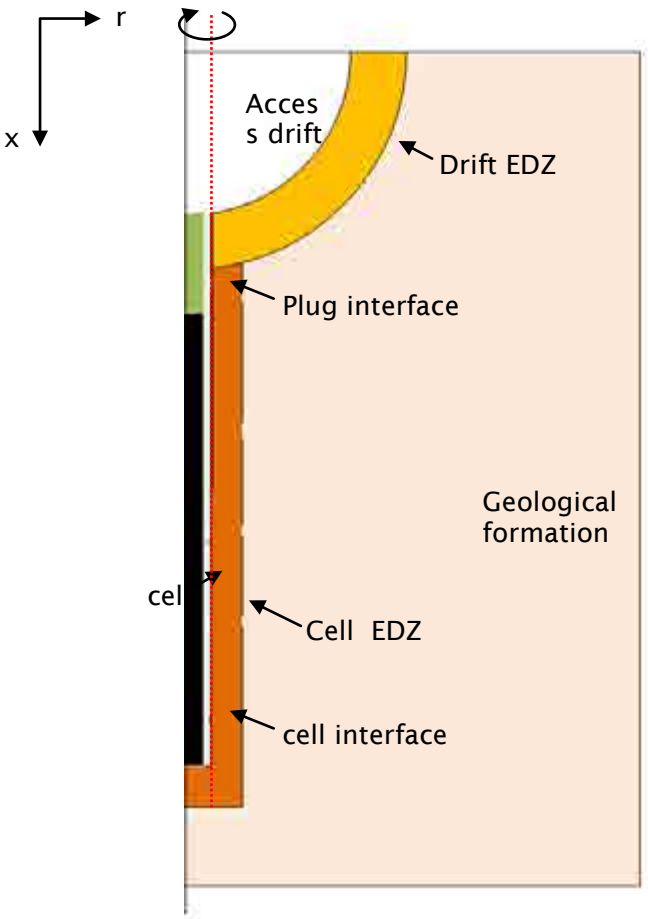

Figure 13 *Problem geometry*

The whole domain is meshed with 2535 triangular linear elements (Figure 14). The Hydrogen produced from the canister cell is considered uniformly distributed within the cell and the time evolution of hydrogen production is illustrated in Figure 14. In the calculation, Hydrogen influx is imposed along the external surface of the waste canister (detailed figure in Figure 14).

Except the outer boundaries with fixed gas and liquid pressure (blue dashed line), the other boundaries are assumed to be no flux boundary (black line). Gas/liquid pressures at the drift boundary (pink line) are time varying. Figure 15 shows the time varying gas/liquid pressure at the drift boundary used in the numerical simulation for the base case.

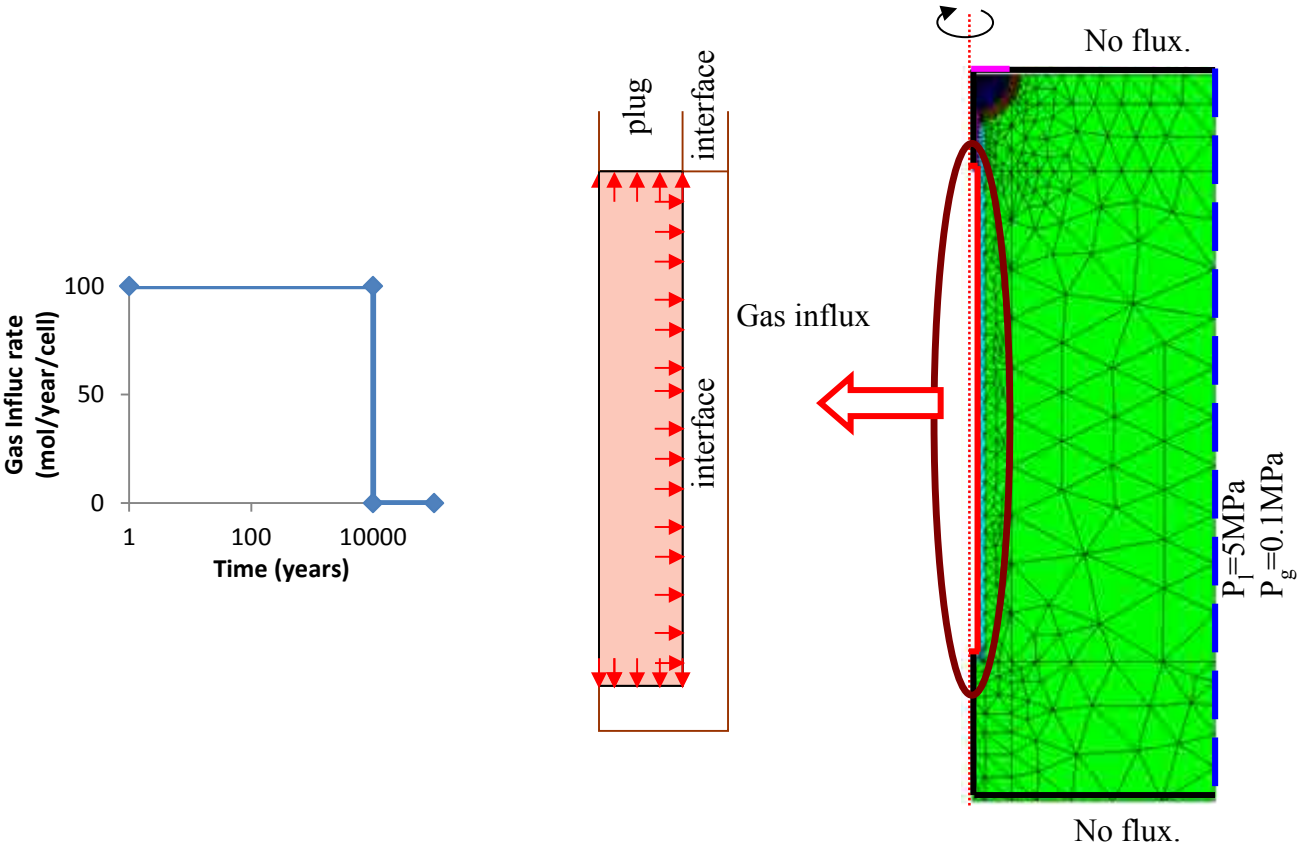

Figure 14 Mesh of the domain and imposed boundary conditions

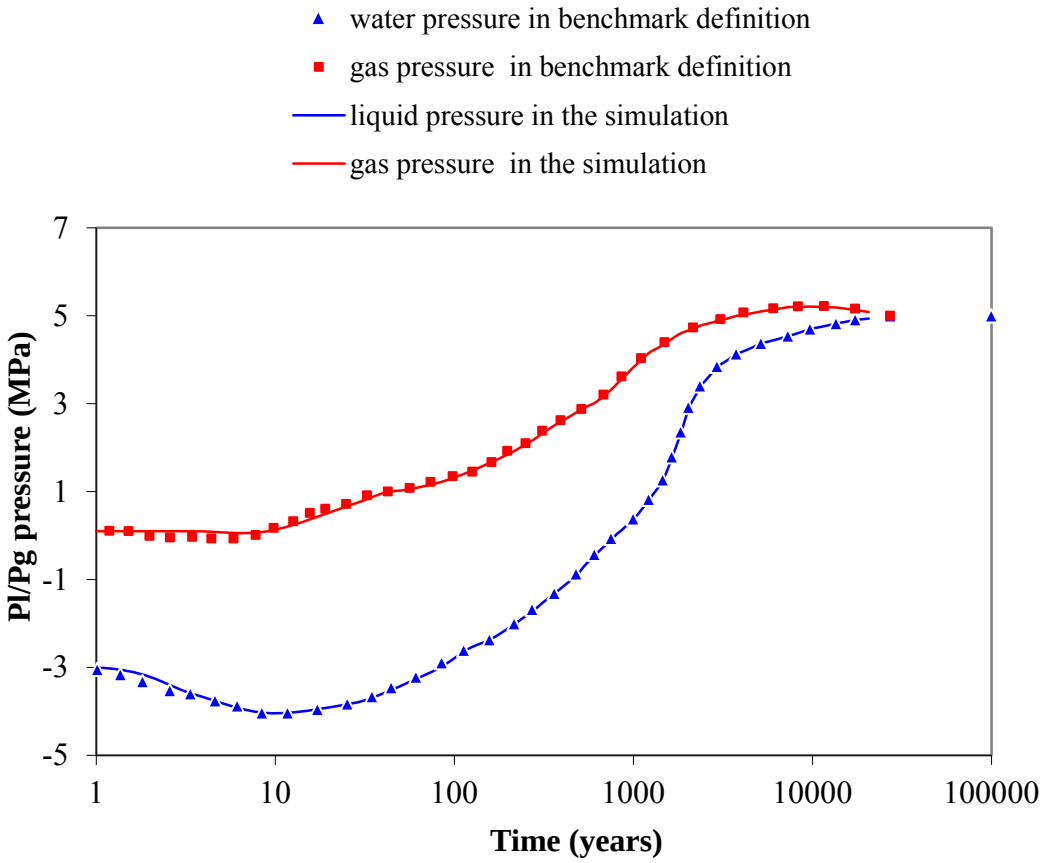

Figure 15 Time variation condition at the boundary of drift

3.2.3 Initial conditions

The geological formation and EDZ are considered to be initially saturated with Pg=0.1 MPa and Pl=5 MPa. Plug is initially 70% saturated with Pg=0.1 MPa and Pl=-21.27 MPa. Drift is initially 70% saturated with Pg=0.1 MPa and Pl=-2.985 MPa. The initial water pressure in the plug interface is assumed to be -40 MPa.

3.2.4 Constitutive models and parameters

The physical models used in the simulation are defined as that required in the benchmark definition including viscosity of gas mixture, diffusion coefficient of dissolved hydrogen and gaseous hydrogen, solubility of hydrogen, retention curve and relative permeability of water and gas. Although great efforts have been made to make the constitutive laws used in CODE_BRIGHT to be the same with what required in the benchmark, there are still the following differences:

- Liquid viscosity:

  In CODE_BRIGHT, liquid viscosity is temperature dependent and obtained from:

$$\mu = A\exp\left(\frac{B}{273.15+T}\right)$$

  where A is a pre-exponential parameter with a default value 2.1×10^{-12} MPa·s for water, B is an exponential parameter with a default value of 1808.5 K for water, T is temperature (°C). It was checked that over the temperature range of 15 °C - 100 °C, as the steam table of 1967 implemented in TOUGH gives quite similar values for water viscosity.

- Liquid density:

Density of water in CODE_BRIGHT is temperature and pressure dependent and expressed as:

$$\rho_l = \rho_{l0} \exp\left(\beta\left(P_l - P_{l0}\right) + \alpha\left(T - T_0\right)\right)$$

where ρ_{l0} is reference liquid density at reference pressure P_{l0} (0.1 MPa) and reference temperature T_0 (0 °C), β is the compressibility coefficient and α is the volumetric thermal expansion coefficient for the liquid phase. Water density calculated using this equation was checked with the function given in the benchmark definition, they give almost the same values.

- Saturation pressure for vapour:

  In CODE_BRIGHT, the saturation pressure of vapour is calculated by:

$$\rho_{v0} = 136075 \exp\left(\frac{-5239.7}{273.15 + T}\right)(MPa).$$

  At 20 °C, saturation pressure for water vapour is calculated to be 2.35 kPa in CODE_BRIGHT, which is very close to the value given in the benchmark definition, 2.34 kPa.

The parameters used in the base case are summarized in Table 1.

Besides the reference case, five among seven sensitivity analyses defined in the benchmark exercise have been carried out by SCK in the exercise:

- Sensitivity analysis 1: all the parameters remain the same as in base case, except that the intrinsic permeability of EDZ is decreased to be the same as the intrinsic permeability of host rock;
- Sensitivity analysis 3: all the parameters remain the same as in base case, except that the diffusion coefficient of dissolved H_2 in liquid phase is increased by one order;
- Sensitivity analysis 5: all the parameters remain the same as in base case, except that gas production starts after one year later;
- Sensitivity analysis 6: all the parameters remain the same as in base case, except that the intrinsic permeability of interface decreases to 10^{-15} m^2;
- Sensitivity analysis 7: all the parameters remain the same as in base case, except that the intrinsic permeability of interface decreases to be the same as the intrinsic permeability of EDZ.

Table 1 *Material properties used in calculations for the base case*

		Unit	Host rock	drift	plug	EDZ	Plug Interface	canister Interface
porosity	η	-	0.15	0.4	0.35	0.15	0.3	0.99
permeability	k_x	m^2	5×10^{-21}	5×10^{-17}	1×10^{-20}	5×10^{-18}	5×10^{-18}	1×10^{-12}
	K_y	m^2	1×10^{-20}	5×10^{-17}	1×10^{-20}	1×10^{-17}	1×10^{-17}	1×10^{-12}
tortuosity	τ	-	2	2	4.5	2	1	
capillary pressure function								
shape parameter	λ	-	0.3333	0.3333	0.375	0.3333	0.75	0.75
residual w saturation	S_{lr}	-	0	0	0	0	0	0
maximum w saturation	S_{ls}	-	1	1	1	1	1	1
air entry pressure	P_0	MPa	15	2	16	1.5	0.01	0.01
liquid density [a]								
Storage coefficient	β	m^{-1}	2.3×10^{-6}	1×10^{-5}	4.4×10^{-6}	2.3×10^{-6}	4.6×10^{-6}	4.6×10^{-6}
Reference density	ρ_{l0}	Kgm^{-3}			1002.6			
Reference pressure	P_{l0}	MPa			0.1			
Volumetric thermal expansion coefficient	α	$^{\circ}C^{-1}$			-3.4×10^{-4}			
Liquid viscosity [b]								
A		MPas			2.1×10^{-12}			
B		K			1808.5			

[a] Liquid density: $\rho_l = \rho_{l0}\exp\left(\beta\left(P_l - P_{l0}\right) + \alpha\left(T - T_0\right)\right)$

[b] Liquid viscosity: $\mu_l = A\exp\left(\frac{B}{273.15 + T}\right)$

3.2.5 Results

Evolution of gas pressure and boundary fluxes, as well as comparisons with results from other teams can be found in the summary report. Figure 16 gives an example of the evolution of nodal gas pressure at two observation points. The nearer does the point locate to the canister, the higher the gas pressure is.

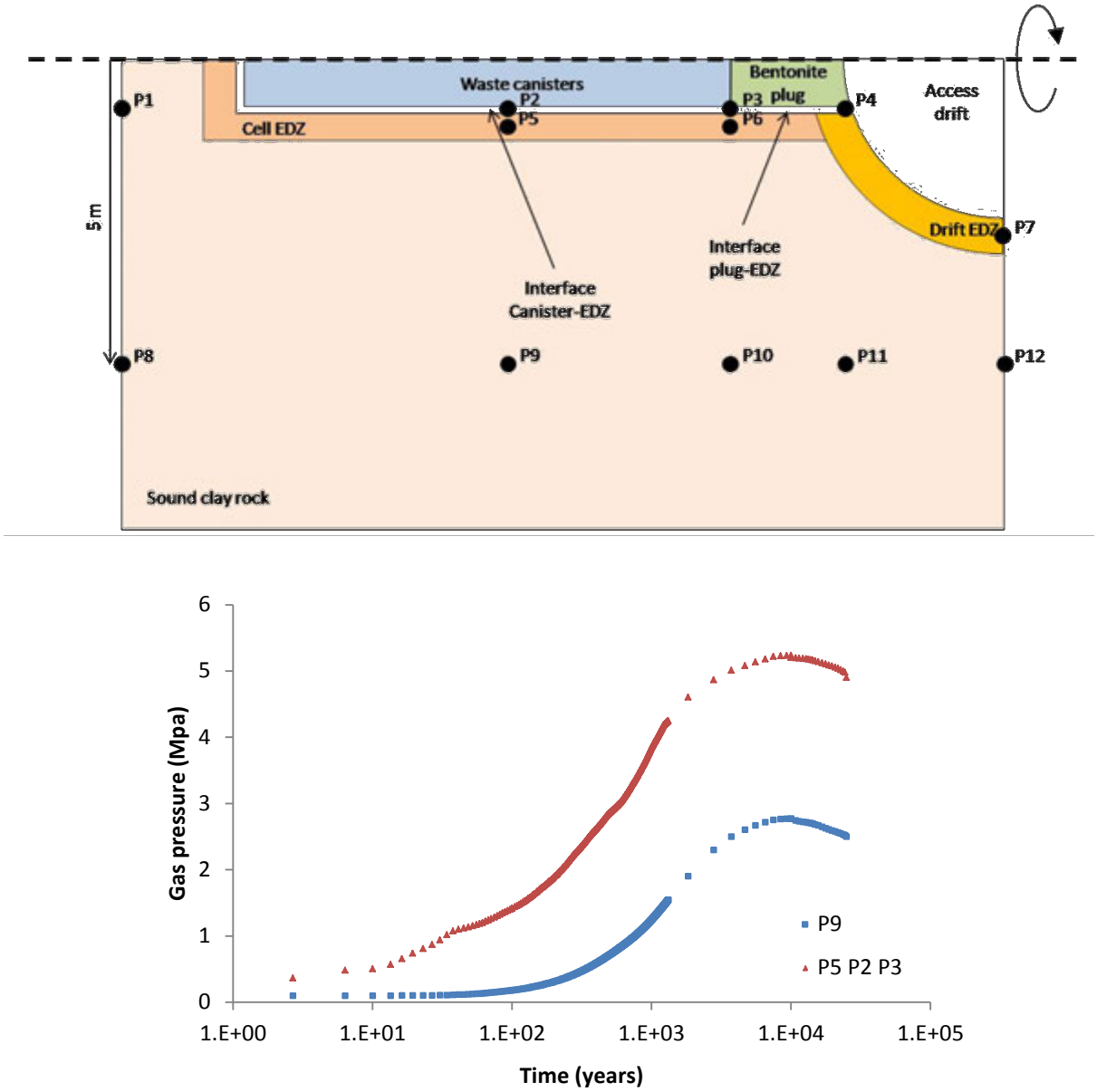

Figure 16 Time evolution of nodal pressure

Figure 17 illustrates gas flux vector at 1000 years. With the existence of very permeable interface, it is evident that the gas migrates preferentially along the interface.

Figure 18 gives the distribution of liquid saturation at 10,000 years. It shows that the interface is quite dry which is due to the steep retention curve defined for the interface. The unsaturated area in the module is limited with EDZ and drift. Most of the host clay and plug remains saturated.

Consistently, the comparison of gaseous fluxes along three boundaries presented in Figure 19 indicates that gas flows preferentially along EDZ and interface towards the drift. After 10,000 years when the gas production stops, gas flows back and dissipates through the host rock.

Time evolution of gas pressure at P2 in five sensitivity analyses is drawn in Figure 20. The first two sensitivity cases i.e. increased D and delayed gas production, do not have too much differences with the reference case. The gas pressure increases obviously with the decreasing of permeability of the interface. Results from all cases converge to very similar values after 1,000 years. The sensitivity analysis with the permeability of EDZ equal to host rock does not yield results due to numerical convergence problems.

Figure 21 compares the evolution of gas pressure contour map in five sensitivity analyses. Besides this, the gas pressure in the case without considering interface is also provided for comparison. The graphs in Figure 21 clearly show that the existence of interface is very efficient in dissipating gas produced in the waste canister. Even when the intrinsic permeability of interface decreases to be the same as EDZ, the gas still migrates preferentially along interface because the retention curve defined for the interface makes this material easy to be desaturated and serves as a preferential pathway for gas migration.

Gaseous flux along EDZ and interface are compared among five sensitivity analyses in Figure 22. The case with increased D lowers the gaseous flux because it makes gas much easier to migrate in the dissolved water. With the increasing of the permeability of interface, gas flows more preferentially along interface. When permeability of EDZ is equal to that of host rock, nearly all the gas flows along the interface.

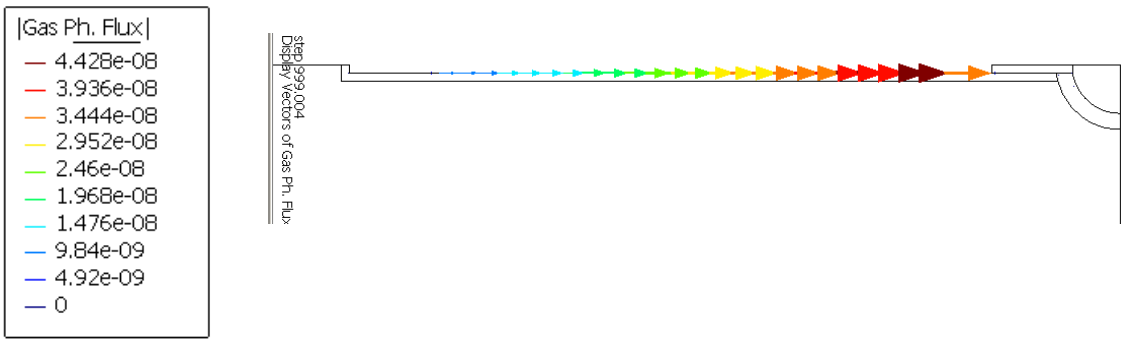

Figure 17 *Gas flux vector at t=1,000 years (Unit: kg/s)*

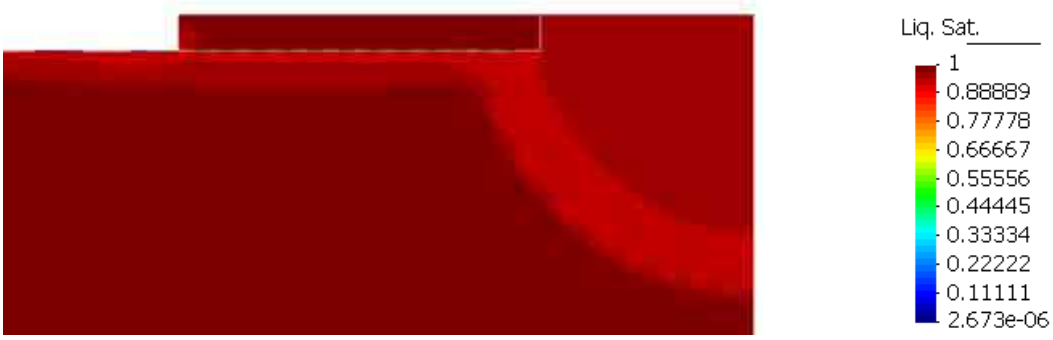

Figure 18 *Liquid saturation contour map at t=10,000 years*

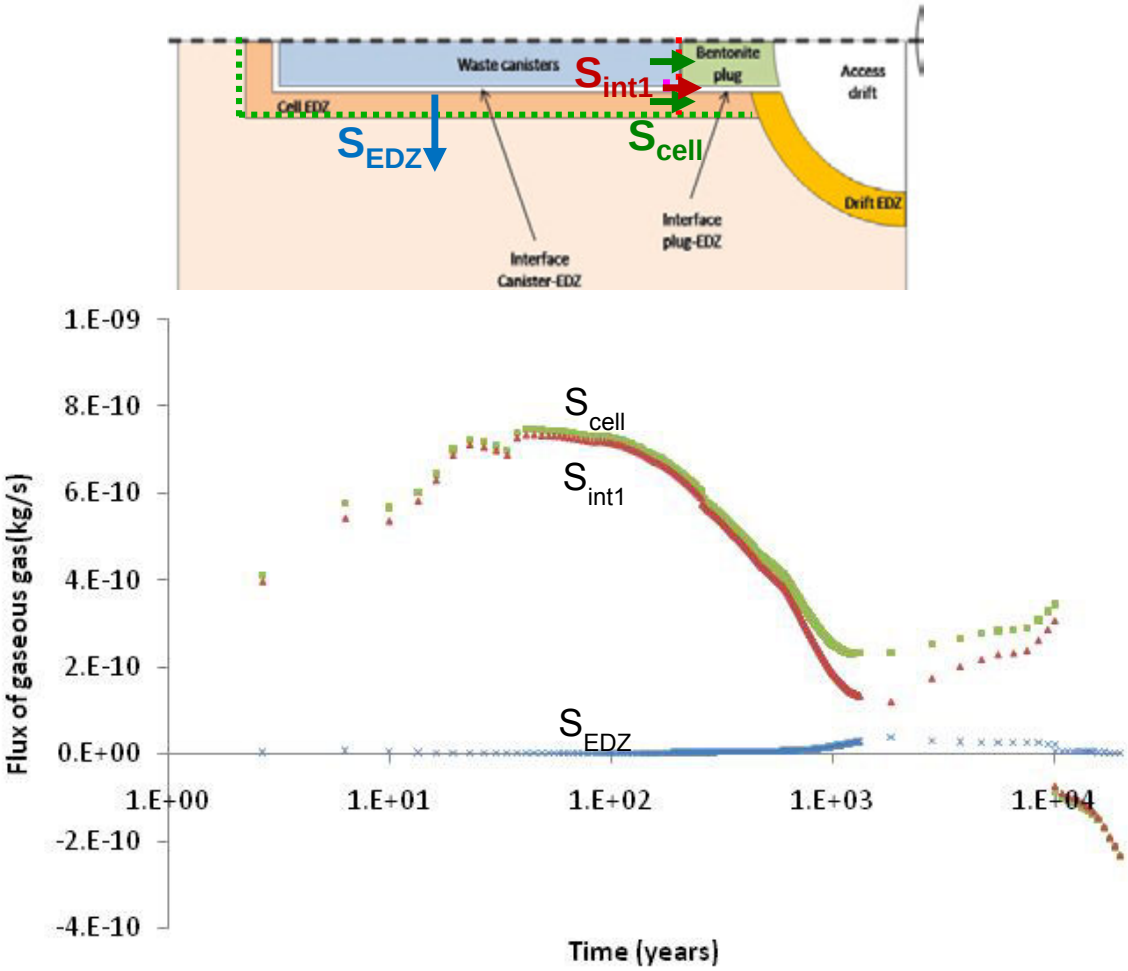

Figure 19 *Comparison of gaseous flux along three boundaries*

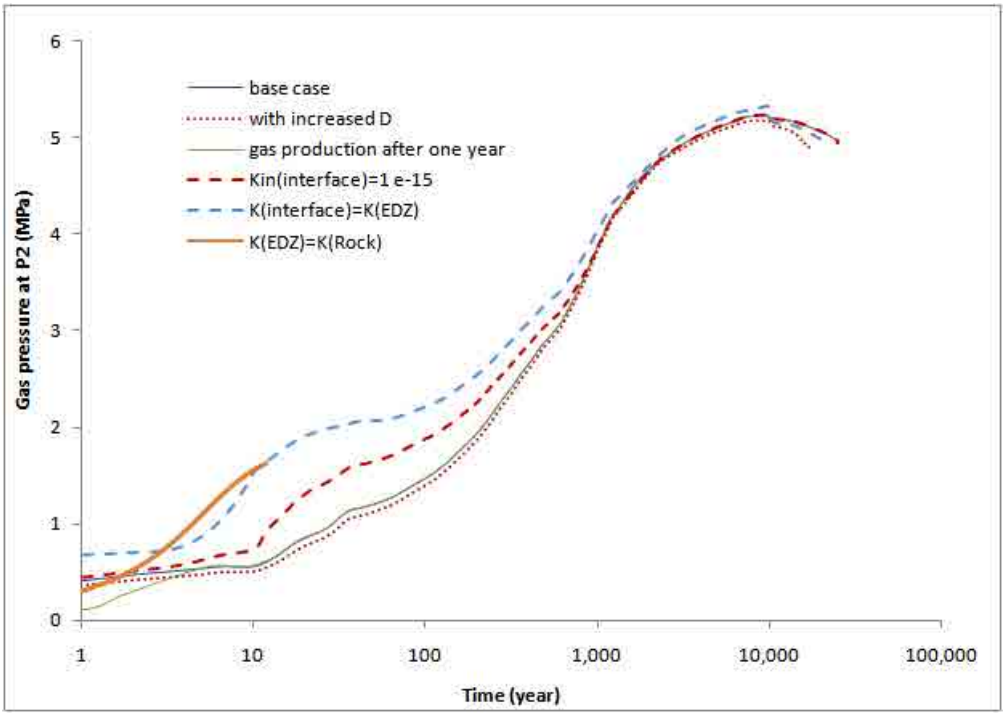

Figure 20 Comparison of the evolution of gas pressure in sensitivity analyses at P2

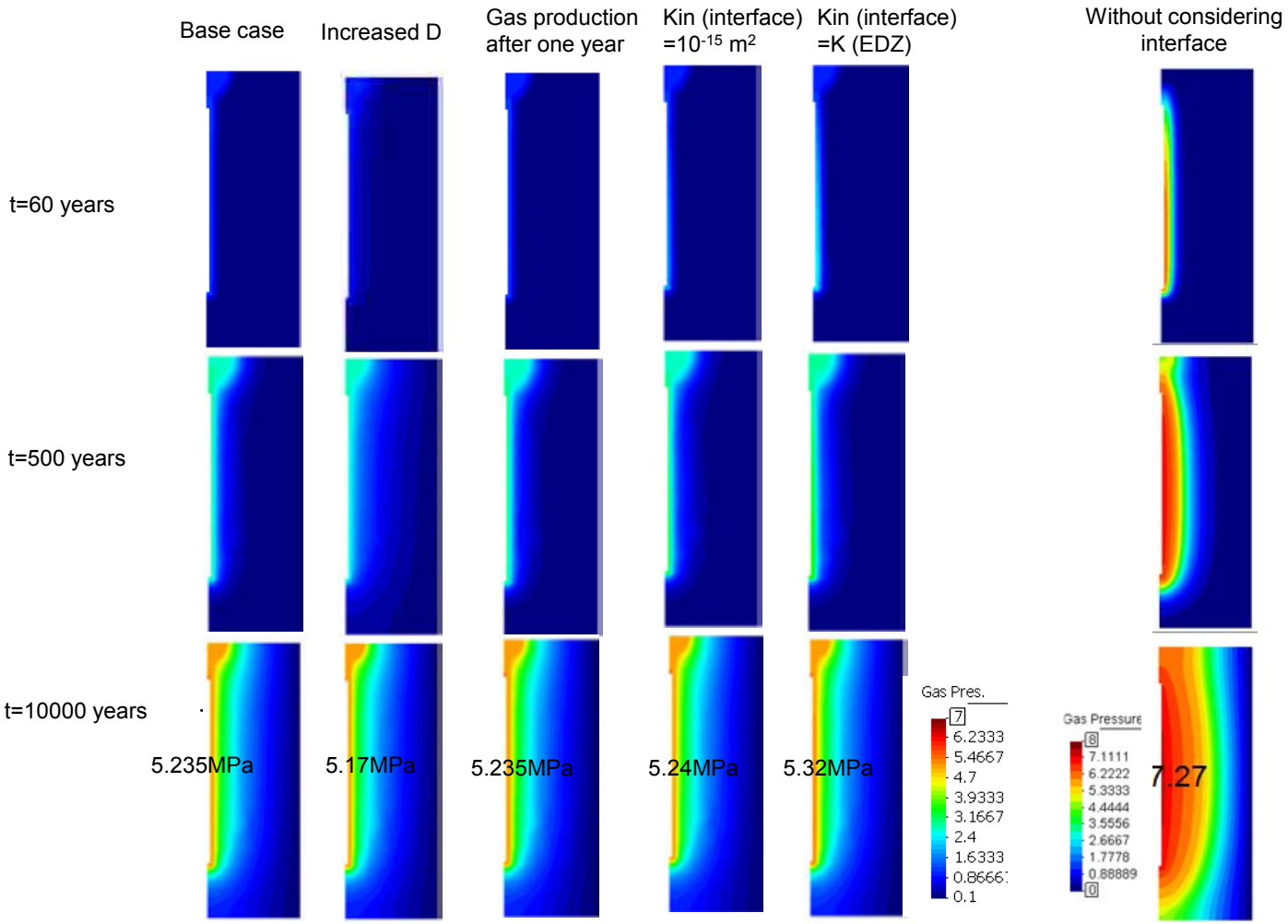

Figure 21 *Comparison of the evolution of gas pressure in sensitivity analysis (Unit: MPa)*

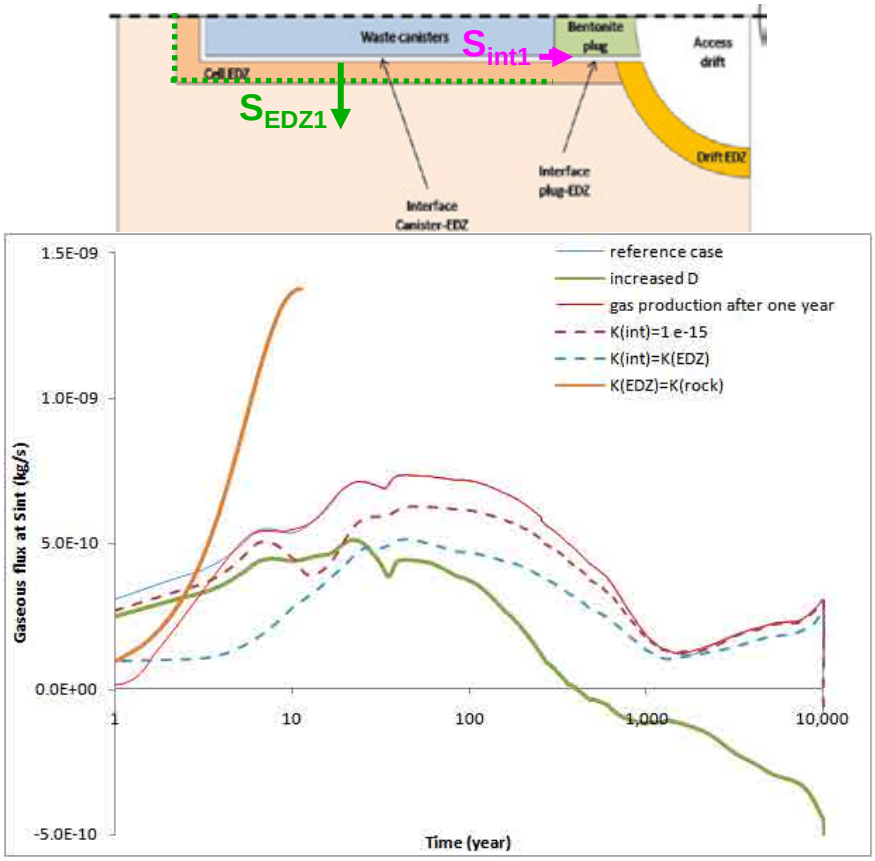

(a)

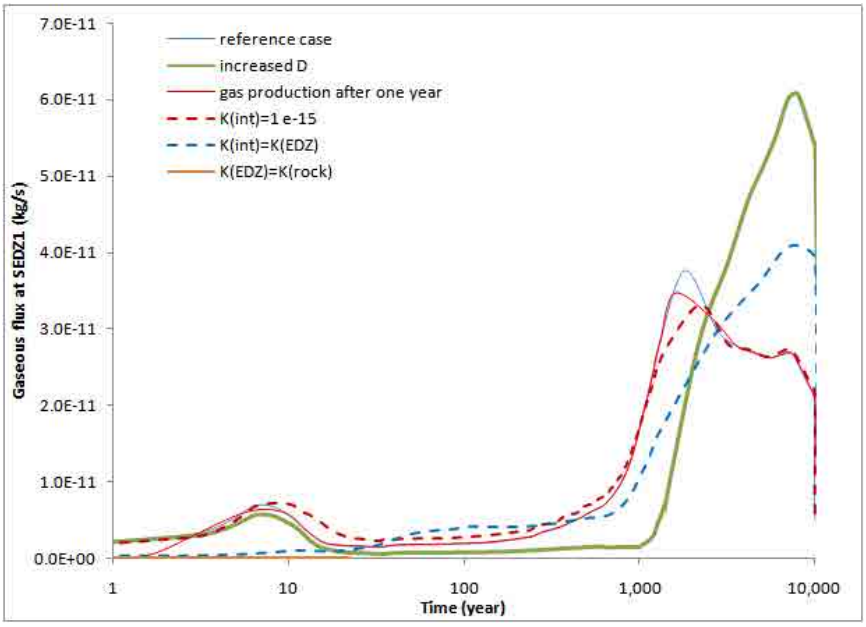

(b)

Figure 22 Comparison of the gaseous flux in five sensitivity analyses through (a) interface S_{int1} and (b) EDZ S_{EDZ1}

3.2.6 Conclusion and remarks

Through the exercise of the first benchmark defined in WP1.2, it is proved that the current numerical tools based on two-phase flow theory are capable of modelling gas migration in a geological repository system. The numerical difficulties such as the very permeable interface, time variable boundary conditions and various distinct materials coexisting in one system and so on have been tackled through this exercise. Hence, upscaling from module scale to repository scale is promising.

The conceptual uncertainty lies on the validity of the boundary condition and the parameterisation of the interface and EDZ. In this benchmark, the interface is modelled as a normal porous media with high permeability. The quite steep retention curve adopted for the interface makes the modelling not easy. It is foreseen that such a peculiar behaviour of interface probably will cause convergence problem when dealing with a complicated repository scale modelling.

Furthermore, how to reflect the time evolution of the EDZ and interface deserves more efforts in the future. However, to what degree does this modelling results reflect the reality in the repository system needs further investigation.

3.2.7 References

[1] L. Yu, J. Wendling, M. Dymitrowska, D. Pellegrini, D. Justinavicius, M. Sentis, S.Norris & A. Bond (2010) Progress report on benchmark studies on repository-scale numerical simulations of gas migration. FORGE delivery D1.3, J. Wendling (eds). http://www.bgs.ac.uk/forge/docs/reports/D1.3.pdf.

[2] L. Yu, E. Weetjens, J. Perko & D. Mallants (in press). Comparison of numerical tools through Thermo-Hydro-Gas transport modelling for a geological repository in Boom Clay. Nuclear Technology.

[3] J. Wendling (2010) Draft report on definition of benchmark studies on repository-scale numerical simulations of gas. FORGE delivery D1.1 Ver.0. http://www.bgs.ac.uk/forge/docs/reports/D1.1.pdf

3.3 Andra contribution

3.3.1 Introduction

This report gives a view of the work done by Andra in the framework of the "cell scale" benchmark of package WP1.2 of the FORGE project. The work done covers most of the prescribed sensitivities, but some specific calculations have not been made mostly because of a lack of available time to complete these before June 2011.

This report first described the code used and the deviations from the benchmark specifications, then the main results of the reference calculation are presented and commented, the sensitivities done are also presented and finally main conclusions for this work are developed.

3.3.2 Code

Numerical simulations rely on TOUGH2, a general-purpose numerical simulation program for multi-phase fluid and heat flow in porous and fractured media. Tough2 was developed at the Earth Sciences Division of Lawrence Berkeley National Laboratory (LBNL).

Simulations have been performed using Tough2-MP, a massively parallel (MP) version of the Tough2 code, designed for computationally efficient parallel simulation of isothermal and non-isothermal flows of multi-component, multiphase fluids in one, two, and three-dimensional porous and fractured media.

Tough2-MP features several fluid property modules [EOS (Equation Of State) modules].

In the framework of this benchmark, numerical simulations are performed using EOS5 module (water, hydrogen).

3.3.2.1 Numerical formulation

TOUGH2(-MP) solves mass and energy balance equations that describe fluid and heat flow in general multiphase, multicomponent systems. Fluid advection is described with a multiphase extension of Darcy's law; in addition there is diffusive mass transport in all phases.

The description of thermodynamic conditions is based on the assumption of local equilibrium for all phases. Fluid and material/formation parameters can be arbitrary nonlinear functions of the primary thermodynamic variables.

One of the specificities of TOUGH2 (-MP) code is that the mathematical formulation is changing from saturated state to unsaturated state, mainly, the primary variables are not the same in the two formulations. For EOS5 module (water, hydrogen), primary variables are as follows:

- single-phase conditions: pressure, air mass fraction, temperature
- two-phase conditions: gas phase pressure, gas saturation, temperature

For numerical simulation the continuous space and time variables must be discretized. InTOUGH2, space discretization is made directly from the integral form of the basic conservation equations, without converting them into partial differential equations. This "integral finite difference" method (IFDM) avoids any reference to a global system of coordinates, and thus offers the advantage of being applicable to regular or irregular discretizations in one, two, and three dimensions.

Time is discretized fully implicitly as a first-order backward finite difference. This together with 100 % upstream weighting of flux terms at interfaces is necessary to avoid impractical time step limitations in flow problems involving phase (dis-) appearances.

The discretization results in a set of strongly coupled nonlinear algebraic equations, with the time-dependent primary thermodynamic variables of all grid blocks as unknowns. These equations are cast in residual form, i.e., {residual} ≡ {left-hand side} - {right-hand side} = 0, and are solved simultaneously, using Newton-Raphson iteration. Time steps can be automatically adjusted (increased or reduced) during a

simulation run, depending on the convergence rate of the iteration process. Automatic time step adjustment is essential for an efficient solution of multiphase flow problems, where intrinsic time scales for significant changes in the flow system may vary by many orders of magnitude during a simulation run.

Different methods are available to solve the linear equations arising at each iteration step, including preconditioned conjugate gradient solvers, as well as sparse direct matrix methods. While direct methods are more predictable and less problem-dependent in their performance, it is only through the application of iterative conjugate gradient methods that solutions for large grid systems (10,000 blocks or more) and three-dimensional problems can be accomplished.

Further description and more details about Tough2/Tough2-MP codes are available from the Tough2 Homepage on the web, at http://esd.lbl.gov/TOUGH2, and from the Tough2-MP Homepage on the web at http://tough2.com.

3.3.2.2 Implementation of benchmark specifications

3.3.3 Mathematics

The mathematical model is the same as described in the benchmark specifications, except for the following processes:

Diffusion terms:

In Tough2/Tough2-MP, diffusive flux of component κ (water or hydrogen for EOS5 module) in fluid phase β (liquid or gas) is expressed as follows $f_\beta^\kappa = -\phi\tau_0\tau_\beta\rho_\beta d_\beta^\kappa \nabla X_\beta^\kappa$

where ϕ is porosity, $\tau_0\tau_\beta$ is the tortuosity which includes a porous medium dependent factor, τ_0 and a coefficient that depends on phase saturation S_β , $\tau_\beta = \tau_\beta(S_\beta)$ ρ_β, is density d_β^κ is the diffusion coefficient of component κ in bulk fluid phase β, and X_β^κ is the mass fraction of component κ in phase β.

Tortuosity effects have a porous medium-dependent part τ_0 and a saturation-dependent part $\tau_\beta(S_\beta)$, with S_β as the fluid phase β saturation. The following three alternative formulations are available in Tough2 / Tough2-MP:

- Relative permeability model: tortuosity will be taken as $\tau_0\tau_\beta = \tau_0 k_{r\beta}(S_\beta)$.
- Saturation model: s $\tau_0\tau_\beta = \tau_0 S_\beta$ will be used.
- Millington-Quirk model: $\tau_0\tau_\beta = \phi^{1/3} S_\beta^{10/3}$, with ϕ as the porosity. This model is used for the benchmark simulations.

Solubility of Hydrogen in water:

In Tough2/Tough2-MP, the solubility of hydrogen in liquid water is represented by Henry's law. Henry's coefficient Kh (expressed in Pa^{-1}) for hydrogen dissolution in water, is the ratio between dissolved hydrogen mass fraction and gaseous hydrogen partial pressure.

It is a linear function of temperature, varying from 1,697 10^{-10} Pa^{-1} at 0 °C to 1,379 10^{-10} Pa^{-1} at 25 °C.

For the 20°C temperature used in the numerical simulations, Kh is equal to 1,443 10^{-10} Pa^{-1}. This value is equivalent to a Henry's constant of 8,0 10^{-6} expressed in $mol.Pa^{-1}.m^{-3}$ (different from the 7.6 10^{-6} $mol.Pa^{1}.m^{-3}$ mentioned in the benchmark description).

Specific storage coefficient:

Tough2/Tough2-MP codes do not use specific storage coefficient S_S as an input parameter, but pore compressibility. Relation between pore compressibility C, expressed in Pa^{-1}, and specific storage coefficient S_S expressed in m^{-1} as follows:

$$C = \frac{S_S}{\rho_w g \phi} - \beta_w$$

With: ρ_w liquid water density (kg/m³)

g magnitude of the gravitational acceleration vector (m/s²)

ϕ porosity (-)

β_w liquid water compressibility (Pa⁻¹)

3.3.4 Boundary Conditions

Boundary conditions can be of two basic types.

Dirichlet conditions prescribe thermodynamic conditions, such as pressure, saturation, temperature, on the boundary. Dirichlet conditions can be implemented by assigning very large volumes (e.g., V = 10^{50} m³) to grid blocks adjacent to the boundary, so that their thermodynamic conditions do not change at all from fluid or heat exchange with finite-size blocks in the flow domain. In addition, a small value (such as D = 10^{-9} m) should be specified for the nodal distance of such blocks, so that boundary conditions are in fact maintained in close proximity to the surface where they are desired, and not at some distance from it.

In the original version of Tough2-MP 2.0, only time dependent pressure boundary conditions are available. Numerical developments have been performed in the Fortran source code of Tough2-MP to provide additional capabilities for a time-dependent gas saturation boundary conditions (gas saturation is one of the primary variables for EO55 module).

Attention must be paid to assume, at every time, coherence between boundary gas saturation, boundary water pressure, capillary pressure in access drift material, and realistic gas pressure.

Neumann conditions prescribe fluxes of mass or heat crossing boundary surfaces. A special case of Neumann boundary conditions is “no flux,” which in the integral finite difference framework is handled with simplicity itself, namely, by not specifying any flow connections across the boundary. More general flux conditions are prescribed by introducing sinks or sources of appropriate strength into the elements adjacent to the boundary. Using this technique, time-dependent hydrogen production term is then applied on a thin specific volume closet to the external surface of the cell.

3.3.5 Initial conditions

Flow systems are initialized by assigning a complete set of primary thermodynamic variables to all grid blocks into which the flow domain is discretized. During the initialization of a TOUGH2-MP run, all grid blocks are first assigned to default thermodynamic conditions. The defaults can then be overwritten for selected domains by assigning domain-specific conditions in specific data blocks.
The primary variables used depend on the fluid phase composition. During phase change primary variables will be automatically switched from one set to another. In multiphase flow systems, therefore, different grid blocks will in general have different sets of primary variables, and must be initialized accordingly.

3.3.6 Other deviations from the specifications

The different conceptual and physical processes and assumptions are in accordance with the benchmark specifications, and/or the original version of Tough2-MP, except for the following aspects:

Physical parameters:

Some physical parameters and fluid properties are internally computed and/or tabulated in Tough2/Tough2-MP Fortran source code. They have not been replaced by the mathematical expressions presented in the benchmark description.

Water vapor pressure:

In standard EOS5 module of Tough2-MP, vapor pressure is equal to saturated vapor pressure of water. It is not expressed by Kelvin's equation. At a 20°C temperature, this vapor pressure is 2337 Pa.

Viscosity of the gas mixture:

Dynamic viscosity of hydrogen is both pressure and temperature dependent in Tough2/Tough2-MP. For the 20°C temperature used in the numerical simulations, values expressed in Pa.s are:

8,8 10^{-6} Pa.s when pressure is lower than 0,1 MPa

8,95 10^{-6} Pa.s at 10,0 MPa and 9,22 10^{-6} Pa.s at 200,0 MPa

Values at intermediate pressures are linearly interpolated.

The dynamic viscosity of hydrogen-vapor mixture is approximated as dynamic viscosity of hydrogen.

Outputs:

In the original version of Tough2-MP 2.0, mass flow rates from diffusion are not printed in the standard output file.

Developments have been performed in the Fortran source code of Tough2-MP to print the diffusive fluxes of each component (water, hydrogen) in both liquid and gas phase. These fluxes are necessary for computing, after the end of the simulation, the total rate of flow for each component.

3.3.7 Base case results

Results for this reference case are presented as time evolution of several variables at specific points and as fluxes through different surfaces. Points, surfaces and variables presented are coherent with the benchmark specifications.

These specifications also give the possibility to represent variation of specific variables along lines for different times. This representation was not used as the results are not adding much to the comprehension of the system.

For description of the base case, one can refer to the benchmark full description in appendix. The main characteristics are as follows :

- 2D axisymmetric cell scale level geometrical domain;
- Explicit representation of an interface between all man made material and clay EDZ, especially around the cell bentonite plug;
- Explicit representation of EDZ and the cell access drift;
- Drift boundary conditions determined from a previous calculation at storage scale.

3.3.7.1 At specific points

Next figure (Figure 23) is representing a schematic view of the geometrical domain with emplacement of the different points used for the results presentation. Figure 24 is presenting some results for points always water saturated and Figure 25 for some points were gas is partially desaturating the porous media.

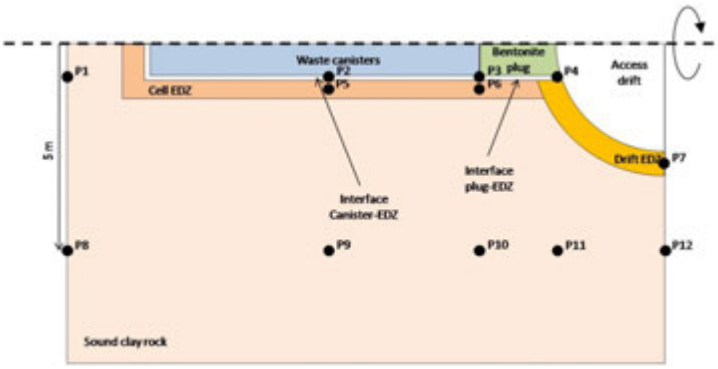

Figure 23 Schematic representation of the points where results are given

These results show that at 5 m from the model axis, all points are always water saturated, even near the access drift. For the saturated points near the drift, dissolved H2 is arriving around 10 years after waste canisters are put in place whereas for points near the end of the cell this time is 10 times higher. This shows that H2 is rapidly present in the drift and dissolves from this element into the clay.

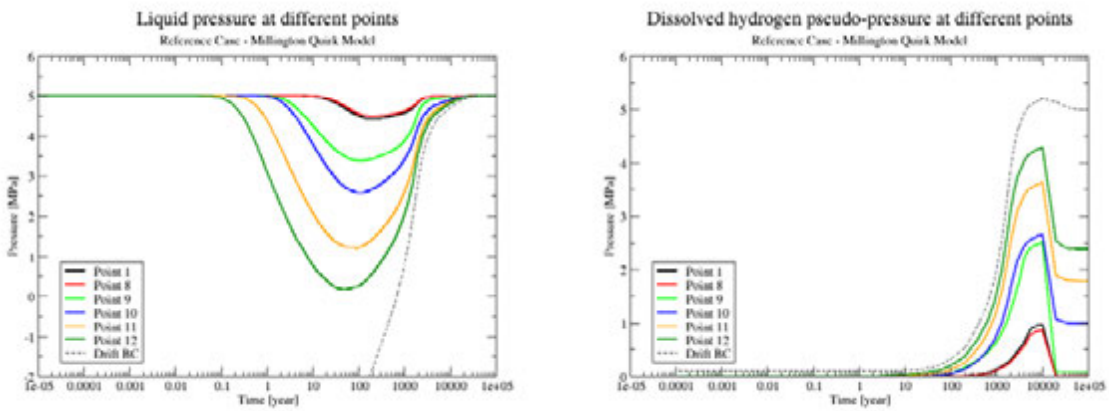

Figure 24 Base case: evolution with time of liquid pressure (left) and dissolved hydrogen pseudo-pressure (right) for points 1 and 8- 12

This can also be shown on gas pressure evolution presented in Figure 25 : expressed gas is arriving in the drift some years after the beginning of the simulation. Maximum gas pressures are in the range of 5 MPa, mainly linked to the value of the imposed boundary condition in the drift.

Concerning water saturation, the interface is initially well desaturated all around the cell, but time evolution is highly position dependent. Near the wastes (point 2), resaturation is reached quite rapidly (several years) before a second desaturation period beginning around 100 years. This can be explained by the arrival of water from the clay, resaturating the interface in a first phase, but after a certain time, gas production is too high and it pushes water away from the interface.

For the interface in front of the bentonite plug (point 3) the evolution is a bit different. In a first phase (more or less 20 years), the bentonite, put in place at 80% water saturation, is resaturating and pulls water out of the interface. In a second phase (from 20 to 50-60 years) the bentonite is quite resaturated and so is the interface. And in a third phase gas production pushes water away from the interface.

For the interface in contact with the drift (point 4), the behavior is mainly linked to the one of the drift backfill which is first desaturating slightly (due to the bentonite succion) and then resaturating very slowly with a resaturation at around 20.000 years. Point 4 remains very desaturated during all this period and resatures rapidly at the same time as the backfill.

For the EDZ, the corresponding points (respectively point 5, 6 and 7 corresponding to point 2, 3 and 4), the influences are the same and the behavior similar except that the permeability of the EDZ is much smaller than the one of the interface and thus desaturation is less important.

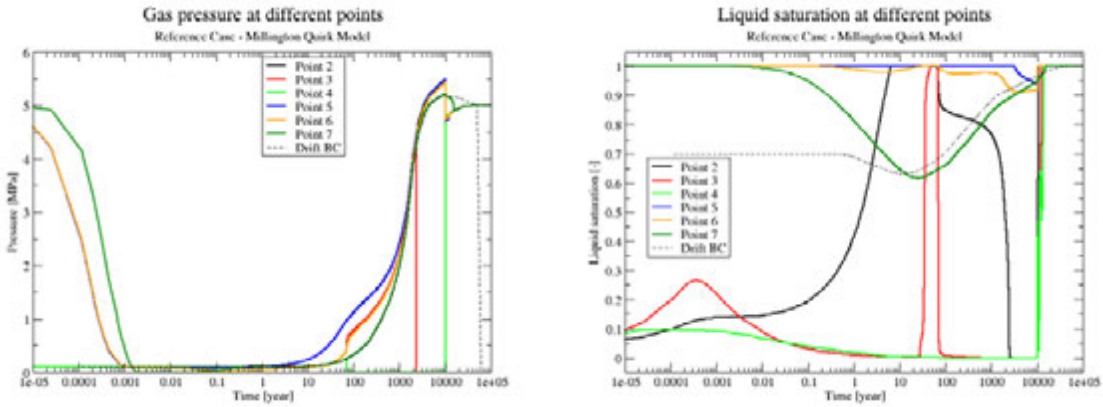

Figure 25 Base case: evolution with time of gas pressure (left) and liquid saturation (right) for points 2- 7

3.3.7.2 For specific fluxes

Concerning the fluxes, Figure 26 is shoving the emplacements of all surfaces through which fluxes are calculated.

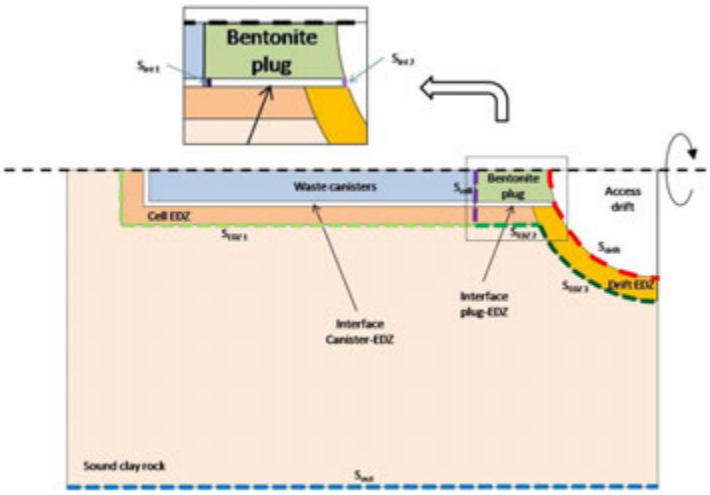

Figure 26 Schematic representation of the surfaces trough which fluxes are calculated

The main water fluxes are during the first years after cell closure (see Figure 27) when water is resaturating the system, and mainly the voids (including the interfaces). During this period, gaseous fluxes can be important as interfaces are still open (see Figure 28), but the main flux is from drift toward the cell (negatives values). This is due to the fact that water is resaturating the drift and gas can only flow toward the cell. As in EOS5 the only possible gas can be water vapor and H2, the air present in the drift is in fact represented by H2. The high negative flux values of H2 before 1 year are in fact representative of the migration of air from the backfilled drift toward the cell. After several years, interface (point 2) can be quite resaturated and gaseous fluxes toward the drift are decreasing dramatically.

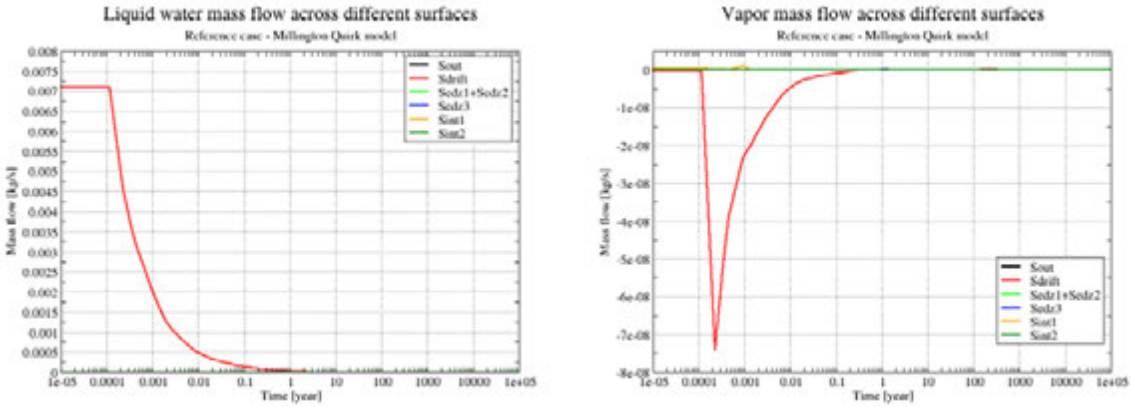

Figure 27 *Base case: evolution with time of liquid water mass flow (left) and vapor mass flow (right) across different surfaces*

After several tens of years, in coherence with the desaturation of point 2, gaseous fluxes are increasing again. This time, H2 fluxes are representative of the corrosion production into the cell and Figure 30 shows that this flux is increasing up to 4 10^{-9} kg/s at several hundred years and then decreasing again down to zero after several tens of thousands of years. For dissolved hydrogen, the pick value is a bit less important (2 10^{-9} kg/s) and is arriving much later several thousands of years). Figure 30 also shows that dissolved hydrogen is reaching the outer boundary, 25 meters radially from the model axis, after around ten thousand years.

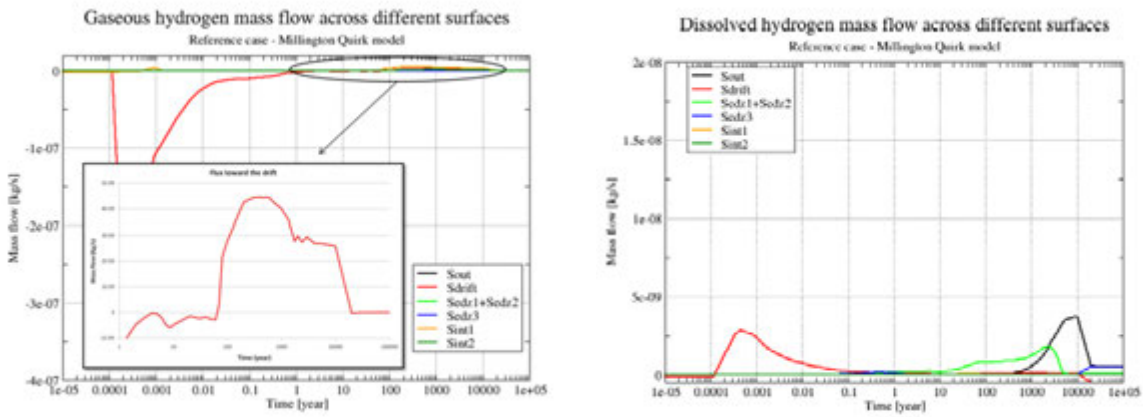

Figure 28 *Base case: evolution with time of gaseous hydrogen mass flow (left) and dissolved hydrogen mass flow (right) across different surfaces*

3.3.8 Global behavior of the cell

The base case behavior can be summarized as follows:

- First period of around 1 year of water and gas exchange between the drift and the cell. During this period the gas is mainly air initially present in the model. During this period the EDZ around the drift is desaturating partially and the interface around the waste storage zone is resaturation, but interface around the bentonite plus is still desaturated and gas pressure is not building up in the cell;

- After several tens of years the resaturation of the plus implies also the restoration of the interface around it. Gas pressure begins to build-up in the cell;

- At around one hundred years the increase of gas pressure inside the cell force a desaturation of the interface around the bentonite plug (and a partial desaturation of the surrounding EDZ). Effective gas (H2) flux is then possible between the waste zone and the drift vie this unsaturated interface. This flow lasts up to the end of the H2 production period (10.000 years);
- Meanwhile, from around 10˚ years to 10.000 years, dissolved H2 is diffusion in the sound clay radially from the waste zone;
- On the average, over the whole H2 production period, there is a co-dominance of the effective gas flow and dissolved gas transfer as the total mass transferred by each of these two processes represent more or less 500% of the total production.

3.3.9 Sensitivity cases results

All sensitivity cases done by Andra are presented below. Only the main differences compared with the base case are commented. If no significant different is seen, no comments are given.

3.3.9.1 Self healing of the EDZ

In this sensitivity case, the EDZ is supposed to have the same intrinsic permeability value as the sound clay. Note that the relative permeability and retention curves are still the ones used for EDZ in the base case as it is assumed that self healing is mainly due to complete resaturation of the material.

<u>At specific points</u>

For saturated points (Figure 29) the global behavior is the same as for the base case, but depressurization is less important and dissolved hydrogen fluxes as well. This is linked to the fact that in this case the EDZ is less desaturated (higher pressures in the point of the figure are directly linked to this), because its permeability is lowered, and so the saturated distance to the different points are more important (dissolved H2 has more travel distance to cross) and hence the concentration is less important.

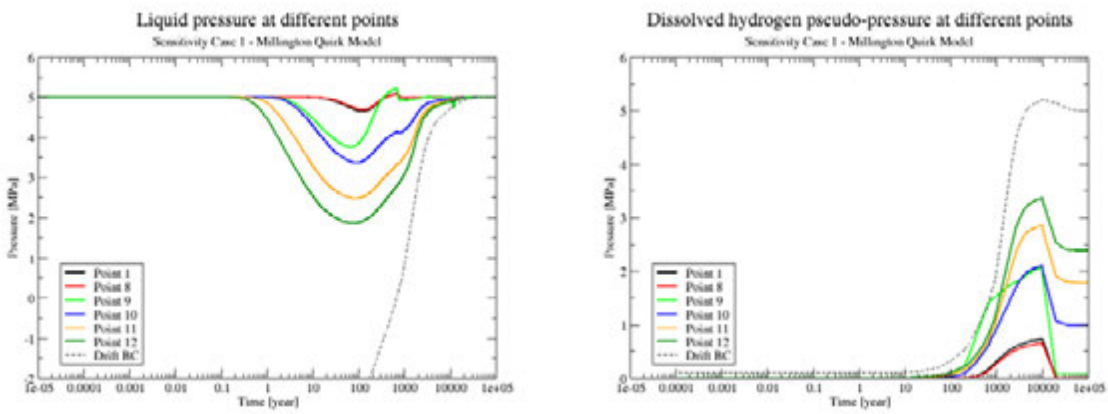

Figure 29 Sensitivity case 1: evolution with time of liquid pressure (left) and dissolved hydrogen pseudo-pressure (right) for points 1 and 8- 12

For points in the EDZ and the interface (Figure 30) the change is more significant. In fact, EDZ is not desaturating at all (points 5, 6 and 7) and water pressure is positive at all times. The gas pressure is building more rapidly near the wastes (point 2 and 5) because gas cannot escape the cell. In the interface (point 2, 3 and 4) desaturation is less important as in the base case and resaturation periods are longer (point 2 and 3).

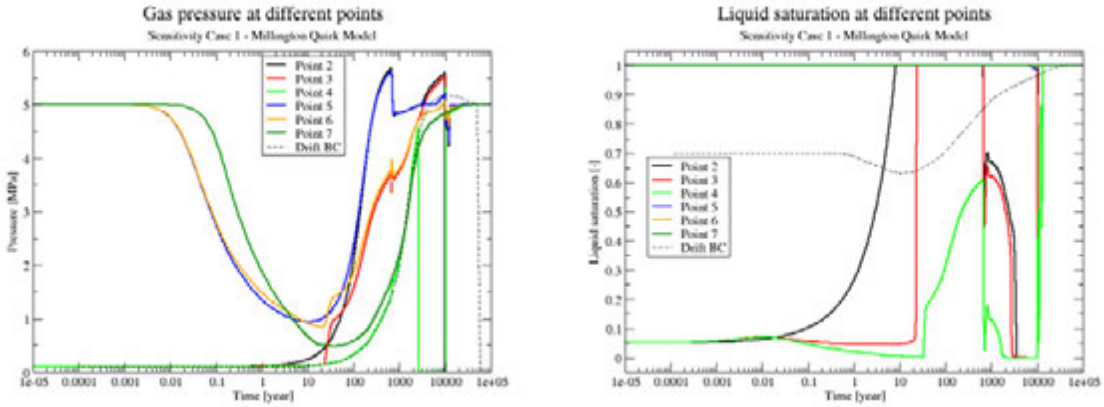

Figure 30 *Sensitivity case1: evolution with time of gas pressure (left) and liquid saturation (right) for points 2- 7*

<u>For specific fluxes</u>

As EDZ is not desaturating, the initial (gas and water) flow during the first years is reduced to (virtually) zero.

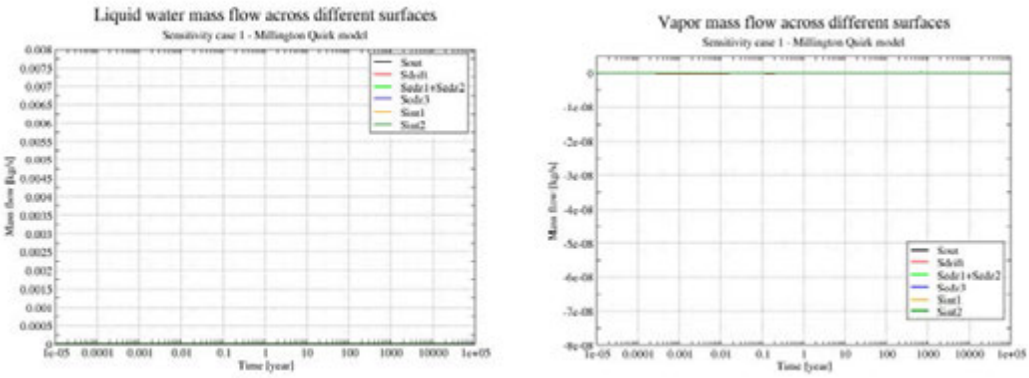

Figure 31 *Sensitivity case 1: evolution with time of liquid water mass flow (left) and vapor mass flow (right) across different surfaces*

But dissolved long term H2 fluxes are significantly modified as there begin a bit later (several tens of years instead of ten years in the base case) but stay at a high level for a much longer time.

For expressed gas fluxes the impact is significant as well, they begin much later (e.g.: around 1000 years against some tens or years in the base case). This is linked to the fact that EDZ and interface around the bentonite plug are saturated before this time. Anyway, on the whole the same mass of expressed gas (around 1000 Kg) is going out of the cell by this process in both cases.

This simulation shows that the long term behavior of the EDZ (e.g.: self-sealing or not, for water and/or gas) is an important issue to understand the hydraulic-gas transient at the cell scale. However, as the global amount of expressed gas is more or less the same in both cases, the global impact at the repository scale could be similar.

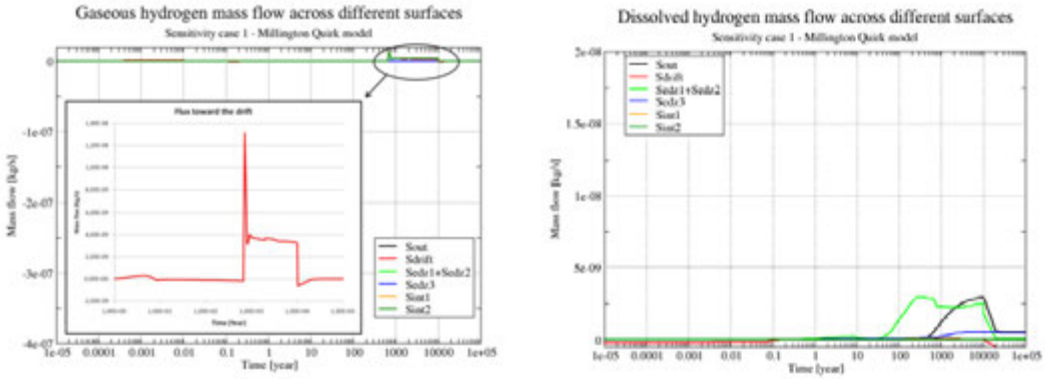

Figure 32 *Sensitivity case1: evolution with time of gaseous hydrogen mass flow (left) and dissolved hydrogen mass flow (right) across different surfaces*

3.3.9.2 Change of relative permeability curve

For this sensitivity, the relative permeability curve has been changed to a power 3 of the water saturation for sound clay and EDZ (instead of a Van Genuchten / Mualem curve). This assumption is made because some data are coherent with it.

<u>At specific points</u>

For saturated points (Figure 33), this sensitivity is changing nothing for dissolved hydrogen concentration but water pressures are slightly lower.

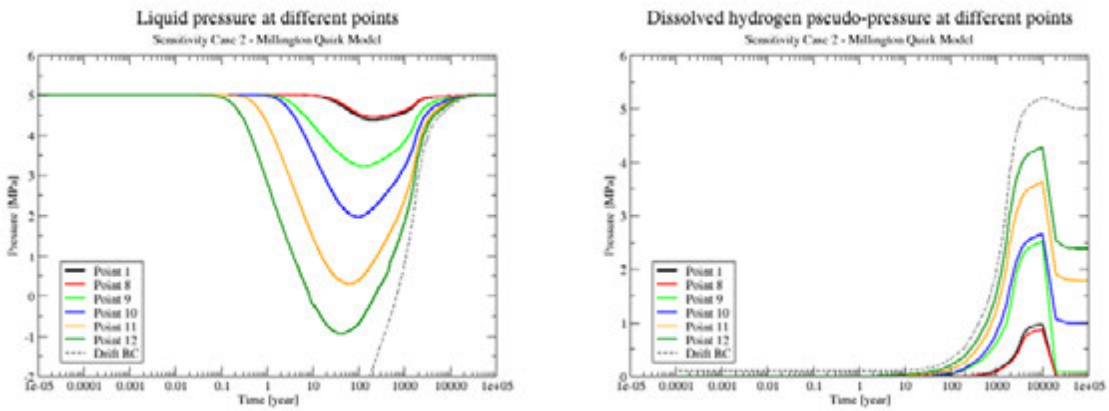

Figure 33 *Sensitivity case 2: evolution with time of liquid pressure (left) and dissolved hydrogen pseudo-pressure (right) for points 1 and 8- 12*

For points in the EDZ (Figure 34), gas pressure is not significantly affected, but water saturation is less important, mainly for point 7. Concerning points in the interface, water saturation is significantly modified and reduced. None of these points is resaturating, gas pressure is never increasing over 1 MPa, before the end of the gas generation period (10.000 years).

This simulation on the change of relative permeability curve in the clay and EDZ emphasize the fact that the shape of this curve (also true for retention curve) around water saturation (e.g.: for water saturation over 95%) is important for the general behavior of the system as clay is never desaturating more than some percent at a most (mainly because of its high gas entry pressure value).

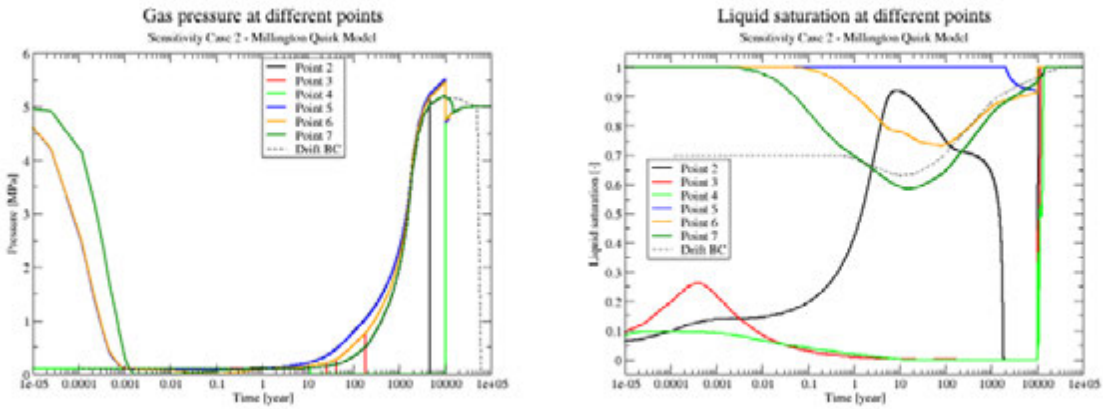

Figure 34 *Sensitivity case2: evolution with time of gas pressure (left) and liquid saturation (right) for points 2- 7*

<u>For specific fluxes</u>

On the whole, for this sensitivity the general behavior is the same. However, the total mass transferred by under effective gas phase is significantly higher (around 30% more) than in the base case, mainly because this process is beginning sooner and thus the dissolved mass transfer is reduced.

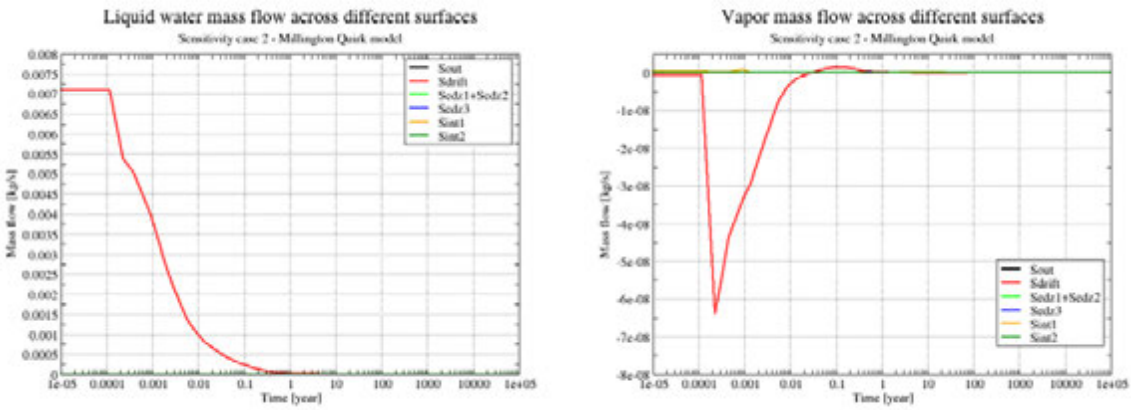

Figure 35 *Sensitivity case 2: evolution with time of liquid water mass flow (left) and vapor mass flow (right) across different surfaces*

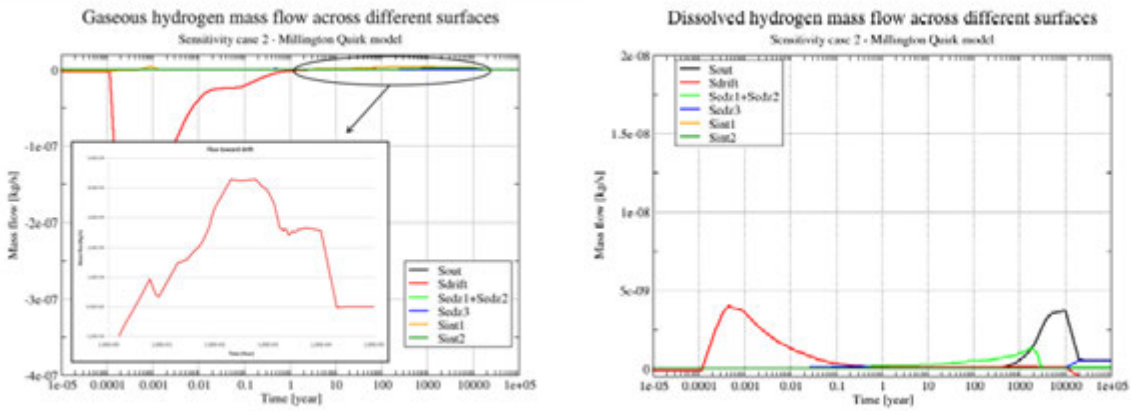

Figure 36 *Sensitivity case2: evolution with time of gaseous hydrogen mass flow (left) and dissolved hydrogen mass flow (right) across different surfaces*

3.3.9.3 Higher diffusion

Diffusion coefficient for dissolved H2 is multiplied by a factor 10 in all materials to take into account the uncertainty on this value.

<u>At specific points</u>

This sensitivity has no noteworthy effect on water pressure at saturated point (Figure 37), but has a significant effect on dissolved hydrogen concentration for which the picks are less sharpen and globally the values less important. This is normal as to transfer the same amount of dissolved gas a less important concentration gradient is needed.

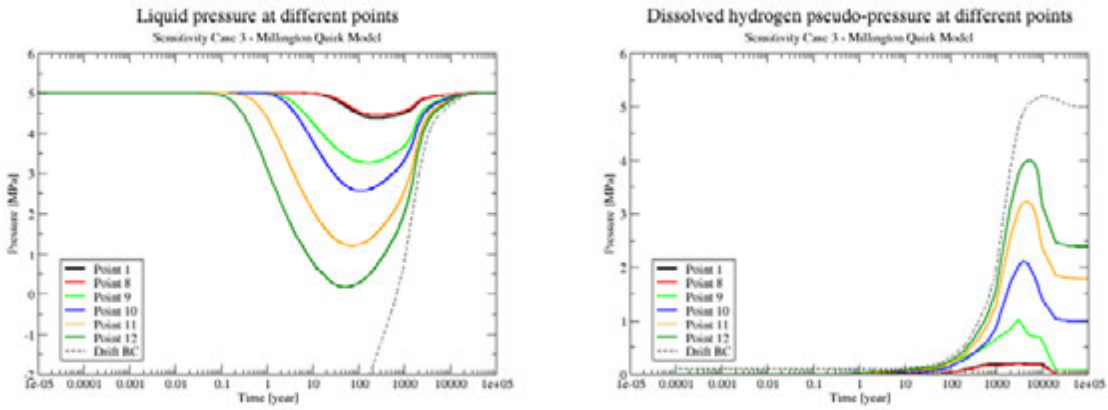

Figure 37 *Sensitivity case 3: evolution with time of liquid pressure (left) and dissolved hydrogen pseudo-pressure (right) for points 1 and 8- 12*

Another significant effect is on water saturation and gas pressure in the EDZ: saturation is higher and gas pressure lower. Once again this is coherent with the assumption of a higher diffusivity for dissolved H2 which implies less expressed gas (more gas being dissolved). For the interface these conclusions are also valid, except for point 3 which saturation around several hundred years is mainly linked to the resaturation of the bentonite plug (not significantly affected by the change of behavior of the dissolved H2).

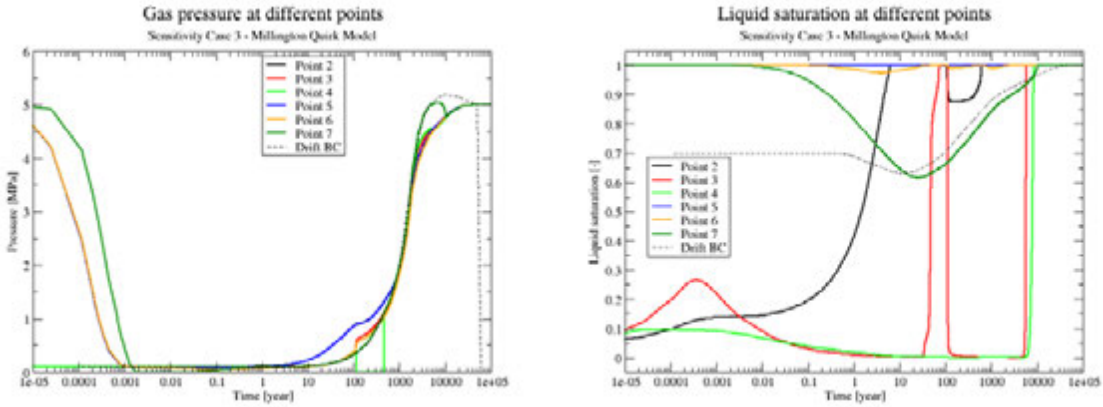

Figure 38 *Sensitivity case3: evolution with time of gas pressure (left) and liquid saturation (right) for points 2- 7*

<u>For specific fluxes</u>

Water fluxes (vapor or liquid) are not significantly affected by the sensitivity, but H2 (dissolved or gaseous) are. The large increase of dissolved H2 flux is coherent with the sensitivity case. The dissolved H2 flux toward the drift is so important, and because the drift is partially desaturated, that part of it is turning to expressed gas (via Henry's law) and coming back in the cell (e.g.: negative values of expressed gas drift flux around several thousand years). In this case, dissolution/diffusion is clearly the dominant process at cell scale, and the global behavior is significantly changed.

This simulation shows that the general behavior of a cell is globally closely linked to the value of the H2 diffusion coefficient. Although this phenomena is, in the base case, not the dominant one, its order of magnitude can modify the way gas is escaping the cell and reducing the uncertainty on this parameter seems worth the deal.

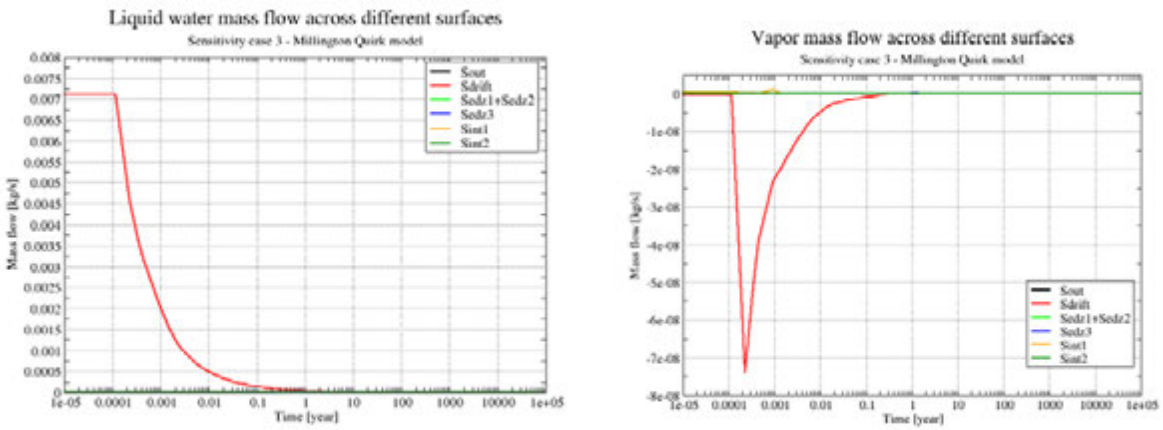

Figure 39 *Sensitivity case 3: evolution with time of liquid water mass flow (left) and vapor mass flow (right) across different surfaces*

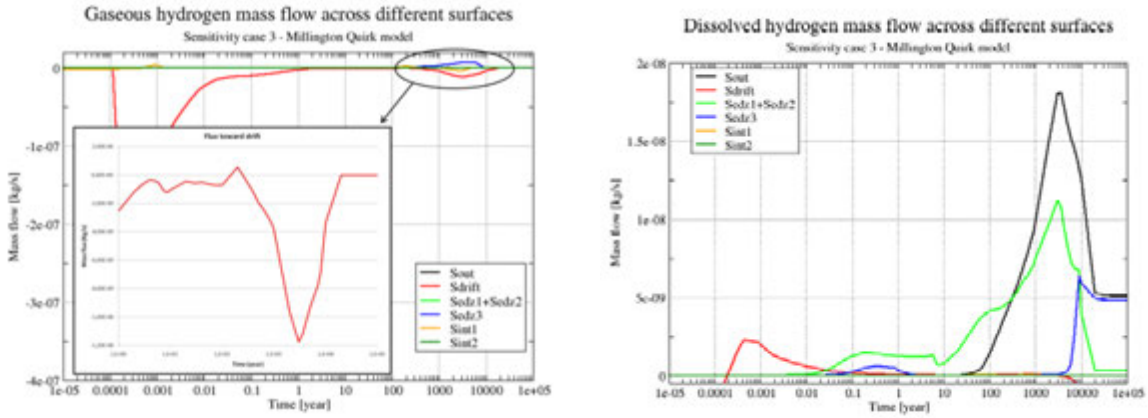

Figure 40 *Sensitivity case3: evolution with time of gaseous hydrogen mass flow (left) and dissolved hydrogen mass flow (right) across different surfaces*

3.3.9.4 Gas generation delayed (1 year and 2 years)

Hydrogen production is linked to metal corrosion in reductive chemical conditions. In a storage, this is possible only in water saturated conditions (roughly). As during a first period the cell is not saturated, hydrogen generation should not be possible. This is why 2 sensitivities taking into account a 1 year and a 5 years delay before enabling H2 production where tested.

The results are not significantly affected mainly so no specific figures are displayed. The explanation lies in the fact that most of the H2 production effect is significant only after several tens of years (or even longer) and a delay of 1-2 years is not changing this characteristic time.

3.3.9.5 Less permeable interfaces (1.e-15 m/s)

Data on interfaces hydraulic parameters are very few so assuming a less permeable interface is something in the range of possible.

<u>At specific points</u>

In the saturated zone of the model there is no significant difference with the base case. But in the unsaturated zone the saturation is significantly affected by the sensitivity, especially for the interface points. Point 2 (near the wastes) is staying resaturated longer between several tens and several thousands of years before desaturating in relation with the increase of gas pressure around the wastes. On the contrary, point 3 (in front of the bentonite plug) is no more affected by the resaturation of the plug, and point 7 (EDZ in front of the bentonite plug) is more desaturated than in the reference case between 10 and 1.000 years : the way is open for gas to go out of the cell (see specific fluxes).

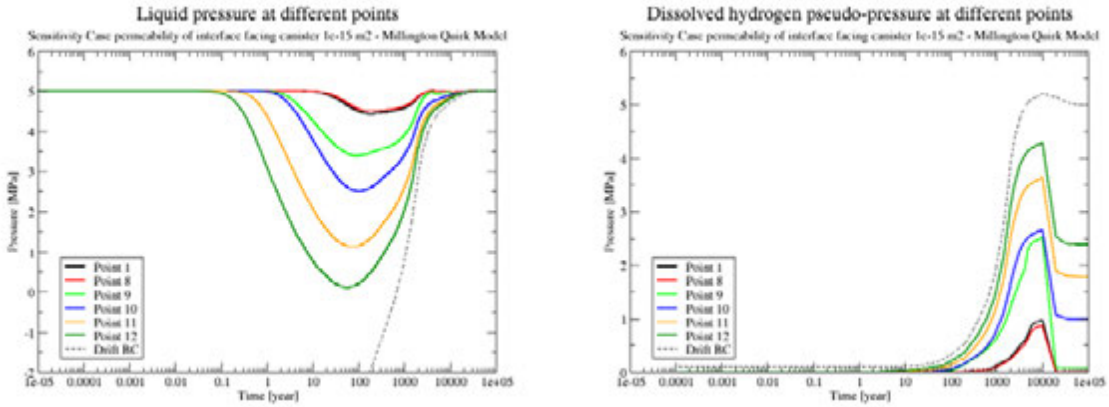

Figure 41 *Sensitivity case less permeable interfaces 1.e-15 m/s: evolution with time of liquid pressure (left) and dissolved hydrogen pseudo-pressure (right) for points 1 and 8- 12*

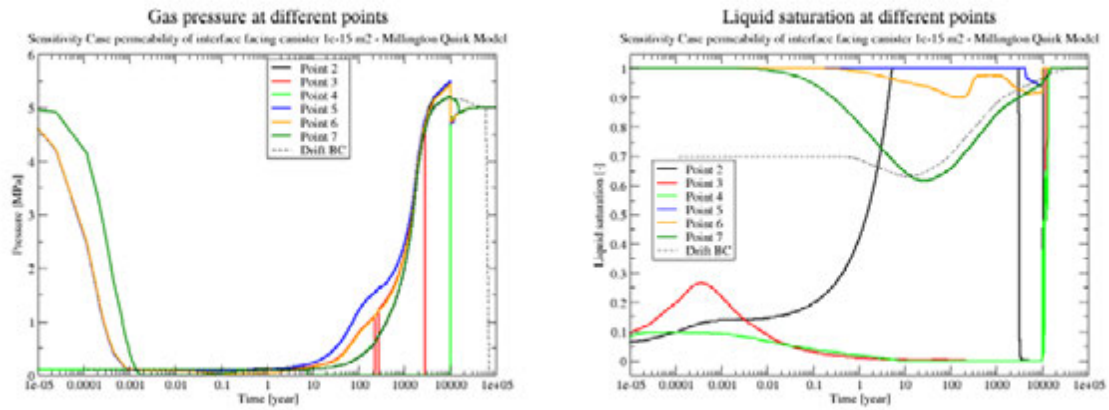

Figure 42 *Sensitivity case less permeable interfaces 1.e-15 m/s: evolution with time of gas pressure (left) and liquid saturation (right) for points 2- 7*

<u>For specific fluxes</u>

Water (liquid and vapor) fluxes are not affected by the permeability change of the interface. No significant change in the dissolved H2 either. But the expressed gas H2 flux is impacted: the maximum value is higher (6 10^{-9} kg/s instead of 4 10^{-9} kg/s) and the shape of the curve is sharper around this maximum. Over the whole simulation time, the total mass of H2 going out of the cell under expressed gas form is 30% more important (more or less 1300 Kg against around 1000 Kg in the reference case).

An explanation of this “non intuitive” behavior is that if gas cannot use interface as escape route, it will be obliged to use the EDZ, and as the width of the EDZ is much more important, on the whole, the escape route will be larger. But this behavior is also linked to the empiric model and parameters values used for relative permeability and retention curves, as well for EDZ as for interface, and there is no direct data about these. So the uncertainty is important and the results could have been different using other empiric models and/or parameters values (e. g.: it is also possible to have an expressed gas volume smaller in this case compared to the base case).

What this simulation shows is that there is a need on EDZ and interface characterization, not only for intrinsic permeability, but also for relative permeability and retention curves. This conclusion can however be tempered by the fact that pressures and water fluxes are not significantly affected and that expressed

gas fluxes is not changing the order of magnitude (e.g.: is in the same range as the uncertainties linked to results comparison between teams in this benchmark).

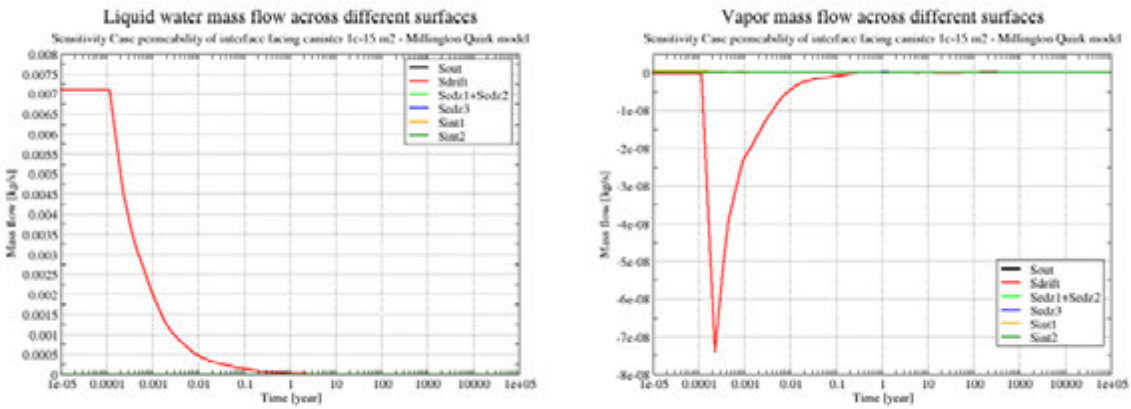

Figure 43 *Sensitivity case less permeable interfaces 1.e-15 m/s: evolution with time of liquid water mass flow (left) and vapor mass flow (right) across different surfaces*

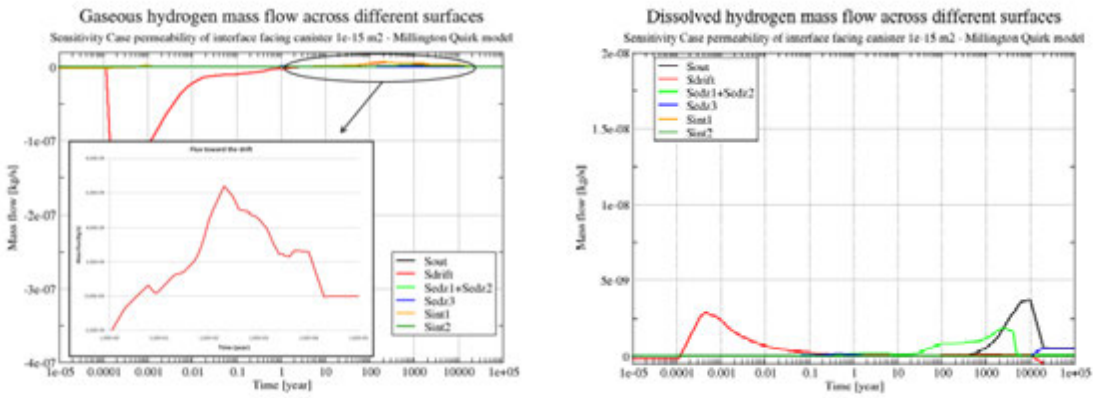

Figure 44 *Sensitivity case less permeable interfaces 1.e-15 m/s: evolution with time of gaseous hydrogen mass flow (left) and dissolved hydrogen mass flow (right) across different surfaces*

3.3.9.6 Less permeable interfaces (1.e-18 m/s)

The results for this case are globally similar to the one for the previous case (interface permeability equal 10^{-15} m/s), so no figures are presented.

An explanation could be that the gas flux was already "derived" to the EDZ as it passes around the bentonite seal and that reducing again the interface permeability is no more changing this phenomenology. This simulation emphasizes the fact that the need of characterization of the interface is relative, but reports the characterization need to the EDZ (which is in this case the preferential gas pathway).

3.3.9.7 Mesh refinement

Sensitivity runs have been performed with different mesh refinements. This analysis is based on the reference case, with anisotropic permeabilities. Four meshes have been used with different refinements:

- 26,346 elements, 10 layers in "Drift EDZ", 13 layers in "Cell EDZ"
- 12,365 elements, 4 layers in "Drift EDZ", 13 layers in "Cell EDZ"

- 6,817 elements, 4 layers in “Drift EDZ”, 4 layers in “Cell EDZ”
- 1,181 elements, 1 layer in “Drift EDZ”, 1 layer in “Cell EDZ”

The pressure and saturation evolutions with time, at the 12 given points defined in the benchmark description, appear to be very similar for the different meshes, except the 1181 cells one. This last mesh seems to be too much coarse for the numerical simulations.

Thus, mesh with 6817 cells is selected for the different cases. A view of this mesh and a close up around the access drift could be seen respectively on Figure 45 and on Figure 46.

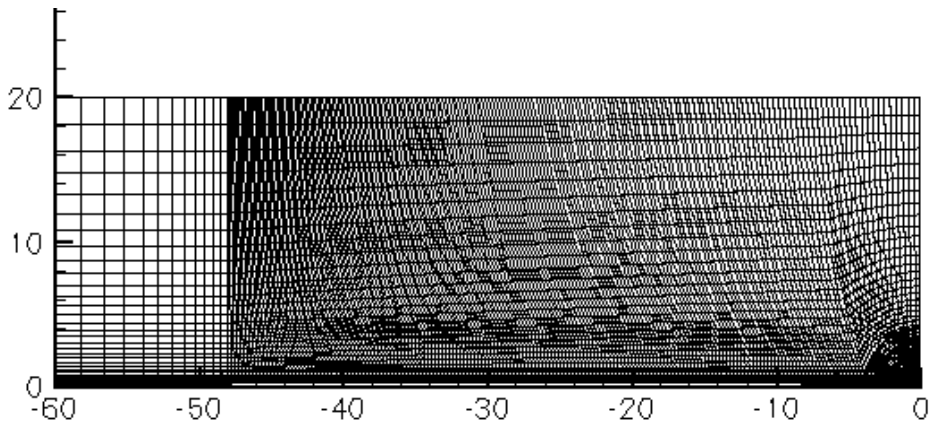

Figure 45 Mesh selected for the different simulations

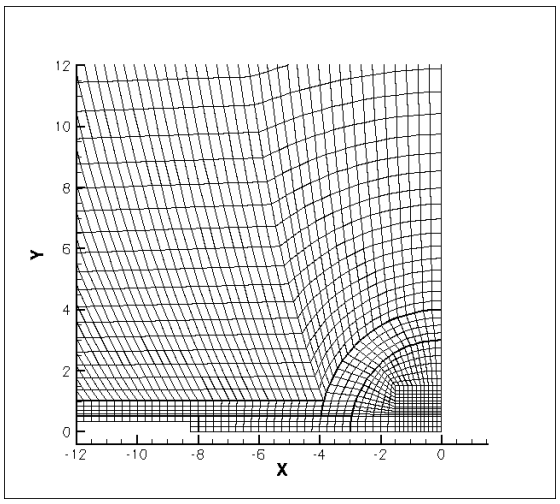

Figure 46 Mesh selected for the different simulations (zoom around the access drift)

However, even if the results are similar, the simulation time and numerical problems are not the same for all the 3 refined meshes. The way to represent (to mesh) the interface is very important and can lead to various problems. The main problem encountered can be summarized as follows :

- TOUGH2(-MP) is changing mathematical formulation and primary variables depending whether an element is saturated or not;
- If there are too many small elements (e.g.; with tiny volumes, especially in the interface) in a region included in the desaturation (resaturation) front the code as difficulties to determine if they are or not saturated;
- In the internal convergence loop these elements are moving from saturated to desaturated on each internal step;

- to deal with this, TOUGH2(-MP) is reducing the time step so as the water exchange between adjacent elements becomes significantly small compared to the necessary volume to pass from desaturation to saturation (or the contrary) in the tiniest elements;

Time steps are reduced to such low values that simulation is not practically possible.

This is why, with TOUGH2(-MP) mesh refinement is not always a synonym of better numerical convergence and why in this benchmark the interface is not very well refined (only 3 elements in its width).

3.3.10 Conclusions

The cell scale benchmark specifications for WP°1.2 of FORGE project has been implemented by Andra on a TOUGH2(-MP) model. Some functionalities described in the specifications were unfortunately not present in this code and some limited development were needed, however some minor differences still persist between specifications and implemented model.

In the process of model implementation some numerical difficulties arise, mainly linked to meshing problems in relation with TOUGH2(-MP) internal way of dealing with time step adjustment. The optimized mesh used in all the simulations is neither to coarse (e.g.: containing too big elements leading to a bad phenomenological representation) nor to fine (e.g.: containing too tiny elements leading to time step reduction incompatible with practical use of the model).

One of the main characteristic of the model is that the interfaces between materials are explicitly represented in the mesh. The base case behavior can be summarized as follows:

- First period of around 1 year of water and gas exchange between the drift and the cell. During this period the gas fluxes is mainly made of air initially present in the model. During this period the EDZ around the drift is desaturating partially and the interface around the waste storage zone is resaturation, but interface around the bentonite plus is still desaturated and gas pressure is not building up in the cell;

- After several tens of years the resaturation of the bentonite plug implies also the restoration of the interface around it. Gas pressure begins to build-up in the cell;

- At around one hundred years the increase of gas pressure inside the cell force a desaturation of the interface around the bentonite plug (and a partial desaturation of the surrounding EDZ). Effective gas (H2) flux is then possible between the waste zone and the drift vie this unsaturated interface. This flow lasts up to the end of the H2 production period (10.000 years);

- Meanwhile, from around 10° years to 10.000 years, dissolved H2 is diffusion in the sound clay radially from the waste zone;

- On the average, over the whole H2 production period, there is a co-dominance of the effective gas flow and dissolved gas transfer as the total mass transferred by each of these two processes represent more or less 50% of the total production.

More than this, some general conclusions can be drawn from the sensitivity process:

- As host clays are very impermeable and gas entry pressures are high, the desaturation is only of some percent and thus there is a need of characterization of the “water saturated tail” of the relative permeability curve (and retention curve) for these materials;

- A better characterization of the EDZ relative permeability and retention curves could also help increase the confidence on the simulation results. This is also true for the interfaces, adding intrinsic permeability values;

- Diffusion process is a key process in the comprehension of a cell hydraulic-gas transient and decreasing the uncertainty on the host clay diffusion coefficient for H2 could also help.

3.4 CEA contribution

3.4.1 Introduction

In the framework of numerical tool development for two-phase flow simulations in porous media, CEA developed a module inside the MPCube code that include several two-phase flow models like two-phase flow with gas phase dissolution in liquid phase as well as multicomponent accounting. The MPCube code is based on the Trio-U kernel **[1]**, also developed by CEA, which allows computation in a parallel environment and high performance computing on massively parallel computers. The benchmark defined in the FORGE project was the opportunity to perform some new numerical developments and to check the efficiency of the MPCube tool.

3.4.2 Model Implementation

The mathematical model implemented in MPCube and used for this benchmark is the two-phase multicomponent one. The multicomponent model is described in **[2]** and is identical to the one described in section 5.5 when we consider water and dissolved hydrogen for the liquid phase and gaseous hydrogen and water vapour for the gas phase.

The mathematical model is then constituted of mass conservation equations for water, gas and hydrogen (Eq. (9), (10), (12) and (15)) where water and gas velocities are of the generalized Darcy form (Eq. (6) and (7)). Gas components are considered to be perfect gases (Eq. (20) and (21)) as well as the gas mixture (Eq. (22)) for which pressure is evaluated considering classical thermodynamic rules (Eq. (19), (23) and (24)). Water and gas pressures are linked via capillary pressure (Eq. (1) and (2)) and hydrogen is considered to diffuse in the gas phase (Eq. (13)) as well as in the liquid phase (Eq. (17)) where dissolved hydrogen concentration follow Henry's law (Eq. (18)). Note that relative permeability curves as well as capillary curve are chosen here of the van Genuchten form (Eq. (4), (5) and (3)).

3.4.2.1 Code and Formulation

The mathematical model presented in section 5.5 is reduced into a matricial one of the form *(1)* using the gas pressure and the liquid saturation as main variables (vector U).

$$M(U)\partial_t U - div[A(U)\nabla U] = F_U \qquad (1)$$

The matrix M and A as well as second member F are then only dependent on the main variables U.

We then used a centered cell finite volume method for the space discretization as presented in **[2]** and an Euler implicit scheme for the time discretization. After discretization, the nonlinear system *(1)* is solved using an iterative attractive fixed point algorithm. Note that the linear solver used is chosen inside the PETSc **[3]** library and we selected the BICGSTAB with an ILU2 preconditioner.

The system resolution is implemented using the Trio-U kernel functionalities allowing parallel computations. The main principle of the parallel computation consists in partitioning the mesh describing the problem in as many parts as requested number of processors to perform the computation.

3.4.2.2 Benchmark Implementation

The benchmark described in section 5 was implemented with some deviations depicted in section 3.4.2.6.

3.4.2.3 Grid

The mesh used for the benchmark computation is presented in Figure 47. The mesh is constituted of 8823 triangles and takes into account all the media depicted in Figure 154 except the interfaces. In Figure 47 bentonite plug in represented in green, waste canisters in yellow, surrounding EDZ cell in red, clay host rock in blue, access drift in red and surrounding drift EDZ in yellow.

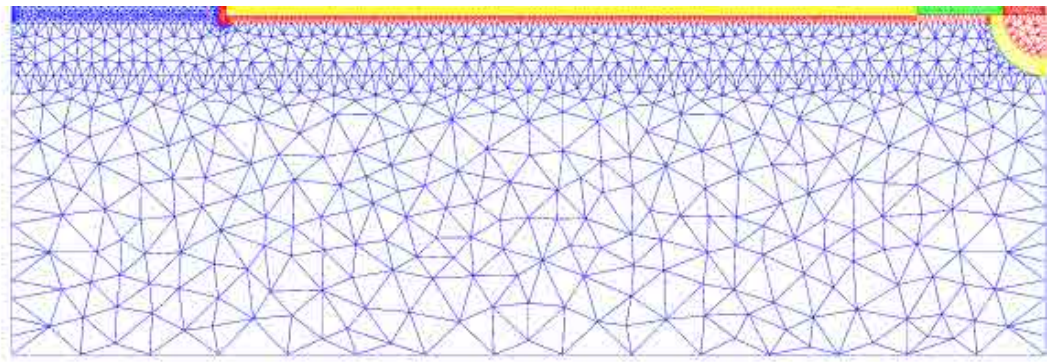

Figure 47 : Mesh used for the benchmark computation.

Note that a mesh taking into account the interfaces was also built but leads to numerical computation problems (non convergence).

3.4.2.4 Boundary Conditions and Sources

The boundary conditions were chosen identical to the ones depicted in section 5 except for the time dependent boundary condition at the right drift border which is kept constant in time with Pg = 1 MPa and Sw = 0.9. The Source term used was identical to the one depicted in section 5.

3.4.2.5 Initial Conditions

The initial conditions in the system were chosen identical to the ones depicted in section 5.

3.4.2.6 Deviations from the specification

The deviations of the conducted calculation from the benchmark depicted in section 5 are listed hereafter:

- Interfaces are not taken into account.
- Boundary conditions for the drift are kept constant over time.
- 2D computation was conducted instead of 2D axisymmetric.

3.4.3 Base Case Results

We performed the benchmark two-phase flow computation over a 20,000 years period and we focused on the temporal liquid saturation evolution of the different components of the system as well as on the temporal gas pressure evolution.

The temporal liquid saturation evolution inside the different components of the system is presented in Figure 48

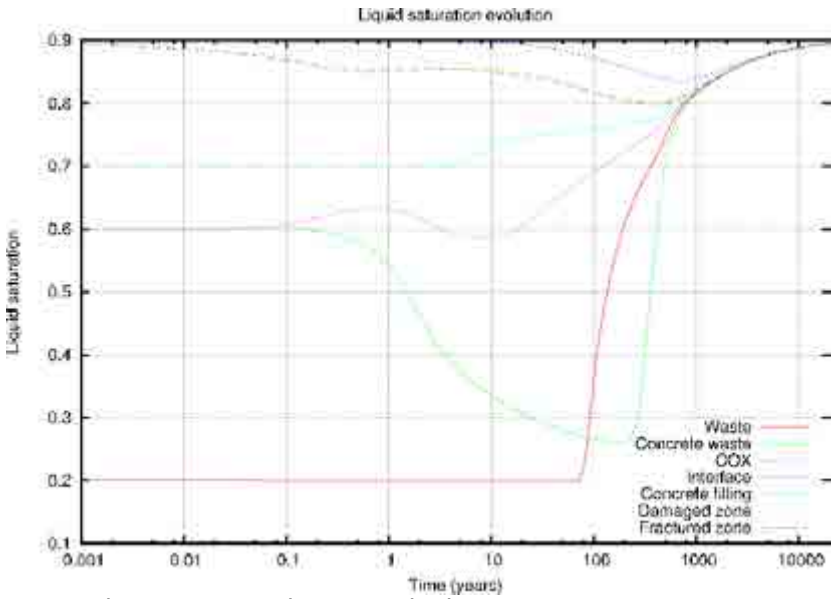

Figure 48: Temporal saturation evolution inside the system

All the system is fully saturated after 20,000 years with some different trends depending on the component. In the vicinity of the disposal cell, the Callovo-Oxfordian argillite (unperturbed, damaged zone and fractured zone) slowly lightly desaturates (with a lower value of 0.8) over the first 1,000 years period before fully resaturating. The concrete filling as well as the interface (considered as EDZ in our case) starts saturating after 10 years and slowly reach full saturation after 20,000 years. The waste starts to saturate after 100 years and rapidly reaches a saturation of 0.8 after 1,000 years before slowly fully saturating. The most interesting trend is the one of the concrete waste were desaturation begin after 1 year before reaching a minimum of 0.25 at about 200 years and increasing to a value of 0.8 at 1,000 years. It is to note that if 20,000 years are needed to fully saturate the system, all the components present a saturation larger than 0.8 after only 1,000 years.

The temporal gas pressure evolution inside the components of the system is presented in Figure 49.

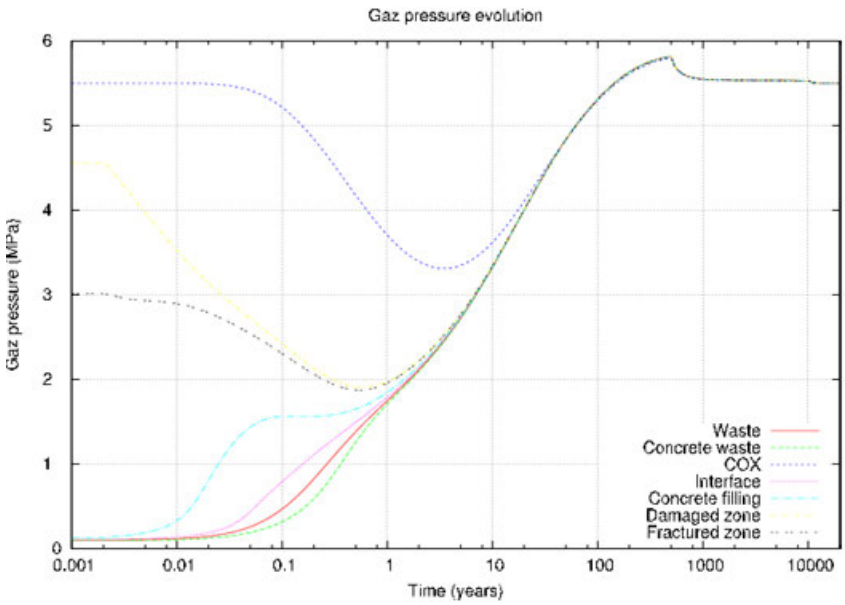

Figure 49: Temporal gas pressure evolution inside the system

Figure 49 indicates that except for the Callovo-Oxfordian argillites (unperturbed, damaged and fractured) the pressure inside the system components slightly increase towards the hydrostatic pressure which is reached in about 200 years. For the argillites in the vicinity of the engineered parts of the system, an hydraulic decompression with a minimum pressure value of about 2 to 3 MPa is observed during the first 100 years.

A small overpressure of about 0.25 MPa is seen after 500 years and is found to be very small in comparison to the overpressure calculated by the other teams. The very low overpressure calculation points out the strong impact of the very small gas residual saturation we introduced in the argillites (which is a deviation from the specified benchmark): even for a very small gas residual saturation inside the argillites, gas is allowed to diffuse in this part of the system and a very low gas pressure buildup is calculated in the repository cell.

3.4.4 Discussion and Conclusions

The performed computations are strongly impacted by the residual gas saturation imposed in the argillites which is a deviation from the specified benchmark. The gas phase, in our case, can migrate inside the argillites leading to a very small overpressure computation in the repository cell in comparison the results obtained by the other teams. Nevertheless, the computed time needed to fully saturate the system seems to be of the same order of magnitude than the one computed by the other teams pointing out that the residual gas saturation hypothesis only affect the gas pressure calculation.

3.4.5 Issues for further consideration

The numerical problems encountered during the numerical computation of the specified benchmark stem from two different points.

The first point, linked to the inability to take into account the interfaces without oscillations computation, stems from the cell centered scheme used to compute the convective part of the system equations. In order to tackle this problem, an upwind scheme must be used to compute the convection.

The second point, linked to the necessity to use residual gas saturation for all the considered materials, stems from the set of variables used (liquid saturation and gas pressure). A new set of variables (like the one prosed in **[4]**) must be used to solve this problem.

3.4.6 References

[1] TrioU: http://www-trio-u.cea.fr.

[2] Caro, F. and Laucoin, E. : Description du module de MPCube permettant la simulation numérique des écoulements diphasiques multicomposants en milieu poreux. Rapport CEA DEN/DANS/DM2S/STMF/LMEC/RT/09-006/B (2009).

[3] PETSC: http://www.ms.anl.gov/pets/pets-as/.

[4] Bourgeat, A., Jurak, M. and Smaï, F.: Two partially miscible flow and transport modeling in porous media; application to gas migration in a nuclear waste repository, *Computational Geosciences* 13(1), 29-42 (2009).

3.5 CNRS contribution

3.5.1 Introduction

This report contains the numerical simulations done in the context of the first benchmark concerning gas generation and migration at repository depth (many hundreds of meters below ground level) and repository scale.

We consider the coupled system describing immiscible compressible two-phase flow, such as water-gas, in porous media without dissolution and evaporation effects. The system is written in a phase flow formulation which consists of a parabolic equation (the gas pressure equation) coupled with a nonlinear degenerated diffusion-convection one (the water saturation equation). A vertex-centred finite volume method on unstructured grids is employed to discretize the coupled system, see e.g. [1, 3]. A Godunov-type method is used to treat the convection terms and a conforming finite element method with piecewise linear elements is used for the discretization of the diffusion terms. Our main focus is on a semi-implicit and sequential scheme. Simulations have been performed using the code 2φICFlow (Immiscible Compressible two-phase Flow) developed by the University of Pau & CNRS in the framework of the French research group MoMaS (http://www.gdrmomas.org/). 2φICFlow is designed for computationally efficient simulation of isothermal two phase flow, such as water-hydrogen, in one and two-dimensional porous media.

A part of this work has been published in [4].

3.5.2 Model Implementation

We use the code 2φICFlow. It is an in-house code for numerical simulation of the two-phase compressible immiscible flow in heterogeneous porous media, based on a finite volume method. The code simulates the two-phase flow equations for gas-water system, with incompressible water and gas satisfying the ideal gas law. The effects of gas dissolution in water and water evaporation are neglected.

3.5.2.1 Code and Formulation

The partial differential equations (PDE) of the model can be written as:

$$\Phi\rho_w\frac{\partial S_w}{\partial t}+\mathrm{div}(\rho_w\mathbf{q}_w)=0 \quad \text{and} \quad \mathbf{q}_w=-\lambda_w(S_w)\mathbb{K}(\nabla p_w-\rho_w\mathbf{g}), \tag{1}$$

$$\Phi\frac{\partial}{\partial t}(\rho_g(p_g)S_g)+\mathrm{div}(\rho_g(p_g)\mathbf{q}_g)=0 \quad \text{and} \quad \mathbf{q}_g=-\lambda_g(S_g)\mathbb{K}(\nabla p_g-\rho_g(p_g)\mathbf{g}), \tag{2}$$

where S_α and p_α, α=w, g, are the phase saturations and the pressures, ρ_w, ρ_g are the phase mass densities and λ_w, λ_g are the phase mobilities, Φ is the porosity and K is the permeability. As primary unknowns we selected the water saturation $S = S_w$ and the gas pressure $p = p_g$, while the water pressure is given by the capillary pressure law $p_w = p_g - p_c(S_w)$. In order to apply the finite volume discretization we rewrite the water equation in a convection-diffusion form:

$$\Phi\frac{\partial S}{\partial t}+\mathrm{div}(f_w(S)\mathbf{q}+a(S)\mathbb{K}\nabla p_c(S)+a(S)(\rho_w-\rho_g(p))\mathbb{K}\mathbf{g})=0, \tag{3}$$

where $q = q_w + q_g$ is the total velocity and new nonlinear functions are: the water fractional flow

$f_w(S) = \lambda_w(S)/(\lambda_w(S)+\lambda_g(S))$ and $a(S) = \lambda_w(S)\ \lambda_g(S)/(\lambda_w(S)+\lambda_g(S))$, the capillary diffusion function. Taking into account that the model is radially symmetric we have transformed the above equations by multiplying the porosity, the permeability, the source terms and the Neumann boundary conditions by $2\pi r$, where r is radial coordinate, and we have neglected the gravity which is incompatible with the radial symmetry assumption. The PDEs are discretized by a **vertex centered finite volume method** (called also finite volume element method). The method uses two grids: the primary grid on which the solution and the material properties of the porous medium are represented, and the secondary grid composed of control volumes used in finite volume integration. Secondary grid cells are centered in the vertices of the primary grid and are formed by connecting the primary grid cell centers with the centers of their edges. Primary unknowns (the water saturation S and the gas pressure p) are computed at the vertices of the primary grid. Since the saturation is discontinuous in the vertices on the boundary of two different materials, we chose for the saturation variable in these vertices the so called **effective saturation** [5]. The effective saturation is defined by the property that it gives the same quantity of water in the control volume as the calculation with limiting values of the saturation in each element of the primary mesh. The time discretization is done by an implicit Euler method. The nonlinear system obtained by the discretization is solved by the Picard iterations. If the values S^n and p^n on the n-th time level are known, then S^{n+1} are calculated by an iterative procedure in which the new value S^+ is obtained from the old iteration S^- by solving:

$$\begin{aligned}
&\rho_w \int_{V_i} \Phi\, dx S_i^+ - \rho_w \int_{V_i} \Phi\, dx S_i^n \\
&+ \Delta t \sum_{T\cap V_i\neq\emptyset} \sum_{j\in\mathcal{N}(T,i)} \frac{p_c^T(S_j^{T,-}) - p_c^T(S_i^{T,-})}{S_j^{T,-} - S_i^{T,-}} \sum_{k\in\mathcal{C}(T,i)} \int_{\gamma_{i,k}^T} a(S^-)\mathbb{K}\nabla\phi_j \cdot \mathbf{n}_{i,k}^T d\sigma \left(\frac{S_j^{T,-}}{S_j^-} S_j^+ - \frac{S_i^{T,-}}{S_i^-} S_i^+\right) \\
&= -\Delta t \sum_{T\cap V_i\neq\emptyset} \sum_{j\in\mathcal{C}(T,i)} \left(f_w(S_i^n) \int_{\gamma_{i,j}^T} \max(0, \mathbf{q}^n \cdot \mathbf{n}_{i,j}^T) d\sigma + f_w(S_j^n) \int_{\gamma_{i,j}^T} \min(0, \mathbf{q}^n \cdot \mathbf{n}_{i,j}^T) d\sigma \right),
\end{aligned}$$

where V_i is the control volume centered in the i-th vertex of the primary grid, and T is an element of the primary grid; $N(T,i)$ is the set of all vertices in the element T except the i-th; $C(T,i)$ is the set of all vertices in the element T connected to the i-th vertex by an edge; $\gamma_{i,k}^T$ is the part of the boundary $\partial V_i \cap T$ between the i-th and the k-th vertex. With $S_j^{T,\pm}$ we denote the local saturation value in the element T corresponding to the effective saturation $S_j^{\pm}$. In the above discretization we use mass lumping in the accumulation terms and explicit upwind calculation of the convective term. The gas equation is treated by summing the gas and the scaled water equations, which makes this equation applicable also in saturated regions. After linearisation the Picard iterations have

$$\begin{aligned}
&c_g p_i^+ (1 - S_i^n) \int_{V_i} \Phi\, dx - \Delta t \int_{\partial V_i \cap \Omega} [\rho_g(p_i^-)\lambda_w(S^+) + \rho_g(p^-)\lambda_g(S^+)]\mathbb{K}\nabla p^+ \cdot \mathbf{n} d\sigma \\
&= c_g p_i^n (1 - S_i^n) \int_{V_i} \Phi\, dx - \Delta t \int_{\partial V_i \cap \Omega} \rho_g(p_i^-)\lambda_w(S^+)\mathbb{K}\nabla p_c(S^+) \cdot \mathbf{n} d\sigma - \Delta t \int_{\partial V_i \cap \Gamma_p^N} Q_g^{n+1}\, d\sigma.
\end{aligned}$$

Here, Γ_p^N is the part of the boundary where the hydrogen is injected, and Q_g^{n+1} is the injection rate.

3.5.2.2 Benchmark Implementation

As mentioned before we do not take into account the gas dissolution and the water evaporation effects. Therefore we do not have the equation for the mass conservation of gaseous hydrogen. We have also taken the water mass density constant.The domain geometry and the boundary conditions are implemented as requested. The gas source term is implemented as a Neumann boundary condition on the border of the interface Canister-EDZ. All porous media material properties are taken as given. The radial permeability is calculated by the formula $K_r = \sqrt{K_h}\sqrt{K_v}$.

3.5.2.3 Grid

The mesh used in the simulations is composed of quadrilaterals and triangles. Quadrilaterals aligned to the coordinate axes are used everywhere except in the Access drift where we use a combination of general quadrilaterals and triangles to match the geometry. The mesh used in the simulations with the Interface has 1915 nodes and 1932 elements, while the mesh used in the simulations without the Interface has 1522 nodes and 1544 elements.

3.5.2.4 Boundary Conditions and Sources

Implemented as requested.

3.5.2.5 Initial Conditions

Implemented as requested.

3.5.2.6 Deviations from the specification

Described in section 3.5.2.2.

3.5.3 Base Case Results

Due to small time steps, caused by the presence of highly permeable interface, we obtained only the first 1000 years of the simulation.

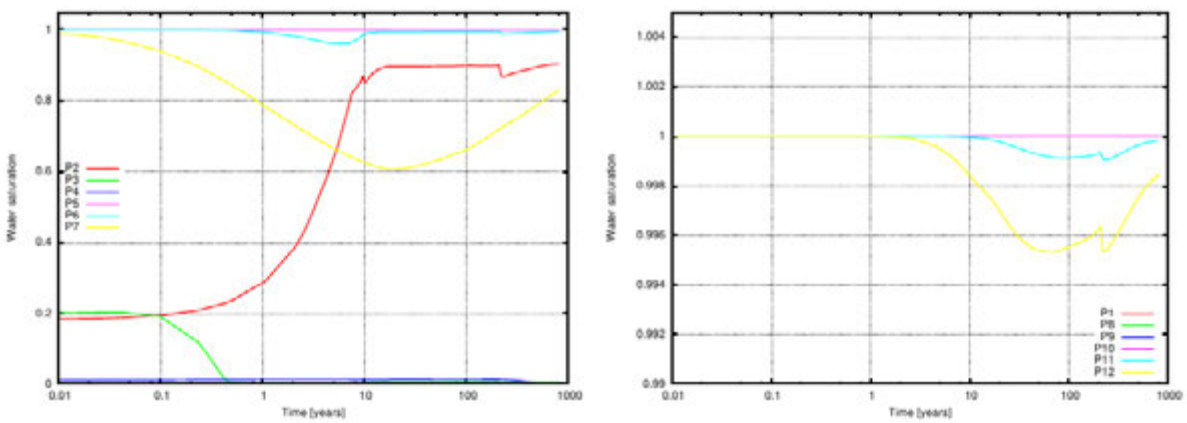

Figure 50 Evolution of the water saturation with time at given points

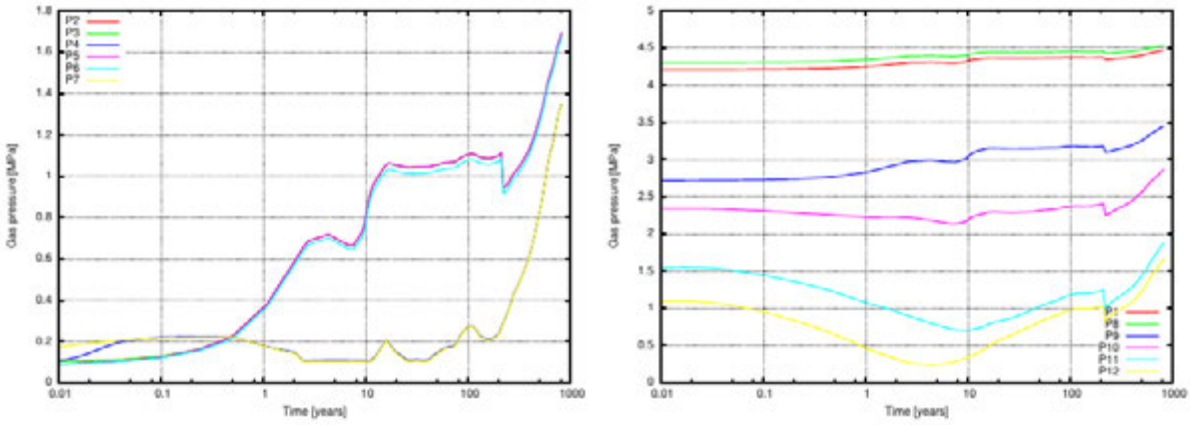

Figure 51 Evolution of the gas pressure with time at given points

3.5.4 Prescribed Sensitivity Cases

Due to small step size in our simulations we could done only the sensitivity with less permeable interface. It seems that the resolution of the flow in the Interface is responsible for small time steps taken by our simulator.

3.5.4.1 Case 1: Self Healing EDZ

Not done.

3.5.4.2 Case 2: Altered Relative Permeability Curves

Not done.

3.5.4.3 Case 3: Increased Diffusion in Water

Not applicable in immiscible simulation.

3.5.4.4 Case 4: Gas Generation Delayed

Not done.

3.5.4.5 Case 5: Less Permeable Interfaces

Case with the interface permeability equal to $10^{-18}\ m^2$. Simulation up to 30,000 years. Maximum gas pressure is 5.42639 MPa.

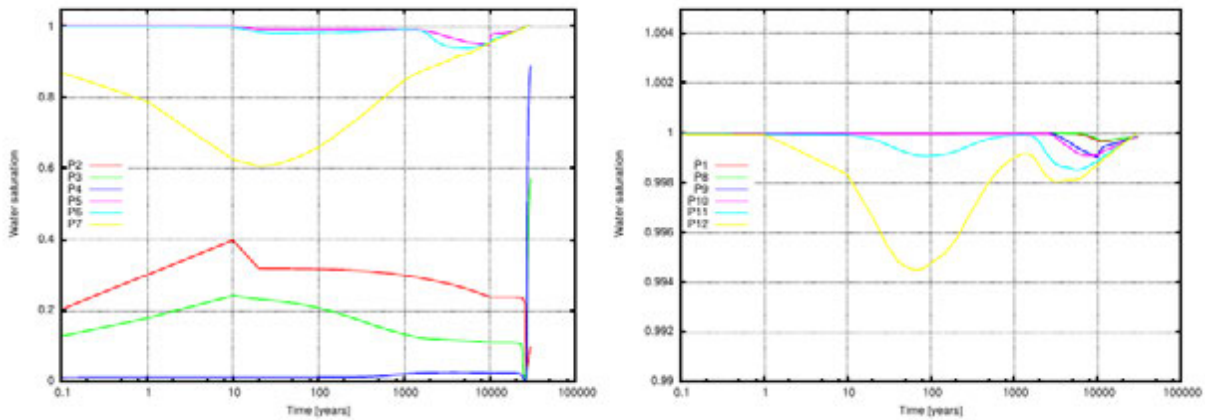

Figure 52 Evolution of the water saturation with time at given points

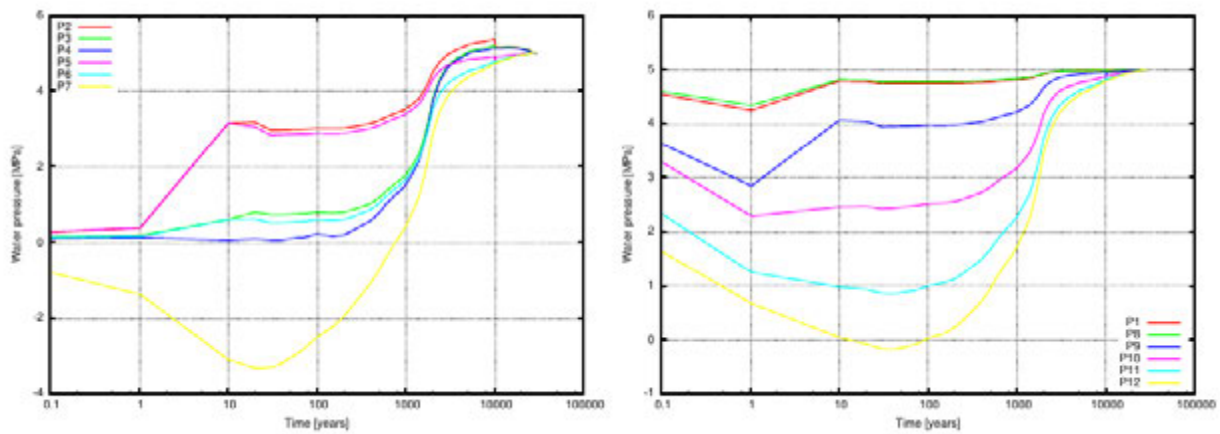

Figure 53 Evolution of the water pressure with time at given points

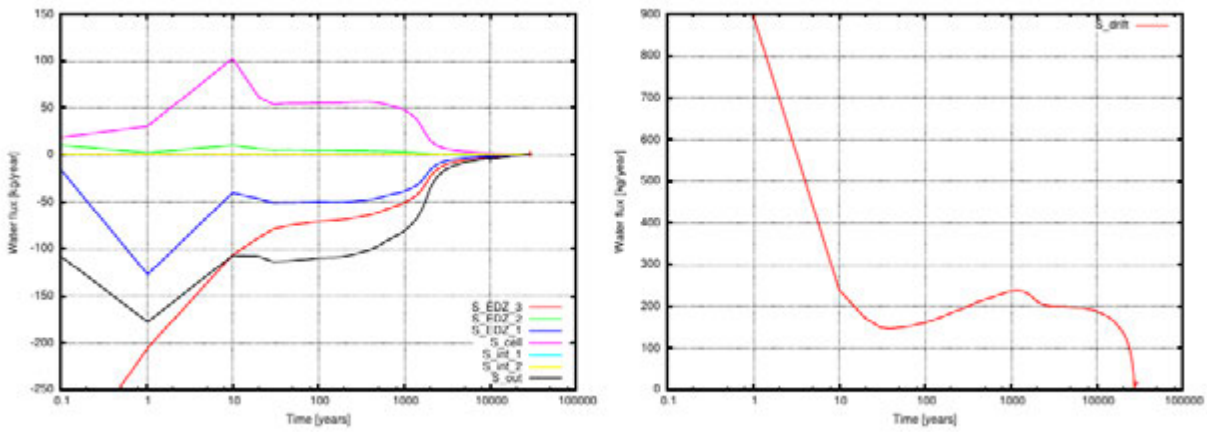

Figure 54 Evolution of the water fluxes with time through surfaces

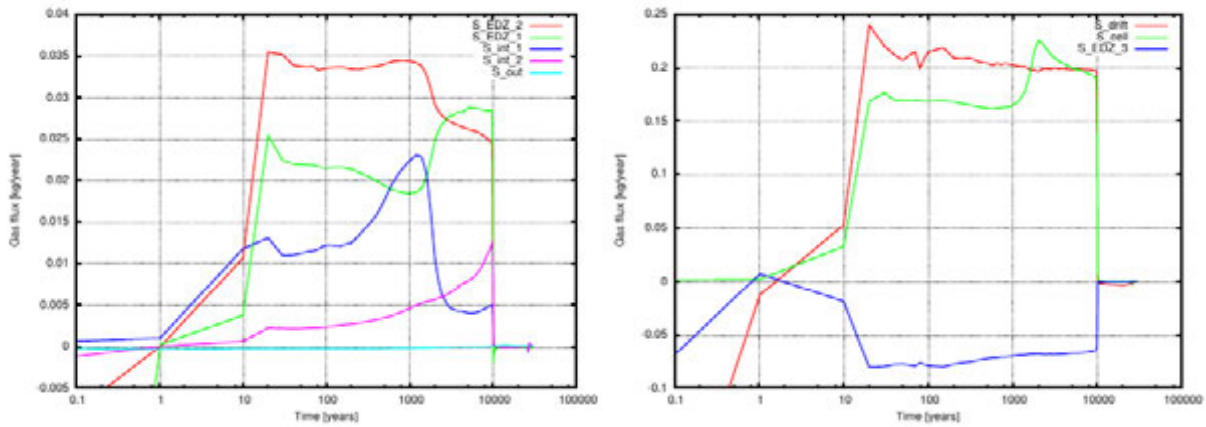

Figure 55 Evolution of the gas fluxes with time through surfaces

3.5.4.6 Case 6: Mesh sensitivities

Not done.

3.5.5 Additional Sensitivities

Not done.

3.5.6 Discussion and Conclusions

From the numerical results presented here, we can conclude that in the test cases with and without the Interface the gas pressure does not increase significantly (about 5.5 MPa). Some oscillations that are visible in calculated fluxes were probably produced by choosing the largest possible time steps. Let us mention that since our code is based on a sequential procedure with a semi-implicit discretization, this does not allow us to choose sufficiently large time steps needed to do the simulation up to 100,000 years. We see that the EDZ is the preferential path for the gas migration toward the Access Drift and out of the computational domain. The Interface is also a path for a gas migration although five times less important (compare the gas fluxes through S_cell and S_int_1). We believe that the gas migration will be very similar also with the original Interface permeability since very permeable gas interface is attached to a less permeable one and the upscaled value of the permeability in the Interface should be obtained by the harmonic mean, which gives the value close to the one we used in this simulation.

In general the gas migration is dominated by imposed boundary condition on the Acces Drift boundary.

3.5.7 Lessons Learnt

We need to upscale (see [2,6]) the Interfaces in the module scale benchmarks in order to avoid problems of flow resolution in very permeable Interface, that can lead to convergence problems leading to small time steps.

3.5.8 Issues for further consideration

Verify imposed boundary condition from the results of the module scale simulation.

3.5.9 References

[1] M. Afif, B. Amaziane, Numerical simulation of two-phase flow through heterogeneous porous media, Numer. Algorithms, 34 (2003) 117–125.

[2] B. Amaziane, S. Antontsev, L. Pankratov, A. Piatnitski, Homogenization of immiscible compressible two-phase flow in porous media : application to gas migration in a nuclear waste repository, SIAM J. Multiscale Modeling & Simulation, 8 (2010) 2023–2047.

[3] B. Amaziane, M. El Ossmani, C. Serres, Numerical modeling of the flow and transport of radionuclides in heterogeneous porous media, Comput. Geosci., 12 (2008) 437–449.

[4] B. Amaziane, M. El Ossmani, M. Jurak, Numerical simulation of gas migration through engineered and geological barriers for a deep repository for radioactive waste, to appear in Computing and Visualization in Science.

[5] B. Amaziane, M. Jurak: Contribution of CNRS/MoMaS to FORGE WP 1.2 Upscaling & Numerical Results of the Benchmark at cell scale, FORGE General Assembly Prague, Nov30th - Dec 2nd, 2010

[6] B. Amaziane, M. Jurak, L. Pankratov, A. Piatnitski, Effective relative permeabilities and capillary pressure of immiscible compressible two-phase flow in porous media, Research Report, 2009.

3.6 IRSN contribution

3.6.1 Introduction

This chapter presents the IRSN contribution to the benchmark at the cell level performed within the Work Package 1.2 of FORGE project.

The presented work consists of two main parts: code development and validation was the first goal and application to the WP1.2 benchmark cases was the second objective. In particular, we wanted to construct an easily adaptable simulation tool capable of taking advantage of new formulations and discretisation schemes and sufficiently modulable to be able to integrate new physical concepts that would receive an agreement of the scientific community in the future.

3.6.2 Model Implementation

IRSN collaborated with University of Claude Bernard in Lyon to develop a 3D simulation tool for gas migration. It takes into account the convective and diffusive transport of N+1 components in 2 phases as well as mass exchanges between phases (dissolution and evaporation). The liquid phase and the solid matrix are assumed incompressible; the other phase follows the ideal gas law. The formulation is based on the classical mass conservation laws for both multi-component phases (g for gas and l for liquid) supplemented with generalized Darcy equations for each phase:

Equation 1

$$\frac{\partial}{\partial t}\left(\Phi \sum_{\alpha} \rho_\alpha X_\alpha^i S_\alpha\right) + div\left(\sum_{\alpha} \rho_\alpha X_\alpha^i \vec{q}_\alpha\right) - div\left(\Phi \sum_{\alpha} \rho_\alpha D_\alpha^i S_\alpha \vec{\nabla} X_\alpha^i\right) = Q_i$$
$$\vec{q}_\alpha = -\lambda_\alpha K\left(\vec{\nabla} P_\alpha - \rho_\alpha \vec{g}\right) \quad \alpha = \{l, g\} \quad i = \{0..N\}$$

where K is the absolute permeability tensor, g the gravity vector, Q_i the source term for the component i, and for each phase α: ρ_α is the density, $\lambda_\alpha = k_{r\alpha}/\mu_\alpha$ the mobility, $k_{r\alpha}$ the relative permeability, μ_α the dynamic viscosity, and we define capillary pressure $P_c = P_g - P_l$. Empirical laws are used for the capillary pressure and relative permeabilities (Brooks-Corey, Brusaert, Van Genuchten, Vauclin …).
These equations are completed by an appropriate set of closure equations related to the hypothesis of the existence of a local thermodynamical equilibrium (Henry law, Raoult-Kelvin law …).

3.6.2.1 Consistent thermodynamical model

We consider that phases are not pure but composed of N+1 components: one solvent (typically water) and N solutes (or gas components, typically hydrogen, nitrogen, oxygen, etc.). Their natural states at standard T, P are liquid for the solvent and gas for the gas components but due to vaporisation and gas dissolution, all components may be present in each phase. Assuming that local thermodynamical equilibrium is satisfied, phase compositions are related by relations of the following general form:

Equation 2

$$X_g^i P_g = K^i X_l^i$$

where i = 0 for the solvent and i = 1…N for the solutes; X^i_α denotes the molar fraction of component i in phase α={g, l}. In the most general case the coefficient K^i depends on temperature and on pressure and composition of each phase but, in the case of ideal gas mixture, dilute liquid solution and moderate pressure, this dependency is reduced to temperature and liquid pressure and Equation 2 recovers the classical relations like Henry's or Raoult-Kelvin's law. Starting with the first principle thermodynamics, e.g. equilibrium of the chemical potentials of each component in both phases, we obtained new thermodynamic equilibrium relations taking into account a higher pressure correction to the infinite dilution limit represented by Henry and Raoult-Kelvin laws. For the solvent we obtain:

Equation 3

$$X_g^s P_g = P_g^s exp\left(\frac{P_l - P_v^s}{RT\rho_l^{s,*}/M^s}\right) X_l^s$$

where P_v^s is the saturated vapour pressure depending only on the temperature, M^s is the molar mass of the pure solvent and $\rho_l^{s,*}$ is the molar mass of the pure solvent. It is easy to verify that the correction with respect to the Kelvin-Raoult law is given by:

Equation 4

$$d_{r,RK} = \left|1 - exp\left(\frac{P_l - P_v^s}{RT\rho_l^{s,*}/M^s}\right)\right|$$

For the solute we get Equation 5 where the exponential term is the correction to the standard Henry law; P0 represents some reference pressure. This is a simplified version of the Krichevsky-Kasarnovsky (KK) equation well known in the liquid mixture theory.

Equation 5

$$X_g^i P_g = K_H^i exp\left(\frac{P_l - P^0}{RT/v_l^{i,\infty}}\right) X_l^i \qquad where \qquad d_{r,H}^i = \left|1 - exp\left(\frac{P_l - P^0}{RT/v_l^{i,\infty}}\right)\right|$$

The corrective exponential terms may become non-negligible in the case of the hydrogen in the repository conditions. The values of corrective terms calculated for water and hydrogen mixture are presented in Figure 56 as a function of liquid pressure.

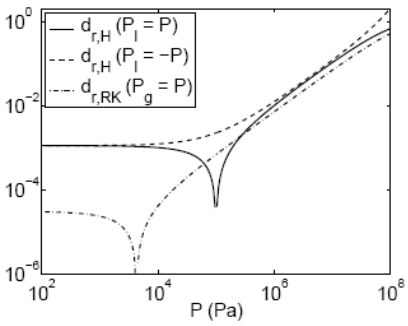

Figure 56 : Relative corrections to the standard Henry constant $d_{r,H}$ and the Raoult-Kelvin relation $d_{r,RK}$ taking into account the existence of the capillary pressure in high pressure limit. The curve where P_l=-P corresponds to the situation where the water pressure is negative as a result of strong capillary pressure. At moderate pressures (10MPa) the relative deviations become non-negligible (10%).

3.6.2.2 Code and Formulation

In order to be able to handle material heterogeneities as well as the changes in the thermodynamical state of the system (one or two phases present), a special set of unknowns has been chosen, namely liquid pressure P_l and molar fraction of dissolved gas (for example hydrogen) X_l^i. They are naturally used to describe fully saturated conditions when only liquid phase is present. However, using thermodynamic equilibrium, it is possible to reconstruct all variables of a two phase system. Thus (P_l, X_l^{H2}) can be used as primary variables with standard physical meaning whenever the liquid phase is present. In the case of zero liquid saturation when only the gas phase is present it is possible to extend these variables using again the thermodynamic equilibrium. On the other hand, the capillary pressure relation $P_c(S_l) = P_g - P_l$ and the thermodynamic equilibrium relations (of the general form of $P_g X_g^i = K_i X_l^i$) must be fulfilled simultaneously in

order to allow the coexistence of the two phases. This fact leads to some simple criteria for discriminating the phase state of the system. The gas pressure candidates are given by two formulae in Equation 6. The superscripts *m* and *t* stand for mechanical and thermodynamical equilibrium conditions.

Equation 6

$$\pi_g^m = P_l - P_c(S_g) \quad and \quad \pi_g^t = \sum_{i=1}^{N} K_l X_l^i$$

Local existence of gas phase is only possible when $\pi^m_g = \pi^t_g$. Thus, given pressure and composition of liquid phase, (P_l, X_l^i), we look for a value of gas saturation S_g such as $P_c(S_g) = \pi^t_g - P_l$. The last equality cannot always be fulfilled, in particular because the capillary pressure curve is positive definite ($P_c \geq 0$). Thus, if $\pi^t_g - P_l$ is smaller than the minimal value of P_c, the two expressions of gas pressure are not compatible and we conclude that the gas phase cannot exist. More generally, assuming that the function P_c is increasing and reversible (with $\max(P_c) \leq \infty$), we can compute S_g as follows:

Equation 7

$$S_g\left(P_l, (X_l^i)_{i=1..N}\right) = \begin{cases} 0 & if \;\; \pi_g^t\left(P_l, (X_l^i)_{i=1..N}\right) - P_l < \min_{S_g} P_c(S_g) \\ 1 & if \;\; \pi_g^t\left(P_l, (X_l^i)_{i=1..N}\right) - P_l > \max_{S_g} P_c(S_g) \\ P_c^{-1}\left(\pi_g^t\left(P_l, (X_l^i)_{i=1..N}\right) - P_l\right) & else \end{cases}$$

In particular for a two component system with linear thermodynamic relations of Henry law $P_g X^1_g = K_H X^1_l$ and constant water vapour $P_g x^0_g = P_v$ the thermodynamic gas pressure is given by $\pi^t_g = K_H X^1_l + P_v$ and the phase diagram in primary variables is defined by two straight lines, as in Figure 57.

This phase diagram may be used to interpret the resulting primary variables values. However it is not necessary to perform that analysis during the simulations, since our formulation is not degenerated. This means that if one of the phases disappears, the system of equations reduces automatically to the flow and transport in the remaining phase, as expected.

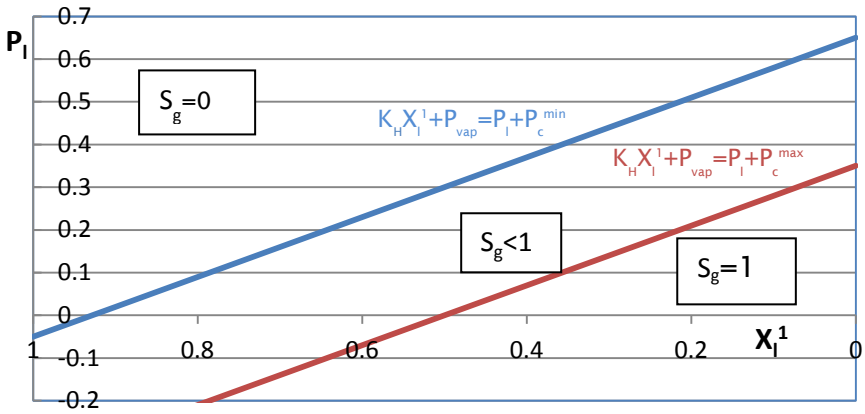

Figure 57 Phase diagram for a two component system with linear thermodynamic equilibrium relations

The resulting system of quasi-linear equations has been treated with fully implicit Euler time discretization and with an exact Newton method to obtain a set of linear equations. The spatial discretization has been done for triangles and tetrahedral elements with a finite element scheme within the Libmesh numerical library. In order to illustrate the ability of the formulation to treat gas appearance or disappearance, the model has been used on synthetic test cases supported by GNR MoMaS aiming at code testing and comparison. Each of those test cases deals with only one physical/numerical problem. We give here the results of two of these test cases sharing the same initial geometry given in Figure 58.

MOMAS Test cases

In the test cases, there are always two components (water and hydrogen); the porous medium is homogeneous. The no flux conditions are imposed on Γ_{imp} (1D flow, but 2D domain!). The initial conditions and left (Γ_{in}) / right (Γ_{out}) boundary conditions differ for each test case. The space discretization scheme used for these calculations is the finite element method of Lagrange P1 with a uniform grid of 200 elements and time steps going from 10 seconds to 15000 years.
Through these two applications, one proves the capacity of the code to simulate diphasic compositional flow where the phases may appear and disappear. The results presented here are in very good agreement with the simulations carried out by other participants to the MoMaS benchmark.

Test case 3b

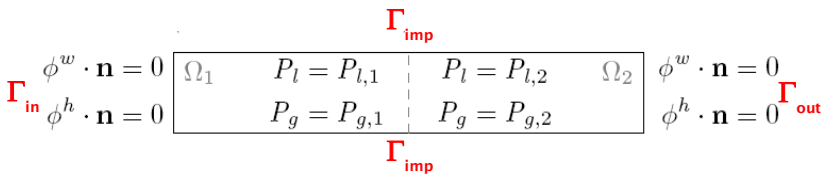

Figure 58 : Definition of the test case 3b. The general dimensions are: the length 1 m, and the height of 0.1m.

In this test case we study the return to equilibrium from an initial out-of-equilibrium state in a homogeneous material. We have no flux boundary conditions and the domain is divided into two parts: water saturated Ω_1 and partially saturated Ω_2. In the results we observe a very sharp desaturation moving to the left which arrives at the left boundary at about 200 000 sec. The precise resolution of such a front is possible due to the continuous treatment of the phase transitions in our model. It can be seen in Figure 59 that this is not necessarily the case for a code using ε switching method to detect the transition between one and two phases state (ToughII).

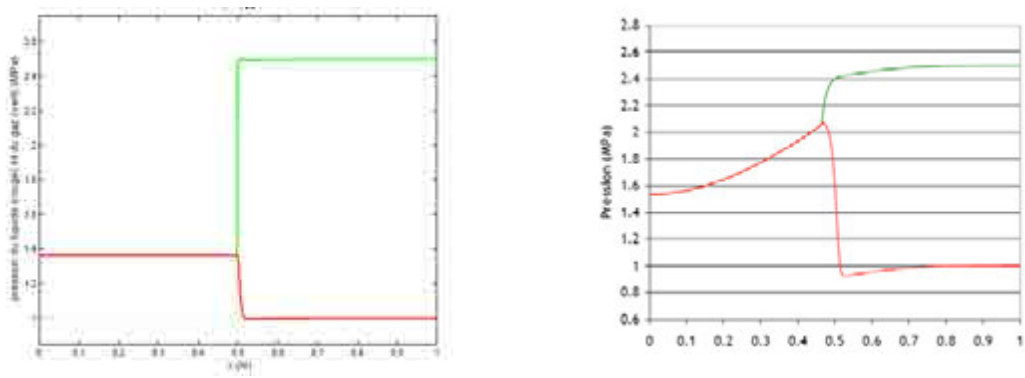

Figure 59 : Test 3b - Results at one time = 100 s; pressure of gas (green) and water (red). On the left Diphpom code, on the right ToughII (courtesy of Z.Saadi, IRSN)

Test case 1b

In this second test case $P_{g,out} > P_{l,out}$, which corresponds to uniform and unsaturated conditions in the whole domain. The general dimensions are: the length 200 m, and the height of 1 m. The injection rate ϕ^h_{in} is constant over the entire simulation period and was adjusted to obtain the required physical phenomena of capillary barrier, which would not appear for smaller or higher injection rates. The results of the simulation of the test 1b are presented in Figure 60. Both phases are initially present in the simulation domain. Inside the domain at some places the pressure of the liquid grows quicker than the gas pressure resulting in the gas phase disappearance. A barrier of liquid appears in the domain and propagates in the direction of the outflow. The unsaturated outflow conditions force the barrier to dissipate. Gradually the saturated zone is being reduced so that both fronts meet and the gas phase is henceforth present in the entire domain, see Figure 60. This test shows the highly non-linear character of the system, which may make hazardous standard interpolation/extrapolation technics used in SA/PA. In practice, for integrated level simulations one uses prescribed hydrogen generation rates which are constant over some periods of time with possibly decreasing steps. This approach is clearly oversimplified and does not take into account many driving factors (temperature, pressure, pH, water composition, gas phase composition, irradiation ...). The usual treatment in PA/SA consisting in use of penalising values leads in this case to considering relatively high generation rates which are supposed to be the upper limit of possible ones. However, due to strongly nonlinear character of the two-phase flow in tight porous media, it may not make sense to simply interpolate between extreme gas generation rates is not necessarily, since maximal gas pressures and gas saturations may be achieved at some intermediate gas generation rate!

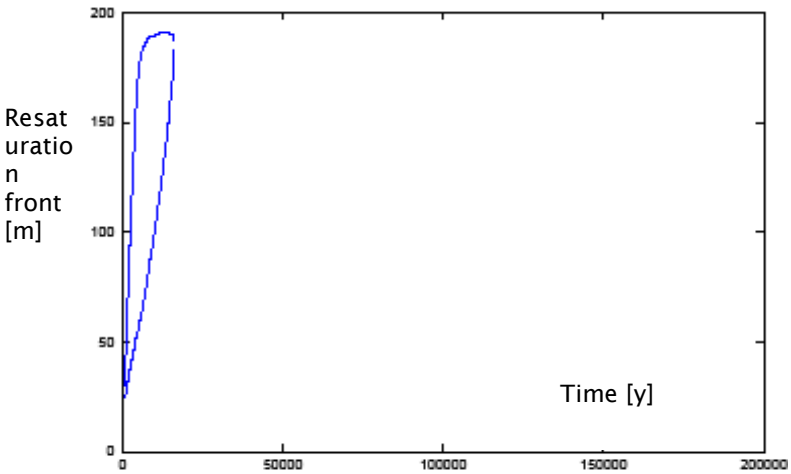

Figure 60: test 1b - position of the limits of the saturated zone as a function of time.

3.6.2.3 Benchmark Implementation

In order to verify the capacity of our simulation code to deal with complex applications we made calculations of 2D version of the FORGE WP1 cell-scale test case. The geometry of this test is presented in Figure 154 together with measure points. The major deviations from the original FORGE benchmark consist in using a plane 2D geometry instead of the 2D axisymmetric one and replacing Van Genuchten liquid relative permeability in technological voids (interfaces) by $k_{r,l}=S_g^{4/3}$ when $S_g<\varepsilon$ in order to avoid degenerescence of flow equations.

3.6.2.4 Grid

The 2D triangular mesh has been constructed with gmsh using both structured (for interfaces) and unstructured (elsewhere) algorithms. The interfaces where represented with 3 layers of elements, in order to be able to capture the permeability jump between the interfaces and the neighbouring materials (EDZ and bentonite). The mesh consisting of 4500 nodes was used for the calculations, see Figure 61.

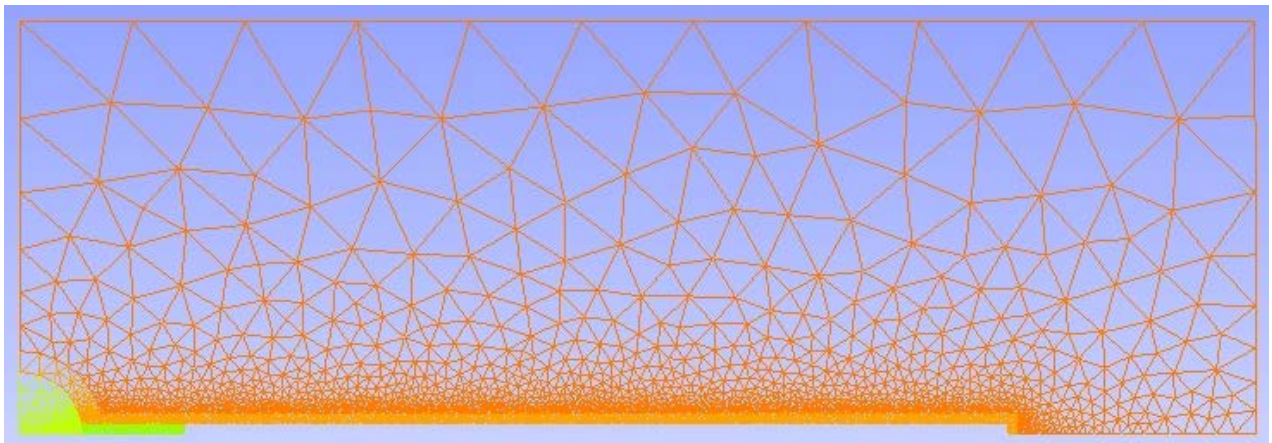

Figure 61 : The mesh used for the cell base case.

The time stepping scheme was created on a basis of an initial time step $dt_0=10^{-8}$ years, and was incremented every 25 time steps by a factor of 1.2. In the case of failure of the Newton iterations, the last time step was divided by 2. After the end of the hydrogen injection at 10^4 years, the time step was dropped to 10^{-8} years in order to resolve the very rapid water resaturation of the interfaces that follows the end of gas injection. This allows solving the base cell test case with 4500 time steps. Still the overall resolution in time shows rather dependent on the time stepping, and in some cases this procedure breaks down. Another important point is the quality of the linear solver used. It has turned out that iterative solvers lead almost always to non-physical solutions. We have used a direct parallelizable solver (Mumps), which allows to split the inversion process over several calculation cores (we have tested the calculations on 4 and 8 cores).

3.6.2.5 Boundary Conditions and Sources

The boundary conditions imposed in the benchmark were expressed either as Dirichlet or Neumann ones. We have used the BC version in terms of liquid pressure P_l and water saturation S_l from which the other variables (P_g, X_l^h) can be deduced.
For the time dependent BC imposed in the drift we needed to interpolate either P_l or S_l since the series of values were not given at the same time moments. Since P_l is one of our primary variables, we have kept the prescribed values of P_l and interpolated linearly the saturations. From the saturations it is possible to calculate the values of liquid molar fraction of hydrogen X^h_l as long as the water saturation is not equal to one. In this later case X^h_l becomes ambiguous. Such a problem appeared for late times of this time dependent BC in the drift and also on the "outer" boundary conditions, where the gas pressure and the liquid pressure were equal to 5MPa, and thus the water saturation was supposed to be 1. The values of X^h_l corresponding to the fully saturated state were chosen in a different way in both cases. For the drift BC it was chosen to be equal to the solubility limit corresponding to the gas phase pressure of 5MPa, and at the "outer" boundary it was set to a lower value in order to represent a sink boundary and to be compatible with the initial conditions, see 3.6.2.6. Finally the value of the source term to be applied on the surface of the waste canister (excluded from the simulation domain) had to be adapted. Since we use a plane 2D, in order to stay as close as possible to the original FORGE benchmark we have to modify the original gas source term Q^h_{3D}. There are several approaches allowing calculating of the equivalent gas term Q^h_{2D}. The reduction

coefficient $R = Q^h_{2D}/Q^h_{3D}$ can be made equal to the ratio between the accessible volumes in both cases or to the ratio of the corroding metal surface present in the systems (in the 2D case the fictitious "depth" of the model is taken to be equal to 1m). Since most of the volume accessible to gas is localised close to the symmetry axis (in the interface) the second possibility has been adopted with the following source term:

- for $0 < t \leq 10000$ years, Q^h_{2D}=322.4mol/year/cell = 1.6 g/m²/year
- for $t > 10000$ years, Q^h_{2D}=0

As in the original case the source term is localised on all over the waste canister external surfaces.

3.6.2.6 Initial Conditions

The initial conditions were specified in the benchmark in terms of gas pressure and water saturation in the materials that were initially partially saturated (backfill in the drift, bentonite plug, interfaces). For these materials it was possible to calculate directly the corresponding water pressure and liquid molar fraction of hydrogen. The obtained values are given in Table 2. However this is not the case for fully saturated materials (EDZ and COx) where the liquid pressure of 5MPa was prescribed. In such a case X^h_l can take any value lower than the one obtained from the equilibrium relation Equation 2. As the X^h_l initial values in desaturated zones are much lower than these limits and very close to each other, we chose to use the same X^h_l value for saturated materials. In this way we avoid discontinuities in initial variables and we ensure that the "top" boundary condition corresponds to an infinite reservoir condition (dissolved hydrogen has a sink at this boundary).

	-21.3MPa	1,33E-05		1,68E-05
	-2.98MPa	1,32E-05		1,37E-05
	72 kPa	1,32E-05		1,32E-05
	5MPa	1,32E-05	*6.9E-4*	*6.5E-4*
	5MPa	1,32E-05	*6.9E-4*	*6.5E-4*

Table 2 The Initial conditions imposed for the base cell case. The limit values are obtained in the case of saturated materials for the hypothetic gas pressure of 1e+4Pa. The last column illustrates the change in solubility limit when the KK equation (Equation 5) is used instead of Henry law.

3.6.2.7 Deviations from the specification

Beside the plane 2D geometry and the modified gas injection rate there are some other minor differences with respect to original specifications.

Absolute permeability

As most of the benchmark participants we have replaced the anisotropic absolute permeabilities of Table 19 by an isotropic ones; for the hostrock $K=10^{-21}m^2$, and for the EDZ and bentonite interface $K=10^{-17}m^2$.

Liquid relative permeability in interfaces

The original definition of the benchmark defined the liquid relative permeability by a standard Van Genuchten function:

$$k_{r,l} = \sqrt{S_{le}}\left[1-\left(1-S_{le}^{1/m}\right)^m\right]^2$$

with the exponent m=0.75. However this function goes very rapidly to zero when S_{le} approaches 0. It has been noticed that the resolution of Equation 1 becomes awesome when $k_{r,l}$ goes to zero quicker that the

inverse of the capillary function P_c^{-1} (which appears in front of the evolution term). For the van Genuchten capillary pressure function this limit is:

$$\lim_{S_{le}\to 0} P_c^{-1} = S_{le}^{1/m}$$

This is especially true in the case of the interfaces, where the convection is a dominant transport mode, and which tend to de- or resaturate very quickly. We have sought thus to regularize the relative liquid permeability in the interfaces by replacing the van Genuchten function near S_{le}=0 by a simple power law:

$$k_{r,l}^{interface} = \begin{cases} S_{le}^{1/2}\left(1-(1-S_{le}^{1/m})^m\right)^2 & S_{le} > 0.38 \\ cst\, S_{le}^{1/m} & S_{le} \leq 0.38 \end{cases}$$

The value of cst is chosen in the way to insure the continuity of the $k_{r,l}$.

Residual water saturation

Another numerical problem was related to the possible complete desaturation of the interfaces which are very permeable and desaturate very easily. In such a case the simulation domain would be divided into two parts which evolve almost separately since the dry interface establish a capillary barrier between them. In this case the numerical resolution becomes tedious and the Newton procedure often converges to an unphysical solution. In order to avoid this problem a small residual water saturation is being imposed in the interfaces (S_{lr}=0.005).

Specific storage

The proposed model of implementation of specific storage was based on the liquid pressure dependency in the liquid density, see 5.5. However the concept of the specific storage was introduced in order to account for the compressibility of the rock and that of the liquid, and thus we consider that we should rather change the porosity than the liquid density, which, if applied as is, would perturb the mass balance calculations. We keep the same functional form and the specific storage coefficients as proposed in the benchmark, but the relation now reads:

$$\Phi_i(P_l) = \Phi_i^0 e^{S_s(P_l - P_0)}$$

where the reference conditions are denoted by an under-script 0 and correspond to the initial conditions.

3.6.3 Base Case Results

Figure 62 presents time evolution of pressures as measured in point P4 (interface), in point P5 (EDZ) and in point P9 (inside undisturbed COX). We find a similar behaviour as the other benchmark participants, namely slow gas pressure increase during gas injection phase (till 10^4 years) accompanied by a decrease of water pressure in the interface (P4). In the case of points P5 and P9, where initially no hydrogen was present, the P_g variable "represents" the amount of dissolved hydrogen. In P5 P_g rises from zero to become equal to P_l which corresponds to the apparition of free gas phase. But as soon as P_g becomes again lower than P_l, gas phase disappears. It can be noted that the value of gas saturation is small (of the order of 0.05%), and would usually not be seen by a code using a switch procedure. This can explain why we obtain some more pronounced minima of liquid pressure as compared to other benchmark participants.

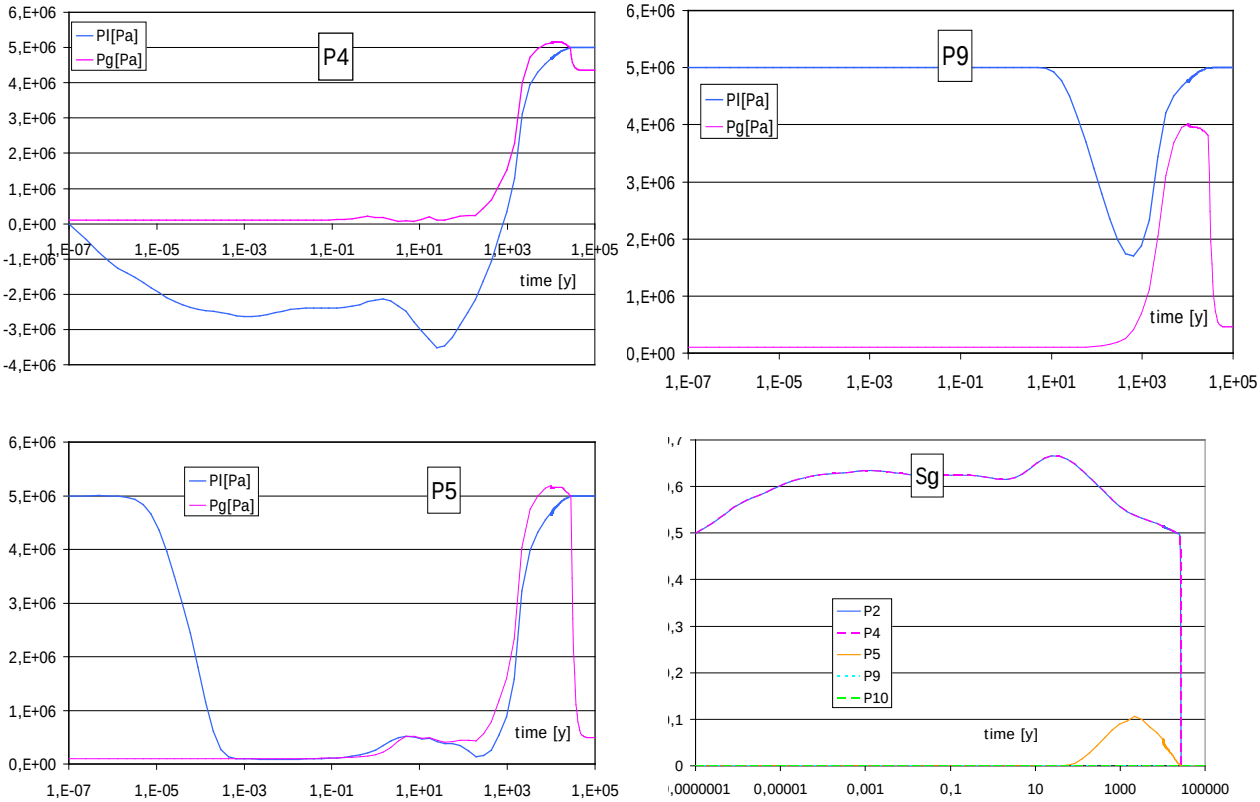

Figure 62 : Selected results of the base case. Points P2 and P4 are in the interface, P5 in EDZ, P9 and P10 in the sound hostrock.

3.6.4 Additional Sensitivities

Outer boundary position

In this additional test we address the question of the possible influence of the boundary conditions which are chosen arbitrary at the outer boundary of the system. As we have seen in 3.6.2.5 there is a certain degree of liberty in choosing the value of X_l^h at this boundary. As the condition is supposed to correspond to fully saturated conditions with a fixed liquid pressure, the amount of dissolved hydrogen is only limited by the solubility limit. Thus there are two possible extreme options. We can choose a low value of X_l^h corresponding to the initial conditions within the cell materials and consistent with the absence of larger amounts of hydrogen before the onset of the corrosion. However this may create a sink conditions for the dissolved hydrogen at this boundary. The second possibility is to use the solubility limit of 6E-4, but this relatively high value must be made consistent with the initial conditions within the hostrock and thus would limit the dissolution of hydrogen in the hostrock. In the base case implementation we have decided to use the first option. As a sensitivity analysis we propose to check if the simulation results would change if we put the outer boundary at 40m instead of 20m as in the base case to limit the influence of the BC values. As it can be seen in Figure 63 there is little change in results with respect to the base case. The desaturation of P5 is a little stronger (12% instead of 10%). However there seems to exist a very strong coupling between the conditions inside the cell and the imposed boundary conditions in the drift. This coupling may shield the effect of the outer boundary values.

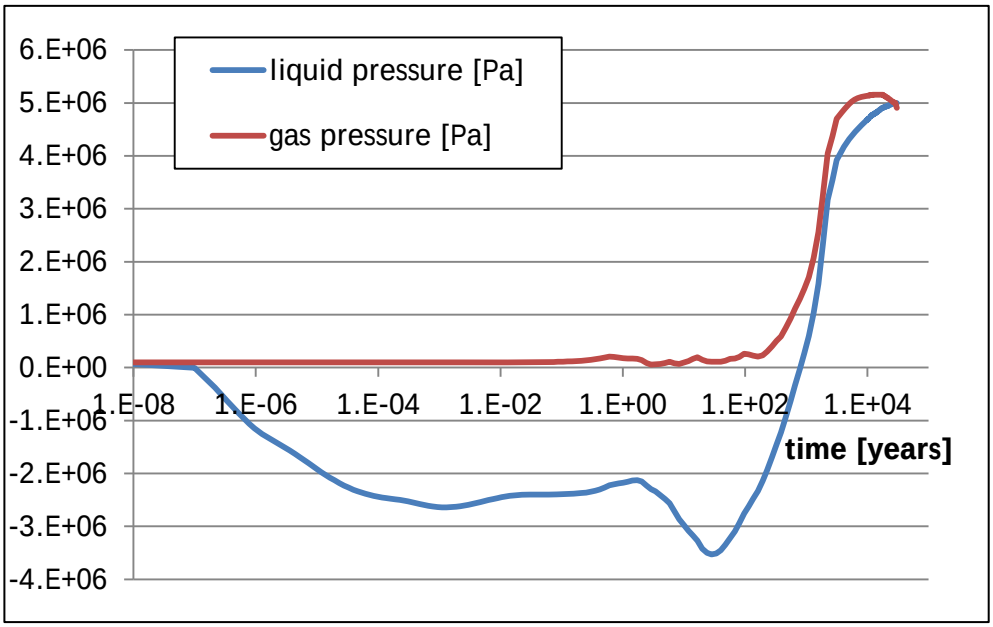

Figure 63 The outer boundary at 40m – results of the sensitivity test case for the point P4.

Drift boundary conditions

In order to verify how the drift time dependent boundary conditions influence the behaviour of the system, we use the liquid pressure and hydrogen liquid molar fraction issued from the calculations on the module scale (courtesy of Quintessa), see Figure 64. The imposed liquid pressure attains values (up to 7.8MPa) higher than the maximal gas pressure in the base case. All other conditions are the same as in the base case. The results of this simulation, Figure 65, confirm that the system is completely driven by these drift boundary conditions. The maximal gas pressure inside the cell rises up to 8.5MPa (instead of 5.5 in the base case). There is also a much stronger desaturation. EDZ is desaturated of more than 25%, and in P9 at 4.5m from the cell in the hostrock we observe 1% of gas saturation.

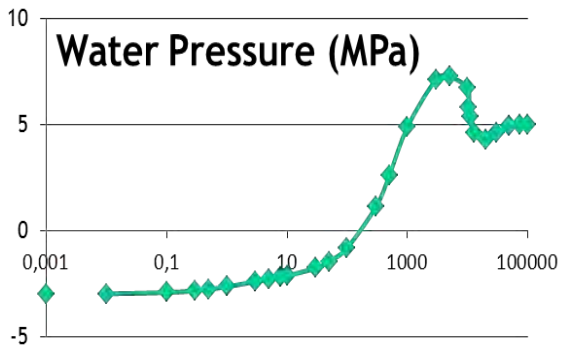

Figure 64 : The drift boundary conditions obtained from the module scale calculations (Quintessa)

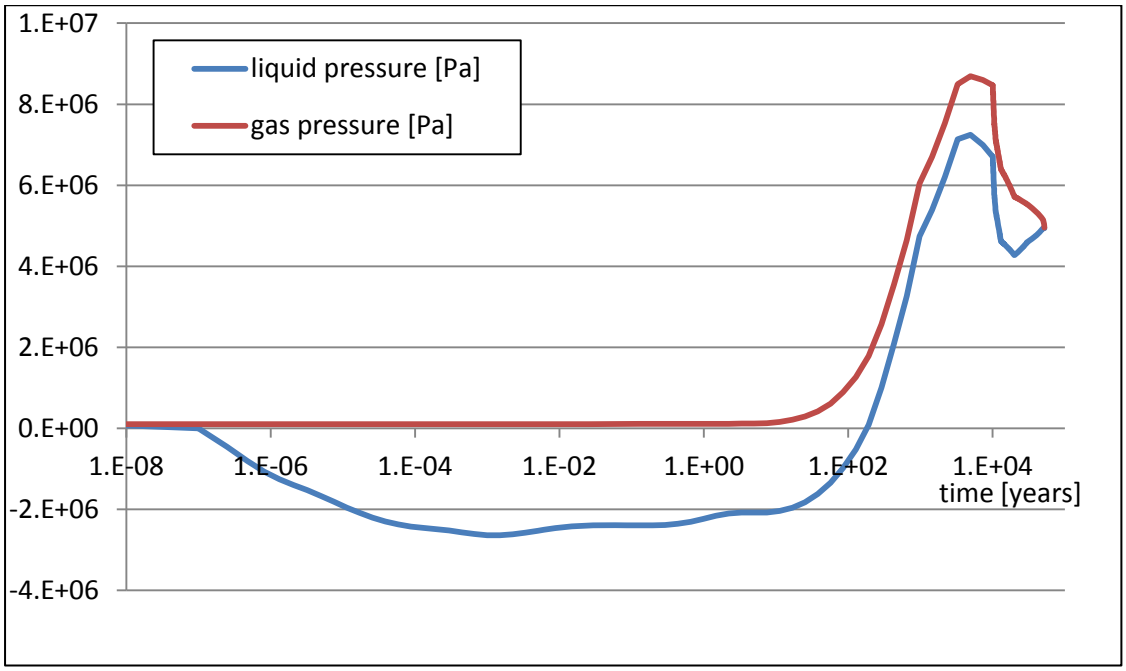

Figure 65 : Drift BCs from the module scale simulations – results for the cell scale simulations in point P4.

Gas entry pressure

In order to accommodate new results from other FORGE WPs, we modify the base case to be able to take into account the existence of gas entry pressures for the hostrock (6MPa) and for the EDZ (2MPa). This minimal capillary pressure P_e at which the desaturation can be initiated must be introduced with some precautions since the capillary pressure function and its derivative need to be continuous and not degenerate. We propose to follow the approach of (Ippich 2006), where the standard Van Genuchten relation is recast into:

$$P_c^e(S_l) = P_c^{VG}(S_c S_l) \quad where \quad P_e = P_c^{VG}(S_c)$$

This insures the continuity of the capillary function and allows us to use the same parameters as in the base case. However, one should keep in mind that the initial and boundary conditions need to be recalculated, since we need to transform the conditions given in terms of gas saturation into X_l^h and we need to calculate the gas pressure $P_g=P_c(S_l)+P_l$.

The results of this sensitivity test are very similar to the base case – the entry pressure of 6MPa is too close to the maximal gas pressure (5.5MPa) resulting from the impact of the drift boundary conditions and the entry pressure into EDZ is low with respect to it. In order to see the true influence of the entry pressure higher values should be tested. The experimental evidence gathered within FORGE points as well towards high entry pressure values for argillites (in the range from 6MPa to 10 MPa, some mesures going as high as 34MPa).

Generalized Henry law

We also wanted to see how the exponential correction to the Henry and Raoult-Kelvin law influences the behaviour of the system. First of all, the initial conditions needed to be adapted to this new relation. It has turned out that due too high capillary pressure in the bentonite (21MPa) the initial value of X_l^h raised to 1.7E-5 while in surrounding materials X_l^h remained close to 1.3E-5. This discontinuity was too steep to be solved with an acceptable time step and only a short period of time (of about 1 year) was simulated during a run lasting about 3 weeks.

3.6.5 Discussion and Conclusions

The first goal of this work was to develop a novel simulation tool for two phase flow in tight porous media that can constitute an alternative to the few existing commercial software. We wanted to obtain a highly flexible tool with a high degree of modularity and controllability, where it would be possible to add new mathematical and physical models. This work has turned out to be much more complicated than what we have expected. Several mathematical formulations (global pressure, pressure-saturation) and discretisation schemes (finite volumes, EFMH) were tested (also by some other teams within FORGE WP1.2) without success on the cell scale benchmark.
Finally, the formulation in liquid pressure and liquid molar fraction discretised by standard Galerkin finite element method and conjugated with a stabilised direct solver for the linear problems (Mumps) has proved to be an adequate choice.
With this tool we were able to solve the cell scale test with about 4500 DoF in a 2D plane. The results obtained are consistent with those from other teams, however not identical. Each team uses somehow different models with modifications of the initial benchmark specifications and there is an important spread of the final results (higher in mass fluxes, lower in maximal gas pressures) even for groups working with the same simulation code.
The code was able to solve the problem on meshes containing three layers of elements inside the interfaces with meaningful values at all positions – even at the connection between the drift and the interface of the plug, which seemed to be problematic for some other teams.
Further conclusions regarding the migration of the gas drawn from the FORGE cell scale benchmark are presented in the following chapter.

3.6.6 Lessons Learnt

On the basis of the work of all teams participating in the benchmark we may conclude about this modelling work on different levels.
First of all, we have noticed that the phenomenological description of the repository cell components exclusively by a generalised Darcy model provokes several conceptual difficulties. One of them is the representation of the interfaces (technological voids), which are the most conductive zones of the system and play an important role in gas transport towards the drift. However it is not clear if it is appropriate to cast them into an equivalent porous medium and what characteristic functions should be associated with them. The definition proposed for the benchmark used a high permeability hypothesis conjugated with a Van Genuchten law for capillary pressure with n=4, which produces a very flat capillary pressure curve at intermediate saturation values, but which becomes very steep (as well as the gas relative permeability) in the vicinity of the full water saturation (S_l=1). Both aspects generate numerical problems (capillary pressure inversion becomes very unstable and the gas permeability goes to zero very fast when approaching full saturation) and what's more the second one is highly unphysical. Second phenomenological question comes from the bentonite which is simply represented by a medium with the capillary pressure law with P_E of one order of magnitude higher than for argillites (hostrock and EDZ). The initial state of bentonite is defined as partially saturated with very high suction (21MPa), which is clearly unphysical from the point of view of the mechanical stability of the solid matrix. The state of the bentonite plug is not correlated with the conductivity of the plug interface and the EDZ, which of course would have an important impact on the results as it has been seen in the sensitivity analysis done initially by some teams.
Due to the existence of the high permeability pathway between the gas source and the sink (drift border) the overall results are totally driven by the imposed boundary conditions masking the possible influence of other design parts.

It should also be noted that a geometry with a high permeability path for gas naturally prevents it from entering into the hostrock; however the transition though the hostrock may be enhanced by applying higher gas pressure as boundary condition in the drift, allowing for stronger gas accumulation within the cell. It has been observed that with the maximal water pressure of about 7.8MPa there was a desaturation of 1% at 4.5m distance from the cell. Taking into account that the experimentally measured entry pressures for argillites are much too high (up to 34MPa) to be considered as physically plausible within Darcy flow model, it has to be concluded that the desaturation of argillites on long distances may not be excluded and thus a more careful modelling of the argillites, including dilatancy flow, should be undertaken in order to be able to predict the actual desaturation degree of the hostrock in the vicinity of the repository.

On the numerical resolution level we have learnt that this relatively simple model becomes difficult to solve without some fine numerical tuning. It consists in most cases in smoothing the relative permeabilities when approaching the full saturation, regularising the capillary pressure curve in order to recover a finite derivative, introducing residual water saturation to prevent creating a capillary barrier in the system. In our particular case, we have shown the crucial importance of the solver for linear systems.

Finally we will repeat here that noticeable variations in results were observed between teams working with the same simulation code (ToughII) but on different meshes and using somehow different strategies to work around numerical problems mentioned before.

3.6.7 Issues for further consideration

On the basis of our work as well as that provided by other participants we consider that in order to construct a simulation case that can be used for performance assessment of a real repository several evolutions are necessary.
The model cannot be considered as realistic without including phenomena that where put aside for this simulation like the influence of the temperature or the coupling of the water supply and the rate of hydrogen generation (some data are available, models exist). We have noticed also that the introduction of the second gas component (representing the air) would help to properly define the initial conditions, especially within the partially desaturated zones where an important capillary pressure may exist (bentonite) and where the liquid phase has to be equilibrated with the dissolved gas (hydrogen) at initial conditions, which limits the dissolution of hydrogen at early times.
The second gas component would also help to implement the initial conditions simultaneously with taking into account the KK equation of thermodynamical equilibrium, which requires very small time step in the 2 component system.
FORGE project has generated an important amount of experimental data about the behaviour of indurated argillites, EDZ and bentonite. The integration of this work into the simulation model should be the next step. To get a full representation of the observed phenomena, such integration will require taking into account the existence of the high entry pressure for all clayey materials and, in a longer time perspective, proposing and validating of dilatancy flow models that can correctly represent the physical phenomena and to be efficient enough to be used on at least metric scale and up to the module and repository scale.

3.6.8 References

Atkins P.W., Physical Chemistry, W.H. Freeman & Company, 6th edition, 1997
Bourgeat A., Jurak M., Smaï F., Two-phase, partially miscible flow and transport modelling in porous media; application to gas migration in a nuclear waste repository, Computational Geosciences, 13, 29-42, 2009
Couplex-gaz, momas.univ-lyon1.fr/cas_test/Cas_test_couplex_gaz_1.pdf
Emmerich W., Thermodynamics of Nonelectrolyte Solubility, in Developments and Applications in Solubility, ed. Trevor M. Letcher, Royal Society of Chemistry, 2007
Gray C.G., Gubbins K.E., Joslin C.G., Theory of Molecular Fluids: Volume 2: Applications, Oxford University Press, 2011
Helmig R, Multiphase Flow and Transport Processes in the Subsurface, Springer-Verlag, 1997
Horseman, S.T., Higgo, J.J.W., Alexander, J., Harrington, J.F., Water, gas and solute movement through argillaceous media, NEA Report CC-96/1, Paris, OECD, 1996

O. Ippisch, H.-J. Vogel, P. Bastian, 2006, Validity limits for the van Genuchten–Mualem model and implications for parameter estimation and numerical simulation, Advances in Water Resources, Volume 29, Issue 12, December 2006, Pages 1780-1789

Kiran E., Levelt Sengers J.M.H., eds., Supercritical Fluids: Fundamentals for Application, Kluwer Academics, 1994

Krichevsky I. R., Kasarnovsky J. S., Thermodynamical Calculations of Solubilities of Nitrogen and Hydrogen in Water at High Pressures, J. Am. Chem. Soc. 57, 2168-2171, 1935

Lassin, A., Dymitrowska, M., and Azaroual, M., Hydrogen solubility in pore water of partially saturated argillites: Application to Callovo-Oxfordian clayrock in the context of a nuclear waste geological disposal, Physics and Chemistry of the Earth, Parts A/B/C 36, 1721-1728, 2011

MoMaS Research group, Mathematical Modelling and Numerical Simulation for Nuclear Waste Management Problems, http://www.gdrmomas.org/pres-en.html

MoMaS test cases: http://sources.univ-lyon1.fr/cas_test.html

Oladyshkin S., Panfilov M., Hydrogen penetration in water though porous medium: application to a radioactive waste storage site, SRC SimTech, Preprint Series, Issue No. 2011-1, 2011

Smaï F., Développement des outils mathématiques et numériques pour l'évaluation du concept de stockage géologique, Ph.D. thesis of University of Claude Bernard of Lyon, 2009

Wu Y.S., Forsyth P.A., On the selection of primary variables in numerical formulation for modelling multiphase flow in porous media, J. Contam. Hydrol., 48(3-4):277-304. 2001

3.7 LEI contribution

3.7.1 Introduction

In this chapter the work done by Lithuanian Energy Institute (LEI) in the first benchmark exercise within the work package WP1.2 of FP7 project FORGE is presented.

This document is describing the modelling tool, model setup and deviation from the benchmark specification [1]. Also the modelling results of reference, prescribed in technical specification and additional sensitivity cases are presented and analyzed.

3.7.2 Model Implementation

The gas transport modelling was started with original version of TOUGH2 [2] code using PETRASIM [3] as the graphical interface. Changes in TOUGH2 source code were not possible due to application of PETRASIM. This limitation determines some deviations from benchmark specification (in gas permeability function and diffusion model). Long computation time and convergence problems in numerical schemes were observed after some test of reference case. The first reason was related to the high contrast of characteristics in different materials (intrinsic permeability, retention and relative permeability functions). The second reason appears when a transition from water saturated flow into two phase flow occurs (the gas saturation appears to get a residual value and the time step critically decrease). In order to avoid this kind of problems it was decided to use massively parallel (MP) version of TOUGH2 code (4) which is also part of PETRASIM software.

3.7.2.1 Code and Formulation

The first benchmark exercise was performed with original and massively parallel version of TOUGH2 code using PETRASIM as the pre- and post-processor. TOUGH2 is a numerical simulator for nonisothermal flow of multicomponent, multiphase fluids in one, two and three-dimensional porous and fractured media. The primary applications for which TOUGH2 is designed are in geothermal reservoir engineering, nuclear waste disposal, environmental assessment and remediation, and unsaturated and saturated zone hydrology. TOUGH2-MP is designed to perform parallel simulation on multi-CPU computational platforms.

The EOS5 fluid property module was selected for the description of the thermodynamics of hydrogen gas in this benchmark. Main features of EOS5 module are:

- Three dimensional transports of water, hydrogen and heat in an anisotropic porous medium;
- Mass conservation equations for each mass component including advection (Darcy law), diffusion (Fick law) in both phases and considering gas solubility (Henry law);
- Darcy equations for liquid and gas phase including relative permeability's and capillary pressure depending upon liquid saturation;
- Water properties using complete water steam table;
- Space discretization employing volume elements;
- Liquid phase: water and dissolved hydrogen;
- Gas phase: water vapour and hydrogen;
- Primary variables:
    - Single phase conditions: gas/water pressure, gas/water saturation, temperature.
    - Two phase conditions: gas pressure, gas saturation, temperature.

Heat transport was not considered in this exercise (isothermal 20 °C conditions were accepted). This means that no energy balance equations were solved and all processes are assumed to be isothermal. The mass balance equations solved by TOUGH2 can be written:

$$\frac{\partial M^{\kappa}}{\partial t} = -div(F_{adv}^{\kappa} + F_{dif}^{\kappa}) + q_k$$

where κ is component index (=1 for water, =2 for hydrogen), M^{κ} are local mass densities, F_{adv}^{κ} and F_{dif}^{κ} are advective and diffusive flow densities, respectively, and q_k is source term for each component. Further description and more details about TOUGH2/TOUGH2-MP are available in [2, 4].

3.7.2.2 Benchmark Implementation

The simulations were performed using a physical model (multiphase Darcy's law, with interaction between each phase: dissolution/evaporation and diffusion) as it prescribed in "ANNEX 1: Mathematical model proposed for the exercise" [1]. The objective of first exercise was to simulate the gas production and migration to a disposal cell and a portion of a drift.

3.7.2.3 Grid

As most of the materials in this benchmark are of very low permeability, the capillary process will be dominant over the gravity. Therefore two-dimensional symmetric disposal cell model in cylindrical r-z system was analyzed. As the scale is quite small (few tens of meters) it is possible to represent fine geometric features and especially the interfaces between waste canisters (or bentonite plug) and disturbed host rock. Both interfaces considered as centimetre-thick regions and are represented with one layer of grid elements.

Currently PETRASIM offers only rectangular grid elements for mesh building. TOUGH2 uses "Integrated finite volume" approach and in order to satisfy convergence criteria, the grid must be a "voronoi grid". Essentially, this means that the cell volumes must be defined by planes normal to the lines drawn between the centres of the adjacent cells. The simplest grid that satisfies this criterion is a rectangular grid. Therefore, the zones defined as "Access drift" and "Drift EDZ" in benchmark specification are not in precise circular domain. These zones were represented by rectangular elements with equivalent cross-sectional areas to the benchmark circular definition:

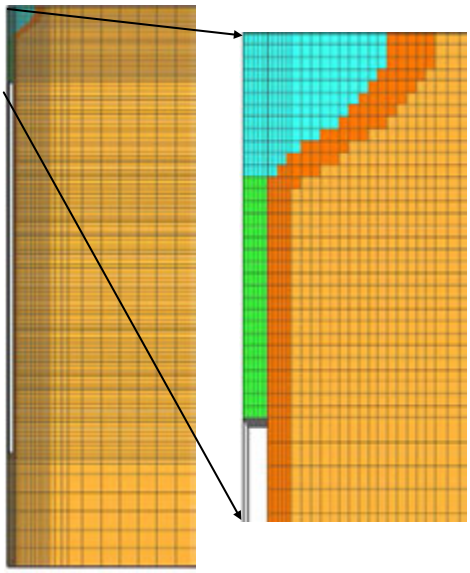

Figure 66 Mesh of LEI model coloured by material type

The whole domain was meshed with 4.836 rectangular elements and is refined in engineered materials due to higher gradients of the physical variables and a finer result resolution required.

Before initiating the benchmark modelling, sensitivity analyses to the grid size have been performed in order to evaluate how different refinement of the grid influences the results at points of interest. Primarily the grid was refined in the interfaces – runs with three and two layers in interfaces facing plug and canister were tested, but these runs ended with convergence problems due critical time step decreasing. Converged results were achieved only in cases where the interfaces are represented only by one layer of grid elements. Then five grids have been tested with different refinement in cell EDZ and drift EDZ:

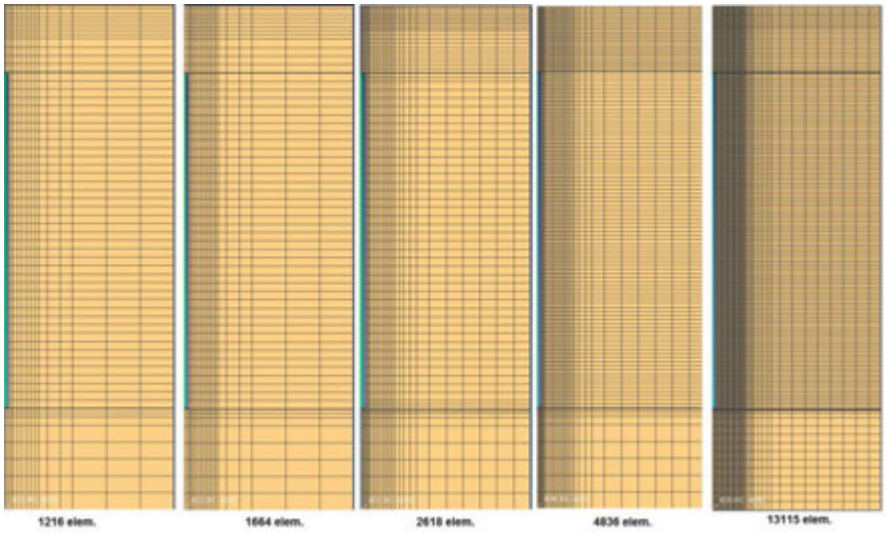

Figure 67 Different grids tested in LEI model

All these cases requite different calculation time – between 0.5 hours and 16 hours. The pressure and saturation evolution with time at 12 points defined in the benchmark specification showed that meshes with 1216, 1664 and 2618 elements are too coarse for numerical simulations in this exercise. The results using 4836 and 13115 grid elements are quite similar. Thus grid with 4836 grid elements was selected for the benchmark exercise.

3.7.2.4 Boundary Conditions and Sources

Boundary conditions when primary variables do not change with time are called Dirichlet boundary conditions. Other type of boundary conditions is called Neumann and prescribes mass or heat fluxes through boundary surfaces. Boundary conditions in LEI model were implemented as described in benchmark specification:

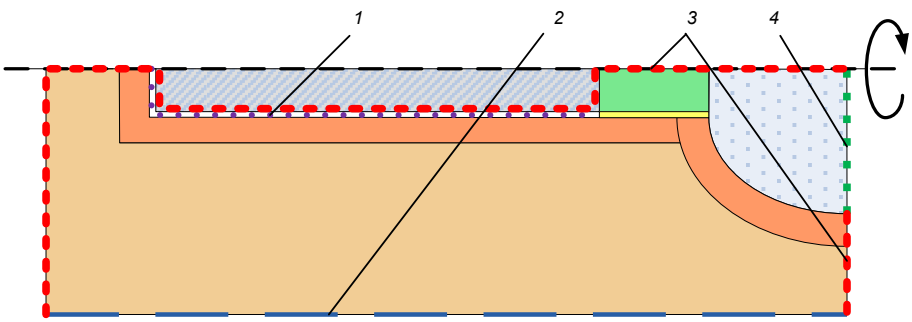

Figure 68 Schematic representation of boundary conditions: 1 – hydrogen gas injection area; 2 – constant water pressure; 3 – no flow boundary conditions; 4 – time varying boundary conditions

Time varying boundary conditions (water pressure and water saturation) at drift boundary are not available in TOUGH2. Using PETRASIM, however, it is possible to implement time varying boundary conditions of gas saturation and gas pressure. The boundary condition cell ("extra" cell) is connected with drift boundary and should be thought of as cell which is not part of the solution. The state variables (gas saturation/pressure)

are not specified explicitly, but initial conditions are defined and then gas/water fluxes into and out of "extra" cell is specified and it results in the desired boundary conditions. The volume of "extra" cell was set very large, so that the thermodynamic conditions do not change due to fluid exchange with the finite-size blocks in the flow domain. Time varying boundary conditions based on benchmark specification and the boundary conditions applied for LEI model are presented in Figure 69:

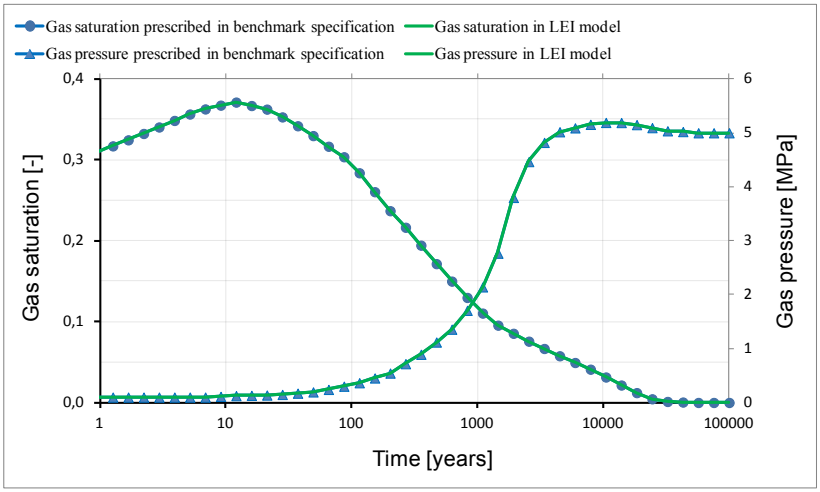

Figure 69 *Comparison of time varying boundary conditions in benchmark specification and LEI model*

The radioactive waste canisters are constituted of a material impermeable to both liquid and gas flow and were not explicitly represented in the model. A gas-source term (100 mol/year/disposal cell) was represented by a simple step function lasting 10.000 years. It was imposed on the external surface of the cylinder that represents disposal canisters. In the numerical model it was assumed that hydrogen is injected into the interface between the canisters and EDZ.

3.7.2.5 Initial Conditions

The assignment of initial conditions for modelling domain is related to the primary variables in TOUGH2. For single phase flow these primary variables are water pressure, water saturation and temperature. For two phase flow – gas pressure, gas saturation and temperature. According to the particularity of TOUGH2 water pressure is reported in the output only in fully water-saturated materials. Gas and capillary pressures are reported in the output in partially-saturated materials.

According to the benchmark specification, gas saturation is 30 % in the bentonite plug and access drift and 95 % in both interfaces. Disturbed and undisturbed rocks are fully water saturated and initial groundwater pressure there was set to be 5 MPa (according to a continuous formulation, the gas and water pressures are the same if only dissolved gas appears). In parts of the model that initially were not fully water saturated, gas pressure is set to be 0.1 MPa. Then water pressure is in capillary equilibrium with the gas pressure and is deduced from the gas pressure and the saturation by applying van Genuchten model associated with each material (see Table 3).

Table 3 : Initial conditions set in LEI model

Material	Gas saturation [%]	Gas pressure [MPa]	Water pressure [MPa]	Capillary pressure [MPa]
Interface facing plug	95	0.1	0.073	0.027
Interface facing canister	95	0.1	0.073	0.027
Backfill	30	0.1	-2.99	3.09
Bentonite plug	30	0.1	-21.3	21.4
EDZ	0	0	5	0
Geological medium	0	0	5	0

3.7.2.6 Deviations from the specification

Anisotropy

In technical specification horizontal and vertical permeability K_h, K_v was given. It is not consistent with supposed radial symmetry of the task. An isotropic permeability K for all materials was used in LEI model:

$$K = \sqrt[3]{K_h K_h K_v}$$

Solubility of hydrogen in water

In the benchmark specification Henry constant is defined to be $7.6 \cdot 10^{-6}$ mol·Pa^{-1}·m^{-3}. In LEI model original value of TOUGH2 Henry constant at 20 °C temperature ($8 \cdot 10^{-6}$ mol·Pa^{-1}·m^{-3}) was used.

Relative permeability of gas phase

Based on the benchmark specification, relative permeability functions for water and gas are expressed by integrating the Mualem prediction model in Van Genuchten capillarity model. The expression for water relative permeability is identical in benchmark specification and original version of TOUGH2. But expressions of gas phase relative permeability are different:

- In benchmark specification $$k_{rg} = \sqrt{1 - S_{we}} \cdot \left[1 - S_{we}^{\frac{1}{m}} \right]^{2m}$$
- In original TOUGH2 (if residual gas saturation S_{gr}=0) $$k_{rg} = 1 - k_{rl}$$
- In original TOUGH2 (if residual gas saturation S_{gr}>0) $$k_{rg} = (1 - S_{we})^2 \cdot (1 - S_{we}^2)$$

Van Genuchten parameters in benchmark specification indicate two groups of materials in point of relative permeability view. First group is for both interfaces and second group is for all remaining materials. Figure 70 shows evolution of gas phase relative permeability functions at logarithmic scale using three above mentioned expressions:

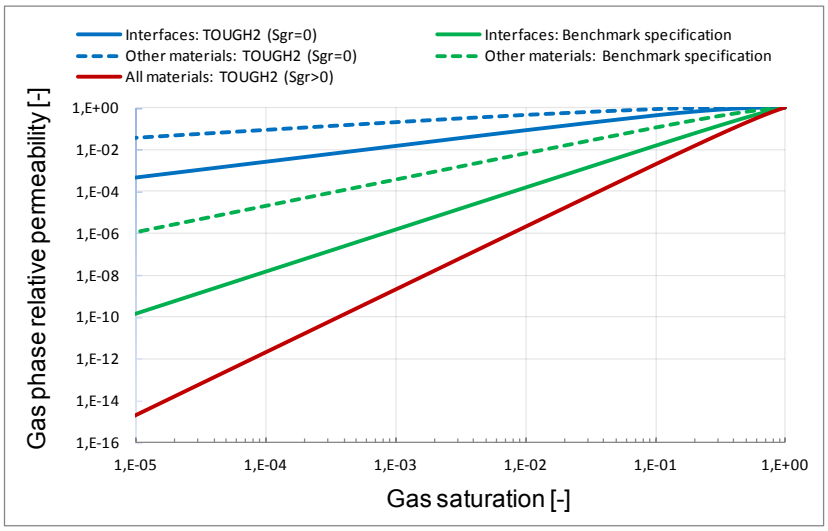

Figure 70 *Relative permeability functions of gas phase for different materials using different expressions*

As it could be seen in Figure 70, different expressions give several orders of magnitude discrepancy of gas phase relative permeability at low saturation. LEI experiences using TOUGH2 showed that assigning of very low residual gas saturations to different materials help to avoid convergence problems in numerical models

and accelerate the computations. Hence non-zero (10^{-6}) residual gas saturation (instead of zero as in benchmark specification) for all materials was assigned and the third expression for relative permeability function was used. Additional non-zero (10^{-5}) residual water saturation (instead of zero as in specification) for both interfaces was assigned too.

Diffusion model

Diffusive flow density of component κ in phase β (β=1 liquid phase, β=2 gas phase) in TOUGH2 is given by

$$F_\beta^\kappa = -\phi\tau_0 \sum_\beta \tau_\beta(S_\beta)\rho_\beta d_\beta^\kappa \nabla X_\beta^\kappa$$

where ϕ denotes porosity, ρ_β the density of phase β, X_β^κ the mass fraction, d_β^κ the molecular diffusion coefficient of component κ in phase β, and $\tau_0\tau_\beta(S_\beta)$ tortuosity. Using effective diffusion coefficients this equation can be rewritten as:

$$F_\beta^\kappa = -\sum_\beta D_{eff,\beta}^\kappa \rho_\beta \nabla X_\beta^\kappa$$

with effective diffusion coefficient:

$$D_{eff,\beta}^\kappa = \tau_0\tau_\beta(S_\beta)\phi d_\beta^\kappa$$

Tortuosity has porous medium dependent factor τ_0 and saturation dependent factor $\tau_\beta(S_\beta)$, where S_β fluid saturation is in phase β. Original version of TOUGH2 offers three tortuosity models:

- Relative permeability (RP): $\tau_0\tau_\beta = \tau_0 k_{r,\beta}(S_\beta)$
- Millington – Quirk (MQ): $\tau_0\tau_\beta = \phi^{\frac{1}{3}} S_\beta^{\frac{10}{3}}$
- Constant diffusivity (CD): $\tau_0\tau_\beta = S_\beta$

In benchmark specification tortuosity model is specified as:

$$\tau_0\tau_\beta = \frac{S_\beta}{\tau_0^2}$$

Simple comparison showed (Figure 71) that dependence of effective diffusion coefficient on liquid saturation is different using different tortuosity models. In comparison to benchmark model, Millington-Quirk model gives higher values of effective diffusion coefficient (especially in high saturations zones) in all materials except interfaces, while using relative permeability model the situation is opposite.

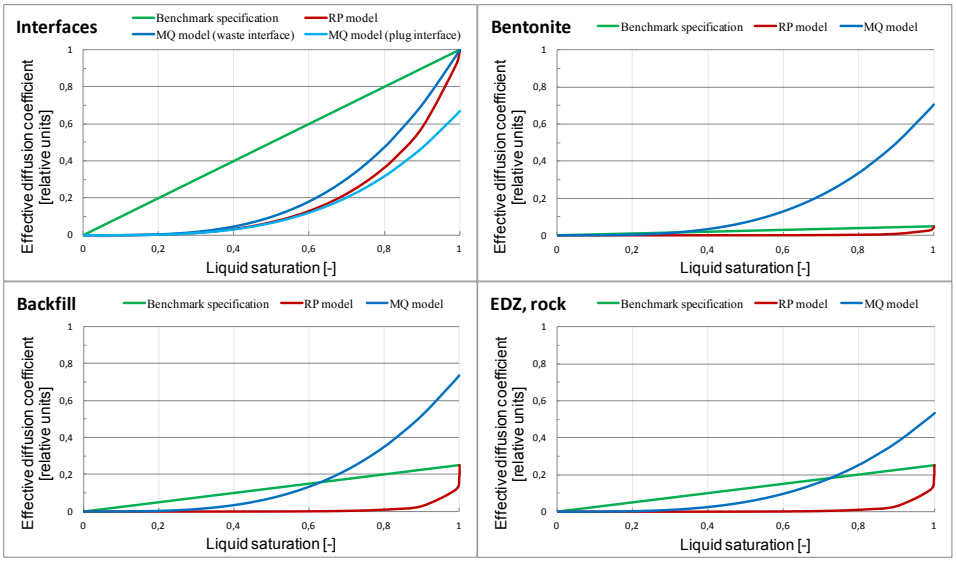

Figure 71 *Dependence of effective diffusion coefficient on liquid saturation for selected materials in benchmark model using different tortuosity expressions*

In order to test the influence of selected tortuosity model on the results, modelling of benchmark exercise was performed using RP and MQ models. Observed peak pressures in the system were 5.7 and 5.6 MPa, respectively. The evolution with time of liquid/gas saturation and pressure at point of interest were very similar in both cases, but concentrations of dissolved hydrogen (and pseudo-gas pressure as well) were slightly higher using MQ model. The main differences were determined in fluid fluxes through surfaces.

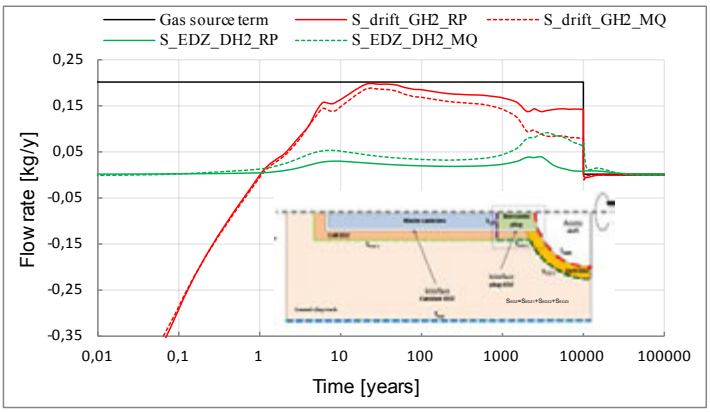

Figure 72 *Comparison of gaseous hydrogen (GH2) flux through S_{drift} and dissolved hydrogen (DH2) flux through S_{EDZ} using RP and MQ tortuosity models*

As it could be seen in Figure 72, gaseous flux is higher using RP model. Total amount of gaseous hydrogen transported to access drift is 1.462 kg using RP model, while using MQ model this mass is much lower (951 kg). In case of dissolved hydrogen flux the situation is opposite – total mass transported out of EDZ is 304 kg and 1.017 kg, respectively. Also it was observed that numerical analysis using RP model has been more stable and run faster (~ 2 times) in comparison to MQ model. Taking into account numerical aspects, LEI team decided to use conservative diffusion approach (lower diffusion, RP model) for first benchmark exercise.

3.7.3 Base Case Results

In order to compare the results with other teams, they were provided in comparable form.

Table 4 presents the description of analysed variables and technique how these variables were assessed by LEI team.

Table 4 : Description of variables used in analyses of the results

Variable	Description	How calculated
Gas pressure (P_{GAS})	In porous medium only, where free gas phase appears. If only dissolved H_2 appears → P_{GAS} =0	$P_{GAS} = P_{WATER} + P_{CAP}$ P_{GAS} is a sum of partial pressures of water vapour and gaseous H_2
Water pressure (P_{WATER})	In porous medium, where liquid phase appears	$P_{WATER} = P_{GAS} - P_{CAP}$ P_{WATER} is a sum of partial pressures of liquid water and dissolved H_2
Liquid water flux	Sum of advective and diffusive flows of liquid water	
Dissolved H_2 flux	Sum of advective and diffusive flows of dissolved hydrogen in water	
Gaseous H_2 flux	Sum of advective and diffusive flows of gaseous hydrogen	
Water vapour flux	Sum of advective and diffusive flows of water vapour	
Total gas flux	Sum of advective and diffusive flows of gaseous hydrogen and water vapour	
Total liquid flux	Sum of advective and diffusive flows of liquid water dissolved hydrogen	

In the original version of TOUGH2-MP, diffusive fluxes of each component (water, hydrogen) in both phases are not reported in the output file. Since these fluxes are necessary for the exercise analysis, MATLAB script was created to compute these fluxes through surfaces predefined in the benchmark specification.

The simulation time is limited up to 100.000 years after the repository closure. The results for comparison were depicted as the gas saturation and gas/liquid pressures profiles at 12 observation locations and drift boundary (Figure 73).

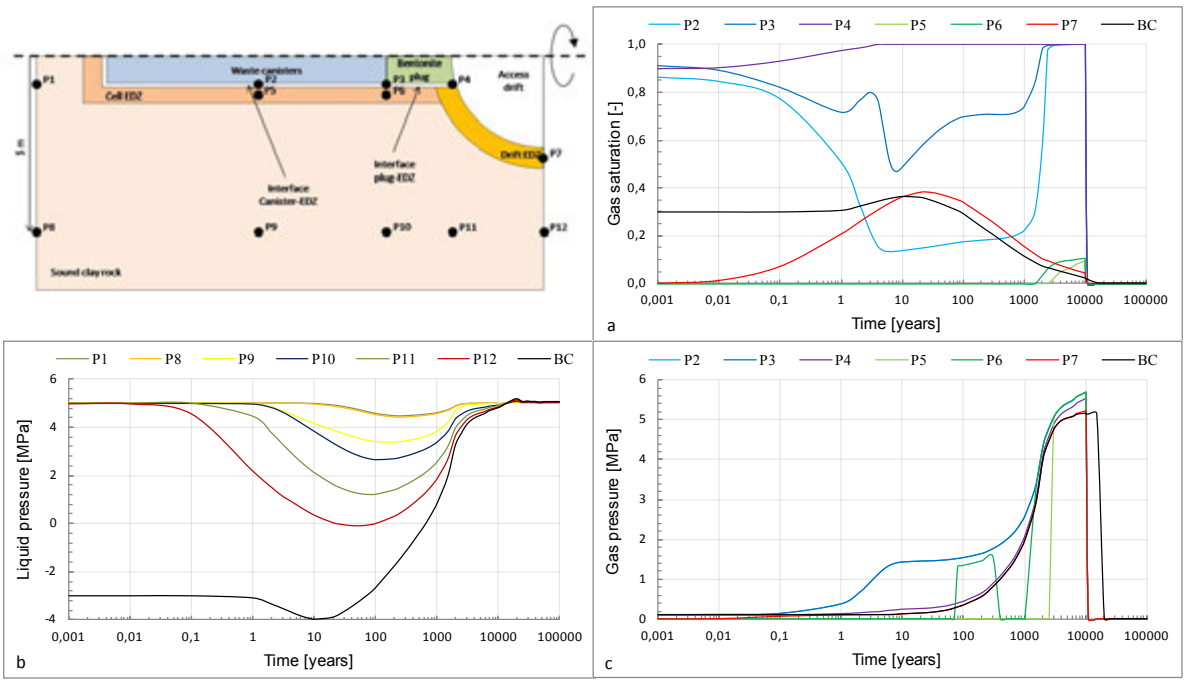

Figure 73 *Base case results: gas saturation (a), liquid pressure (b) and gas pressure (c) evolution with time*

Significant levels of gas saturation were reached in the interfaces (Figure 73a). The interfaces are almost fully desaturated, but the evolution of gas saturation with time depends on the position of particular observation point. The interface near waste canisters (point P2) is resaturated up to ~15-20 % from 5 up to 1.000 years due to the water inflow from the surrounding clay rock. Gas builds-up and completely pushes water away after 3.000 years. Similar evolution was observed at point between both interfaces (P3). The evolution in the interface near bentonite plug (P4) is somewhat different: within first 4 years the interface becomes fully gas saturated and keeps such till the end of gas generation. Full resaturation at all three

points (P2, P3, P4) is reached after 11.000 years past repository closure. Gas saturation in the EDZ never exceed 10 % and exist only for particular time periods: in the cell EDZ (P5) from 2.500 up to 11.000 years, in the bentonite plug EDZ (P6) from 70 up to 350 and from 1.400 up to 11.000 years and in the drift EDZ (P7) gas saturation history is very closely related to saturation history at drift boundary. No free gas was observed in the undisturbed clay rock.

As it could be seen in Figure 73b and Figure 73c peak pressure of 5.7 MPa was observed and is much lower than lithostatic pressure (~10 MPa) in modelling domain. Thus mechanical effects on repository and rock structures caused by the pressure build-up that may follow from gas generation are not presumable. These results show that Darcy, Fick and Henry laws are sufficient to describe gas behaviour in single disposal cell and continuous fluid flow approach realized in TOUGH2 code could be used.

The results of gaseous hydrogen fluxes (Figure 74) show that hydrogen is transported from the disposal cell toward access drift during the period of gas generation (up until 10.000 years). Positive flow rate indicate H_2 flow toward the drift. As it could be seen, great part of generated hydrogen (1.694 kg out of 2.000 kg) flows through surface S_{cell} toward the access drift and major part of this hydrogen (1.617 kg) flows over very thick interface (surface S_{int1}). As H_2 access to the plug interface, whose permeability is much lower (equal to permeability of the EDZ), part of this hydrogen (990 kg) flows through plug interface (surface S_{int2}) and remaining part (472 kg out of 1.462 kg) flows toward the drift over the EDZ. Overall, 73 % of generated hydrogen is transported from disposal cell toward the access drift in gaseous form while remaining part is dissolved in pore-water.

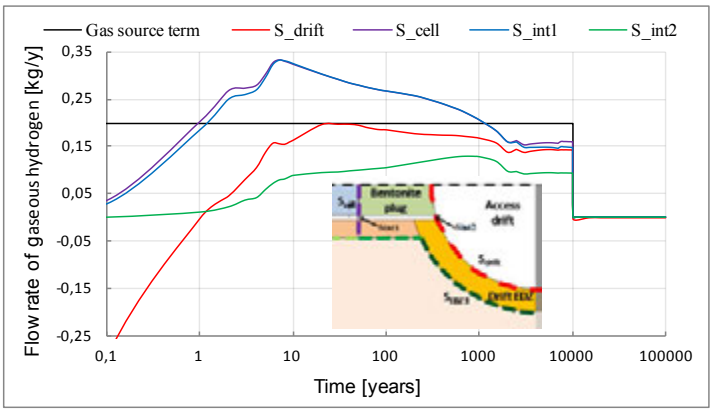

Figure 74 *Base case results: comparison of gaseous hydrogen flow rates through 4 different surfaces*

Advective flow is the primary transport mechanism of gaseous hydrogen during gas generation period (Figure 75). The diffusion process has a significant impact on gaseous hydrogen transport only during the first hundreds of years. Diffusive flow is the primary transport mechanism of dissolved hydrogen into the clay rock.

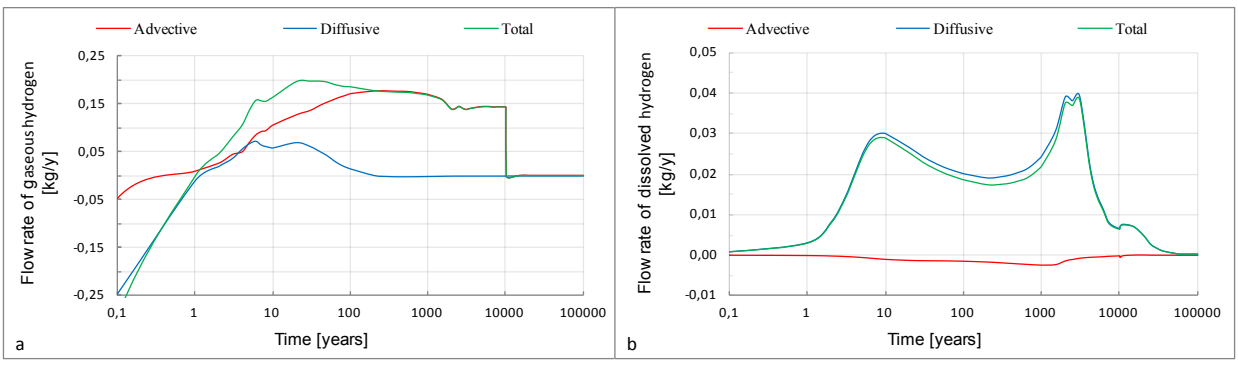

Figure 75 *Base case results: flow rates of gaseous hydrogen through S_{drift} (a) and dissolved hydrogen through S_{EDZ} (b)*

3.7.4 Sensitivity Analysis

Besides reference case, seven sensitivity analyses defined in the benchmark specification and nine additional analyses were performed by LEI team at cell scale. All analysed cases are grouped into six groups and described in Table 5:

Table 5 : Description of analyzed sensitivity cases

Analysis no.	Analysis ID	Description
1. Characteristics of disturbed and undisturbed rock		
1	S11*	**Self healing EDZ**. Intrinsic permeability of EDZ is supposed equal to undisturbed rock permeability
2	S12*	**Altered relative permeability curve**. Van Genuchten – Mualem relative permeability function has been changed to Fatt and Klikoff function (cubic law) for clay rock and the EDZ
2. Diffusion		
3	S21	**Alternative diffusion model**. Millington-Quirk expression instead of relative permeability model for tortuosity is used
4	S22*	**Increased diffusion**. Diffusion coefficient of dissolved hydrogen under water saturated conditions multiplied by 10 for all simulated porous media
5	S23	**Decreased diffusion**. Diffusion coefficient of dissolved hydrogen under water saturated conditions divided by 10 for all simulated porous media
6	S24	**Without diffusion**. Only advective mass transport is considered
3. Gas generation		
7	S31*	**Gas generation delay for 10 years**
8	S32	**Gas generation delay for 100 years**
9	S33	**Without gas generation**
4. Characteristics of interfaces		
10	S41*	**Less permeable interface1**. Decreasing the intrinsic permeability value of the waste interface from the base value of 10^{-12} m^2 to 10^{-15} m^2
11	S42*	**Less permeable interface2**. Decreasing the intrinsic permeability value of the waste interface from the base value of 10^{-12} m^2 to 10^{-18} m^2
12	S43*	**Without waste interface**. Waste interface have the same properties as the EDZ
13	S44	**Without both interfaces**. The characteristics of waste interface are the same as the EDZ and characteristics of plug interface are the same as bentonite plug
5. Boundary conditions		
14	S5	**Without time varying boundary conditions**. No flow boundary conditions applied for drift boundary
6. Numerical aspects		
15	S61	**Higher convergence tolerance**. Increasing value of relative convergence criterion (RE1) in TOUGH2 from the base value of 10^{-4} to 10^{-5}
16	S62	**Lower convergence tolerance**. Decreasing value of relative convergence criterion (RE1) in TOUGH2 from the base value of 10^{-4} to 10^{-3}

* cases defined in the benchmark specification

The summary results for analyzed cases are given in the following sections.

Characteristics of disturbed and undisturbed rock

Lower permeability of EDZ limits gas access there from gas source (waste interface) and from drift. As it could be seen in Figure 76a, free gas flux at point P6 is delayed and gas saturation here is lower. This results in the higher pressures in disturbed and undisturbed rock (Figure 76b) in comparison to reference case.

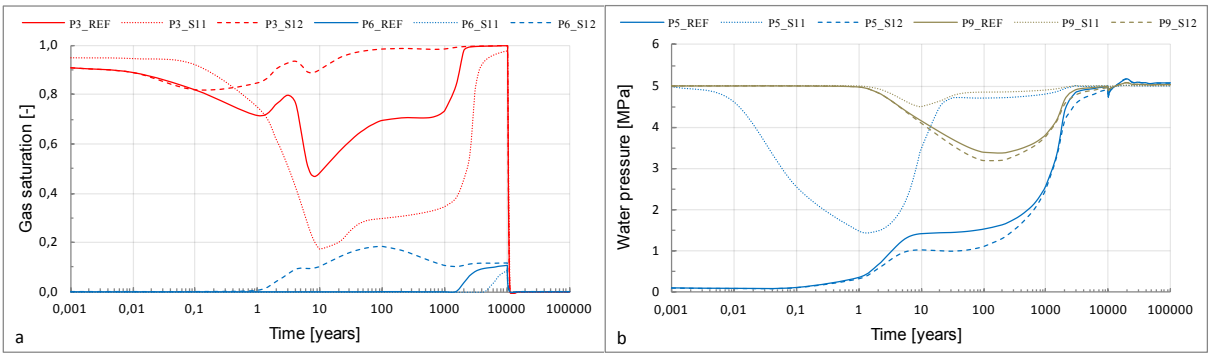

Figure 76 *Sensitivity 11-12 results: comparison of gas saturation (a) and water pressure (b) evolution with time at selected points*

Concerning specific fluxes (Figure 77 and Table 6), no free gas flow out of EDZ, but higher flux of dissolved H_2 toward undisturbed host rock is observed in comparison to reference case. In case of gaseous H_2 flux out of disposal cell, self healing EDZ reduces the importance of second transport pathway over EDZ, but the primary pathway through interfaces is more dominant in this case. However, despite different shape of the profile, only ~50 kg more of total gaseous H_2 mass is transported toward the drift due to lower permeability of EDZ.

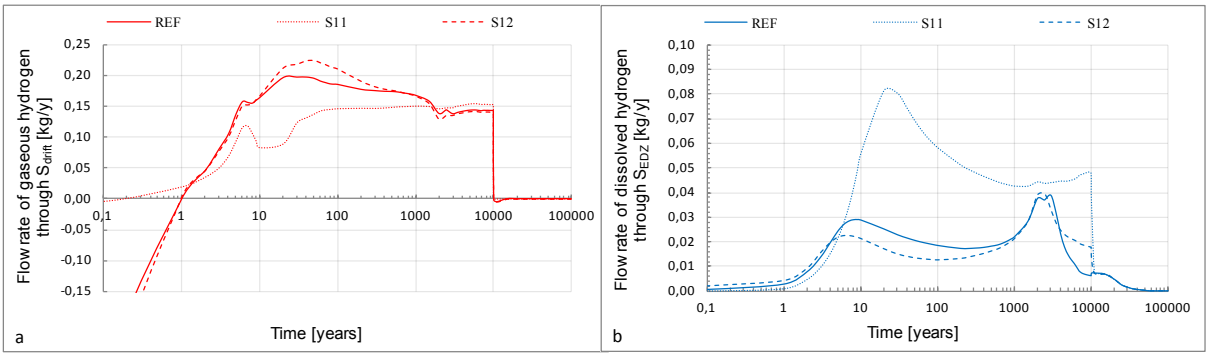

Figure 77 *Sensitivity 11-12 results: comparison of flow rate for gaseous hydrogen through S_{drift} (a) and dissolved hydrogen through S_{EDZ} (b)*

Different relative permeability curve for disturbed and undisturbed rock determines earlier and higher gas saturation in the EDZ (P6 in Figure 76a) and slightly lower water pressures in these media (Figure 76b) in comparison to reference case. Gas saturation level in interfaces (P3 in Figure 76a) is much higher during gas generation period in this case. Concerning fluxes, shapes of the profiles and total transported mass through different surfaces are very similar in comparison to reference case.

Table 6 : Sensitivity 11-12 results: comparison of total transported mass through different surfaces

Type of flux	Total transported mass, kg		
	REF	S11	S12
Gaseous H_2 through S_{drift}	1.464	1.514	1.450
Gaseous H_2 through S_{EDZ}	338	0	300
Dissolved H_2 through S_{EDZ}	304	590	365
Dissolved H_2 through S_{out}	659	595	678

Sensitivity analyses of disturbed and undisturbed rock characteristics showed that gas saturation in the EDZ could vary significantly and so influence on gas preferential pathways. However, the total amount of transported gaseous H_2 toward the drift or dissolved H_2 to the host rock is very similar.

Diffusion

Results of Millington – Quirk diffusion model (S21) were discussed in Section 3.7.2.6. The increased or decreased value of effective diffusion coefficient for dissolved hydrogen determines lower or higher amount of free gas in the system, respectively. As it could be seen in Figure 78a, the evolution of gas saturation at point P2 during gas generation period is very similar in all cases except the case of higher diffusivity. However, resaturation periods in cases of lower/without diffusion are very different in comparison to reference case. Gas saturation evolution with time in the EDZ (Figure 78b) is different in all analyzed cases. Higher saturation levels are obtained in cases of lower/without diffusion. No gaseous hydrogen observed in case of higher diffusivity.

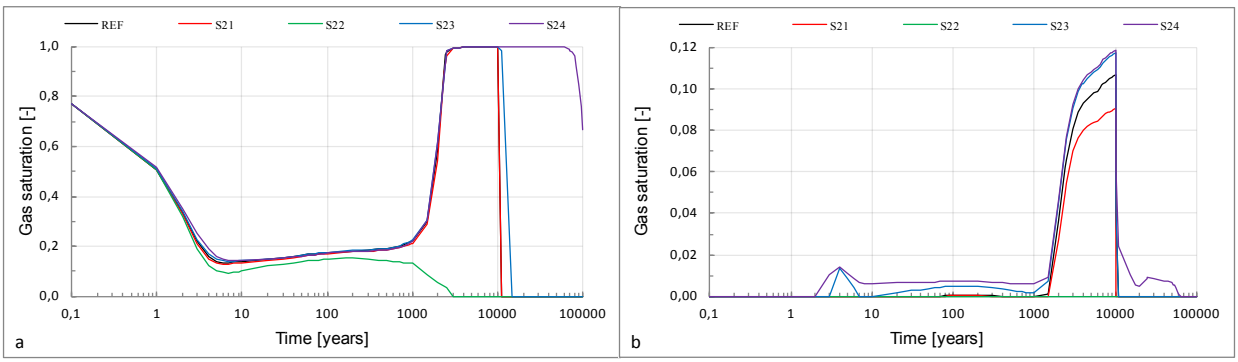

Figure 78 Sensitivity 21-24 results: comparison of gas saturation evolution with time in waste interface (a) and EDZ (b)

Diffusion process affects dissolved and gaseous hydrogen fluxes significant (Table 7). As diffusion process is neglected (S24), all generated gases are transported toward the drift by advective flow. In case of lower diffusivity (S23) higher amount of gaseous H_2 flows toward the drift and much lower amount of gaseous/dissolved H_2 flows out of EDZ in comparison to reference case. In case of higher diffusivity (S22) important changes in global behaviour of the system were obtained as the dissolution/diffusion is dominant process. Total amount of gaseous H_2 toward the drift is negative and free gas flows from access drift to the disposal cell and due to very strong diffusion are transported toward the radial boundary. Total amount of dissolved H_2 transported out of radial boundary is ~2 times higher than total mass of generated gas in the system. It indicates that in case of higher diffusivity additional ~2.000 kg of gas comes into the system via drift boundary due to implemented time varying boundary conditions in the model.

Table 7 : Sensitivity 21-24 results: comparison of total transported mass through different surfaces

Type of flux	Total transported mass, kg				
	REF	S21	S22	S23	S24
Gaseous H_2 through S_{drift}	1.464	951	-559	1.905	1.992
Gaseous H_2 through S_{EDZ}	338	304	141	71	6
Dissolved H_2 through S_{EDZ}	304	1017	3743	26	0
Dissolved H_2 through S_{out}	659	1365	3921	97	0

Gas generation

Gas generation delay by 10 and 100 years (S31 and S32) reduces hydrogen mass injected in the system only by 2 kg and 20 kg, respectively. It is a minor part in comparison to total gas mass (2.000 kg) injected in the system during first 10.000 years. Hence the impact to pressures and saturations at analysed points is minor and only for the first hundreds of years. Concerning total fluxes through surfaces (Table 9), the differences are very small in comparison to reference case.

Table 8 : Sensitivity 31-33 results: comparison of total transported mass through different surfaces

Type of flux	Total transported mass, kg			
	REF	S31	S32	S33
Gaseous H_2 through S_{drift}	1.464	1.461	1.430	-246
Gaseous H_2 through S_{EDZ}	338	328	321	57
Dissolved H_2 through S_{EDZ}	304	313	313	280
Dissolved H_2 through S_{out}	659	659	656	335

Sensitivity analysis without considering gas generation (S33) was performed in order to examine time varying boundary conditions influence on the results. Negative value of total gaseous H_2 mass transported through S_{drift} shows that free gas flow from access drift toward the disposal cell. Total mass of dissolved H_2 transported out of EDZ (280 kg) is very similar to this mass determined in reference case (304 kg). This could mean that the diffusive flux originates from the partial desaturation of the access drift rather than from the gas generation around the canister. These results clearly show that boundary conditions imposed at the drift can have strong impact on the results.

Characteristics of interfaces

Decreased intrinsic permeability value of waste interface (S41 and S42) influence on similar or shorter resaturation period at point P2 in the interface (Figure 79a) and earlier and higher gas saturation at point P5 in the EDZ (Figure 79b). Without considering waste interface and both interfaces (S43 and S44), evolution of gas saturation with time is different in comparison to reference case. However, evolution of gas saturation is similar and saturation peak is ~20 % in both cases.

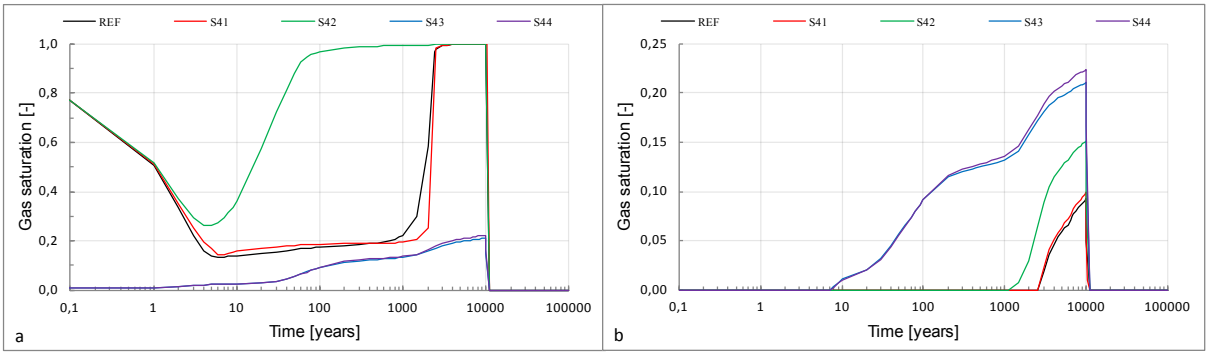

Figure 79 *Sensitivity 41-44 results: comparison of gas saturation evolution with time in waste interface (a) and EDZ (b)*

As it could be seen in Table 9, the results of S41 and reference case are very similar. It is consistent with fact, that the interface is still the most permeable component in the system. In other analysed cases slightly lower mass transport of gaseous H_2 toward the drift and higher gaseous H_2 transport out of EDZ were observed. Concerning dissolved hydrogen mass transport out of radial boundary, higher amount was observed in three cases (S42, S43 and S44) in comparison to reference case. Besides, the results of S43 and S44 are very similar, hence having no interface near bentonite plug does not change the behaviour of the system significantly.

Table 9 : Sensitivity 41-44 results: comparison of total transported mass through different surfaces

Type of flux	Total transported mass, kg				
	REF	S41	S42	S43	S44
Gaseous H_2 through S_{drift}	1.464	1.451	1.422	1.363	1.357
Gaseous H_2 through S_{EDZ}	338	347	468	616	628
Dissolved H_2 through S_{EDZ}	304	307	222	142	146
Dissolved H_2 through S_{out}	659	674	678	777	795

Boundary conditions

Sensitivity analysis without considering time varying boundary conditions was performed to find potential peak pressure in the fully sealed system due to the gas generation. Only way for gas to leave the system is flow toward the radial boundary in gaseous/dissolved form. The observed peak pressure in this case is 12.7 MPa. It is the highest pressure over all analysed cases. Such high pressure could cause mechanical effects on the repository and rock structures. As it could be seen in Table 10, all generated hydrogen is transported toward the undisturbed host rock in gaseous form, but leaves the system in dissolved form.

Table 10 : Sensitivity 5 results: comparison of total transported mass through different surfaces

Type of flux	Total transported mass, kg	
	REF	S5
Gaseous H_2 through S_{drift}	1.464	-5
Gaseous H_2 through S_{EDZ}	338	2.000
Dissolved H_2 through S_{EDZ}	304	26
Dissolved H_2 through S_{out}	659	2.039

Numerical aspects

Numerical analyses using different value for convergence tolerance (RE1) in TOUGH2 have tremendous impact on calculation time (Table 11):

Table 11 : Sensitivity 61-62 results: comparison of computation speed

Sensitivity case	Calculation time, hours	Numbers of time steps
REF (RE1=$1\cdot10^{-4}$)	8	27.928
REF (RE1=$1\cdot10^{-3}$)	4	12.965
REF (RE1=$1\cdot10^{-5}$)	93	639.716

Achieved results show any observable discrepancy of pressures and saturations evolution with time at the points of interest. However very minor differences were observed between total transported mass through different surfaces, but they are not essential. All other sensitivity analyses in the first benchmark exercise were done using convergence tolerance RE1=$1\cdot10^{-4}$.

Table 12 : Sensitivity 61-62 results: comparison of total transported mass through different surfaces

Type of flux	Total transported mass, kg		
	REF	S61	S62
Gaseous H_2 through S_{drift}	1.464	1.459	1.461
Gaseous H_2 through S_{EDZ}	338	336	331
Dissolved H_2 through S_{EDZ}	304	308	306
Dissolved H_2 through S_{out}	659	664	655

3.7.4.1 Comparison of the results

Comparing observed peak pressure over all analyzed cases (Figure 80), it could be seen, that pressure increases by 0.2-7.7 MPa from initial groundwater pressure. In all cases, except without considering time varying boundary conditions, peak pressure do not exceed allowed (lithostatic) pressure which is ~10 MPa in this repository concept. In most of cases, the peak pressure is achieved in waste interface by the end of gas generation (after 10.000 years). In two cases peak pressure (5.2 MPa) is very close to the initial pressure (5 MPa) and is observed on the outer boundary of access drift after 20.000 years. This is related with time varying boundary conditions implemented in the model. These results are coherent, because the most optimistic cases – of higher diffusivity and without considering gas injection were analyzed. The higher pressure in comparison with reference case (5.7 MPa) is observed in cases of self healing EDZ, without considering interface(s) and when permeability of waste interface is equal to the permeability of EDZ. Results of other cases are very similar to the reference case.

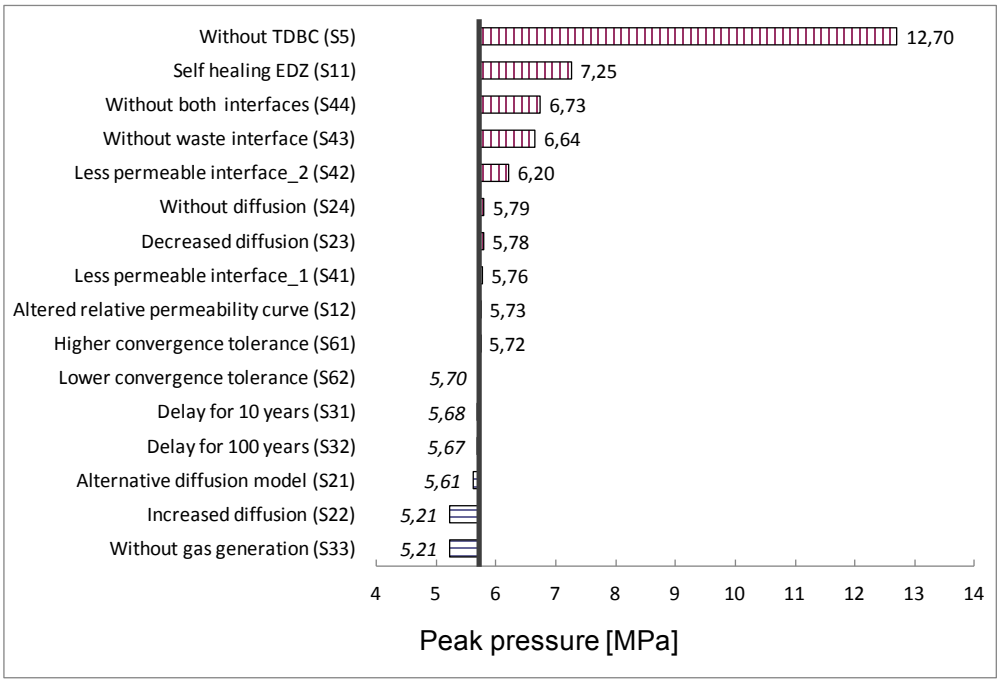

Figure 80 Comparison of peak pressure in the system for all analysed cases

Concerning gaseous hydrogen flux toward the drift (Figure 81), the higher amount of total transported mass were observed in three cases – without diffusion, with lower diffusivity and in case of self healing EDZ – in comparison to the reference case (1.464 kg). In three cases – without considering time varying boundary conditions, without gas generation and with higher diffusivity – negative total fluxes were observed. Important, that alternative diffusion model in TOUGH2 (Millington-Quirk) gives lower results.

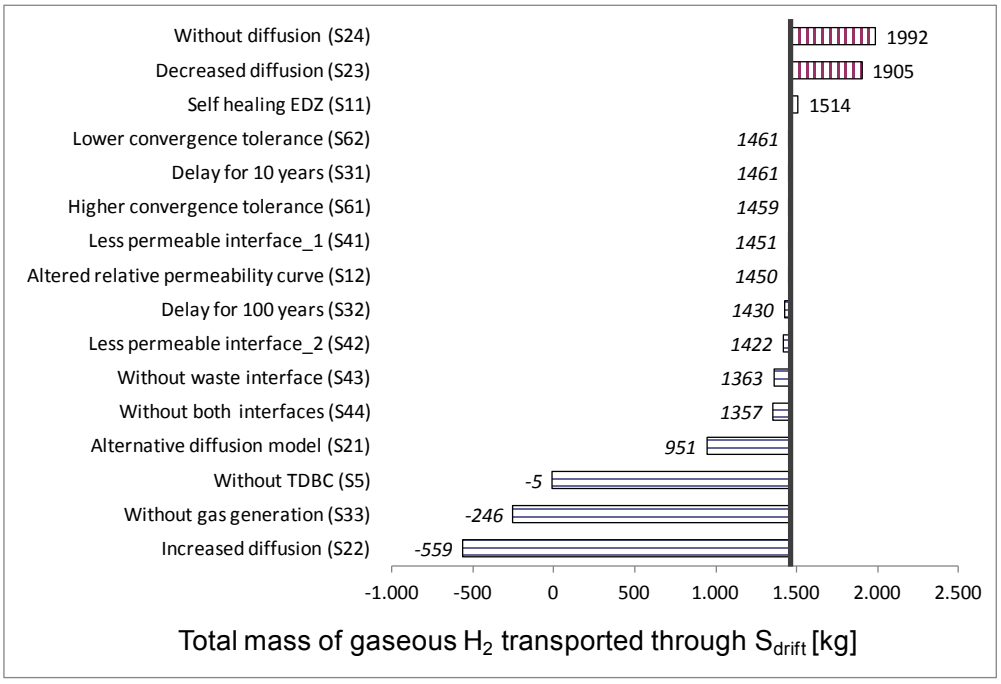

Figure 81 Comparison of gaseous H_2 flux through S_{drift} for all analysed cases

As it could be seen in Figure 82, the highest fluxes of dissolved H_2 out of radial boundary were determined in cases of higher diffusivity, without considering time varying boundary conditions, using Millington-Quirk

model for diffusion and without considering interface(s). The lower fluxes, in comparison to reference case (659 kg), were determined in cases without diffusion, with lower diffusivity, without gas generation and in case of self healing EDZ.

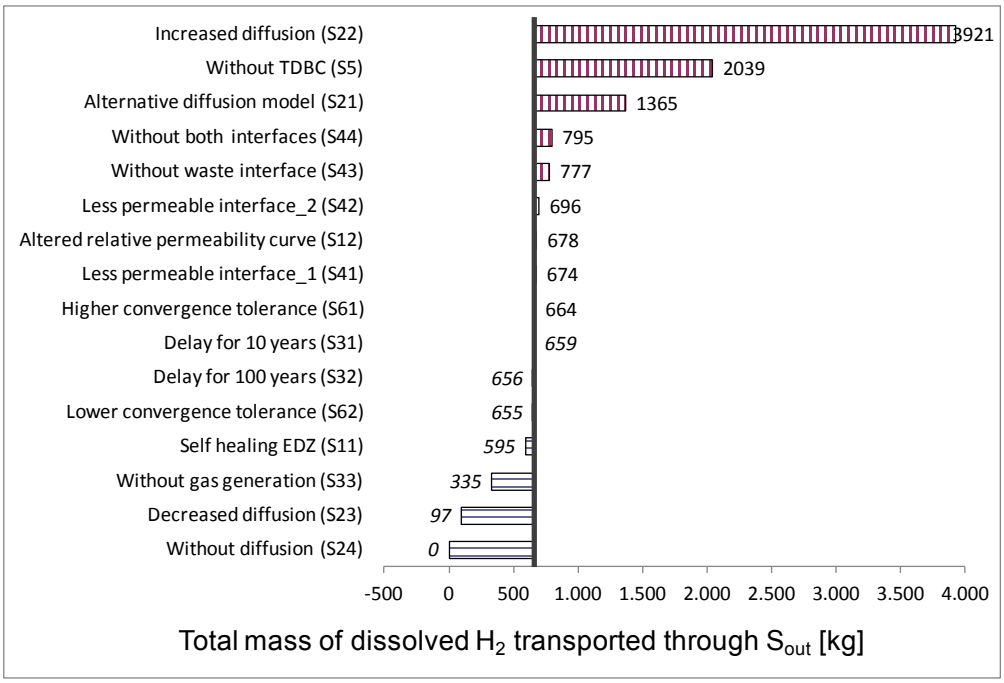

Figure 82 Comparison of dissolved H_2 flux through S_{out} for all analysed cases

3.7.5 Conclusions

The first benchmark exercise has been performed with original version of TOUGH2-MP code using PETRASIM as the graphical interface. Since modifying of TOUGH2 source code were not possible due to application of PETRASIM, some deviations from technical specification, related to the estimation of gas phase relative permeability and tortuosity model could not be avoided in LEI model.

The main results of the reference case could be summarised as follows:

- Peak pressure (5.7 MPa) was observed in waste interface by the end of gas generation (10.000 years);
- Significant levels of gas saturation is reached in the interfaces, access drift and engineered disturbed zone (EDZ). Minor amount of gas concentrates in some parts of undisturbed geological media;
- Most of generated gas (~73 %) is transported in gaseous phase by advective flow toward the drift while the rest part is dissolved and is transported by diffusion into the host rock. The interfaces and EDZ play an important role for gaseous hydrogen movement from the disposal cell toward the drift. The primary transport pathway is over the interface (~50 % of total generated gas transported) while the second transport pathway is over EDZ (~24 % of total generated gas transported);

The obtained results of sensitivity analysis allow concluding:

- The peak pressure increases by 0.2-2.25 MPa from initial groundwater pressure and these values do not exceed allowed (lithostatic) pressure (~10 MPa). The results suggest that the numerical tool based on two-phase flow approach is appropriate to model the gas transport in such geological repository system;

- Different diffusion models in TOUGH2 (relative permeability and Millington-Quirk) could affect the results significantly;
- The time varying boundary conditions imposed at the access drift boundary have strong impact on the results at cell scale.

3.7.6 References

1. FORGE WP 1.2: first step toward a benchmark for 3D modelling of a disposal area for vitrified waste
2. K. Prues, C. Oldenburg, G. Moridis. TOUGH2 Users's guide, Version 2.0. Lawrence Berkeley National Laboratory, LBNL-43134, 1999,198 p.
3. PetraSim user manual, Version 5.0, Thunderhead engineering, 2010.
4. K. Zhang, Y. Wu, K. Prues. 2008. User's Guide for TOUGH2-MP - A Massively Parallel Version of the TOUGH2 Code. LBNL-315E. 108 p.

3.8 ENSI/IFSN contribution

3.8.1 Introduction

Hydrogen gas is formed by anaerobic corrosion of metal components in a deep geological repository. FORGE aims to investigate the importance in relation to nuclear safety of the processes caused by gases in the near and far field of a deep geological repository. This includes the gas generation and the gas transport. The project lasts 4 years from 2009 to 2013 and is divided into five work packages. ENSI participates in the first work package WP1 (Treatment of gas in performance assessment). This work package is divided into two parts WP1.1 and WP1.2. The objective of WP1.1 is to review the state of the art of gas generation and transport in a geological repository for nuclear waste. Based on research coming from inside and outside of FORGE a compilation of technical and scientific knowledge has been made regarding gas aspects in a deep geological repository. WP1.2 aims to define and perform comparative safety-relevant calculations regarding gas transport in a stepwise approach from a cell scale, module scale until the repository scale. In this report the results of ENSI concerning the first benchmark will be presented. The cell scale benchmark [1] is represented in the Figure 83. In this stepwise approach each model is included in the next one.

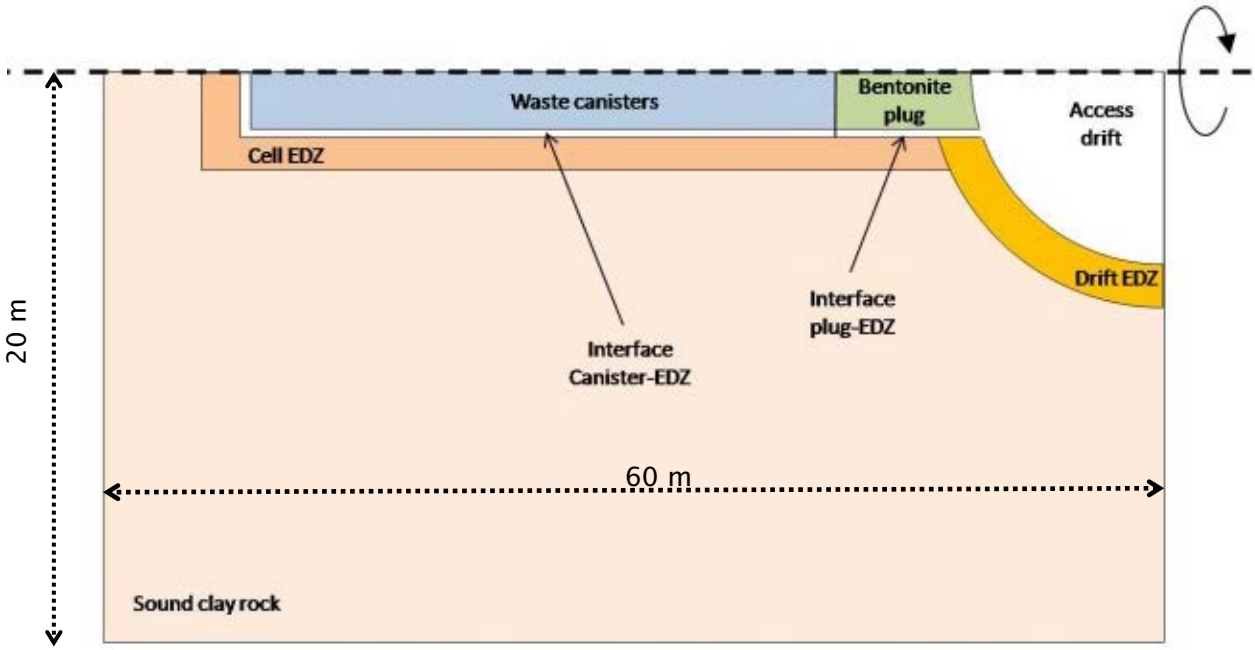

Figure 83 Domain of the model proposed for the first benchmark exercise (cell scale) [1].

During its participation in FORGE, ENSI performed calculations for the first and second benchmark. Calculations similar to the cell scale were already performed in the firs stage of the sectoral plan in Switzerland [2]. The sectoral plan (divided into three stages between 2008 and 2020) is a stepwise process for a site selection of a geological repository for radioactive waste in Switzerland. The cell scale model for the FORGE project contains additional features in particular the interfaces between the EDZ and the waste canister as well as the interface surrounding the bentonite plug. It contains also different parameters and models from the ones used for the calculations of the first stage of the sectoral plan. The interface and some of the models and parameters compromised the stability of the numerical calculations performed in the first benchmark.

Work package 1.2 proposed three very challenging benchmarks related to the transport of gas in a deep geological repository. ENSI started with the work related to the first exercise within FORGE WP1.2 with a delay caused by the review by ENSI of the first stage of the sectoral plan in Switzerland. The experience gained by ENSI with the simulation of the gas transport in a nuclear waste geological repository during the first stage of the sectoral plan could be used for the simulation of the first benchmark exercise. The above mentioned delay was already corrected between the end of 2009 and 2010, when ENSI results were presented in the meeting of Kaunas in June 2010. A lot of effort was put by ENSI in order to obtain the results within the specified deadline.

It was clearly established from the beginning of the project by the team members that these benchmarks do not represent the reality of a particular disposal concept of a country but they represent a numerical exercise to compare results of different teams. The preparation and the realization of the benchmark were made in view of future reviews of similar calculation by ENSI during the sectoral plan. In this respect the priority was set on the preparation of the technical tools to perform this kind of calculations instead of trying to analyze the correct models and parameters. It is in this sense that the results presented here by ENSI have to be understood and not as the definitive results about the complete behaviour of the gas in a deep geological repository. They have to be seen as results of a numerical exercise performed by several teams and ENSI with currently available software tools. These numerical calculations allow us the acquisition and preparation of the necessary software tools and its implementation by comparing with the results of other teams, in particular to determine the order of magnitude of the results and of their course of variation. There are some statistical errors related to the programs and also to the simplifications used by the different teams. Moreover, the results of the calculations were not compared to measurements coming from laboratory or field experiments what reinforces the thesis of the no interpretation of the results as the definitive behaviour of the gas in a geological repository but as reference for the order of magnitude of what in principle the measurements will provide. ENSI would like to remark here the importance of the combination of numerical results with measurements in order to understand correctly the processes occurring in the underground.

The benchmark exercises were from the numerically point of view very challenging and therefore all teams have to use different, sometimes code depending, kind of simplifications and approximations to obtain results. This explains together with the use of different codes the differences in some of the results. Despite these simplifications the results show concerning their range and their course of variation a good agreement. A lot of effort was put by ENSI into the correct implementation of the exercises avoiding as much as possible the use of simplifications. That was possible in the first exercise but in the second exercise some simplifications had to be made in order to avoid convergence problems. These convergence problems have to be understood more as a decrease of the speedup of the calculation rather than convergence problems causing a breakdown of the calculations, what sometimes but rarely happened.

The results obtained by ENSI in the first (cell benchmark) benchmark exercise within the work package WP1.2 of FORGE will be described in this chapter. This chapter is divided into seven parts. In the next two chapters 3.8.2 and 3.8.3 a general description of the codes used and of the mathematical models will be presented. The third part 3.8.4 will deal with the implementation of the specifications of the benchmark. The fourth part 3.8.5 will show a selection of some results of the first benchmark exercise. The fifth part 3.8.6 will show the results of the sensitivity cases. The sixth part 3.8.7 will show results of an additional sensitivity case and finally the seventh part 3.8.8 will show the conclussions.

3.8.2 Codes Used for the Calculation

The code chosen to perform the numerical simulations is TOUGH2 (Transport of unsaturated groundwater and heat), a general purpose numerical simulation program for multi-dimensional fluid and heat of flows of multiphase, multicomponent fluid mixtures in porous and fractured media [3]. It is applicable in geothermal reservoir engineering, nuclear waste isolation, environmental assessment and remediation and flow and transport in variably saturated media and aquifers. It is specially the two-phase flow capabilities, which are of concern in the calculations envisaged in this report. The program is developed and provided by the Lawrence Berkeley National Laboratory.

The first simulations for the FORGE project were conducted with TOUGH2 but after some difficulties such as the time-dependent boundary conditions or the long computational times it was decided to use the recently acquired program TOUGH2-MP to perform the numerical simulations for this exercise. TOUGH2-MP is a parallel version of the TOUGH2 code developed also by the Lawrence Berkeley National Laboratory [4].

ENSI acquired the program TOUGH2-MP in November 2009 and in January 2010 was decided to use TOUGH2-MP to implement the time-dependent boundary conditions and to increase the speedup of the calculations. The compilation and installation of the code took longer than expected. Our computer cluster consists of an IBM AIX machine with 4 nodes and each with 32 processors. This system was not included among the systems in which the program was tested. Therefore the compiling options had to be adapted to our system and additional features had to be installed in our system. The code needs also the external libraries AZTEC and METIS. The compilation of these libraries was also system-dependent and besides no compiling option was specified for our system.

After the installation of TOUGH2-MP some tests were performed successfully with inputs included in the distribution. The input for FORGE was implemented and adapted to the code TOUGH2-MP; in fact there are some slight differences between the inputs for the two codes TOUGH2 and TOUGH2-MP. Unfortunately many problems were found, related to the installation of the code and also related to the input file and our simulations could not be run with the program TOUGH2-MP. The input file was refined and the installation and compilation options were optimize but there were still problems. The input file was checked by the authors of the code in LBNL and no problem was found except that it run a little slow. In the meantime the input was tested again but with the module EOS3 (TOUGH2 module in which the gas phase consists of air instead of hydrogen like in the EOS5 module) and the code worked with this input. After some months of extensively checking of the code, a bug related to our computer architecture was found in the code, after the correction of this bug the input worked perfectly. In comparison with other gas transport simulations performed by ENSI, we soon realized that the input run relatively well at the beginning but after more or less 100 years the code starts slowing down. The reason of that was that ENSI used in the first simulations two layers of mesh elements for the interface. Due to the small dimensions of the node elements of the grid especially in the interface the code run very slowly. To increase the size of the elements the two layers of interface were reduced to one layer and the computational time of the simulations was then improved.

3.8.3 Numerical Formulation

The basic mass- and energy balance equations solved by TOUGH2 can be written in the general form [3]:

$$\frac{d}{dt}\int_{V_n} M^k dV_n = \int_{\Gamma_n} F^k \cdot n d\Gamma_n + \int q^k dV_n \qquad (1)$$

The integration is over an arbitrary subdomain V_n of the flow system under study, which is bounded by the closed surface Γ_n. The quantity M appearing in the accumulation term (left hand side) represents mass or energy per volume, with κ = 1… NK labeling the mass components (water, air, H_2, solutes, etc.), and κ = NK + 1 the heat "component." F denotes mass or heat flux and q denotes sinks and sources. A normal vector n is defined on surface element $d\Gamma_n$, pointing inward into V_n.

The continuum equations (1) are discretized in space using the integral finite difference method (IFD; [5, 6]). Introducing appropriate volume averages, we have:

$$\frac{dM_n^k}{dt} = \frac{1}{V_n}\sum_m A_{nm} F_{nm}^k + q_n^k \qquad (2)$$

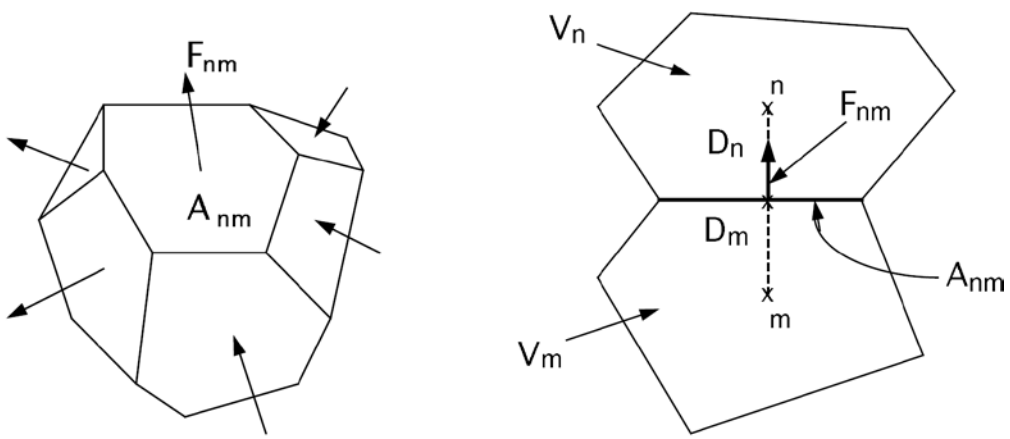

Figure 84 Space discretization in the integral finite difference method [3].

Time is discretized as a first-order finite difference. The flux and sink and source terms on the right-hand side of Eq. (2) are evaluated at the new time level, $t_{k+1} = t_k + \Delta t$, to obtain the numerical stability needed for an efficient calculation of multiphase flow. There are NEL nodes for which Eq. (2) has to be solved and NK+1 equations. Accordingly there are NEL x NK+1 independent primary variables {xi; i = 1... NEL x NK+1} which completely define the state of the flow system at time level t_{k+1}. The time discretization results in the following set of coupled non-linear, algebraic equations:

$$R^k_{n,t+1} = M^k_{n,t+1} - M^k_{n,t} - \frac{\Delta t}{V_n}\left\{\sum_m A_{nm} F^k_{nm,t+1} + q^k_{n,t+1}\right\} = 0 \qquad (3)$$

These equations are solved by Newton/Raphson iteration, which is implemented as follows. An iteration index p is introduced and the residuals $R^k_{n,t+1}$ in Eq. (3) are expanded at iteration step p + 1 in a Taylor series in terms of those at index p. Retaining only terms up to first order, for each volume element (grid block) V_n, there are NEQ equations (κ = 1, 2, ..., NEQ; usually, NEQ = NK + 1), so that for a flow system with NEL grid blocks Eq. (4) represents a total of NEL x NEQ coupled non-linear equations for the increments $(x_{i,p+1} - x_{i,p})$:

$$-\left.\frac{\partial R^k_{n,t+1}}{\partial x_i}\right|_p (x_{i,p+1} - x_{i,p}) = R^k_{n,t+1}(x_{i,p}) \qquad (4)$$

3.8.4 Benchmark Implementation

In order to be able to compare the results of different teams, under the same assumptions, ENSI put a lot of effort in the implementation of the parameters and models as prescribed in the exercise [1]. Some of them like the thin interfaces and like the time-dependent boundary conditions were extremely difficult to implement and without them, the calculations would have been much easier to perform but on the other hand it would have been much more difficult to compare with other teams within the scope of this benchmark exercise. That is why ENSI proposed for next exercises to use identical specifications and in case some specifications result to be problematic to inform all the teams in order to use the same changes of the specifications. The reality is that sometimes some specifications cause problems with some codes but not with others, an example is the variable boundary condition.

In Figure 85 a representation of the model and its dimensions is shown. The dimensions are listed on Table 13.

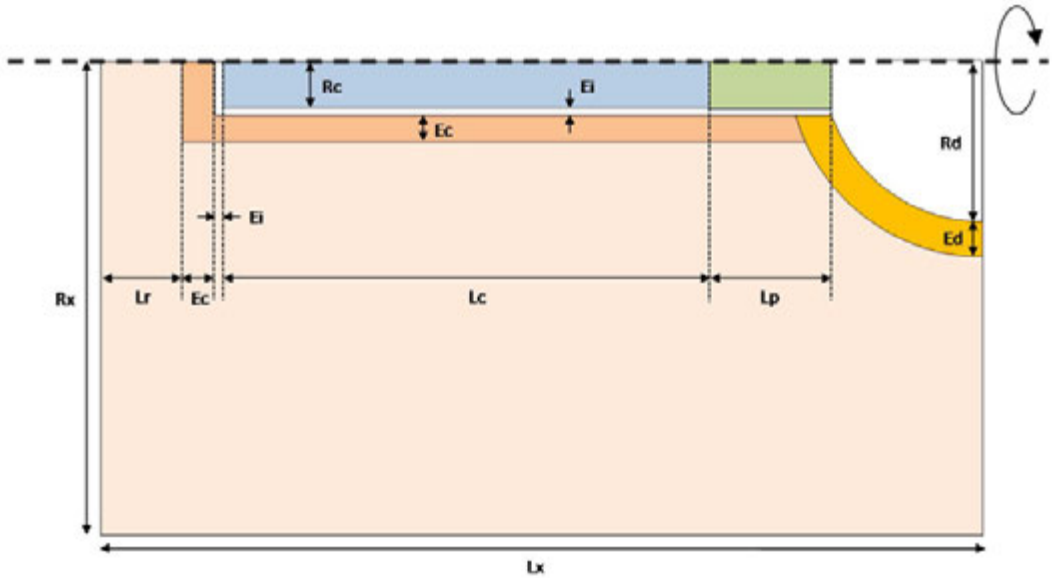

Figure 85 *Model and dimensions for the first benchmark [1].*

Table 13 *Dimensions of the model for the first benchmark [1].*

Name of parameter	Parameter	Value
Length of the domain (cell axis direction)	Lx	60 m
Radius of the domain	Rx	20 m
Radius of access drift	Rd	3 m
Thickness of the access drift EDZ	Ed	1 m
Length of the plug	Lp	5 m
Length of the canister zone	Lc	40 m
Thickness of the cell EDZ	Ec	0.5 m
Plug and canisters radius	Rc	0.5 m
Thickness of the interface	Ei	0.01 m
Distance between end of cell EDZ and boundary	Lr	11.5 m

In Table 14 the main physical parameters for the first benchmark exercise are listed. A detailed description of the exercise can be seen in [1].

Table 14 *Physical parameters for the materials [1] in the first benchmark.*

Parameter (at 20°C)	Materials		
	Interface facing plug	Interface facing canister	Backfill (access drift)
K_v [m^2]	$5.0\ 10^{-18}$	$1.0\ 10^{-12}$	$5.0\ 10^{-17}$
K_h [m^2]	$1.0\ 10^{-17}$	$K_v=K_h$	
Porosity [%]	30	100	40
Specific storage coefficient [m^{-1}]	$4.6\ 10^{-06}$	$4.6\ 10^{-06}$	$1.0\ 10^{-05}$
Two-phase flow parameters			

Parameter (at 20°C)	Materials		
	Interface facing plug	Interface facing canister	Backfill (access drift)
S_{gr} [%]	0	0	0
S_{wr} [%]	0	0	0
Van Genuchten parameters			
n [-]	4	4	1.5
P_r [Pa]	10^4	10^4	$2\ 10^6$
□ (Tortuosity)	1	1	2

Parameter (at 20°C)	Materials		
	Bentonite plug	EDZ	Geologial Medium
K_v [m²]	$1.0\ 10^{-20}$	$5.0\ 10^{-18}$	$5.0\ 10^{-21}$
K_h [m²]	K_v=K_h	$1.0\ 10^{-17}$	$1.0\ 10^{-20}$
Porosity [%]	35	15	15
Specific storage coefficient [m⁻¹]	$4.4\ 10^{-06}$	$2.3\ 10^{-06}$	$2.3\ 10^{-06}$
Two-phase flow parameters			
S_{gr} [%]	0	0	0
S_{wr} [%]	0	0	0
Van Genuchten parameters			
n [-]	1.6	1.5	1.5
P_r [Pa]	$1.6\ 10^7$	$1.5\ 10^6$	$1.5\ 10^7$
□ (Tortuosity)	4.5	2	2

In this chapter the implementation and in some cases the adaptations of the code in order to fulfil the required specifications for the benchmark exercise will be explained.

3.8.4.1 Models for the Gas Relative Permeability and Diffusion

The parameters for the first benchmark of WP1.2 are indicated in table 2 of the document with the specifications [1]. The parameters were implemented into the input of TOUGH2-MP. The code has to be modified in order to be able to implement the diffusion coefficient, the gas relative permeability and slight modifications have also to be made in the solubility coefficients for hydrogen in the Henry's law.

According to the prescriptions in the exercise [1], the relative permeability for water is expressed by integrating the Mualem prediction model in the Van Genuchten model:

$$k_r^w = \sqrt{S_{we}}\left[1-\left(1-S_{we}^{1/m}\right)^m\right]^2 \qquad (5)$$

k_r^w : Water relative permeability (-)

This expression is the same as the one for the Van Genuchten-Mualem model in the TOUGH2 code.

The relative permeability for gas is expressed similarly in the exercise as:

$$k_r^g = \sqrt{1-S_{we}}\left[1-S_{we}^{1/m}\right]^{2m} \qquad (6)$$

k_r^g : Gas relative permeability (-)

In the TOUGH2 code there are several options for the gas relative permeability, the relation of Van Genuchten-Mualem is usually used:

$$k_r^g = (1-S_{we})^2\left[1-S_{we}^2\right] \qquad (7)$$

The prescribed gas relative permeability is given by the Van Genuchten-Mualem relation with γ=0.5:

$$k_r^g = (1-S_{we})^\gamma\left[1-S_{we}^{1/m}\right]^{2m} \qquad (8)$$

This option is not available in TOUGH2; therefore the code was modified to make this option available. The use of the option caused a slowdown and instabilities of the simulations and for some calculation cases even a crash of the simulation after 10'000 years.

The diffusion coefficient of dissolved H2 in the binary H2/water-vapour mixture of the porous medium is specified in the exercise as:

$$D_{H_2/vap}^g = (1-S_w)\left(\frac{\phi}{\tau^2}\right)D_0\left(\frac{P_0}{P}\right)\left(\frac{T}{T_0}\right)^{1.75} \qquad (9)$$

The diffusion coefficient of dissolved H2 in the water of the porous medium is specified in the exercise as:

$$D_{H_2}^w = S_w\left(\frac{\phi}{\tau^2}\right)\times 1.5710^{-14}\frac{T}{\mu_{water}(T)} \qquad (10)$$

In TOUGH2 the corresponding values are defined as:

$$D_{H_2/vap}^g = \phi\tau_0\tau_\beta\left(\frac{1}{\tau^2}\right)D_0\left(\frac{P_0}{P}\right)\left(\frac{T}{T_0}\right)^{1.75} \qquad (11)$$

$$D_{H_2}^{w} = \phi \tau_0 \tau_\beta \left(\frac{1}{\tau^2} \right) \times 1.5710^{-14} \frac{T}{\mu_{water}(T)} \qquad (12)$$

Some changes were made in the TOUGH2 code in order to define the diffusion coefficients as specified in (9) and (10).

The proposed expression for the Henry's law in FORGE has some differences with the used in the TOUGH2 code. Namely the expression in FORGE contains the concentration of hydrogen in mol/m3 und the expression in TOUGH2 uses the mole fraction of hydrogen. A conversion factor was implemented in the TOUGH2 code to use the in FORGE suggested expression.

3.8.4.2 Initial and Boundary Conditions

The boundary conditions as well as the initial conditions prescribed in the FORGE WP1.2 were implemented in the TOUGH2 input file. The behaviour of the system depending on the initial conditions was studied with numerical simulations. It was seen that the numerical convergence of the simulations is improved if the initial conditions in the different nodes between the interface, EDZ and rock vary smoothly. The best convergence was obtained when the initial conditions of the EDZ and interface are the same.

The results of ENSI and of other teams confirm that initially a transient of pressure occurs during the first thousandth of a year as shown in Figure 86. The gas pressure in the EDZ changes during this transient from 5MPa to about 0.1 MPa. ENSI proposed therefore to change the initial conditions of the EDZ to this last value in order to avoid numerical oscillations at the beginning.

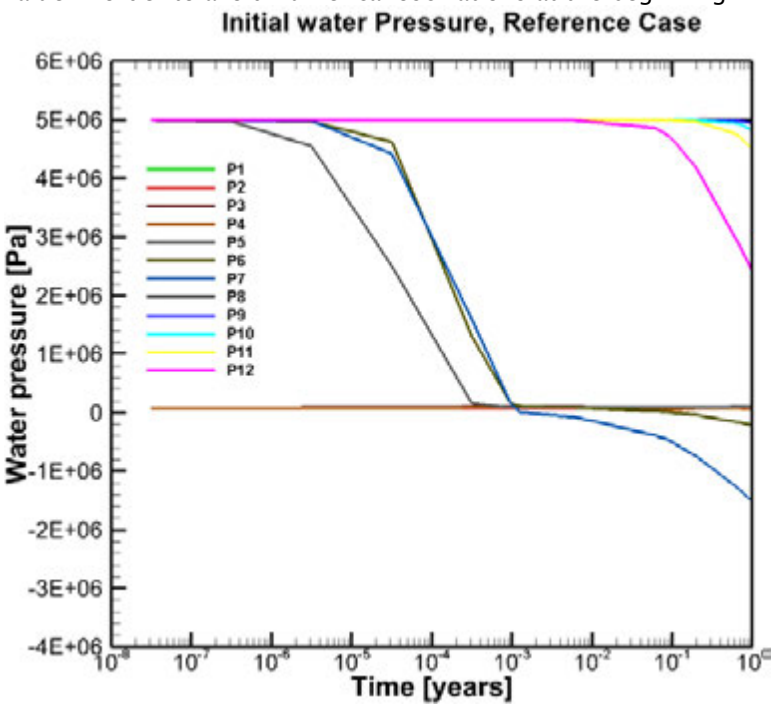

Figure 86 *ENSI Results for liquid pressure during the first year at different points of the model.*

ENSI used at the beginning the code TOUGH2 to perform the simulations for this exercise; the variable boundary condition, see Figure 87, were implemented with a time-dependent source term. In this way the prescribed pressure and saturation variation was implemented but on the other hand also a variable mass of gas was introduced into the system, how this mass can affect the properties of the system has to be analysed.

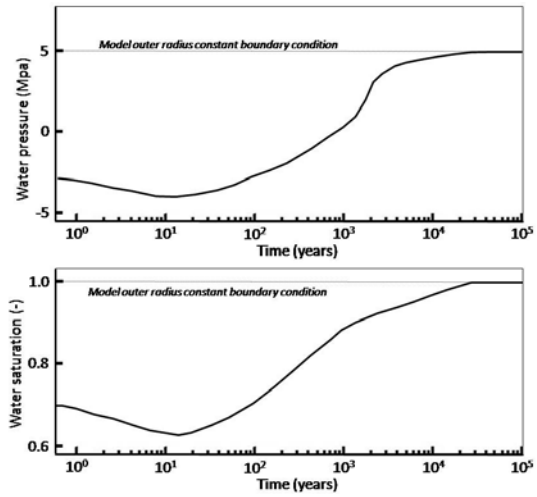

Figure 87 Time variable boundary conditions to be used in the drift.

To avoid possible problems with the indirectly inserted gas, the code TOUGH2-MP was used because this code includes a capability to implement time-dependent boundary conditions for the pressure. Since in the exercise not only time-dependent boundary conditions for the pressure but also for the saturation were prescribed, the code had to be modified to allow the implementation of time-dependent saturation values.

The time-dependent boundary conditions cause the code to slow down. Comparisons were made between the calculation times of two inputs, one with boundary conditions and the other without them. The calculation time decreases significantly for the case without time-dependent boundary conditions. The boundary conditions at the bottom of the domain were implemented in TOUGH2-MP by means of large volume elements.

3.8.4.3 Deviations from the specification

Since the model is axisymmetric around the axis of the cell, each element of the grid includes all elements generated by rotating each planar element around this axis. Therefore the horizontal intrinsic permeabilities are implemented in the input as prescribed but the vertical intrinsic permeabilities have to include all the rotated elements. An average value around the rotation was taken for the vertical intrinsic permeabilities. For the isotropic materials the prescribed intrinsic permeabilities did not change, for the anisotropic materials the following changes were made:

Table 15 Changes made in the intrinsic permeabilities.

	k_x (m^2)	k_y (m^2)	k_z (m^2)
Interface facing plug	$1.0*10^{-17}$	$7.49*10^{-18}$	$7.49*10^{-18}$
EDZ	$1.0*10^{-17}$	$7.49*10^{-18}$	$7.49*10^{-18}$
Rock formation	$1.0*10^{-20}$	$7.49*10^{-21}$	$7.49*10^{-21}$

3.8.5 Base Case Results

In the next subchapters the results for the pressure at different points and along lines in the domain as well as the results of the mass flows of water and of hydrogen will be shown.

The Figure 88 shows the results for the water saturation after 10'000 years. It can be observed that the whole domain is close to full saturation.

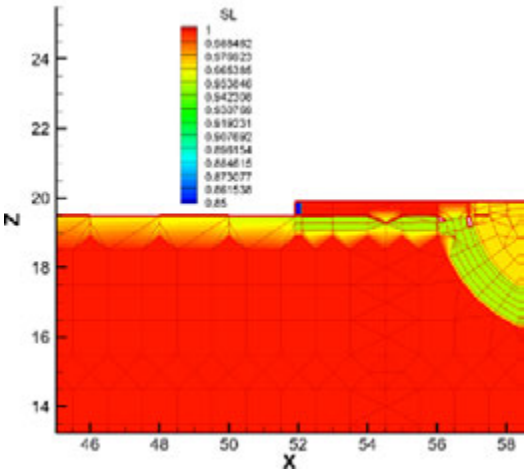

Figure 88 *Results for the water saturation after 10'000 years for the reference case.*

3.8.5.1 Results at Specific Points

In Figure 89 are represented the points for which a selection of results will be provided.

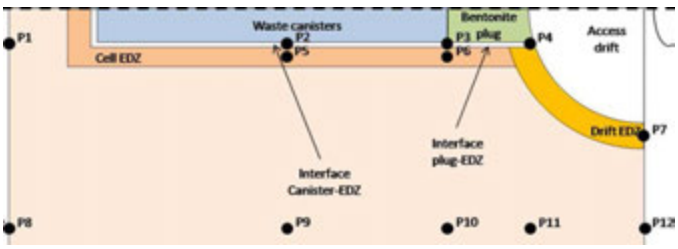

Figure 89 *Position of the points at which the results of the calculations are shown.*

The results in Figure 90 show the variation of the gas pressure with the time. The variation occurs between 10 and 10'000 years. The results clearly indicate an increase of the gas pressure as consequence of a larger amount of gas in the system. The maximal gas pressure is about 5.2 MPa and is reached at 10'000 years when the gas injection stops. In this benchmark it was taken the convention of considering the gas pressure as zero when the gas saturation is zero. This convention can cause some oscillations when the saturation is zero and close to it because in this case there is a transition from two-phase to one-phase flow and vice versa. Another convention is to take the gas pressure even in the case of a one-phase flow as equal to the water pressure. This convention was taken in the second benchmark because most of the teams used it. The reason in this case is to preserve the continuity of the solution for the transition from a two-phase flow, where the gas pressure is the difference between the capillary and liquid pressure, to a one-phase flow where the capillary pressure disappears. Taking into account these conventions the change from one to the other convention can be calculated easily. Based on these considerations it is the most appropriate to speak about the pressure of the system in order to avoid misunderstandings.

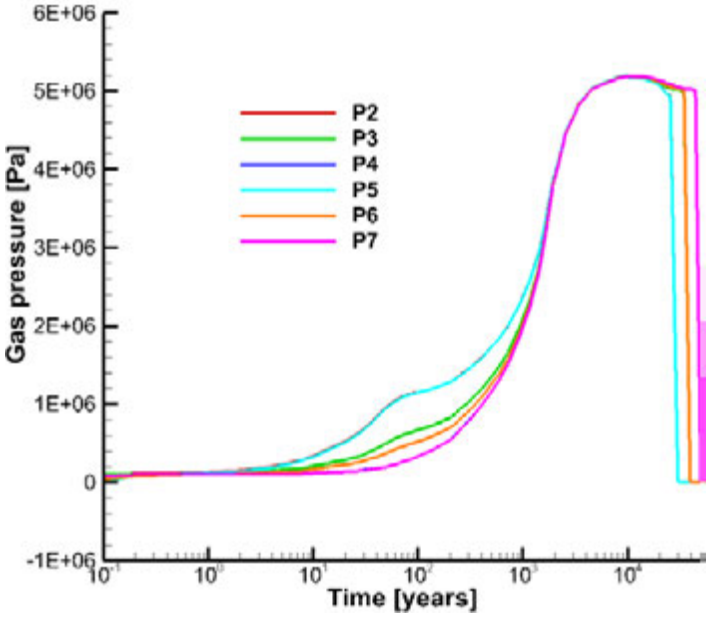

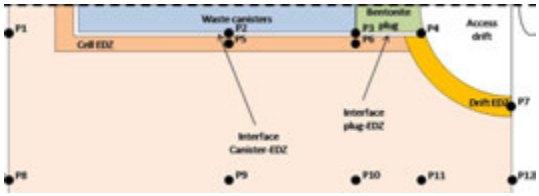

Figure 90 Gas pressure at the points where there is a gas phase.

The gas pressure decays some years after 10'000 years to zero because the points P5, P6 and P7 in the EDZ saturate after that time. The results of the variation of the gas saturation in the prescribed points are represented in the Figure 91.

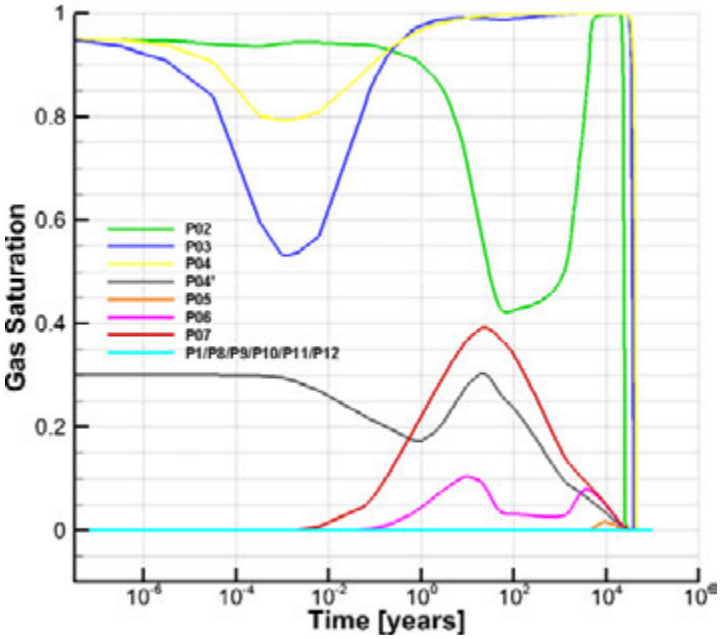

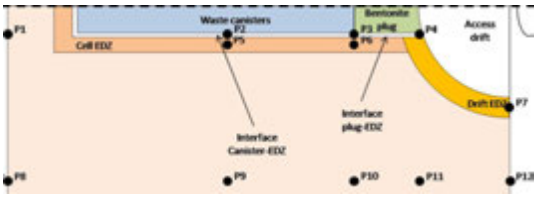

Figure 91 Variation of the gas saturation at the prescribed points.

The initial gas saturation in the interface points (P2, P3 and P4) is 95%, in the EDZ points (P5, P6 and P7) is 0%. It was also represented a point P4' close to the interface but in the access drift where the initial gas saturation is 30%. The EDZ tends to desaturate a little and the interface tends to saturate. In the EDZ, there is a balance between the water that tries to saturate the interface and the gas that tries to expand. Therefore, when the injection finishes at 10'000 years the interface becomes fully saturated.

In the next picture are shown the values of the water pressure in function of time for the points selected. The pressure decreases very quickly the closer the points are to the interface and to the access drift. The

gas flows in the direction towards the access drift from the waste canister along the interface and along the EDZ. The initial transient of Figure 86 can also be observed in this figure.

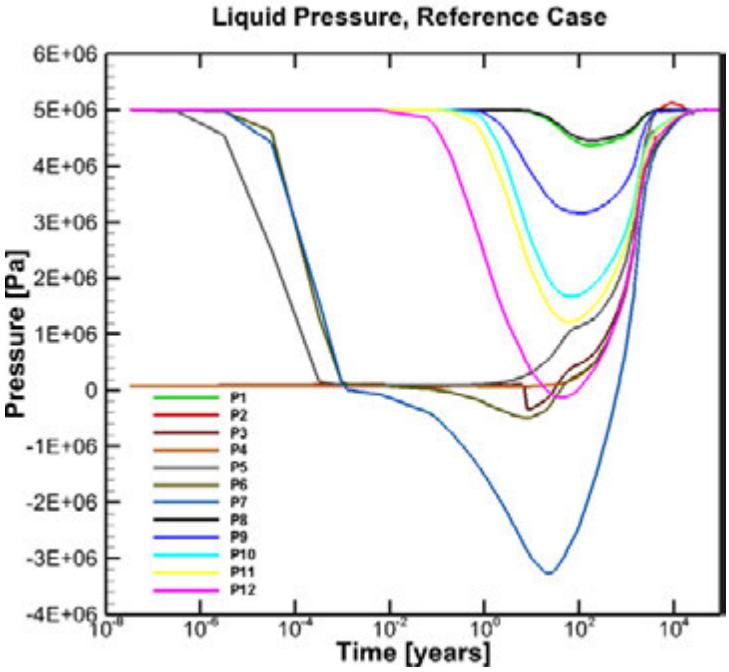

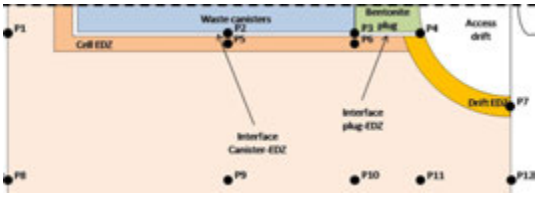

Figure 92 Water pressure at different points.

3.8.5.2 Results along Lines of the Domain

In the next two pictures is shown the change in the gas pressure along the interface and the cell EDZ. The interface spans from the x coordinate 11.5 m to about 55 m. The value of the gas generation in the waste canister at 10'000 years is zero what causes an immediate change of the gas pressure as it can be seen in the Figure 93 and Figure 94.

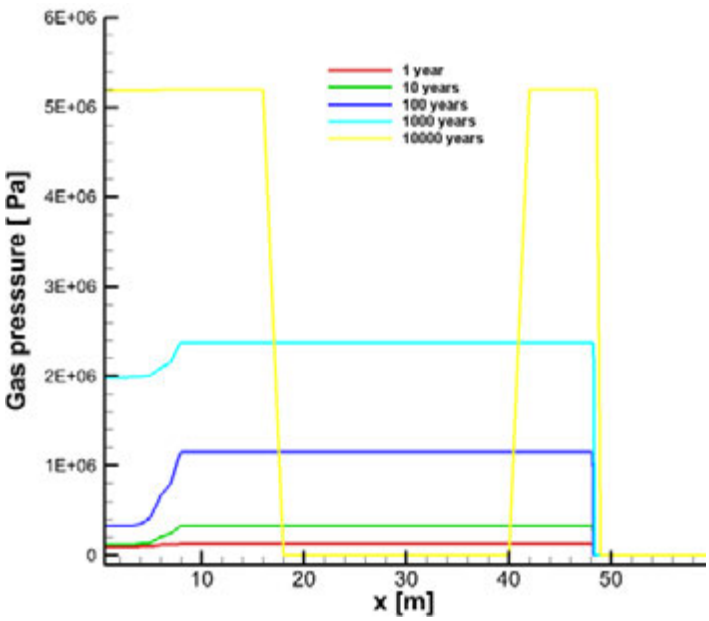

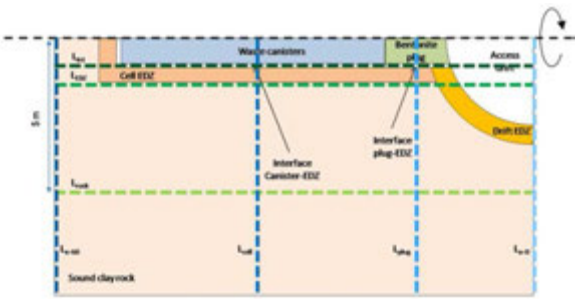

Figure 93 Gas Pressure along the line marked as L_{int} on the right part.

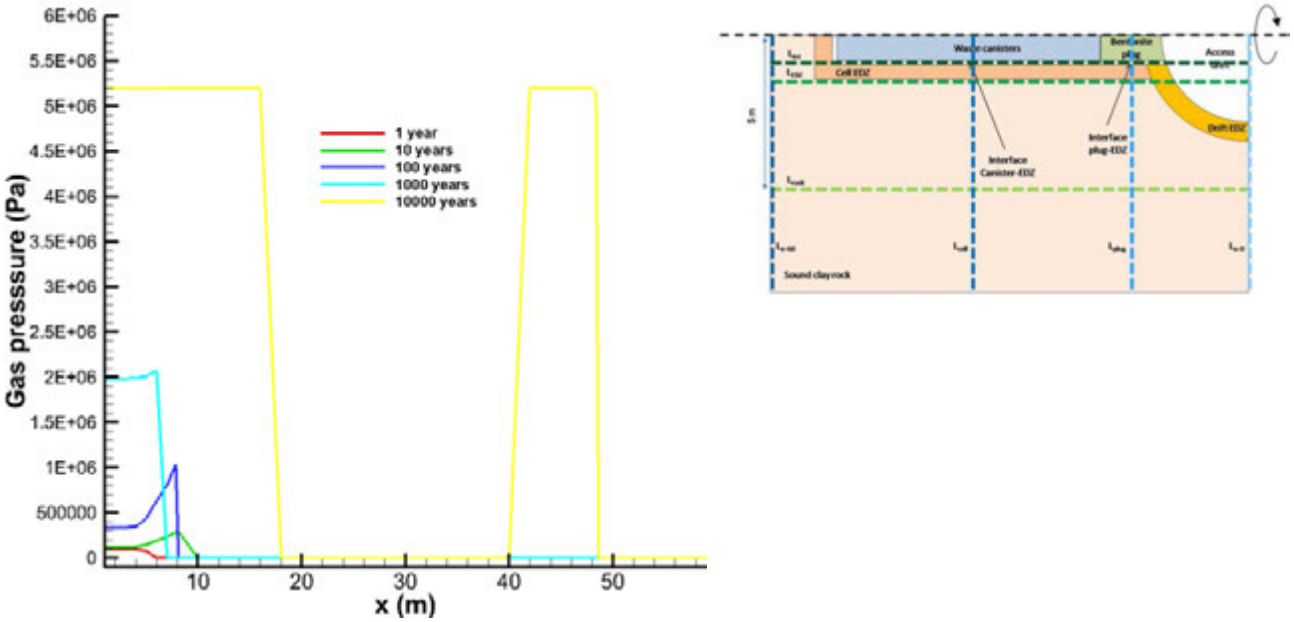

Figure 94 *Gas Pressure along the line marked as LEDZ on the right part.*

In Figure 95 is shown the variation of the gas saturation along a line perpendicular to the waste cell. The line starts at a distance of 0.495 m from the axis (the cell has a radius of 0.5 m). The saturation varies only in the interface and very close to it. The saturation of the EDZ and of the host rock close to the EDZ decreases at at time between 1'000 and 10'000 years.

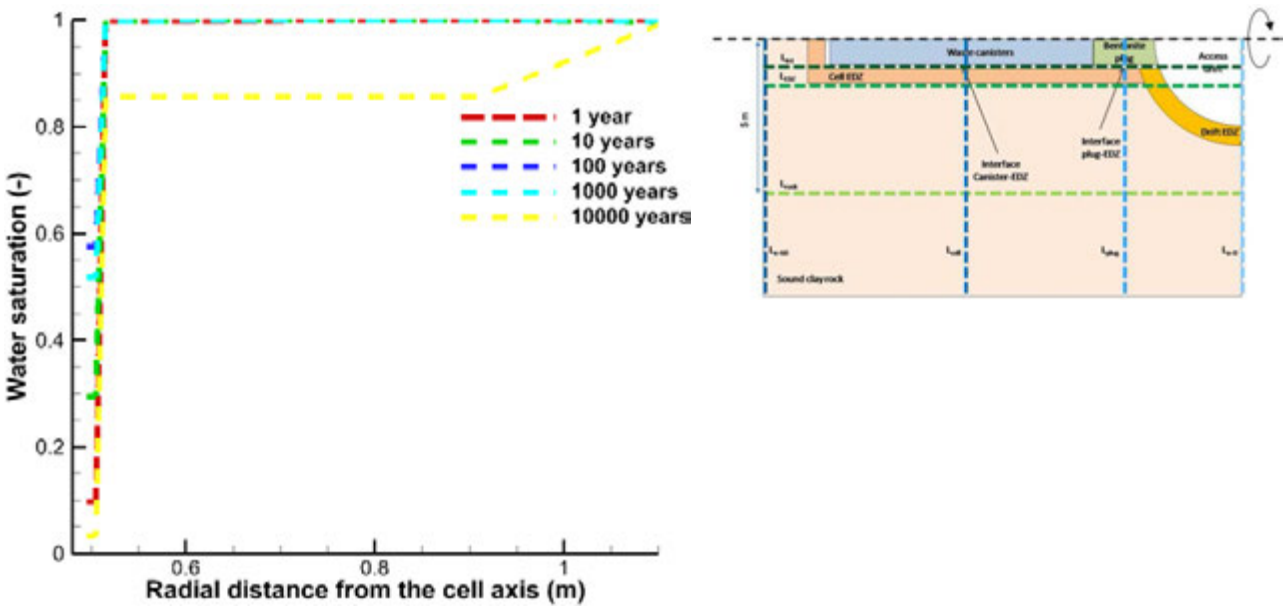

Figure 95 *Variation of the water saturation along a perpendicular line L_{cell} to the cell starting in the surface of the waste canister at coordinate y =0.495 m from the axis.*

The plot was cut at about 1.1 m from the cell axis because the saturation of the host rock does not vary beyond this distance.

3.8.5.3 Results for the Mass Flow Rates

In Figure 96 and Figure 97 are shown the values of the mass flow of water through the EDZ and through the drift. The negative mass flow indicates a flow towards the EDZ from the host rock. The evolution of the mass flow of water through the EDZ corresponds to the suddenly change in the pressure seen in Figure 92.

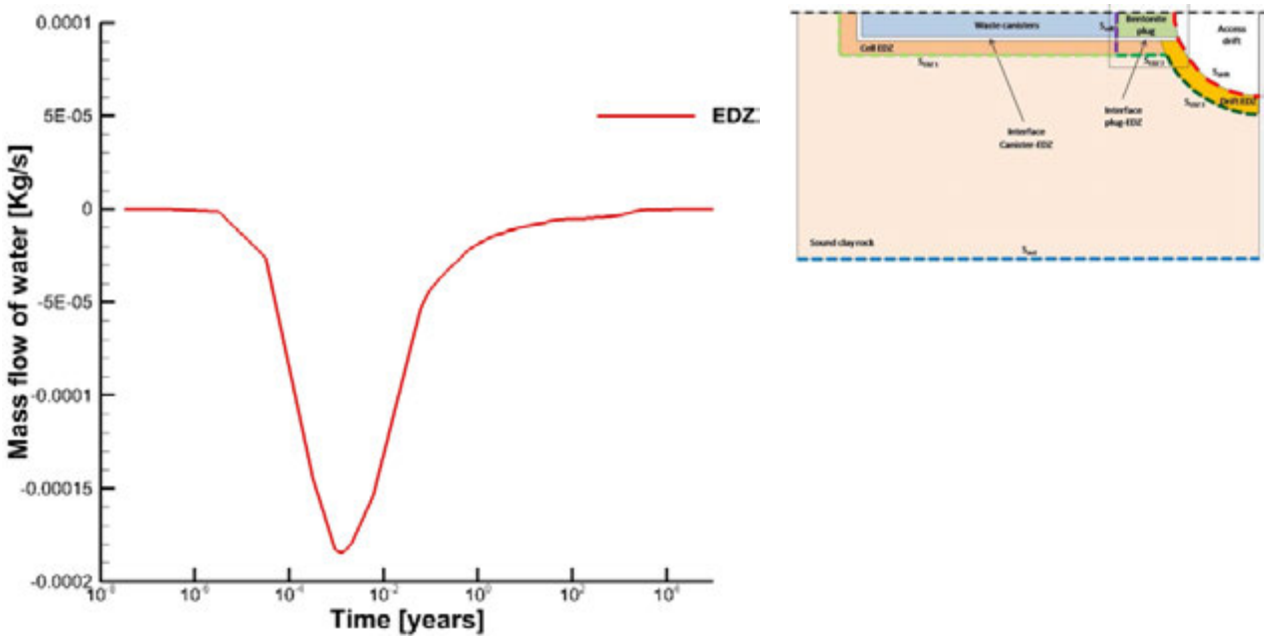

Figure 96 Mass flow of water in kg/s through the EDZ.

The mass flow of water through the drift decreases gradually as it can be seen in Figure 97. These two figures show on the one hand a pulse of water towards the EDZ caused by the initial conditions and the small desaturation of the EDZ and on the other hand a flow of water from the saturated host rock to the backfill of the drift that is not saturated. This mass flow decreases until about 100 years when it increases a little due to the increase of the gas pressure and correspondingly decrease of the water pressure close to the EDZ as it can be seen in Figure 90 and Figure 91 and that makes the water to drain into the drift afterwards is the gas that takes this preferential pathway.

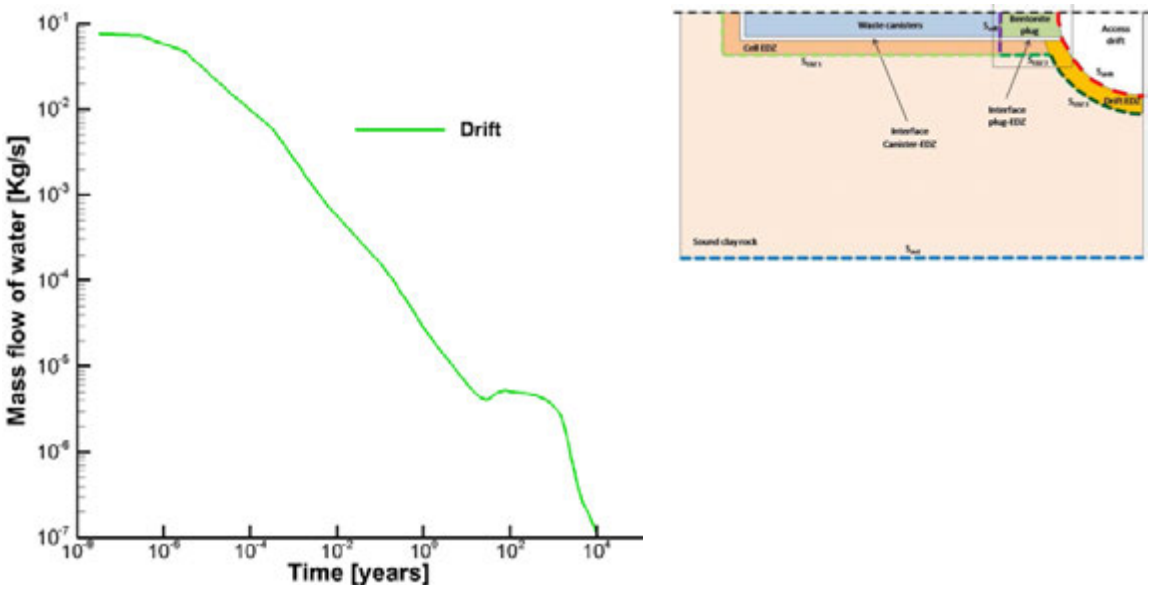

Figure 97 Mass flow rates of water in kg/s through the drift.

The results of the mass flow rate of hydrogen dissolved in water and in the gas phase are shown in the next picture. To calculate these values post-processing scripts were created and the code was modified because TOUGH2 does not deliver results for dissolved hydrogen in water.

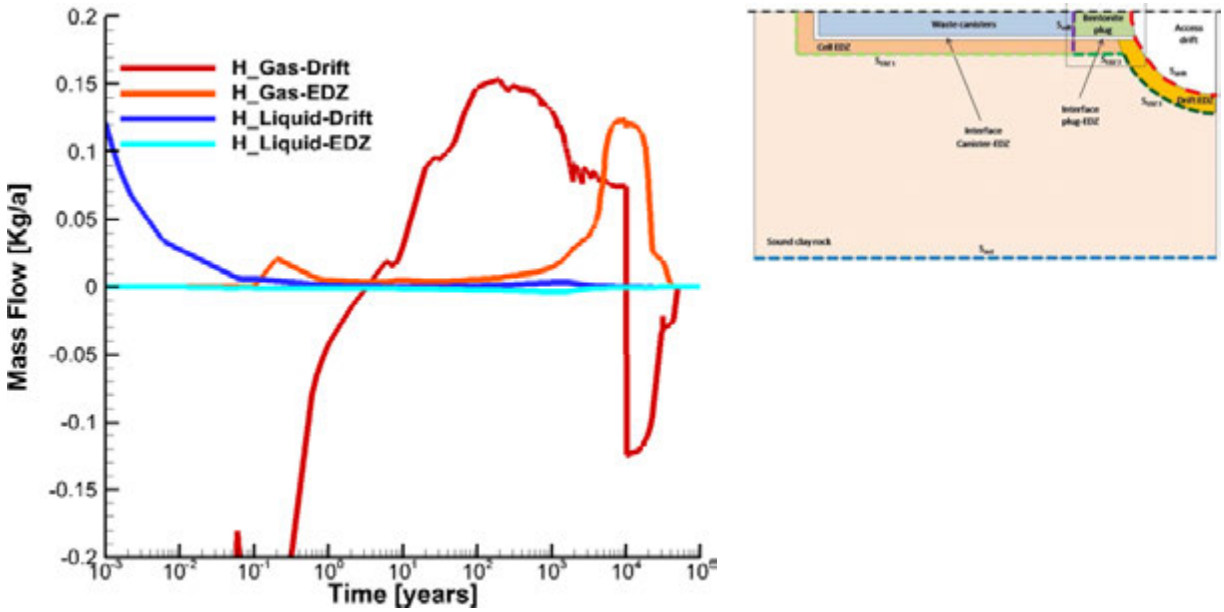

Figure 98 Hydrogen mass flow rates in kg/a through the EDZ and through the drift.

The maximal mass flow rate of around 0.15 kg/a is obtained after 200 years. Afterwards the mass flow decreases slowly up to the end of the gas generation period at 10'000 years. Comparing with the values of the liquid mass flow it can be concluded that, except at the beginning when a transport of dissolved hydrogen occurs, most of the hydrogen is being transported in a gas phase and only a small fraction is transported dissolved in a liquid phase. The gas is transported initially through the drift along the interface and then when the peak of mass flow is reached, the mass flow through the EDZ starts increasing to reach a maximum at 10'000 years.

3.8.6 Prescribed Sensitivity Cases

Besides the reference case the following sensitivity analysis were defined in the first exercise:

Table 16 Calculation cases for the cell scale benchmark

Reference Case	Parameter and conditions as specified before
Sensitivity analysis 1	EDZ intrinsic permeability equal to the one of the undisturbed rock (reduction of EDZ intrinsic permeability)
Sensitivity analysis 2	Power law for EDZ and host rock intrinsic permeability
Sensitivity analysis 3	Increase of diffusion coefficient of dissolved hydrogen
Sensitivity analysis 4a/4b	Delay of gas production of 1 year/ 2 years
Sensitivity analysis 5a/5b	Intrinsic permeability interface = $10^{-15}m^2$/ Intrinsic permeability of the interface equal to the one of the EDZ
Sensitivity analysis 6	Mesh refinement
Sensitivity analysis 7	Additional sensitivity

A selection of results for the different sensitivity analysis will be presented in the next subchapters.

3.8.6.1 Case 1: Self Healing EDZ

For this sensitivity analysis the EDZ intrinsic permeability (for both drift and cell) is supposed equal to undisturbed rock permeability, that is to say smaller than in the reference case, everything else is the same as in the reference case. In this case from the comparison between the Figure 92 and

Figure 99 it can be seen that the variation of the water pressure is not as quick as in the reference case and the water pressure takes negative values but close to zero.

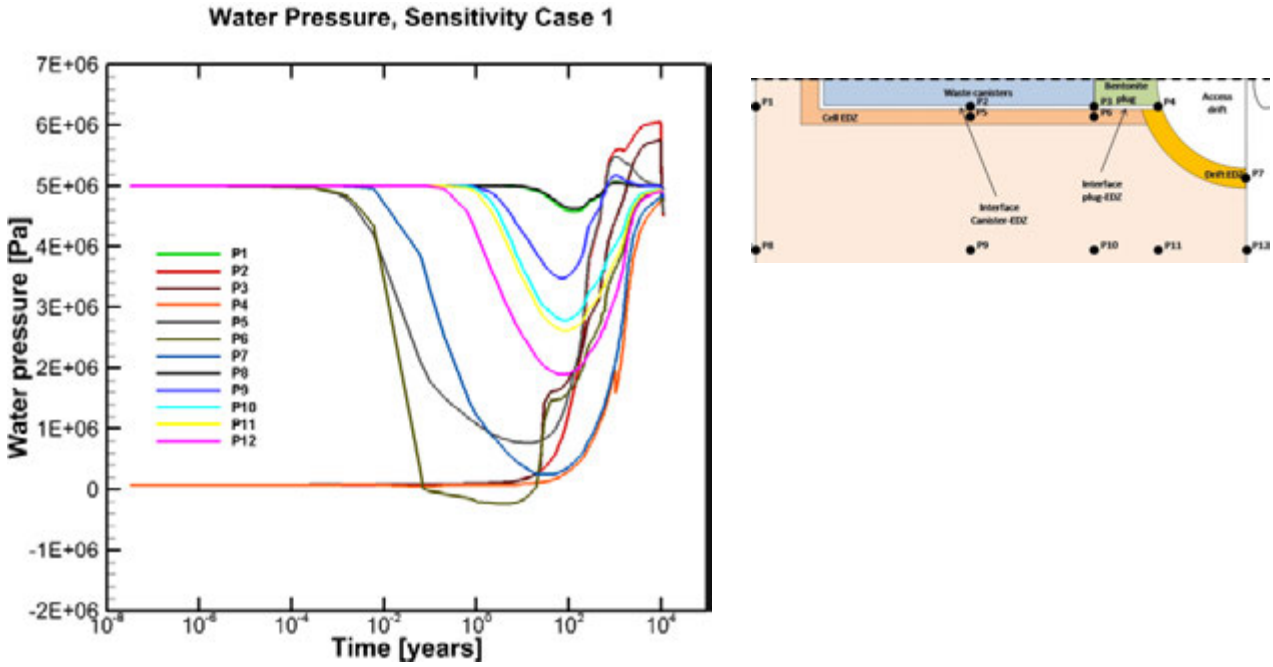

Figure 99 Water pressure at different points.

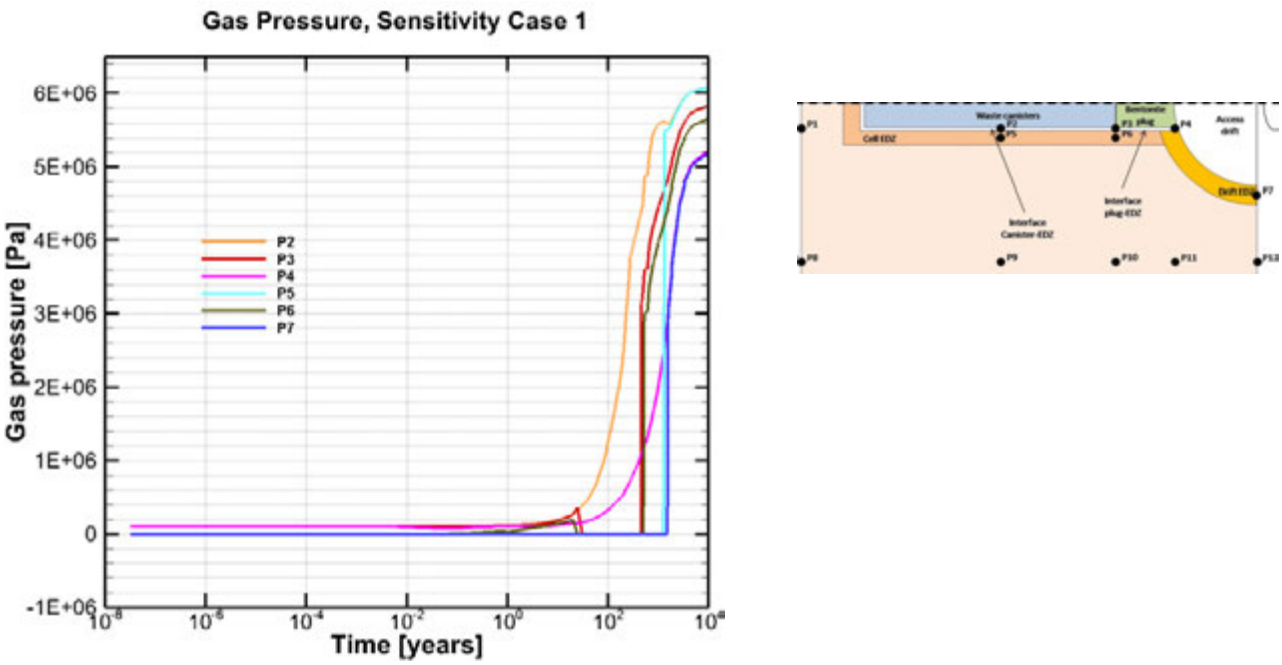

Figure 100 Gas pressure at different points.

As the permeability of the EDZ has decreased the gas continues flowing preferentially through the interface but in the reference case part of the gas flows through the EDZ and in this case the second preferential way is through both rock and EDZ. There is less change in water mass flow through the EDZ. Part of the water mass flow goes through the rock.

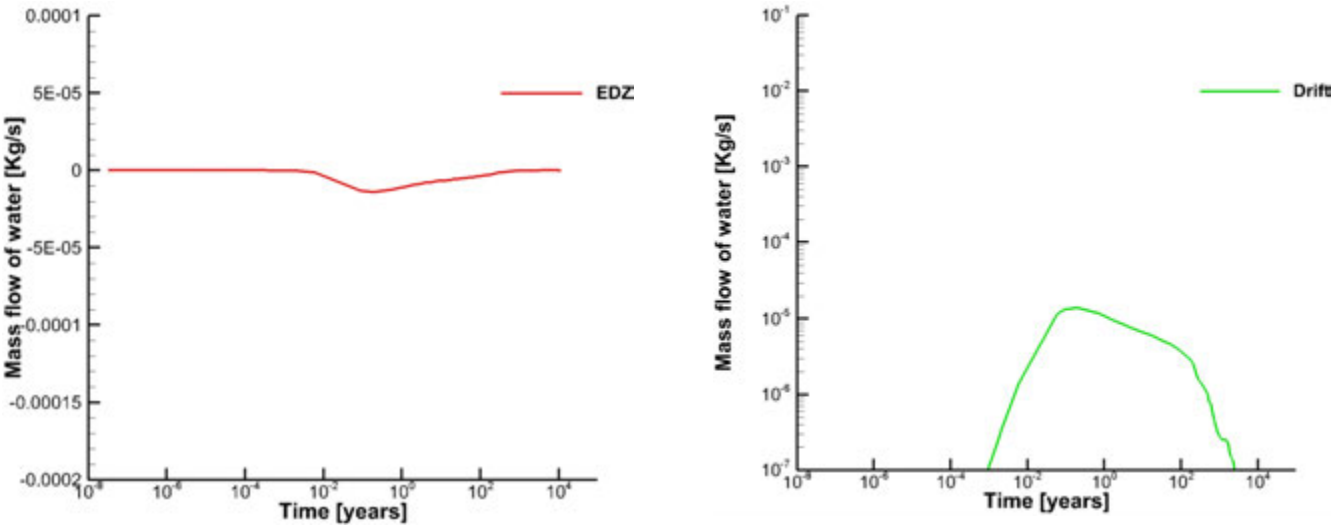

Figure 101 *Mass flow of water through the EDZ and through the drift. In order to compare them with Figure 96 and Figure 97 the same scale was used.*

3.8.6.2 Case 2: Altered Relative Permeability Curves

For this sensitivity analysis, everything else being equal to the reference case, relative permeability curve for water and gas of undisturbed host rock and EDZ (for both drift and cell) is supposed to follow saturation at the power 3:

$$K_r^w = S_w^3 \qquad K_r^g = S_g^3 = (1 - S_w)^3$$

Where K_r^w is the relative permeability for water (-),K_r^g is the gas relative permeability (-), S_w is the saturation for water (-) and S_g is the gas saturation.

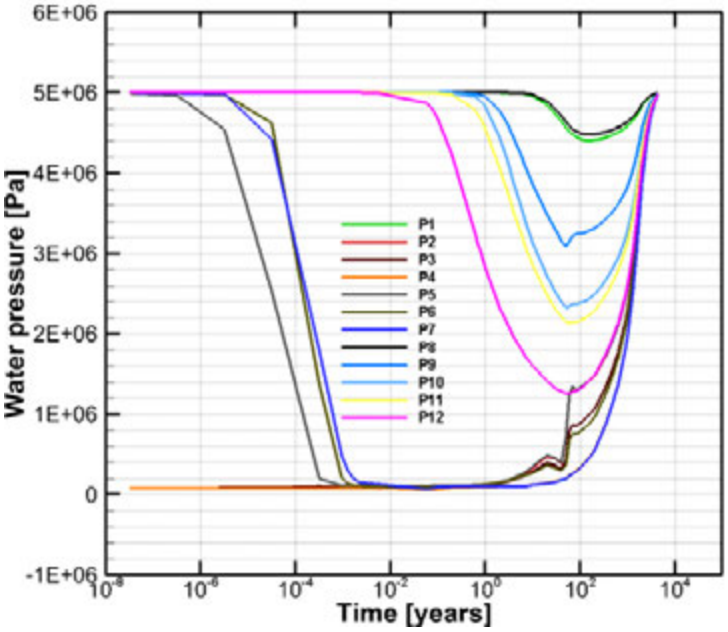

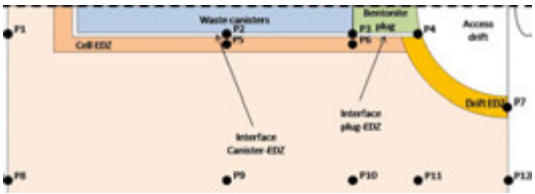

Figure 102 Water pressure at different points.

The water pressure does not take in this sensitivity analysis negative values as in Figure 92 and Figure 99.

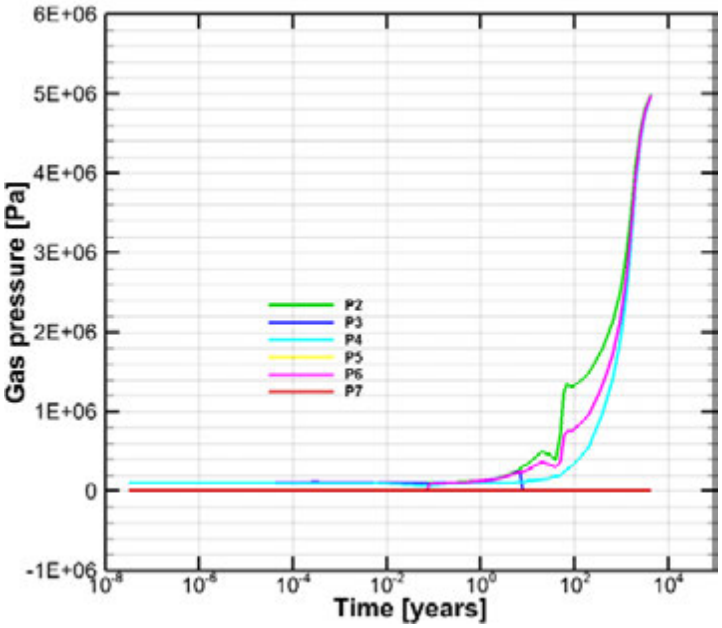

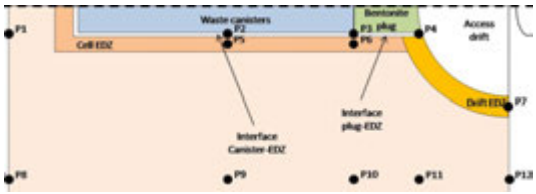

Figure 103 Gas pressure at different points.

The variation of the gas pressure for the points with a gas phase is shown in Figure 103. The maximal values for the gas pressure are lower than in the reference case (see Figure 90) and in the sensitivity case 2 (see Figure 100).

3.8.6.3 Case 3: Increased Diffusion in Water

In this sensitivity case the diffusion coefficient of dissolved hydrogen under water saturated conditions is multiplied by 10 for all simulated porous media, everything else is the same as in the reference case. In this

case as the gas can be transported dissolved in water the maximal pressure decreases in comparison with the reference case as it can be in the Figure 104.

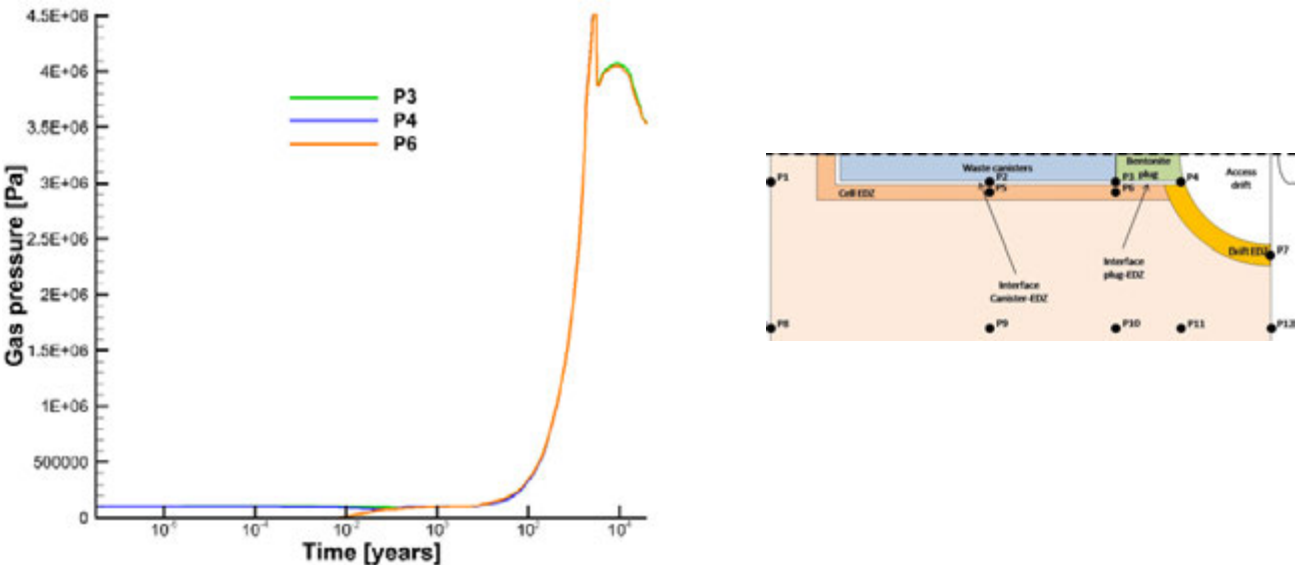

Figure 104 *Results of the gas pressure for the sensitivity case 3.*

In Figure 105 the gas flow through the drift is represented and compared with the equivalent values in the reference case and in the sensitivity case 1.

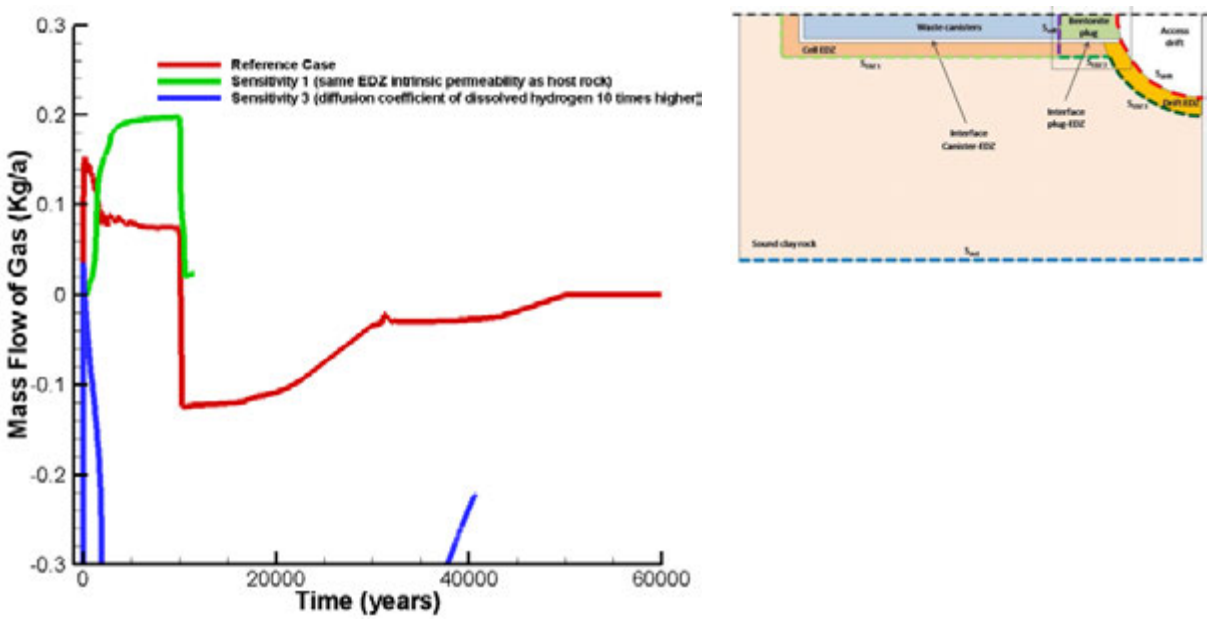

Figure 105 *Mass flow rates of gas in kg/a through the drift for the reference case and for the sensitivity cases 1 and 3.*

In the sensitivity case 1 the gas flow increases as the gas tends to go along the interface towards the drift. More gas is transported dissolved in water in the sensivity case 2 and therefore the mass flow of gas decreases.

3.8.6.4 Case 4: Gas Generation Delayed

Sensitivity case 4a and 4b represents a delay in the gas production of 1 and 2 years respectively. The results of the water pressure are shown in the Figure 106. The results show that a delay of 1, 2 or even 10 (also calculated but not shown here) years does not make a big difference in the results.

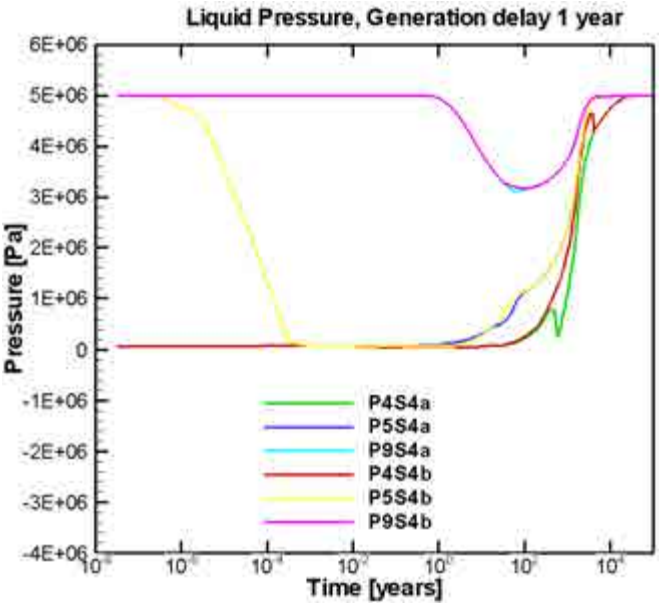

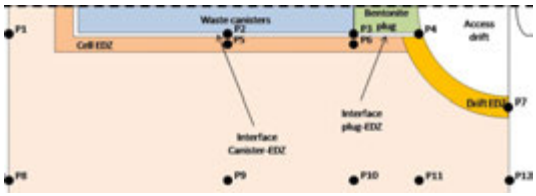

Figure 106 Water pressure at different points.

3.8.6.5 Case 5: Less Permeable Interfaces

In this sensitivity analysis the permeability of the interface was changed from 10^{-12} m² (reference case) to 10^{-15} m² (sensitivity analysis 5a) and to 10^{-18} m² (sensitivity analysis 5b). The comparison of these three calculation cases are shown in the next picture for three points P4, P5 and P9 close to the interface.

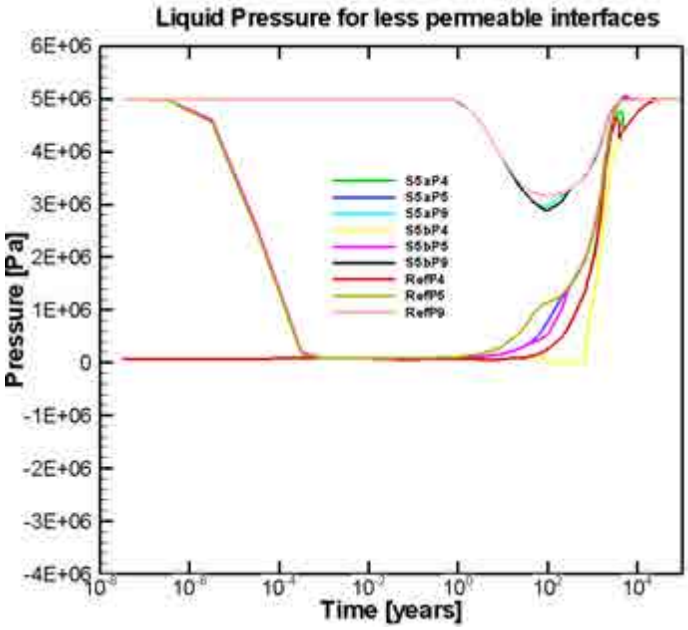

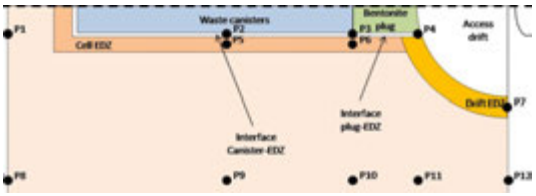

Figure 107 Water pressure in different points.

It can be seen in this picture that the results of the pressure do not change much with the change of the permeability of the interface.

3.8.6.6 Case 6: Mesh sensitivities

The program Wingridder [7] was used to create the mesh for TOUGH2. At the beginning ENSI created a very fine mesh of about 12000 elements, with two layers in the interfaces facing plug and canister. Due to these small volume elements the simulations run slowly and there were some numerical convergence problems. It was then decided to use a coarser grid with about 8000 elements but still we found that the numerical simulations were still too slow. The mesh was again reduced to 6300 elements (a detail of this mesh is shown in Figure 108 and Figure 109) and the two layers in the interfaces were reduced to only one layer, additionally the program TOUGH2-MP was used for the calculations. This causes a reduction in the calculation time of the simulations. The results of the simulations with the different meshes were similar; the differences were rather the time until the simulation could be run, because sometimes the simulation crashed.

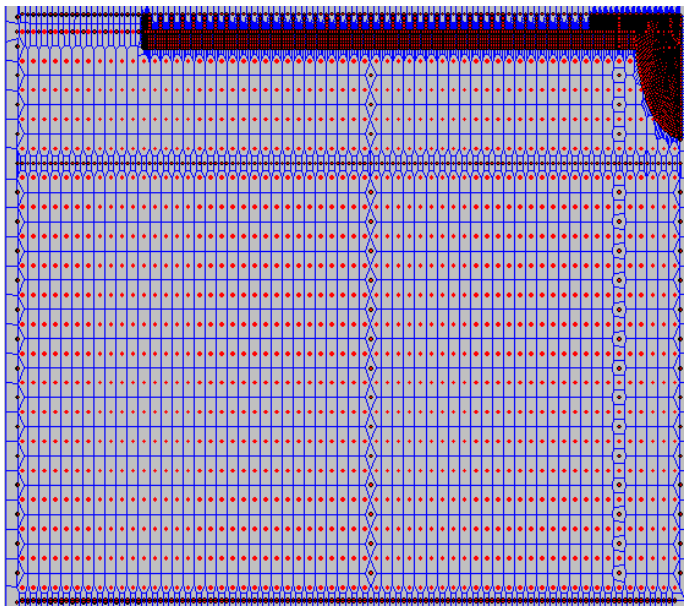

Figure 108 *Mesh used for the numerical simulations with TOUGH2 and TOUGH2-MP, the mesh consists of 6300 nodes.*

A detail of the mesh close to the bentonite plug is shown in Figure 109. The mesh is coarser in the less permeable domains like the host rock than in the bentonite and in the access drift domain. The source term was integrated by means of small volume elements all around the cell domain.

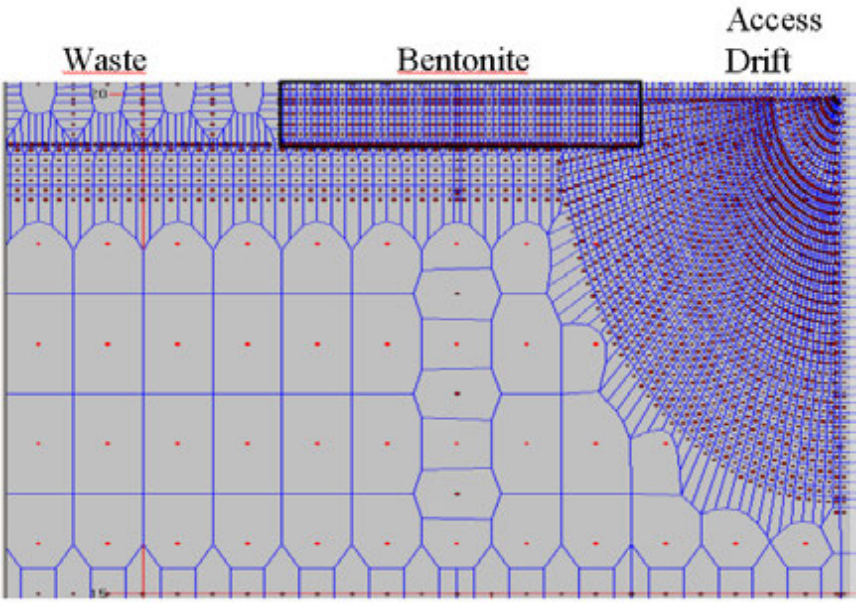

Figure 109 *Detail of the mesh (6300 elements) in the common region of the EDZ, bentonite and access drift. The differences in sizes of the nodes for the different materials are noticeable.*

In the Figure 110 a detail of the layer in the interface facing the cell is shown. Originally there were two layers in the interfaces facing the plug and the canister but due to numerical problems it was reduced to one layer as it can be seen in Figure 110. In this picture it can be seen that special care had to be taken in order to be able to represent exactly the volume of the elements in the interface. As shown in Figure 84 in TOUGH2 the mesh (Voronoi mesh) are created starting from the nodes after drawing the perpendicular to the nodes and taking the middle point between the two nodes. With this method and to fulfil the requirements of the prescribed volume of the interface the nodes in the interface have to be defined exactly with the same horizontal coordinates.

In order to check the areas of the material domains (cell, drift, bentonite, interface, etc.) scripts were created. These scripts allow calculating the sum of the volumes of all nodes, which have the same material properties and then they compare it with the specifications. As explained before the way of creating these mesh elements creates some differences in the effective volume elements for a given material. For big volumes it does not make a big difference but for small volumes like for the interface can be critical. One of the objectives of this exercise is to study whether the changes in the dimensions of the interface affect indeed the results. In which case, as the dimensions of the interfaces are so small, the use of other values for the areas of the interfaces than the specified ones may produce different results.

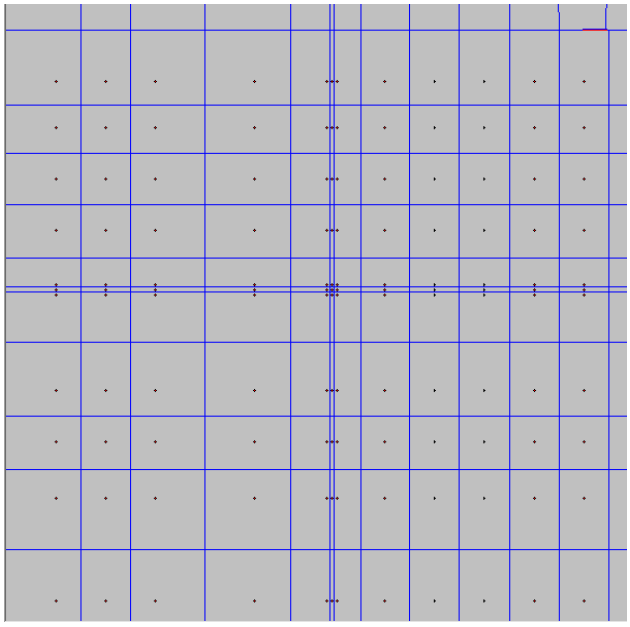

Figure 110 *Detail of the mesh close to the corner in the interface facing canister.*

The small volumes of the nodes, especially in the interfaces, may explain the numerical instabilities of some simulations; the volumes are in the order of 10^{-2} m^2. These volumes are situated in a region of wide change in the hydrological properties of the materials between the cell and the bentonite and thus some numerical convergence problems are expected.

The calculation time is affected by the refinement of the mesh for a 12000 nodes mesh the calculations took between 6 and 14 days (depending on the calculation case). For 6300 nodes it took from 2 to 7 days and finally for a 2500 nodes mesh it took from 1 to 3 days to complete the calculations. The following table shows the results of this sensitivity analysis.

Table 17 Different Meshes used for the calculations in the sensitivity analysis 6.

	Computation time (depending on the calculation case)
Mesh 1: 2500 nodes	1-3 days
Mesh 2: 6300 nodes	2-7 days
Mesh 3: 12000 nodes	6-14 days

In Figure 111 the mesh used for the calculations in this report is shown. The mesh consists of 2500 nodes and only a layer of mesh elements for the interfaces.

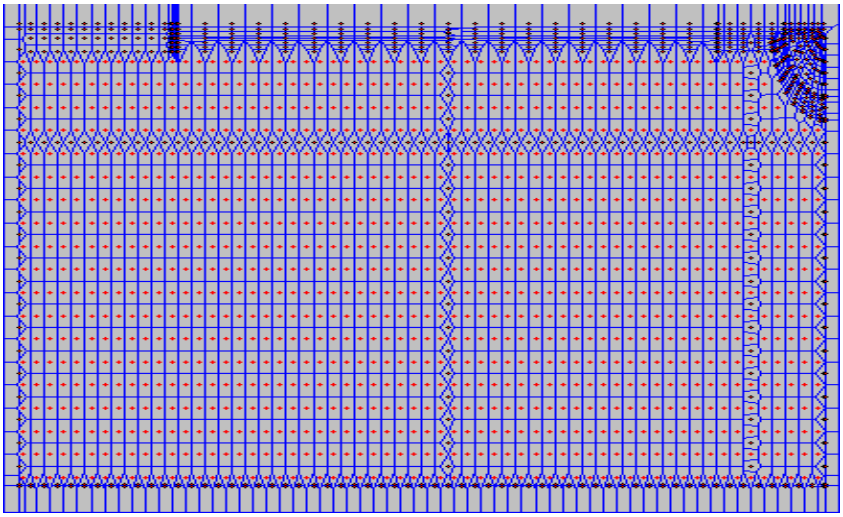

Figure 111 *Mesh consisting of 2500 nodes used for the calculations shown in this report.*

3.8.7 Additional Sensitivities

It is important to remark here that the calculations of ENSI were so performed that the gas was generated in a tiny layer of elements in the waste canister close to the interface. The elements were defined in such a way, that the gas flow was always perpendicular to the waste canister. In this way it was avoided the formation of a second interface with nodes belonging to the waste materials. ENSI made some calculations without this hypothesis and some differences in the results could be seen. This could also explain some differences between the different teams.

In this sensitivity case the permeability of the tiny source elements around the waste canister was reduced with respect to the value used in the reference case (in which case the permeability of the canister is the same as the one of the interface) to a new value of 10^{-25} m^2. The results of this analysis together with the results of the reference case are shown in the next picture. The results show that there is a decrease in the gas pressure at the beginning in comparison with the results for the reference case and then for times after 1'000 years the pressure becomes higher than the one in the reference case.

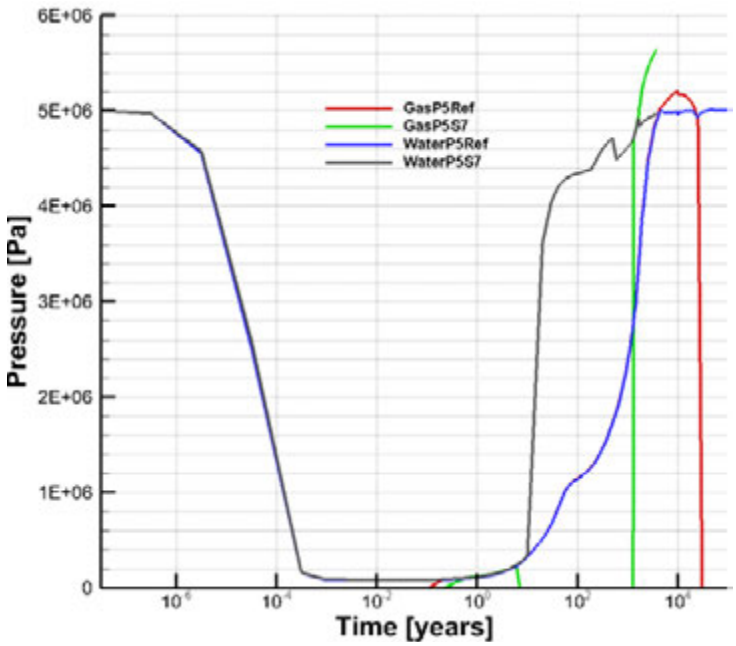

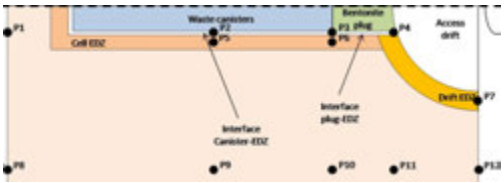

Figure 112 *Gas und water pressure in point 5 for the sensitivity case 7, in which the permeability of the elements of the source term in the waste canister is Kwaste=10^{-25} m^2. The results are compared with the ones of the reference case.*

3.8.8 Conclusions

The results and the numerical convergence of the simulations are affected by the presence of an interface close to the waste canister. The implementation into the code of these tiny elements in the interface has to be performed carefully; otherwise the results or its convergence can be affected.

The results of the two benchmarks show that in order to obtain a good convergence of the results an adequate mesh has to be used, what means adequate depends on the problem. For the first exercise it was seen that a mesh with 12'000 elements was too fine and finally a mesh with 2'400 elements was used.

A lot of work of ENSI was dedicated to install and compile TOUGH2-MP, to the modification of the code, to the acquisition and adaptation of a mesh program, to the creation of the respective input and finally to the control of the instabilities of the simulation. An important part of the work was also dedicated to the post processing of the results. On the one hand there were many results to process specially for the second benchmark with outputs of size of about 20 GB and on the other hand many of the results could not be obtained directly from the output of the code but by means of scripts or modifications of the code.

From the results of the two benchmarks it can be concluded that the interface and the EDZ represent the main pathway for the migration of the hydrogen to the drift in these conceptual models. The hydrogen is transported mainly in gas form and through the interface and EDZ to the drift.

The implementation of the expression for the relative permeability as specified in the exercise caused many convergence problems. These problems disappeared using the original expression used in the TOUGH2/TOUGH2MP code.

The gas mass flow toward the drift increases with a low permeable EDZ (sensitivity 1). Increasing the diffusion coefficient of dissolved hydrogen by a factor 10 (sensitivity 3) decreases the gas mass flow rate toward the drift in this conceptual model.

The results of the different teams are in general similar and in the same order of magnitude. In the case of pressure and saturation the differences in the values were not very important and the differences could be explained due to the various approaches and simplification taken in the model. Less clear are the

differences in the values of the mass flow rates that could not be explained only by the use of different approaches and simplifications.

3.8.9 Issues for further consideration

The results of the calculations were not compared to measurements coming from laboratory or field experiments and therefore the results cannot be seen as the definitive behaviour of the gas in a geological repository but as reference for the order of magnitude of what in principle the measurements should provide. ENSI would like to remark here the importance of the combination of numerical results with measurements in order to understand correctly the processes occurring in the underground.
Another important point in opinion of ENSI is the explanation of the differences obtained by the different teams in the values of the mass flow rates. More effort should be made in this aspect in order to be able to explain these differences.

3.8.10 References

1. Wendling, J., et al., *FORGE WP1.2: First step toward a benchmark for 3D Modelling of a disposal area for vitrified waste*. 2010, Euratom 7th Framework project: FORGE 2010.

2. ENSI, *Sachplan geologische Tiefenlager, Etappe 1: Gasproduktion, Gastransport und deren Folgen für das SMA-Lager*, M.L. Sentis and A.-K. Leuz, Editors. 2012, Eidgenössisches Nuklearsicherheitsinspektorat: Brugg.

3. Pruess, K., C. Oldenburg, and G. Moridis, *TOUGH2 USER'S GUIDE, VERSION 2.0*. 1999, Lawrence Berkeley National Laboratory: Berkeley, California.

4. Zhang, K., Y. Wu, and K. Pruess, *User's Guide for TOUGH2-MP, A massively Parallel Version of the TOUGH2 Code*. 2008, Lawrence Berkeley National Laboratory.

5. Narasimhan, T.N. and P.A. Witherspoon, *An integrated finite difference method for analyzing fluid flow in porous media*, in *Water Resources Research*. 1976. p. 57-64.

6. Narasimhan, T.N., P.A. Witherspoon, and A.L. Edwards, *Numerical model for saturated-unsaturated flow in deformable porous media, part 2: the algorithm*, in *Water Resources Research*. 1978. p. 255-261.

7. Pan, L., *Users Manual for WinGridder V2.0*. 2001, Lawrence Berkeley national laboratory.

3.9 NWMO contribution

3.9.1 Introduction

Geofirma Engineering Ltd. conducted the cell-scale benchmark modelling on behalf of the Nuclear Waste Management Organization (NWMO) in Canada.

3.9.2 Model Implementation

3.9.2.1 Code and Formulation

T2GGM (Quintessa and Geofirma, 2011 [1]), a modified version of TOUGH2 v2.0 with optional gas generation model, was selected as the two-phase flow modelling code. The gas generation model (GGM) capabilities were turned off, and TOUGH2-MP was not used. TOUGH2 is a general-purpose numerical simulation program for multi-phase fluid and heat flow in porous and fractured media developed by Lawrence Berkeley National Laboratory (Pruess et al. 1999 [2]). The EOS3 equation of state module used in T2GGM simulates the transport of a single separate gas phase in water (note that T2GGM allows for specification of alternate gases to air, the EOS3 default). EOS3 also models the transport of dissolved gas in water by diffusion and advection. Dispersive processes are not modelled.

Two minor modifications were made to the T2GGM code to facilitate the benchmark modelling studies:

- Time-dependent Dirichlet boundary conditions were added based on the implementation within TOUGH2-MP. TOUGH2-MP only allows for time-dependent pressure changes (assuming saturation and temperature remain constant), while this new implementation allows both time-dependent pressure and saturation as required by the benchmark specification.
- A new time-stepping scheme, based on the scheme within TOUGH2-MP with minor modifications, was implemented. This time stepping scheme allows for smaller increases in time step (when the simulation converges within a specified number of iterations) and smaller decreases in time step (when the simulation does not reach convergence within the maximum number of iterations). The scheme also minimizes the occurrence of oscillations between time step increases and decreases (e.g. when a time step decrease results in a time step solving within the specified number of iterations, this causes a subsequent time step increase that cannot be solved, requiring the time step to be decreased etc.) by preventing time step increases for five time steps following a reduction in time step.

mView, developed by Geofirma Engineering, was used for pre- and post-processing.

3.9.2.2 Grid

Please note that the benchmark defines the model domain in the negative X and negative Y quadrant, but the models described here are defined in the positive X and positive Y quadrant. X, Y and Z axes are assumed as usually defined, with the Z axis representing the vertical axis. The central axis of the cell is defined along the X axis, with the origin in the middle of the access drift.

A 2D grid was developed, with both radial and rectangular components within the 2D grid. Block volumes and connection areas were calculated by rotating the 2D grid around the X axis, effectively including the full 3D volume of the model domain. Figure 113 shows the overall grid discretization, and Figure 114 shows a detail of the grid discretization near the bentonite plug. The grid has 3391 nodes, with grid refinement around the interface area. The irregular nature of the grid allows for grid refinement only where required.

Originally, a simple 2D radial grid with rectangular discretization was developed. With rectangular discretization, the discretization in the X and Y directions is fixed, resulting in small grid blocks where not required. Simulations with this grid encountered significant stability issues unless diffusion was removed. The final model grid was developed to alleviate potential gridding issues resulting from transitions from small to large block sizes, which is exacerbated in a rectangular grid by the fixed X and Y discretizations, resulting in grid refinement in areas where it is not required. It should also be noted that the irregular grid of the final model grid does not strictly adhere to the TOUGH2 integral finite difference requirements; some

nodal connections are not perpendicular to the connection area, resulting in shorter connection distances for these connections. The impact of these inaccuracies is expected to be small, and this is confirmed by the comparison of results between the two grids for the no diffusion case, see Figure 115. In this figure, note that the gas flows greater than the generation rate are due to gas flowing into the model from the access drift boundary before year 10. Integration of gas flows confirms that the quantities of gas are consistent.

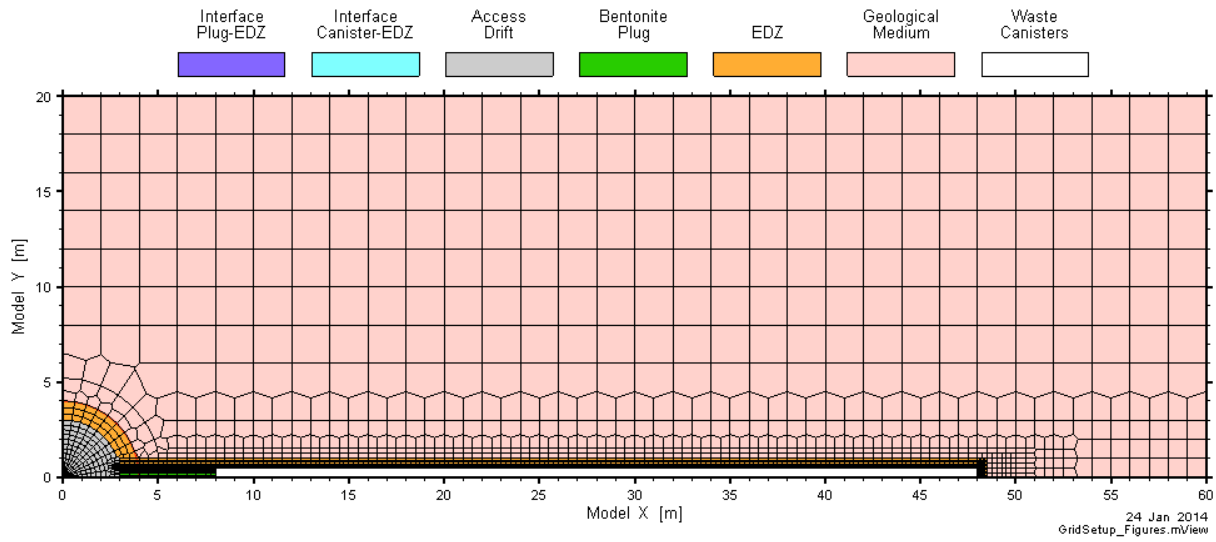

Figure 113: Grid discretization

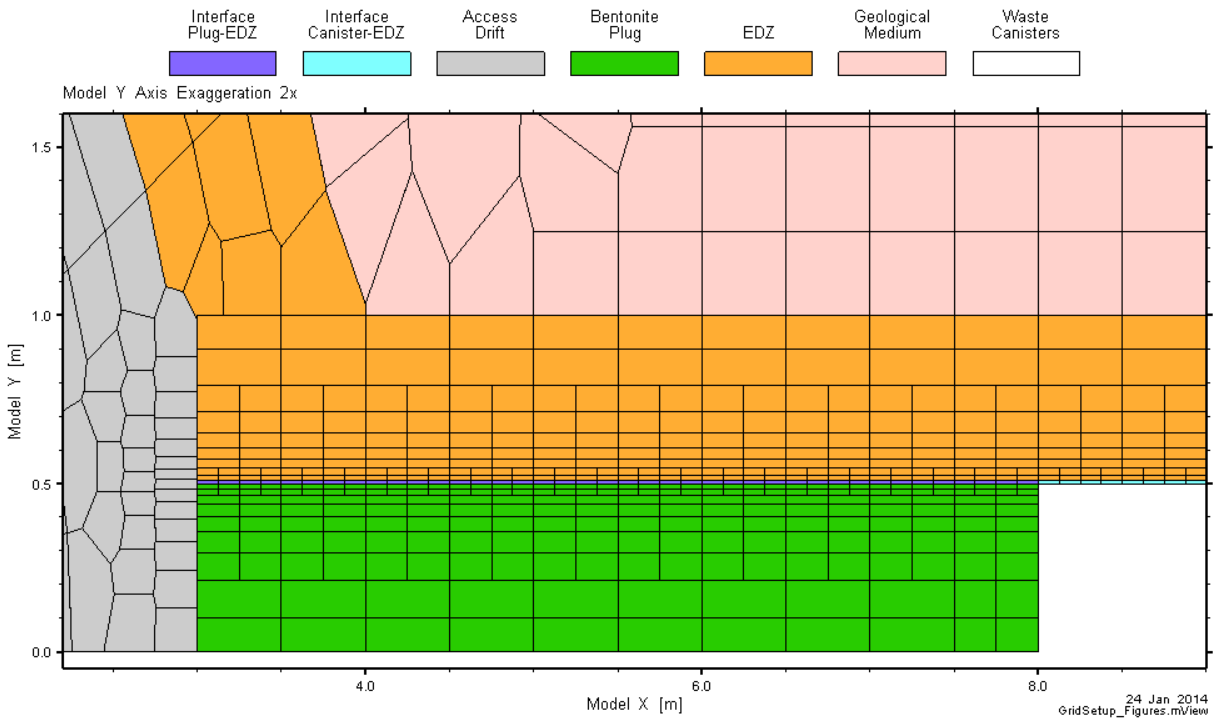

Figure 114: Detail of grid discretization around the bentonite plug

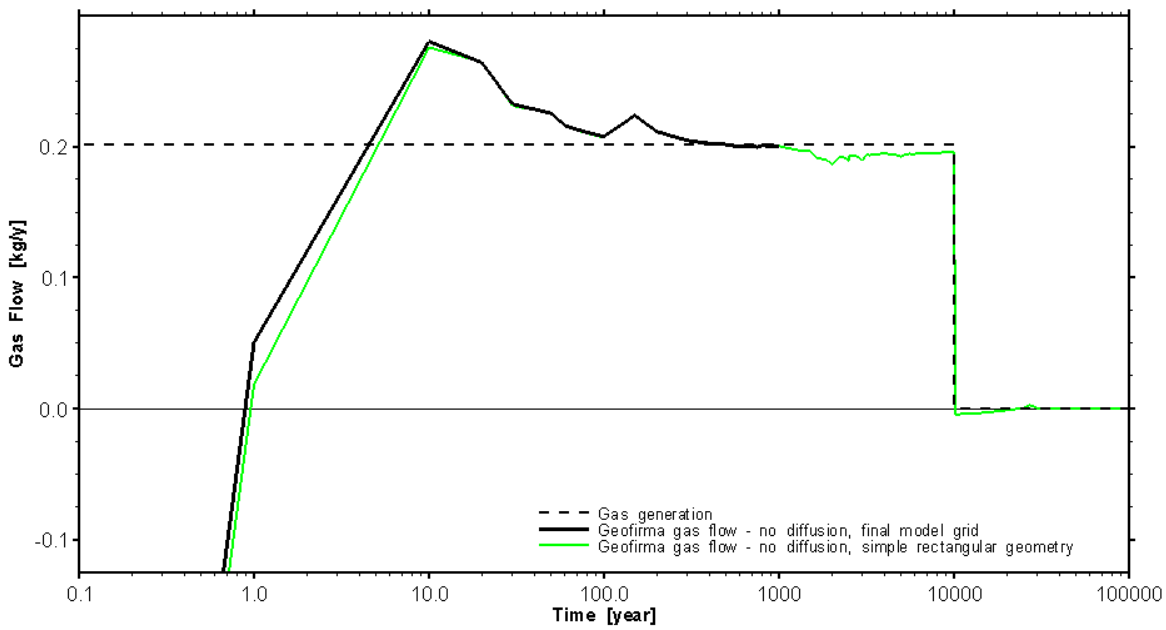

Figure 115: Comparison of final model grid and simple rectangular model grid gas flows through the access drift for the base case with no diffusion.

3.9.2.3 Boundary Conditions and Sources

The benchmark specified H_2 gas to be generated at the surface of the waste containers, with the waste containers specified as a no-flow feature. Gas is generated at a rate of 100 mol/year for the first 10 000 years, with no gas generation after 10 000 years. As the waste containers were not included in the model, gas generation was specified at the nodes immediately adjacent to the waste container, mainly the interface between canister/EDZ and the bentonite plug nodes adjacent to the waste container. The generation term was proportioned between nodes according to connection area between the generation node and the waste container.

The access drift boundary condition was provided as a water pressure and water saturation curve. As the TOUGH2 inputs require a gas pressure curve, gas pressures were calculated using the van Genuchten parameters for the access drift backfill. The resulting gas pressure curve had a few small bumps which were smoothed out to improve numeric stability.

3.9.2.4 Deviations from the specification

A limitation of a 2D model discretization is the specification of anisotropic permeability for the plug-EDZ interface, EDZ and geologic medium is inaccurate. In the 2D model grid, all connections are horizontal (in the XY plane), and therefore anisotropic media is represented solely by their horizontal permeability, which is half an order of magnitude greater than the vertical permeability. Results are therefore conservative, resulting in faster transport of gas and water away from the cell (radially, which includes both horizontal and vertical components) than would be represented by an anisotropic model representation. However, transport along the cell in the x-direction, which model results presented below suggest is the primary direction of transport, is correct. Due to the small difference in horizontal and vertical permeabilities, the differences are expected to be small. Many of the other modelling groups also used 2D models, and therefore were unable to represent the anisotropy of the system.

Another deviation from the benchmark is the relative gas permeability model. The benchmark defines the relative gas permeability using the Mualem model:

$$k_{rg} = (1 - S^*)^{1/2}(1 - S^{1/m})^{2m} \qquad \textit{Equation 8}$$

However, the modified van Genuchten model option in T2GGM, used in the models presented here, is the Luckner model, identical to the Mualem model except the 1/2 exponent is replaced by a 1/3 exponent:

$$k_{rg} = (1 - S^{*})^{1/3}(1 - S^{1/m})^{2m} \qquad \textit{Equation 9}$$

A comparison between relative permeability curves is shown in Figure 116.

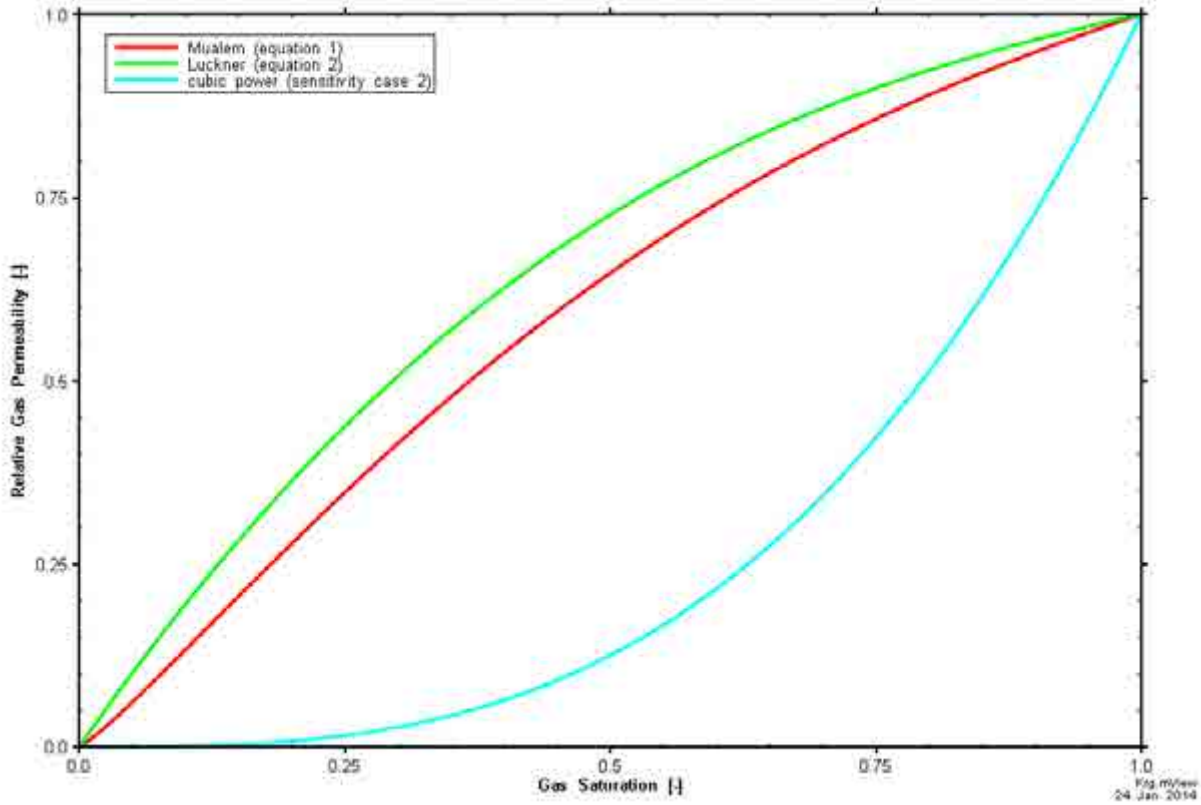

Figure 116: Relative gas permeability curves for the EDZ/Rock (n=1.5) represented by the benchmark and T2GGM

Stability issues were encountered for the final model grid. Stability was improved by adding a residual gas saturation in the EDZ of 10^{-6}, minimizing oscillations of phase generation and disappearance that can occur.

3.9.3 Base Case Results

Gas and water pressures are shown for various times in Figure 117 through Figure 123. Gas saturations and dissolved gas mass fractions are shown in Figure 124 through Figure 130. Each plot shows empty space within the canisters, and a ring defining the outer limits of the access drift. Note that for gas pressures, empty space is also shown in areas where gas is not present (and therefore there is no gas pressure). Note that some of the contours appear jagged or wavy; this is entirely due to the grid discretization.

By 1 year, gas has migrated out of the interface and into the EDZ surrounding the cell. Gas generated in the cell primarily migrates through the interface and EDZ towards the access drift, and is removed out of the access drift boundary condition. Gas also migrated slowly out into the host rock, with gas saturations reaching their peak at 10 000 years (the time at which gas injection stopped). At this time, the interface was almost completely saturated with gas (gas saturation > 0.999), the maximum gas saturation in the EDZ was 0.05 and free phase gas spread approximately 0.5 to 1 m into the host rock (beyond the EDZ), at very small saturations (less than 0.002).

The low initial pressures within the cell reduced pressures out into the host rock. These low pressures are almost dissipated by 10 000 years, and gas pressures begin to exceed initial undisturbed water pressures (5 MPa). The maximum gas pressure reached was 5.7 MPa in the bentonite plug adjacent to the canisters. This maximum occurred at 10 000 years, the time at which gas injection stopped. Water pressures returned to initial undisturbed conditions (5 MPa) by approximately 20 000 years.

Over the course of the simulation, dissolved gas migrates out away from the cell into the host rock and towards the access drift. This migration of dissolved gas is diffusion dominated, as water flows towards the cell from the host rock, rather than away from the cell. In the first 100 years, initial dissolved gas is removed from the access drift by the access drift boundary condition and dissolved gas near the cell has not migrated far enough out to reach the access drift. By 1000 years, the access drift is full of dissolved gas generated from the cell. By the end of the simulation, dissolved gas continues to migrate towards the access drift, with the greatest concentration of dissolved gas near the access drift boundary condition.

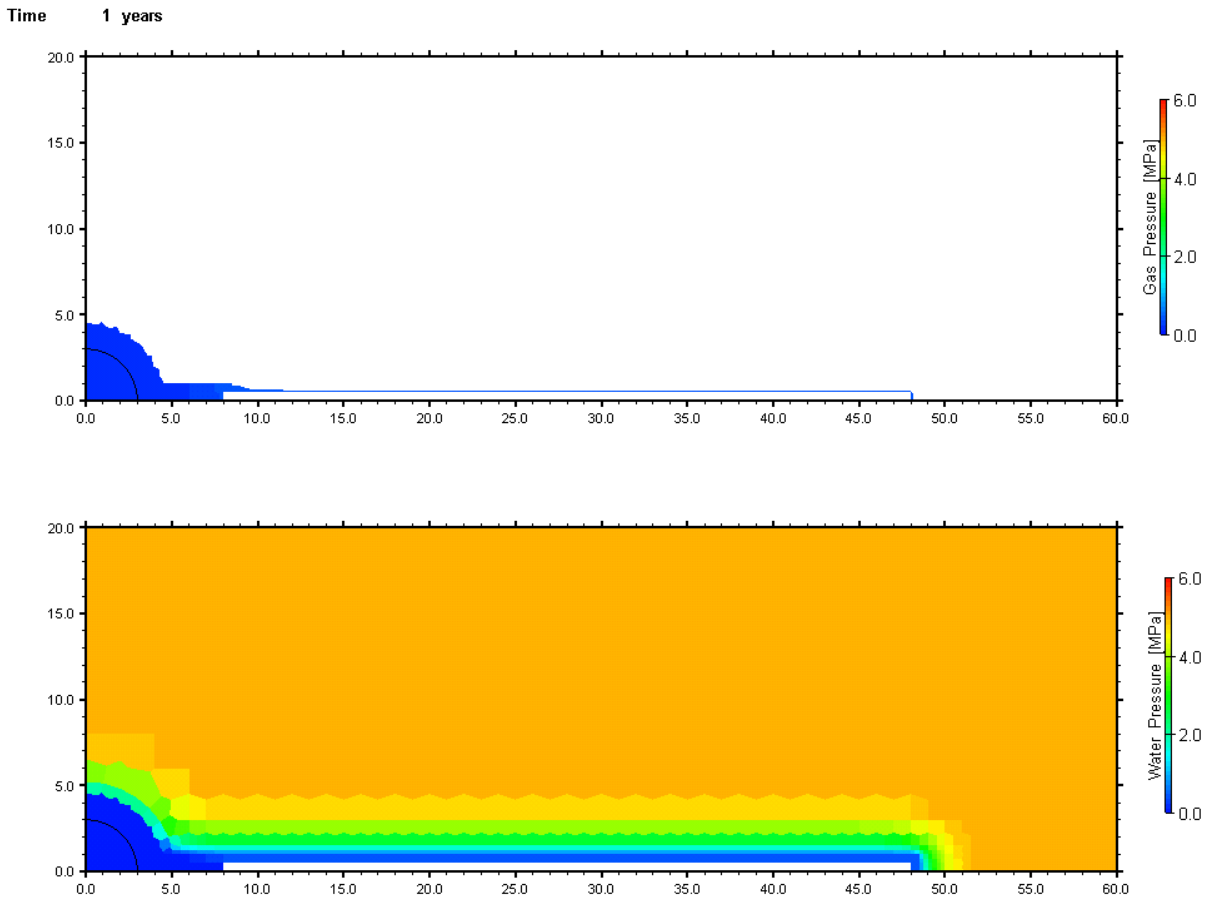

Figure 117: Gas and water pressures for the base case at 1 year

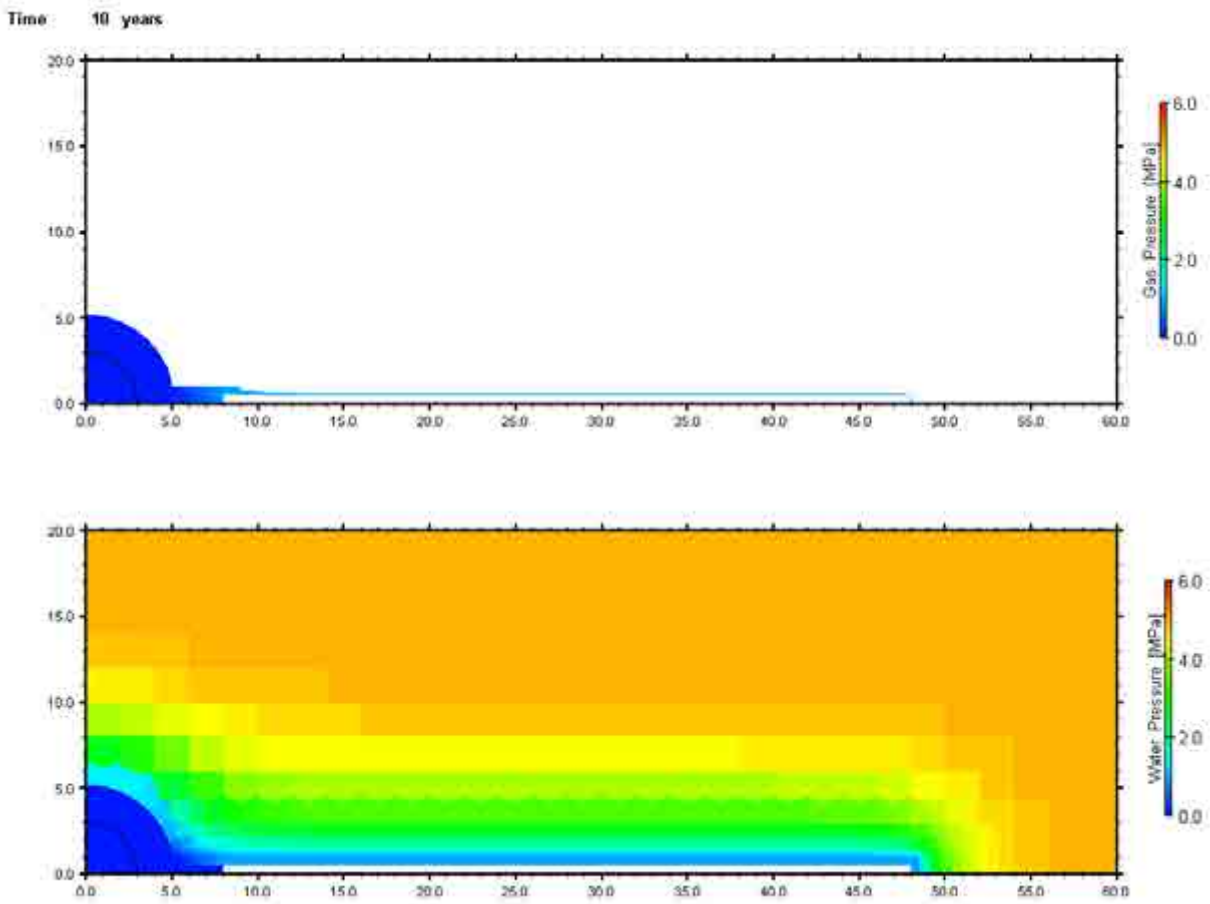

Figure 118: Gas and water pressures for the base case at 10 years.

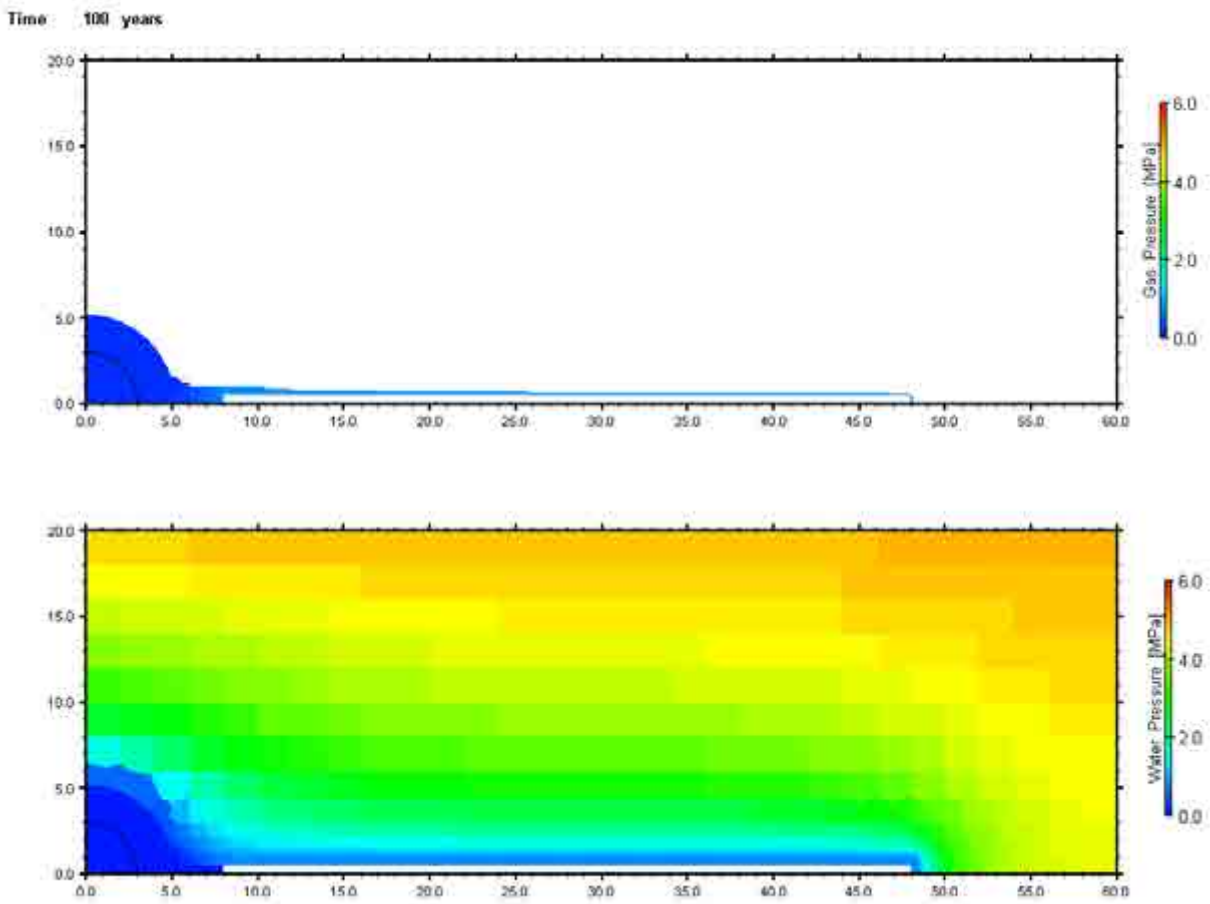

Figure 119: Gas and water pressures for the base case at 100 years.

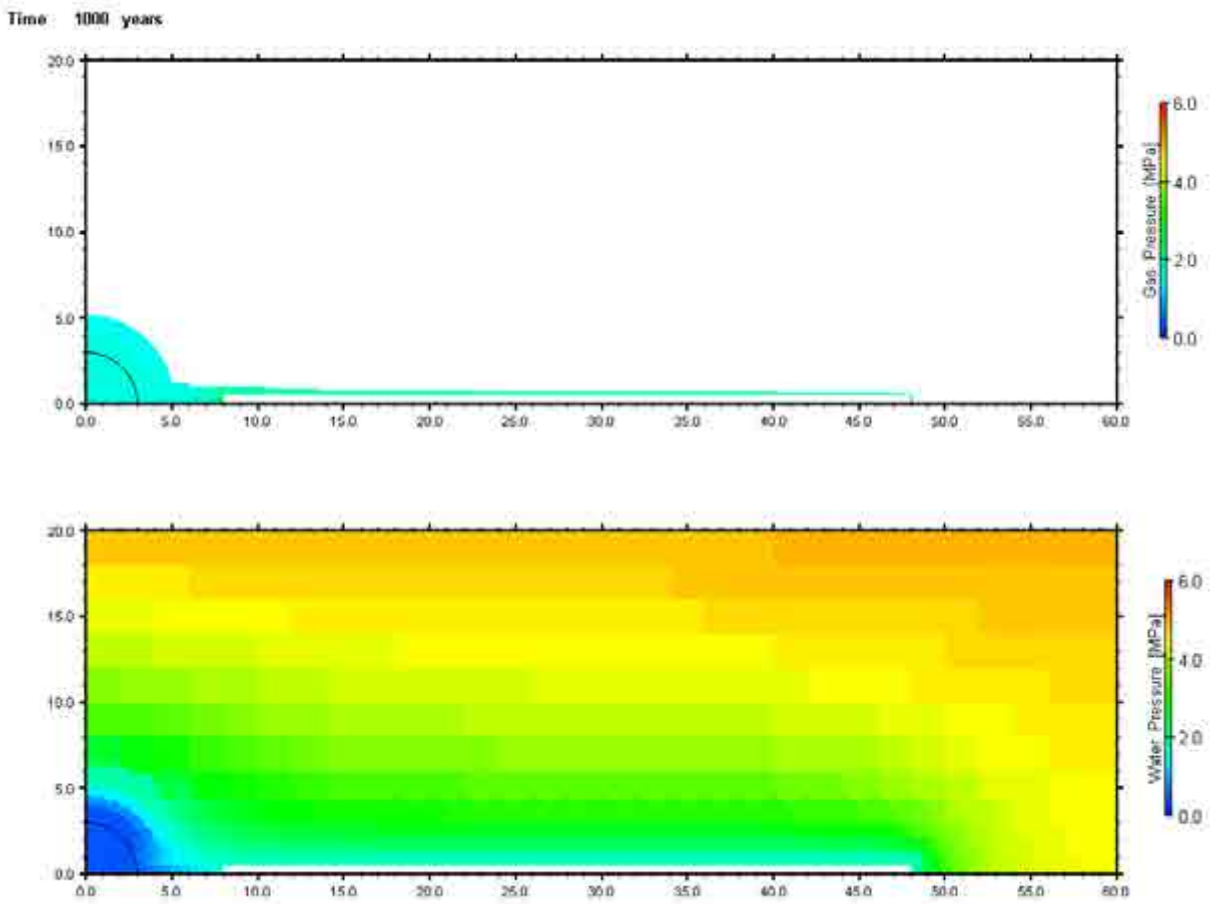

Figure 120: Gas and water pressures for the base case at 1000 years.

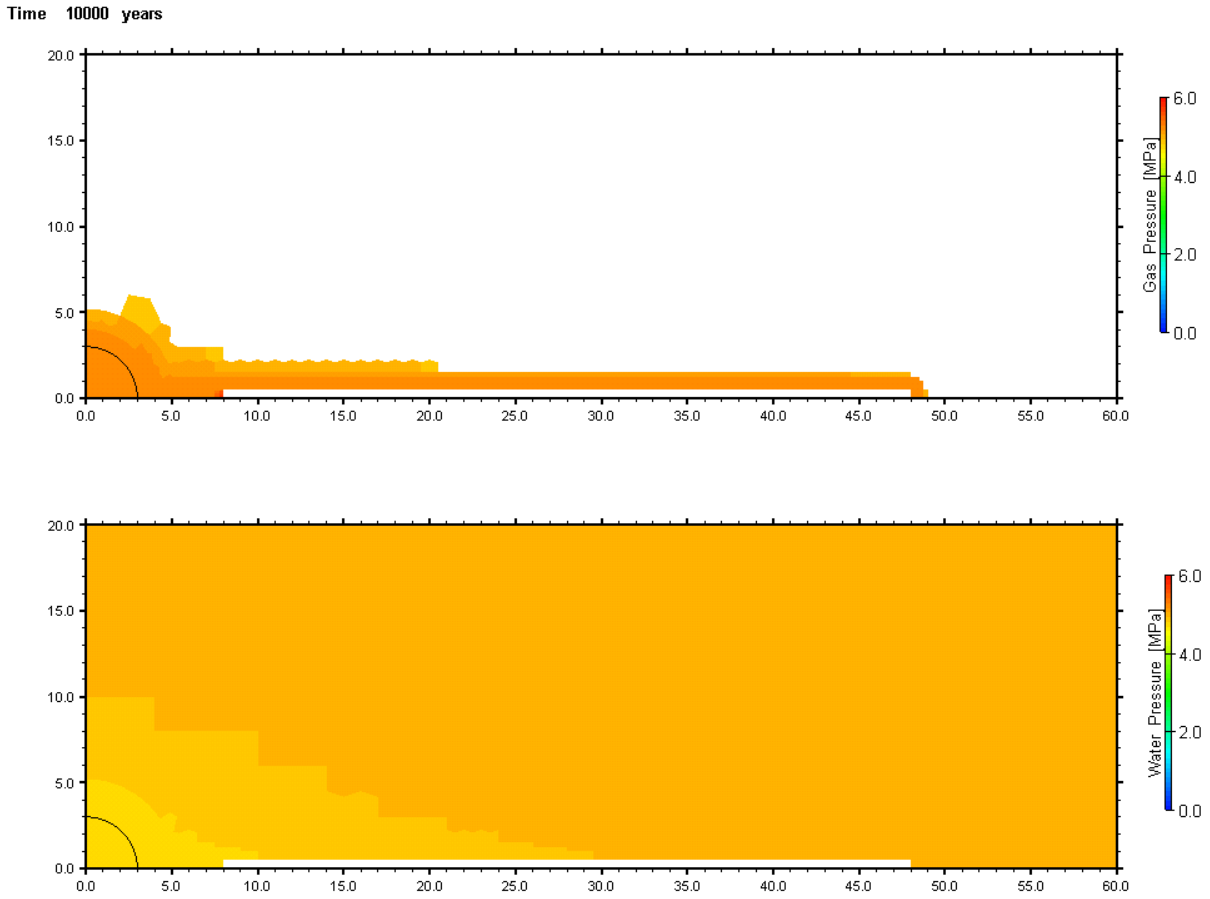

Figure 121: Gas and water pressures for the base case at 10 000 years.

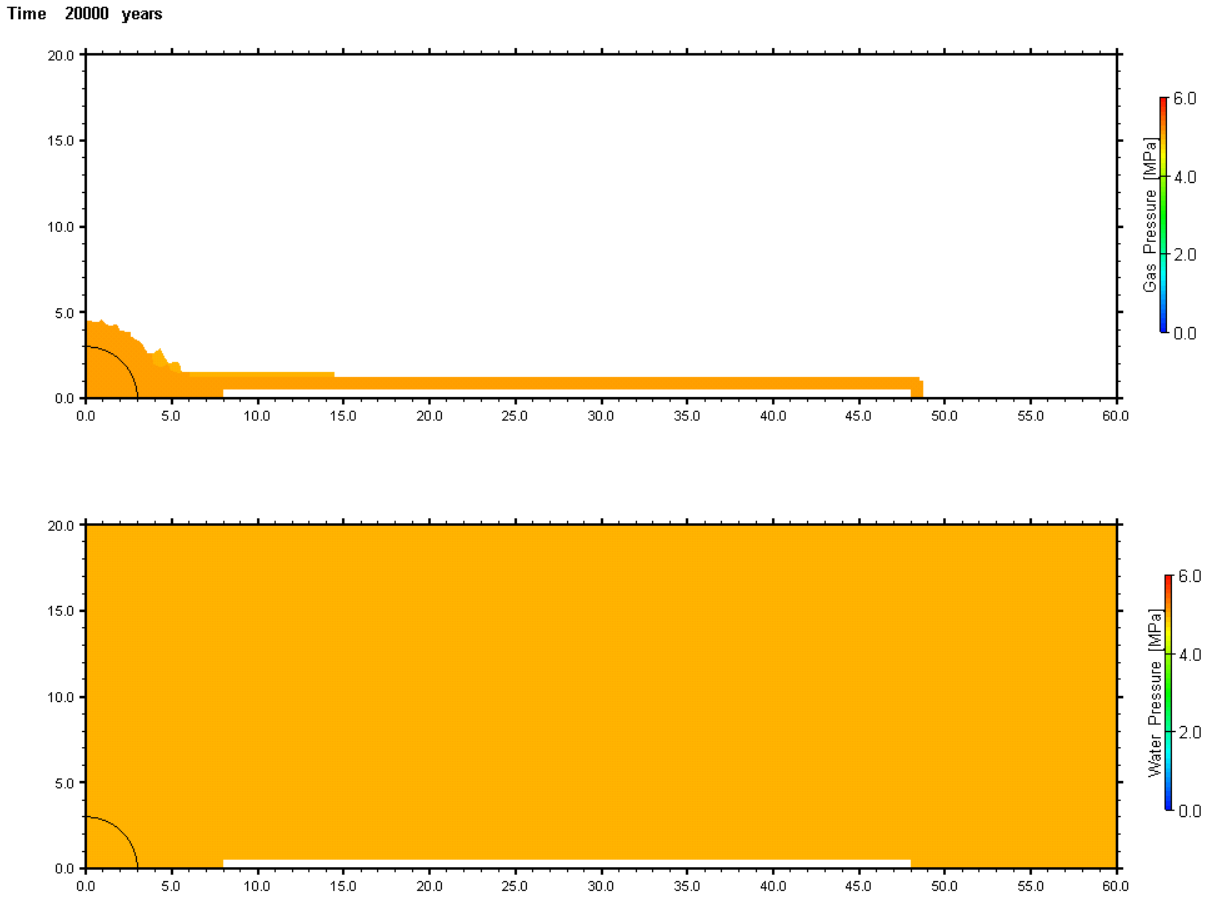

Figure 122: Gas and water pressures for the base case at 20 000 years.

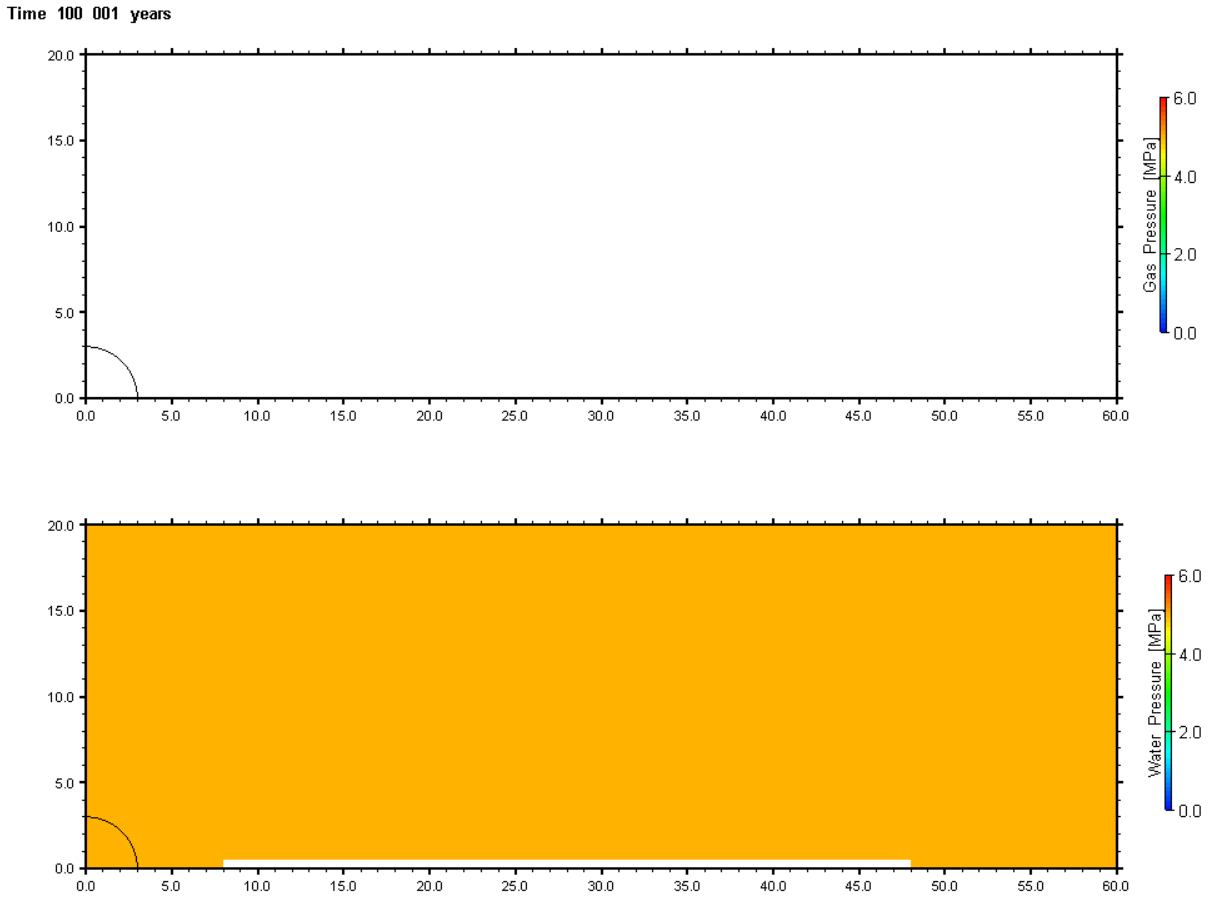

Figure 123: Gas and water pressures for the base case at 100 000 years.

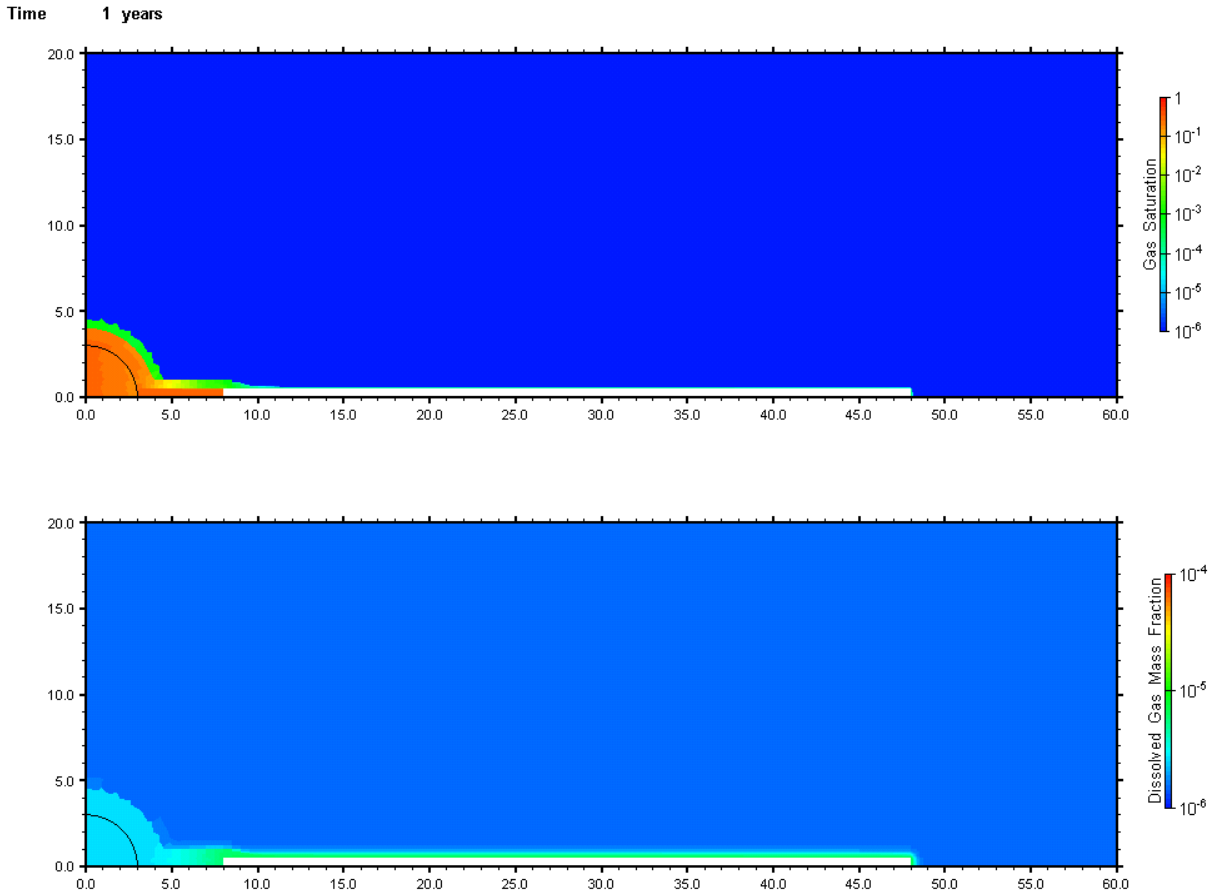

Figure 124: Gas saturations and dissolved gas mass fraction for the base case at 1 year.

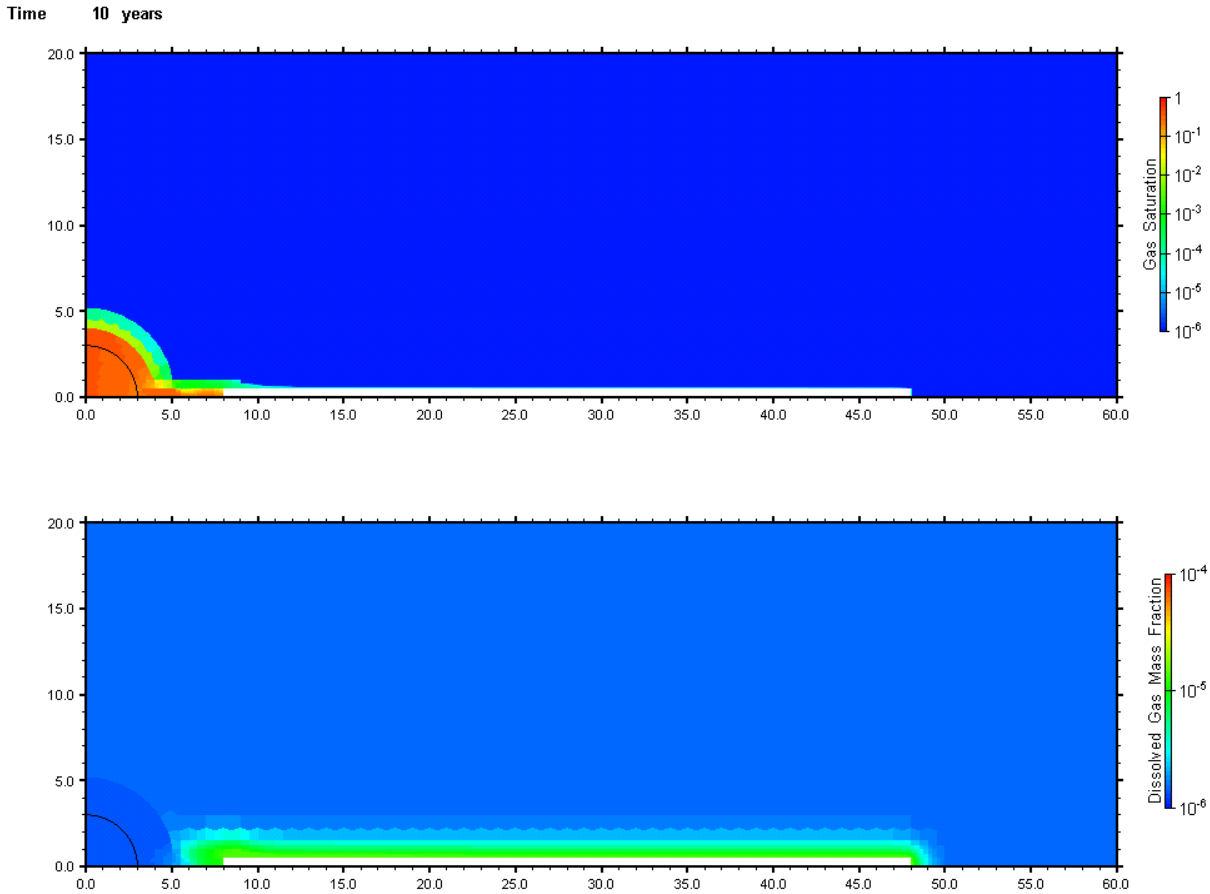

Figure 125: Gas saturations and dissolved gas mass fraction for the base case at 10 years.

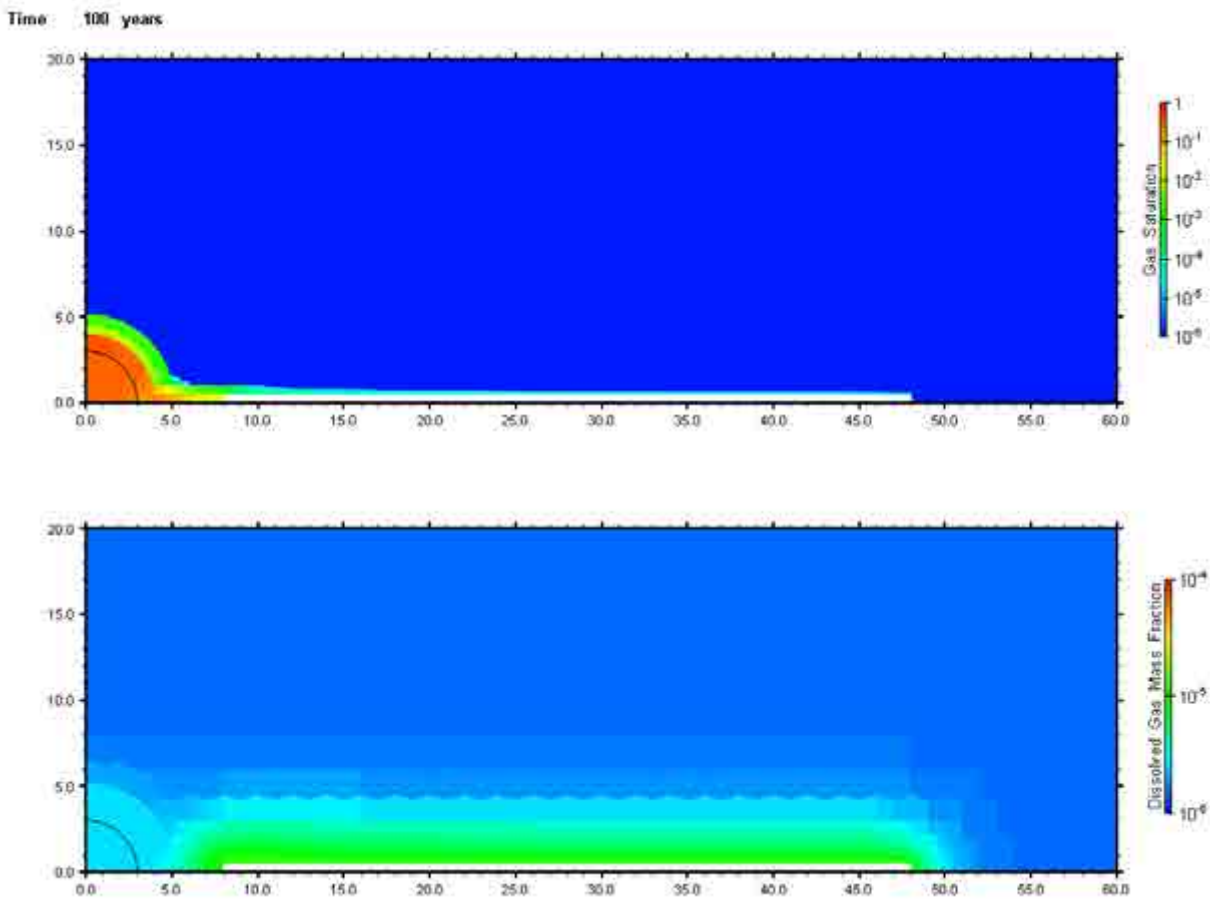

Figure 126: Gas saturations and dissolved gas mass fraction for the base case at 100 years.

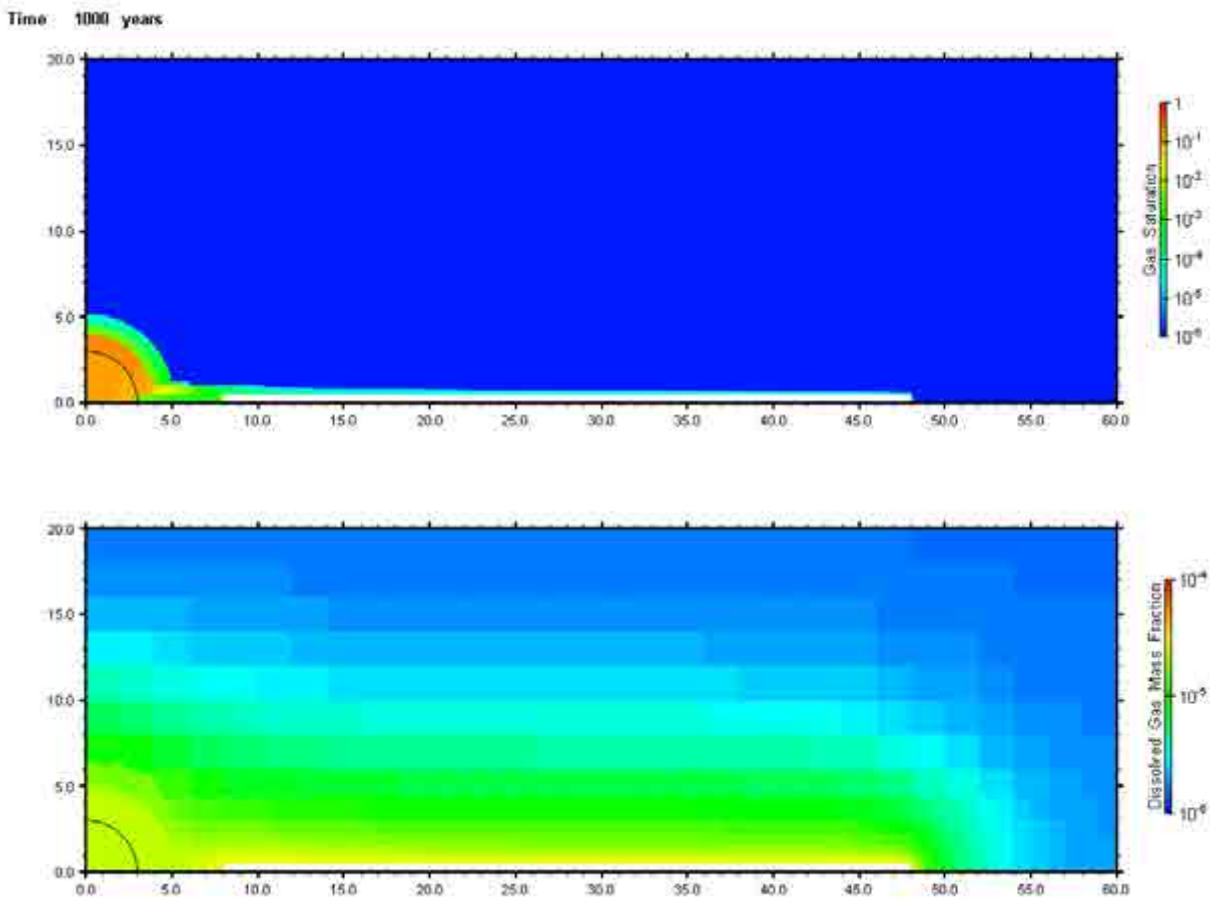

Figure 127: Gas saturations and dissolved gas mass fraction for the base case at 1000 years.

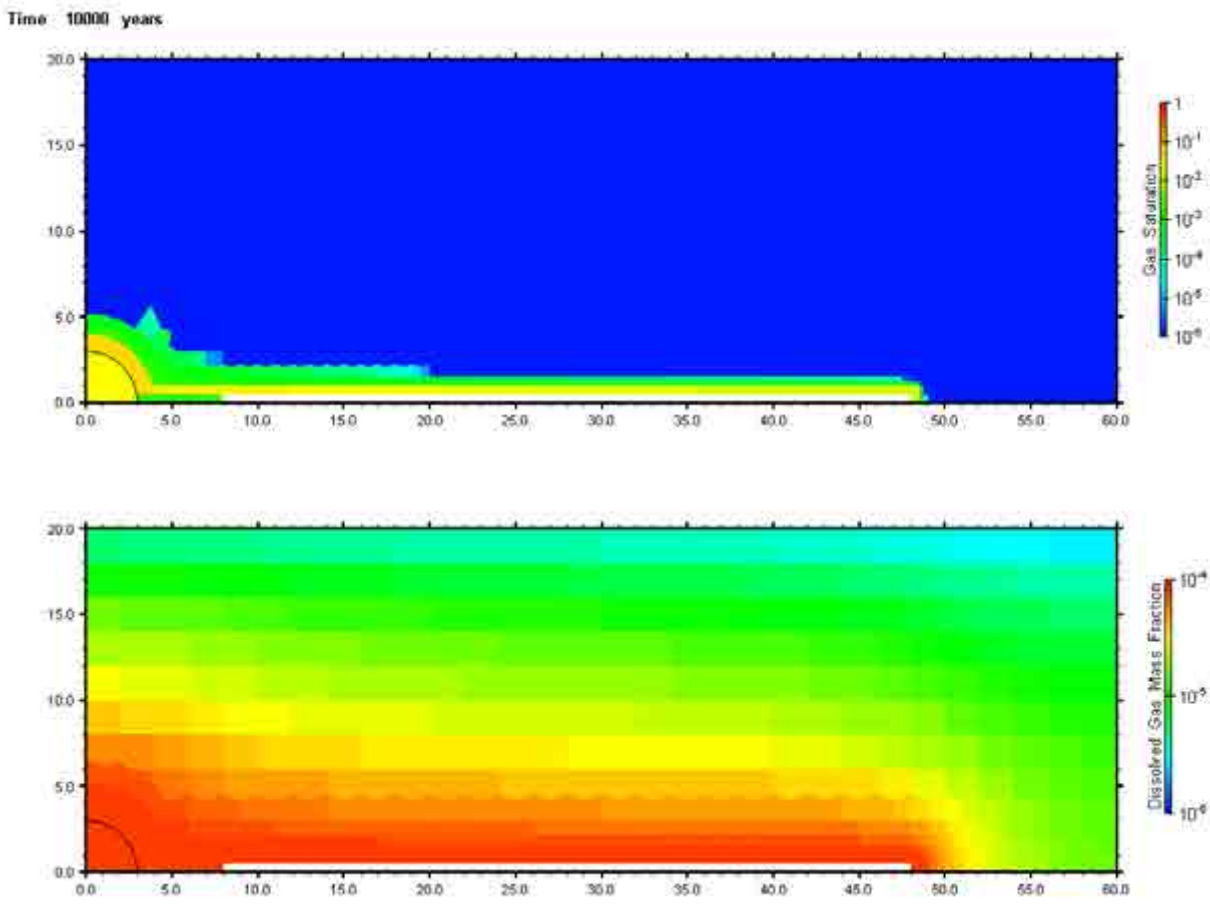

Figure 128: Gas saturations and dissolved gas mass fraction for the base case at 10 000 years.

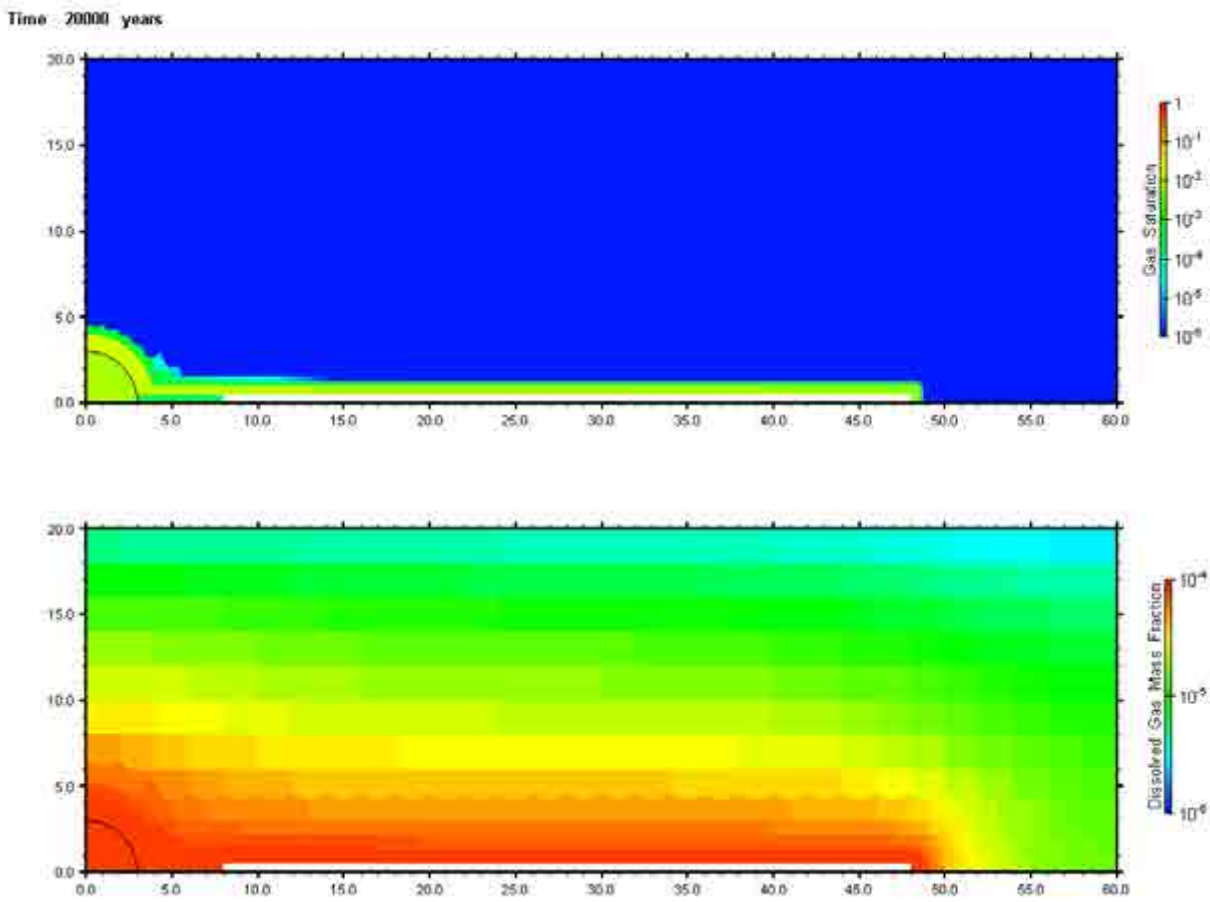

Figure 129: Gas saturations and dissolved gas mass fraction for the base case at 20 000 years.

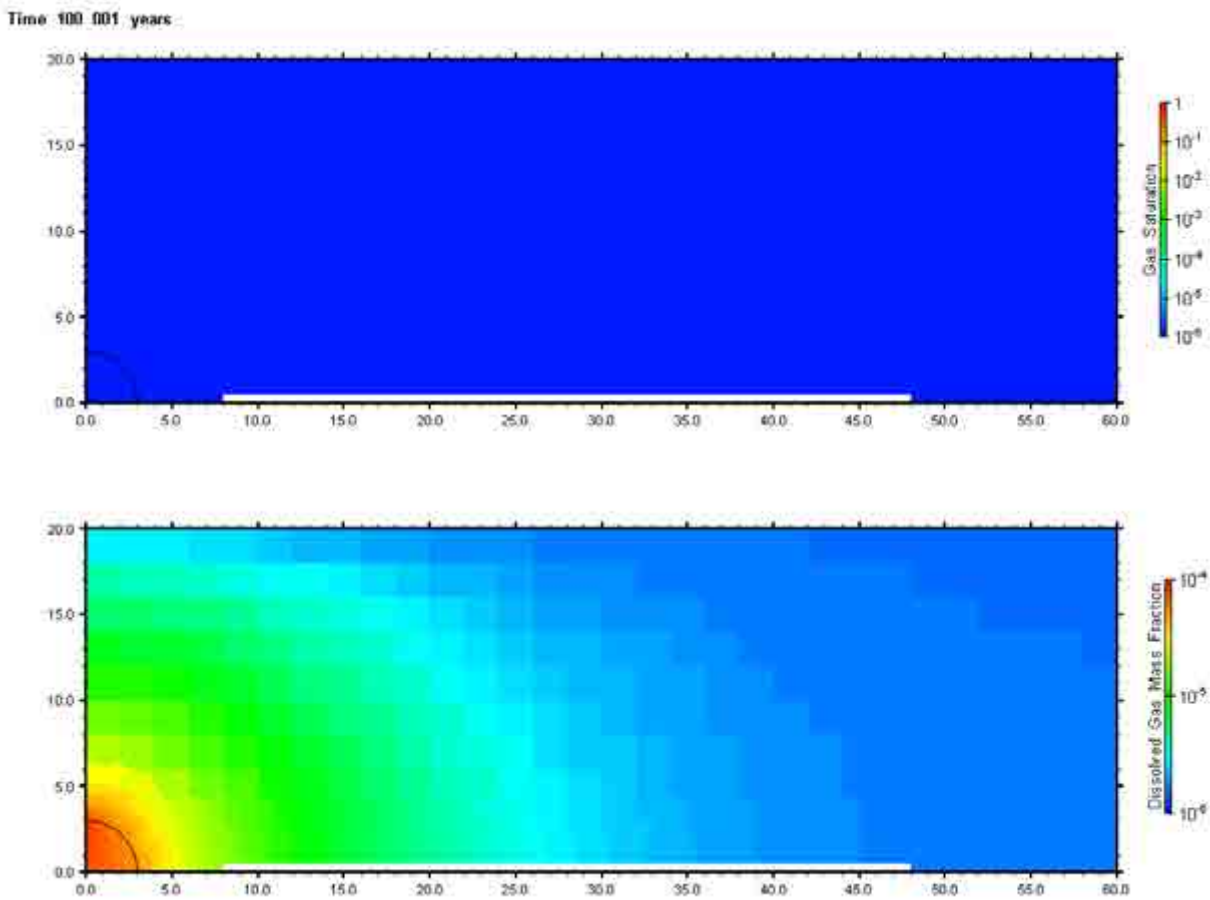

Figure 130: Gas saturations and dissolved gas mass fraction for the base case at 100 000 years.

Pressure time series at three points are provided in Figure 132 through Figure 134. The locations of these pressure points are shown in Figure 131, highlighted by red circles and lines.

The boundary condition at the access drift clearly dominates behaviour in the system: for the gas pressure curves at point 4 and point 5 (Figure 132 and Figure 133), the shape of the curve matches that of the pressure boundary at the access drift; as well, water pressures at point 5 (no gas present at point 5 at this time) matches those of the boundary by 2000 years.

Water pressure at point 4 increases slightly at 10 000 years, the time at which gas injection stops. This is a result of gas pressures matching the access drift boundary condition, and gas saturations in the interface decreasing very slightly since gas is no longer being generated in the cell (gas saturations at point 4 decrease from 0.999 at 10 000 years to 0.998 at 25 000 years), resulting in lower capillary pressures and consequently higher water pressures. This change in water pressure when gas generation stops is not observed by the other model groups; which suggests that they do not see the very small drop in gas saturation at point 4. This could be due to a number of differences between models such as grid discretization, differences in point 4 location, or relative gas permeability models.

Figure 135 shows the gas flow into the access drift, divided into cell components: bentonite plug, interface and EDZ. It can be seen that gas flow from the containers into the access drift is dominated by flow through the EDZ. While the interface is more permeable than the EDZ and contains a greater concentration of gas, the area of the interface is much smaller than the EDZ, resulting in a relatively small amount of flow. The bentonite plug flows are negligible compared to those in the EDZ and interface, due to lower permeabilities and higher air-entry pressures,

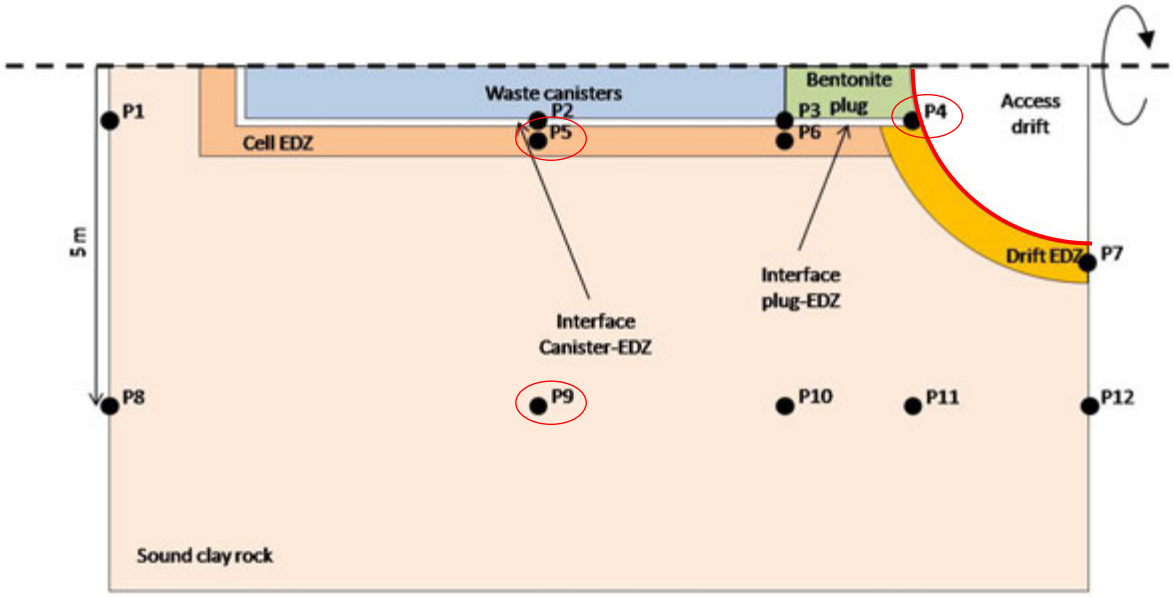

Figure 131: Location of pressure and flow time series. Points (point 4, 5 and 9) are circled in red, and the interface for the access drift flow is highlighted in red.

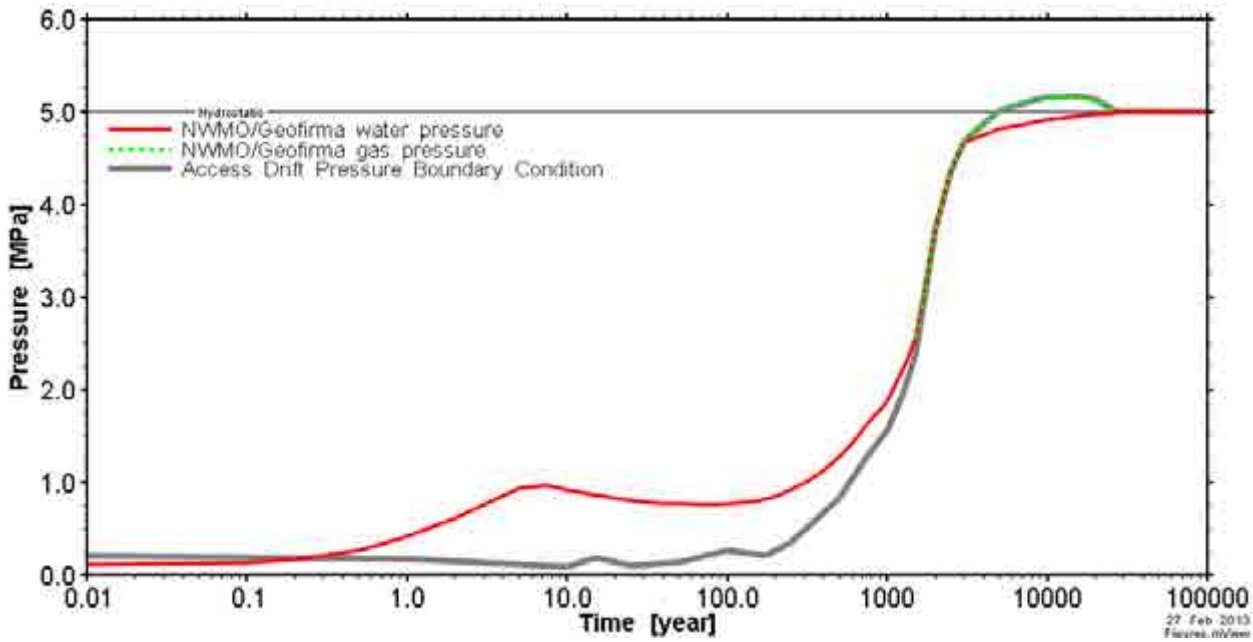

Figure 132: Base case water and gas pressures at point 5, located in the middle of the EDZ, half way along the canister.

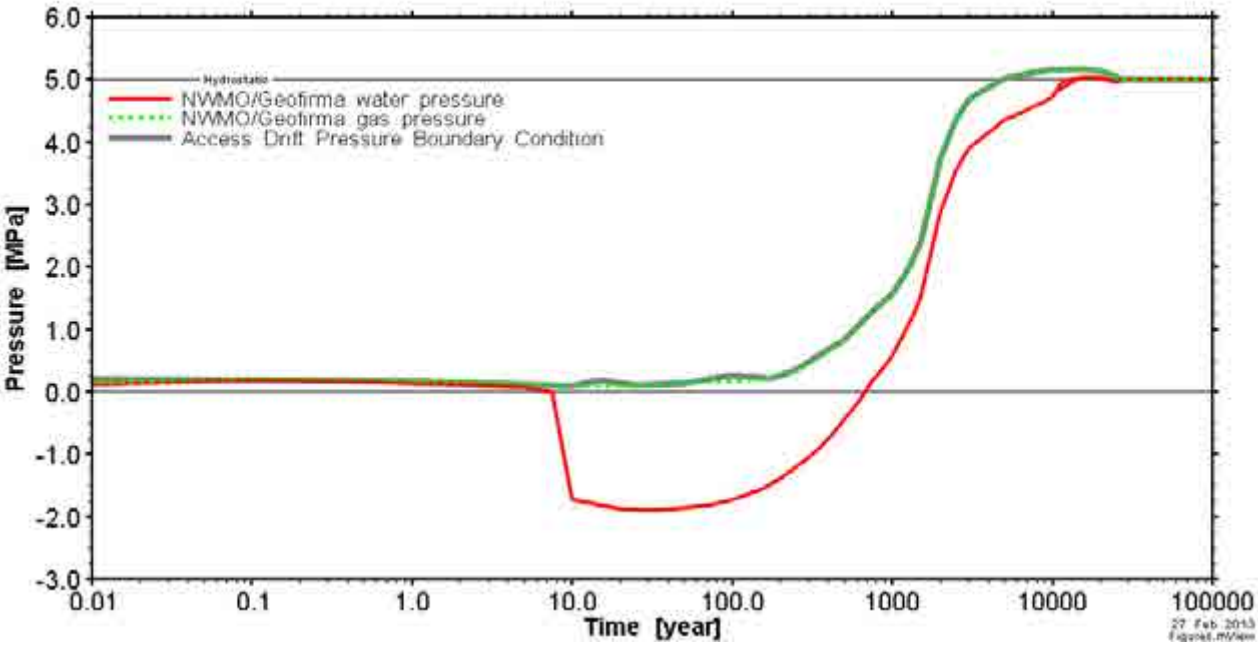

Figure 133: Base case water and gas pressures at point 4, located in the EDZ, at the intersection of the access drift and the bentonite plug.

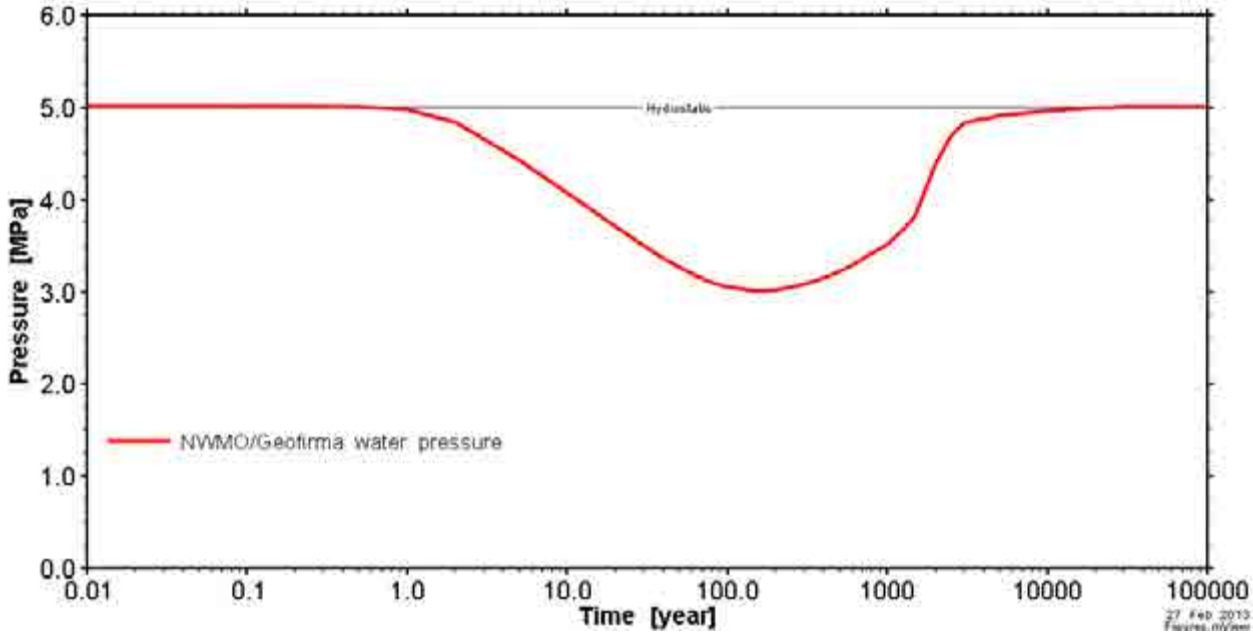

Figure 134: Base case water pressures at point 9, located in the host rock, 5 m away from the center of the cell.

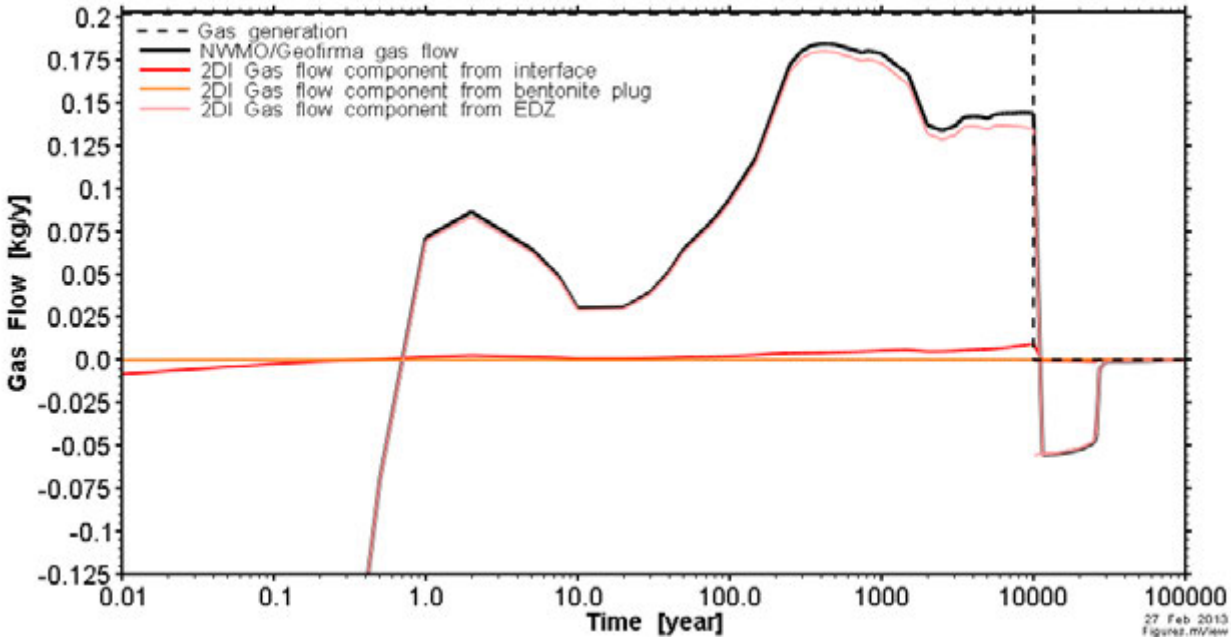

Figure 135: Base case gas flux into the access drift, from the EDZ, interface and bentonite plug.

3.9.4 Prescribed Sensitivity Cases

3.9.4.1 Case 1: Self Healing EDZ

In this sensitivity case, the permeability of the EDZ is set equal to that of the host rock. This case has only completed to approximately 25 000 years.

Figure 136 shows the gas flows into the access drift for this sensitivity case, compared to the base case. The low permeability of the EDZ resulted in gas flow towards the access drift occurring through the interface rather than the EDZ. Virtually no gas enters the EDZ surrounding the cell. The amount of gas flow is not significantly reduced, but rather simply shifted to flow through the interface. There is a small reduction in the peak gas flow, but the peak occurs for a longer period of time. There is a small amount of gas flow away from the access drift through the EDZ.

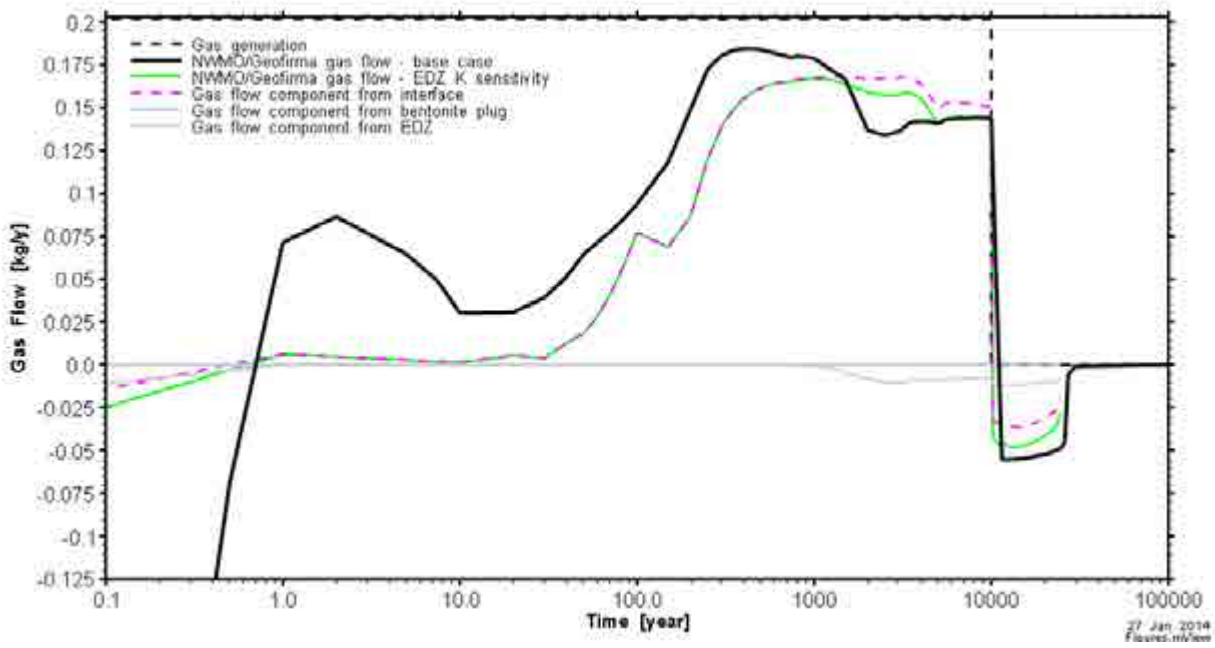

Figure 136: Sensitivity case 1 (EDZ K equivalent to rock K) gas flux into the access drift, from the EDZ, interface and bentonite plug.

3.9.4.2 Case 2: Altered Relative Permeability Curves

In this case, the relative permeability curve for both the host rock and the EDZ is changed from the van Genuchten relationship to a cubic power relationship (TOUGH2 refers to this relationship as the Verma et al. (1985) relationship):

$$K_r^w = S_w^3 \qquad K_r^g = S_g^3 = (1 - S_w)^3$$

K_r^w : relative permeability for water (-)

K_r^g : relative permeability for the total gas phase (-)

S_w : saturation for water (-)

S_g : saturation for the total gas phase (-)

The relative gas permeability curve for this cubic power relationship is shown in Figure 116, compared to the benchmark van Genuchten relative gas permeability curves.

This simulation is only complete until approximately 2000 years. Numerical issues were encountered with this simulation, particular at nodes where gas saturation was very small and gas was no longer migrating into the node. While similar numerical difficulties were encountered in other simulations, the very flat relative gas permeability curve at low gas saturations of the cubic power law exacerbated the numeric issues.

Compared to the base case, changing the relative permeability curve had minimal impact on results. Figure 137 shows the gas flow into the access drift. Small differences occur mainly at early times; peak gas flows after 100 years are very close between the two cases.

While at early times, the changes in relative gas permeability in the EDZ and host rock has resulted in less flow to the access drift, it has correspondingly resulted in greater flow out of the EDZ and into the host rock at early times (except for a short peak in gas flow in the base case at 1 year), as show in Figure 138.

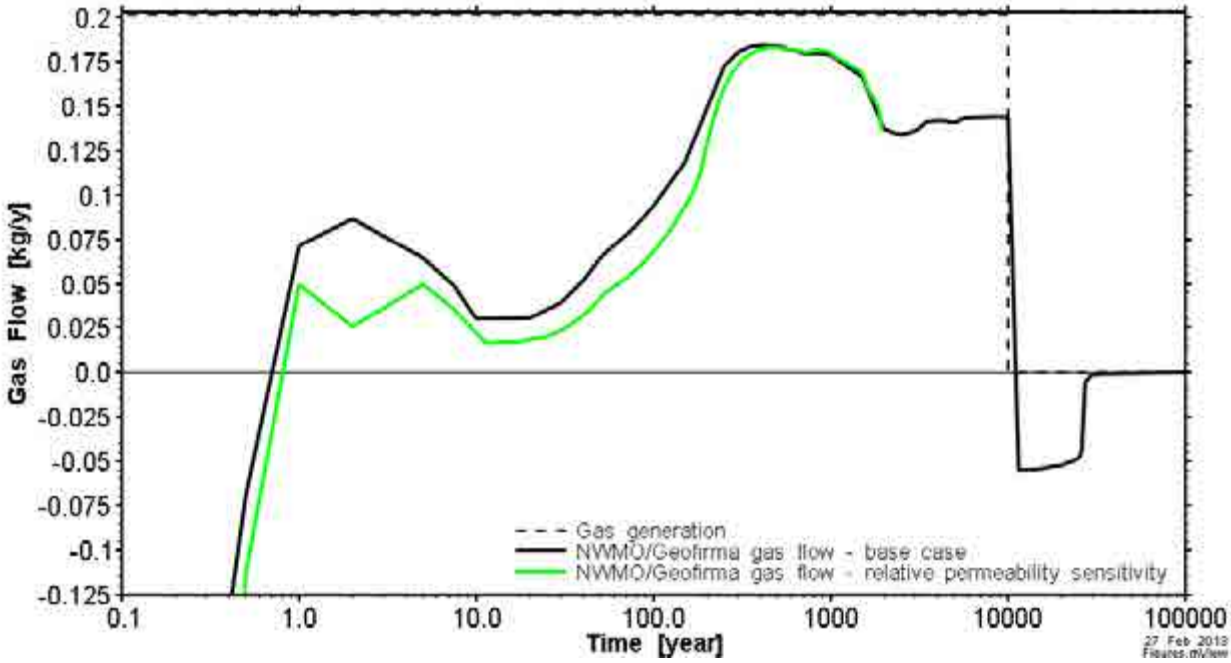

Figure 137: Sensitivity case 2 (Cubic power law relative permeability curve in host rock and EDZ) gas flow into the access drift.

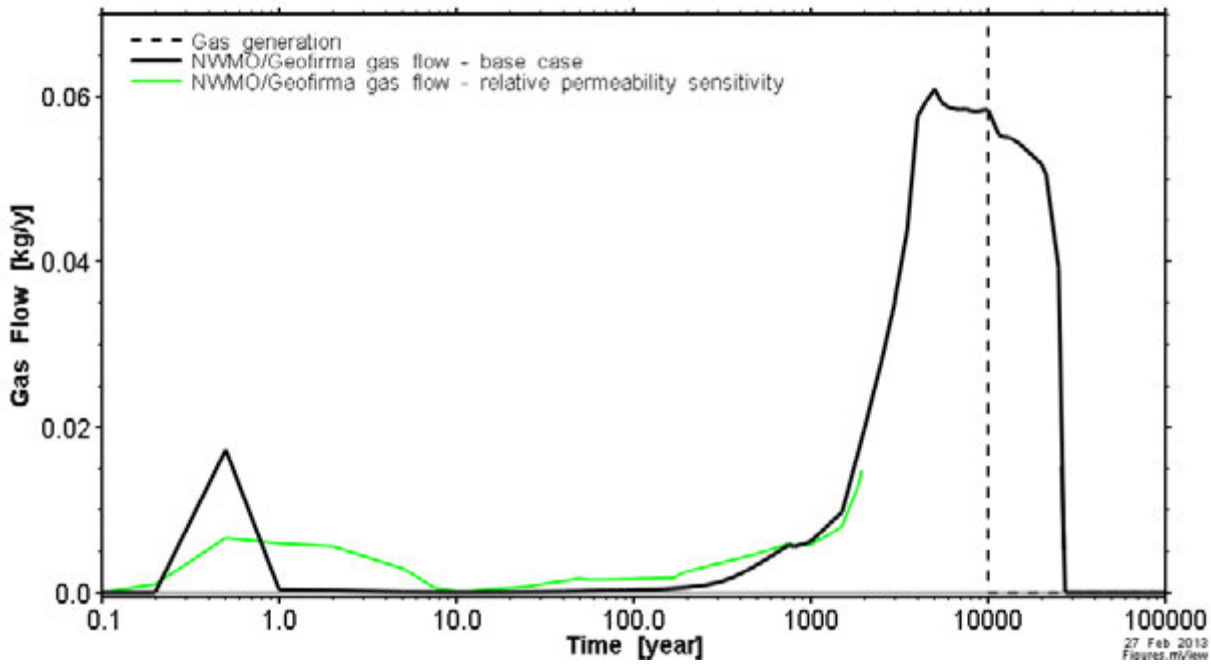

Figure 138: Sensitivity case 2 (Cubic power law relative permeability curve in host rock and EDZ) gas flow out of EDZ surface into host rock.

3.9.4.3 Case 3: Increased Diffusion in Water

In this sensitivity case, the diffusion coefficient for dissolved hydrogen is increased by a factor of 10. The base case diffusion coefficient is 4.59×10^{-9} m^2/s. This simulation is only complete to 23 000 years.

Increasing diffusion has a substantial impact on results. A greater amount of dissolved gas migrates out away from the cell and into the host rock, resulting in less gas travelling towards the access drift. It should

be emphasized that the greater amount of gas migrating away from the cell is dissolved gas, not actual gas phase. This greater amount of dissolved gas travelling away from the cell results in greater dissolution of gas near the cell, and consequently the gas phase does not travel as far away from the cell as in the base case. By 10 000 years, the gas phase has only extended 0.25 to 0.5 m into the host rock (compared to 0.5 and 1 m in the base case).

With less gas travelling towards the access drift, gas actually travels out of the access drift from the boundary condition and into the cell, EDZ and host rock, as shown in Figure 139. As in the base case, all of the gas flow is through the EDZ, not the interface or the bentonite plug. Based on these gas fluxes, it is not clear that this diffusion scenario is realistic, whether the access drift would actually provide this quantity of gas (greater than gas generation in the cells).

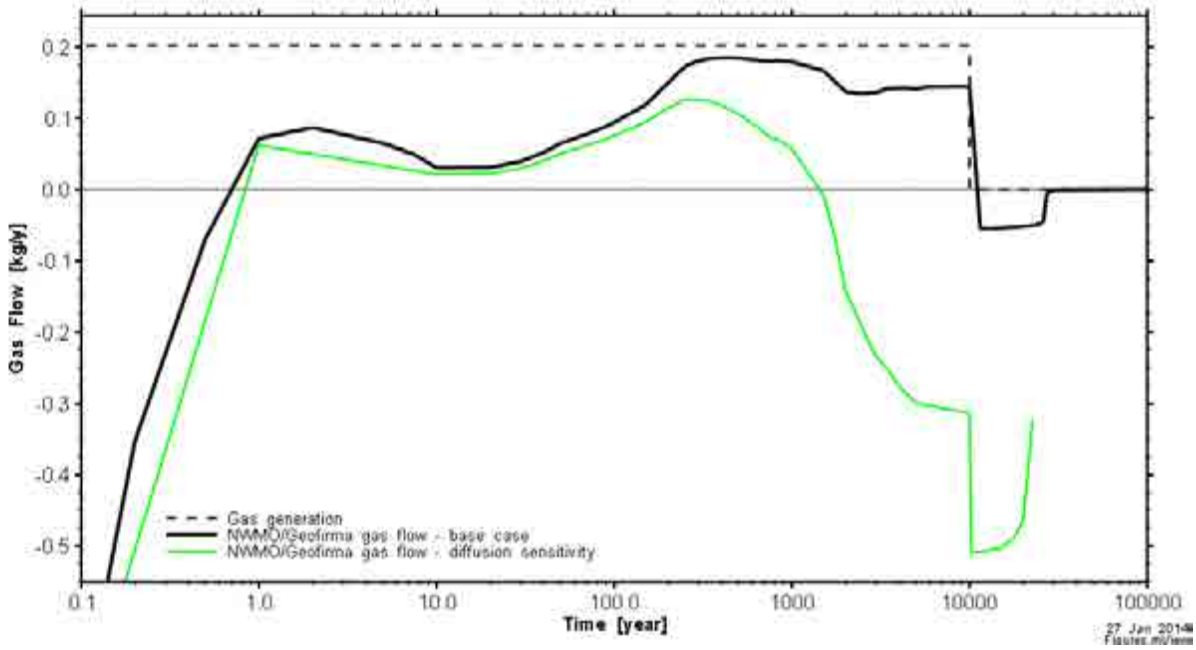

Figure 139 : Sensitivity case 3 (increased diffusion coefficient) and base case gas flux into the access drift.

3.9.4.4 Case 5: Less Permeable Interfaces

In this sensitivity case, the permeability of the interface facing the canister is reduced to 10^{-15} m^2 (base case canister interface permeability is 10^{-12} m^2).

Figure 140 shows the gas flow into the access drift compared to the base case. Gas flows through the access drift are very similar to the base case, with flow through the interface reduced to negligible amounts.

The gas flow results of this interface permeability and the EDZ permeability sensitivity cases suggest that the interface is only an important feature of the system if the EDZ permeability is small. It is possible that the interface plays a role in distributing the gas out into the EDZ. A further sensitivity case, removing the interface entirely, would be required to confirm that the interface can effectively be ignored for the reference case.

Water pressures at point 5 (Figure 141) are approximately double the water pressures in the base case by 10 years, and by 1000 years, water pressures are the same as the base case. These high water pressures at early times can be explained by slightly more gas migrating out into the EDZ in the low interface permeability case, instead of migrating along the interface to the access drift. This slightly greater amount of gas will result in slightly lower water pressures near the cell, resulting in a greater gradient of water towards the cell, and a faster resaturation of the EDZ. The effect is small, and once the access drift

pressures increase, the effect is negligible. This explanation is confirmed by the gas flow rates to the access drift in Figure 140.

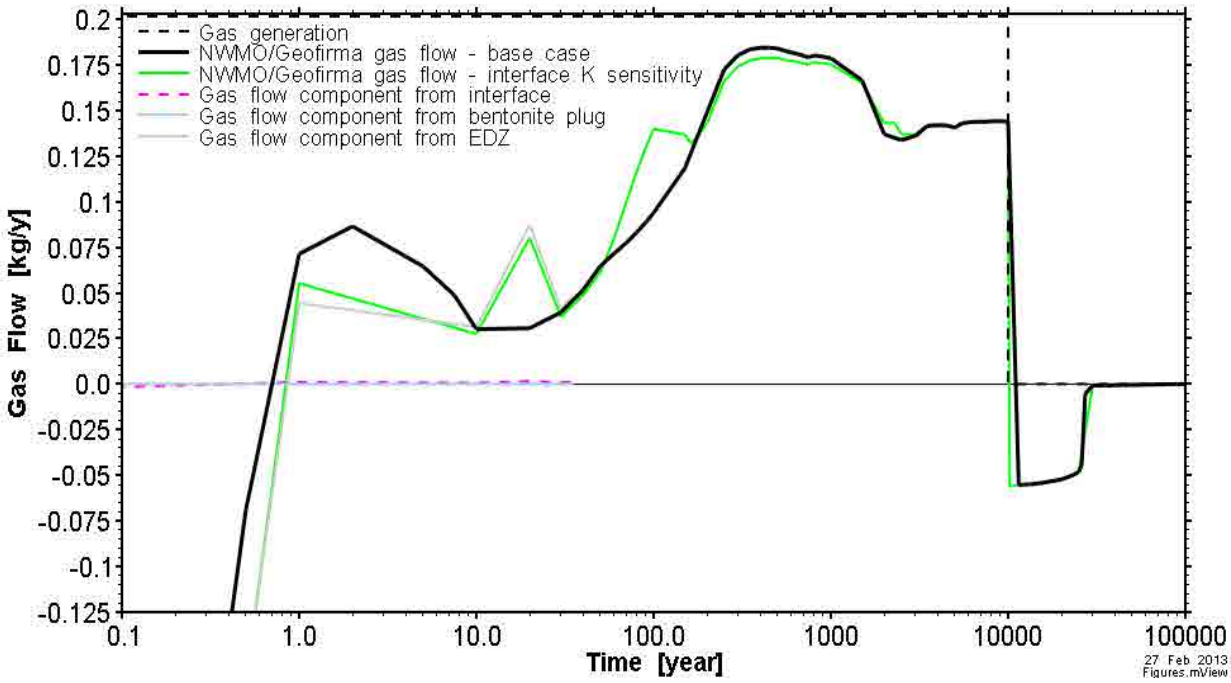

Figure 140: Sensitivity case 5 (interface permeability increased to 10^{-15} m^2) gas flux into the access drift, from the EDZ, interface and bentonite plug.

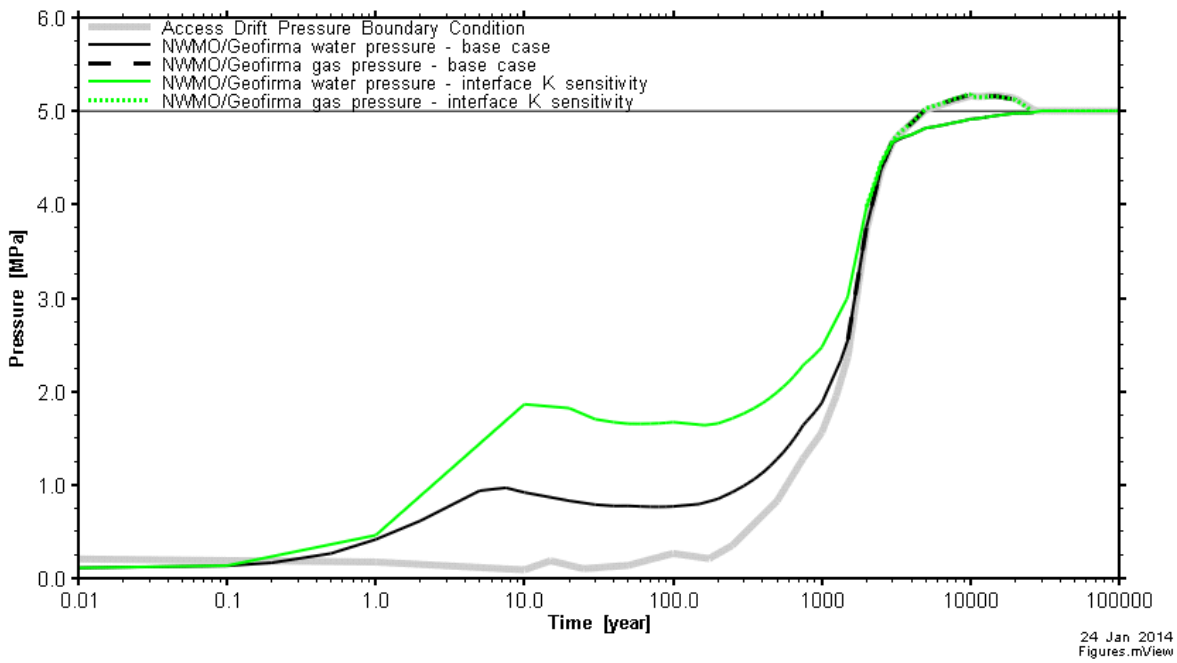

Figure 141: Water pressures at point 5 for sensitivity case 5 (interface permeability decreased to 10^{-15} m^2) and base case. Point 5 is located in the middle of the EDZ, half way along the canister.

3.9.5 Additional Sensitivities

Two additional sensitivity cases were simulated to help define the impact of potential grid simplifications for the future module and repository scale models:

(A) No interface. The interface (both cell and plug) was removed from the model simulation, and replaced with EDZ. It should be noted that gas is injected directly into the EDZ in this case.

(B) Upscaled interface. The interface (both cell and plug) was combined with the EDZ, effectively forming an inner EDZ 25 cm thick. Upscaled parameters for the inner EDZ and other interface combinations were developed by weighting parameters by the relative volume of the contributing materials. This was the first approach used in the module-scale modelling; a more conventional upscaling scheme was subsequently applied to the module-scale model resulting in little difference in both parameters and results. Initial pressures in the upscaled interface elements are the same as the EDZ.

These cases are compared to the base case, defined in Section 3.9.3 Two metrics were used to compare the differences between these two cases and the reference case: gas flow into the access drift and gas flow out of the EDZ and into the host rock. Dissolved gas flows across these surfaces were also examined; however, differences between the cases were negligible, and consequently results are not presented.

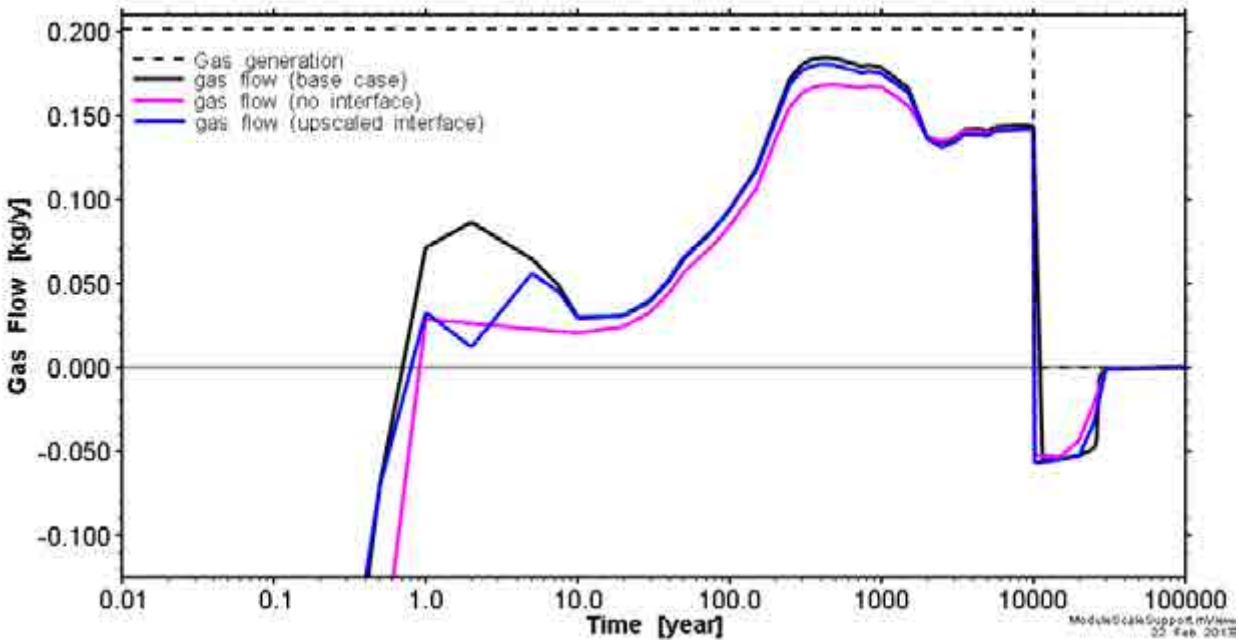

Figure 142 shows the gas flows to the access drift for the base case, compared to the two additional sensitivity cases described above. Removal of the interface entirely had surprisingly little impact on gas flows to the access drift, particularly after 2000 years. However, the upscaled results provide an improved approximation to the reference case results, particularly at early times. Neither case was able to duplicate the peak in gas flows shortly after 1 year, indicating that this peak gas flow is strongly related to the high permeability of the interface.

Figure 143 shows the gas flows out of the EDZ and into the host rock for the reference case and the two cases described above. Removal and upscaling of the interface resulted in a marginally greater amount of gas flow out the EDZ into the host rock, at an earlier time. This is perhaps not unexpected, as it corresponds to the slightly smaller flows out of the access drift, confirming that gas flows into the host rock are directly affected by the access drift boundary condition. Note that the bulk of the gas flow out the EDZ originates from the EDZ adjacent to the cell, rather than adjacent to the access drift. The small peak in gas flow for the upscaled interface case at 0.5 years is not apparent in either of the other cases due to

coarse output discretization in the other cases (only data points at 0.1 and 1 years). This small peak in gas flow is also a result of gas flow out the EDZ adjacent to the access drift.

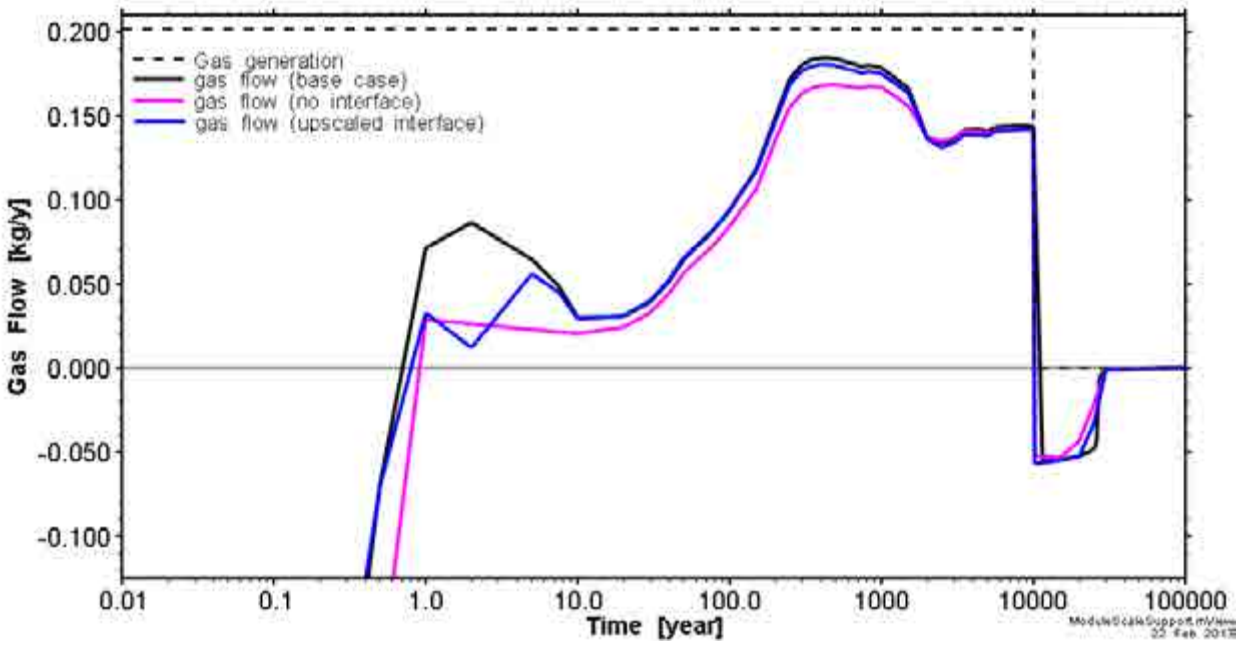

Figure 142: Gas flows to the access drift for the base case, no interface case and upscaled interface case.

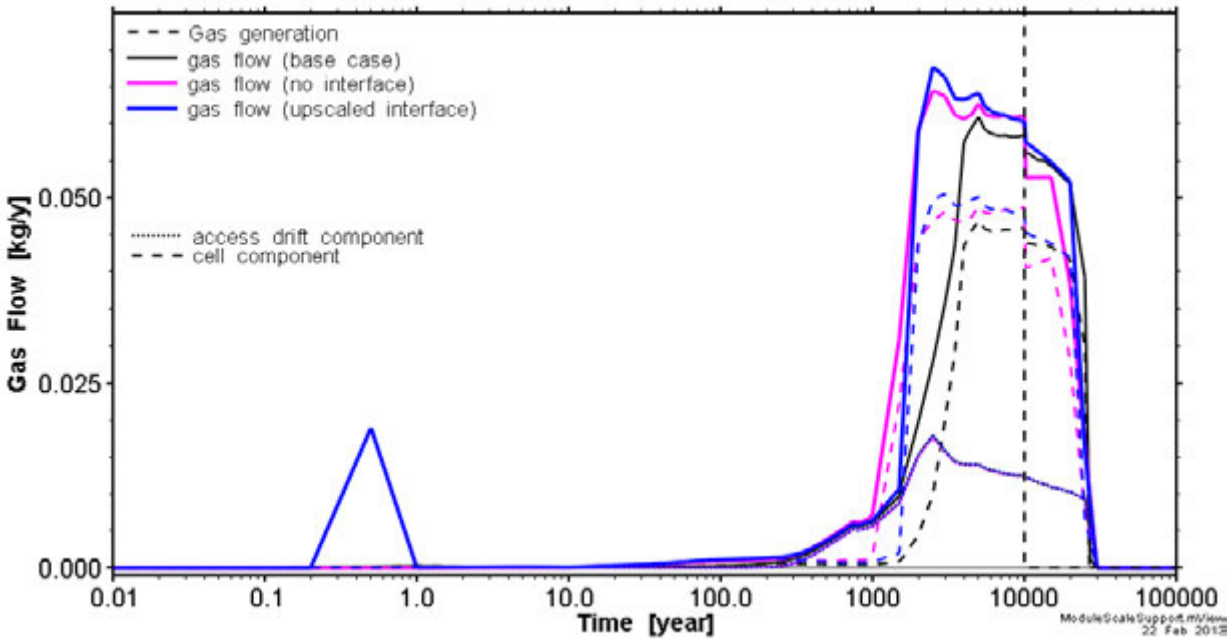

Figure 143: Gas flows out the EDZ into the host rock for the base case, no interface case and upscaled interface case.

Pressures at points 4, 5 and 9 were also examined, shown in Figure 144, Figure 145 and Figure 146. Higher initial pressures (5 MPa rather than atmospheric) for the no interface and upscaled interface simulations explain the differences in pressure. Initial pressures are higher in these two cases by definition: the benchmark defines initial pressures of 5 MPa in the EDZ, and atmospheric in the interface. Since the no interface case is only EDZ, and the upscaled interface case is mostly EDZ, initial pressures were assumed to be 5 MPa. At point 5, pressures for the no interface case are very close to the reference case after approximately 10 years. At point 4, pressures for the upscaled interface case are almost identical to the reference case, reinforcing the importance of the boundary condition in the access drift for this case. For the no interface case at point 4, note that the negative water pressures before 10 years is a result of the location of the point. This point is located within the interface for the other cases (interface has low capillary pressures), and within the EDZ for the no interface case (EDZ has large capillary pressures).

The results of these additional sensitivies suggest that while an upscaled interface approach is more accurate representation of the system, the contribution of the interface is relatively small and could potentially be ignored. Sensitivity cases ignoring the interface at the module or repository scale would provide further evidence of the relative unimportance of the interface.

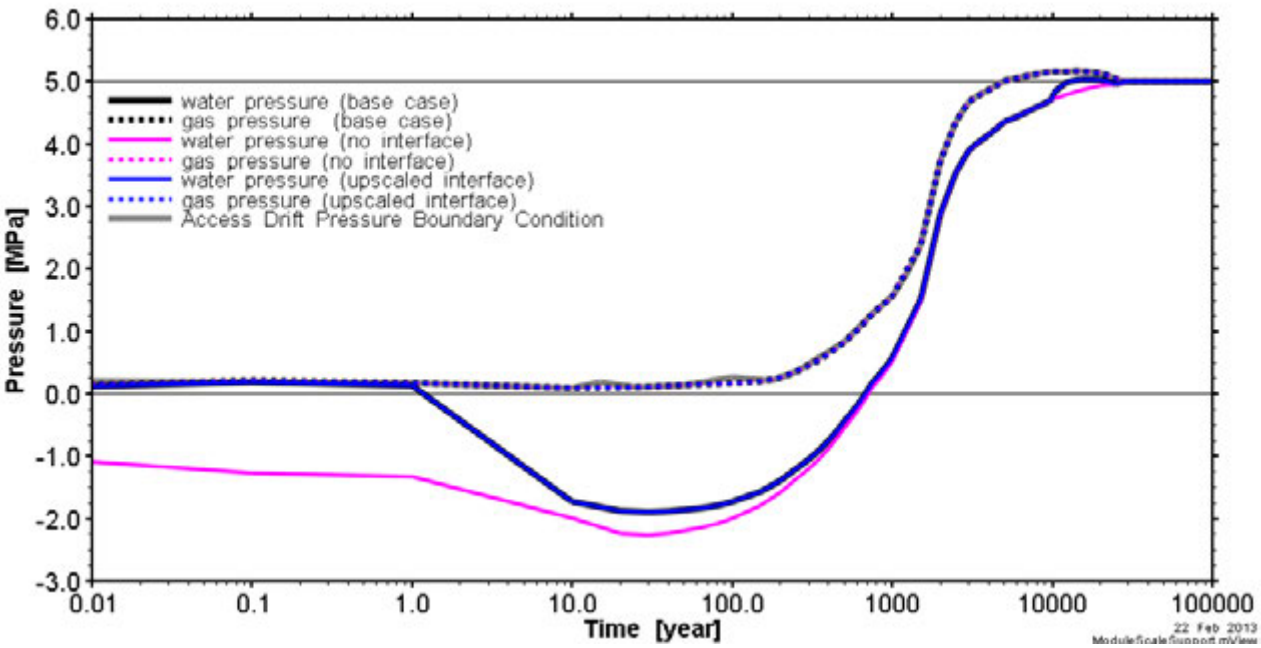

Figure 144: Water and gas pressures at point 4 for the base case, no interface case and upscaled interface case.

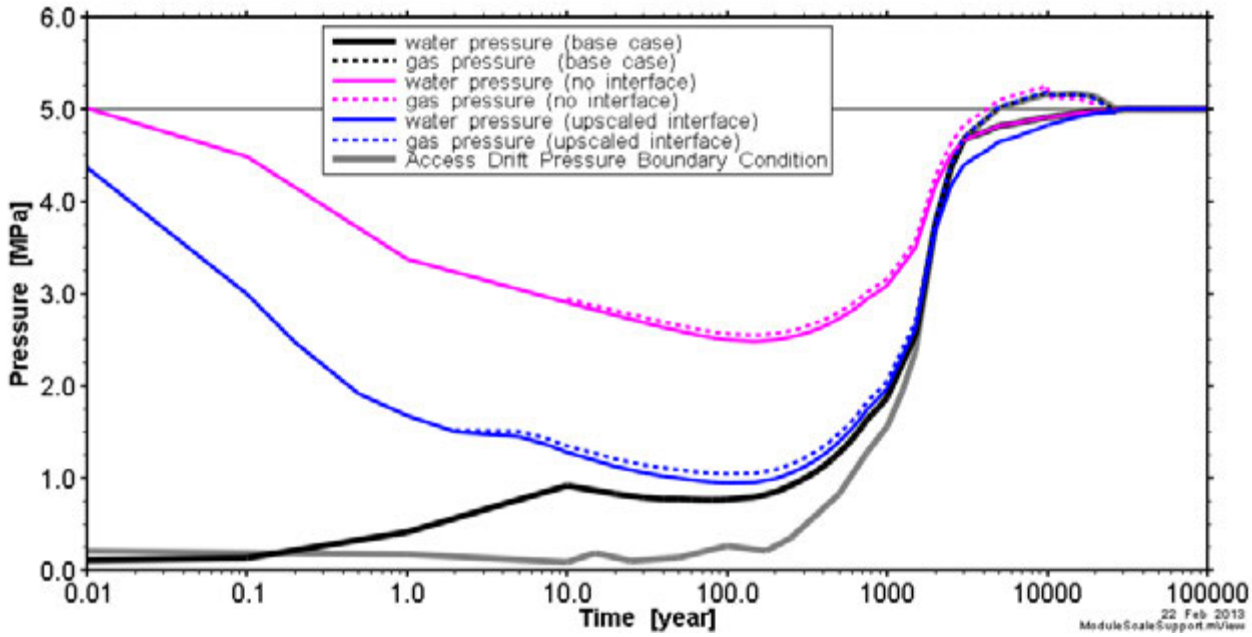

Figure 145: Water and gas pressures at point 5 for the base case, no interface case and upscaled interface case.

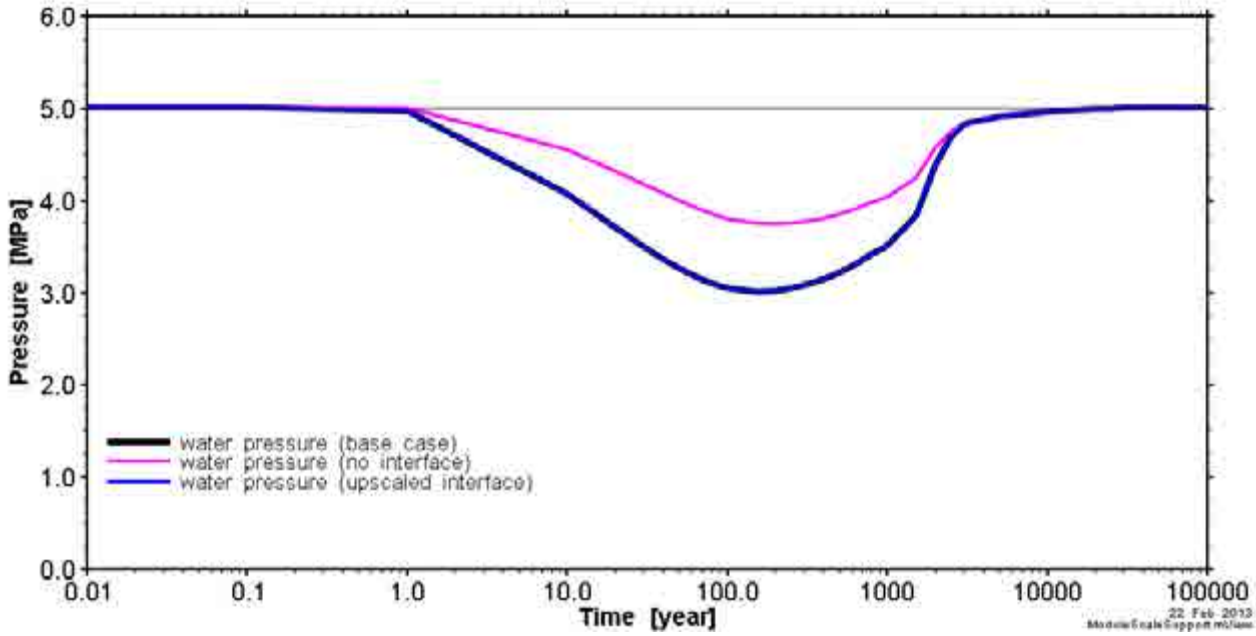

Figure 146: Water pressures at point 9 for the base, no interface case and upscaled interface case.

3.9.6 Discussion and Conclusions

The boundary condition at the access tunnel is a strong driver in this model, ensuring flow along the cell and towards the access drift. As well, pressures in the interface and EDZ develop towards pressures at this boundary condition. At the mid-point of the cell, in the middle of the EDZ (point 5), pressures match the access drift boundary condition by 2000 years.

Free gas flow occurs mainly in the cell EDZ, due to the greater cross-sectional area for flow compared to the more permeable 1 cm interface. The maximum gas pressure reached was 5.7 MPa in the bentonite plug adjacent to the canisters, at 10 000 years, the time at which gas injection stopped.

The sensitivity cases demonstrated the following important points about the cell-scale system:

(1) The importance of the EDZ is limited by permeability. Reducing the permeability of the EDZ (to the same as the host rock) shifts gas flow into interface (towards the access drift).

(2) The interface has a minor importance. The small size of the interface means that the bulk of the gas flow occurs through the EDZ. Decreasing the permeability of the interface, removing the interface or upscaling the interface with the EDZ, has minimal to no impact on results.

(3) Changing the relative gas permeability model to the cubic power relationship resulted in minimal differences.

(4) Increasing the diffusion coefficient had a dramatic effect on results. Greater dissolved gas diffusion resulted in greater dissolution of gas, and free phase gas no longer migrating towards the access drift.

3.9.7 References

[1] Quintessa and Geofirma. 2011. T2GGM Version 2: Gas Generation and Transport Code. Quintessa Ltd. and Geofirma Engineering Ltd. report for the Nuclear Waste Management Organization NWMO DGR-TR-2011-33 R000. Toronto, Canada.

[2] Pruess, K., C. Oldenburg and G. Moridis. 1999. TOUGH2 User's Guide, Version 2.0. Lawrence Berkeley National Laboratory LBNL-43134. Berkeley, USA.

4. Global synthesis of the benchmark at cell scale

This benchmark study is not particularly aimed at comparing amoung codes, but rather aims to consider how relevant global phenomenological behavior associated with gas generation and migration in a repository are considered by participating teams. However, as each team is using its own code, some code specificity has been introduced into the benchmark study regarding how it is represented in the participants' respective codes, especially in relation to boundary conditions. Therefore, direct comparison of all results produced by participants is not always possible.

However, in order to obtain an order of magnitude of the results, a comparison of the results of the different teams will be shown and a summary of the general behavior of the hydraulic-gas transient of a cell based on these results will follow. The sensitivity cases conclusions are also presented briefly as well as the main problems encountered in the simulation process by the different teams. Finally, some discussion on the hypothesis made and the representativity of the benchmark is proposed.

N.B. *: there are two other document linked to this one, on module scale (report FORGE D1.6-R part 2: module scale benchmark) and repository scale (report FORGE D1.6 –R part 3: repository scale benchmark) benchmark. The repository scale benchmark has a final conclusion synthethising all the conclusions of the global benchmark work*

4.1 Base case results

The results of some teams are not used in this section for the following reasons:

- the results of IRSN cannot be directly compared with those of the other teams as the model used is not the same (2D plane geometry);
- the model used by CNRS is simplified (immiscible compressible two phase flow : no dissolution/diffusion process), comparison is therefore not easy and is not preformed;
- The model used by CEA differs significantly from the benchmark specifications: no interface, constant boundary conditions, and 2D plane geometry.

So only the results of 6 teams are compared in this section: NDA/Quintessa, CEN/SCK, Andra, LEI, ENSI and NWMO/Geofirma.

4.1.1 Comparison of the available results and main phenomenological results

Despite some minor differences in the way to represent varying boundary conditions at the drift, and some minor phenomenology, the ways the 6 teams have represented the model are quite comparable. Overall, the results are in good agreement for water and gas pressure (and therefore as well for water saturation).

Figure 147 represents the time evolution of water pressure at point 4, in the interface Bentonite/EDZ near the drift (see annex for more details on P4 position).

All teams have found that gas is not generating groundwater overpressures: the maximum pressure is reached after a long time, when water pressure is reaching initial undisturbed conditions at 5 MPa. This time is in the order of 20,000 - 40,000 years and correspond to the moment of water saturation of the cell (gas pressure is equal to water pressure; e. g. capillary pressure is equal to zero). Gas pressure is never very high, the maximum being achieved just before resaturation at around 5 to 5.5 MPa.

At the beginning (from one year up to one thousand years), the capillary pressure calculated by the different teams in the interface can be quite different (up to 2 MPa of difference before one hundred years). This can be due to the type of meshing (one or more element in the interface) and/or the way the model is averaging the permeabilities between adjacent cells. Although this may seem a significant difference, it does not have a major influence on the global behavior of the cell.

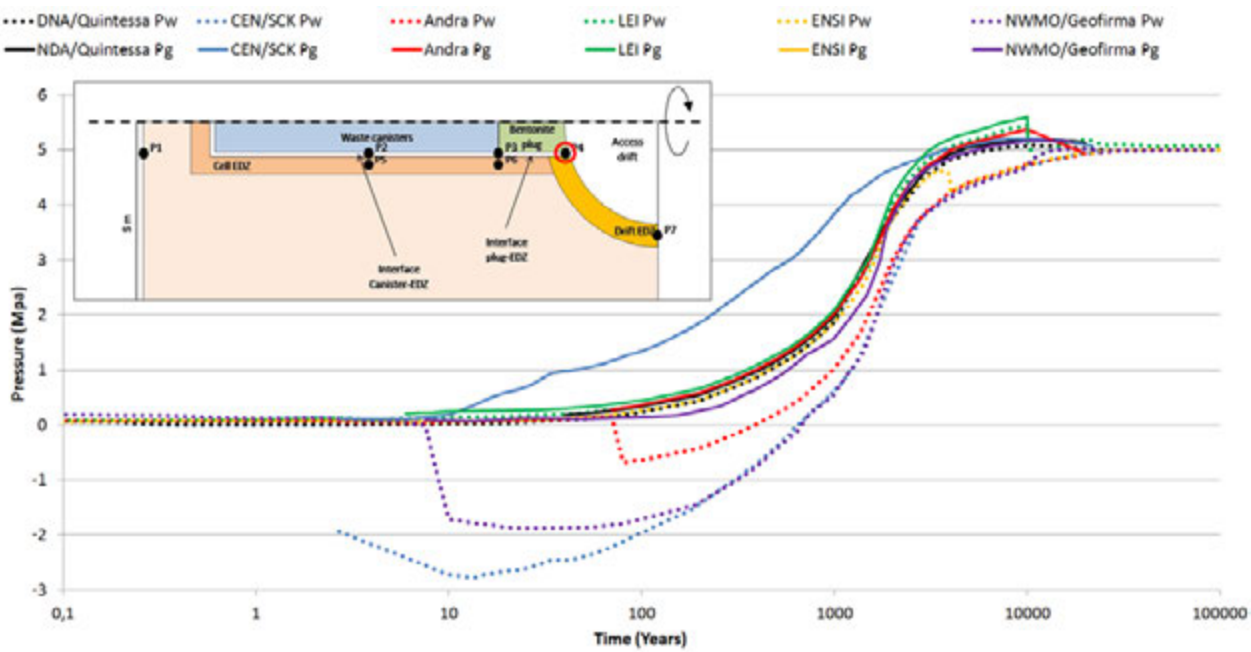

Figure 147 Evolution with time of water and gas pressures at point 4

Another interesting result is the fact that a gas phase is maintained in the access drift during several tens of thousands of years after the end of the gas production phase (gas production ends at 10,000 years) before dissolution/diffusion processes lead to its removal. Convection along the access drift is certainly also a dominant process during this period but, as it is (at least pratly) driven by boundary conditions, this will have to be tested at a larger scale.

In the EDZ (see Figure 148 for point 5 time evolution) the evolution is more or less the same and results are even more coherent. Due to a smaller permeability of the EDZ compared to the interface, desaturation is less important, e. g. gas phase is only present for a short time period and only after approximately one thousand years.

For points in the clay far from the cell, the results are also coherent (see Figure 149 for water pressure time evolution at point 9, 5 m in the clay radially from cell center). The fact that water pressure only decreases by around 2 MPa from the initial undisturbed natural pressure means that the geoelogical medium is not desaturating at all at this distance from the cell. In fact, due to the very small permeability of the argillites and to its high capillary entry pressure, desaturation is mainly occurring inside the cell and EDZ, but the sound clay is not significantly desaturated (a desaturation of some % is possible over some decimeters in the undisturbed clay, but not more than this).

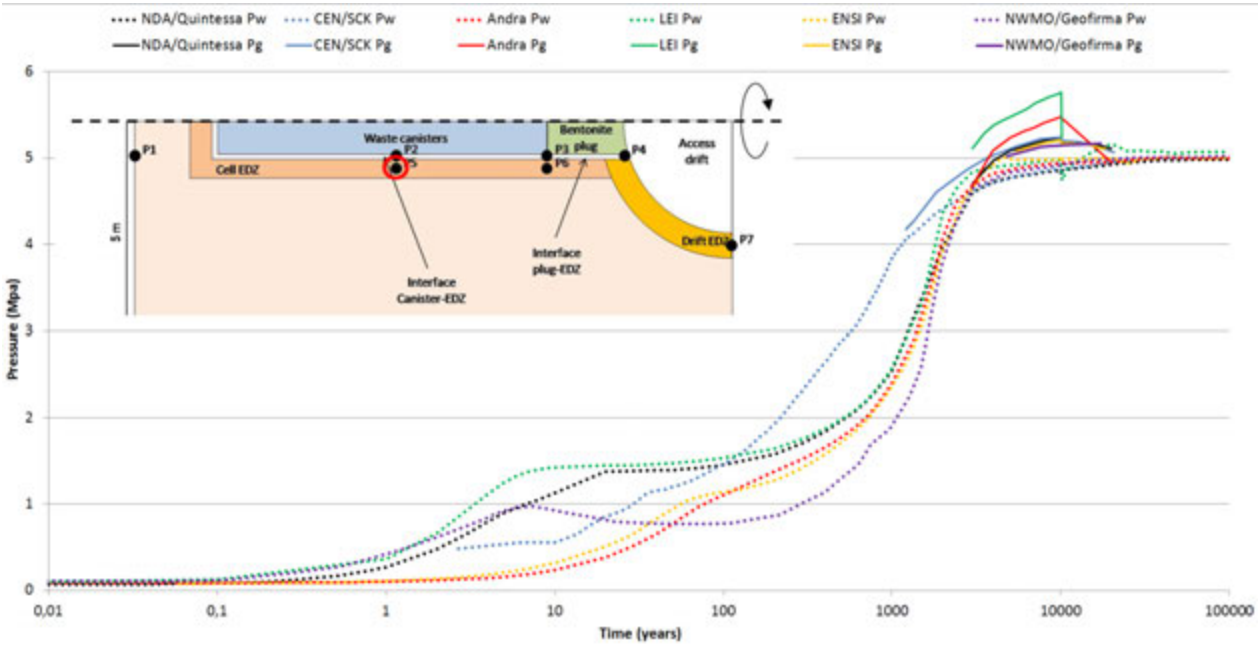

Figure 148 *Evolution of water and gas pressures with time at point 5*

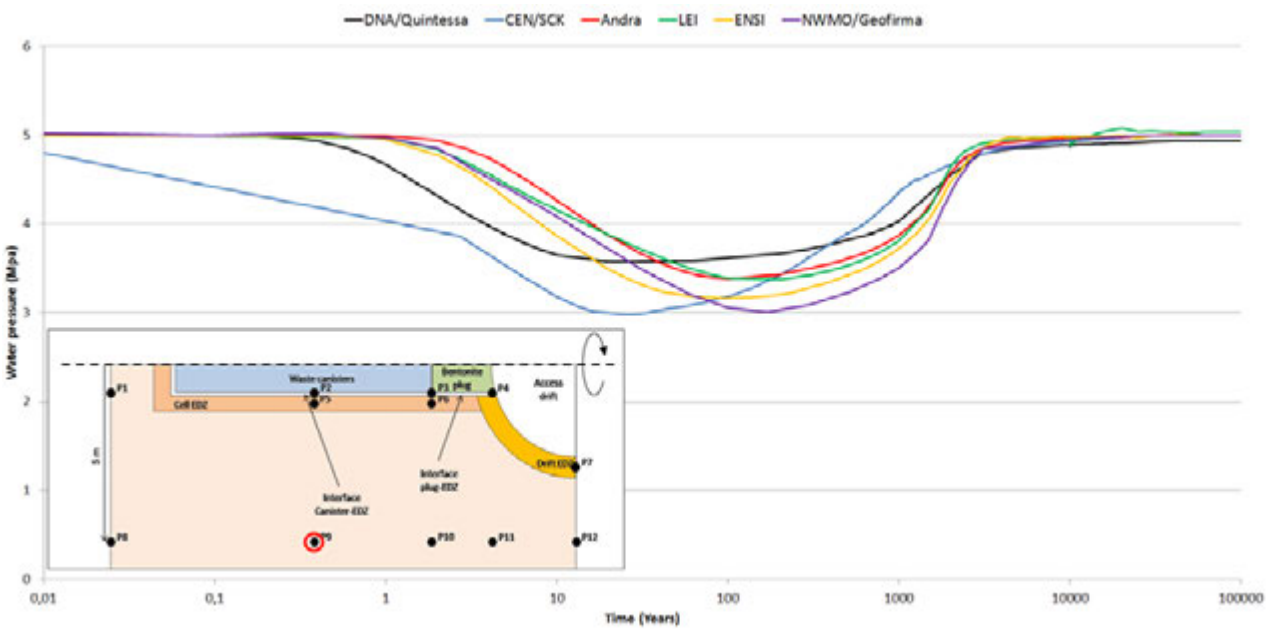

Figure 149 *Evolution of water pressure with time at point 9*

Concerning gas fluxes, the simulations are also coherent as shown in Figure 150 (CEN/SCK was not able to compute gas fluxes the way stated in the benchmark specifications, so their results are not presented in the graphs on fluxes). At the beginning, for around one year, the gas (initially air brought in during drilling of the cell/drift and ventilation of the drift) flux is directed from the access drift toward the cell (negative flux values), but rapidly, due to the generation of the gaseous H_2 the direction of the flux is inverted and hydrogen is going out of the cell toward the access drift (positive values). The maximum flux (around 0.1 to 0.18 kg/y) is reached after several hundreds of years and a high flux level is maintained up to the end of the gas generation period (10,000 years).

The average flux value is differing from one team to the other, but is significant compared with the generation rate (0.2 kg/y) although not quite as high as this value. This implies :

- That an important part of the hydrogen is moving under gas phase. On the other hand, this also implies that a significant part is dissolving and diffusing in the clay water around the cell;
- That the interface and the EDZ are playing an important role in enabling the gaseous hydrogen to move easily from the end of the cell toward the drift.

After the gas production period, the gas flux toward the drift is decreasing rapidly to zero. A reverse flow (from drift to cell) is eventually possible at a small rate for several tens of thousands of years, the gas stored in the drift moving back to the cell as pressure drops due to the dissolution/diffusion process (which become dominant after gas production period).

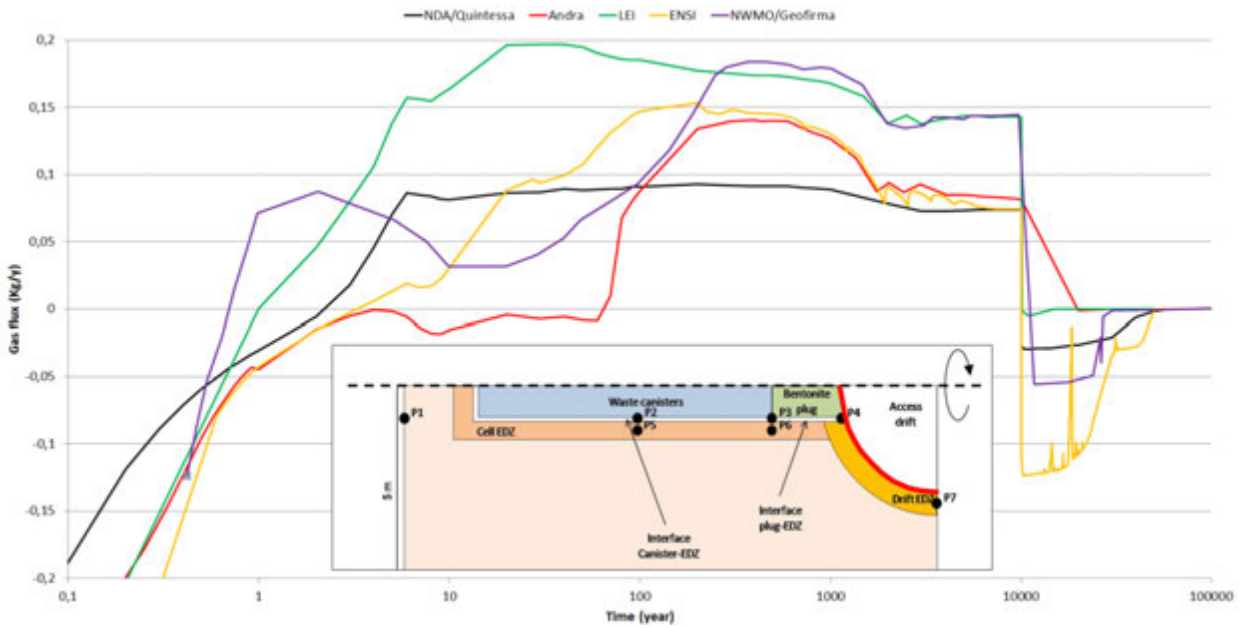

Figure 150 *Evolution with time of the gas flux toward the access drift for all teams except CEN/SCK*

This globally coherent scheme should not mask the fact that some specific results are significantly different without any phenomenological explanation. Concerning the results presented in Figure 151 (expressed gas flux through the global EDZ), this may be due to the definition of the surface over which the flux is calculated. This surface (S_{EDZ}) is integrating 3 sub bits of the EDZ in 3 different regions of the cell (waste zone for S_{EDZ1}, in front of the bentonite plug for S_{EDZ2} and the drift EDZ for S_{EDZ3}). It may be that between teams, the synchronization of these 3 sub-fluxes are different and that for a team they are adding during a certain period whereas for another team they are of different signs, even if the global behavior is similar.

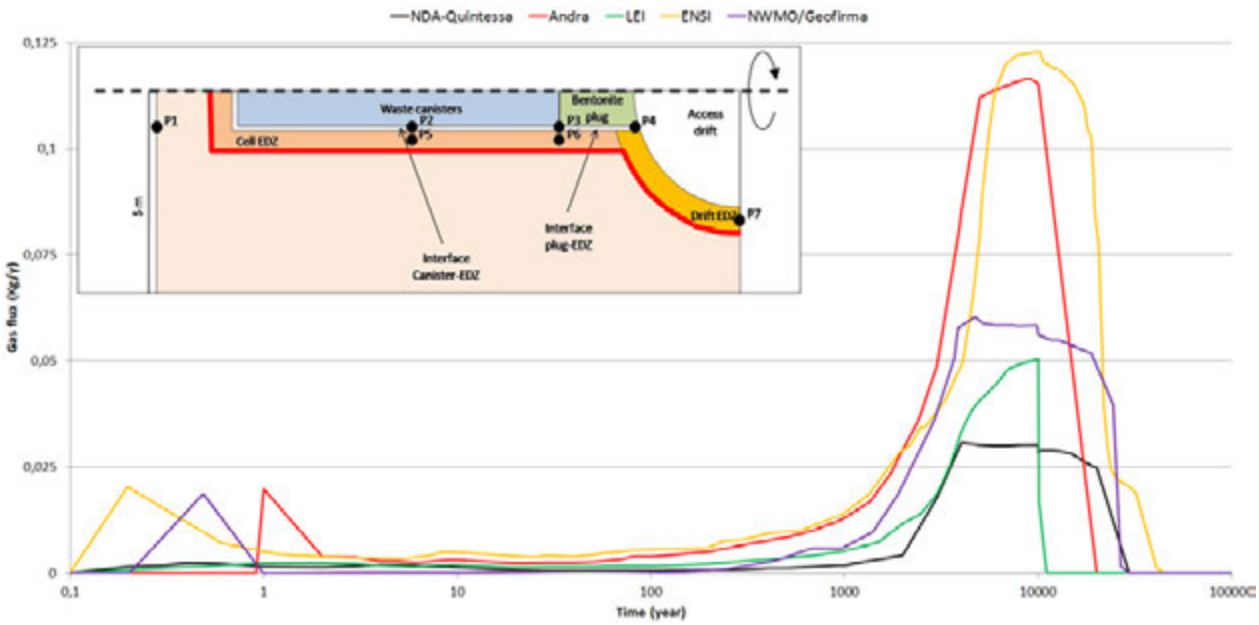

Figure 151 *Evolution with time of the gas flux through the entire EDZ for all teams except CEN/SCK*

4.1.2 Main conclusions for the base case

On the whole, the results from the different teams are globally coherent and give the same general vision of the hydraulic-gas evolution at the cell scale defined by the benchmark.

However, significant discrepancies exists, and an important conclusion of this benchmark, consolidating similar ones in the past, is that numerical simulation is a powerful tool (if not the only one) to give a trend, a tendency, a general evolution but has to address uncertainty of the gas modeling analysis to help bounding the results, only way to enable a representative phenomenological analysis.

Another important fact is that the results of the base case of this benchmark was done assuming no uncertainties on the real phenomenology, parameters values, simplification of the geometry (e.g., despite some minor changes in the implementations, all teams had the same already "simplified" specifications assuming two phase flow for all materials, axisymmetric geometry, ...) and thus, the results, in terms of real behavior in the field, can only be taken in order of magnitude.

Having this in mind, the base case behavior can be summarized as follows:

- First period of around 1 year of water and gas exchange between the drift and the cell. During this period the gas fluxes is mainly made of air initially present in the model. During this period the EDZ around the drift is desaturating partially and the interface around the waste storage zone is resaturating, but interface around the bentonite plug is still desaturated and gas pressure is not building up in the cell;

- After several tens of years the resaturation of the bentonite plug implies also the resaturation of the interface around it. Gas pressure begins to build-up in the cell. The gas pressure is never much higher than the water pressure, and at its maximum (after several thousands of years), the capillary pressure is only around 1 Mpa;

- At a period of several years to several tens of years the increase of gas pressure inside the cell forces a desaturation of the interface and a partial desaturation of the surrounding EDZ around the bentonite plug. Effective gas (H2) flux is then possible between the waste zone and the drift via this unsaturated interface/EDZ section. This flow lasts up at least to the end of the H2 production period (10.000 years);

- Meanwhile, dissolved H2 is diffusing in the sound clay radially from the waste zone;
- Over the whole H2 production period two-phase flow and dissolved gas transport play both an important role in the gas transfer.

4.2 Sensitivity analysis results

This part is not describing each sensitivity made during the benchmark, but is summarizing the different results and conclusion of all teams:

- As host clays are very impermeable and gas entry pressures are high, the desaturation is only of some percent and thus there is a need of better characterization of the "water saturated tail" of the relative permeability and retention curves for these materials;
- A better experimental characterization of the EDZ relative permeability and retention curves could also help increase the confidence on the simulation results.
- This is also true for the interfaces, adding intrinsic permeability values as well;
- Diffusion process is a key process in the comprehension of a cell hydraulic-gas transient and decreasing the uncertainty on the host clay diffusion coefficient for H2 could also help.

4.3 Main problems encountered

Most of the teams have had problems to conceive a simulation fulfilling all the benchmark specifications. This is mainly true for the representation of the time varying boundary conditions, but also for some part of the mathematical description of the phenomenology to be represented. So at the first meeting between the modeling teams part of the discussion was about how to fulfill the benchmark specifications. So some modifications of these specifications were adopted and most of the teams could implement this new model. However, some minor discrepancies are still pending for some teams (see each team description of their work).

After this first adjustment period, some general problems where still pending. On the basis of input from all participating teams, the main problems encountered with the current benchmark study can be subdivided into 3 major groups, all closely linked with numerical issues:

4.3.1 Boundary conditions representation

For some teams, it was a real challenge to take into account the varying prescribed pressure boundary conditions, because their specific code does not allow the integration of these types of boundary conditions. In such a case, the boundary conditions had to be adapted to the code capabilities and the results were therefore affected, sometimes significantly.

A way to resolve this problem is to transform pressure-varying boundary conditions into time-dependent flux boundary conditions: this type of boundary condition is more widely supported by the codes used for this exercise.

4.3.2 Time step management

Although the benchmark geometry is not very complicated, its definition is really demanding in terms of numerical behavior. The main difficulties are the highly heterogeneous properties of the different material, especially in terms of permeability (interface 10^{-12} m^2, argillite 10^{-21} m^2). A second difficulty, linked to model geometry, is the different sizes of the different materials (thickness of the interface is 0.01 m whereas radius of the domain is 20 m).

This causes numerical problems especially in the management of the shift between water saturated flow and two-phase flow. Sometimes element/node is near the shift from one situation to another and depending on the internal numerical iteration there is a movement back and forth between the two stages. Trying to solve this uncertainty, the code reduces the numerical time step and this can result in a time step

so small that a simulation over some tens of thousands of years is computationally impossible to manage; for extreme situations, the model-run can cease.

This problem is linked to several factors:

- Specific complexity of the model (high heterogeneity of parameters, high differences in characteristic dimension, ...);
- Mesh optimization (see next point) : the smallest the numerical elements, the higher the number of elements where this type of problems can appear;
- Code capability to cope with this type of numerical problem.

The two first items can be modified by the user when working on a specific simulation, but the third one is more difficult to modify and can need specific numerical development within the code structure.

4.3.3 Mesh optimization

This problem is related to the preceding point, and is a real issue on itself. There are several ways to define meshes that are coherent with the numerical requirement of the code and the model to simulate (Figure 152 and Figure 153). Simple regular meshes can be defined by hand, but complex unstructured and/or non uniform meshes can only be generated by specific numerical codes and sometimes it is difficult to optimize the parameters of these meshes.

If the mesh is not sufficiently refined, the numerical diffusion can be high, and the results are no longer representative of the physics that the code is trying to solve. On the other hand, if the mesh is too refined, the time needed for the simulation can be too high for practical use (due to power limitation of the computers) or numerical problems, like time step reduction (see preceding point), can occur.

To solve this problem, one approach is to use an automatic and adaptive mesh generator, optimizing the mesh at each numerical time step by refining it where fronts are present and coarsening it where refinement is less necessary (front has passed or is not yet arrived).

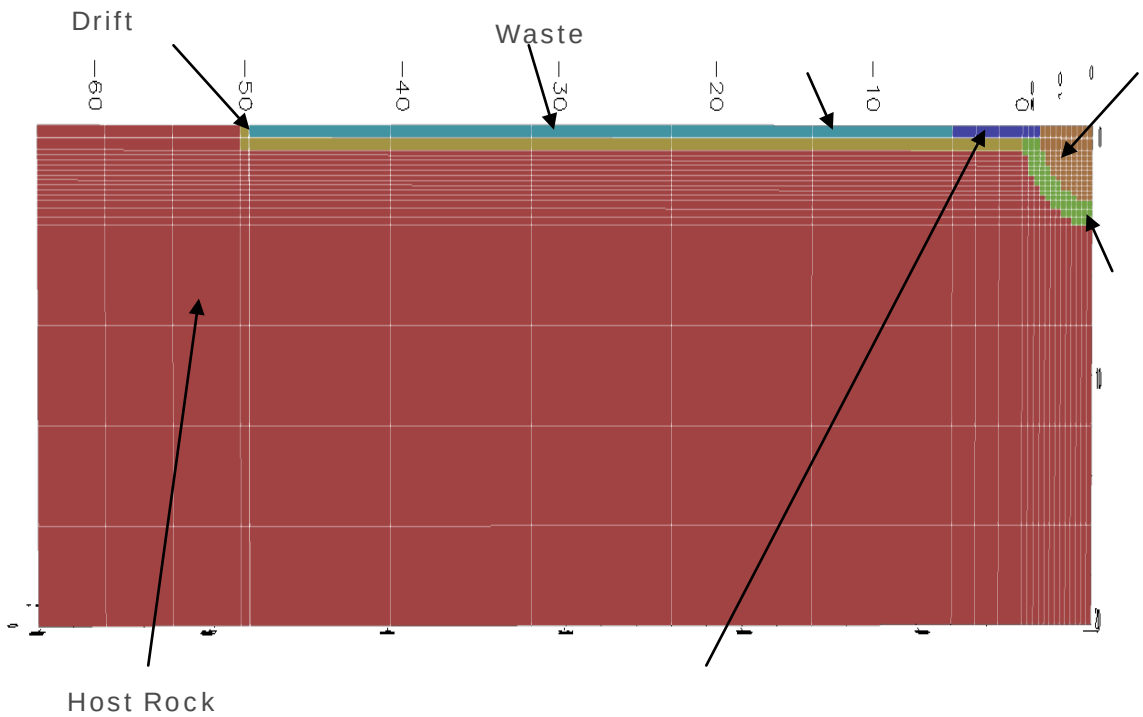

Figure 152 Example of a coarse regular mesh

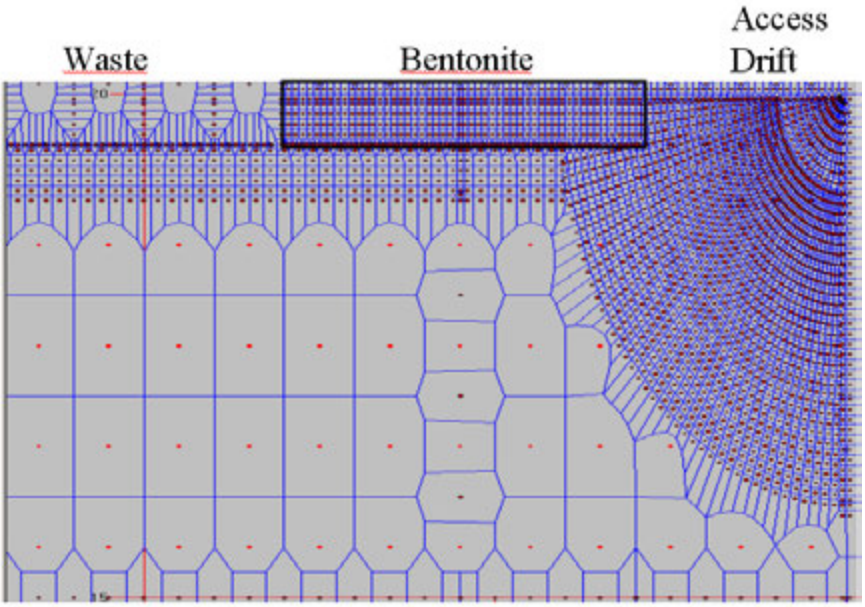

Figure 153 Example of a refined unstructured non conform mesh

4.4 Model and code development in the frame work of this cell scale benchmark

Part of the goals of FORGE WP1.2 is trying to develop models and codes more suitable for two-phase flow transport and also to work on upscaling technics.

As for simulation at the cell scale upscaling is not an issue, this point will be developed in the module and repository scale benchmark document.

Concerning model development IRSN has made a contribution integrating a special set of unknown to avoid numerical problems linked to phase changes. This new set of variable and the method used to implement it in a new code is fully described in chapter 3.6 as well as a first trial of application on the cell scale benchmark. It shows that such approaches are viable and worth developing although for the FORGE project a full complete 3D code was not available due to the timeframe of the exercise.

CEA has also developed a new code but aiming toward high performance computing on massively parallel computers (see chapter 3.4 for more details). This way is also worth developing as two phase flow being highly nonlinear this type of development can significantly reduce the computing time. One again, due to the limited time in the framework of FORGE, the code is not fully operational and will continue to be developed on the following years.

4.5 Discussion on the representativity of the models used and Interactions with other FORGE WP's

The mathematical representation of the phenomenology specified of the benchmark is based on simple equations widely used over the world (e.g., two-phase flow associated with dissolution/diffusion processes). This formulation has the advantage of been implemented in most of the hydraulic-gas codes available but on the other hand it is missing some more complex behavior that could be significant in some particular situation. The main simplifications needing some comments are :

- No coupling with other processes, mainly mechanic and thermic. In the clay, and especially in the EDZ, mechanical processes like creep are changing significantly the hydraulic conditions over long periods of time. In the bentonite, during resaturation, the poral structure is largely modified and this implies also mechanical interaction with the hydraulic processes. The high level wastes been

exothermal, some thermal coupling could also be important during the first hundred years of the repository time evolution.

- Very crude gas (H2) source term description. The source term used is a step function over 10 000 years representing very crudely the real gas flux generated by corrosion. This flux should be variable in time according to water availability and consumption as well as with the relative humidity of the gas phase. But as this execice is generic (not linked to any national architectural concept) this remark is secondary as most of the processes linked to gas migration are not linked to source term.

- Seal representation. The seal, bentonite plug, is represented as a homogeneous porous media which hydraulic behavior is represented by Darcy two phase flow equations. More than a mechanical coupling problem, this representation is not taking into account the eventual mixing of the bentonite with sand and/or the way the seal was put in place (brick, pellets, powder). This could have significant impacts on the general hydraulic behavior of the seal, especially concerning the gas entry pressure. But once again as this exercise is somehow generic, real seals concept cannot be taken into account and the results are to be interpreted on a general trend point of view.

Another point is that the boundary conditions are inherited from a simulation at total repository scale, therefore they should be representative, but as the global model was not integrating interfaces of any sort and has not exactly the same hydraulic parameter values either, the bias could be significant. More than this, these conditions are imposed in the access drift and are affecting an important part of the model. This problem should be overcome when simulations at higher scales will be performed (module scale and repository scale benchmarks) and is therefore not a real issue.

Concerning the other points mentioned before (coupling, source term, seal), one must keep in mind that the final result is to be produced (i) at total repository scale and (ii) in a PA/SA vision. These two elements requires a simple as possible mathematical/phenomenological model to reduce the calculation time and computer power to a reasonable level and eventually to apply a stochastic approach. Another practical point is that most of (if not all) the available numerical codes able to compute PA/SA (including radionuclides chains decay) are based on Darcy two-phase flow (and dissolution/diffusion processes) and it is not part of FORGE work to develop PA/SA codes based on more sophisticated approaches.

Nevertheless, the model implemented should be as representative as possible of the experimental data. In this context, some conclusions of cell scale benchmark can be directly linked to the work done in other FORGE Work Packages:

- The interface between canisters, cell liner or cell seal (bentonite or concrete) and EDZ is a very important feature for gas behavior at an HLW cell scale in argillite media. Thus improving the knowledge about these interfaces is important. This links to part of the work done in WP3 and WP4.
- The EDZ permeability is also an important parameter concerning gas migration at an HLW cell scale in argillite media. Having more confidence in hydraulic parameters in this material is of real importance, especially for intrinsic permeability, initial values but also its evolution with time. Having data on the relative permeability and retention curves is also important. This links to part of the work done in WP4.
- Another potentially important process is diffusion. A good estimation of the parameters defining this process is to be found especially in the EDZ and in the undisturbed argillites, for saturated and unsaturated conditions. This links to part of the work done respectively in WP4 and WP5.

One last point that should be addressed for a complete PA/SA process is concerning the probabilistic distribution of the parameters values, for all important processes (two-phase flow and dissolution/diffusion). This point is actually not directly addressed in FORGE. However, having reliable data on probabilistic distribution functions for the main parameters of a safety case is a question that is still to be addressed.

5. ANNEX : Full description of the benchmark

5.1 CONTEXT AND OBJECTIVES

From WP1 participants point of view, the aim of the benchmark should less be a comparison of numerical codes then an exercise trying to answer some precise questions in a PA logic (for example, which could be the relative role of the EDZ, interfaces, backfill in the migration of gas at storage scale?). This clearly includes numerical considerations, but they are a mean and not an objective.

One of the difficulties is to find a common playground for all participants, which allows bringing some add-on for each one. After discussion, a general agreement was that the reference exercise will be as generic as possible (without targeting precisely on national concepts) and to propose sensitivity analyses making it possible to cover national specificities. What is aimed is more to feel how the systems react and why they can react differently rather than an inter-comparison of codes. A second agreement was that, although the final aim of the benchmark studies is to represent repository-scale simulations, the first exercise should be rather simple and at cell scale.

In this context, one of the major problems in representing gas transfers in a repository for radioactive waste is to model simultaneously all gas sources (generally located in the disposal cells) and the transfer pathways constituted by the network of interfaces, plugs and undergrounds drift.

5.2 REFERENCE TEST CASE

The objective of this first test case is to simulate the gas production and migration in a disposal cell and a portion of the drift (Figure 154).

The calculation domain is axisymetric. In the direction of the cell axis, the extension takes into account the length of the cell, the distance between the bottom of two adjacent cells in this direction and the radius of the access drift (Figure 155 and Table 18). The radius of the axisymetric domain is a compromise between the inter-cell distance along the access drift and the thickness of the geological layer.

A gas-production term is provided for the disposal cell. It is imposed on the external surface of the cylinder that represents schematically the canisters. The cell is constituted of a material impermeable to both water and gas, and is not explicitly represented in the model (the external surface of the canister is a no flux boundary). The materials to be taken into account in that simulation include the EDZ of both the cell and the access drift, the cell plug, the backfill of the access drift and the geological medium. Moreover the interface between the cell and the cell EDZ should be represented (general retention behaviour similar to a sand), taking into account a different behaviour whether the interface is facing the bentonite plug (same permeability as EDZ) or the canisters (same permeability as a sand).

The aim of this test case is to better understand the mechanisms of the gas migration (transport, diffusion and dissolution) at the cell scale and in particular to analyze the effect of the presence of different material and interfaces on such mechanisms.

For this first exercise, isothermal hypothesis at 20°C were considered, even in the sensitivity analysis.

The main constraints of the case are to give a detailed representation of all the elements of the proposed problem and to maintain compatible calculation times with the simulation tools while complying with the physics of the problem. Moreover special attention should be paid at the effect of the size and form of the mesh on the results of the simulation.

The simulations should be performed using a full physical model (multiphase darcy's law, with interaction between each phase: dissolution/evaporation and diffusion), a consistent example can be found in paragraph 5.5 "Mathematical model proposed for the exercise".

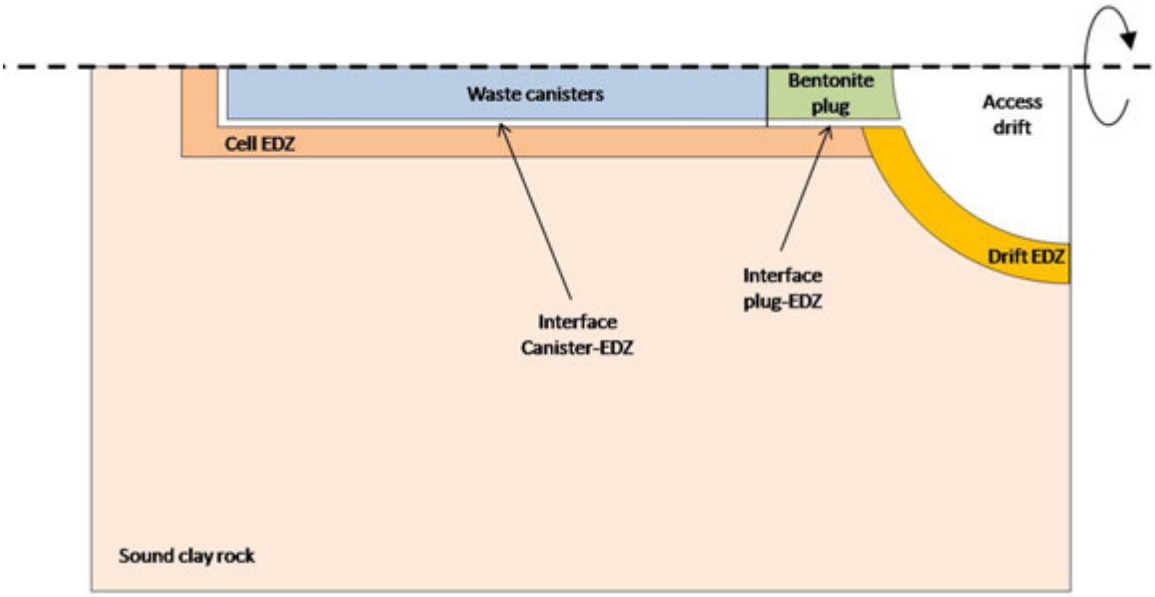

Figure 154: Representation of the axisymetric calculation domain

5.2.1 GEOMETRY

The canister and the plug share the same circular section.

The section of the access drifts is circular. Disposal cell is positioned at half-height in the access drift.

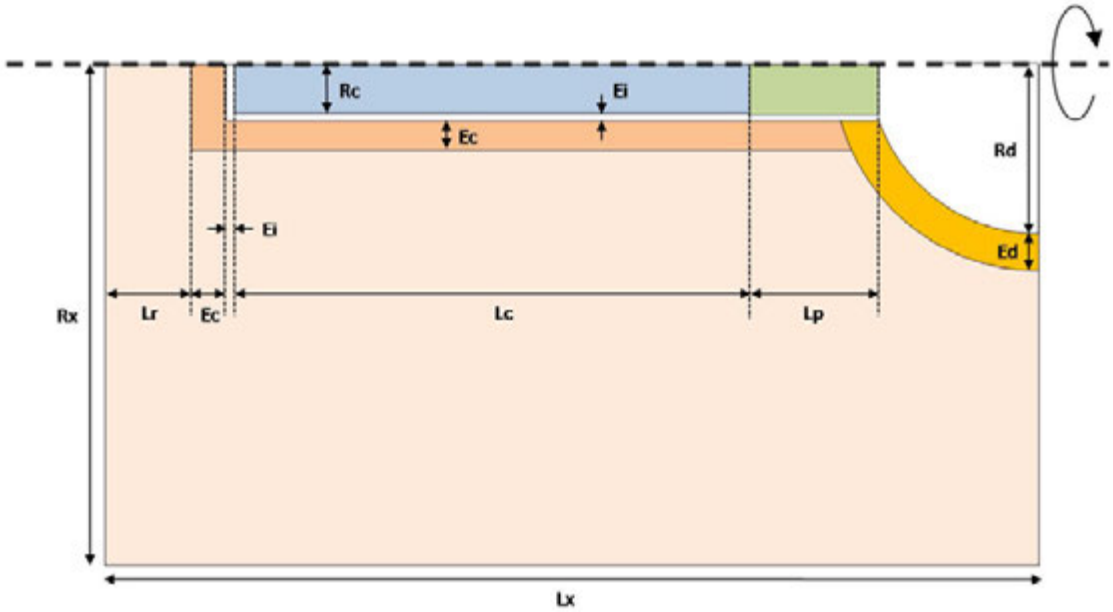

Figure 155: Dimensions in the calculation domain

Table 18 : Size of items in the calculation domain

Name of parameter	Parameter	Value
Length of the domain (cell axis direction)	Lx	60 m
Radius of the domain	Rx	20 m
Radius of access drift	Rd	3 m
Thickness of the access drift EDZ	Ed	1 m
Length of the plug	Lp	5 m
Length of the canister zone	Lc	40 m
Thickness of the cell EDZ	Ec	0.5 m
Plug and canisters radius	Rc	0.5 m
Thickness of the interface	Ei	0.01 m
Distance between end of cell EDZ and boundary	Lr	11.5 m

5.2.2 PHYSICAL PARAMETERS

Physical parameters at 20°C are shown in Table 19 (for this first exercise, all calculations are isotherm and temperature is set at 20°C throughout the simulation period).

Table 19 : Physical characteristics of materials

Parameter (at 20°C)	Materials		
	Interface facing plug	Interface facing canister	Backfill (access drift)
K_v [m^2]	$5.0\ 10^{-18}$	$1.0\ 10^{-12}$	$5.0\ 10^{-17}$
K_h [m^2]	$1.0\ 10^{-17}$	Kv=Kh	
Porosity [%]	30	100	40
Specific storage coefficient [m^{-1}]	$4.6\ 10^{-06}$	$4.6\ 10^{-06}$	$1.0\ 10^{-05}$
Two-phase flow parameters			
S_{gr} [%]	0	0	0
S_{wr} [%]	0	0	0
Van Genuchten parameters			
n [-]	4	4	1.5
P_r [Pa]	10^4	10^4	$2\ 10^6$
□ (Tortuosity)	1	1	2

Parameter (at 20°C)	Materials		
	Bentonite plug	EDZ	Geologial Medium
K_v [m^2]	$1.0\ 10^{-20}$	$5.0\ 10^{-18}$	$5.0\ 10^{-21}$
K_h [m^2]	Kv=Kh	$1.0\ 10^{-17}$	$1.0\ 10^{-20}$
Porosity [%]	35	15	15

Parameter (at 20°C)	Materials		
	Bentonite plug	EDZ	Geologial Medium
Specific storage coefficient [m^{-1}]	4.4 10^{-06}	2.3 10^{-06}	2.3 10^{-06}
Two-phase flow parameters			
S_{gr} [%]	0	0	0
S_{wr} [%]	0	0	0
Van Genuchten parameters			
n [-]	1.6	1.5	1.5
P_r [Pa]	1.6 10^7	1.5 10^6	1.5 10^7
□ (Tortuosity)	4.5	2	2

- Viscosity of the gas mixture:

The viscosity of the gas mixture (water vapour + hydrogen) can be estimated by a classical Wilke approximation or by a simplified formula as follows:

$$\mu_g = \frac{1}{\frac{X^g_{H_2}}{\mu^g_{H_2}} + \frac{X^g_{wvap}}{\mu^g_{wvap}}} \quad \text{with} \quad \mu^g_{H_2}(T=293K) = 9\ 10^{-6}\ Pa.s \qquad \mu^g_{wvap}(T=293K) = 10^{-5}\ Pa.s$$

- Diffusion coefficient of dissolved H_2 in water:

$$D_{H_2/water} = 1.57\ 10^{-14} \frac{T}{\mu_{water}(T)} \qquad (m^2/s)$$

- Diffusion coefficient of gaseous H_2 in water vapour:
(T_0=293 K and at P_0=1.0·10^5 Pa: D_0=9.5·10^{-5} m^2/s)

$$D^g_{H_2-H_2O} = D_0 \left(\frac{P_0}{P}\right)\left(\frac{T}{T_0}\right)^{1.75} \qquad (m^2/s)$$

- Diffusion coefficient of dissolved H_2 in the water of the porous medium:

$$D^w_{H_2} = S_w \left(\frac{\omega}{\tau^2}\right) D_{H_2/eau}$$

- Diffusion coefficient of dissolved H_2 in the binary H_2/water-vapour mixture of the porous medium:

$$D^{g}_{H_2/vap} = (1 - S_w)\left(\frac{\omega}{\tau^2}\right) D^{g}_{H_2 - H_2O}$$

- Solubility of hydrogen in water: $H_{H_2}(T = 293K) = 7.610^{-6}\ mol.Pa^{-1}.m^{-3}$

Note: Temperature in diffusion models is stated in Kelvin.

5.2.3 Initial conditions

Water saturation:

- in the geological medium is equal to 100%;
- in the cell and drift EDZ is equal to 100%
- in the interface (facing canister and plug) equal to 5%;
- in the bentonite plug is equal to 70%;
- in the backfill of the access drifts is equal to 70%.

Pressure:

- in the water-saturated materials at 100%, the water and gaz pressure are equals to the value at radial outer boundary (respectively 5 MPa and 0.1 MPa, see Boundary limits);
- in partially-saturated materials, the gas pressure is equal to 1 atmosphere. The water pressure is deduced from the gas pressure and the saturation by applying Van Genuchten models associated with each material.

5.2.4 Boundary conditions

Figure 156 is a schematic representation of the boundary conditions to be used.

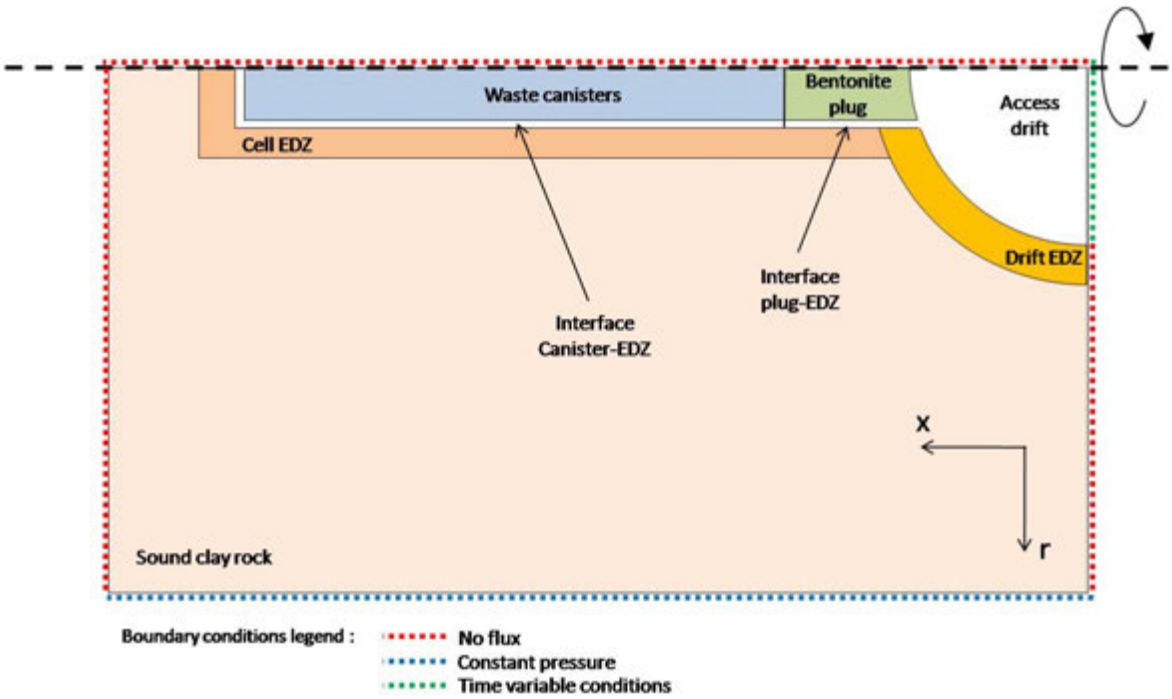

Figure 156: schematic representation of the boundary conditions

- Conditions at the outer radius of the calculation domain:

$P_w(x,r=20,t)=5.0\,10^6\,Pa \quad S_w(x,r=20,t)=1 \qquad P_g(x,r=20,t)=1.0\,10^5\,Pa \quad x\in[0,60],\ t\in[0,t_{fin}]$

As gaseous phase is not expressed, the gas pressure corresponds also to a concentration via Henry's law (see "Mathematical model proposed for the exercise" for details).

- Conditions at the centre (r=0) of the calculation domain:

$Flux_w(x,r=0,t)=0 \qquad Flux_g(x,r=0,t)=0 \qquad x\in[0,60] \quad t\in[0,t_{fin}]$

- Conditions on the lateral side, x=60 of the calculation domain:

$Flux_w(x=60,r,t)=0 \qquad Flux_g(x=60,r,t)=0 \qquad r\in[0,20] \quad t\in[0,t_{fin}]$

- Conditions on the lateral side, x=0 of the calculation domain:

$Flux_w(x=0,r>3,t)=0 \qquad Flux_g(x=0,r>3,t)=0 \qquad r\in]3,20] \quad t\in[0,t_{fin}]$

For r ≤ 3, the boundary conditions are variable in time for water and gas. The representation of these variations can be found in Figure 157.

The boundary conditions represented in Figure 157 are extrapolated from a study made by Andra at a module scale (several hundred of cells). The hypothesis used in this study are a bit different from the one assigned here (especially, the generation term for hydrogen is more complex), but the general behaviour should be the same.

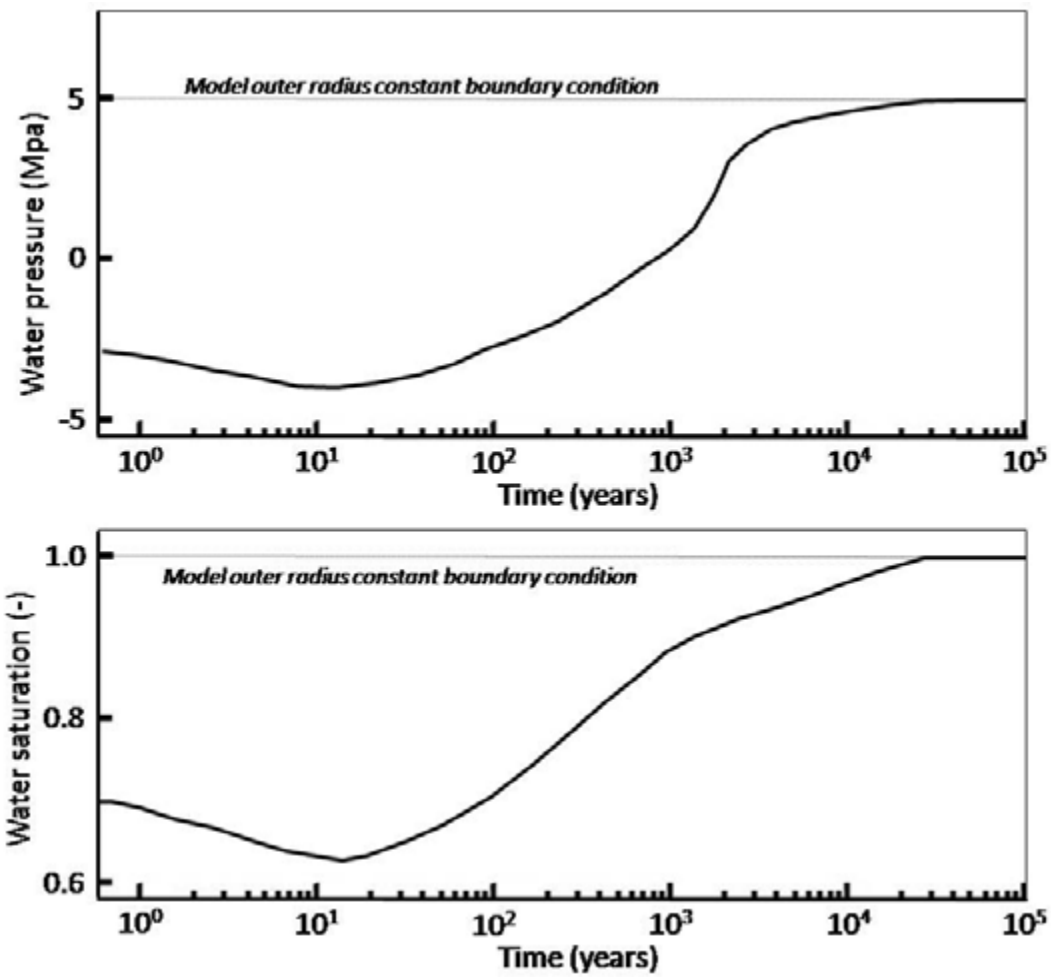

Figure 157: Time variable boundary conditions to be used in the drift

5.2.5 Production term for hydrogen

The hydrogen-production term is to be distributed over the external surface of the cell, as follows:

- for 0 < t ≤ 10000 years, $Q_{H_2}^{g} = 100\ mol/year/cell$ $\quad Q_{H_2}^{w} = 0$ $\quad Q_{H_2}^{w} = 0$
- for t > 10000 years $Q_{H_2}^{g} = 0\ mol/year/cell$

5.2.6 Simulation period

The simulation will be performed between moment $t_0=0$ and moment t_{fin}=100.000 years.

5.3 SENSITIVITY ANALYSIS

For this first exercise, the sensitivity analysis is concentrated oround uncertainties concerning the EDZ, the host rock permeability and the diffusion of H2 in porous media :

- Sensitivity 1 :

The evolution of the EDZ intrinsic permeability with time is not well known, some data however show a reduction of permeability with time down to values similar to those of the undisturbed rock. Concerning the evolution with time of the retention and relative permeability curve of the EDZ, no consistent data are available.

For this sensitivity analysis, everything else being equal to the reference case, EDZ intrinsic permeability (for both drift and cell) is supposed equal to undisturbed rock permeability

- Sensitivity 2 :

Depending of the type of clay rock, Mualem / Van Genuchten curve is not always the best choice for relative permeability of the host rock and EDZ. For certain data a power law fits quite well the measures.

For this sensitivity analysis, everything else being equal to the reference case, relative permeability curve for water and gas of undisturbed host rock and EDZ (for both drift and cell) is supposed to follow saturation at the power 3 :

$$K_r^w = S_w^3 \qquad K_r^g = S_g^3 = (1 - S_w)^3$$

- K_r^w : Relative permeability for water (-)
- K_r^g : Relative permeability for the total gas phase (-)
- S_w : saturation for water (-)
- S_g : saturation for the total gas phase (-)

- Sensitivity 3 :

Uncertainties for the diffusion coefficient of dissolved hydrogen in porous media is quite high and this parameter can have a real impact on the percentage of H2 turning effectively to gas.

For this sensitivity analysis, everything else being equal to the reference case, the diffusion coefficient of dissolved hydrogen under water saturated conditions will be multiplied by 10 for all simulated porous media.

5.4 OUTPUT RESULTS

The output will be the same for the reference case and the sensitivity cases.

- Evolution with time of fluxes through surfaces (see Figure 158)

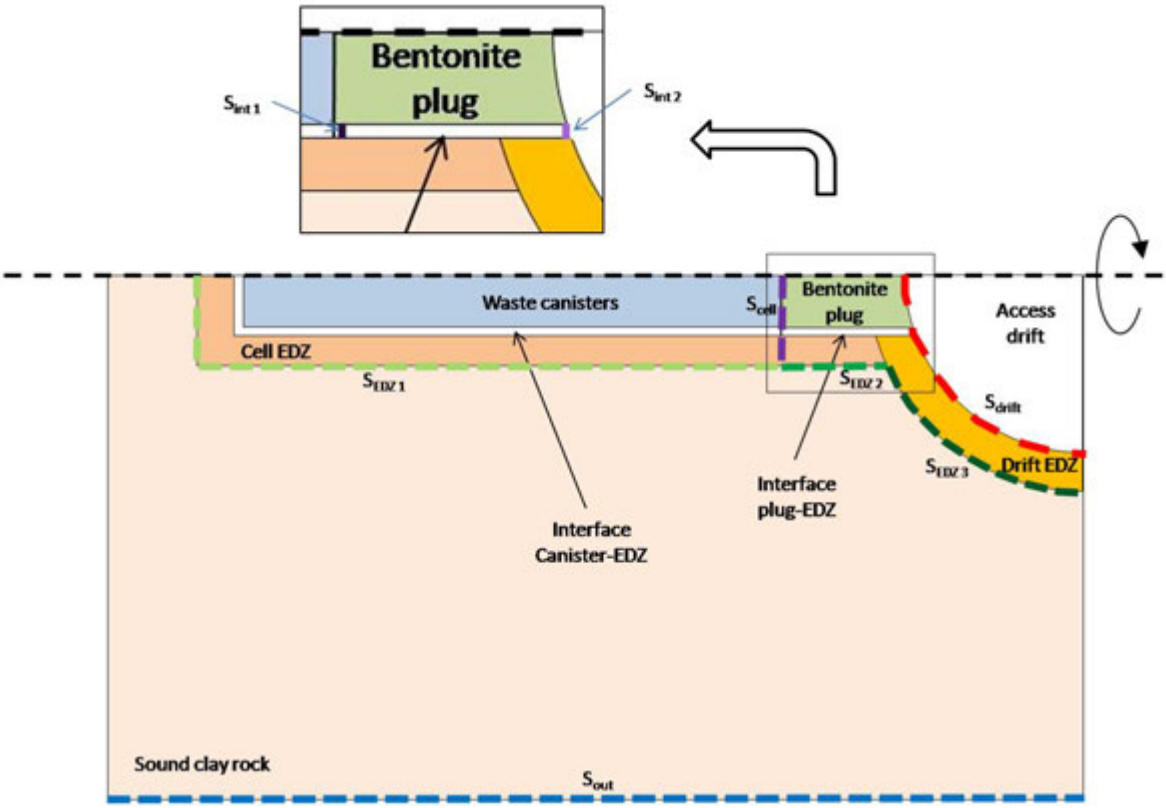

Figure 158: schematic representation of the surfaces trough which fluxes will be calculated

Type of fluxes :

- Liquid water flux
- Water vapor
- Gaseous H2
- Dissolved H2

Type of surfaces :

- Outer boundary of the model at r=20 m (S_{out} in Figure 158), fluxes counted positively out of the model.
- Drift wall (S_{drift} in Figure 158), fluxes counted positively toward the drift
- Outside surface of the EDZ, separated in 3 sections (see Figure 158): S_{EDZ1} (around canister), S_{EDZ2} (around plug), S_{EDZ3} (drift EDZ). Fluxes counted positively out of the EDZ toward the undisturbed rock
- Inner cell surfaces (see Figure 158) : Scell (section including interface and EDZ at canister-plug junction), Sint1 (interface at canister-plug junction), Sint2 (interface at the drift wall). Fluxes counted positively toward the drift.

- Evolution with time along lines (see Figure 159)

Evolution with time of :

- Water saturation
- Water pressure
- Gas pressure (in the gas phase when it exists)
- Dissolved H2 pseudo-pressure (see Henry's law in paragraph 5.5 "Mathematical model proposed for the exercise" for details)
- Capillary pressure

Type of lines

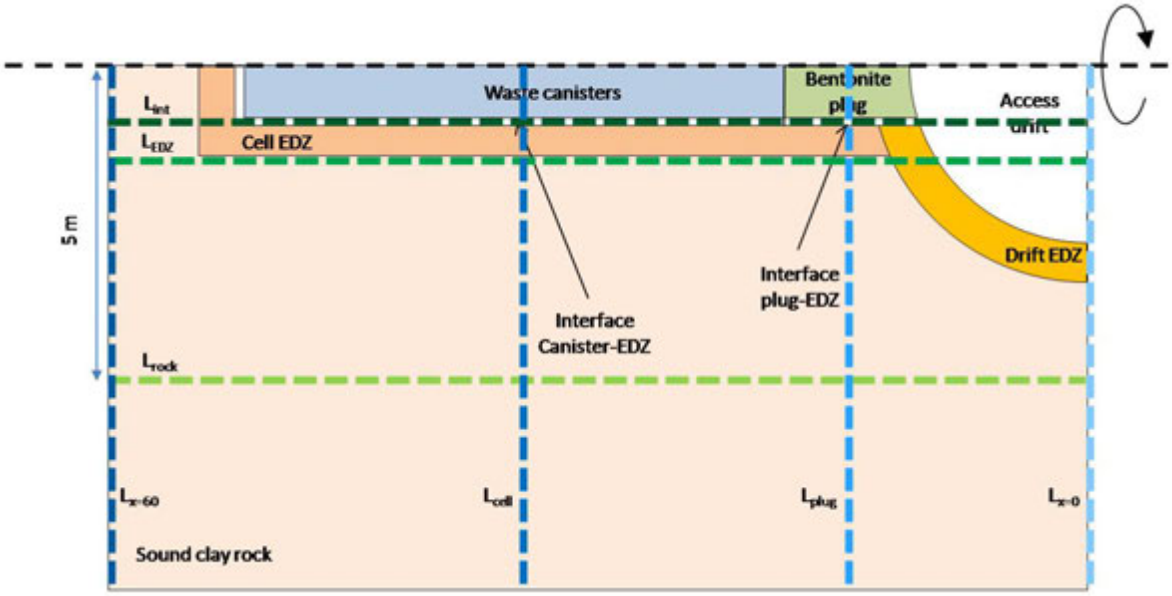

Figure 159: schematic representation of the lines along which results should be given

- Lines at constant radius (see Figure 159) : L_{int} (passes through the interface), L_{EDZ} (just outside the cell EDZ), L_{rock} (inside the rock at a 5 m radius)
- Lines at constant x (see Figure 159) : $L_{x=0}$ and $L_{x=60}$ (boundaries of the model), L_{plug} (in the middle of the plug), L_{cell} (in the middle of the canister)

- Evolution with time at given points (see Figure 160)

Evolution with time of :

- Water saturation
- Water pressure
- Gas pressure (in the gas phase when it exists)
- Dissolved H2 pseudo-pressure (see Henry's law in paragraph 5.5"Mathematical model proposed for the exercise" for details)
- Capillary pressure

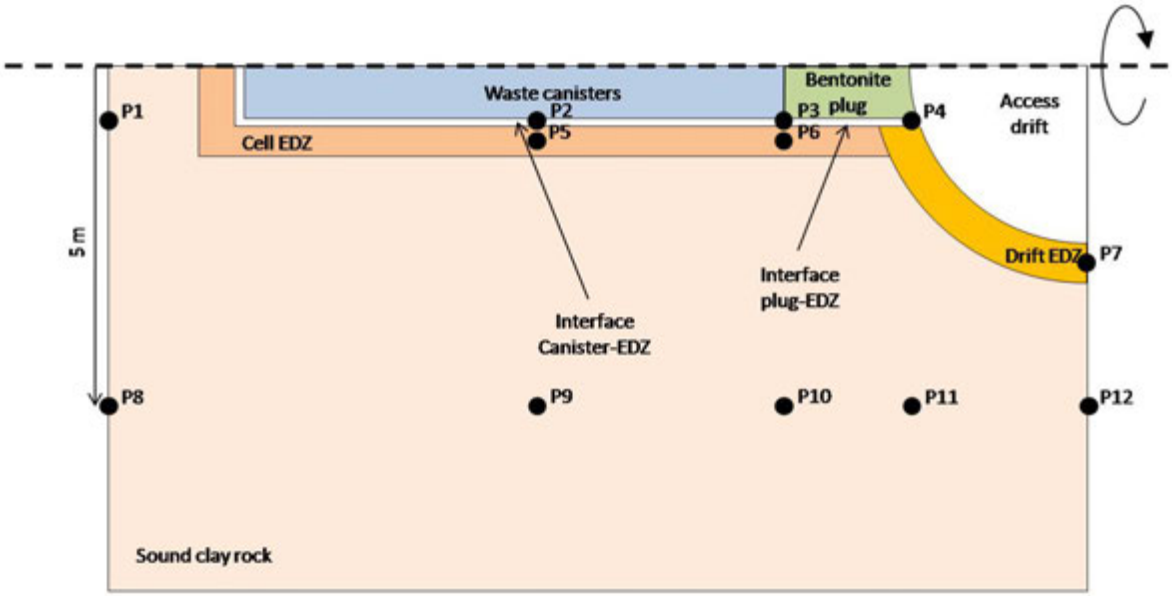

Figure 160: schematic representation of the point where results should be given

Type of points :

- Points 1 to 4, at the same radius as the centre of the interface (see Figure 160) : P1 and P4 (at the boundaries), P2 (in the middle of the canister), P3 (in the middle of the plug)
- Points 5 and 6, at the same radius as the centre of the cell EDZ (see Figure 160) : P5 (in the middle of the canister), P6 (in the middle of the plug)
- Point 7 (see Figure 160) in the middle of the drift EDZ on the x=0 boundary
- Points 8 to 12, at a 5 m radius (see Figure 160) : P8 and P12 (at the boundaries), P9 (at the same x as the middle of the canister), P10 (at the same x as the middle of the plug), P11 (at the same x as the intersection of the drift and the interface)

5.5 MATHEMATICAL MODEL PROPOSED FOR THE EXERCISE

The capillary pressure is defined as the difference between gas pressure and water pressure :

$$P_C = P_g - P_w \qquad (1)$$

- *Pc* : capillary pressure (Pa)
- *Pg* : total pressure of the gas phase(Pa)
- *Pw* : water pressure (Pa)

The dependence between water and gas saturation in each porous media is expressed by :

$$S_g + S_W = 1 \quad \text{with} \quad S_g = \frac{V_g}{V_p} \text{ and } S_w = \frac{V_w}{V_p}$$

- Sg : gas saturation (-)
- Sw : water saturation (-)
- Vg : gas volume (m3)
- Vw : water volume (m3)
- Vp : pore volume (m3)

Van Genuchten model is used to express capillary pressure function of the effective saturation in a given porous media :

$$S_{we} = \frac{S_w - S_{wr}}{1 - S_{wr} - S_{gr}} \quad (2)$$

$$S_{we} = \frac{1}{\left[1 + \left(\frac{P_c}{P_r}\right)^n\right]^m} \quad (3)$$

- Swe : Effective water saturation (-)
- Swr = residual water saturation (-)
- Pr : reference pressure for Van genuchten law (Pa). Generally the value for this coefficient is higher than the gas entry pressure for a given porous media
- n, m : coefficient for Van genuchten law. We have $m = 1 - \frac{1}{n}$

The relative permeability for water is expressed by integrating the Mualem prediction model in the Van Genuchten capillarity model :

$$k_r^w = \sqrt{S_{we}}\left[1 - \left(1 - S_{we}^{1/m}\right)^m\right]^2 \quad (4)$$

- k_r^w : relative permeability for water (-)

The relative permeability for gas is expressed similarly :

$$k_r^g = \sqrt{1 - S_{we}}\left[1 - S_{we}^{1/m}\right]^{2m} \quad (5)$$

- k_r^g : relative permeability for gas (-)

The water and gas movement in a porous media is represented by the mass conservation law and the energy conservation law (reduced to the generalized Darcy law) :

$$U_w = -\frac{kk_r^w(S_w)}{\mu_w}(\nabla P_w + \rho_w g \nabla z) \quad (6)$$

$$U_g = -\frac{kk_r^g(S_g)}{\mu_g}(\nabla P_g + \rho_g g \nabla z) \quad (7)$$

- K : intrinsic permeability of the porous media (m2)
- μg : viscosity of the total gas phase (kg.s-1.m-1)
- μw : viscosity of water (kg.s-1.m-1)
- ρg : volumetric mass of the total gas phase (kg.m-3)
- ρw : volumetric mass of water (kg.m-3)

$$\rho_w(P_w) = \rho_{atm} \exp\left[S_s(P_w - P_{atm})\right] \quad (8)$$

ρatm : volumetric mass of water at atmospheric pressure (kg.m-3)
Patm : atmospheric pressure (Pa)
Ss : specific storage (Pa-1)

- g : gravity (m.s-2)
- z : altitude (m)
- Ug : Darcy velocity for the gas phase (m.s-1)
- Uw : Darcy velocity for water (m.s-1)

Equation of conservation for water :

$$\frac{\partial(\rho_w \omega S_w)}{\partial t} + \nabla(\rho_w U_w) = Q^w \quad (9)$$

- ω : porosity (-)
- Qw : consumption/production of water (kg.m-3.s-1)

Equation of conservation for the total gas phase :

$$\frac{\partial(\rho_g \omega S_g)}{\partial t} + \nabla(\rho_g U_g) = Q^g \qquad (10)$$

- Qg : consumption/production for the total gas phase (kg.m-3.s-1)

The mass fraction of gaseous hydrogen is expressed as :

$$X_{H_2}^g = \frac{\rho_{H_2}^g}{\rho_g} \qquad (11)$$

With $\rho_{H_2}^g = \frac{m_{H_2}^g}{V_g}$ and $\rho_g = \frac{m^g}{V_g}$

- $X_{H_2}^g$ is the mass fraction of hydrogen in the total gas phase (-)
- $m_{H_2}^g$ is the hydrogen mass in the gaz phase (kg)
- m^g is the total mass of the gas phase (kg)
- $\rho_{H_2}^g$ is the volumetric mass of gaseous hydrogen in the gas phase (kg.m-3)

Mass conservation law for gaseous hydrogen :

$$\frac{\partial}{\partial t}(\omega S_g \rho_g X_{H_2}^g) + \nabla(\rho_g X_{H_2}^g U_g - J_{H_2}^g) + \Omega_{H_2}^{g/l} = Q_{H_2}^g \qquad (12)$$

- $\Omega_{H_2}^{g/l}$ is the exchange term from the gaseous phase to the liquid phase for H2 (kg.m-3.s-1)
- $Q_{H_2}^g$ is the consumption/production term for gaseous hydrogen (kg.m-3.s-1)
- $J_{H_2}^g$ is the diffusive term for gaseous hydrogen (kg.m-2.s-1)

Diffusive flux for a binary mixture of gas (H2 and water vapor) can be expressed by Kick law :

$$J_{H_2}^g = \rho_g D_{H_2 vap}^g \nabla X_{H_2}^g \qquad (13)$$

- $D_{H_2 vap}^g$ is the diffusion coefficient for gaseous hydrogen in water vapor (m2.s-1)

The mass fraction of dissolved hydrogen is expressed as :

$$X_{H_2}^w = \frac{\rho_{H_2}^w}{\rho_w} \qquad (14)$$

With $\rho_{H_2}^w = \frac{m_{H_2}^w}{V_w}$ and $\rho_w = \frac{m^w}{V_w}$

- $X_{H_2}^w$ is the mass fraction of dissolved hydrogen (-)
- $m_{H_2}^w$ is the dissolved hydrogen mass (kg)
- m^w is the total mass of the liquid phase (kg)
- $\rho_{H_2}^w$ is the volumetric mass of dissolved hydrogen in the liquid phase (kg.m-3)

Mass conservation law for dissolved hydrogen is expressed as :

$$\frac{\partial}{\partial t}(\omega S_w \rho_w X_{H_2}^w) + \nabla(\rho_w X_{H_2}^w U_w - J_{H_2}^w) + \Omega_{H_2}^{l/g} = Q_{H_2}^w \qquad (15)$$

- $\Omega_{H_2}^{l/g}$ is the exchange term from the liquid phase to the gas phase for H2 (kg.m-3.s-1)
- $Q_{H_2}^{w}$ is the consumption/production term for dissolved hydrogen (kg.m-3.s-1)
- $J_{H_2}^{w}$ is the diffusive term for dissolved hydrogen (kg.m-2.s-1)

The exchange terms from between liquid and gaseous phase are linked by the following relation :

$$\Omega_{H_2}^{l/g} = -\Omega_{H_2}^{g/l} \qquad (16)$$

Diffusive flux for dissolved hydrogen can be expressed by Kick law :

$$J_{H_2}^{w} = \rho_w D_{H_2 vap}^{w} \nabla X_{H_2}^{w} \qquad (17)$$

- $D_{H_2 vap}^{w}$ is the diffusion coefficient for dissolved hydrogen in water vapor (m2.s-1)

Part of the gas will be dissolved in the pore water. The solubility limit for the gas depend mainly on thermodynamic conditions and can be expressed by Henry's law :

$$C_{H_2}^{w} = H_{H_2}(T) P_{H_2}^{g} \qquad (18)$$

Where $C_{H_2}^{w} = \dfrac{X_{H_2}^{w} \rho_w}{M_{H_2}}$

- $C_{H_2}^{w}$ is the maximum concentration of hydrogen in water (mol.m-3)
- H_{H_2} is the constant of Henry's law for hydrogen (mol.m-3.Pa-1)
- $P_{H_2}^{g}$ is the partial pressure of hydrogen in the total gaseous phase (Pa)
- M_{H_2} is the molar mass for hydrogen (kg.mol-1)

The relation between partial pressure of each gas present in the total gas phase and total gas pressure is given by Dalton law that writes for a binary mixture (H2 and water vapor) :

$$P_g = P_{H_2}^{g} + P_{wvap}^{g} \qquad (19)$$

- P_{wvap}^{g} is the partial pressure of water vapor in the total gas phase (Pa)

Each of the gas is supposed perfect :

$$P_{H_2}^{g} = \frac{\rho_{H_2}^{g}}{M_{H_2}} RT \text{ and } P_{wvap}^{g} = \frac{\rho_{wvap}^{g}}{M_{wvap}} RT \qquad (20,21)$$

For the gas mixture this writes :

$$P_g = \frac{\rho_g}{M_g} RT \qquad (22)$$

- Mg : molar mass for the total gaseous phase (H2 + water vapor) (kg.mol-1)
- R : constant of the perfect gas (J.mol-1.K-1) : R = 8.314 J.mol-1.K-1
- T : temperature (°K)

Saturation pressure for water vapor is only depending on temperature and can by expressed by :

$$\log_{10}(P_{sat}) = 2.786 + 0.031514 T_c - 1.2373 x 10^{-4} T_c^{2} + 4.2267 x 10^{-7} T_c^{3} - 8.1308 x 10^{-10} T_c^{4} \qquad (23)$$

- Psat : saturation pressure for water vapor (Pa)
- Tc : Temperature (°C)

Kelvin law is giving a relation between saturation pressure for water vapor, effective pressure for water vapor and capillary pressure :

$$P^{g}_{wvap}(T,S_w) = \exp\left(\frac{M_w P_c(S_w)}{\rho_w RT}\right) P_{sat}(T) \tag{24}$$

FORGE

Fate Of Repository Gases

European Commission FP7

Final report on benchmark studies on repository-scale numerical simulations of gas migration Part 2: module scale benchmark

FORGE Reports D1.4R and D1.6-R pt 2

Keywords.

Benchmark, module scale, numerical simulation, repository

Bibliographical reference

WENDLING, J (COMPILER). 2013. Final report on benchmark studies on repository-scale numerical simulations of gas migration Part 2: module scale benchmark .

FORGE Reports D1.4R and D1.6-R pt 2. 169pp.

Euratom 7th Framework Programme Project: FORGE

EURATOM

FORGE Deliverable D1.6-R

Final report on benchmark studies on repository-scale numerical simulations of gas migration Part 2: module scale benchmark[1]

September 2013

Authored by:

France	Eloi Treille & Jacques Wendling (ANDRA)
	Magdalena Dymitrowska & Delphine Pellegrini (IRSN)
	Etienne Ahusborde, Mladen Jurak & Brahim Amaziane (CNRS)
	Florian Caro & Alain Genty (CEA)
Lithuania	Povilas Poskas & Darius Justinavicius (LEI)
Switzerland	Manuel Sentis (ENSI)
United Kingdom	Simon Norris (NDA RWMD)
	Alex Bond (Quintessa)
Canada	Helen Leung (NWMO)
	Nicola J. Calder (Geofirma)

Compiled by:	Jacques Wendling	Date: September 2013
Checked by:	Simon Norris	Date: 28th March 2014
Approved by:	Richard Shaw	Date: 30th April 2014

[1] J. Wendling, E. Treille, M. Dymitrowska, D. Pellegrini, E. Ahusborde, M. Jurak, B. Amaziane, F. Caro, A. Genty, P. Poskas, D. Justinavicius, M. Sentis, S. Norris, A. Bond, H, Leung, N.J. Calder, *Final report on benchmark studies on repository-scale numerical simulations of gas migration, Part 2 : module scale benchmark*, European Commission FORGE Deliverable D1.6-R, 2013..

Fate **O**f **R**epository **G**as**E**s (FORGE)

The multiple barrier disposal concept is the cornerstone of all proposed schemes for geological disposal of radioactive wastes. The concept is based on a series of passive complementary barriers, both engineered and natural, that act to achieve the required level of safety for radioactive waste disposed in a geological repository.

Demonstrating an appropriate understanding of gas generation and migration is a key component in a safety case for a geological repository for radioactive waste. On the basis of work to date, the overall behaviour of waste-derived gas and its influences on repository system performance require improved understanding. Key issues to be further examined relating to an enhanced understanding of gas-related processes include: dilational versus visco-capillary flow mechanisms; long-term integrity of seals, in particular gas flow along contacts; role of the EDZ as a conduit for preferential flow; and laboratory to field up-scaling. Such issues are the focus of the integrated, multi-disciplinary European Commission FORGE project.

The FORGE project links international radioactive waste management organisations, regulators and academia, and is specifically designed to tackle the key research issues associated with the generation and movement of repository gases associated with waste disposed in a geological repository. Of particular importance are the long-term performance of bentonite buffers, plastic clays, indurated mudrocks and crystalline formations. Further experimental data are required to reduce uncertainty relating to the quantitative treatment of gas in performance assessment.

FORGE will address these issues through a series of laboratory and field-scale experiments, including the development of new methods for up-scaling allowing the optimisation of concepts through detailed scenario analysis. The FORGE partners are committed to training and CPD through a broad portfolio of training opportunities and initiatives which form a significant part of the project.

Further details on the FORGE project and its outcomes can be accessed at www.FORGEproject.org.

Contact details:

EC FORGE Work Package 1 Leader:

Dr Simon Norris

Nuclear Decommissioning Authority – Radioactive Waste Management Directorate

Tel +44 1925 802891

Fax +44 1925 802948

Email simon.norris@nda.gov.uk

Web address: www.nda.gov.uk

Address NDA Harwell
Building 587
Curie Avenue
Harwell Science and Innovation Campus
Didcot
Oxon OX11 0RH
United Kingdom

Table of content

1. Context and introduction 1

2. Definition of the benchmark 2

3. Summary of the work done by the different teams 4

3.1 NDA RWMD contribution 4

3.1.1 Introduction 4
3.1.2 Model Implementation 4
3.1.3 Base Case Results 9
3.1.4 Sensitivity Cases on the Base Case (50 HA Cells) 15
3.1.5 Variant Case – 100 Cells 20
3.1.6 Sensitivity Cases on the Variant Case (100 HA Cells) 22
3.1.7 Discussions and Conclusions 24
3.1.8 References 25

3.2 SCK-CEN contribution 26

3.3 Andra contribution 27

3.3.1 Introduction 27
3.3.2 Model Implementation 27
3.3.3 Base Case Results 31
3.3.4 Discussion and Conclusions 35

3.4 CEA contribution 36

3.4.1 Introduction 36
3.4.2 Model Implementation 36
3.4.3 Base Case Results 38
3.4.4 Discussion and Conclusions 40
3.4.5 Issues for further consideration 40
3.4.6 References 40

3.5 CNRS contribution 41

3.5.1 Introduction 41
3.5.2 Model Implementation 41
3.5.3 Base Case Results 62
64
3.5.4 Sensitivity Cases 76
3.5.5 Discussion and Conclusions 78
3.5.6 References 79

3.6 IRSN contribution 80

3.6.1 Introduction 80
3.6.2 Model Implementation 80
3.6.3 Base Case Results 85
3.6.4 Sensitivity Cases 89
3.6.5 Discussion and Conclusions 89
3.6.6 Lessons Learnt 89
3.6.7 References 89

3.7 LEI contribution 91

3.7.1 Introduction 91
3.7.2 Model Implementation 91
3.7.3 Base Case Results 94
3.7.4 Conclusions 98

3.7.5 References 98
3.8 ENSI/IFSN contribution 99
3.8.1 Introduction 99
3.8.2 Codes Used for the Calculation 101
3.8.3 Numerical Formulation 102
3.8.4 Benchmark Implementation 103
3.8.5 Base Case Results 108
3.8.6 Conclusions 119
3.8.7 Issues for Further Consideration 119
3.8.8 References 119
3.9 NWMO contribution 120
3.9.1 Introduction 120
3.9.2 Model Implementation 120
3.9.3 Base Case Results 128
3.9.4 Sensitivity Cases 141
3.9.5 Discussion and Conclusions 146
3.9.6 Issues for further consideration 146
3.9.7 References 146
4. Global synthesis of the benchmark at module scale 147
4.1 Comparison of the available results at module scale and main phenomenological understandings 147
4.1 Numerical and upscaling technics used in the frame work of this module scale benchmark 149
4.2 Representativity of the evaluation 150
5. ANNEX: Full description of the benchmark at module scale 151
5.1 Context and Objectives 151
5.2 Benchmark General specification at module scale 151
5.3 Detailed description of the test case 155
5.3.1 Geometry 155
5.3.2 Boundary Conditions 157
5.3.3 Physical Parameters 160
5.3.4 Initial conditions 161
5.3.5 Production term for Hydrogen 162
5.3.6 Simulation period 162
5.4 Output results 162
5.4.1 Evolution with time of mass flows across surfaces 163
5.4.2 Evolution along lines at different times 164
5.4.3 Evolution with time at given points 165
5.5 Mathematical model proposed for the exercise 167

List of figures

Definition of benchmark

Figure 1 Schematic representation of a repository for HLW 2
Figure 2 Schematic representation of the module to be simulated. 3
Figure 3 QPAC geometry definition. 4
Figure 4 Plan illustration of the model showing the half not considered in this initial model. 6
Figure 5 Visualisation of the 3D Cartesian grid with compartments coloured by material type (left). Close-up of the access drift and main drift junction with the top half of the model removed (right) 7
Figure 6 Visualisation of the 3D Cartesian grid with compartments coloured by material type and the host rock removed (left) and only interfaces visible (right) 7
Figure 7 Process of inserting cylindrical grid sections for the waste cells into the Cartesian grid. Grey=Host Rock, Green=EDZ, Red=Interfaces, Blue=Plug. 8
Figure 8 Gas pressure and saturation result points. Note the Pu-1 and Pu-2 are not present in the base case. 10
Figure 9 Flux locations and indication of positive flow directions in the waste module. Note the F_PU is not present in the base case. 11
Figure 10 Gas pressure at key measurement points. 11
Figure 11 Water saturations at key measurement points. 12
Figure 12 Free gas fluxes in the module compared with total gas generation and cell generation rates. 12
Figure 13 As per Figure 12, but zoomed in to the scale of individual cell fluxes. 13
Figure 14 Free gas and dissolved gas fluxes (+ve = outflow) across the top and bottom of the model compared with total gas generation and cell generation rates. 14
Figure 15 Upscaling approach for sensitivity case 5 and 6. 16
Figure 16 Water saturation at Pd-1 for the three interface sensitivity cases (Group A) and the base case. 17
Figure 17 Gas pressure at Pd-1 for the three interface sensitivity cases and the base case. 18
Figure 18 Water saturation at Pd-1 for the three grid sensitivity cases (Group B), the base case and sensitivity case 1. 19
Figure 19 Gas pressure at Pd-1 for the three grid sensitivity cases (Group B), the base case and sensitivity case 1. 19
Figure 20 Visualisation of the 3D Cartesian grid for 100 HA Cells with compartments coloured by material type and the host rock removed (left) and only interfaces visible (right) 20
Figure 21 Water saturations at key measurement points for the 100 Cell variant case. 21
Figure 22 Gas pressure at key measurement points for the 100 Cell variant case. 21
Figure 23 Fractional difference in upstream versus downstream plug gas fluxes (+ve = more flux downstream) 22
Figure 24 Gas pressure and water saturation for the 100 Cell case at 10,000 years. 22
Figure 25 Gas pressure at Pd-1 and Pu-1 for case 7 and the 100 cell variant (labelled Base here) 23
Figure 26 Water saturation at Pd-1 and Pu-1 for case 7 and the 100 cell variant (labelled Base here) 23
Figure 27 : examples of different parts of the mesh 29
Figure 28 : Liquid pressure at different points 31
Figure 29 : gas pressure at different points 32
Figure 30 : mass flow of gaseous hydrogen across cell interface and EDZ. Positive values means of flow directed from cell toward the drift 33
Figure 31 : mass flow of gaseous hydrogen across access drift. Positive values means a flow directed toward the main drift 34

Figure 32 : mass flux of gaseous hydrogen across the main drift plugs 35
Figure 33: Mesh of the whole system (2,500,000 tetrahedrons) 37
Figure 34: Mesh of the repository cells and access galleries. 37
Figure 35: Liquid saturation evolution for different components of the system. 38
Figure 36: Liquid saturation horizontal cross-section (z=75 m) at t=10 years (top) and t=300 years (bottom). 39
Figure 37: Gas pressure horizontal cross-section (z=75 m) at t=300 years. 39
Figure 38: Gas pressure vertical cross-section (y=73 m) at t=300 years. 40
Figure 39 Computation of effective capillary pressure law. 47
Figure 40 Different upscaling steps near canisters and in the drifts. 50
Figure 41 Effective relative permeability and the capillary pressure curves of the EDZ upscaled with the Interface. 51
Figure 42 Effective tortuosity of the EDZ upscaled with the Interface. 52
Figure 43 Effective relative permeability curves of the Backfill upscaled with the Interface. 53
Figure 44 Effective tortuosity curves of the Backfill upscaled with the Interface. 53
Figure 45 Effective curves of the Main drift plug upscaled with the Interface. 54
Figure 46 Effective tortuosity curves of the Main drift plug upscaled with the Interface. 54
Figure 47 Grid for U1 model. 55
Figure 48 Effective relative permeability curves of the domain containing the Canister, Interface and EDZ. 56
Figure 49 Effective tortuosity curves of the domain containing the Canister, Interface and EDZ. 57
Figure 50 Effective relative permeability curves of the domain containing the Plug, Interface and EDZ. 57
Figure 51 Effective tortuosity curves of the domain containing the Plug, Interface and EDZ. 58
Figure 52 Effective relative permeability curves of the domain containing the Backfill, Interface and EDZ. 59
Figure 53 Effective tortuosity curves of the domain containing the Backfill, Interface and EDZ. 59
Figure 54 Grid for U2 model. 60
Figure 55 Effective relative permeability curves of the domain containing block of canisters. 61
Figure 56 Effective tortuosity curves of the domain containing block of canisters. 61
Figure 57 Grid for U3 model. 62
Figure 58 Water flux for U3 immiscible simulation. 63
Figure 59 Gas flux for U3 immiscible simulation. 64
Figure 60 Water saturation in points for U3 immiscible simulation. 64
Figure 61 Gas pressure in points for U3 immiscible simulation. 64
Figure 62 Liquid water total flux for U3 simulation 65
Figure 63 Liquid water total flux for U3 miscible simulation. 66
Figure 64 Gaseous Hydrogen total flux for U3 miscible *simulation.* 66
Figure 65 Gaseous Hydrogen total flux for U3 miscible simulation. 67
Figure 66 Gas saturation in points for U3 miscible simulation. 68
Figure 67 Gas pressure in points for U3 miscible simulation. 68
Figure 68 Water pressure in points for U3 miscible simulation. 69
Figure 69 Capillary pressure in points for U3 miscible simulation. 69
Figure 70 Comparison of the solutions in the point C25-3. 70
Figure 71 Comparison of the solutions in the Main drift at t=1000 years. 70
Figure 72 Liquid water total flux for U2 simulation. 71
Figure 73 Water vapor total flux for U2 simulation. 71
Figure 74 Gaseous hydrogen total flux for U2 miscible simulation. 72
Figure 75 Dissolved hydrogen total flux for U2 miscible simulation. 72
Figure 76 Gas saturation in points for the U2 miscible simulation. 73
Figure 77 Gas pressure in points for the U2 miscible simulation. 73
Figure 78 Water pressure in points for the U2 miscible simulation. 74
Figure 79 Capillary pressure in points for the U2 miscible simulation. 74
Figure 80 Solutions in the points Pu-1 for both U2 and U3 miscible simulations. 75
Figure 81 Solution in the point P-C25-3 for both U2 and U3 miscible simulations. 75

Figure 82 Solution in the Main drift at t=10000 years for both U2 and U3 miscible simulations. 76
Figure 83 Flux comparison over section D1. 77
Figure 84 Comparison of the solutions in the point C25-3. 78
Figure 85 The mesh used for the module case: the part containing the main drift and a zoom at the interfaces around the plug in this drift. 81
Figure 86 Boundary conditions for the drift in terms of X_i^h. 82
Figure 87 Time series of Pl, Pg and Sg in prescribed output points for the 2D module case. 86
Figure 88 Base case results at 1y and 10y for prescribed lines L-AD and L-MD and a zoom on primary variables in the main plug interface along the L-MD. 87
Figure 89 Base case results at 1y and 10y for prescribed lines along three cells (1, 25 and 50) in terms of phase pressures (left axis [Pa]) and saturation (right axis). 88
Figure 90 Modelling domain simulated by LEI team 91
Figure 91 Grid of LEI model coloured by material type: full model (left) and model pattern without considered host rock (right) 92
Figure 92 Visualisation of interfaces (left) and engineered materials (right) in LEI model 92
Figure 93 Schematic representation of points where results are given: P-Cxx-1 in the undisturbed clay medium; P-Cxx-2 in the waste interface; P-Cxx-3 in the backfill interface; P-PU-1 in the bentonite plug; P-PU-2 in the plug interface; P-BC in the end of main drift backfill (time varying boundary condition) 94
Figure 94 Gas saturation evolution with time 95
Figure 95 Gas pressure (left) and liquid pressure (right) evolution with time for specific fluxes 95
Figure 96 Schematic representation of flux surfaces and directions of positive flow: F-Dxx through access drift backfill, interface and EDZ toward the main drift; F-Cxx through waste interface and EDZ toward the cell; F-PU through main drift plug and interface toward the end of main drift 96
Figure 97 Flow rate of gaseous hydrogen through different surfaces 96
Figure 98 Flow rate of dissolved hydrogen out of the module 97
Figure 99 Domain of the model proposed for the second benchmark exercise (module scale) [1]. 99
Figure 100 Domain of the model proposed for the third benchmark exercise (repository scale) [2]. 100
Figure 101 Space discretization in the integral finite difference method [3]. 102
Figure 102 Horizontal and vertical dimensions as well as boundary conditions for the model of the second benchmark [1]. 103
Figure 103 Detail of the mesh: Transversal cut of the cylindrical waste tunnels. 105
Figure 104 Detail of the mesh: Longitudinal cut of the module close to the main drift. 105
Figure 105 Gas pressure (left) and water pressure (right) time varying boundary conditions on the backfill 107
Figure 106 Points of the model for which results were required. 108
Figure 107 Variation of the gas saturation with the time at the points shown in Figure 106. 109
Figure 108 Variation of the gas pressure with the time at the points shown in Figure 106. 110
Figure 109 Variation of the water pressure with the time at the points shown in Figure 106. 110
Figure 110 Lines of the model along which results are provided. 111
Figure 111 Variation of the water saturation along the access drif; line L-AD in Figure 110. 111
Figure 112 Variation of the gas pressure along the access drift; line L-AD in Figure 110. 112
Figure 113 Variation of the water saturation perpendicular to the access drift; line L-C25 in Figure 110. 113
Figure 114 Variation of the gas pressure perpendicular to the access drift; line L-C-25 in Figure 110. 114
Figure 115 Variation of the water saturation perpendicular to the access drift; line L-C-25 in Figure 110. 114
Figure 116 Variation of the water saturation along the main drift; line L-MD in Figure 110. 115

Figure 117 Variation of the gas pressure along the main drift; line L-MD in Figure 110. 116
Figure 118 Position of the surfaces used for the calculation of the mass flow rates. 117
Figure 119 Results for the mass flow rates of water through the different surfaces. 117
Figure 120 Results for the mass flow rates of gas through the different surfaces. 118
Figure 121 Results for the mass flow rates of dissolved H2 through the different surfaces. 118
Figure 122 : 3D model domain with boundary conditions, cells and drifts. Note that variable pressure and saturation boundary conditions exist at the upstream (Y= 0) and downstream (Y= 126) ends of the main drift. 121
Figure 123: Grid discretization detail: cross-section of a cell. Note that cell areas and volumes for the inner cell EDZ have been corrected to remove the inactive waste containers, as described in the text. 122
Figure 124: Grid discretization detail: cross-section of a cell plug. 123
Figure 125: Grid discretization detail: plan view of the access drift. 123
Figure 126: Grid discretization detail: plan view of the main drift. 124
Figure 127: Capillary pressure curve for cell interface, EDZ and cell inner EDZ (combined interface and EDZ) at high liquid saturations 126
Figure 128: Relative gas permeability curves for the interface represented by the benchmark and T2GGM 127
Figure 129: Gas saturation and dissolved gas mass fraction at 1 year, at a plan slice through the middle of the repository. 128
Figure 130: Water saturation with time at L-MD points between the bentonite plugs (Y= 35 to Y= 90), compared to the main drift boundary condition. 129
Figure 131: Water pressure with time at L-MD points between the bentonite plugs (Y= 35 to Y= 90), compared to the main drift boundary condition. 129
Figure 132: Evolution of water saturation, water pressure and gas pressure for various times along the L-MD line. 130
Figure 133: Evolution of water and H_2 gas with time across F-P surfaces. 131
Figure 134: Plan view of gas saturations at 300 years, through the middle of the repository. 131
Figure 135: Evolution of liquid water with time across F-C (cell) and F-D (access drift) surfaces. 132
Figure 136: Evolution of liquid water with time across F-P (main drift) surfaces. 132
Figure 137: Evolution of H_2 gas with time across F-C (cell) surfaces. 133
Figure 138: Evolution of H_2 gas with time across F-D (access drift) and F-P (main drift) surfaces. 133
Figure 139: Water pressures at all output points. 134
Figure 140: Gas pressure at all output points. 135
Figure 141: Gas saturation and at 100 years, at a plan slice through the middle of the repository. 136
Figure 142: Gas saturation and at 300 years, at a plan slice through the middle of the repository. 136
Figure 143: Gas saturation and at 1000 years, at a plan slice through the middle of the repository. 136
Figure 144: Gas saturation and at 3000 years, at a plan slice through the middle of the repository. 137
Figure 145: Gas saturation and dissolved gas mass fraction at 10 000 years, at a plan slice through the middle of the repository. 137
Figure 146: Gas saturation and dissolved gas mass fraction at 10 000 years, for a vertical XZ slice at Y = 72 (just above the bentonite plugs in the cells). Note that locations of cells are shown as black circles for clarity with dissolved gas mass fraction. 138
Figure 147: Gas saturation at 30 000 years, for a vertical XZ slice at Y = 72 (just above the bentonite plugs in the cells). Note that locations of cells are shown as black circles for clarity. 138
Figure 148: Gas saturation at 300 years, at a detail of a plan slice through the middle of the repository. Green blocks are either bentonite plugs at the end of cells, or host rock. White areas are areas with gas saturation less than 1E-6. Reminder that cell centers of upscaled interface and EDZ have modified block volumes similar to the adjacent EDZ blocks. 139
Figure 149: H2 gas flow across F-C slices, shown for material components in the slice, upscaled interface (IF)/EDZ and EDZ. 140

Figure 150: H_2 gas flow across F-D slices, shown for material components in the slice, backfill, upscaled interface (IF)/backfill and EDZ. 141
Figure 151: H_2 gas flow across F-P slices, shown for material components in the slice, upscaled interface (IF)/bentonite and bentonite. 141
Figure 152: Comparison of alternate parameters to reference case: evolution of liquid water with time across F-C (cell) and F-D (access drift) surfaces. 142
Figure 153: Comparison of alternate parameters to reference case: evolution of liquid water with time across F-P (main drift) surfaces. 143
Figure 154: Comparison of alternate parameters to reference case: evolution of H_2 gas with time across F-C (cell) surfaces. 143
Figure 155: Comparison of alternate parameters to reference case: evolution of H_2 gas with time across F-D (access drift) and F-P (main drift) surfaces. 144
Figure 156: Comparison of alternate parameters to reference case: water saturation at all output points. 144
Figure 157: Comparison of alternate parameters to reference case: water pressure at all output points. 145
Figure 158: Comparison of alternate parameters to reference case: gas pressure at all output points. 145
Figure 159 : comparison of gas pressure at point P_C25-2 for all teams 147
Figure 160 : Comparison of gas fluxes across the main drift for all teams 148
Figure 161 : comparison of gas fluxes across section F_D50 (for teams showing this result in their contribution) 149
Figure 162 Schematic representation of a repository for HLW 152
Figure 163 Schematic representation of the module to be simulated. Definition of the A-A', B-B', C-C' and D-D' cross sections 152
Figure 164 Schematic representation of the A-A' vertical cross section (see figure 2 for definition) 153
Figure 165 Schematic representation of the B-B' vertical cross section (see figure 2 for definition) 153
Figure 166 Schematic representation of vertical cross section C-C' and D-D' (see figure 2 for definitions) 154
Figure 167 Schematic representation of the main drift plugs and backfills interfaces 154
Figure 168 Horizontal dimensions and boundary conditions 155
Figure 169 Vertical dimensions and boundary conditions on cross section A-A' 156
Figure 170 Vertical dimensions and boundary conditions on cross section B-B' 156
Figure 171 Gas pressure time varying boundary conditions on the backfill of the main drift 159
Figure 172 Water pressure time varying boundary condition 159
Figure 173 Schematic representation of the surfaces across which flows will be calculated 163
Figure 174 Schematic representation of the lines on which results should be given 164
Figure 175 Schematic representation of the points where results should be given 165

List of tables

IRSN contribution

Table 1 The Initial conditions imposed for the base cell case. The limit values are obtained in the case of saturated materials for the hypothetic (atmospheric) gas pressure of 1e+4Pa. 83

LEI contribution

Table 2 : Total mass of gaseous hydrogen transported through different surfaces 97

ENSI contribution

Table 3 : List of all parameters about the dimensions of the model for the second benchmark [1]. 104

NWMO contribution

Table 5: Parameters and Initial Conditions for Upscaled Interface Materials 126
Table 6: Alternate Parameters for Upscaled Interface Materials 127

Annex

Table 7 Dimensions relative to the simulated domain 157
Table 8 Values for physical parameters 160

1. Context and introduction

This document is the second part (out of three) of the final report on the work done for FORGE WP1.2 in the context of a benchmark simulation concerning gas generation and migration at repository depth (many hundreds of metres below ground level) and repository scale.

The work presented is linked to the second benchmark proposed in the FORGE WP1.2 context. The first one was realised at cell scale and the present one is to be made at a module scale (several tens on cells). This is the intermediate scale toward a full repository representation.

One of the main problems in dealing with different teams from different countries, who have different disposal concepts, is to find a common representation as a basis for the benchmark. This implies simplifications are necessary to real concepts, in order that they be represented at a basic level that has some degree of consistency to all participants. Another point is to find a common benchmark definition that can satisfy any team, so something quite simple is needed at the outset, so that teams can have a first trial and, in comparing the respective results thus obtained, verify that basics are well understood by each team.

At the start of WP1.2 activities, after discussion, there was a general agreement that the reference exercise will be as generic as possible (without targeting precisely on national concepts), with sensitivity analyses making it possible to cover national specificities. The aim here is more to understand the behaviour of the modeled system as understood by each participant, rather than to undertake an inter-comparison of codes.

To give some added value to this first exercise, a feature not yet well represented in usual gas simulations was introduced: the explicit representation of the interface between canisters and cell walls.

After a brief description of the benchmark definition (see Section 2), Section 3 of this report collates the results to date of each WP1.2 participant. To conclude, some very preliminary conclusions are drawn and the proposed work programme up to the first semester of 2012 is presented.

N.B. *: there are two other document linked to this one, on cell scale (report FORGE D1.6-R part 1: cell scale benchmark) and repository scale (report FORGE D1.6 –R part 3: repository scale benchmark) benchmark. The repository scale benchmark has a final conclusion synthethising all the conclusions of the global benchmark work*

2. Definition of the benchmark

N.B. *: The complete definition of the benchmark can be found in the Annex*

N.B. 2 *: This benchmark is the second proposed in the context of FORGE WP1.2. The first one was defined at cell level. The type of cell considered is a somehow generic high level waste cell in a clay host rock. The results can be found in the reports FORGE D1-6 part 1: "cell scale benchmark".*

One of the major difficulties in the representation of gas transfer in a repository is to take into account simultaneously all the sources terms (generally located inside the storage cells) and to represent at the same time the transfer network constituted by the different drifts and cells.

For this second exercice of FORGE WP1.2 we assume a repository having a simple architecture (see Figure 162). This architecture is more or less representative of some general concepts for HLW repository zones but without any national specificity. The main features are:

- Subdivision of the all repository into several modules linked by a main drift;
- All the modules are equal and contains an access drift serving 50 cells on each side;
- All modules are separated from their neighbors by a drift seal.

This test case is limited to a portion of such a repository containing an access drift serving a number of cells (see Figure 162). This portion is called a module (a drift serving two rows of vitrified HLW cells containing each 50 cells, see Figure 163).

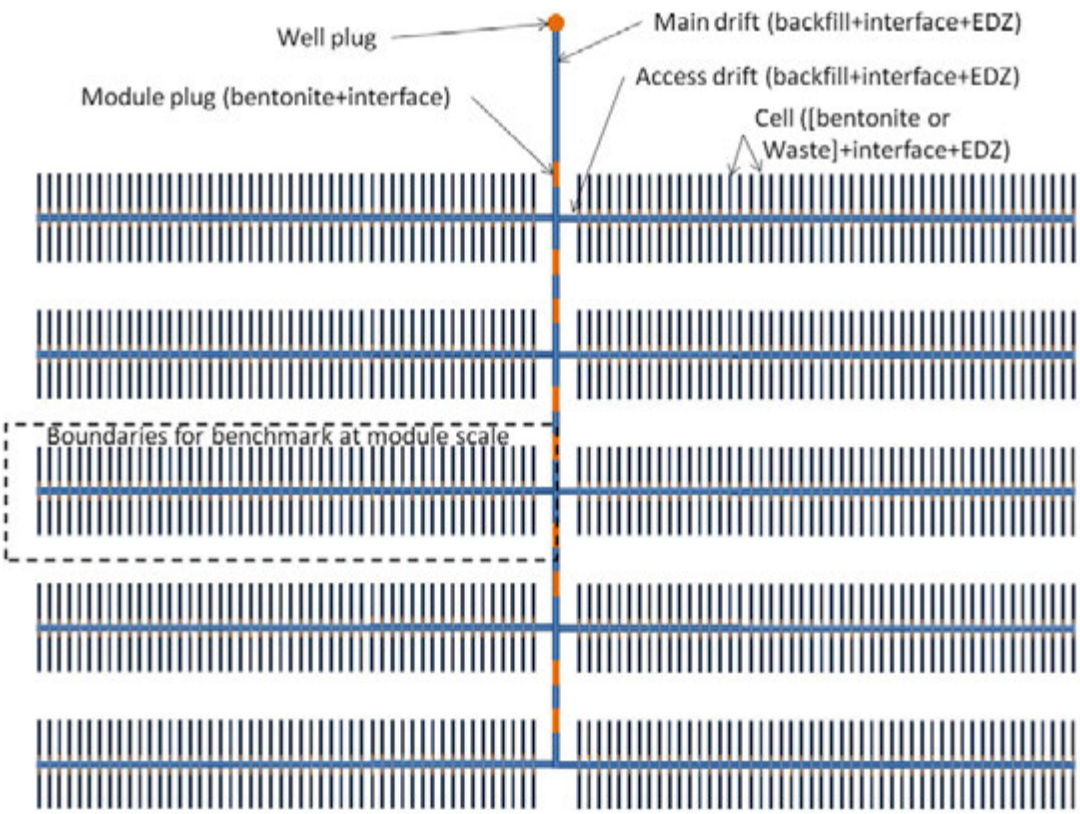

Figure 1 Schematic representation of a repository for HLW

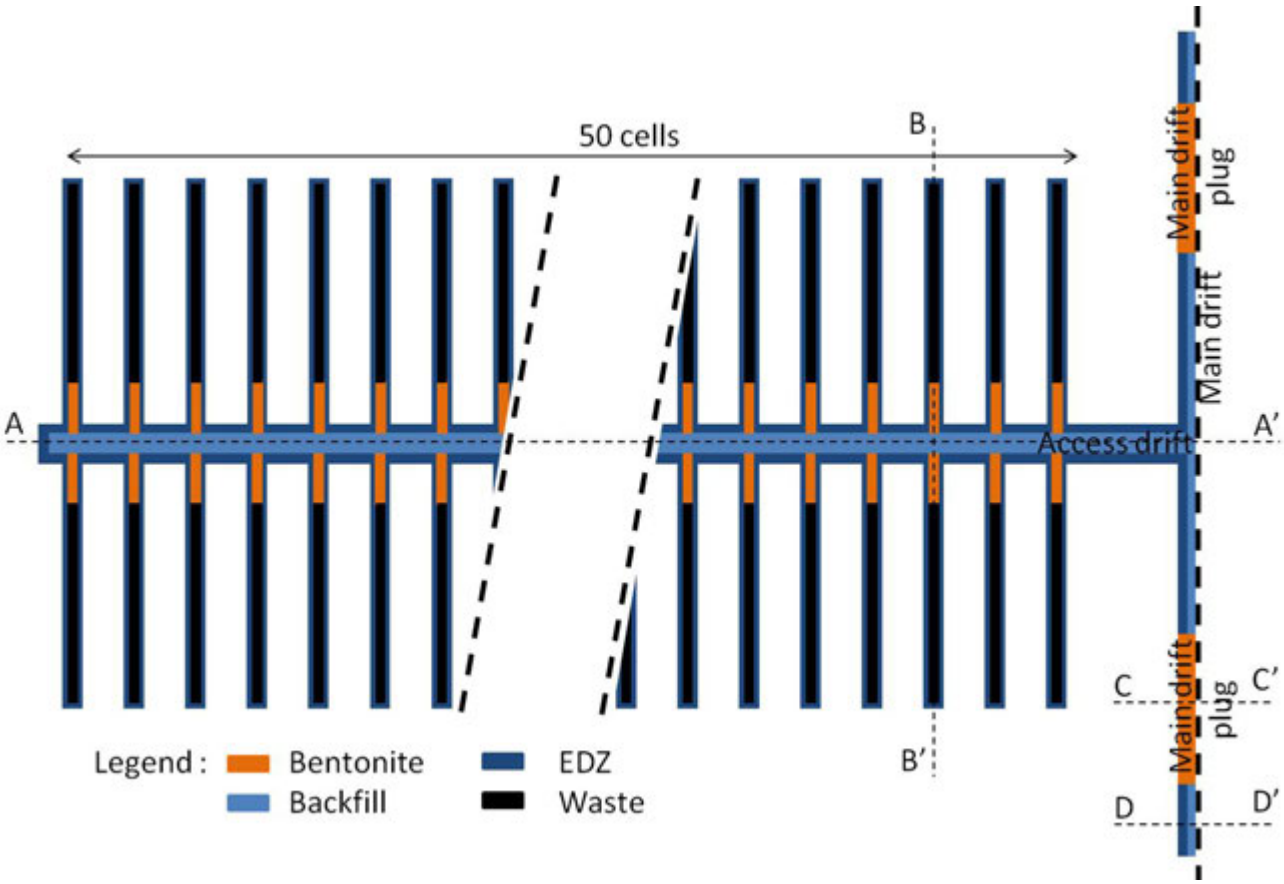

Figure 2 Schematic representation of the module to be simulated.

To stay as generic as possible, the gas flux rate in this benchmark is represented by a simple step function lasting 10,000 years; the simulation time is limited to 100,000 years. To understand the distinct role of each phenomenon, the reference case is not considering any coupling. This will be done further on in the sensitivity analysis.

More details and the complete benchmark definition can be found in the Annex

3. Summary of the work done by the different teams

3.1 NDA RWMD contribution

3.1.1 Introduction

This document presents the model setup, results, sensitivity cases and key learning points from the second benchmark (see Annex) produced by the UK Nuclear Decommissioning Authority (NDA) and Quintessa team.

3.1.2 Model Implementation

3.1.2.1 Code and Formulation

QPAC is a general purpose modeling tool designed for flexibility and robustness. The 'model as input' approach for the input syntax allows the user to adjust all aspects of the model formulation and to create couplings in internal parameters so that, within certain limitations, any one input parameter can be a function of any other, and such couplings can be expressed naturally through the input language. Problems are solved monolithically and using a time-implicit method supported by automatic time-stepping. Collections of user-input can be compiled to create 'modules'. Such modules (e.g. thermal transport, reactive transport, simple Darcy flow, Multi-Phase-Flow etc.) can be tested and quality assured much like a conventional code and then used in a modular fashion in new models. The Multi-Phase-Flow module used in this exercise is one example of such a module.

QPAC does not impose a numerical method on the user, but rather provides a rather generic concept of compartments (volumes) and interfaces (faces between volumes) on which variables (unknowns for the calculation) and properties can be defined (Figure 3). Regions where different process models (sub-systems) are represented are connected via 'joiners'. Most QPAC models and modules use a Finite Volume formulation, however Mixed Element and Finite Difference schemes can also be adopted. The Multi-Phase-Flow module uses a conventional Finite Volume formulation.

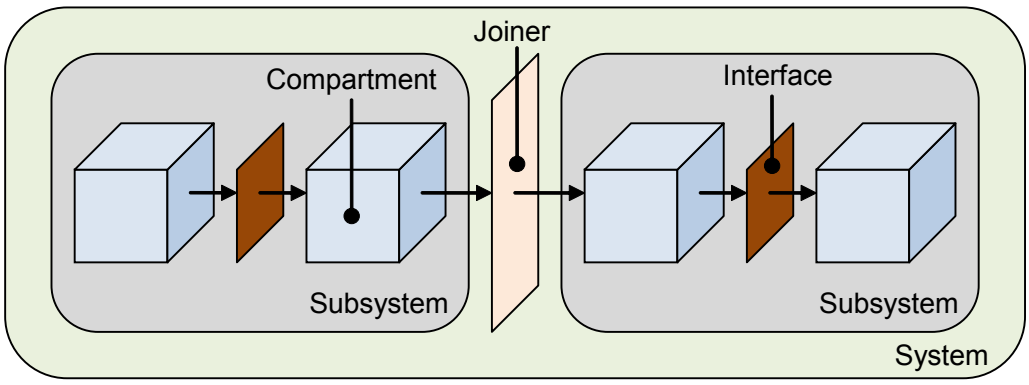

Figure 3 QPAC geometry definition.

Grids of compartments and interfaces can be created using the standard QPAC input language on both axi-symmetric (cylindrical) and Cartesian grids. Also abstract geometries of arbitrary or abstract compartment and interface structures can be created, and attached to the more conventional gridded structures.

The benchmark was implemented in the Quintessa multi-physics code "QPAC" using the benchmark specification (see Annex) as the only source of input. The standard QPAC Multi-Phase-Flow (MPF) module includes all the process model functionality required by this case [1], and hence the process and geometry could be implemented exactly as described in the specification, i.e. multiphase flow of water with a gas phase (hydrogen) together with consideration of dissolved hydrogen and water vapour diffusion. Consistent with the specification there is no distinction between the initially present gas (air) and hydrogen generated during the model run. QPAC uses a control volume approach for spatial discretisation.

The MPF module uses a continuous formulation for water and gas; this means that for numerical reasons, when fully water saturated, small amounts of immobile gas are assumed to be present and that this gas is in pressure equilibrium with the water (i.e. capillary pressure is zero).

Dissolution is considered to proceed according to Henry's law:

$$p = k_H . c$$

where

p is the pressure of the gas phase (this is equal to the total pressure of the gas phase when only a single gas is present, or the partial pressure when a mixture of gases are present) (Pa)

c is the concentration of the gas in the solution (mol m^{-3})

k_H is Henry's constant for the gas (Pa m^3 mol^{-1})

In a two-phase (or multi-phase) system, comprising gas and water, as the amount of free gas becomes increasingly small the gas pressure tends to the water pressure. When only very small amounts of free gas are present the gas pressure is equal to the water pressure, but there may not be sufficient gas to satisfy the equilibrium dissolved gas concentration calculated using the equation above. This implies that all the gas will dissolve, there will be no free gas, and the system will transition to a single phase system (water partially saturated with dissolved gas).

Two mathematical approaches are available to model this phase transition:

- Apply different mathematical models for multi-phase and single phase conditions, with discontinuous change between models according to defined criteria.
- Apply a single mathematical model, so there is no discontinuity, but appropriately modify the mathematical model when single phase conditions are implied.

In the QPAC code the latter approach is taken. The amount of gas that can be dissolved is given by:

$$Amount\ dissolved\ gas = \min\left(\frac{p}{k_H} V_w m_g,\ Hf\ A_g\right)$$

Where

V_w is the volume of water (m^3)

m_g is the molar weight of gas (g mol^{-1})

A_g is the total amount of gas either as free gas or dissolved gas (in the given model compartment) (kg)

Hf is the Henry's law scaling factor which defaults to 0.99 (-)

Since QPAC primarily solves for the amount of gas present in any compartment, the above equation is simple to evaluate and restricts the amount of dissolved gas when there is very little gas in a given compartment. When there is a very small amount of gas, 1% (by default) of the total gas is always free gas to maintain the continuous formulation. Under these conditions, QPAC calculates a gas pressure that is equal to the water pressure. The Hf parameter can be adjusted to increase or decrease the strength of this effect, and the user will ensure that the parameterisation of the residual gas phase is effectively immobile once the water becomes under-saturated with respect to dissolved gas.

This approach is similar to some other multi-phase codes (e.g. Eclipse) and is consistent with other physic-chemical mathematical models, for example it is possible to calculate a vapour pressure for a single phase (liquid only) system. It also has a conceptual basis: dissolved gas molecules will have a range of energies, and some molecules will have sufficient energy to effectively be disassociated from water, even if the number of such molecules is too small for a distinct free gas phase to form.

3.1.2.2 Benchmark Implementation

Grid

The full geometry consists of an 'upstream' and 'downstream' half of the module of disposal cells (100 cells in total) with time variant boundary conditions specified on the upstream and downstream ends of the main drift. As discussed in FORGE (see Annex) the difference in gas pressure and saturation from the upstream to the downstream end is relatively small, thus for this first version of the model it was decided that a pragmatic simplification would be to assume vertical symmetry along the centre of the access drift and only model the downstream side of the system (Figure 4). This reduces the size of the case to be modelled. However, a full 100 cell case was attempted as a variant case, with a separate set of sensitivity calculations.

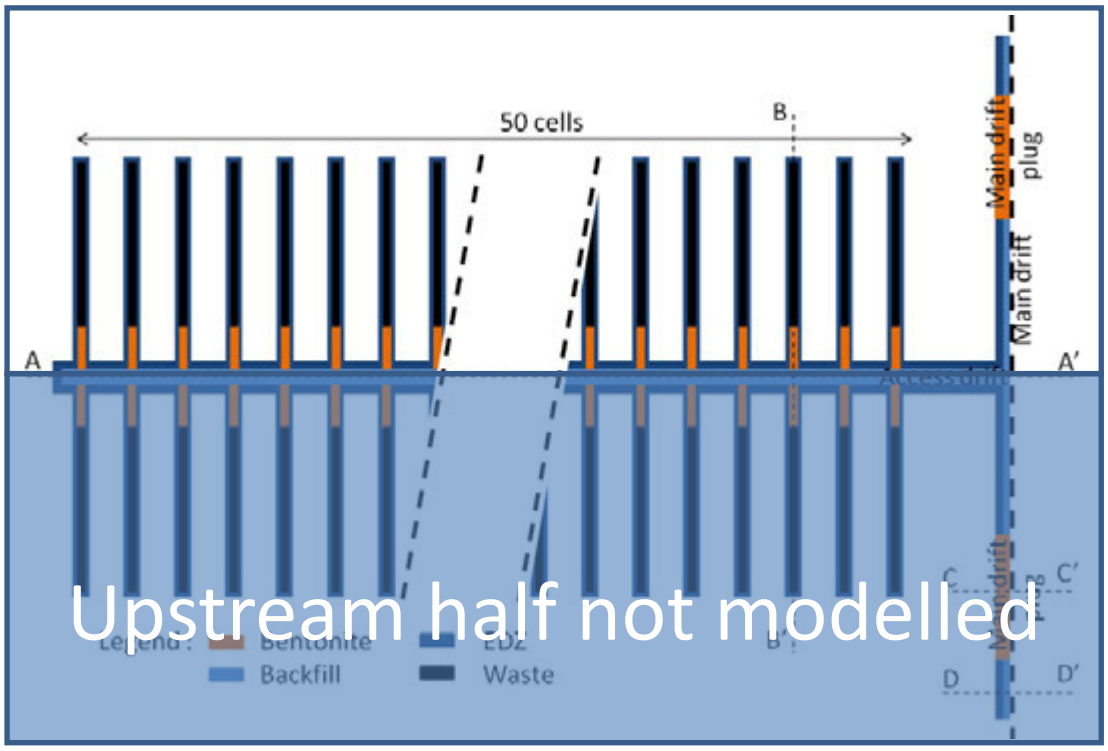

Figure 4 *Plan illustration of the model showing the half not considered in this initial model.*

For the base case the model geometry was implemented using a combination of Cartesian and cylindrical grid sections, which are joined together. The general domain including the host rock, access drift, main drift and main drift plug (with associated EDZs) was modelled using a Cartesian approach and a reasonable minimum spatial discretisation (Figure 5). Figure 6 shows the structure of the model without the host rock present and more importantly the structure of the interfaces in the model. Unlike the first benchmark [2], the interfaces completely surround whole sections of the model, effectively isolating the backfill and plugs (cells and main drift) from the remainder of the model. Given the high permeability and low capillary pressure parameterisation of the interfaces this could lead to partial hydraulic isolation of parts of the model from each other.

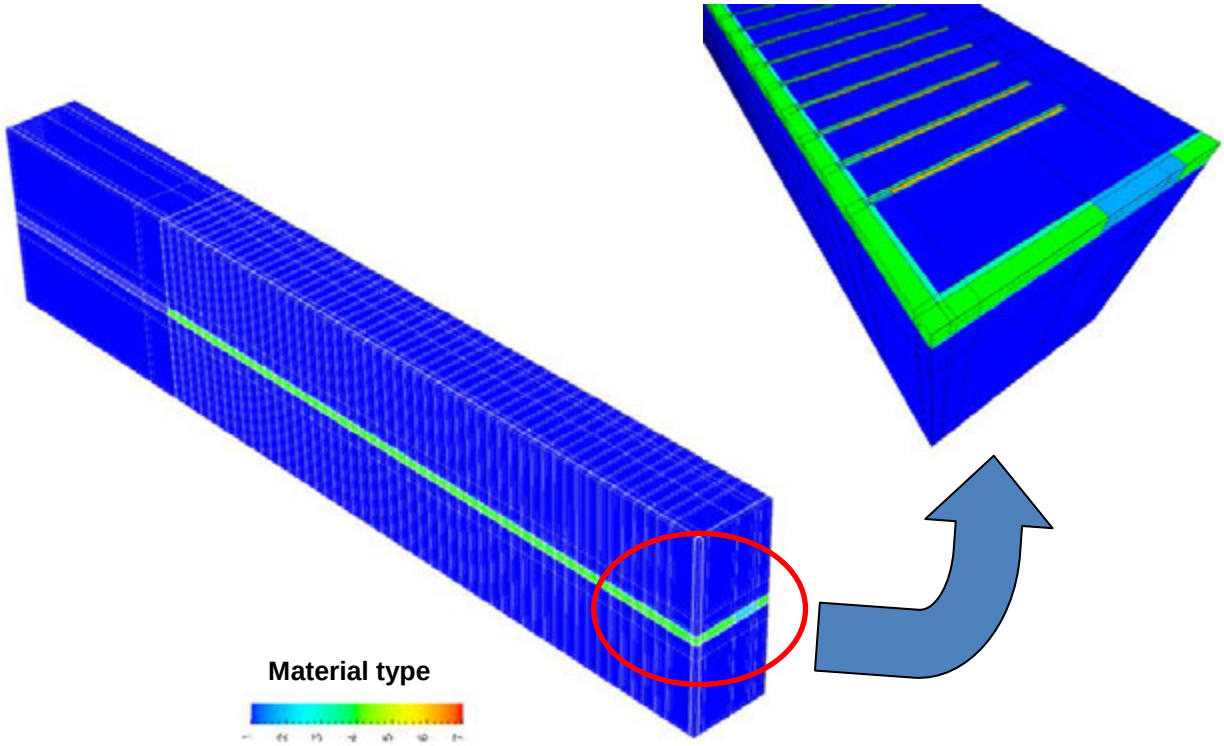

Figure 5 *Visualisation of the 3D Cartesian grid with compartments coloured by material type (left). Close-up of the access drift and main drift junction with the top half of the model removed (right)*

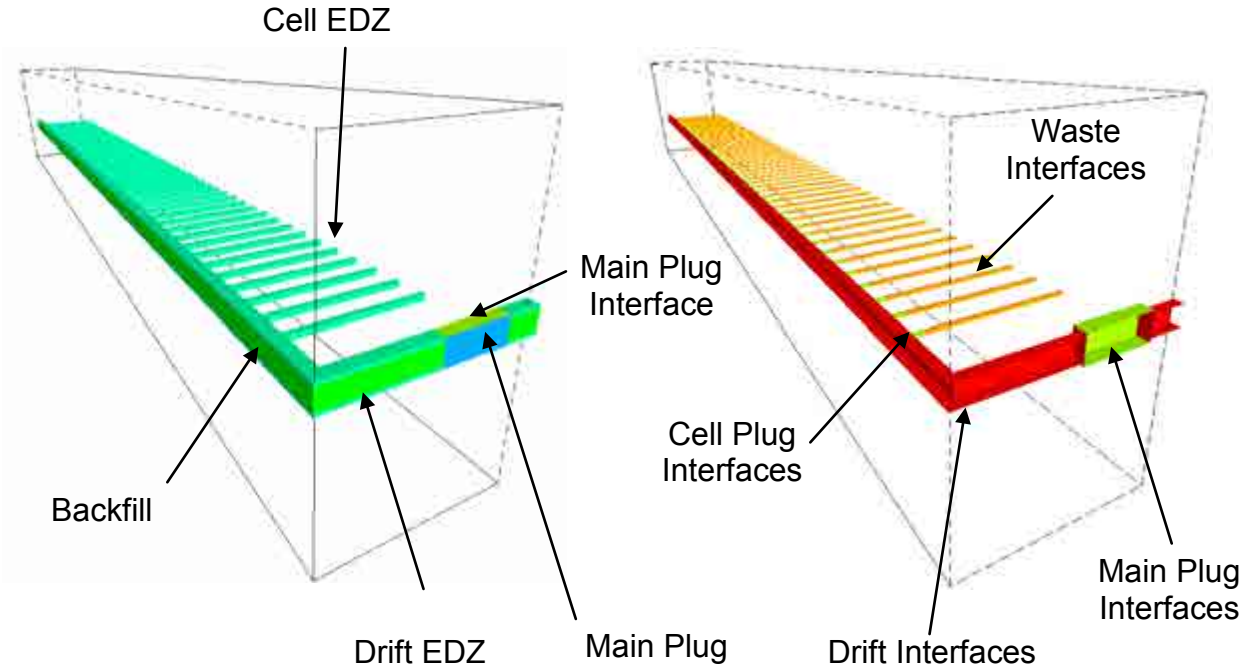

Figure 6 *Visualisation of the 3D Cartesian grid with compartments coloured by material type and the host rock removed (left) and only interfaces visible (right)*

Each waste cell was then removed from the Cartesian model and replaced with a cylindrical representation of the waste cell. The cylindrical and Cartesian sections were then connected together and the volumes of the compartments in the Cartesian grid adjusted to account for the space-filling mis-match between the cylindrical grid and the equivalent Cartesian volume that was removed (see Figure 7).

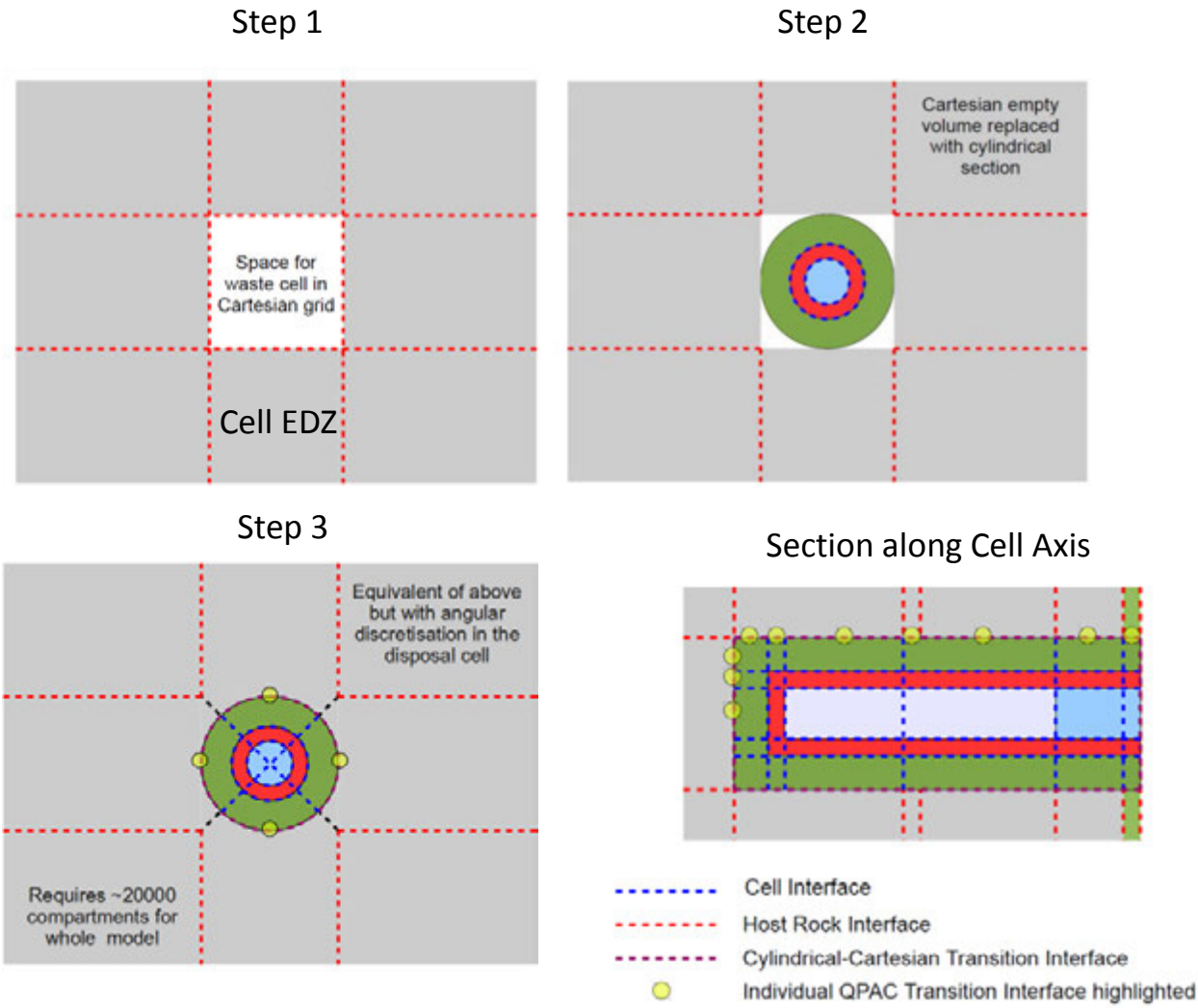

Figure 7 *Process of inserting cylindrical grid sections for the waste cells into the Cartesian grid. Grey=Host Rock, Green=EDZ, Red=Interfaces, Blue=Plug.*

It is noted that the gridding approach creates non-conformant connections between the cells, implemented using the cylindrical grid, and the rest of the domain, implemented using the Cartesian grid. This has the potential to introduce numerical issues. However after experimenting with a number of different grid types for this case, the potential numerical issues associated with non-concordant grids were felt to be acceptable when weighed against known issues concerning very high aspect ratio grid compartments and prohibitively refined discretisation. The grid refinement shown here is consistent with the coarsest of grids used in grid convergence testing for the cell-scale benchmark [2] and hence was expected to be sufficient for this application.

Boundary Conditions and Sources

As specified in the benchmark specification, the interface between the waste and EDZ received the H_2 gas, generated as a result of corrosion of the disposal canister, at a total rate of 100 mol/y per cell. For

simplicity and robustness of model setup in this early case, and unlike the first benchmark, gas was injected only into the waste interface surrounding the waste, not into the cell plug. Some testing using the first benchmark indicated that the first benchmark was almost completely insensitive to whether gas was input directly to the interface or as a surface flux across the entire surface of the canister (i.e. also injecting gas into bentonite plug). However, it is planned to use the surface flux model in later versions of the second benchmark.

The boundary condition for water (water pressure, gas pressure and fluid saturation) at the downstream main drift was implemented as specified using the tabulated data provided as part of the specification to create linearly interpolated time-dependent lookups for each property.

The upper and lower boundaries were implemented precisely as described; all other boundaries were designated as no-flow, consistent with the specification.

Initial Conditions

Initial conditions used were exactly as in the specification.

Initially the air saturation is 0.3 in the bentonite plugs (cell and main drift) and backfilled drifts and 0.95 in the waste and plug interfaces. The remainder of the domain is fully water saturated. Because of the continuous formulation, it is numerically convenient to prevent zero phase saturations, hence the starting saturation of air in the model is 1e-6 in all fully saturated water compartments.

As per the specification, the initial saturated water pressure varies linearly from 6 MPa at the base to 4 MPa at the top of the model (note that with a continuous formulation the gas and water pressures are the same when there is only residual gas present). In other parts of the model that are not initially fully saturated with water, gas pressures are at 1e5 Pa and water pressures in capillary equilibrium with the gas pressure.

Deviations from the specification

There were two deviations from the model specification for the reference case:

1. Only the downstream portion of the domain was modelled, assuming symmetry with the upstream half.
2. Gas was generated only into the waste interfaces, not across the whole surface of the canister and hence directly into the bentonite plug.

Both of these issues are to be addressed through variant cases, although neither are expected to result significant changes to the overall behaviour of the system.

3.1.2.3 Implementation Issues and Model Stability

The single largest problem in producing stable results was the choice of interface parameterisation. Because of the low capillary pressures in the interfaces they act as a capillary barrier between the porous media they sit between. As a consequence large sections of the model only have a weak hydraulic communication. This tends to make the solution matrices highly compartmentalised and pushed towards singularity. As such, significant care was required in order set the solver parameters such that stable solutions could be obtained while retaining timestep progress and stability.

Despite these issues, the model runs showed no sign of instability and the results (in conjunction with the sensitivity cases) were found to be conceptually reasonable with respect to the input parameterisation.

3.1.3 Base Case Results

Results for the second benchmark are shown in Figure 8 to Figure 14. In contrast to the first benchmark, the degree of control that the boundary conditions exert on the model evolution is relatively weak. The initial conditions of low pressures and saturations in the engineered structures dominate causing a drawdown of local host-rock and EDZ pressures. Resaturation is slow due to the interfaces around the drifts acting as capillary barriers and for the disposal cells becomes overwhelmed by the gas generation

within about 10 years of the start of the run (Figure 11). The relative impermeability of the main plug compared with the combined conductance of the cell plugs means that while advective flow of gas into the drift is important, the pressure in the drifts rises above background after approximately 1000 years (Figure 10). This causes the majority of gas to be lost via dissolution and diffusion in the host rock rather than by advection through the plugs. This is clearly a contrast to the first benchmark where the boundary condition to the access drift prevented pressurisation of the drift, hence resulting a rather different behaviour. Once gas generation has ceased at 10,000 y, the gas pressures drops away to background at approximately 30,000 y, and the very slow process of water resaturation starts (Figure 10, Figure 11– note log scale on time axis). One of the main sources of water is from the downstream boundary, where water pressure, gas pressure and water saturation are prescribed, which acts as the primary source of water for resaturating the main plug. The remaining dissolved gas diffuses and advects out of the top and bottom of the model, the upper surface receiving the largest flux, but at 100,000 y (the specified end of the model run) significant quantities of gas remain in the system.

The location of key result points and flux surfaces are shown in Figure 8 and Figure 9. Selected, but representative, pressure responses are shown Figure 10 and associated water saturations given in Figure 11. The results illustrate the degree to which temporary pressurisation occurs behind, and to some extent, in the main plug and that the resaturation process is very slow, with resaturation only occurring very late on in the model run.

The flux results in the module (selected outputs in Figure 12 and Figure 13) show that the free gas flux through the main drift plug is small in comparison with the total amount of gas being generated. The remainder of the gas dissolves. It also shows that, once pressurisation starts to occur, at least one of the cells furthest away from the main drift (observed in Cell 50) sees a reversal of gas fluxes as the pressurised gas overwhelms the cell gas generation pressures causing the cell to act as a net sink for dissolved gas.

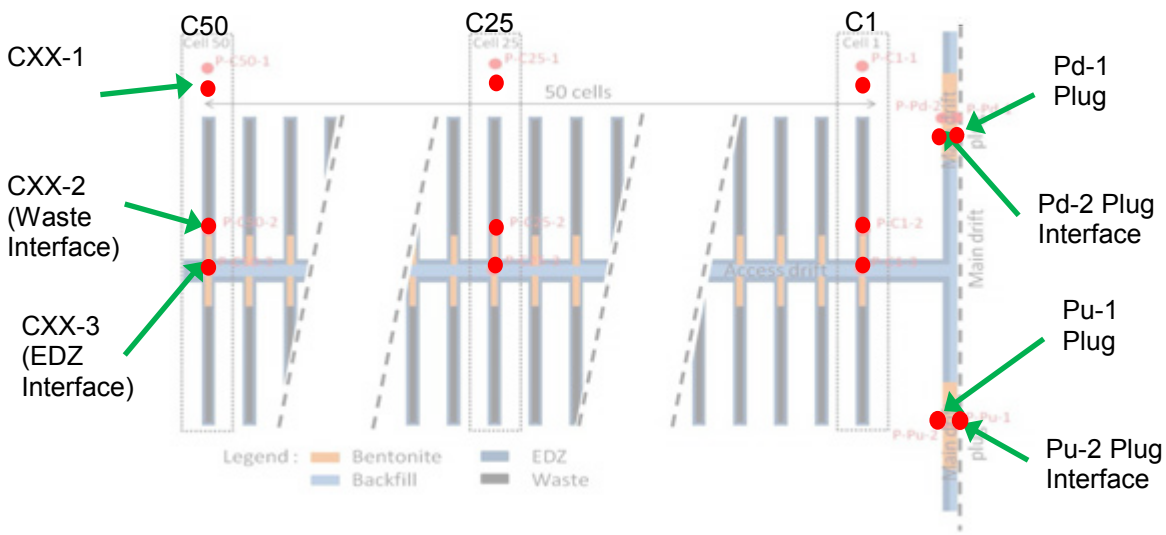

Figure 8 Gas pressure and saturation result points. Note the Pu-1 and Pu-2 are not present in the base case.

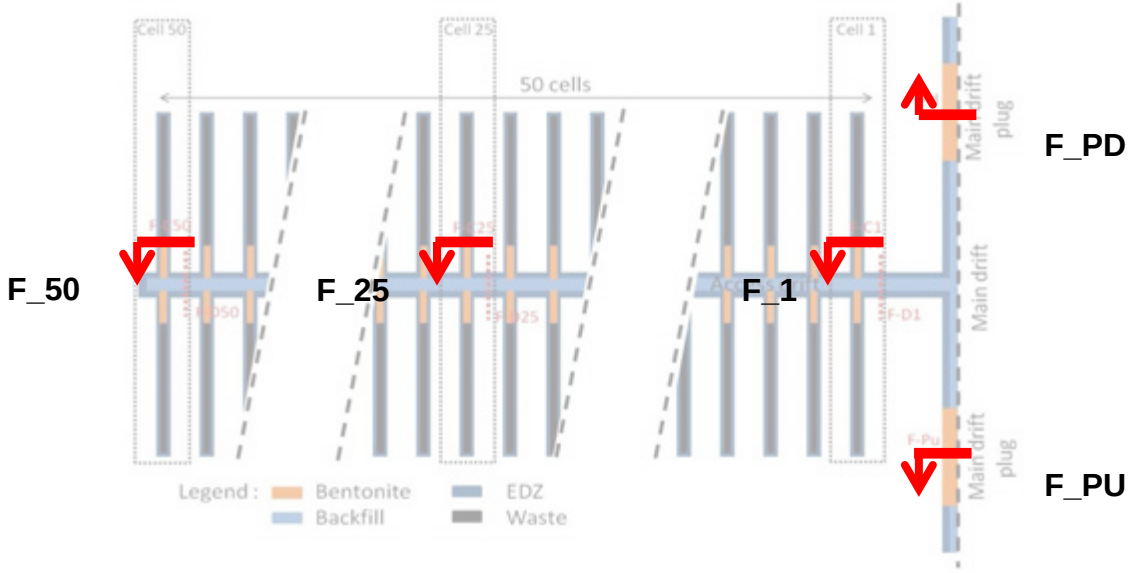

Figure 9 *Flux locations and indication of positive flow directions in the waste module. Note the F_PU is not present in the base case.*

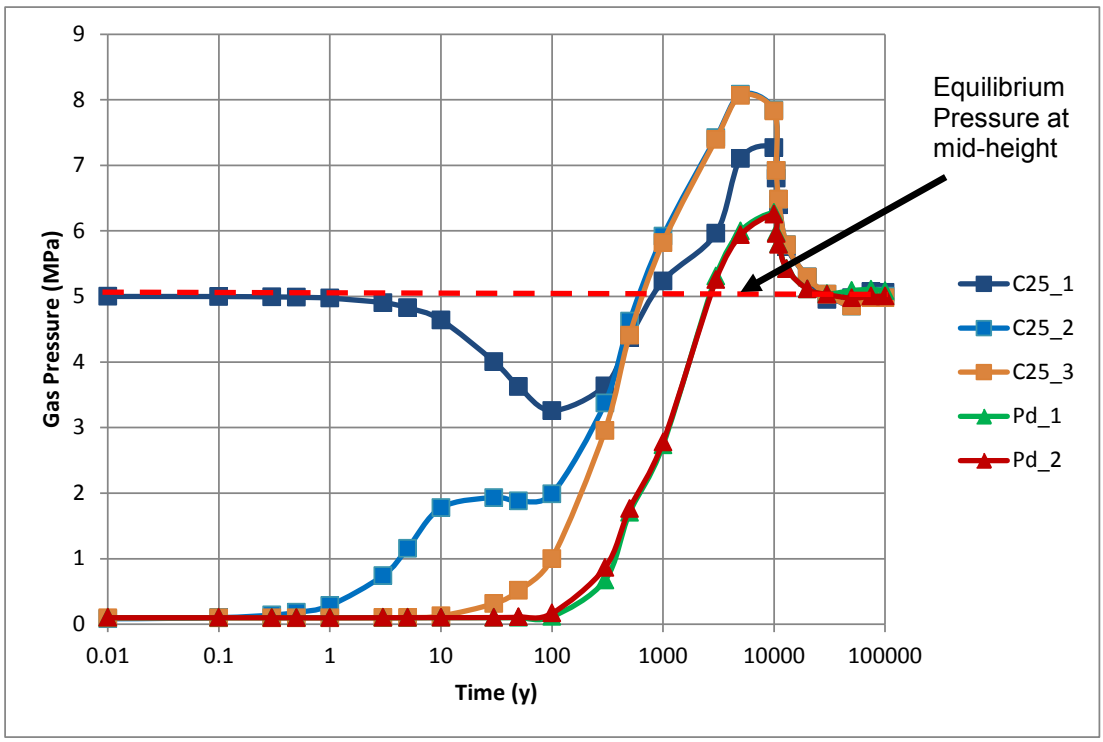

Figure 10 *Gas pressure at key measurement points.*

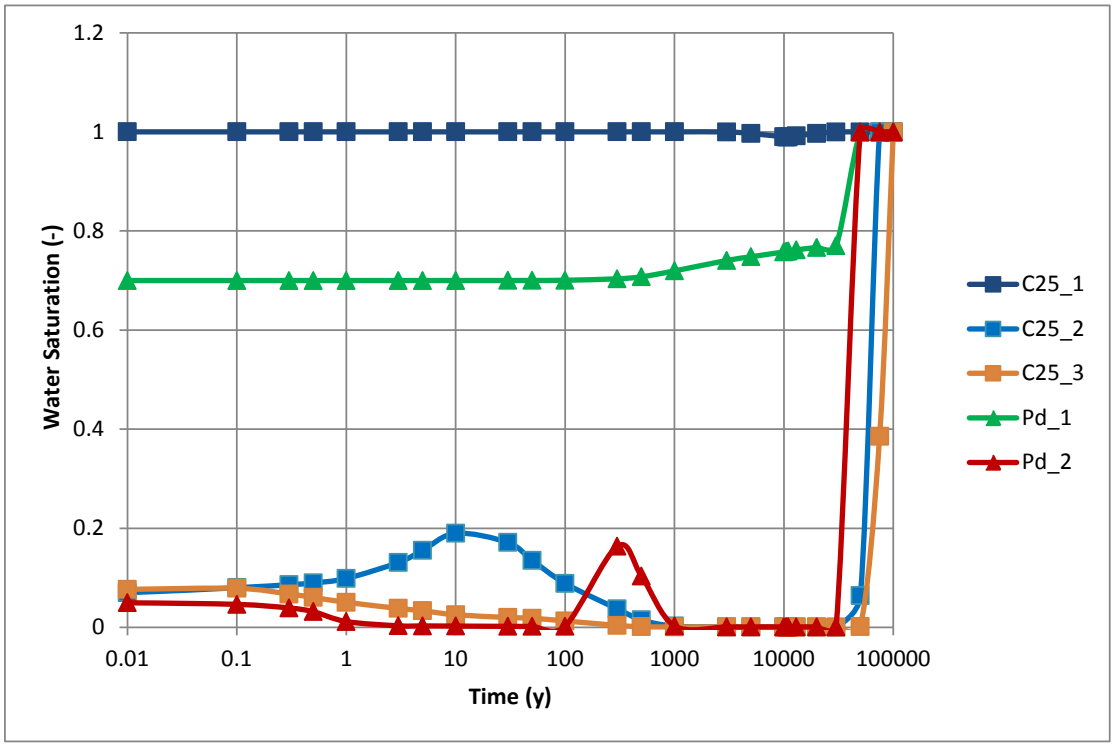

Figure 11 *Water saturations at key measurement points.*

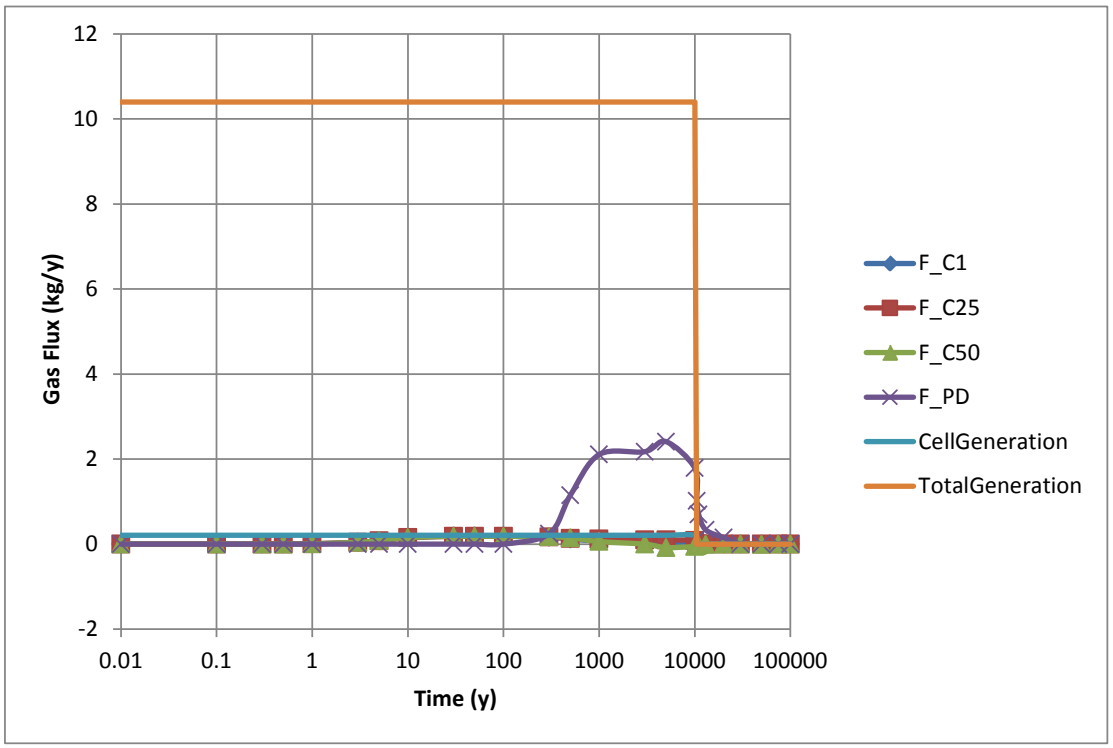

Figure 12 *Free gas fluxes in the module compared with total gas generation and cell generation rates.*

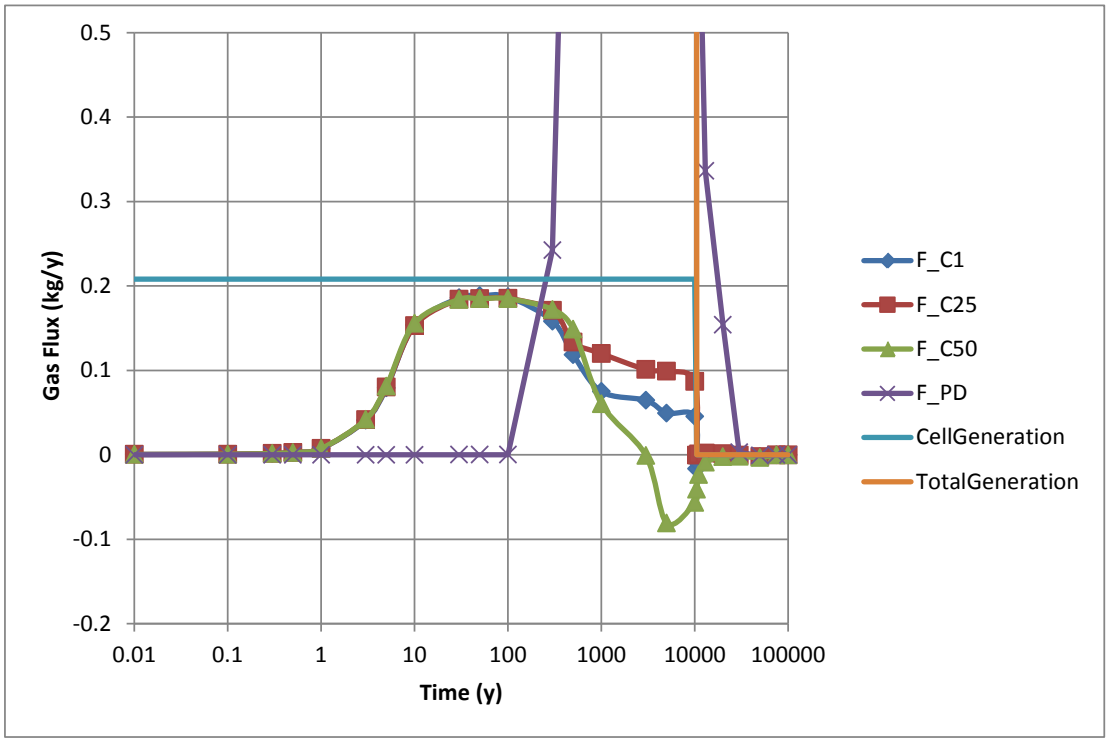

Figure 13 *As per Figure 12, but zoomed in to the scale of individual cell fluxes.*

Figure 13 also shows that before the pressure builds up in the main drift and access drift, advective loss of free gas around the cell plug dominates the fate of the generated gas – this is consistent with the first benchmark results. Gas fluxes through the top and bottom of the model (Figure 14) show that losses are small in comparison with generation rates but are persistent after 4000 y and gas continues to be lost via this route at the end of the model run. Small amounts of free gas loss are seen through the top boundary while the gas pressurises in the engineered system are high, but the flux of free gas quickly drops to zero after approximately 30,000 y.

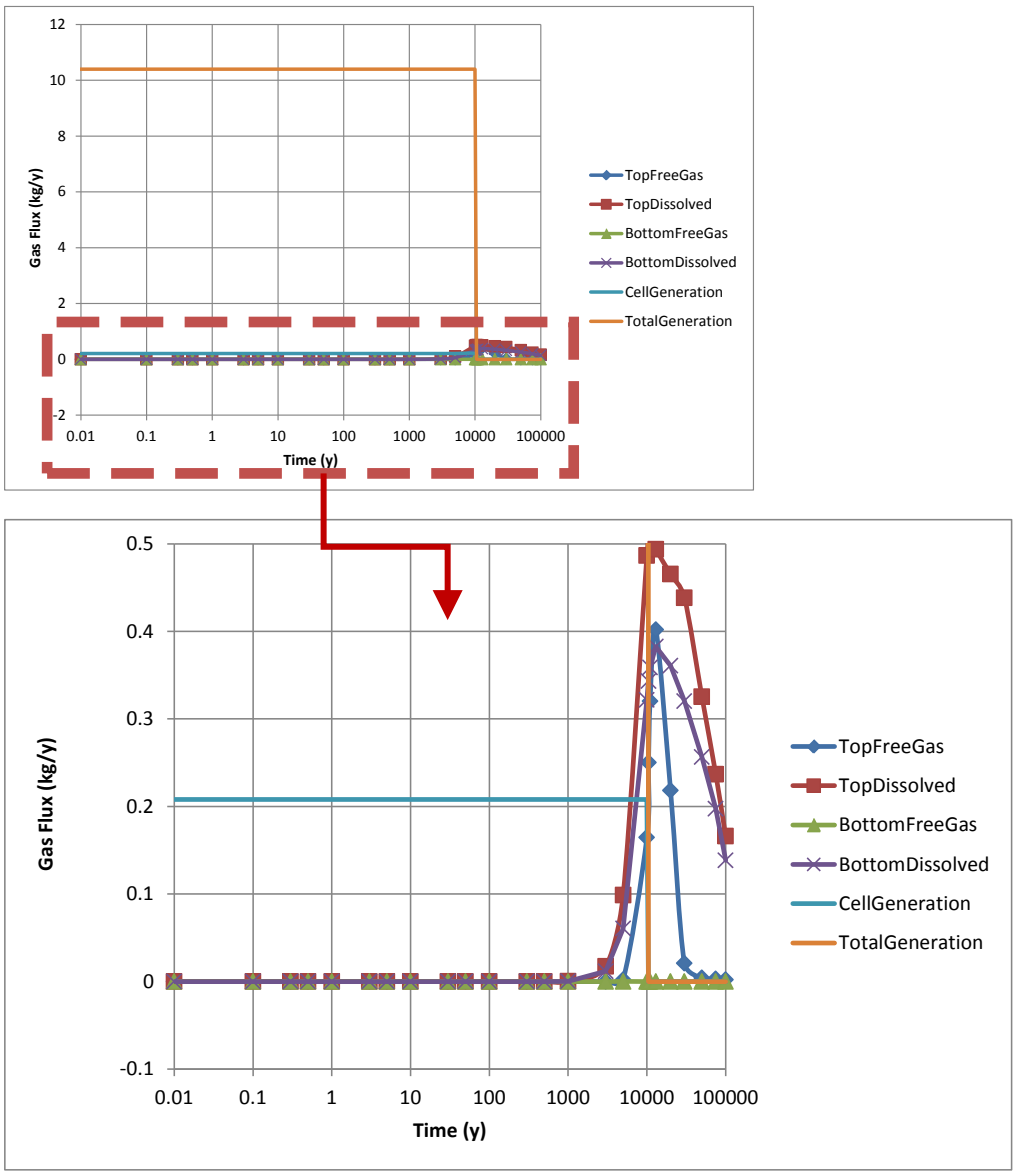

Figure 14 *Free gas and dissolved gas fluxes (+ve = outflow) across the top and bottom of the model compared with total gas generation and cell generation rates.*

3.1.4 Sensitivity Cases on the Base Case (50 HA Cells)

No sensitivity cases were prescribed in the specification. However six additional cases were conducted as a first step towards developing a further understanding of system behaviour. The first three cases dealt with the representation of the interfaces (group A), while the second three dealt (group B) dealt with changes in resolution and the impact of upscaled representations of the HA cells (hence reducing computational overhead).

Group A

1. Case 1 (NoInt): No drift interfaces.
2. Case 2 (NoInt_NoPEDZ): No drift interfaces, and no EDZ overcut around the main plug.
3. Case 3 (HalfInt): Interfaces only on the upper half of all features (Z>75m)

Group B

1. Case 4 (NoInt_UpscaledCells): No drift interfaces and HA cells are reprsented using a homgenised, upscaled approach.
2. Case 5 (NoInt_UpscaledCellsNoCellInt): No drift interfaces and HA cells are reprsented using a homgenised, upscaled approach, but the effects of interfaces in the HA cells are neglected.
3. Case 6 (Refined_NoInterfaces): Grid refinement is increased generally in the model (factor of 1.5 more compartments in each coordinate direction), but with interfaces neglected.

The specification of each case is discussed below; the results are presented together in Figure 16 and Figure 17 for comparison afterwards.

3.1.4.1 Case 1 (NoInt): No drift interfaces

This case removes all the interfaces associated with the drifts and main plug. The purpose of this case is to test the degree to which the interfaces act as barriers to wider resaturation from the host-rock and to what extent they act as conduits for gas flow, especially around the main plug.

3.1.4.2 Case 2 (NoInt_NoPEDZ): No drift interfaces and no EDZ overcut

This case is identical to Case 1, except that the main plug is no-longer assumed to have been constructed by cutting into the EDZ around the plug. Instead the main drift EDZ remains intact around the plug and the plug only fills the main tunnel of the drift.

3.1.4.3 Case 3 (HalfInt): Interfaces only on the upper part of features

In this case all interfaces (including those in the cells) are eliminated if they reside below or equal to the height of 75m, i.e. the mid-height of the module. This case is designed to investigate the impact of partial interfaces, which have been partially eliminated by the weight of backfill etc.

3.1.4.4 Case 4 (NoInt_UpscaledCells): No drift interfaces and HA cells are reprsented using a homgenised, upscaled approach.

This case removes all the interfaces associated with the drifts and main plug and simplifies the structure of the model representing the HA cells. The simplification is shown in Figure 15. This case allows us to test the importance of the explicit representation of the HA cells for this model.

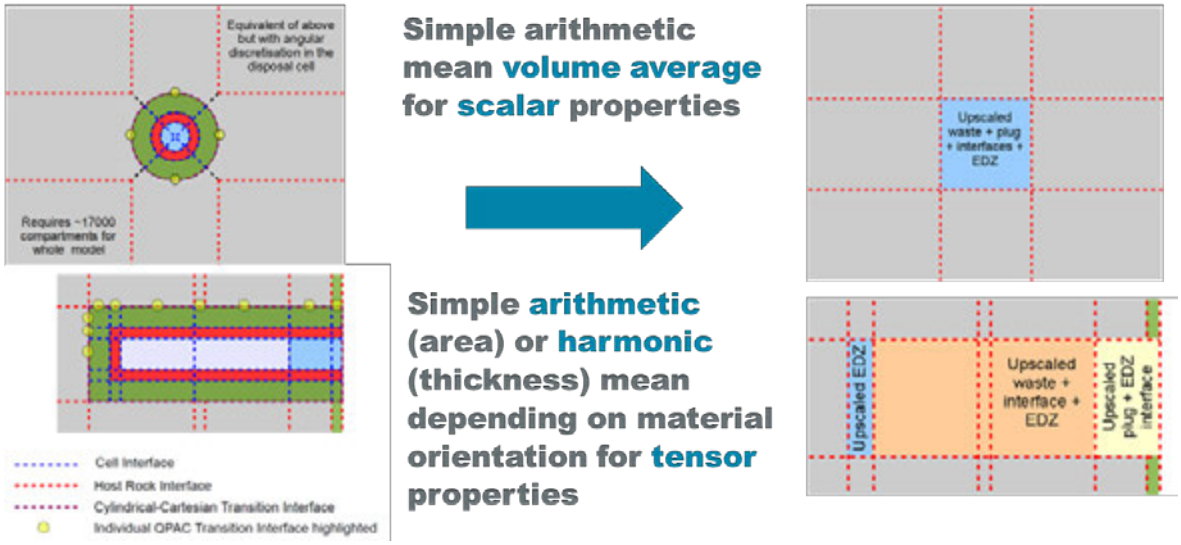

Figure 15 Upscaling approach for sensitivity case 5 and 6.

3.1.4.5 Case 5 (NoInt_UpscaledCellsNoCellInt): No drift interfaces and HA cells are reprsented using a homgenised, upscaled approach, but the effects of interfaces in the HA cells are neglected.

This case is identical to Case 4, except that the effect of the HA cell interfaces is removed from the upscaling process.

3.1.4.6 Case 6 (Refined_NoInterfaces): Increased grid refinement with no interfaces

The purpose of this case is to test the sensitivity of the key model results to changes in grid density, acknowledging that the grid used for the base case is coarse and may produce numerical artefacts. This model raises the number of compartments to approximately 30000, from ~17000 for the base case in increases the number compartments in each of the principal directions by a factor of approximately 1.5.

3.1.4.7 Comparison of Results – Group A (Sensitivity Cases 1-3)

Water saturation (Figure 16) and gas pressure (Figure 17) results are compared at point Pd-1 between the sensitivity cases and the base case. In terms of water saturation it is quite clear that the presence of interfaces around the drift is significantly retarding resaturation of the drifts and main plug. Even having only half the interfaces in place results in much faster resaturation.

From the gas pressures it is clear that the removal of interfaces around the main plug has a significant impact on pressurisation, adding over 1 MPa of pressurisation above the base case in the plug (and other results show more pressurisation behind the plug). Removing only half the interfaces shows approximately 0.5 MPa of pressurisation, again highlighting the plug interfaces as a major flow path. Reintroducing the plug EDZ, even without the plug interface, shows a dramatic reduction in pressurisation, with a peak gas pressure in the plug of only ~6.5 MPa, or only ~0.5 MPa above the peak downstream boundary gas pressure. Examination of the results in more detail for all the cases confirmed that in the drifts themselves that the interfaces were not significant in terms of free gas transport and the majority of free gas was transported through the backfill in the drifts.

Overall it appears that the presence of interfaces all around the drifts is having a major effect on the resaturation behaviour of the system, causing the system to take an unexpectedly long time to resaturate. Given the need to keep these interfaces intact all the way around the drift to retain this isolating effect, it is questionable whether the specification as it stands is physically reasonable and the results are representative.

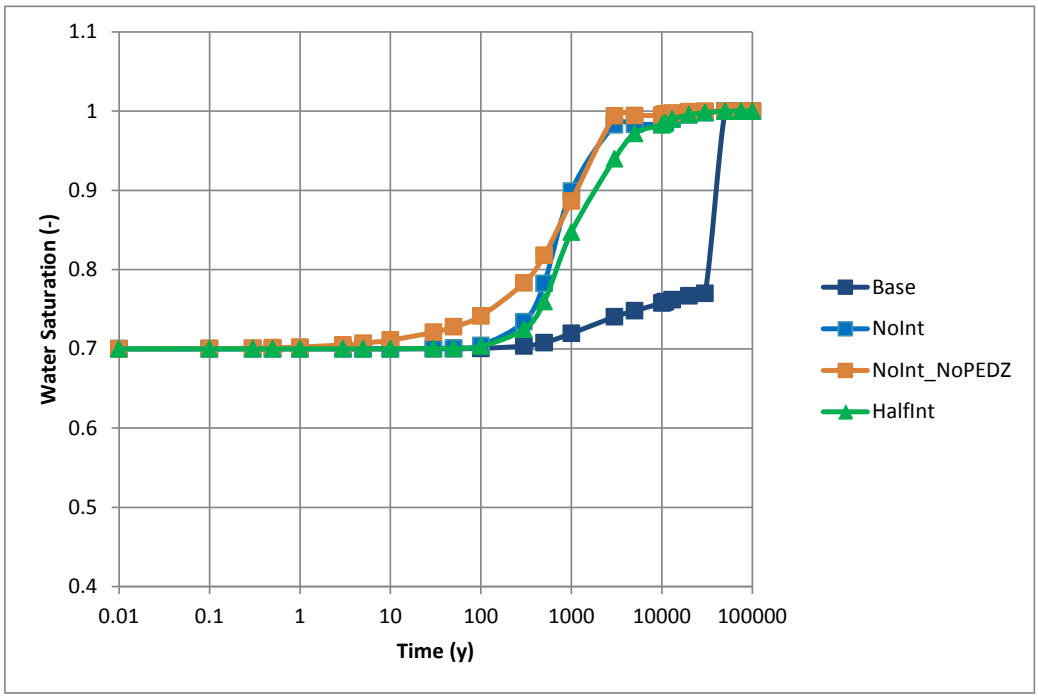

Figure 16 *Water saturation at Pd-1 for the three interface sensitivity cases (Group A) and the base case.*

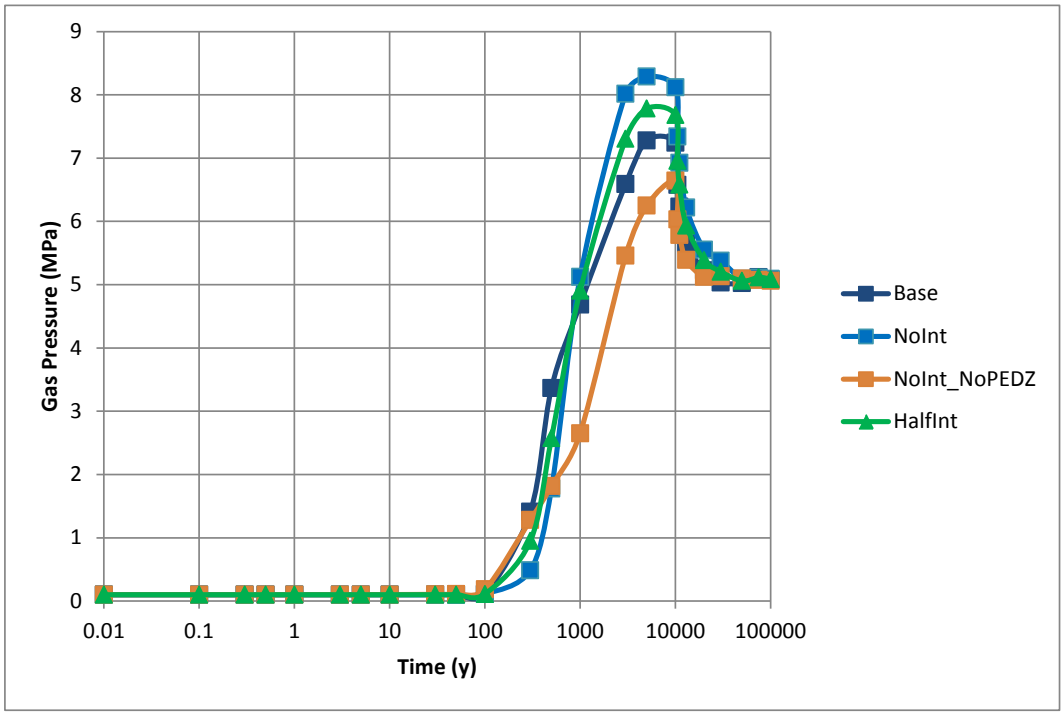

Figure 17 *Gas pressure at Pd-1 for the three interface sensitivity cases and the base case.*

3.1.4.8 Comparison of Results – Group B (Sensitivity Cases 4-6)

The comparison of evolution for water saturations and gas pressures are shown in Figure 18 and Figure 19 respectively at Pd-1 (centre of the downstream main plug) as a representative point – all other points showed similar levels of coherence across cases. In terms of water saturation, the results show a very high degree of similarity, all illustrating the effects of neglecting the prescribed interfaces from the model. In terms of pressures, there is a slight variation between the cases with upscaling and no upscaling of the HA cells, with the upscaled models showing a peak in gas pressure slightly earlier and lower than the other cases. This is probably because of the effects of numerical dispersion on the gas source, tending to broaden the pulse of free gas moving through and around the HA plugs, hence giving rise to the wider peak in pressure.

The additional refinement for case 6 appears to have had a minimal impact on results. Some minor variations were seen in the fluxes when considering free gas and dissolved gas separately (maximum of a factor of 1.5), especially at the top of the model, but it was later determined that these were all variations caused by artefacts associated with the different grid refinement close to this upper boundary. When comparing the total flux of H_2 across the top of the model, there was found to be very little difference the base case and case 6.

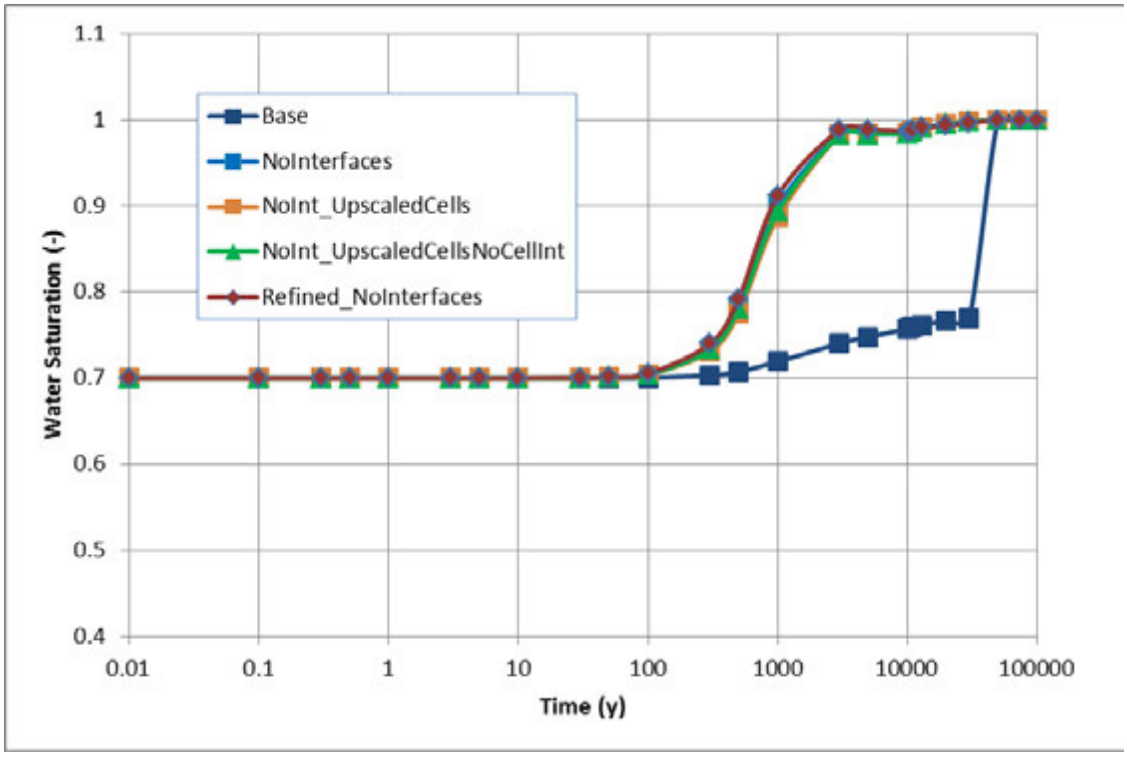

Figure 18 *Water saturation at Pd-1 for the three grid sensitivity cases (Group B), the base case and sensitivity case 1.*

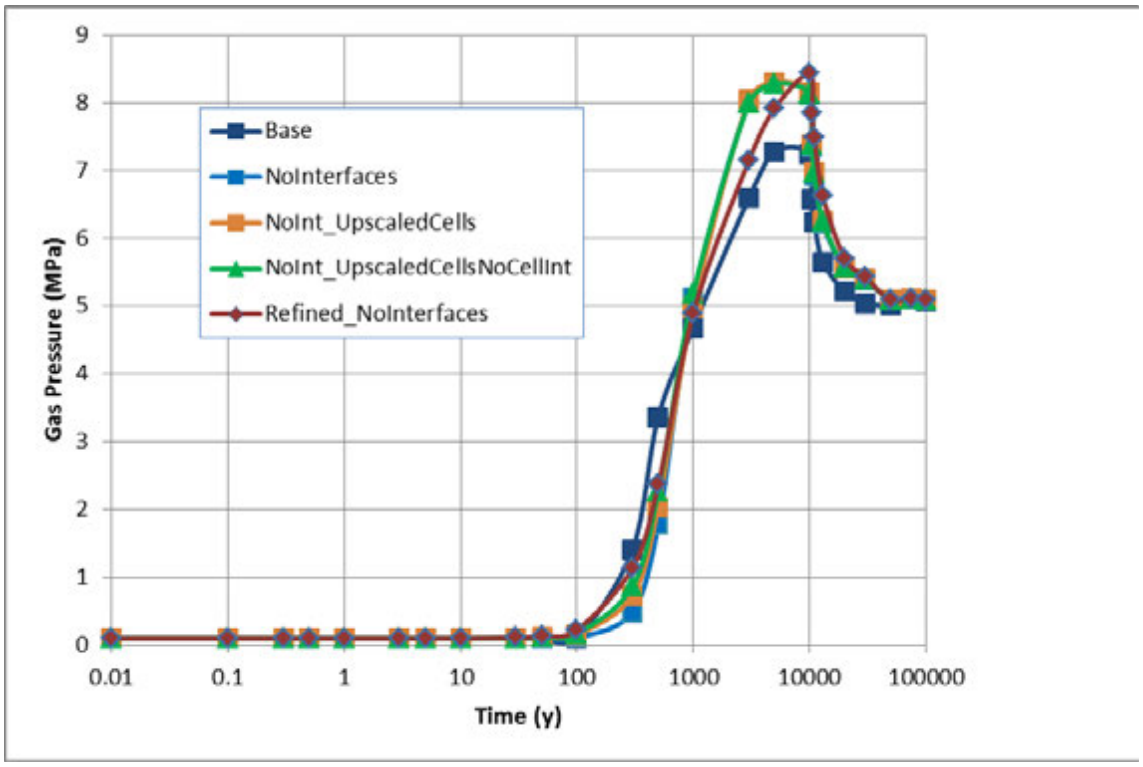

Figure 19 *Gas pressure at Pd-1 for the three grid sensitivity cases (Group B), the base case and sensitivity case 1.*

3.1.5 Variant Case – 100 Cells

To supplement the base case a full 100 Cell case was constructed, with associated sensitivity cases, in order to investigate the impact of the assumption of symmetry down the access tunnel. The grid was constructed in exactly the same way as the 50 cell case, but included both sides of the access tunnel and different boundary conditions on the upstream and downstream sides of the main drift (Figure 20). Consistent with the base case of 50 cells, interfaces were included in the model Output locations are the same as those shown in Figure 8 and Figure 9, but including the equivalent upstream points for the main plug (Pu-1, Pu-2) and upstream plug fluxes (F-PU).

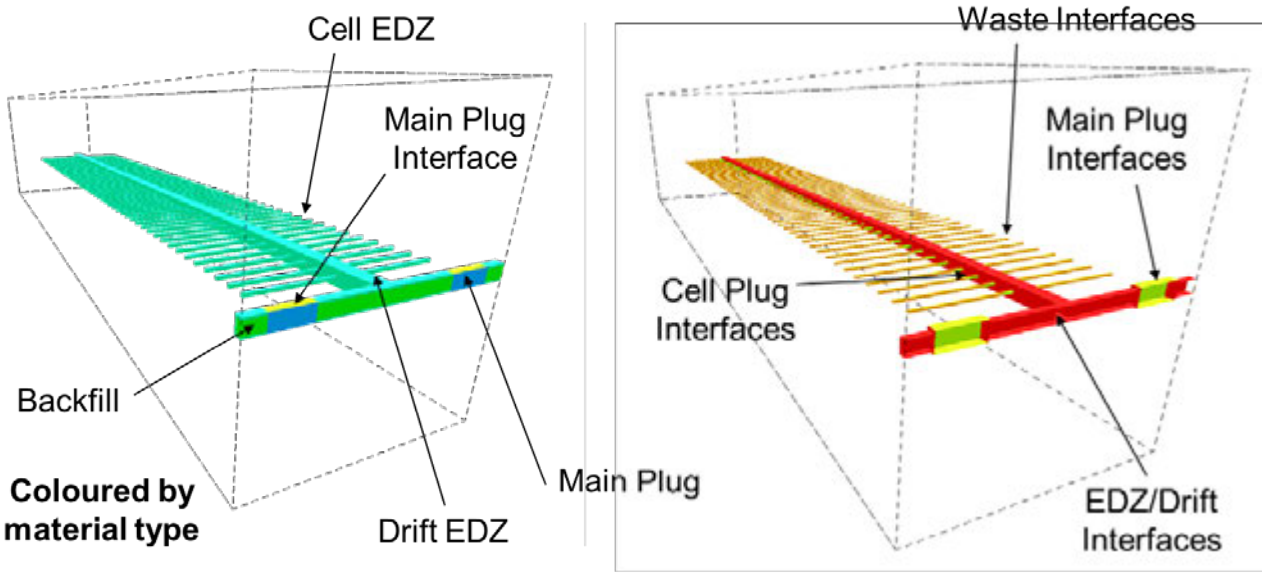

Figure 20 *Visualisation of the 3D Cartesian grid for 100 HA Cells with compartments coloured by material type and the host rock removed (left) and only interfaces visible (right)*

Results for the 100 Cell case were extremely similar to the base case, with evolution of fluxes and pressures on the downstream side being functionally identical. Differences in gas pressure and water saturation between the upstream and downstream sides of the model are very minor as shown in Figure 21 and Figure 22. Further estimates of asymmetry we obtained by comparing the magnitudes if the upstream and downstream fluxes through the plugs. The fractional difference (1-F_PU/F_PD) is shown in Figure 23, which is less than 6%, equally plots of water saturation and gas pressure at 10,000 years (peak pressure - Figure 24) show very little asymmetry. Such small differences are well within the bounds of parametric, process and numerical uncertainty for this case.

Overall the 100 cell case with the reference paramterisation behaves in an almost identical manner to the 50 cell case, justifying the reference assumption of symmetry down the access drift for the base case.

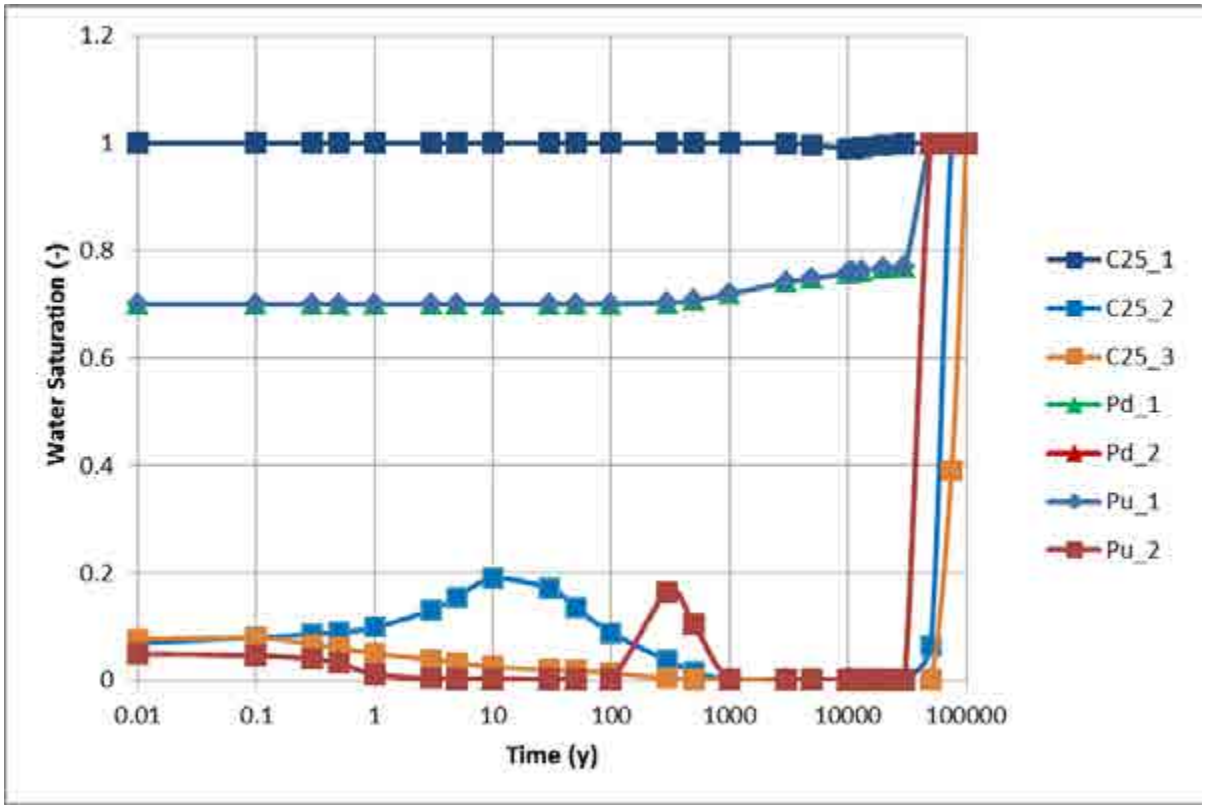

Figure 21 *Water saturations at key measurement points for the 100 Cell variant case.*

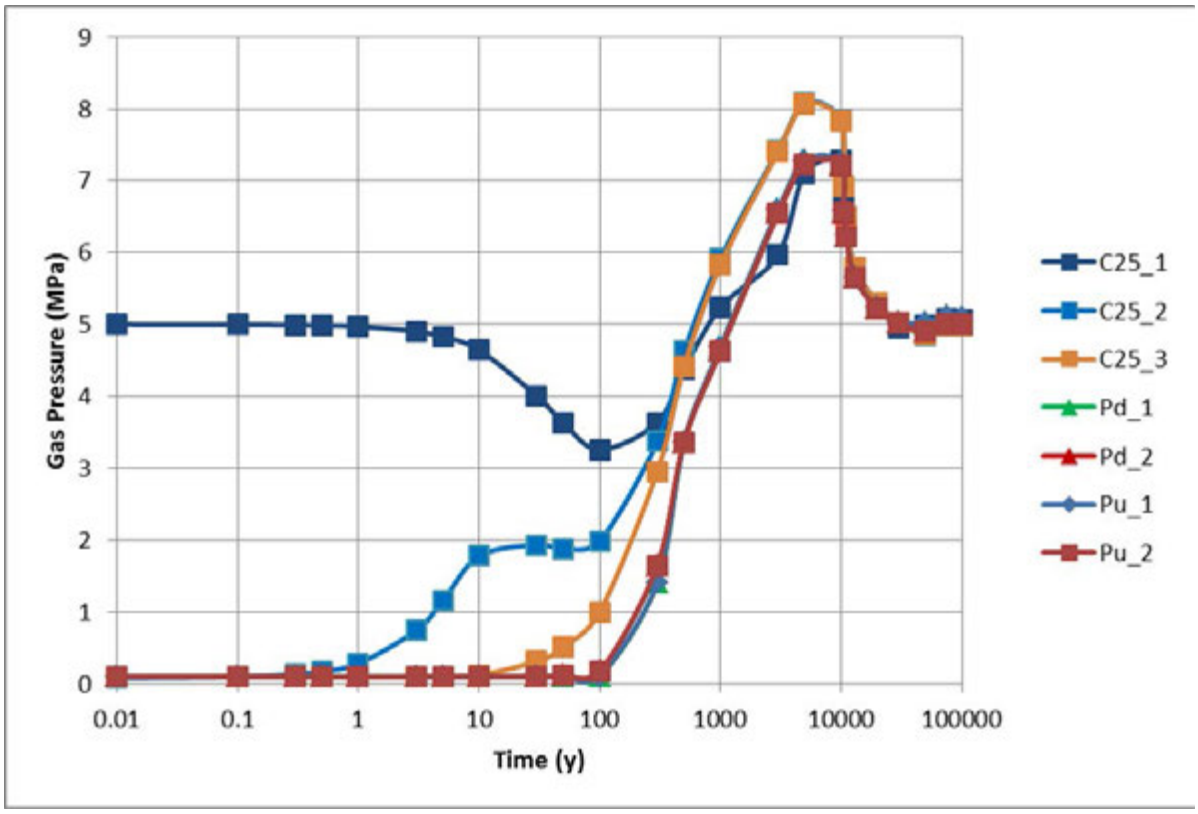

Figure 22 *Gas pressure at key measurement points for the 100 Cell variant case.*

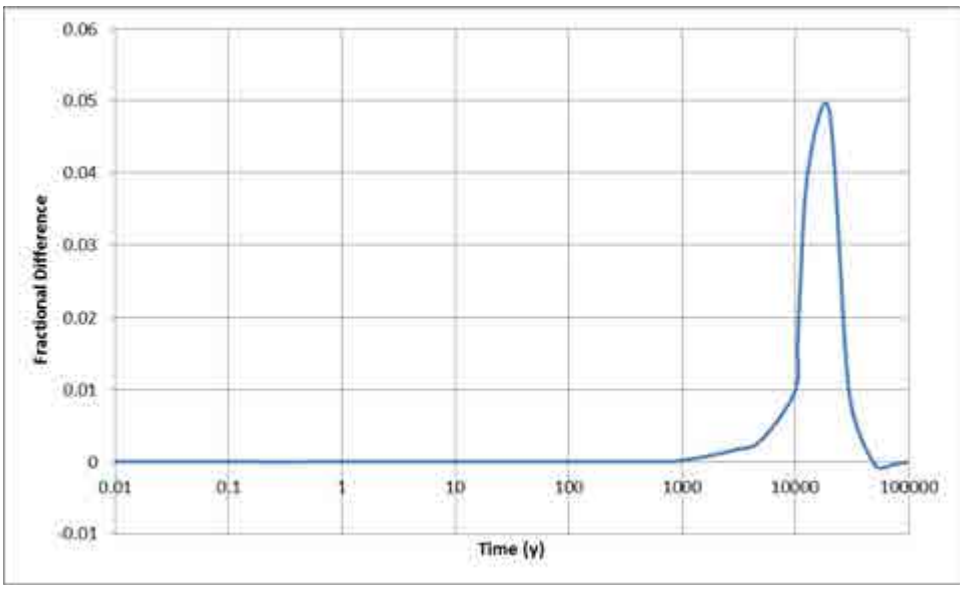

Figure 23 *Fractional difference in upstream versus downstream plug gas fluxes (+ve = more flux downstream)*

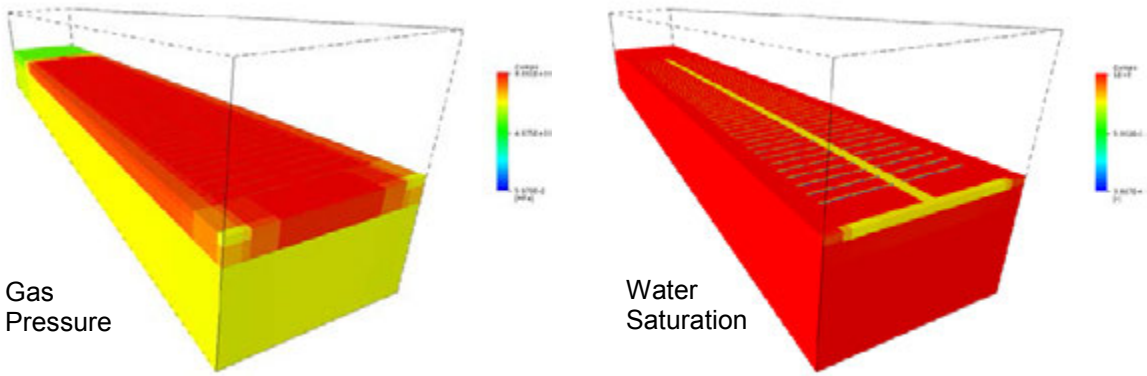

Figure 24 *Gas pressure and water saturation for the 100 Cell case at 10,000 years.*

3.1.6 Sensitivity Cases on the Variant Case (100 HA Cells)

For comparison with and to complement the base case sensitivities, two additional sensitivity cases were run on the 100 cell model. These were

1. Case 7 (NoDriftInterfaces): No drift or plug interfaces
2. Case 8 (NoInterfaces) : All interfaces elminated from the model (including the HA cells)

Selected results are plotted below in Figure 25 and Figure 26. Note that the results of Case 8 were virtually identical to Case 7, hence they are not included on the diagrams below to improve clarity. The results show that the symmetry across the access drift is retained in these configurations and that the changes in gas pressures are completely consistent with the equivalent variants for the 50 cell model (compare Figure 25 and Figure 26 with Figure 17and Figure 16 respectively).

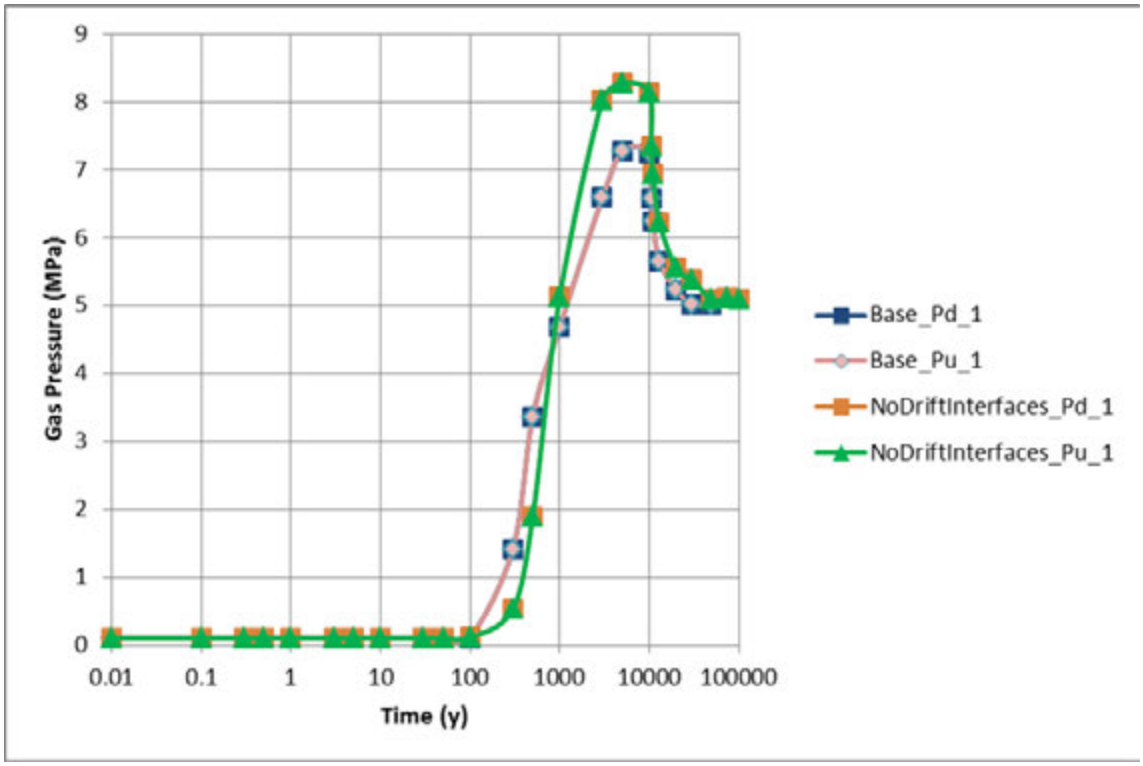

Figure 25 *Gas pressure at Pd-1 and Pu-1 for case 7 and the 100 cell variant (labelled Base here)*

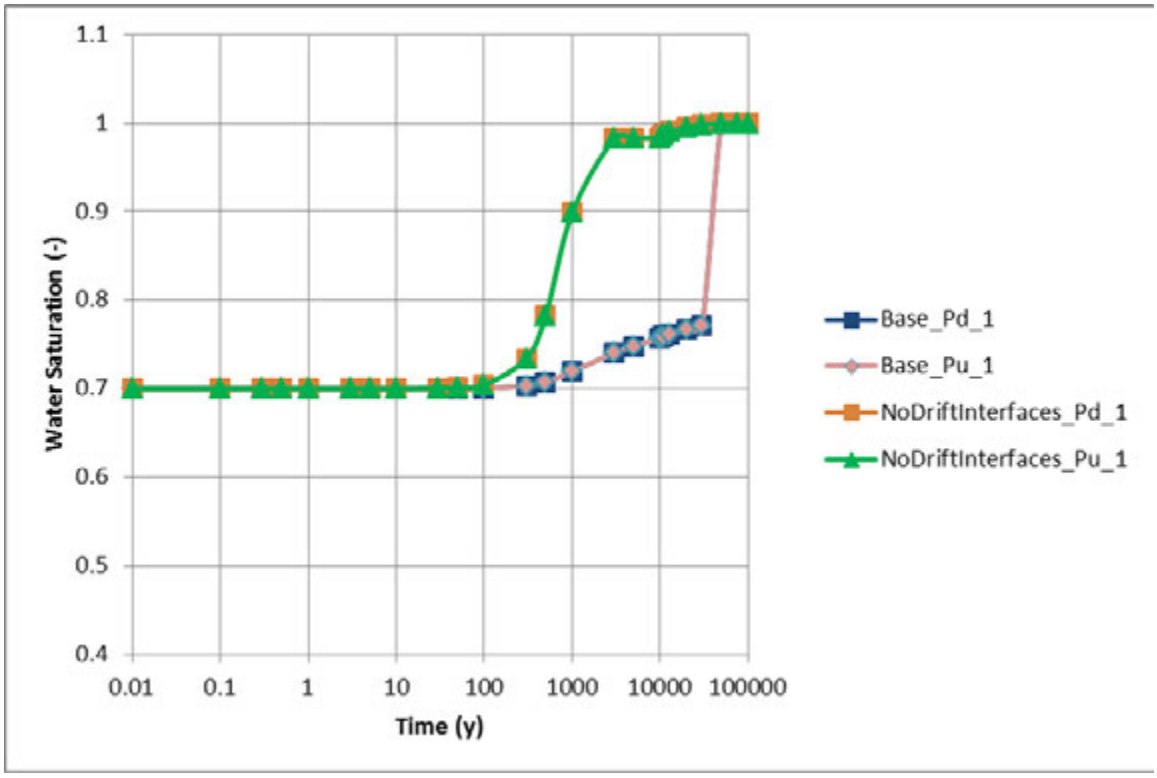

Figure 26 *Water saturation at Pd-1 and Pu-1 for case 7 and the 100 cell variant (labelled Base here)*

3.1.7 Discussions and Conclusions

3.1.7.1 Lessons Learnt

During the process of constructing the model and clarifying potential ambiguities in the specification a number of potentially significant points were identified.

1. It has been demonstrated that, using QPAC with conventional gridding approaches, it is possible to construct a full multi-phase flow model at the module-scale including all prescribed features without recourse to conventional upscaling techniques. Furthermore the run-times were sufficiently managable that a wide range of sensitivity calcutions and numerical stability tests could be conducted, increasing the confidence and value of the results.

2. The presence of high permeability, low capillary pressure interfaces has a major impact on the bulk behaviour of the system. The interfaces act as a capillary barrier and hence restrict water flow normal to the plane of the interfaces. They also act as major gas flow paths for free gas around the plugs and waste. The impact is far more prominent in this case than in the first benchmark.

3. Elimination of the interfaces around the backfill gave much faster resaturation than seen in the base case.

4. The structure of the interfaces tends to make the solution matrices extremely stiff by effectively compartmentalising the model.

5. Despite the numerical issues, stable, conceptually sensible results were obtained using a relatively coarse gridding scheme.

6. There is a mismatch between the access drift boundary condition used in the first benchmark and the behaviour of the access drift in this second benchmark. Therefore there may be a requirement to revisit the first benchmark boundary condition parameterisation to investigate the impacts of the observed pressurisation at the cell scale. Equally, it will be expected that at the whole facility scale there may be a mismatch between the boundaries used at this module scale and the larger scale calculations.

7. Despite the coarse grid selected, refinement of the problem did not significantly change the results.

8. The initial assumption of symmetry between the upstream and downstream sides of the module was demonstrated to be robust by modelling the complete module as a variant case.

3.1.7.2 Issues for further consideration

1. The behaviour of the system, especially including the interfaces, gave a significantly different response to that assumed for the cell-scale benchmark. This is largely an artefact of the parameterisation selected for the interfaces, as static, open structures with a very low capillary pressure. and should not be regarded as realistic. The evolution of interfaces and their potential to act as relatively fast pathways (either when open, or as a line of 'weakness' for the creation of dilation pathways) is potentially of interest in terms of the of bentonite seals acting consistent with their required safety functions. The issue of dilation is discussed further in the repository scale report and the cell scale report [2,3],

2. In this case, upscaling via homogenisation for the HA cells did not significantly change the evolution of the system. While not a general conclusion, it suggests that such approaches may be appropriate under certain circumstances. This issue is revisited on a much larger scale in the repository scale modelling [2].

3.1.8 References

1 Bond AE. and Benbow SJ. (2009). QPAC Multi-Phase Flow Module Functional Specification and Architectural Design. Quintessa Report QRS-3000C-4 v1.0.

2 FORGE (2013). Deliverable D1.6 Final report on benchmark studies on repository-scale numerical simulations of gas migration. Part 1 : cell scale benchmark

3 FORGE (2013). Deliverable D1.6 Final report on benchmark studies on repository-scale numerical simulations of gas migration. Part 3 : repository scale benchmark

3.2 SCK-CEN contribution

No contribution

3.3 Andra contribution

3.3.1 Introduction

This report gives a view of the work done by Andra in the framework of the "module scale" benchmark of package WP1.2 of the FORGE project. The work done covers only the reference case.

This report first describes the code used and the slight deviations from the benchmark specifications, then the main results of the reference calculation are presented and finally main conclusions for this work are developed

3.3.2 Model Implementation

3.3.2.1 Code and Formulation

Numerical simulations rely on TOUGH2, a general-purpose numerical simulation program for multi-phase fluid and heat flow in porous and fractured media. Tough2 was developed at the Earth Sciences Division of Lawrence Berkeley National Laboratory (LBNL).

Simulations have been performed using Tough2-MP, a massively parallel (MP) version of the Tough2 code, designed for computationally efficient parallel simulation of isothermal and non-isothermal flows of multi-component, multiphase fluids in one, two, and three-dimensional porous and fractured media.

Tough2-MP features several fluid property modules [EOS (Equation Of State) modules].

In the framework of this benchmark, numerical simulations are performed using EOS5 module (water, hydrogen).

TOUGH2(-MP) solves mass and energy balance equations that describe fluid and heat flow in general multiphase, multicomponent systems. Fluid advection is described with a multiphase extension of Darcy's law; in addition there is diffusive mass transport in all phases.

The description of thermodynamic conditions is based on the assumption of local equilibrium for all phases. Fluid and material/formation parameters can be arbitrary nonlinear functions of the primary thermodynamic variables.

One of the specificities of TOUGH2(-MP) code is that the mathematical formulation is changing from saturated state to unsaturated state, mainly, the primary variables are not the same in the two formulations. For EOS5 module (water, hydrogen), primary variables are as follows:

- single-phase conditions: pressure, air mass fraction, temperature
- two-phase conditions: gas phase pressure, gas saturation, temperature

For numerical simulation the continuous space and time variables must be discretized. InTOUGH2, space discretization is made directly from the integral form of the basic conservation equations, without converting them into partial differential equations. This "integral finite difference" method (IFDM) avoids any reference to a global system of coordinates, and thus offers the advantage of being applicable to regular or irregular discretizations in one, two, and three dimensions.

Time is discretized fully implicitly as a first-order backward finite difference. This together with 100 % upstream weighting of flux terms at interfaces is necessary to avoid impractical time step limitations in flow problems involving phase (dis-)appearances.

The discretization results in a set of strongly coupled nonlinear algebraic equations, with the time-dependent primary thermodynamic variables of all grid blocks as unknowns. These equations are cast in residual form, i.e., {residual} ≡ {left-hand side} - {right-hand side} = 0, and are solved simultaneously, using

Newton-Raphson iteration. Time steps can be automatically adjusted (increased or reduced) during a simulation run, depending on the convergence rate of the iteration process. Automatic time step adjustment is essential for an efficient solution of multiphase flow problems, where intrinsic time scales for significant changes in the flow system may vary by many orders of magnitude during a simulation run. Different methods are available to solve the linear equations arising at each iteration step, including preconditioned conjugate gradient solvers, as well as sparse direct matrix methods. While direct methods are more predictable and less problem-dependent in their performance, it is only through the application of iterative conjugate gradient methods that solutions for large grid systems (10,000 blocks or more) and three-dimensional problems can be accomplished.

Further description and more details about Tough2/Tough2-MP codes are available from the Tough2 Homepage on the web, at http://esd.lbl.gov/TOUGH2, and from the Tough2-MP Homepage on the web at http://tough2.com.

3.3.2.2 Benchmark Implementation

The mathematical model is the same as described in the benchmark specifications, except for the following processes:

Diffusion terms:

In Tough2/Tough2-MP, diffusive flux of component κ (water or hydrogen for EOS5 module) in fluid phase β (liquid or gas) is expressed as follows: $f_\beta^\kappa = -\phi\tau_0\tau_\beta\rho_\beta d_\beta^\kappa \nabla X_\beta^\kappa$.

where ϕ is porosity, $\tau_0\tau_\beta$ is the tortuosity which includes a porous medium dependent factor, τ_0 and a coefficient that depends on phase saturation S_β, $\tau_\beta = \tau_\beta(S_\beta)$, ρ_β is density, d_β^κ is the diffusion coefficient of component κ in bulk fluid phase β, and X_β^κ is the mass fraction of component κ in phase β.

Tortuosity effects have a porous medium-dependent part τ_0 and a saturation-dependent part $\tau_\beta(S_\beta)$, with S_β as the fluid phase β saturation. The following three alternative formulations are available in Tough2 / Tough2-MP:

- Relative permeability model: tortuosity will be taken as $\tau_0\tau_\beta = \tau_0 k_{r\beta}(S_\beta)$.
- Saturation model: s $\tau_0\tau_\beta = \tau_0 S_\beta$ will be used.
- Millington-Quirk model: $\tau_0\tau_\beta = \phi^{1/3} S_\beta^{10/3}$, with ϕ as the porosity. This model is used for the benchmark simulations.

Solubility of Hydrogen in water:

In Tough2/Tough2-MP, the solubility of hydrogen in liquid water is represented by Henry's law. Henry's coefficient Kh (expressed in Pa^{-1}) for hydrogen dissolution in water, is the ratio between dissolved hydrogen mass fraction and gaseous hydrogen partial pressure.

It is a linear function of temperature, varying from 1,697 10^{-10} Pa^{-1} at 0 °C to 1,379 10^{-10} Pa^{-1} at 25 °C.

For the 20°C temperature used in the numerical simulations, Kh is equal to 1,443 10^{-10} Pa^{-1}. This value is equivalent to a Henry's constant of 8,0 10^{-6} expressed in $mol.Pa^{-1}.m^{-3}$ (different from the 7.6 10^{-6} $mol.Pa^{-1}.m^{-3}$ mentioned in the benchmark description).

Specific storage coefficient:

Tough2/Tough2-MP codes do not use specific storage coefficient S_S as an input parameter, but pore compressibility. Relation between pore compressibility C, expressed in Pa^{-1}, and specific storage coefficient S_S expressed in m^{-1} as follows:

$$C = \frac{S_S}{\rho_w g \phi} - \beta_w$$

With: ρ_w liquid water density (kg/m³)

g magnitude of the gravitational acceleration vector (m/s²)

ϕ porosity (-)

β_w liquid water compressibility (Pa⁻¹)

All the specifications of the benchmark are taken into account

Some slight developments have been performed to take into account time dependent boundary conditions

and to add some additional quantities in the output data file

3.3.2.3 Grid

All the cells, on the both sides of the access drift, and their plugs, interfaces and EDZ are explicitly represented

The cells and their environment (interfaces, EDZ) are represented with square cross sections

This allows using a regular, structured mesh

As waste packages are considered as gas- and water-tight components, they are not represented in the geometric model

No upscaling technique or approximation was used (no merge of materials or geometric cells)

This leads to a mesh of up to 600, 000 cells

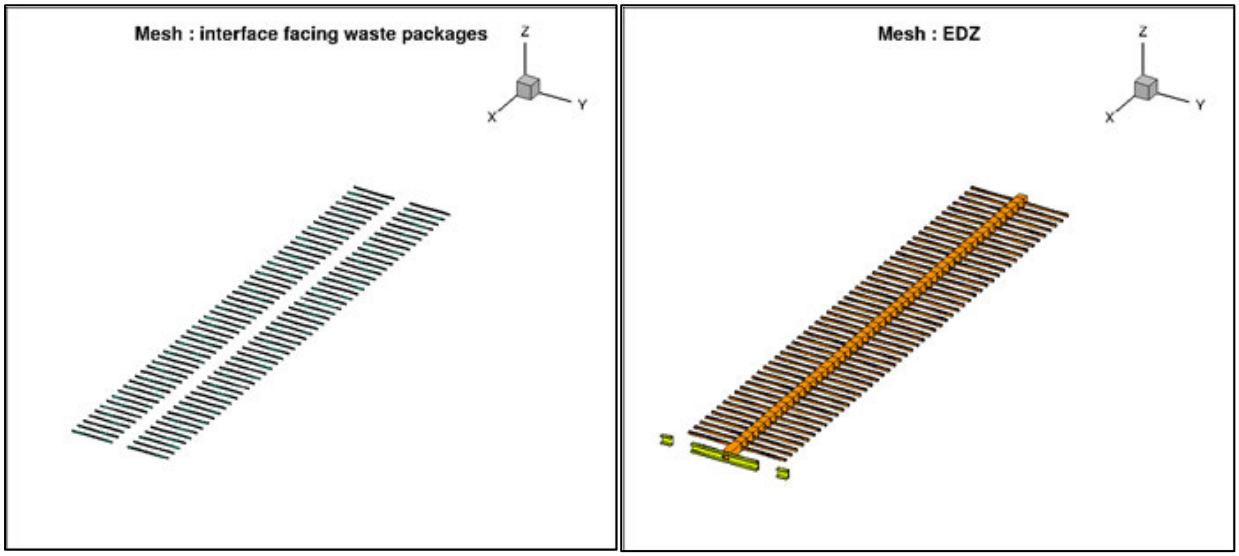

Figure 27 : examples of different parts of the mesh

3.3.2.4 Boundary Conditions and Sources

Boundary conditions can be of two basic types.

Dirichlet conditions prescribe thermodynamic conditions, such as pressure, saturation, temperature, on the boundary. Dirichlet conditions can be implemented by assigning very large volumes (e.g., $V = 10^{50}$ m^3) to grid blocks adjacent to the boundary, so that their thermodynamic conditions do not change at all from fluid or heat exchange with finite-size blocks in the flow domain. In addition, a small value (such as $D = 10^{-9}$ m) should be specified for the nodal distance of such blocks, so that boundary conditions are in fact maintained in close proximity to the surface where they are desired, and not at some distance from it.

In the original version of Tough2-MP 2.0, only time dependent pressure boundary conditions are available. Numerical developments have been performed in the Fortran source code of Tough2-MP to provide additional capabilities for a time-dependent gas saturation boundary conditions (gas saturation is one of the primary variables for EO55 module).

Attention must be paid to assume, at every time, coherence between boundary gas saturation, boundary water pressure, capillary pressure in access drift material, and realistic gas pressure.

Neumann conditions prescribe fluxes of mass or heat crossing boundary surfaces. A special case of Neumann boundary conditions is "no flux," which in the integral finite difference framework is handled with simplicity itself, namely, by not specifying any flow connections across the boundary. More general flux conditions are prescribed by introducing sinks or sources of appropriate strength into the elements adjacent to the boundary. Using this technique, time-dependent hydrogen production term is then applied directly in the interface volumes which are besides the external surfaces of the different waste packages.

3.3.2.5 Initial Conditions

Flow systems are initialized by assigning a complete set of primary thermodynamic variables to all grid blocks into which the flow domain is discretized. During the initialization of a TOUGH2-MP run, all grid blocks are first assigned to default thermodynamic conditions. The defaults can then be overwritten for selected domains by assigning domain-specific conditions in specific data blocks.
The primary variables used depend on the fluid phase composition. During phase change primary variables will be automatically switched from one set to another. In multiphase flow systems, therefore, different grid blocks will in general have different sets of primary variables, and must be initialized accordingly.

3.3.2.6 Deviations from the specification

The different conceptual and physical processes and assumptions are in accordance with the benchmark specifications, and/or the original version of Tough2-MP, except for the following aspects:

Physical parameters:

Some physical parameters and fluid properties are internally computed and/or tabulated in Tough2/Tough2-MP Fortran source code. They have not been replaced by the mathematical expressions presented in the benchmark description.

<u>Water vapor pressure:</u>

In standard EOS5 module of Tough2-MP, vapor pressure is equal to saturated vapor pressure of water. It is not expressed by Kelvin's equation. At a 20°C temperature, this vapor pressure is 2337 Pa.

<u>Viscosity of the gas mixture:</u>

Dynamic viscosity of hydrogen is both pressure and temperature dependent in Tough2/Tough2-MP. For the 20°C temperature used in the numerical simulations, values expressed in Pa.s are:

$8{,}8\ 10^{-6}$ Pa.s when pressure is lower than 0,1 MPa

$8{,}95\ 10^{-6}$ Pa.s at 10,0 MPa and $9{,}22\ 10^{-6}$ Pa.s at 200,0 MPa

Values at intermediate pressures are linearly interpolated.

The dynamic viscosity of hydrogen-vapor mixture is approximated as dynamic viscosity of hydrogen.

Outputs:

In the original version of Tough2-MP 2.0, mass flow rates from diffusion are not printed in the standard output file.

Developments have been performed in the Fortran source code of Tough2-MP to print the diffusive fluxes of each component (water, hydrogen) in both liquid and gas phase. These fluxes are necessary for computing, after the end of the simulation, the total rate of flow for each component

3.3.3 Base Case Results

Due to numerical problems, the simulation was performed only up to a time of 10 000 years. Thus the end of the hydraulic-gas transient is not simulated, but the available results are sufficient to give a general view of this phenomenon.

- **Gas and liquid pressure**

Figure 28 and Figure 29 represent respectively the evolution with time of liquid and gas pressures at different points inside cells and inside the access drift. One can see that the behavior is very similar in each cell, as well as all along the access drift, whatever the position inside the module, for gas and water pressures.

This means that the drift plug is efficient and after several hundred years the gas pressure and the water pressure is homogenized inside the module at a value linked to plug « gas entry pressure ». This is the case although the bentonite of the plus is not completely saturated as its water pressure is largely negative (values for P_Pu-1 and P-Pd-1)

Gas is implying a water over pressure of 2 MPa (compared with the 4 MPa hydrostatic pressure) at 10 000 years, time at which gas pressure is also at its maximum. Maximum gas pressure is around 7 MPa, so only 3 MPa over the hydrostatic water pressure.

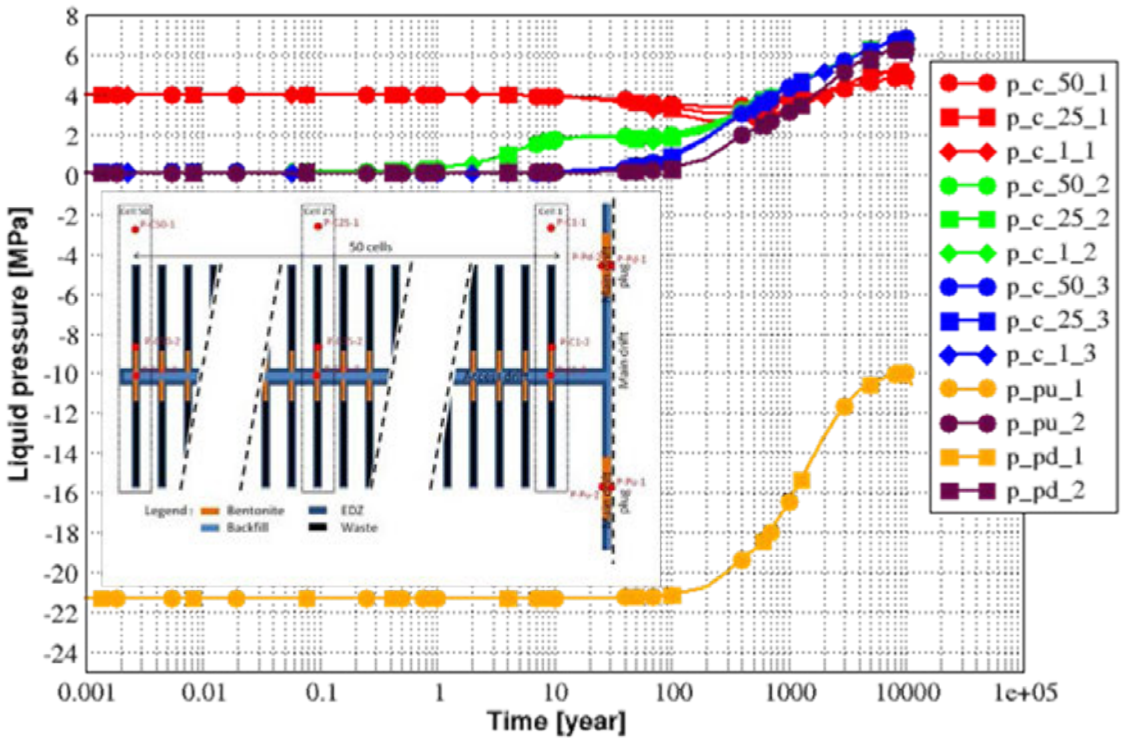

Figure 28 : Liquid pressure at different points

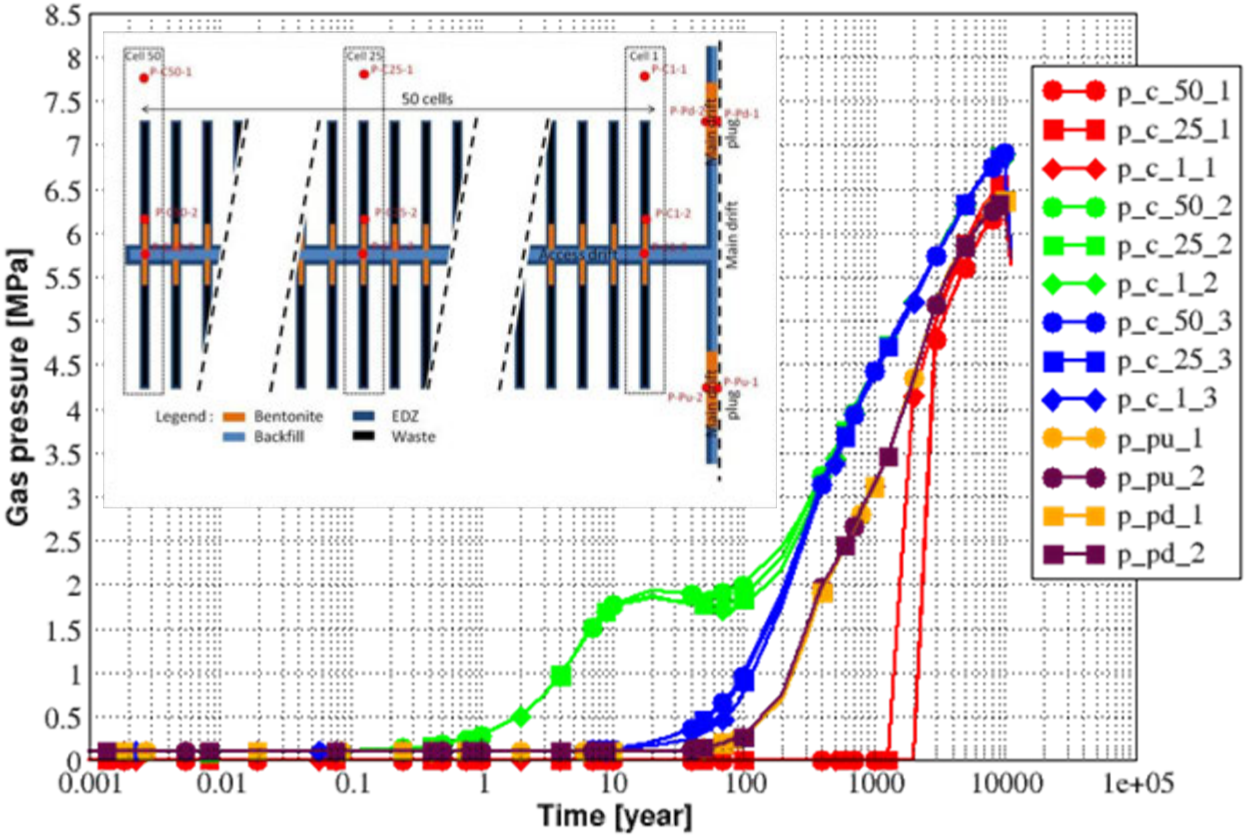

Figure 29 : gas pressure at different points

- **Hydrogen flows**
  - **Across interface and EDZ**

On the folloving plot (Figure 30), flow is positive when directed towards the drift and negative when directed towards the end of the cell.

For the cells near the main drift (red and green curves) free H2 flux is always directed towards the drift, meaning that the gas produced inside the cells is flowing toward the access drift.

On the contrary, for the cells near the end of the module, after several thousand years free H2 flux is directed towards the cell meaning that the end of the module cells are acting as sinks for the free gas (dissolution/diffusion): these cells are too far from the main drift and it is easier for gas to move toward the end of the module and to dissolve in the water in contact with the far end cells.

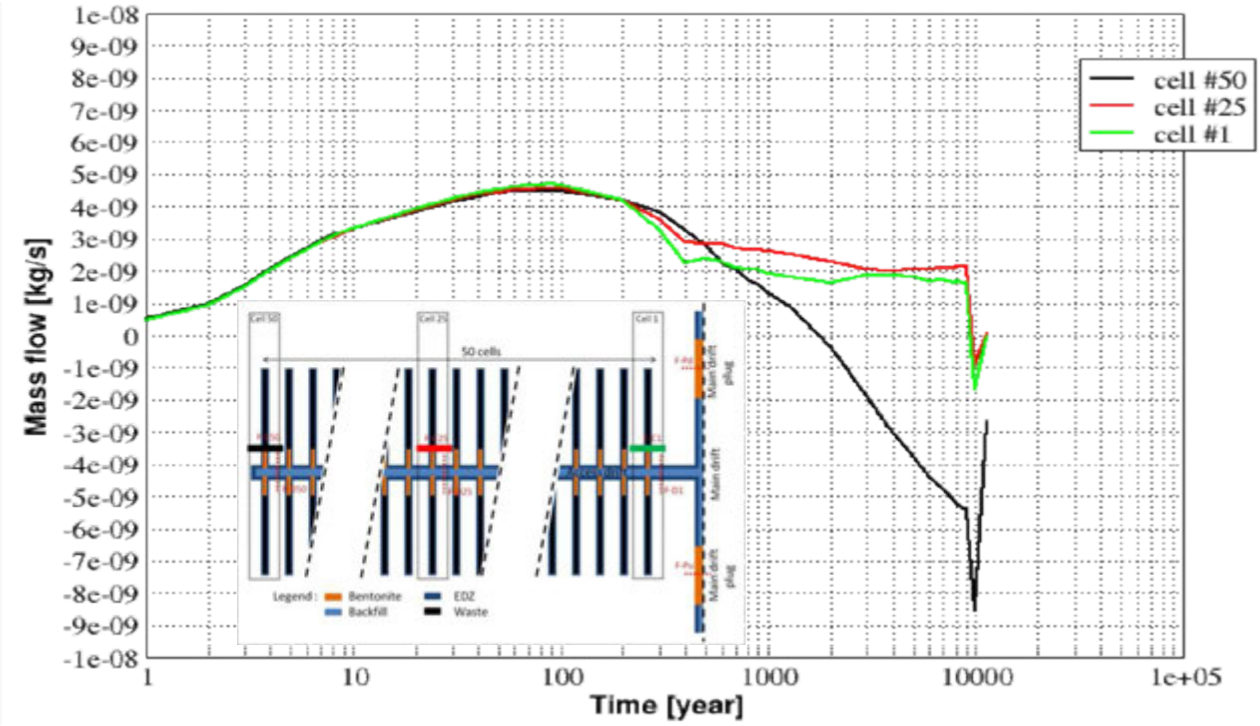

Figure 30 : mass flow of gaseous hydrogen across cell interface and EDZ. Positive values means of flow directed from cell toward the drift

- **Across access drift**

The general behavior (Figure 31) shows a flux directed toward the main drift for the majority of the access drift length. But near the end of this drift, after several hundred years, fluxes are changing directions and are directed toward the end of the drift instead of being directed toward the main drift. This means that the main drift plug (10^{-11} m/s) is impermeable enough to force part of the free gas to move away from it before dissolving.

This behavior is similar to the one described for fluxes across cell interfaces and EDZ: after several hundred years and near the end of the module free gas flux is directed towards the end of the module. Around 10 000 years, the part of the total gaseous hydrogen flux directed toward the end of the module is up to 30% of the gaseous hydrogen flux directed toward the main drift: an important part of the free gas produced inside the module is dissolving in the end of the module without leaving the module under gaseous form.

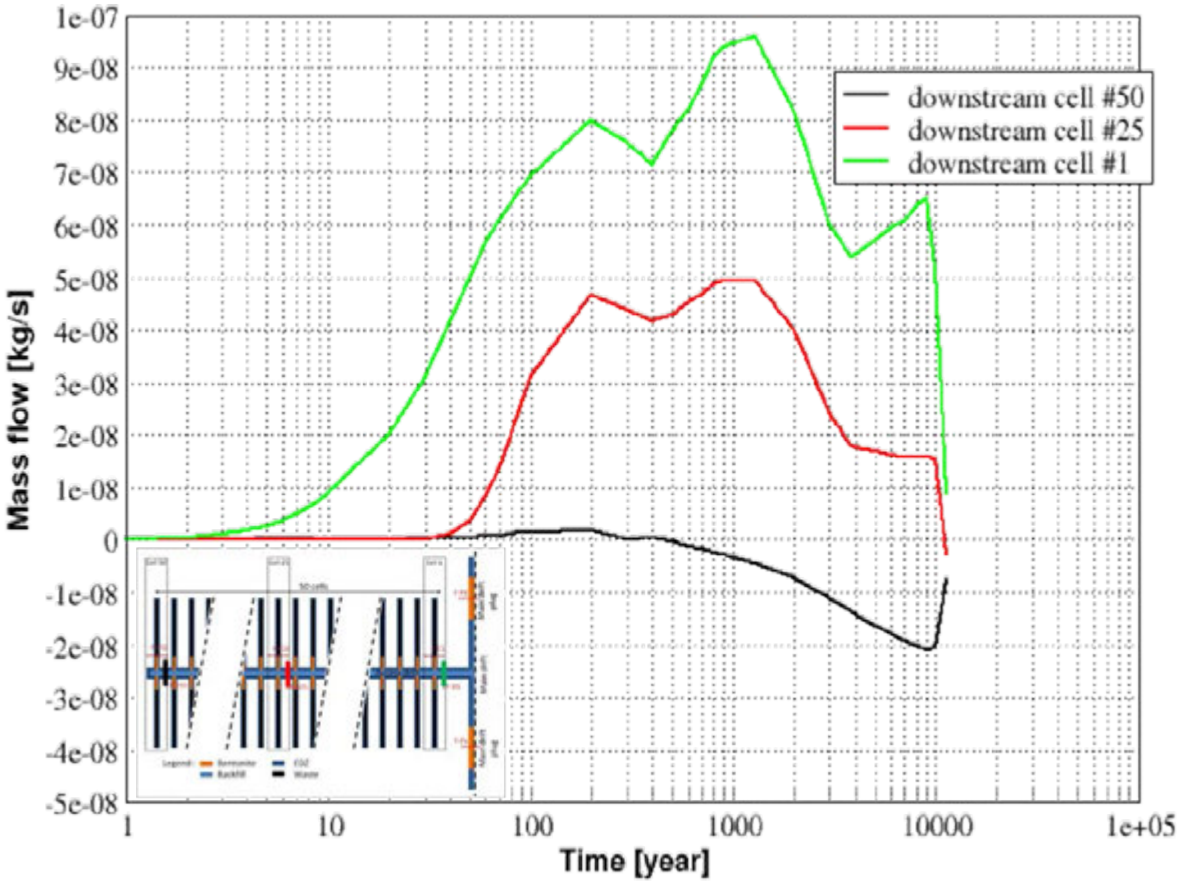

Figure 31 : mass flow of gaseous hydrogen across access drift. Positive values means a flow directed toward the main drift

- **Across main drift plugs**

Figure 32 represent the free gas flux across the main drift plugs. The downstream flux and the upstream flux are quite the same, reflecting the boundary conditions. Such a module can be representative of a module in the middle of several other of the same type. This issue is addressed in the "repository scale" benchmark.

The figures also shows that across the main drift plugs the total flux of free gas going out of the module is less than an order of magnitude smaller than the total gas production rate. This attests that at the module scale dissolution/diffusion is the main process for hydrogen migration; most of the hydrogen produced inside the module is never going out of it under gaseous form.

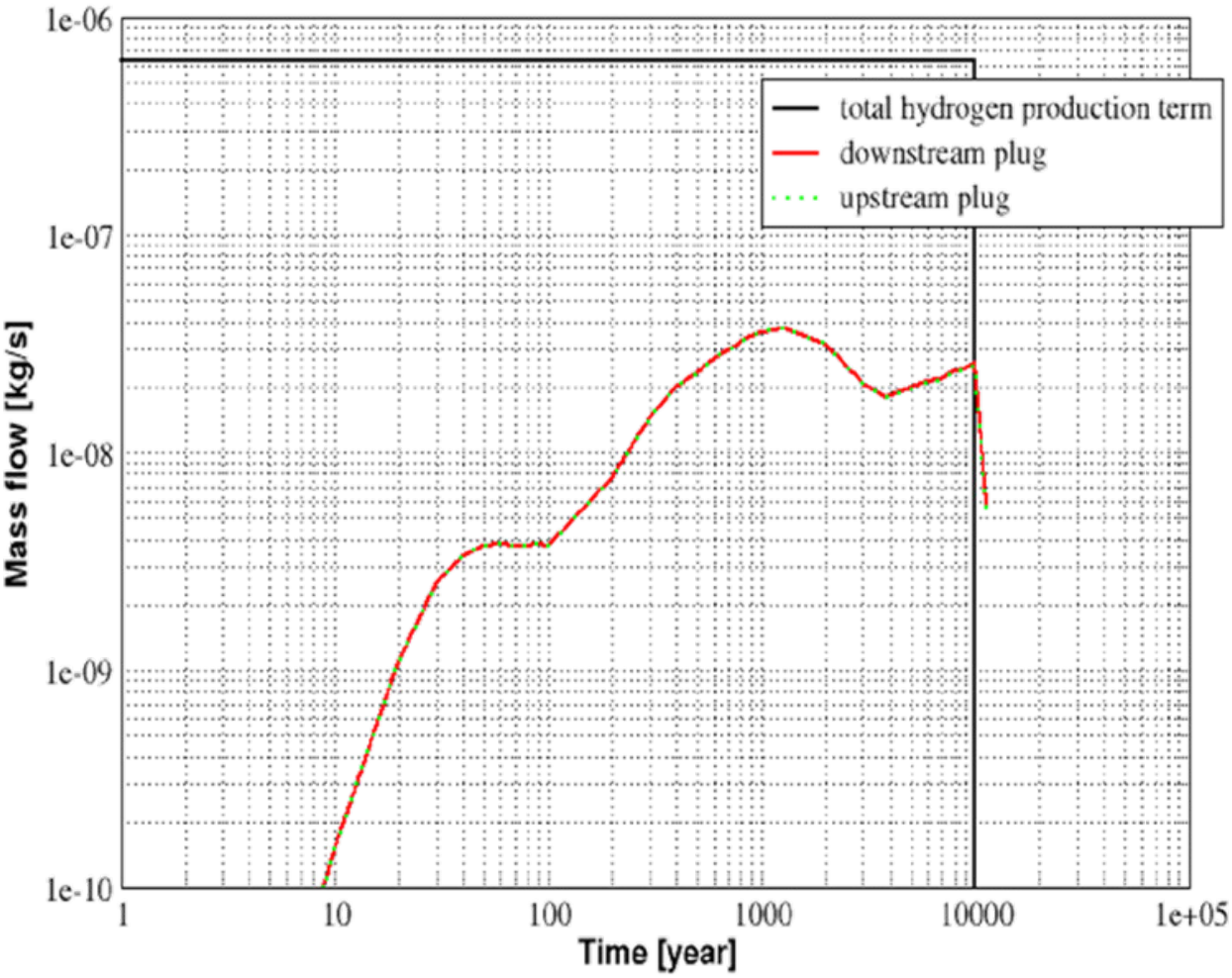

Figure 32 : mass flux of gaseous hydrogen across the main drift plugs

3.3.4 Discussion and Conclusions

Due to numerical problems, only 10 000 years of the reference case have been performed and no sensitivity analysis was done. Nether the less, some general conclusions can be drowned out of the available results.

The first one is that the gaseous hydrogen produced inside the module is not entirely moving toward the main drift, part of it is moving toward the end of the module where it dissolves in the argillites water.

The second one is that the total gaseous flux across the main drift seals are small compared to the total generated hydrogen flux.

Both these conclusions are coherent with the fact that the module seal is impervious enough (permeability of 10^{-11} m/s) to force the hydrogen to dissolve inside the module and move mainly by diffusion inside the host rock water.

3.4 CEA contribution

3.4.1 Introduction

In the framework of numerical tool development for two-phase flow simulations in porous media, CEA developed a module inside the MPCube code that include several two-phase flow models like two-phase flow with gas phase dissolution in liquid phase as well as multicomponent accounting. The MPCube code is based on the Trio-U kernel **[1]**, also developed by CEA, which allows computation in a parallel environment and high performance computing on massively parallel computers. The benchmark defined in the FORGE project was the opportunity to perform some new numerical developments and to check the efficiency of the MPCube tool.

3.4.2 Model Implementation

The mathematical model implemented in MPCube and used for this benchmark is the two-phase multicomponent one. The multicomponent model is described in **[2]** and is identical to the one described in the annex (§ 5) when we consider water and dissolved hydrogen for the liquid phase and gaseous hydrogen and water vapour for the gas phase.

The mathematical model is then constituted of mass conservation equations for water, gas and hydrogen (Eq. (9), (10), (12) and (15)) where water and gas velocities are of the generalized Darcy form (Eq. (6) and (7)). Gas components are considered to be perfect gases (Eq. (20) and (21)) as well as the gas mixture (Eq. (22)) for which pressure is evaluated considering classical thermodynamic rules (Eq. (19), (23) and (24)). Water and gas pressures are linked via capillary pressure (Eq. (1) and (2)) and hydrogen is considered to diffuse in the gas phase (Eq. (13)) as well as in the liquid phase (Eq. (17)) where dissolved hydrogen concentration follow Henry's law (Eq. (18)). Note that relative permeability curves as well as capillary curve are chosen here of the van Genuchten form (Eq. (4), (5) and (3)).

3.4.2.1 Code and Formulation

The mathematical model presented in the annex (§ 5) is reduced into a matricial one of the form *(1)* using the gas pressure and the liquid saturation as main variables (vector U).

$$M(U)\partial_t U - div[A(U)\nabla U] = F_U \qquad (1)$$

The matrix M and A as well as second member F are then only dependent on the main variables U.

We then used a centered cell finite volume method for the space discretization as presented in **[2]** and an Euler implicit scheme for the time discretization. After discretization, the nonlinear system *(1)* is solved using an iterative attractive fixed point algorithm. Note that the linear solver used is chosen inside the PETSc **[3]** library and we selected the BICGSTAB with an ILU2 preconditioner.

The system resolution is implemented using the Trio-U kernel functionalities allowing parallel computations. The main principle of the parallel computation consists in partitioning the mesh describing the problem in as many parts as requested number of processors to perform the computation.

3.4.2.2 Benchmark Implementation

The benchmark described in the annex (§ 5) was implemented with some deviations.

3.4.2.3 Grid

The mesh used for the benchmark computation is presented in Figure 33 for the whole mesh and in Figure 34 for the repository cells and access galleries system. The mesh is constituted of 2,500,000 tetrahedrons and takes into account a half part of the system described in the annex (§ 5) (using symmetry properties of the system).

Note that the interfaces and the EDZ are not considered in our computations and that the total number of repository cells is reduced to 60 (2x30) instead of 100 (2x50).

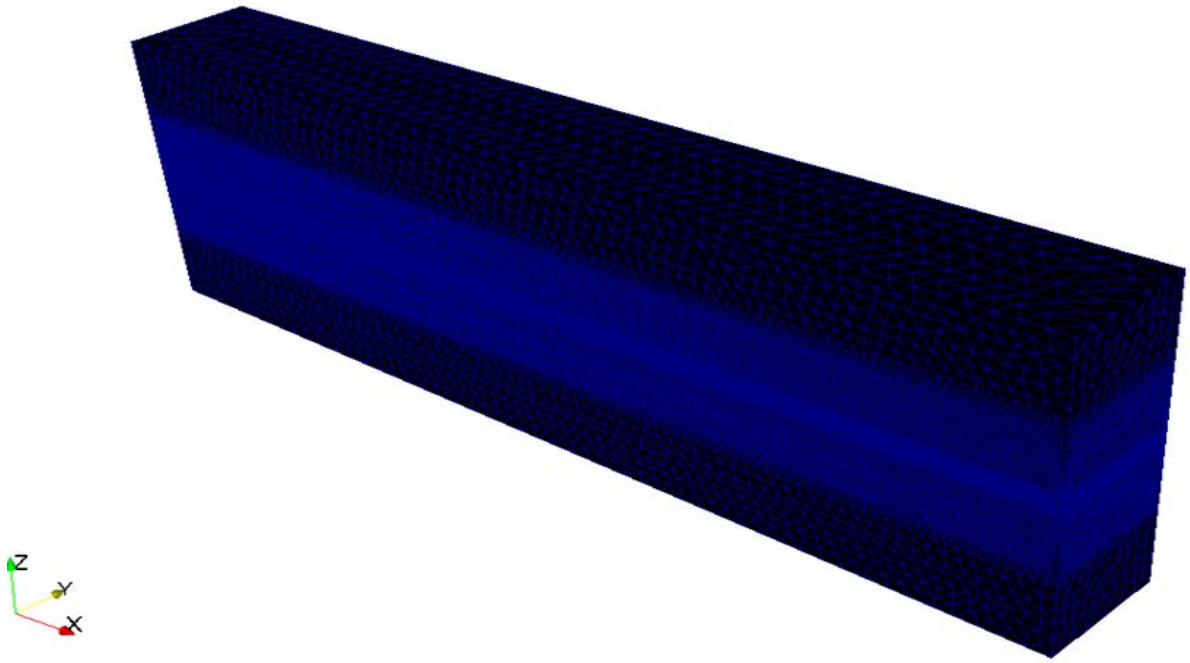

Figure 33: Mesh of the whole system (2,500,000 tetrahedrons)

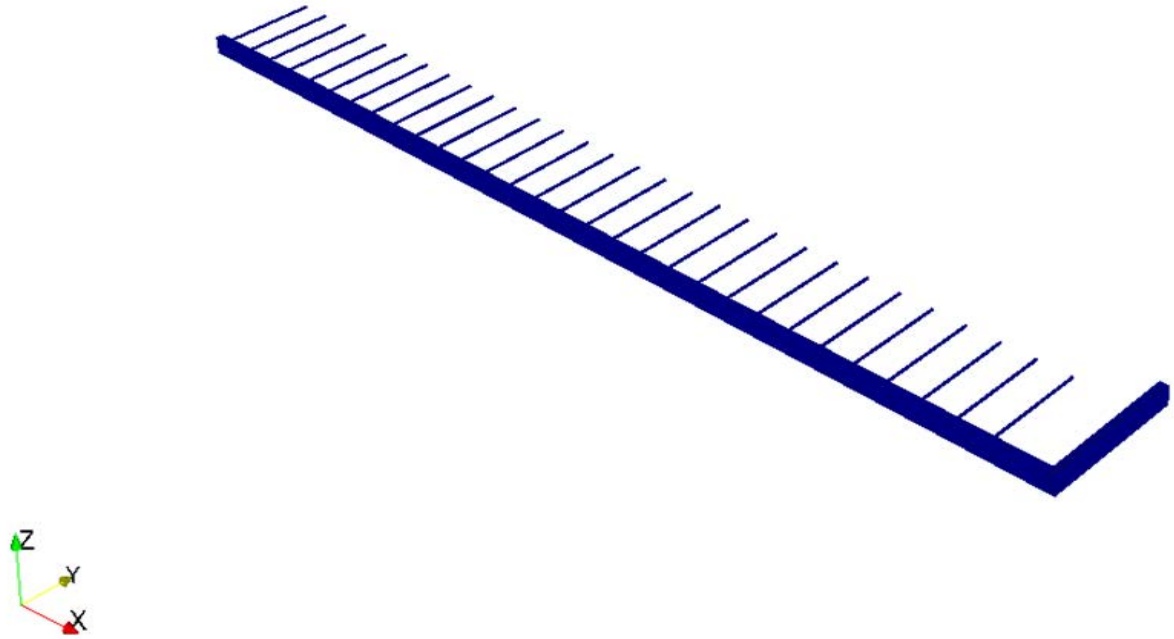

Figure 34: Mesh of the repository cells and access galleries.

3.4.2.4 Boundary Conditions and Sources

The boundary conditions were chosen identical to the ones depicted in the annex (§ 5) except for the time dependent boundary conditions which are kept constant in time. The Source term used was identical to the one depicted in the annex (§ 5).

3.4.2.5 Initial Conditions

The initial conditions in the system were chosen identical to the ones depicted in the annex (§ 5) except for the Callovo-Oxfordian argillites where residual gas saturation was introduced.

3.4.2.6 Deviations from the specification

The deviations of the conducted calculation from the benchmark depicted in the annex (§ 5) are listed hereafter:

- Only a half part of the system is considered for symmetry reasons.
- Number of repository cells is reduced to 60 instead of 100.
- Interfaces are not taken into account.
- EDZ is not taken into account.
- Residual gas saturation is introduced for the argillites.
- Boundary conditions were kept constant over time.

3.4.3 Base Case Results

We performed the benchmark two-phase flow computation over a 100,000 years period and we focused (for the first 10,000 years) on the temporal liquid saturation evolution of the different components of the system as well as on the temporal gas pressure evolution. The code development using a parallel architecture allows a calculation in about 15 hours for 312 computation time steps on 24 processors.

The temporal liquid saturation evolution inside the different components of the system is presented in Figure 35.

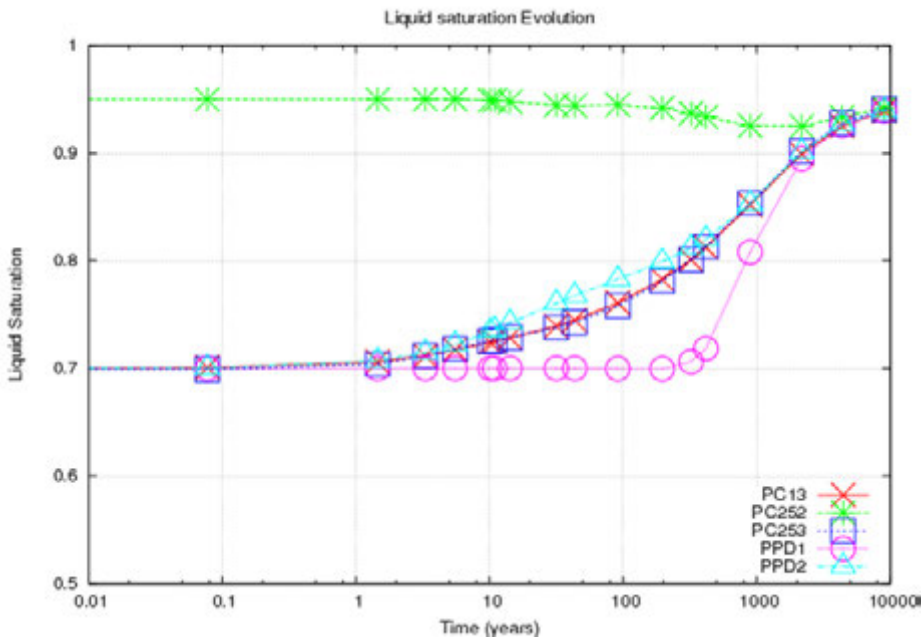

Figure 35: Liquid saturation evolution for different components of the system.

All the system is fully saturated after 20,000 years with some different trends depending on the component. In the vicinity of the disposal cells, the Callovo-Oxfordian argillite slowly lightly desaturates over the first 1,000 years period before fully saturating. The other components of the system start to saturate after at last few hundred years and slowly reach full saturation after 20,000 years.

Two horizontal cut sections of liquid saturation in the system are presented in Figure 36.

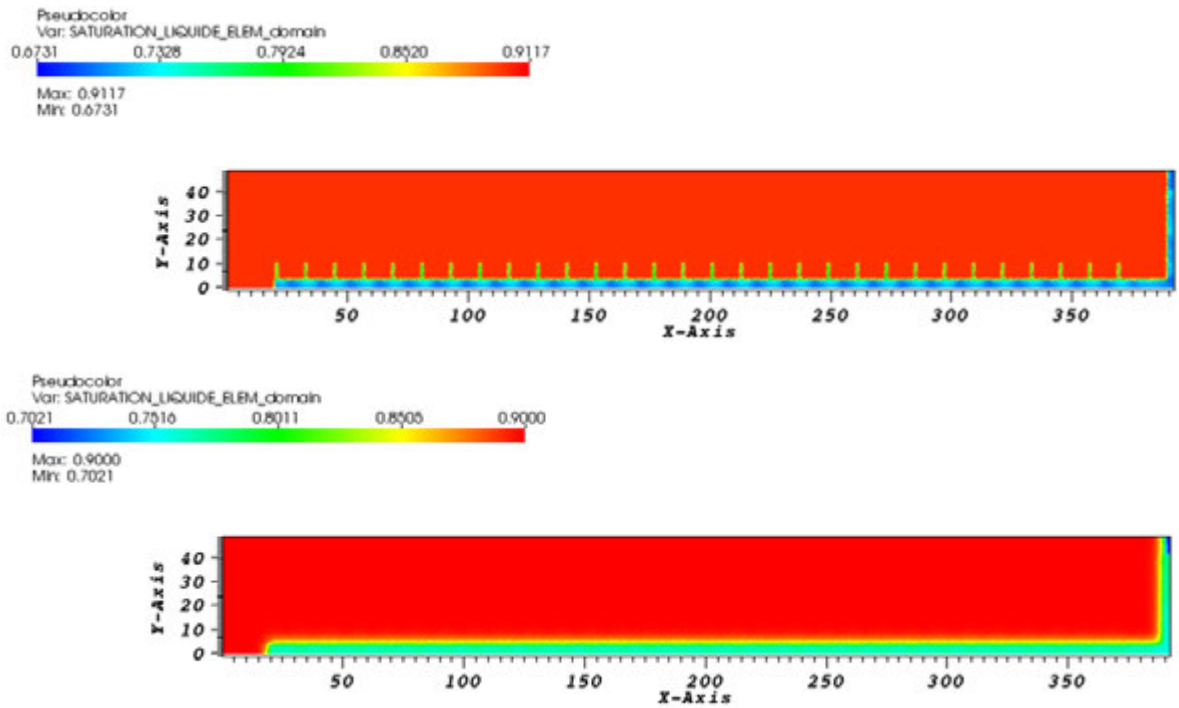

Figure 36: Liquid saturation horizontal cross-section (z=75 m) at t=10 years (top) and t=300 years (bottom).

Concerning the temporal gas pressure evolution inside the components of the system, a gas pressure map at t=300 years is presented for a horizontal cross-section in Figure 37 and for a vertical cross-section in Figure 38.

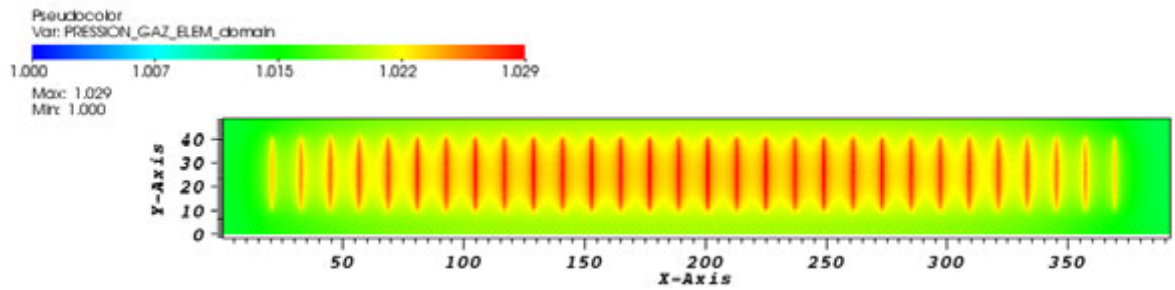

Figure 37: Gas pressure horizontal cross-section (z=75 m) at t=300 years.

The maximum gas overpressure is reached after 10,000 years inside de repository cells but the computed value is very small in comparison to the overpressure calculated by the other teams due on the first hand to the residual gas saturation introduced in the argillites (0.05) and on the other hand to the low gas constant pressure boundary condition for the backfill of the main drift.

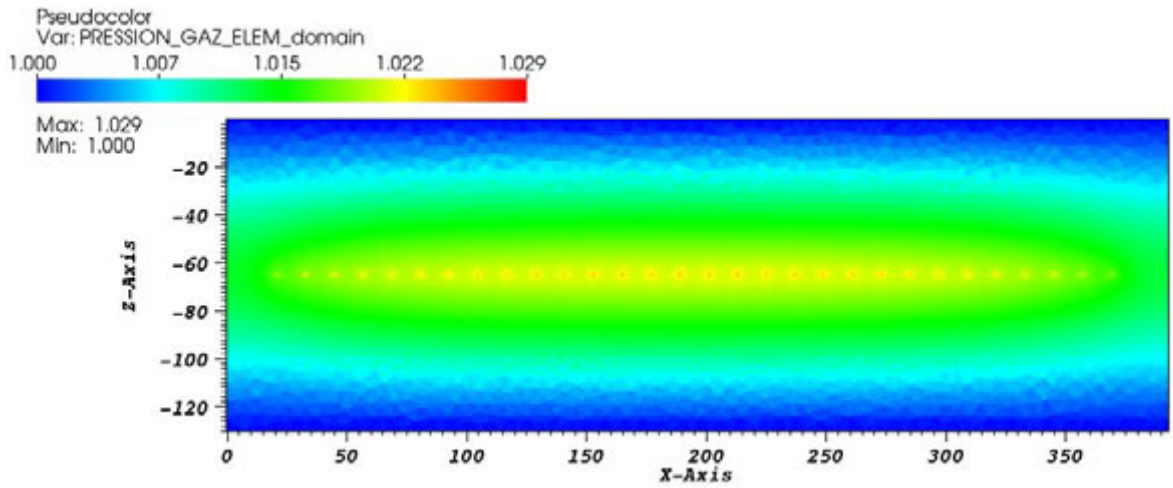

Figure 38: Gas pressure vertical cross-section (y=73 m) at t=300 years.

3.4.4 Discussion and Conclusions

The performed computations are strongly impacted by the residual gas saturation imposed in the argillites which is a deviation from the specified benchmark. The gas phase, in our case, can migrate inside the argillites leading to a very small overpressure computation in the repository cell in comparison to the results obtained by the other teams. Nevertheless, the computed time needed to fully saturate the system seems to be of the same order of magnitude than the one computed by the other teams pointing out that the residual gas saturation hypothesis only affects the gas pressure calculation.

3.4.5 Issues for further consideration

The numerical problems encountered during the numerical computation of the specified benchmark stem from two different points.

The first point, linked to the inability to take into account the interfaces without oscillations computation, stems from the cell centered scheme used to compute the convective part of the system equations. In order to tackle this problem, an upwind scheme must be used to compute the convection.

The second point, linked to the necessity to use residual gas saturation for all the considered materials, stems from the set of variables used (liquid saturation and gas pressure). A new set of variables (like the one prosed in **[4]**) must be used to solve this problem.

3.4.6 References

[1] TrioU: http://www-trio-u.cea.fr.

[2] Caro, F. and Laucoin, E. : Description du module de MPCube permettant la simulation numérique des écoulements diphasiques multicomposants en milieu poreux. Rapport CEA DEN/DANS/DM2S/STMF/LMEC/RT/09–006/B (2009).

[3] PETSC: http://www.ms.anl.gov/pets/pets-as/.

[4] Bourgeat, A., Jurak, M. and Smaï, F.: Two partially miscible flow and transport modeling in porous media; application to gas migration in a nuclear waste repository, *Computational Geosciences* 13(1), 29-42 (2009).

3.5 CNRS contribution

3.5.1 Introduction

Numerical simulation of the module scale benchmark presents a challenge by its size and heterogeneities. In order to reduce the size of the numerical model we use mathematical upscaling technique which replaces a heterogeneous material with an equivalent homogeneous material. In that way the size of the numerical model is reduced since one does not need to grid the heterogeneities that are removed from the model by upscaling. By replacing a heterogeneous material by an homogeneous one, we lose the small scale variations of the solution. The mathematical upscaling technique guaranties that during this process the large scale characteristics of the solution will be preserved. Thus, the homogeneous material that replaces the heterogeneous one is called equivalent, since it will reproduce the same macroscopic behavior.

It is possible to perform different levels of upscaling for the module scale benchmark. By the level of upscaling we mean a quantity of heterogeneities that were replaced by an equivalent homogeneous material. Each upscaling produces one numerical model and more upscaled models (models with less heterogeneities) can be solved on smaller grid, therefore offering more efficient solution process, at the price the loss of small scale variations of the solution.

We have constructed three levels of upscaling. The first one only eliminates the Interfaces from the model by upscaling it with other materials (the EDZ and the Backfill). The numerical model thus constructed is called U1. In the second level of upscaling we eliminate the EDZ from the model. In that model the Access drift becomes an homogeneous material and the Canisters and closing Plugs are replaced by an equivalent homogeneous material. The corresponding numerical model is called U2. This process then forces us to redistribute the gas source (the Canister surface is not represented in the model any more) and to upscale the initial conditions (initial pressure discontinuity cannot be represented). Finally, in the last level of upscaling we replace all 50 canisters on each side of the Access drift by homogeneous blocks. This model is called U3. In this most upscaled model we do not need to grid individual canisters. However, we us grid fine enough to be able to calculate the fluxes which are requested in the benchmark.

In this report, numerical simulations are presented only for the U2 and U3 models. We will present immiscible and miscible simulations. In the miscible simulation full physical model with gas dissolution and water evaporation is implemented. In the immiscible simulation there is no mass exchange between gaseous and liquid phases, meaning that the gas is composed only of the hydrogen and the liquid only of the water. The immiscible simulation is presented since it is faster and allow us to make grid sensitivity analysis, and also for validation/measurements of the effects of the gas dissolution. We plan to present simulations for U1 models in our future work and to compare then in order to verify the effects of the upscaling. The goal is to verify if the U2 and U3 models are sufficient for a reliable simulation of the whole repository.

The rest of this contribution is organized as follows.

Firstly, we describe the implementation of the model used in our simulations. We use **DuMu**^{x} [2,3] a free and open-source simulator and some small differences with the proposed mathematical model are considered. Then, we describe the technique of mathematical upscaling. By applying this technique to the module scale benchmark, we define U1, U2 and U3 models mentioned aboves. Finally we present the numerical results of immiscible simulation for the U3 model and miscible simulations for both U2 and U3 models. For the U3 immiscible simulation we present a grid sensitivity and we give a small comparison between miscible and immiscible simulations. Then we present results for the U2 miscible simulation and compare both U2 and U3 simulations. We finish with conclusions and the bibliography.

3.5.2 Model Implementation

3.5.2.1 Code and Formulation

We describe here the differences between the proposed mathematical model for the second benchmark and the one used in our simulations which are performed with **DuMu**^{x}.
DuMu^x : DUNE for Multi-{Phase, Component, Scale, Physics, ...} flow and transport in porous media [2,3] is a free and open-source simulator for flow and transport processes in porous media, based on the Distributed and Unified Numerics Environment **DUNE**. **DuMu**^{x} is developed at the University of Stuttgart and is accessible at http://www.dumux.org, while **DUNE** environment can be found at http://www.dune-project.org/. **DuMu**^{x} is also a part of the OPM (Open Porous Media) initiative.

DuMu^x has several mathematical flow models implemented in different modules. Here we use **2p2c** module which implements two-phase flow with two components.

There are some small differences in implementation of the phase equilibrium in the proposed model and the one implemented in **DuMu**^{x}.
In the sequel, the index $\alpha \in \{w, g\}$ refers to the phase (w for water = liquid and g for gas = hydrogen), while the superscript $\kappa \in \{H_2O, H_2\}$ refers to the component.
Let us denote the fugacity of the component κ in the phase α by f_α^κ, and the molar fraction of the component in the phase α by x_α^κ.

The phase equilibrium in **DuMu**^{x} is implemented as equality of component fugacities in both phases:

$$f_w^{H_2O} = f_g^{H_2O},\ f_w^{H_2} = f_g^{H_2}. \tag{1}$$

The fugacities in the gas phase are just the component partial pressures:

$$f_g^{H_2O} = x_g^{H_2O} P_g,\ f_g^{H_2} = x_g^{H_2} P_g,$$

and the fugacities in the water (liquid) phase are given in **DuMu**^{x} as

$$f_w^{H_2O} = P_{sat}(T) x_w^{H_2O},\ f_w^{H_2} = K(T) x_w^{H_2},$$

where $P_{sat}(T)$ is the saturation pressure of water vapor [Pa], and K(T) is the Henry constant [Pa]. From (1), we get the following system of equations that **DuMu**^{x} solves in order to get component distribution over the phases:

$$P_{sat}(T) x_w^{H_2O} = x_g^{H_2O} P_g = P_g^{H_2O}, \quad K(T) x_w^{H_2} = x_g^{H_2} P_g = P_g^{H_2}. \tag{2}$$

The connection between mass fractions X_α^κ and the molar fractions x_α^κ is given by

$$X_\alpha^\kappa = \frac{M_\kappa}{\overline{M_\alpha}}, \quad \overline{M_\alpha} = M_{H_2O} x_\alpha^{H_20} + M_{H_2} x_\alpha^{H_2},$$

($\overline{M_\alpha}$ is the average molar mass of the phase). By comparing (2) with the form of the Henry law defined in the benchmark, we get

$$K(T) = \frac{\rho_w}{H_{H_2}(T)\overline{M_w}}.$$

Approximatively we have

$$K(T) = \frac{\rho_w}{H_{H_2}(T)\overline{M_w}} \approx \frac{\rho_{atm}}{H_{H_2}(T) M_{H_20}} = \frac{10^3}{7.6 \cdot 10^{-6} \cdot 18.0153 \cdot 10^{-3}} = 7.3037 \cdot 10^9\, Pa.$$

- Given value of $H_{H_2}(T)$ is not used in the simulations. Instead we used **DuMu**^{x} default, which is to calculate K(T) by an IAPWS formula [5] that gives $K(293) = 6.94053 \cdot 10^9\, Pa$;

- Similarly, we did not use the proposed formula for the saturation pressure, but the one built into **DuMu**^{x} giving the water vapor pressure of 2317.57 Pa. Kelvin's correction is not taken into account (maximum of the correction factor is only 1.08).

The pseudo pressure of the dissolved hydrogen, $\tilde{P}_g^{H_2}$ is transformed by using the following identity

$$K(T) = \frac{\rho_w}{H_{H_2}(T)\overline{M}_w}. \tag{3}$$

which gives, by inversion of Henry's law:

$$\tilde{P}_g^{H_2} = \frac{\rho_w}{M_{H_2} H_{H_2}(T)} X_w^{H_2} = \frac{\overline{M}_w}{M_{H_2}} K(T) X_w^{H_2} \approx \frac{M_{H_2O}}{M_{H_2}} K(T) X_w^{H_2}, \tag{4}$$

where $\frac{M_{H_2O}}{M_{H_2}} K(T) = 6.2029 \cdot 10^{10}$.

- Approximation (4) is used in the output as the value of the pseudo pressure.

Diffusion coefficients are taken into account as given.

- For the water density and the gas viscosity we have used formulas built in **DuMu**^{x} which depends on the pressure and the temperature. This means that the gas viscosity is independent of its composition. All water properties in **DuMu**^{x} are based on IAPWS standards. Gas viscosity is taken equal to the hydrogen viscosity which is implemented from [7].
- The tortuosity in **DuMu**^{x} is calculated by an upscaling strategy.
- Finally, let us mention that the Van Genuchten functions were regularized near 1 and 0 in order to avoid the singularities in the derivatives.

3.5.2.2 Mathematical upscaling

Using different mathematical techniques, such as formal asymptotic expansions or the two-scale convergence, it is possible to develop mathematical upscaling procedures applicable to the two-phase flow in heterogeneous porous media, such as water-gas flow in an underground repository. These methods can be applied to the case of a single rock-type media, i.e. where one scales up the porosity, absolute permeability and tortuosity while assuming the capillary pressure and relative permeability curves independent of the space position. One can then rigorously justify these mathematical upscaling processes by using the two-scale convergence.

The same techniques can be extended to a more general model where capillary pressure and relative permeability curves are different in different regions of the porous media (different rock types). This model contains nonlinear transmission conditions representing the continuity of phase pressures and fluxes, at the interfaces that separate different media, while the saturation and some other flow characteristics are then getting discontinuous at the interfaces.

Applying the mathematical upscaling technique to a heterogeneous flow problem, one obtains a global or effective model of an *equivalent* homogeneous porous domain. It is then shown, that the mathematically upscaled model has almost the same form as the initial model but with spatially heterogeneous parameters replaced by homogeneous, *effective values*. Definitions of the effective values in the upscaled model are based on computing the solution of some partial differential equations in a *Representative Elementary Volume* (REV) with imposed appropriate boundary conditions; for instance periodic, Dirichlet, or Neumann boundary conditions. For more details see report [1] and references therein.

In the following sections we described the procedure of upscaling of different characteristics of the two-phase flow model.

3.5.2.2.1 Upscaling absolute permeability and porosity

Let us denote the upscaling REV by $V=(0,L_1)\times(0,L_2)\times(0,L_3)$. The sides of this volume will be denoted $S_i^{\min}=\{x_i=0\}$, $S_i^{\max}=\{x_i=L_i\}$ for i=1,2,3. We assume that the volume is composed of N different materials $V_1,\ldots,V_N$, and we denote by χ_{V_i} the characteristic indicator function of i-th material ($\chi_{V_i}(\mathbf{x})=1$ for $x\in V_i$ and 0 otherwise).

All material properties, such as the absolute permeability $k(\mathbf{x})$, porosity $\Phi(\mathbf{x})$ and tortuosity $\tau(\mathbf{x})$, are piecewise constant in the volume, that is, of the form

$$k(\mathbf{x})=\sum_{j=1}^{N}k^j\chi_{V_j}(\mathbf{x}),\quad \Phi(\mathbf{x})=\sum_{j=1}^{N}\Phi^j\chi_{V_j}(\mathbf{x}),\quad \tau(\mathbf{x})=\sum_{j=1}^{N}\tau^j\chi_{V_j}(\mathbf{x}), \tag{5}$$

where k^j is the absolute permeability in the material V_j etc.

The effective porosity, Φ^h, is just the arithmetic mean value of the porosity $\Phi(\mathbf{x})$:

$$\Phi^h=\frac{1}{\mathrm{vol(V)}}\int_V\Phi(\mathbf{x})d\mathbf{x}=\sum_{j=1}^{N}\Phi^j\frac{\mathrm{vol(V_j)}}{\mathrm{vol(V)}}. \tag{6}$$

For the upscaling of the absolute permeability $k(\mathbf{x})$, we have to solve three elliptic problems

$$\begin{cases}-\mathrm{div}(k(\mathbf{x})\nabla P_i)=0 \text{ in V},\\ \qquad P_i=x_i \text{ on } \mathrm{S_i^{min}},\mathrm{S_i^{max}},\\ k(\mathbf{x})\nabla P_i\cdot\mathbf{n}=0 \text{ on } \mathrm{S_j^{min}},\mathrm{S_j^{max}} \text{ for } \mathrm{j}\neq\mathrm{i},\end{cases} \tag{7}$$

for all space directions i=1,2,3 and calculate the effective absolute permeability matrix K^h given by

$$K^h\mathbf{e}_i=\frac{1}{\mathrm{vol(V)}}\int_V k(\mathbf{x})\nabla P_i d\mathbf{x}. \tag{8}$$

Here the i-th row of the matrix is calculated using i-th solution to the problem (7).
The boundary conditions in problem (7) chosen for upscaling, so called *confined boundary conditions,* produce very small extra-diagonal terms that we will neglect in simulations. The diagonal terms of the effective permeability are then given by formula:

$$K_{i,i}^h=\frac{1}{\mathrm{vol(V)}}\int_V k(\mathbf{x})\frac{\partial P_i}{\partial x_i}d\mathbf{x}, \tag{9}$$

for i=1,2,3.

The procedure described here is developed in [1] and in references therein, and it has a simple physical interpretation. The problem (7) is a stationary flow through upscaling REV, with pressure drop $-L_i$ in the direction i. Formula (8) gives a constant permeability (equivalent homogeneous medium) that will produce the same mean flow (in the direction i) for given uniform pressure drop as the original, heterogeneous medium. The whole effective permeability tensor is constructed considering all three space directions.

Remark: *Instead of using confined boundary conditions in problem (7) one can use linear boundary conditions, leading to the following problem*

$$\begin{cases} -\mathrm{div}(k(\mathbf{x})\nabla P_i) = 0 \text{ in V}, \\ P_i = x_i \text{ on } \partial \mathrm{V}, \end{cases} \tag{10}$$

where the condition $P_i = x_i$ *is applied to the whole boundary. The advantage of the linear boundary condition compared to the confined boundary conditions is that it can be applied to geometrical shapes other than rectangular. We will apply it the domain composed of the Canister, Interface and the EDZ around it.*

When the heterogeneous medium is l*ayered* then it is easy to see that the solutions of problem (7) simplify and the formula (8) gives arithmetic or harmonic mean; arithmetic in the directions parallel to the layers and harmonic in the direction perpendicular to the layers.

Let us take that the materials is layered in i-th direction. This means that $k = k(x_i)$ and it does not depend on other space variables. Then, the solution P_i of (7) depends only on the variable x_i, and satisfies the equation

$$\begin{cases} \frac{d}{dx_i}(k(x_i)\frac{dP_i}{dx_i}) = 0, \\ P_i = 0 \text{ for } x_i = 0, P_i = L_i \text{ for } x_i = L_i. \end{cases} \tag{11}$$

Now, from (11) it follows

$$k(x_i)\frac{dP_i}{dx_i} = k^H, \tag{12}$$

for some constant k^H, and by using the boundary conditions in (12) we have

$$L_i = \int_0^{L_i} \frac{k^H}{k(x_i)} dx_i = k^H \Rightarrow k^H = L_i / \int_0^{L_i} \frac{dx_i}{k(x_i)}. \tag{13}$$

This gives $K^h \mathbf{e}_i = k^H \mathbf{e}_i$, where the value k^H, given by (13), is the harmonic mean of the permeability k. If we look the solution P_j of (7) for $j \neq i$, we see that $P_j = x_j$ and $K^h \mathbf{e}_i = k^A \mathbf{e}_i$ where

$$k^A = \frac{1}{L_i} \int_0^{L_i} k(x_i) dx_i$$

is the arithmetic mean of the permeability k .

From these calculations we see that the upscaled absolute permeability tensor is diagonal with the arithmetic mean on the diagonal at places corresponding to space directions parallel to the material layers and the harmonic mean in the direction perpendicular to the material layers.

3.5.2.2.2 Upscaling relative permeabilities and capillary pressure

As before, the upscaling REV, V is composed of N different materials $V_1, \ldots, V_N$, and to the i -th material we associate the capillary pressure function $p_c^i(S)$ and the relative permeability functions $kr_w^i(S)$ and $kr_g^i(S)$.

We can then introduce the following functions,

$$p_c(\mathbf{x},S)=\sum_{j=1}^{N} p_c^j(S)\chi_{V_j}(\mathbf{x}), \quad kr_\alpha(\mathbf{x},S)=\sum_{j=1}^{N} kr_\alpha^j(S)\chi_{V_j}(\mathbf{x}), \quad \alpha\in\{w,g\}. \tag{14}$$

The procedure of scaling up of the relative permeability functions and the capillary pressures is based on the local capillary equilibrium hypothesis. By this hypothesis one distributes the saturation in upscaling REV in such way that the capillary pressure in the REV is constant. The assumption is realistic if the capillary forces are dominant, which is the case in largest part of the repository.

The first step in the upscaling is to calculate for given capillary pressure value u a distribution of the saturation $S(\mathbf{x})$corresponding to u. This saturation is given by

$$S(\mathbf{x})=\sum_{j=1}^{N} S^j\chi_{V_j}(\mathbf{x}), \tag{15}$$

where S^j are given by the capillary pressure equilibrium hypothesis:

$$u=p_c^j(S^j), \mathrm{j}=1,\ldots,N \tag{16}$$

For this distribution of the saturation we calculate the effective saturation

$$S^h=\int_V \Phi(\mathbf{x})S(\mathbf{x})d\mathbf{x} \Big/ \int_V \Phi(\mathbf{x})d\mathbf{x}. \tag{17}$$

Note that the effective saturation is calculated such that one preserves volume of the phase present in the porous media, namely

$$\mathrm{vol}(V)\Phi^h S^h=\int_V \Phi(\mathbf{x})S(\mathbf{x})d\mathbf{x}.$$

The point (S^h,u) represents one point on the *effective capillary pressure curve* $S^h\to p_c^h(S^h)$ which is defined by $p_c^h(S^h)=u$. To calculate this curve in form of a table we simply choose a number of capillary pressure values u and for each value we calculate corresponding effective saturation S^h, building in that way the effective capillary pressure curve. An example of such calculation for two materials is given in Figure 39.

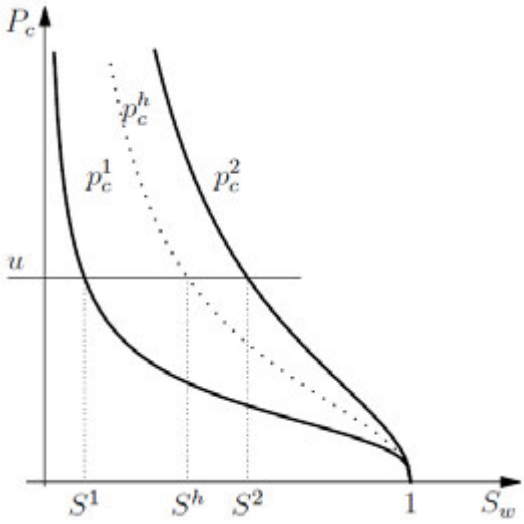

Figure 39 Computation of effective capillary pressure law.

For upscaling of relative permeability $kr_\alpha(S), \alpha \in \{w, g\}$, we apply the procedure developed for upscaling the absolute permeability to the total permeability $k(\mathbf{x})kr_\alpha(\mathbf{x}, S(\mathbf{x}))$. In the calculation of total permeability we use a distribution of the saturation S(**x**) which corresponds to given capillary pressure u. This procedure is then repeated for chosen number of the capillary pressure values, building in that way effective relative permeability curves point by point.

Therefore, we need to solve the problems:

$$\begin{cases} -\mathrm{div}(k(\mathbf{x})kr_\alpha(\mathbf{x}, S(\mathbf{x}))\nabla P_i) = 0 \text{ in V}, \\ \qquad P_i = x_i \text{ on } \mathrm{S}_\mathrm{i}^{\min}, \mathrm{S}_\mathrm{i}^{\max}, \\ k(\mathbf{x})kr_\alpha(\mathbf{x}, S(\mathbf{x}))\nabla P_i \cdot \mathbf{n} = 0 \text{ on } \mathrm{S}_j^{\min}, \mathrm{S}_\mathrm{j}^{\max} \text{ for j}\neq\text{i}, \end{cases} \tag{18}$$

where S(**x**) is the saturation distribution corresponding to the capillary pressure value u, given by (15) and (16). The *effective relative permeability* function $kr_\alpha^h(S^h)_i$, in the space direction i, is defined in the effective saturation S^h (given by (17)) by the formula:

$$kr_\alpha^h(S^h)_i = \frac{1}{\mathrm{vol(V)}} \int_V k(\mathbf{x})kr_\alpha(\mathbf{x}, S(\mathbf{x}))\nabla P_i \cdot \mathbf{e}_i \, d\mathbf{x} / K_{i,i}^h. \tag{19}$$

The mathematical upscaling procedure produces, in general, a full tensor of relative permeability functions. As already mentioned, the extra-diagonal terms in that matrix are small and they can be safely neglected, as we did, keeping only the diagonal terms.

Remark: *By neglecting extra-diagonal terms in the matrix of relative permeability functions we obtain directional effective relative permeabilities. Generally, in each space direction we have different effective relative permeability curves. Since the simulation software we use is not capable of taking into account directional relative permeability curves we have to make a choice between the curves calculated in different directions. We always chose the curve in dominant flow direction and apply chosen curve to all directions. Note, however, that we do not do the same approximation with the absolute permeability: we keep different effective absolute permeabilities in different space directions.*

In the case of layered materials, the results for absolute permeability can be easily applied. We obtain the effective relative permeability curves calculated as the arithmetic mean ($kr_\alpha^A(S^h)$) in the direction of layers, and calculated as the harmonic mean ($kr_\alpha^H(S^h)$) in the direction perpendicular to the layers:

$$K_{i,i}^h kr_\alpha^H(S^h)_i = L_i \Big/ \int_0^{L_i} \frac{dx_i}{k(x_i) kr_\alpha(x_i, S(x_i))},$$
$$K_{i,i}^h kr_\alpha^A(S^h)_i = \frac{1}{L_i} \int_0^{L_i} k(x_i) kr_\alpha(x_i, S(x_i)) dx_i, \tag{20}$$

where L_i is the length of the upscaling REV in chosen direction; $K_{i,i}^h$ is the effective absolute permeability in i -th direction.

3.5.2.2.3 Upscaling tortuosity

Although the tortuosity τ in the benchmark does not depend on the saturation, the upscaled tortuosity will depend on the effective saturation. This is a consequence of the fact that the tortuosity must be upscaled together with the saturation and the porosity. For the same reason, effective tortuosity depends on the phase in which it is considered, so that we will obtain two effective tortuosities, τ_w^h and τ_g^h.

The procedure for scaling up the tortuosity is similar (see [8]) to upscaling the relative permeability functions and is based on the local capillary equilibrium hypothesis. The only difference is in the function that is upscaled: instead of total permeability we upscale here the product of porosity, saturation and tortuosity.

Therefore, we need to solve the problems :

$$\begin{cases} -\mathrm{div}(\Phi(\mathbf{x}) \dfrac{S_\alpha(\mathbf{x})}{\tau^2(\mathbf{x})} \nabla \xi_i^\alpha) = 0 \text{ in V}, \\ \xi_i^\alpha = x_i \text{ on } \mathrm{S_i^{min}}, \mathrm{S_i^{max}}, \\ \Phi(\mathbf{x}) \dfrac{S_\alpha(\mathbf{x})}{\tau^2(\mathbf{x})} \nabla \xi_i^\alpha \cdot \mathbf{n} = 0 \text{ on } \mathrm{S_j^{min}}, \mathrm{S_j^{max}} \text{ for j}\neq\text{i}, \end{cases} \tag{21}$$

where $S_\alpha(\mathbf{x})$ is α-phase distribution corresponding to the capillary pressure value u, given by (15) and (16). The *effective tortuosity* function $\tau_\alpha^h(S^h)_i$, in the space direction i, is defined for the effective saturation S^h (given by (17)) by the formula:

$$\frac{\Phi^h S_\alpha^h}{(\tau_\alpha^h(S^h)_i)^2} = \frac{1}{\mathrm{vol}(V)} \int_V \Phi(\mathbf{x}) \frac{S_\alpha(\mathbf{x})}{\tau^2(\mathbf{x})} \nabla \xi_i^\alpha \cdot \mathbf{e}_i \, d\mathbf{x}. \tag{22}$$

As for the effective relative permeabilities we have neglected any possible extra-diagonal terms in the effective tortuosity matrix, keeping only diagonal terms.

In the case of layered materials, the results for absolute and relative permeability can be easily applied here. We obtain the effective tortuosity calculated as the arithmetic mean ($\tau_\alpha^A(S^h)$) in the direction of layers, and calculated as the harmonic mean ($\tau_\alpha^H(S^h)$) in the direction perpendicular to the layers:

$$\frac{\Phi^h S_\alpha^h}{(\tau_\alpha^H (S^h)_i)^2} = L_i \Big/ \int_0^{L_i} \frac{\tau(x_i)^2 dx_i}{\Phi(x_i) S_\alpha(x_i)},$$
$$\frac{\Phi^h S_\alpha^h}{(\tau_\alpha^A (S^h)_i)^2} = \frac{1}{L_i} \int_0^{L_i} \frac{\Phi(x_i) S_\alpha(x_i)}{\tau(x_i)^2} dx. \tag{23}$$

where L_i is the length of the upscaling REV in chosen direction; Φ^h and S_α are the effective porosity and the α-phase saturation.

3.5.2.3 Upscaling results for module scale benchmark

Heterogeneitis of the module scale benchmark lead to a very large numerical model that makes simulation of the whole repository very difficult, if not impossible. It is therefore of interest to reduce the size of the module scale numerical model by use of an appropriate upscaling technique which will reduce the heterogeneity of the repository and allow numerical representation of the module by a coarser grid.

By upscaling we replace several different materials present in the REV by one equivalent homogeneous material that we call the effective material. We calculate for each REV effective permeability, porosity, relative permeability curves, effective capillary pressure curve and effective tortuosity. After replacing several different materials with an effective one we need to upscale also the initial conditions in order to keep given initial quantity of water, gas and dissolved hydrogen. When the upscaling changes the geometry of the model in such a way that the upscaled model does not represent the Canister surface (hydrogen source), we need to do a repartition of the hydrogen source in a suitable way.

Here we propose three levels of upscaling, denoted U1, U2 and U3, each producing less heterogeneous model than preceding one. Simulation software that we use, and the most of the simulation software in use presently, cannot take directional/tensorial relative permeability functions into account. This is a big obstacle for mathematical upscaling technique since it produces generally tensorial and, in practice, at least directional relative permeabilities. In this situation we have to make a choice between different curves, and we use the curves in dominant flow direction, loosing in that way a part of the information from the small scale. For a discussion on tensorial relative permeabilities and its numerical discretization we refer to [6].

3.5.2.3.1 U1. Elimination of the Interfaces

The aim of this first upscaling step is to eliminate the Interfaces from the model, keeping all other heterogeneities. This will be done in the following way:

- Near the canisters and the bentonite plugs that are close to them we upscale the Interface with the EDZ;
- In the drifts (main and access) the Interface is upscaled with the Backfill;
- The main drifts plugs are upscaled with the Interface which surrounds them.

Upscaling steps used in U1, but also in U2 and U3, are represented in Figure 40.

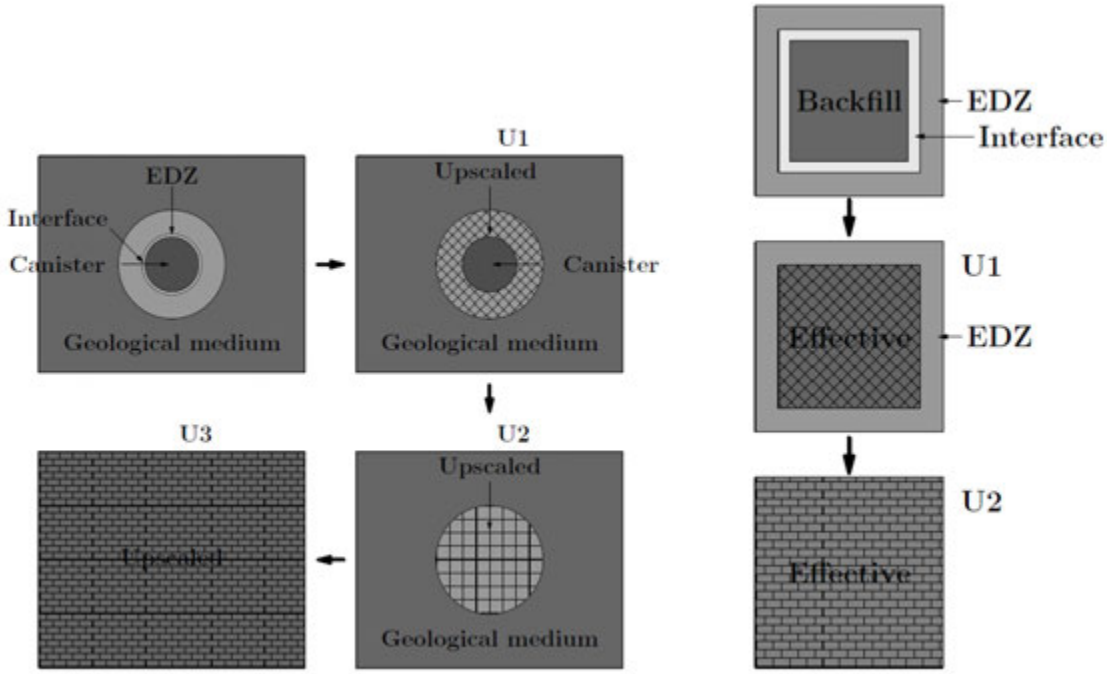

Figure 40 Different upscaling steps near canisters and in the drifts.

Upscaling of EDZ-Interface

Here we describe the upscaling of the EDZ and the Interface near the Canister and near the Plug. After the upscaling of the EDZ and the Interface near the Canister, it will form one homogeneous domain, and the EDZ and the Interface near the Plug will form an other homogeneous domain.

The upscaling of the absolute permeability in x and z directions near the Canister is done by using linear boundary conditions, that is by solving problem (11). On the Canister boundary we put no flow conditions since the Canister is not a part of computational model.

In the y direction we use the arithmetic average (layered material case). Before upscaling of the EDZ and the Interface in y direction we upscale the Interface, which is composed of the Interface near the Canister and the Interface near the Plug. The Interface near the Canister has much higher permeability (10^{-12} m^2) than the Interface near the Plug ($5 \cdot 10^{-18}$ m^2) but, since the flow in the Interface is mostly unidirectional, we judge that this large value near the Canister is not representative for the y direction flow and we do the harmonic average of the two Interface permeability values before the upscaling with the EDZ. As a consequence, after upscaling with the EDZ, we will obtain the same value of effective permeability in y direction near the Canister and near the Plug. In order to stay consistent we also upscale the porosity of the Interface (obtaining $\Phi = 0.8891$) before upscaling the relative permeability curves. As a consequence, after upscaling the Interface and the EDZ, we obtain the same effective relative permeability functions near the Canister and near the Plug in the y direction.

The effective permeability, porosity and the initial saturation values are given here. The values near the Canister are denoted by the superscript c, and the values near the Plug are denoted by the superscript p. Since the Interface is upscaled before upscaling with the EDZ, we obtain the same porosity and the initial saturation near the Canister and near the Plug.

$$K^C_{x,x} = 10.963 \cdot 10^{-18}, \quad K^C_{y,y} = 5.4342 \cdot 10^{-18}, \quad K^C_{z,z} = 10.963 \cdot 10^{-18},$$
$$K^P_{x,x} = 5.0 \cdot 10^{-18}, \quad K^P_{y,y} = 5.4342 \cdot 10^{-18}, \quad K^P_{z,z} = 5.0 \cdot 10^{-18},$$
$$\Phi = 0.159628, \quad S_{w,\,init} = 0.987624.$$

When upscaling capillary pressure and relative permeability functions, we take into account that the principal flow in the EDZ and the Interface goes in direction of y-axis, and since the simulation software cannot work with directional relative permeabilities, we use the effective curves calculated in the y direction in all space directions.

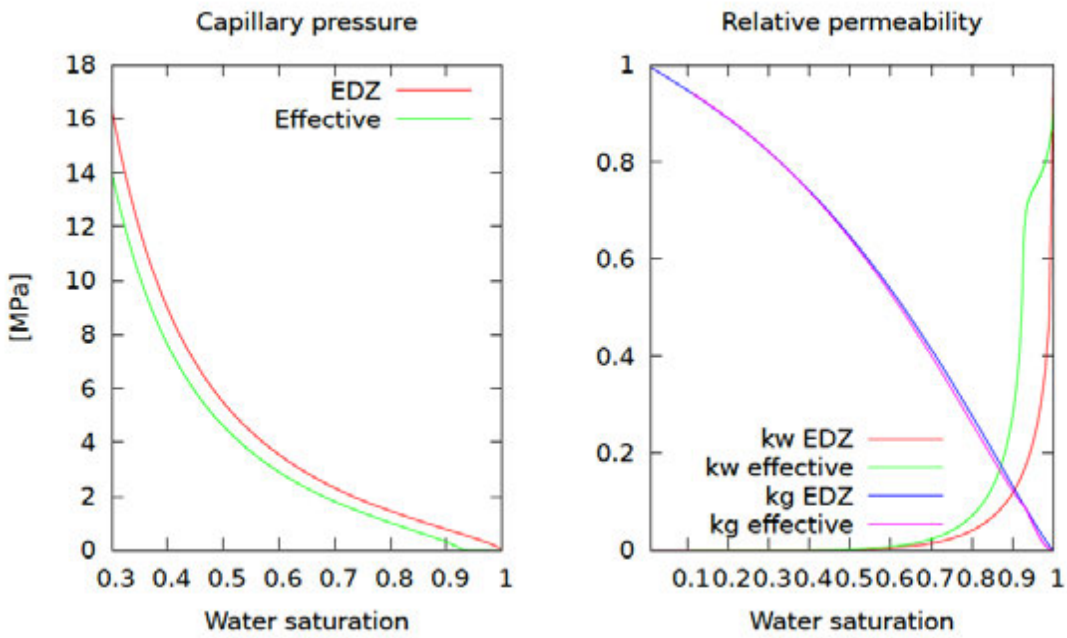

Figure 41 Effective relative permeability and the capillary pressure curves of the EDZ upscaled with the Interface.

The arithmetic average is used to upscale the relative permeabilities in the y direction, and since the Interface is upscaled before upscaling with the EDZ, we obtain the same curves near the Canister and near the Plug. The effective relative permeability curves are shown in Figure 41 compared to the EDZ curves.

Upscaling of the tortuosity proceeds in the same way as for the relative permeability. We retain only the curve in the y direction shown in Figure 42.

Upscaling of Backfill-Interface

Due to the geometry of drifts, upscaling of the Backfill with the Interface can be done completely by use of arithmetic and harmonic means.

When upscaling the absolute permeability in x, y or z directions, we first upscale the Backfill and the Interface by the harmonic mean, taking into account the Interface in front and behind of the Backfill. Then we proceed with one application of the arithmetic mean in order to take into account parts of the Interface which are below and above the Backfill (parallel to the flow direction). The values obtained in each direction are very similar, and we take one of the values as representative.

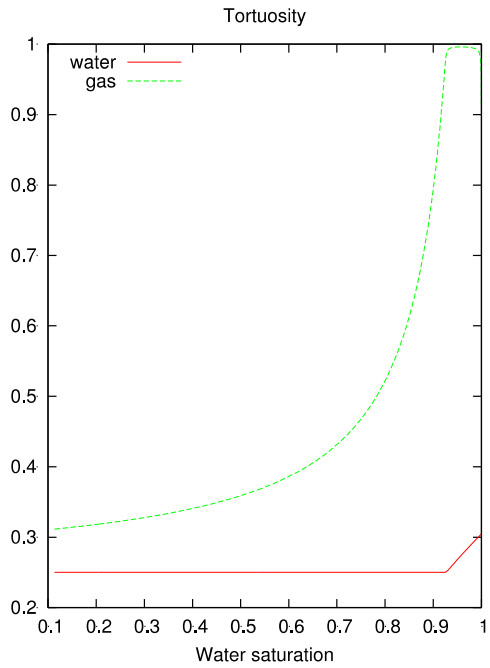

Figure 42 Effective tortuosity of the EDZ upscaled with the Interface.

This procedure, applied also to the relative permeability functions, leads to a very steep relative permeability curves because of extreme characteristics of the Interfaces. Since complete isolation of the Backfill (and the Plug) by the Interface is not realistic, we further take into account that 30 % of the Backfill area is not covered by the Interface (30 % is taken somehow arbitrary). To that aim we make one more arithmetic average between completely surrounded Backfill and a non-surrounded one in 70-30 % proportion. We obtain the following characteristic of the Backfill:

$$K = 5.22167 \cdot 10^{-17},\ \Phi = 0.4,\ S_{w,init} = 0.701.$$

The effective relative permeability curves, upscaled with this procedure, are shown in Figure 43 compared with the original Backfill curves. In this case we have taken the curves calculated in the y-direction as representative. The effective tortuosity curves are presented in Figure 44.

Upscaling of Main drift plug-Interface

Upscaling of the main drift plug with the Interface is done by the same procedure that is used for upscaling of the Backfill with the Interface. Here we have taken that the Plug is covered 50 % by the Interface. We obtain the following characteristic of the Main drift plug:

$$K = 1.87262 \cdot 10^{-20},\ \Phi = 0.349912,\ S_{w,init} = 0.7005.$$

The effective relative permeability curves are shown in Figure 45 compared with the original Bentonite curves.

Let us note that the effective relative permeability curves in neighborhood of $S_w = 1$ are very steep and that they will not be exactly represented in the simulator since some regularisation of the curves in that area is always done. The effective tortuosity curves are presented in Figure 46.

Simulation grid

In griding the module we have used a structured grid. To that aim we have transformed cylindrical canisters into rectangular shaped canister, by preserving cross-sectional area of the canister. An example of the grid used in U1 simulation is shown in Figure 47.

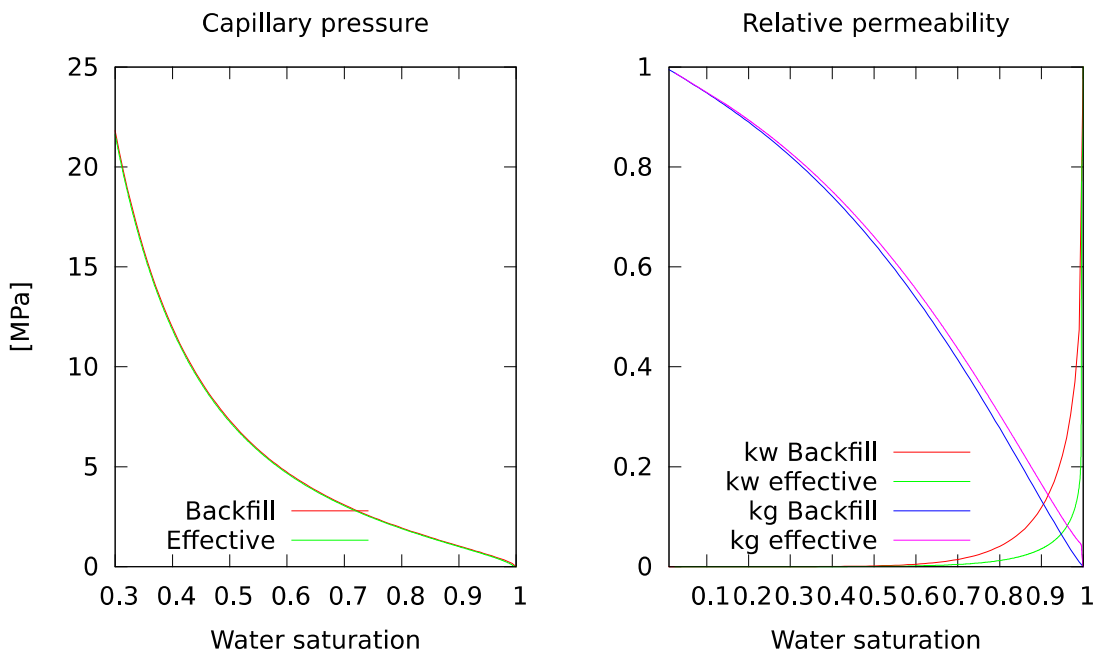

Figure 43 Effective relative permeability curves of the Backfill upscaled with the Interface.

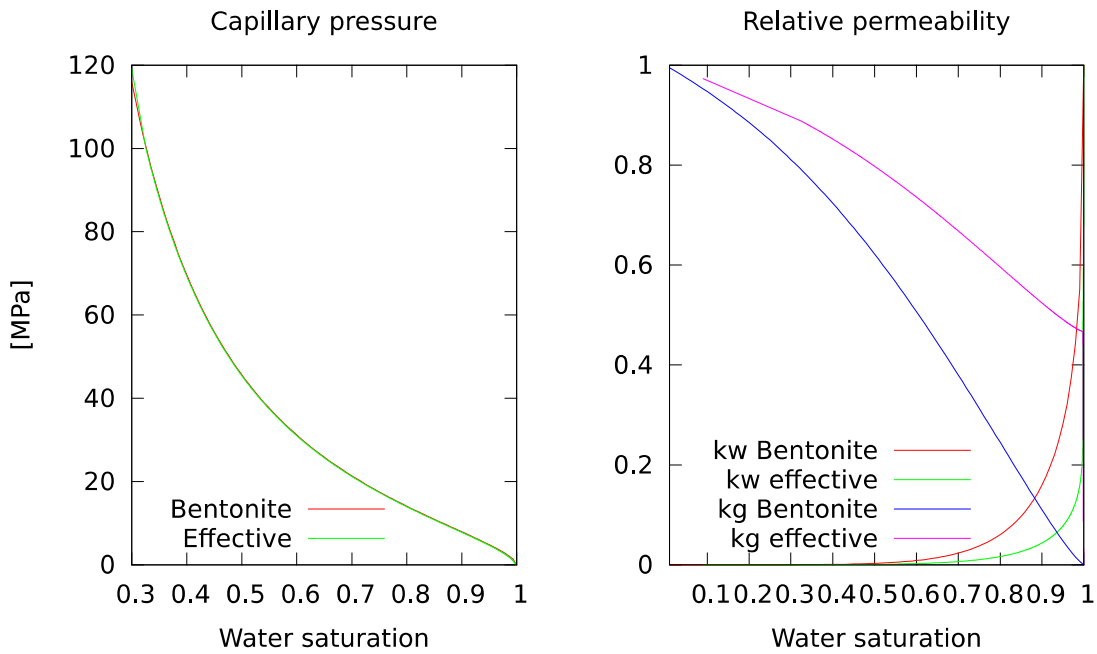

Figure 44 Effective tortuosity curves of the Backfill upscaled with the Interface.

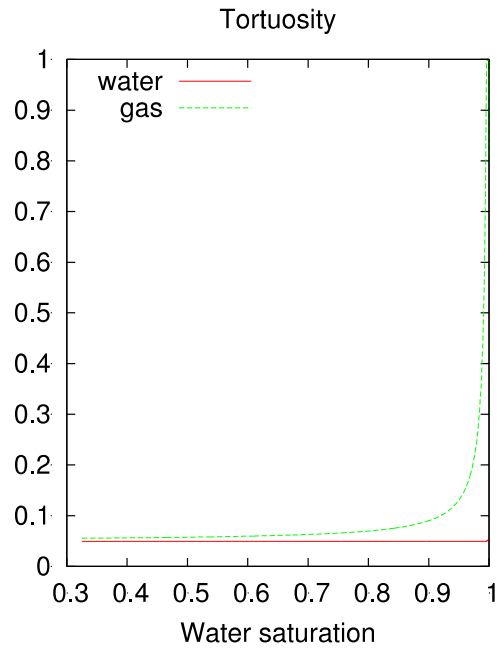

Figure 45 Effective curves of the Main drift plug upscaled with the Interface.

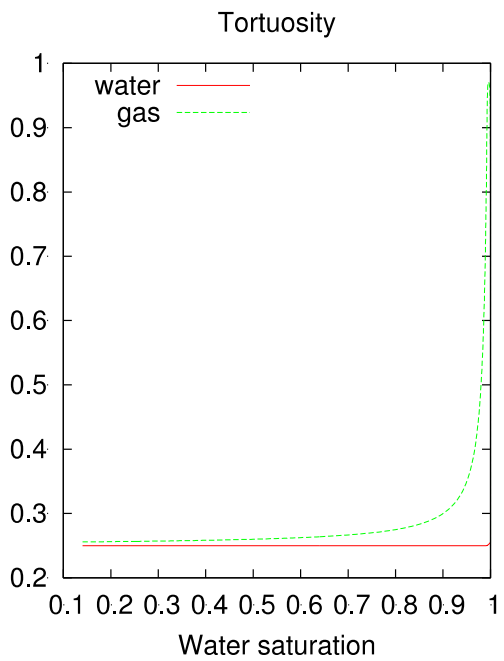

Figure 46 Effective tortuosity curves of the Main drift plug upscaled with the Interface.

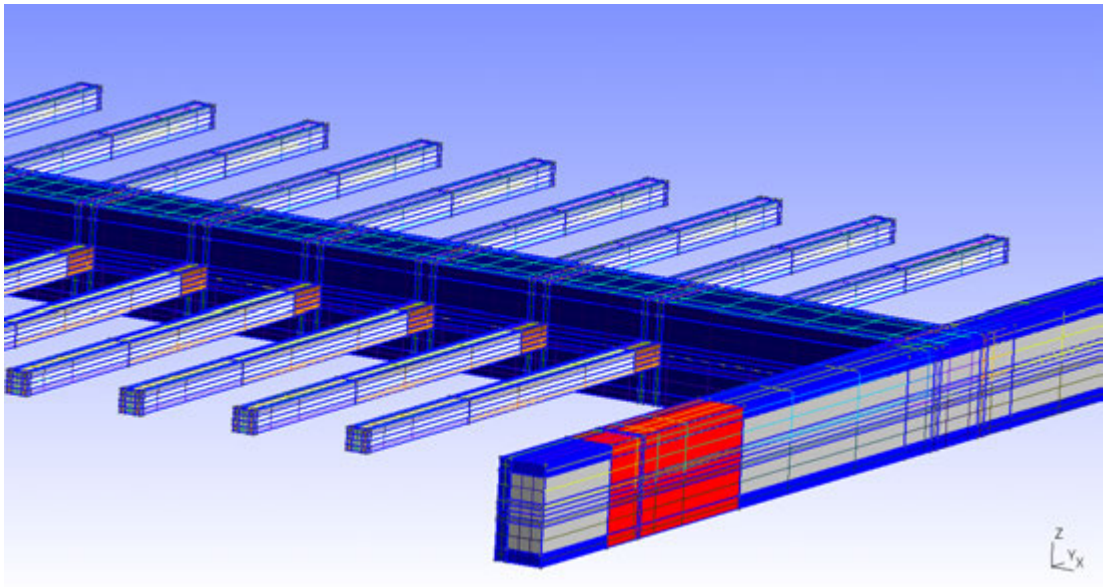

Figure 47 Grid for U1 model.

3.5.2.3.2 U2. Intermediate Upscaling

This second level of upscaling eliminates the EDZ from the model. It also eliminates the canisters (empty space) and the bentonite plugs near the canisters by forming homogeneous (upscaled) blocks out of them.

In this model

- Canister, interface and EDZ form a homogeneous block;
- Bentonite plug (near the canister), interface and EDZ form a homogeneous block;
- Access drift backfill, interface and EDZ form a homogeneous block;
- Main drift backfill, interface and EDZ form a homogeneous block;
- Main drift plugs are already upscaled with the Interface and they do not change in U2 and U3 models.

After this stage of upscaling we need to distribute the source term over larger domain since the canister boundary does not exist in this model. We choose to distribute the source term over whole Canister-interface-EDZ block.

Upscaling of Canister-Interface-EDZ

We start from the EDZ upscaled with the Interface and we take into account presence of the Canister, which is an empty space in the simulation model. Upscaling of the porosity and the absolute permeability in the y direction amounts to scaling of these values with the factor 3/4. The values of absolute permeability in x and z directions are already upscaled taking into account that the Canister is not present in computational domain (no flow boundary condition on the Canister in upscaling of the EDZ and the Interface). We only need to multiply them by 3/4 to make a volume correction. The relative permeability curves are also calculated in y the direction and applied in all directions.

Effective values are given here:

$K_{x,x}=8.2225\cdot10^{-18}$, $K_{y,y}=4.07565\cdot10^{-18}$, $K_{z,z}=8.2225\cdot10^{-18}$

$\Phi=0.119721$, $S_{w,init}=0.987624.$

The effective relative permeability curves, presented in *Figure 48* are compared to the EDZ curves.

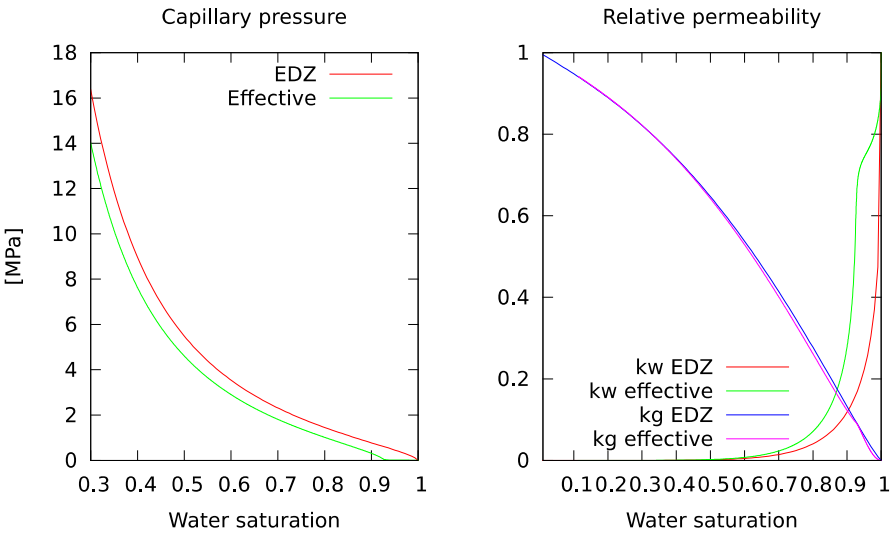

Figure 48 Effective relative permeability curves of the domain containing the Canister, Interface and EDZ.

The effective tortuosity curves are presented in Figure 49.

Upscaling of Plug-Interface-EDZ

We start from the EDZ upscaled with the Interface and we make further upscaling with the bentonite plug. The upscaling of the absolute permeability is done by solving problem (10) with linear boundary conditions. The arithmetic average is used in the y direction. The effective relative permeability curves are taken in the y direction. Note that, due to the presence of the plug, these curves are now different from corresponding curves in the Canister-interface-EDZ domain.

Effective values are given below:

$K_{x,x}=3.07\cdot10^{-18}$, $K_{y,y}=3.81\cdot10^{-18}$, $K_{z,z}=3.07\cdot10^{-18}$,

$\Phi=0.207221$, $S_{w,init}=0.915718.$

The effective curves, shown in Figure 50 are compared to the bentonite curves.

The effective tortuosity curves are presented in *Figure 51*.

Upscaling of Backfill-Interface-EDZ

We start from the Backfill upscaled with the Interface and we make further upscaling with the EDZ. This upscaling for the absolute permeability and for the relative permeabilities is done in x direction by arithmetic averaging, and in the y and the z directions by solving problem (7). The same values are used for upscaled main drift backfill, with exchanging values in the x and the y directions.

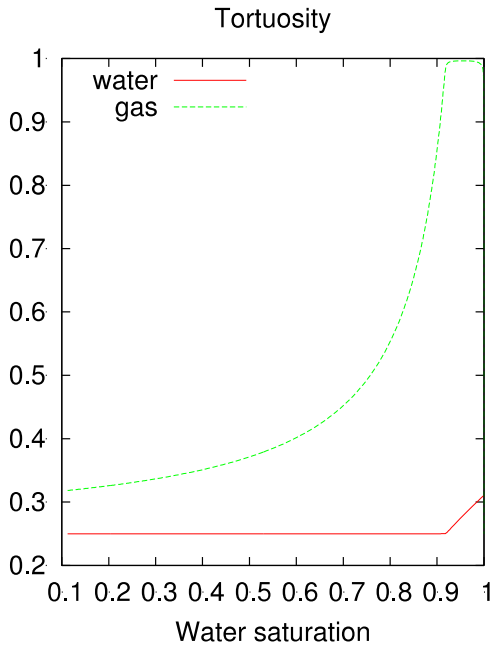

Figure 49 Effective tortuosity curves of the domain containing the Canister, Interface and EDZ.

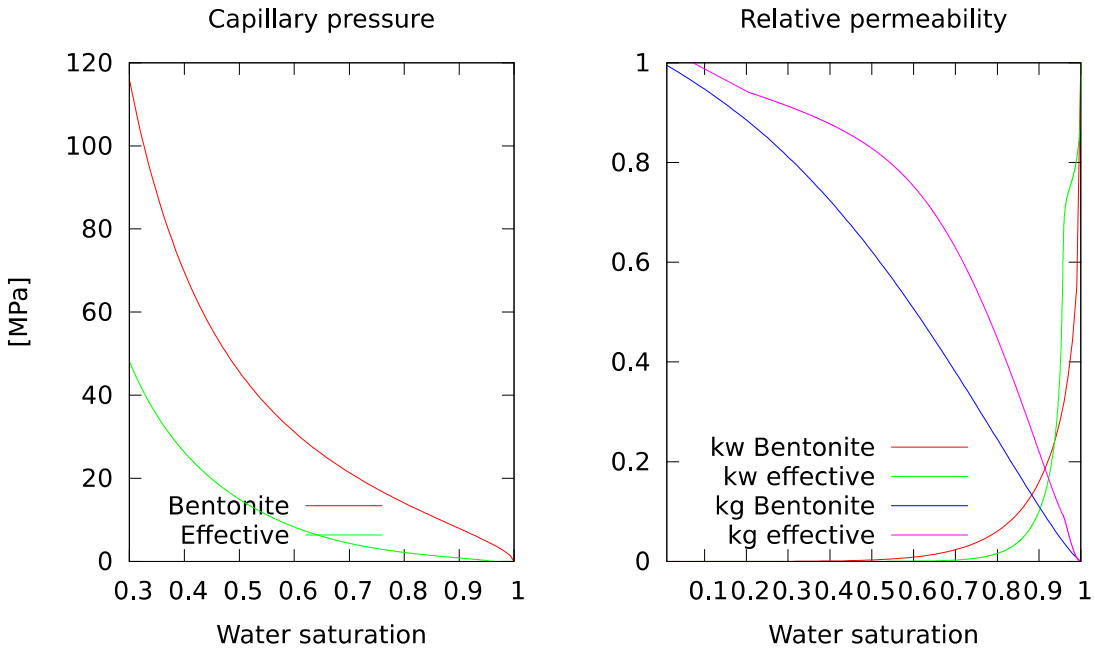

Figure 50 Effective relative permeability curves of the domain containing the Plug, Interface and EDZ.

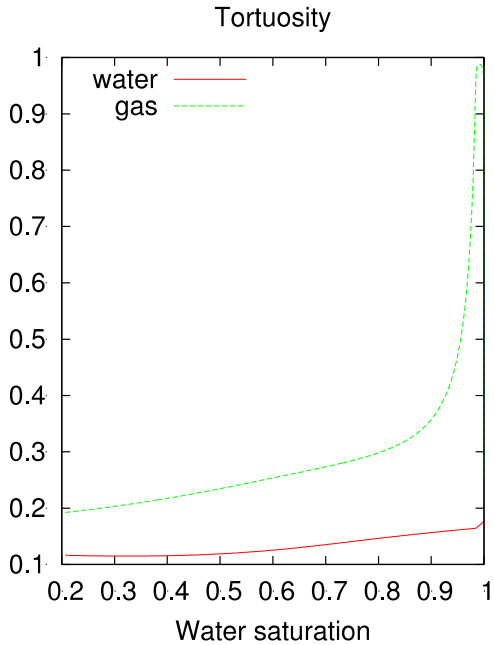

Figure 51 Effective tortuosity curves of the domain containing the Plug, Interface and EDZ.

Effective values are given below:

$$K_{x,x}=3.15594\cdot 10^{-17},\quad K_{y,y}=1.39\cdot 10^{-17},\quad K_{z,z}=1.3924\cdot 10^{-17},$$
$$\Phi=0.2906,\quad S_{w,init}=0.835187.$$

The effective curves are computed in the x (dominant) direction and are shown in *Figure 52* compared to the backfill curves.

Let us note that in this upscaling procedure we have neglected the part of the bentonite plugs that enters into the Access drift EDZ, but which cannot disturb significantly the flow in the Access drift. In that way we obtain completely homogeneous Access drift.

The effective tortuosity curves are presented in Figure 53.

Simulation grid

An example of the grid used in U2 simulation is shown in Figure 54.

3.5.2.3.3 U3. Full Upscaling

The third upscaling step eliminates all individual upscaled canisters making of all canisters with surrounding geological medium a homogeneous block (see Figure 57). This level of upscaling does not change the drifts, which stay the same as in U2 model.

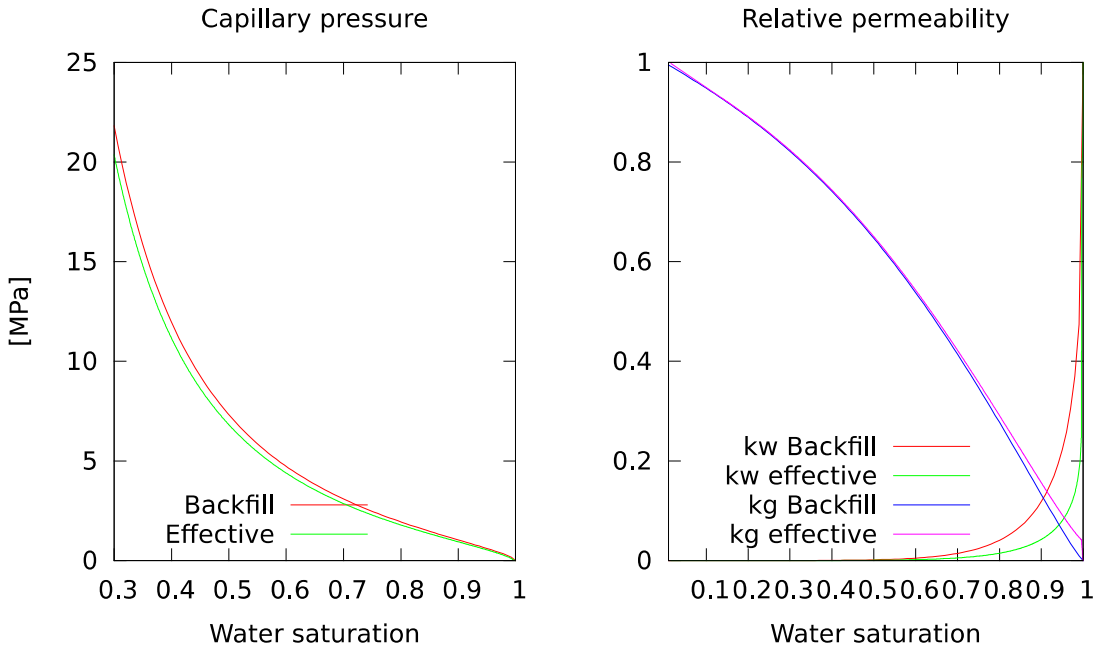

Figure 52 Effective relative permeability curves of the domain containing the Backfill, Interface and EDZ.

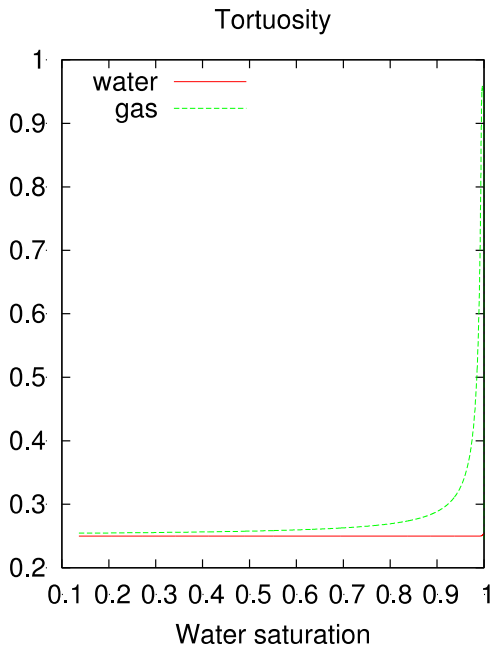

Figure 53 Effective tortuosity curves of the domain containing the Backfill, Interface and EDZ.

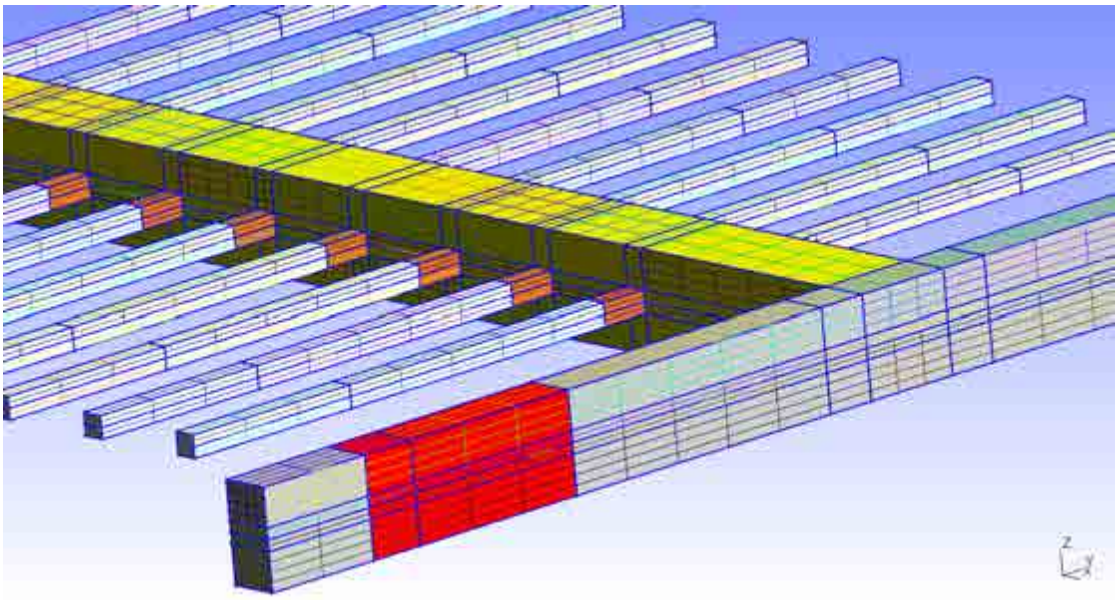

Figure 54 Grid for U2 model.

Block off canisters

Note that in U2 upscaling two domains Canister-Interface-EDZ and Plug-Interface-ED have different properties, including the functions of the saturation. Since we want to have one homogeneous block that will represent all the canisters (see Figure 40), we need to eliminate this heterogeneity before upscaling with the Geological medium that surrounds the Canisters. This upscaling is performed by the harmonic mean in the y direction and by the arithmetic mean in the x and z directions. Since the relative permeabilities are calculated in the y direction, they are upscaled by the harmonic mean.

After this intermediate upscaling we pass to the upscaling with the Geological medium, as indicated in Figure 40. The absolute permeability is upscaled as an arithmetic mean in the y direction, and by solving problem (7) in the x and z directions. The relative permeability curves are upscaled in the y direction, by using the arithmetic mean.

Effective values are given below:

$$K_{x,x}=1.08\cdot 10^{-20},\quad K_{y,y}=14.9118\cdot 10^{-20},\quad K_{z,z}=1.08\cdot 10^{-20},$$
$$\Phi=0.149118,\quad S_{w,init}=0.999262.$$

The effective relative permeability curves are shown in *Figure 55*, compared to the geological medium curves.

The effective tortuosity curves are presented in Figure 56.

Since in U3 model the individual cells (Canister and the Plug) are not presented, we distribute the hydrogen source uniformly over the whole block of upscaled cells.

Simulation grid

An example of the grid used in U3 simulation is shown in Figure 57.

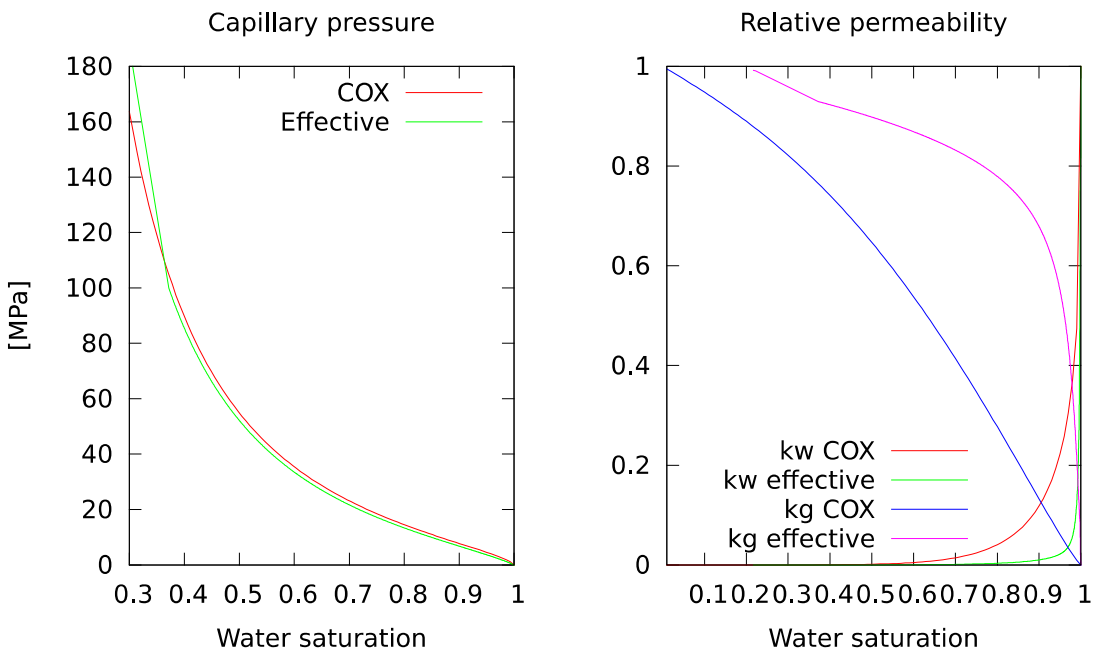

Figure 55 Effective relative permeability curves of the domain containing block of canisters.

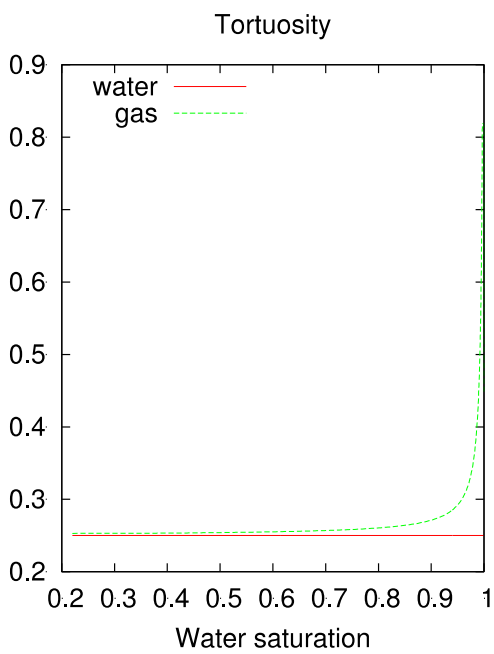

Figure 56 Effective tortuosity curves of the domain containing block of canisters.

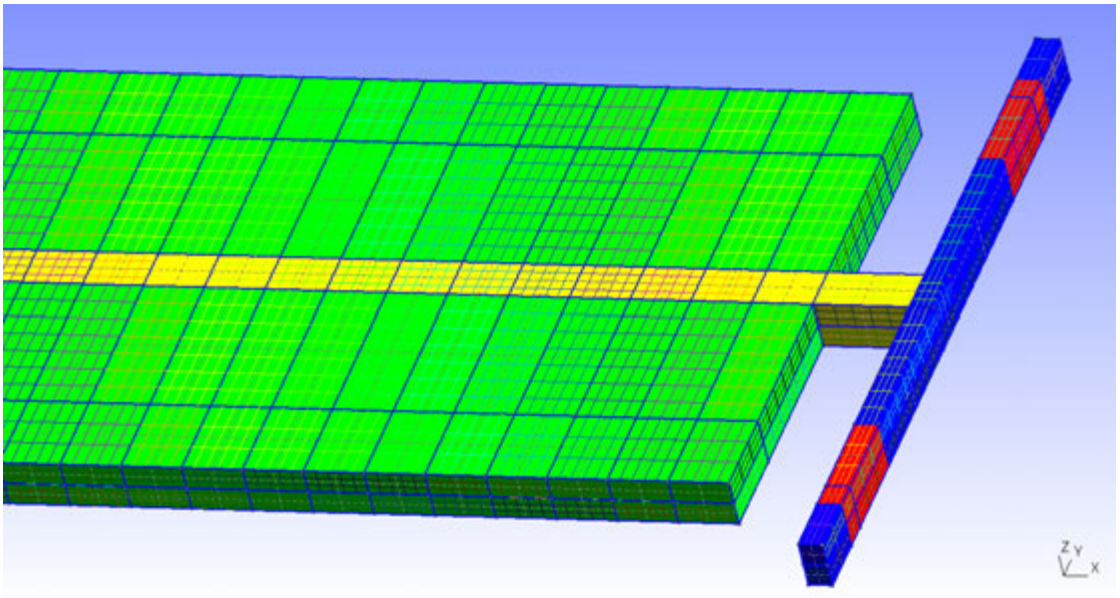

Figure 57 Grid for U3 model.

3.5.3 Base Case Results

In this section we will present results of numerical simulations of U2 and U3 model. The U3 model is the most homogenized one and it requires the smallest grid while the U2 model is the intermediate model of homogenization.

Firstly, we present immiscible simulation (without dissolution of hydrogen and evaporation of water) for only the model U3 and then miscible simulation for both U2 and U3 models, where dissolution of hydrogen and evaporation of water are taken into account.

3.5.3.1 U3 Immiscible simulation

3.5.3.1.1 Fluxes

Since there is no exchange of the mass between the phases in this simulation, the liquid phase is composed only of the water and the gas phase is composed only of the hydrogen. We present, therefore, only the liquid and the gas convective fluxes in Figure 58 - Figure 59.
Since in the U3 model the hydrogen source is uniformly distributed over the domain of all 50 cells, it does not make sense to calculate the fluxes over surfaces F-C1, F-C25 and F-C50 as given in the specifications. Instead, we calculate the fluxes over equally centered surfaces, but with the section of 10 m x 8 m.

3.5.3.1.2 Solution in points

Solutions are given in all prescribed points in Figure 60 - Figure 61. Since we could use only the grid points, there may be small differences in the point coordinates. This does not change the results significantly since the U3 model does not represent the Interfaces and the EDZ.

We should also note that the initial saturations in the model are upscaled such that the initial quantity of the gas is preserved. With the initial pressure there is no such criteria for upscaling. We have thus taken in the Geological medium and in the blocks of the cells the initial water pressure equal to the hydrostatic pressure, and the gas pressure is then calculated form the capillary pressure law. In the drifts and the Main drift bentonite blocks the initial gas pressure is 0.1 MPa, and the water pressure is calculated from the capillary pressure law.

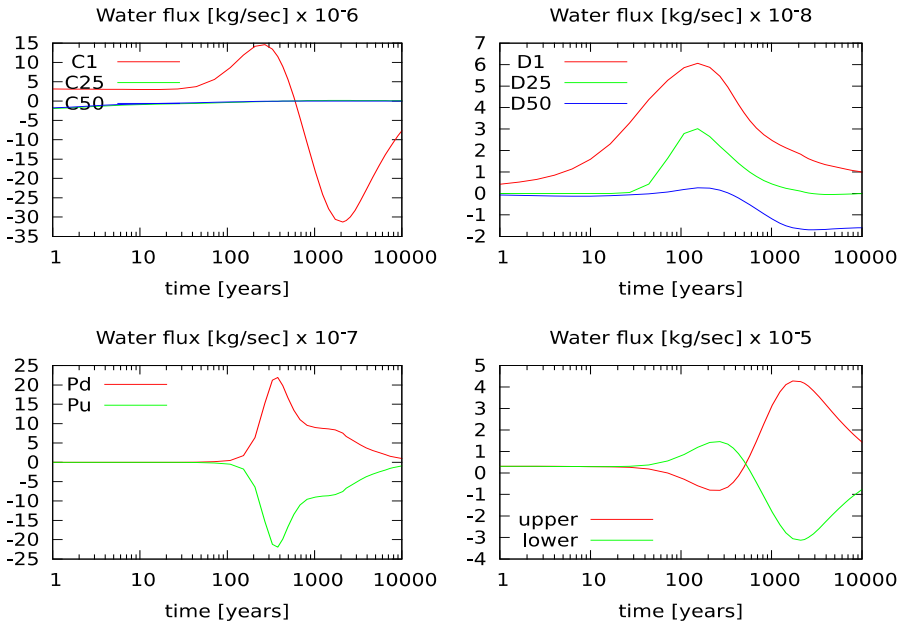

Figure 58 Water flux for U3 immiscible simulation.

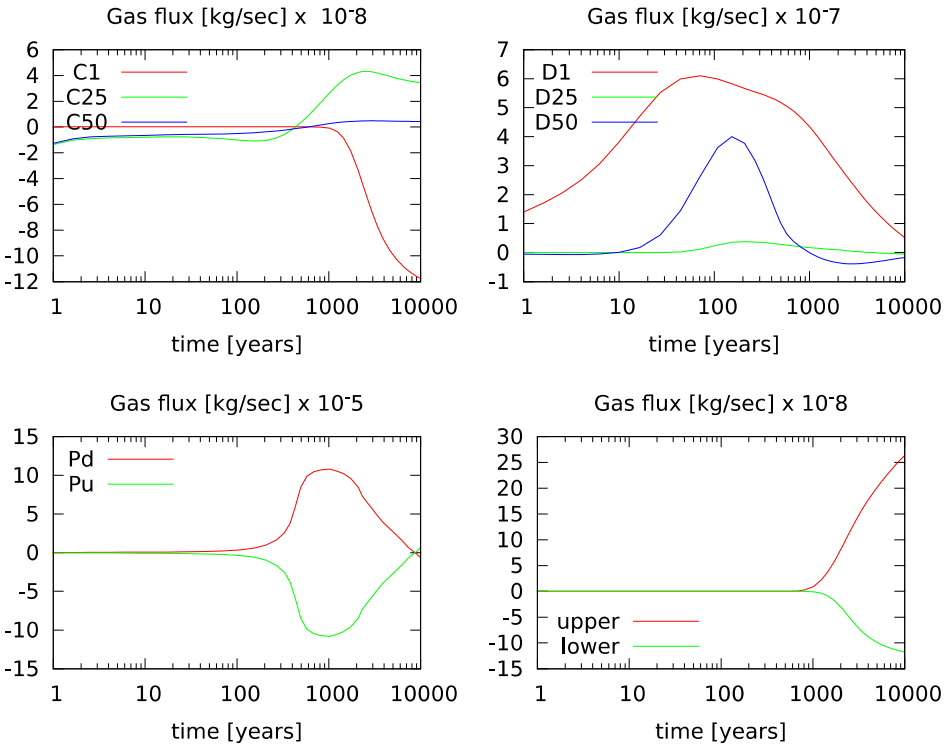

Figure 59 Gas flux for U3 immiscible simulation.

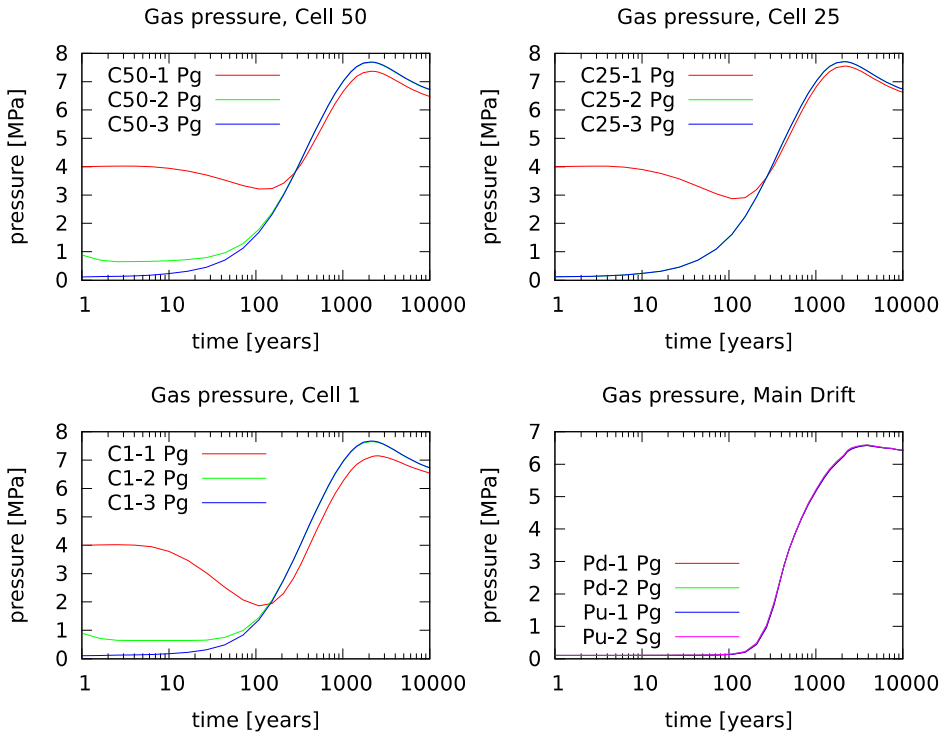

Figure 60 Water saturation in points for U3 immiscible simulation.

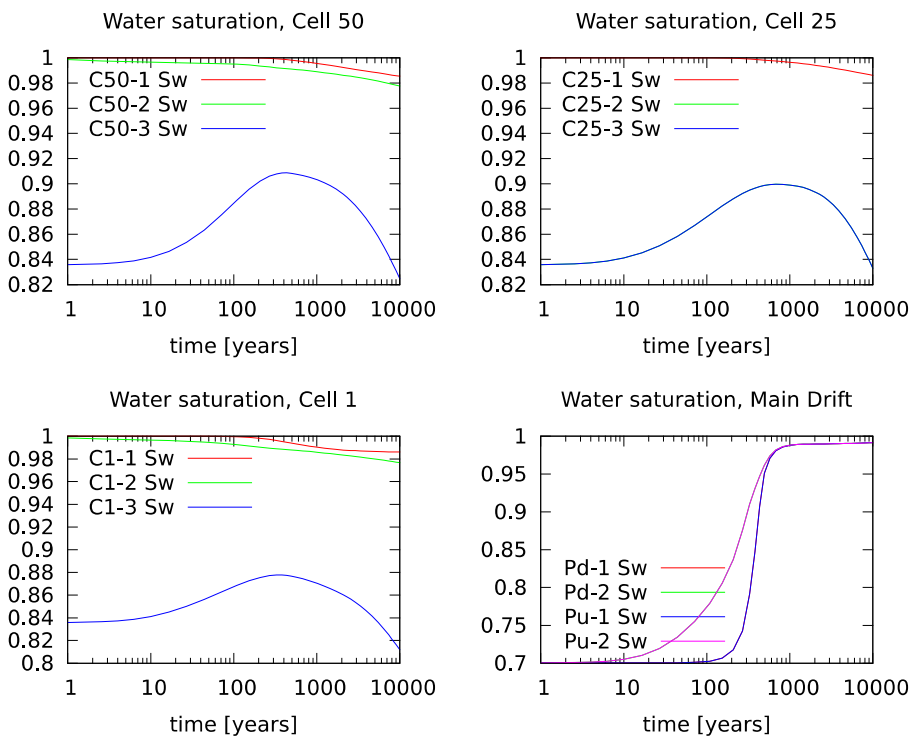

Figure 61 Gas pressure *in points for U3 immiscible simulation.*

3.5.3.2 U3 Miscible simulation

In this section we present results of numerical simulation of the miscible model for the U3 level of upscaling. Details of the implementation of the miscible model are given previously. In the sequel we present some requested output: Fluxes and solutions in points. Then we make a short comparison of immiscible and miscible simulations.

3.5.3.2.1 Fluxes

Here we present some requested fluxes in *Figure 62* - Figure 65. The same remark concerning flux calculations as in immiscible case holds. We note that gaseous hydrogen total flux is two order of magnitudes larger than dissolved hydrogen total flux. Also we can note that convection fluxes dominates diffusive fluxes by several order of magnitudes, except in the bentonite plugs where they are of the same order of magnitude in the gas phase.

Some oscillations are present in dissolved hydrogen fluxes, but they are of small amplitude. What is surprising in these results, compared to the immiscible case, is the very different behavior of the Main drift plugs. They appear here much less permeable, for the gas and the water, than in the immiscible simulation. This is difficult to explain by higher pressures in the Main drift in the immiscible simulation.

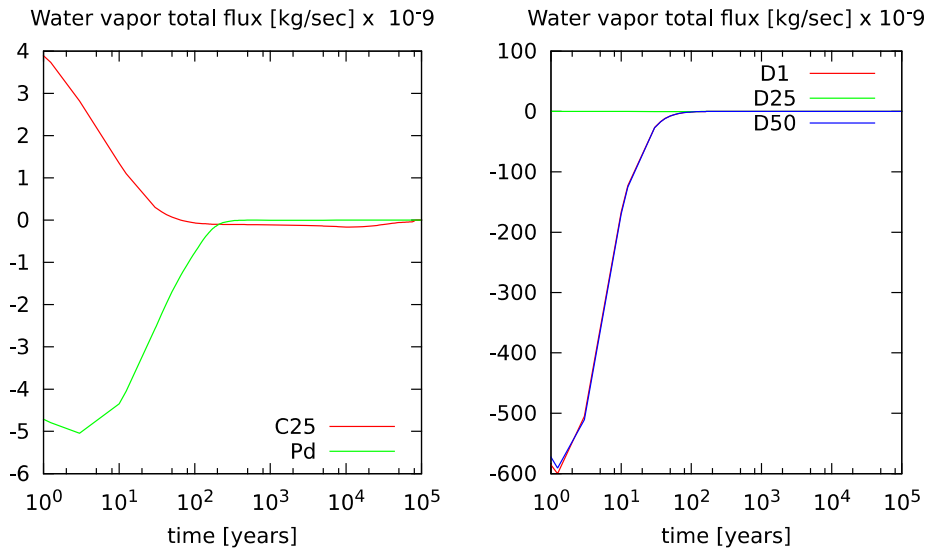

Figure 62 Liquid water total flux for U3 simulation

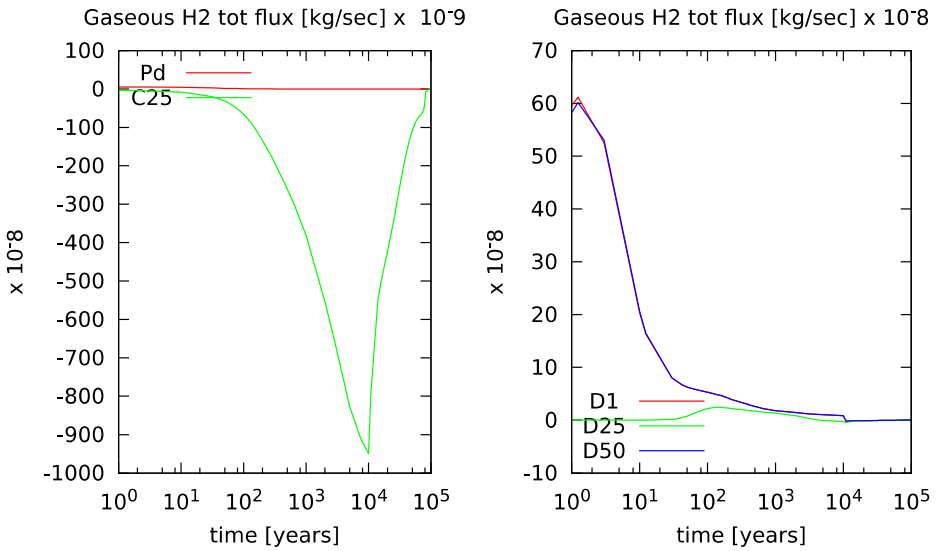

Figure 63 Liquid water total flux for U3 miscible simulation.

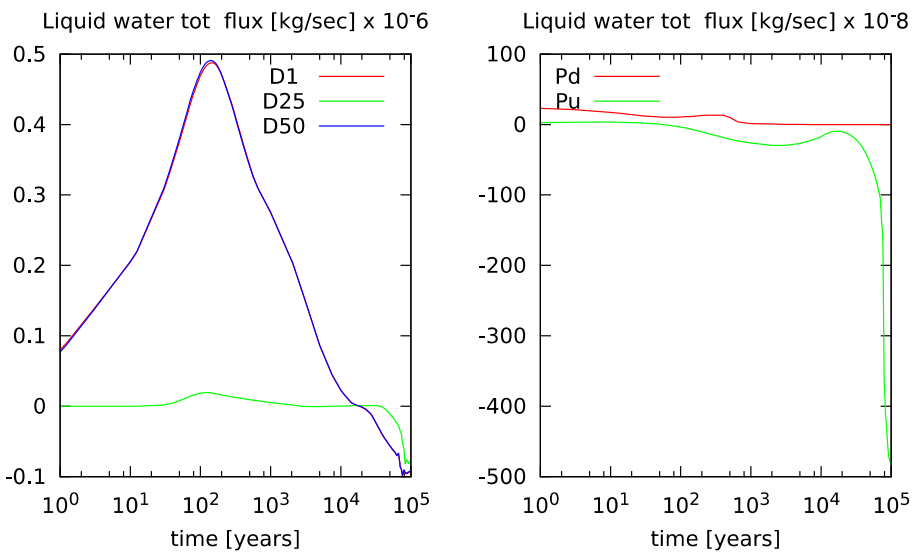

Figure 64 Gaseous Hydrogen total flux for U3 miscible *simulation.*

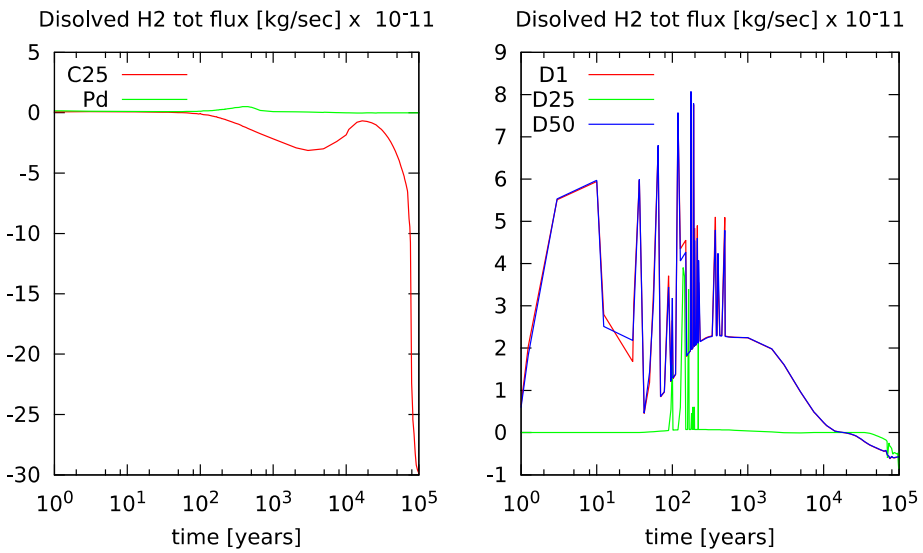

Figure 65 Gaseous Hydrogen total flux for U3 miscible simulation.

3.5.3.2.2 Solutions in points

Here we give solutions in some points in Figure 66. Remarks made previously for immiscible are valid in the miscible simulation too.

Note that the resaturation time of the main drifts is about 1000 years and that this resaturation is not complete. The phase pressures attain their maximum before 10,000 years, the last time of hydrogen source activity.

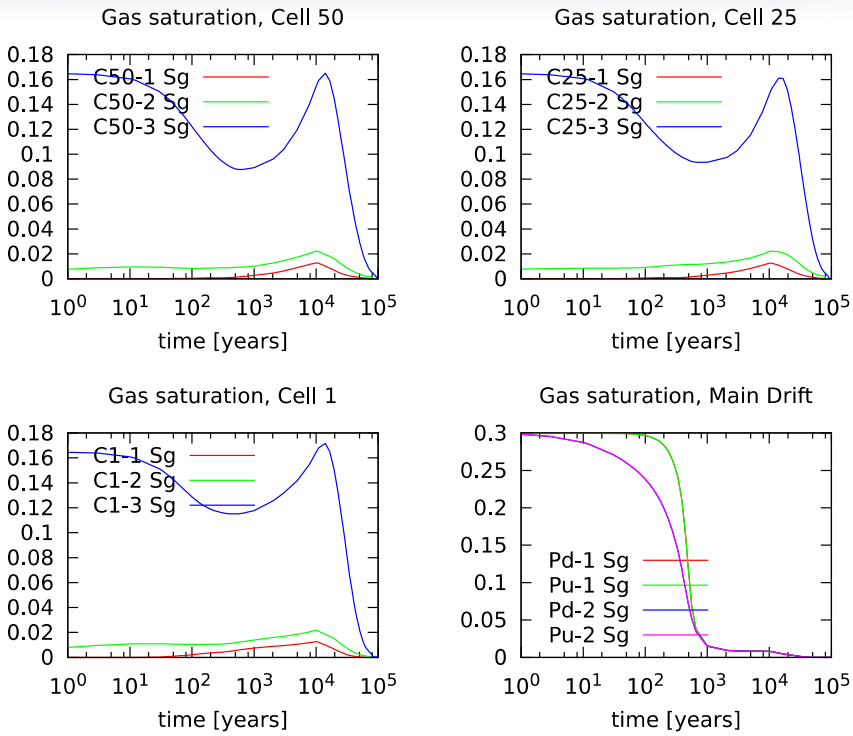

Figure 66 Gas saturation in points for U3 miscible simulation.

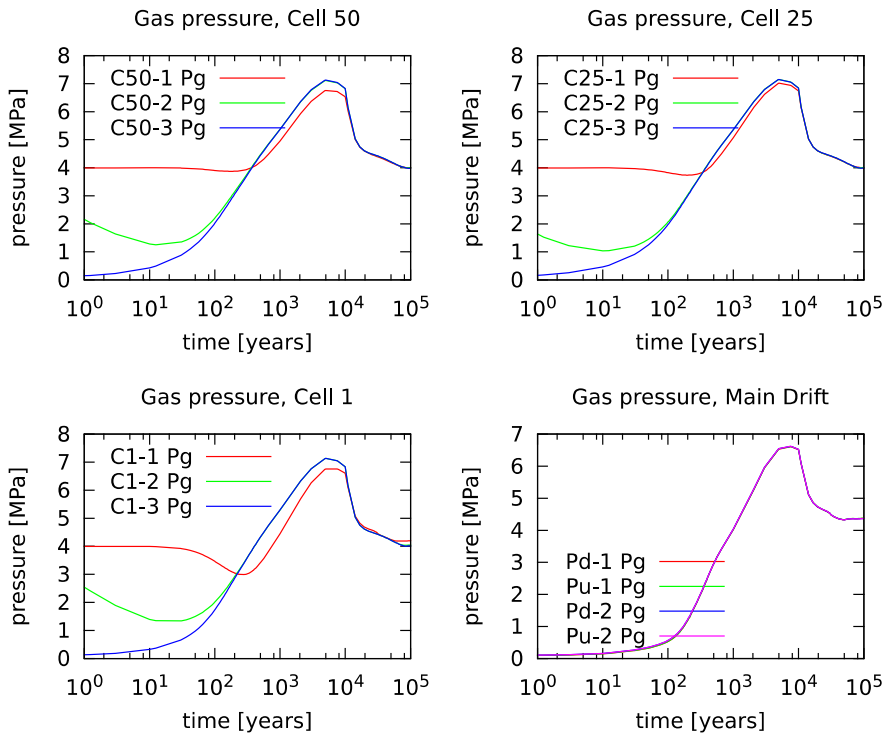

Figure 67 Gas pressure in points for U3 miscible simulation.

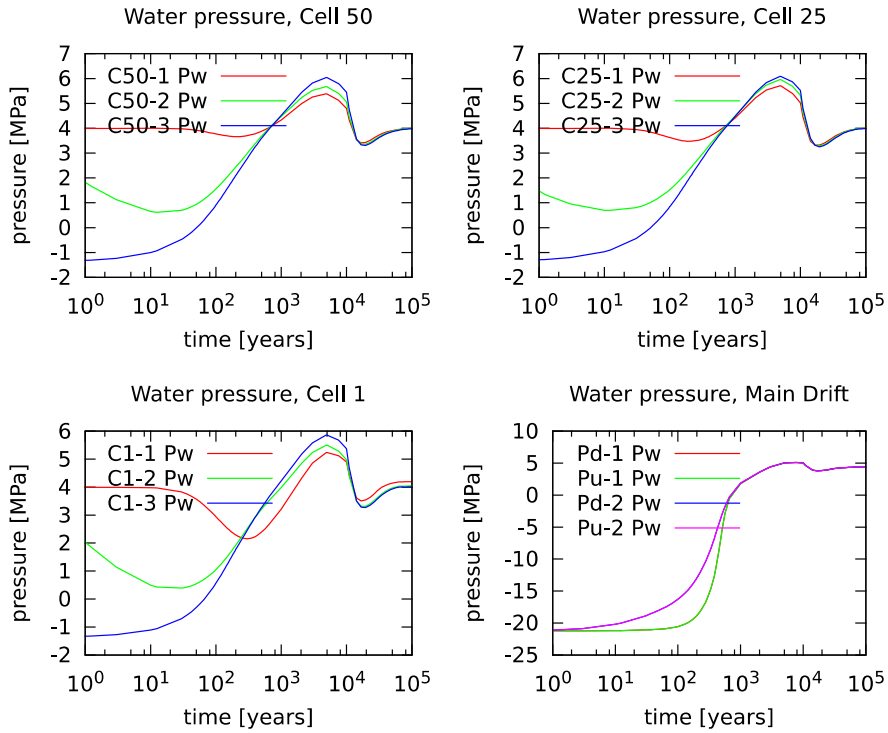

Figure 68 Water pressure in points for U3 miscible simulation.

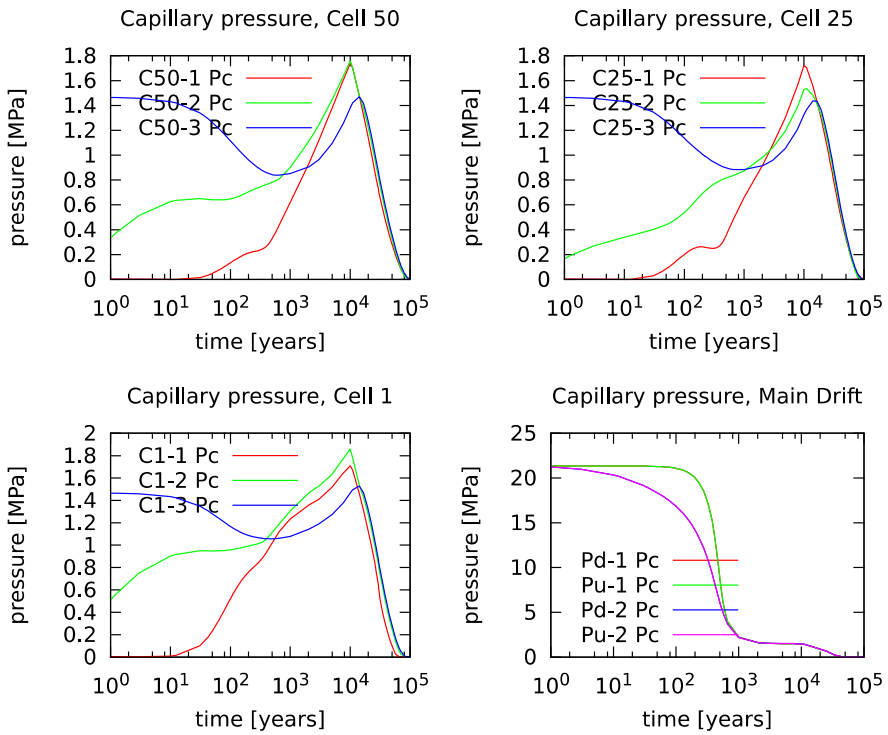

Figure 69 Capillary pressure in points for U3 miscible simulation.

3.5.3.2.3 Comparison of miscible and immiscible simulation

Here we compare some results of the miscible and the immiscible simulation. Both simulations are performed on the coarse grid of 27776 elements with the U3 model.

We present the solution in the point C25-3 in Figure 70 and solution on a line over the Main drift in *Figure 71*. The red line represents immiscible simulation and the green one represents miscible simulation.

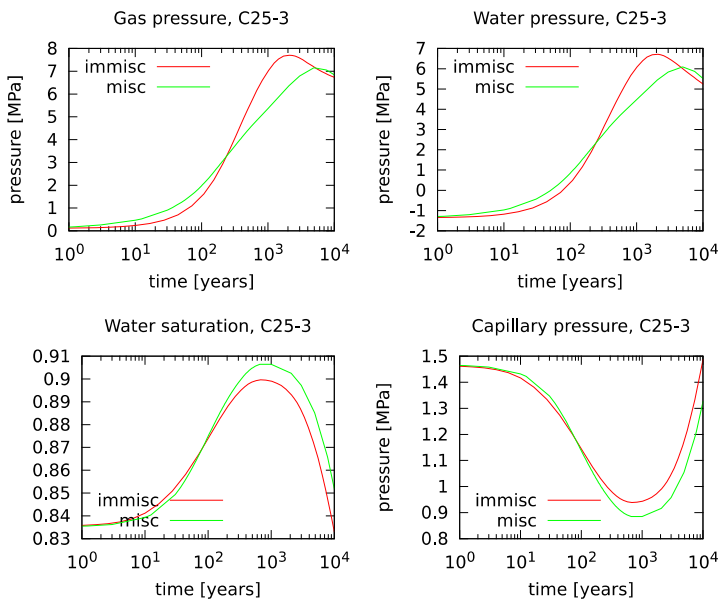

Figure 70 Comparison of the solutions in the point C25-3.

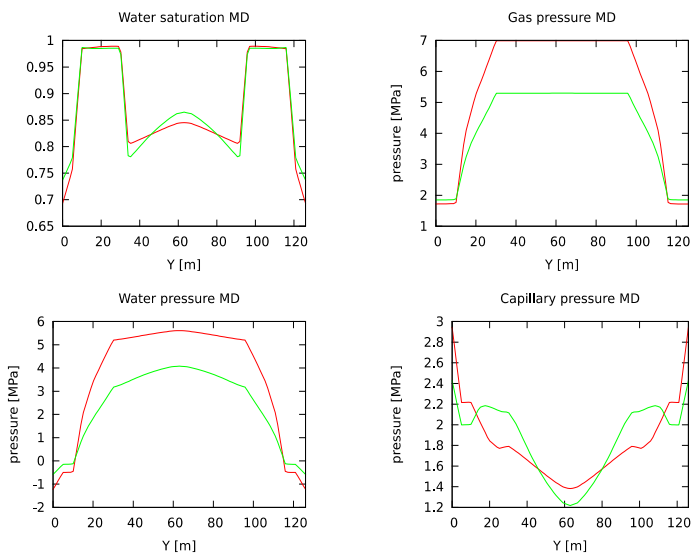

Figure 71 Comparison of the solutions in the Main drift at t=1000 years.

As we can see from the solutions in points, the pressure increase in the miscible simulation has some retardation compared to the pressure increase in the immiscible simulation. The maximum pressures in the immiscible simulations are higher than in the miscible simulation and the difference is of the order of 1 MPa.

3.5.3.3 U2 Miscible simulation

In this section we present results of (miscible) simulation of the U2 model. The simulation is performed on the grid with 188298 elements. In the following sections we present some requested output: Fluxes, and solutions in points. Then we make a short comparison of the U2 and the U3 (miscible) simulations.

3.5.3.3.1 Fluxes

In Figure 72 - Figure 75, we present the same fluxes as for the U3 miscible simulation

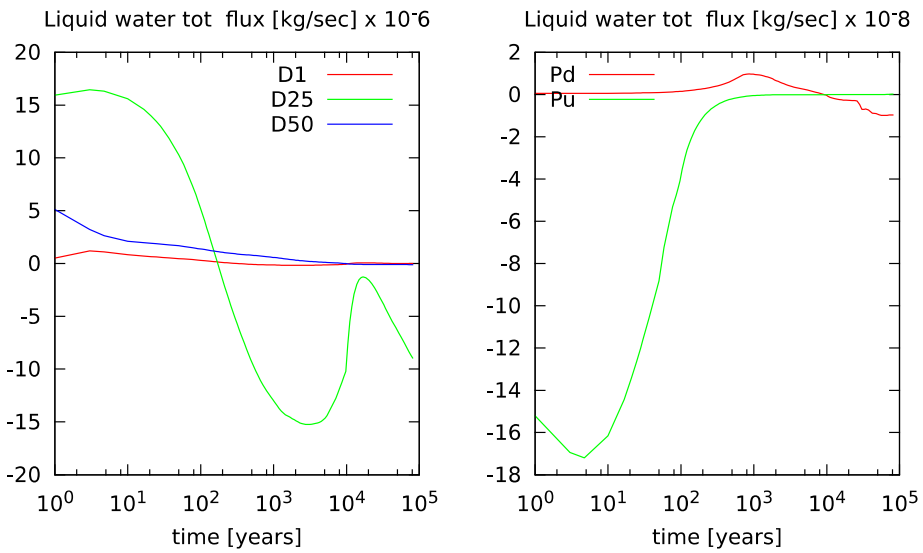

Figure 72 Liquid water total flux for U2 simulation.

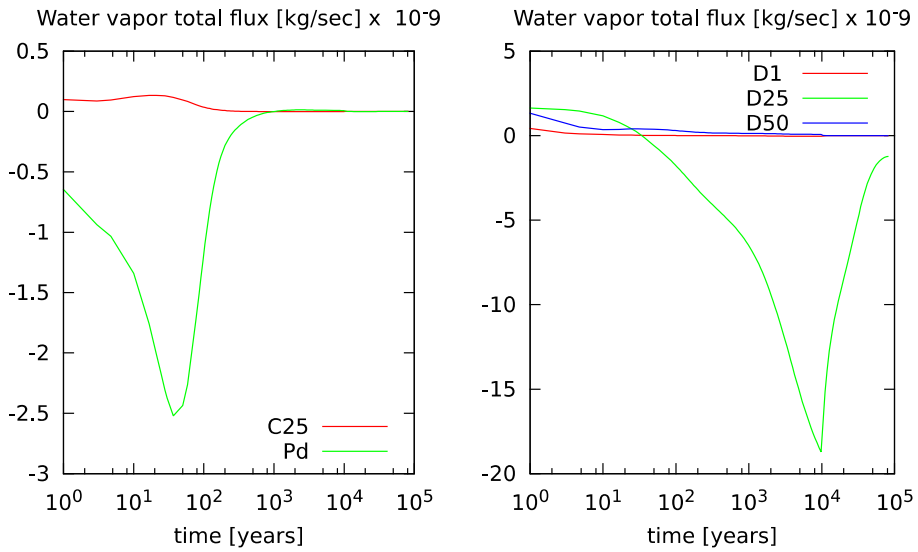

Figure 73 Water vapor total flux for U2 simulation.

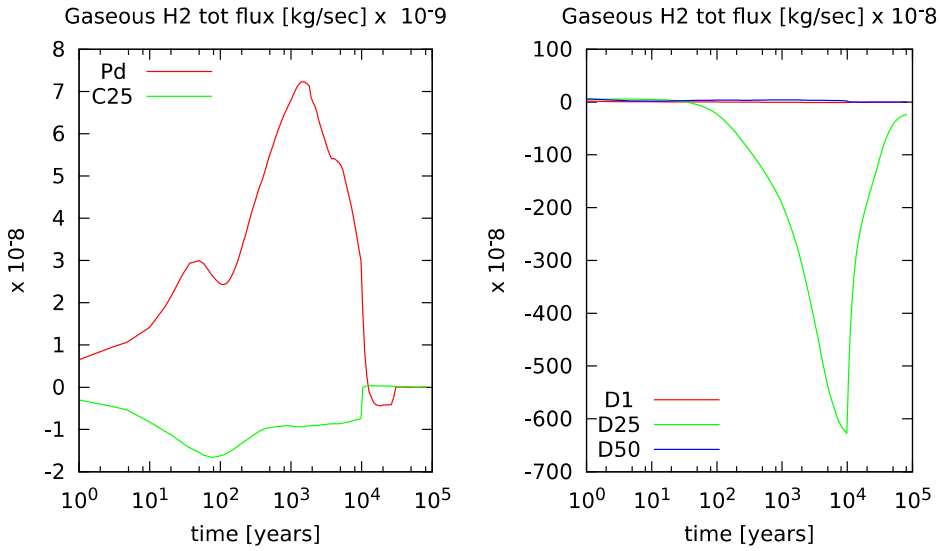

Figure 74 Gaseous hydrogen total flux for U2 miscible simulation.

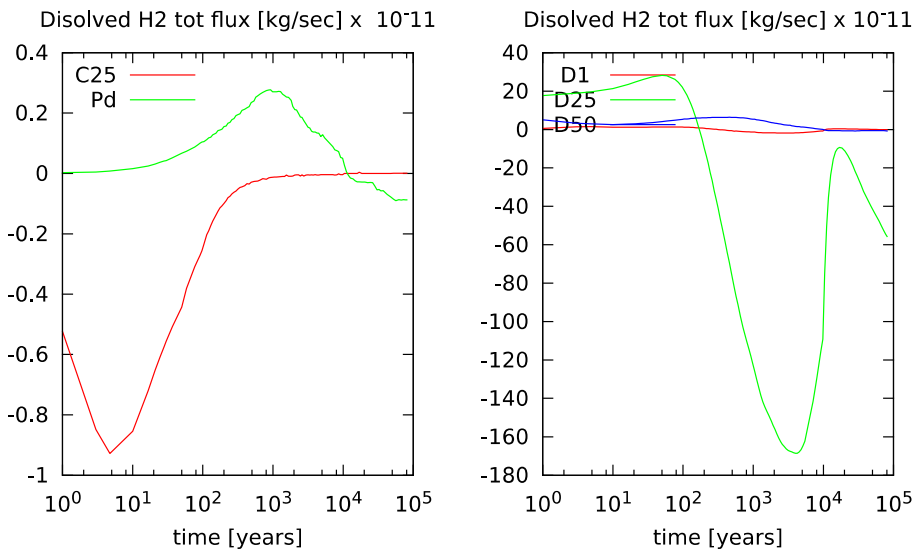

Figure 75 Dissolved hydrogen total flux for U2 miscible simulation.

3.5.3.3.2 Solution in points

In Figure 76 - Figure 79, we give solutions in the same points as the simulation U3.

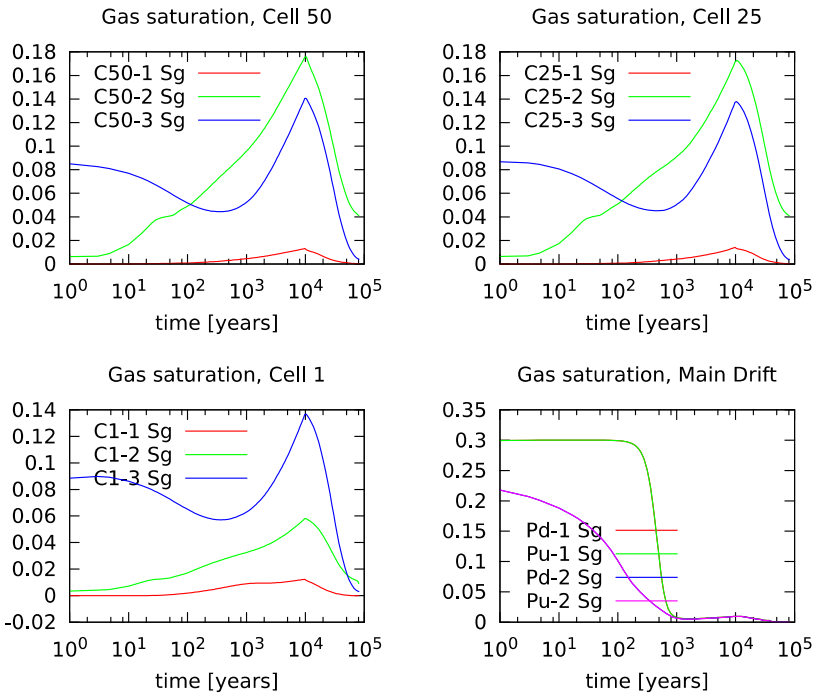

Figure 76 Gas saturation in points for the U2 miscible simulation.

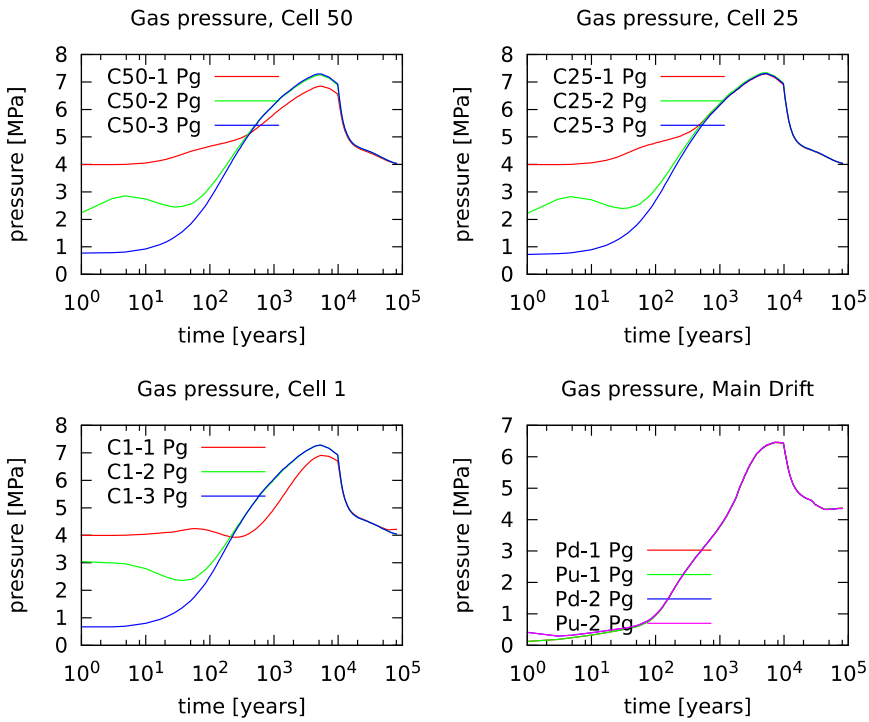

Figure 77 Gas pressure in points for the U2 miscible simulation.

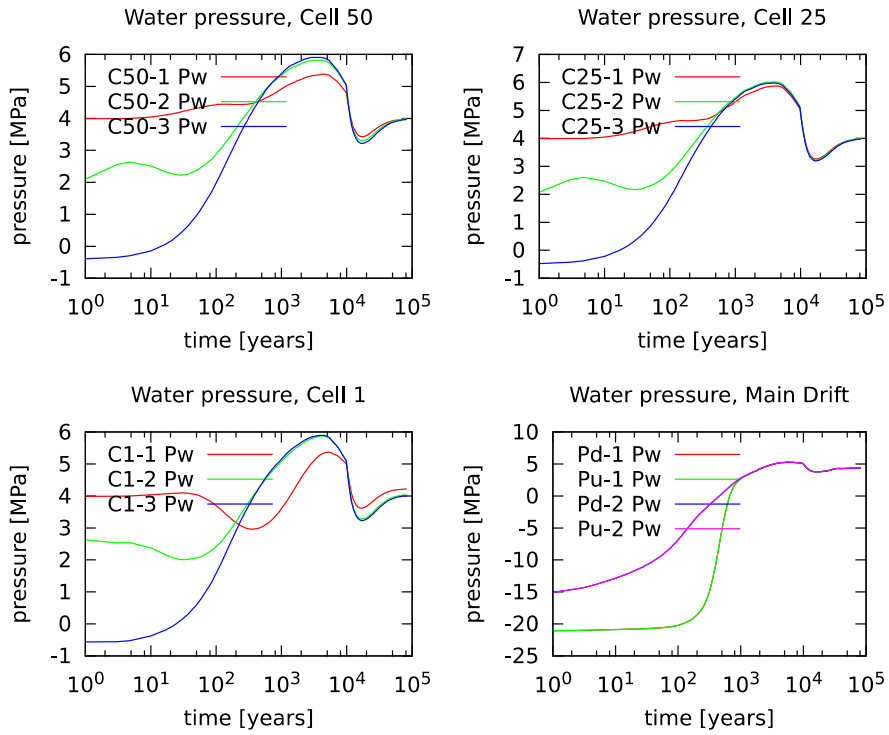

Figure 78 Water pressure in points for the U2 miscible simulation.

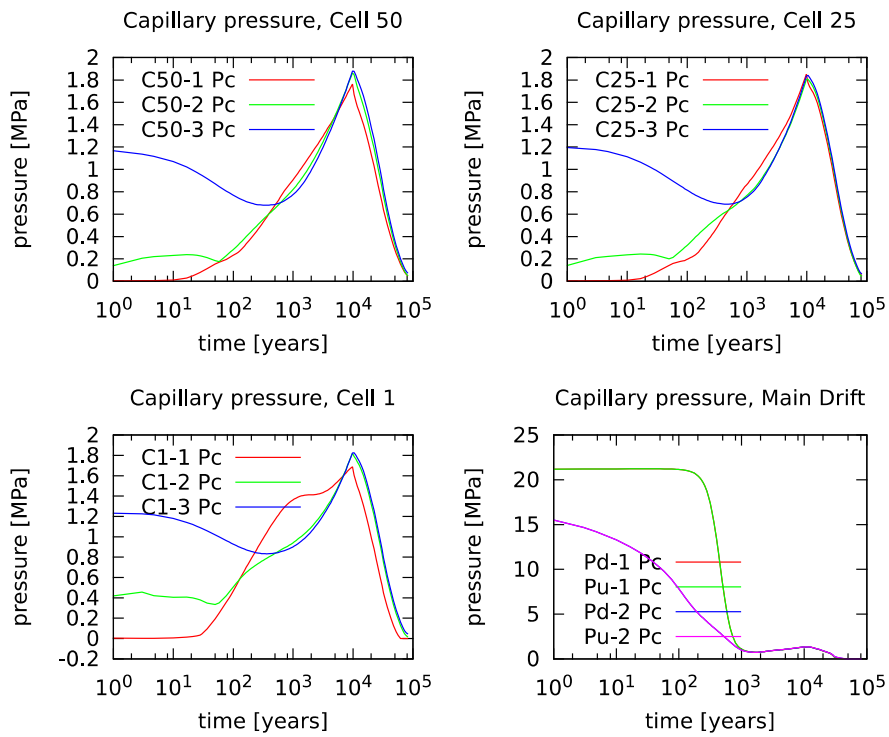

Figure 79 Capillary pressure in points for the U2 miscible simulation.

3.5.3.3.3 Comparison of U2 and U3 simulation

The results show that locally the differences between the U2 and the U3 simulations can be large, but global behavior is enough similar to confirm the same conclusions about response of the system to migration of generated gas. In *Figure 80* - Figure 82 we show several comparisons.

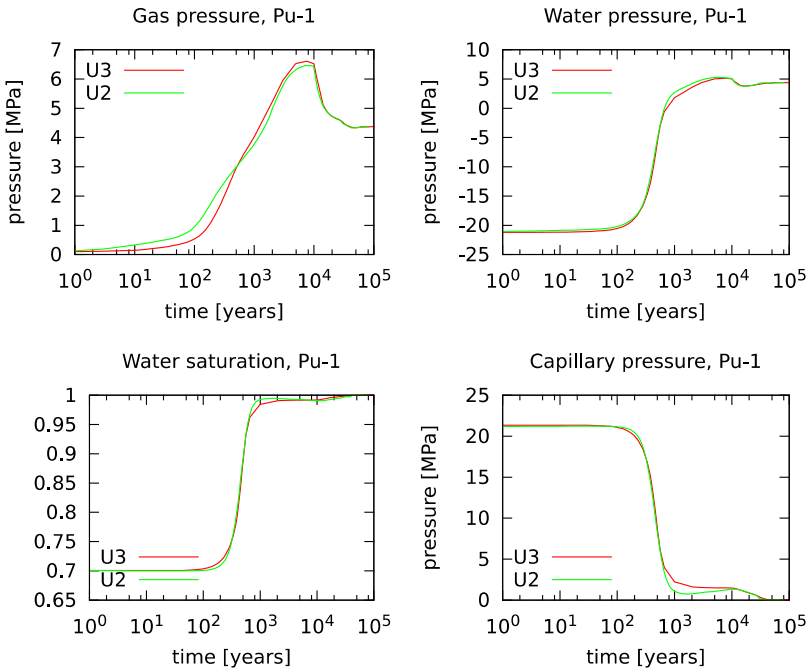

Figure 80 Solutions in the points Pu-1 for both U2 and U3 miscible simulations.

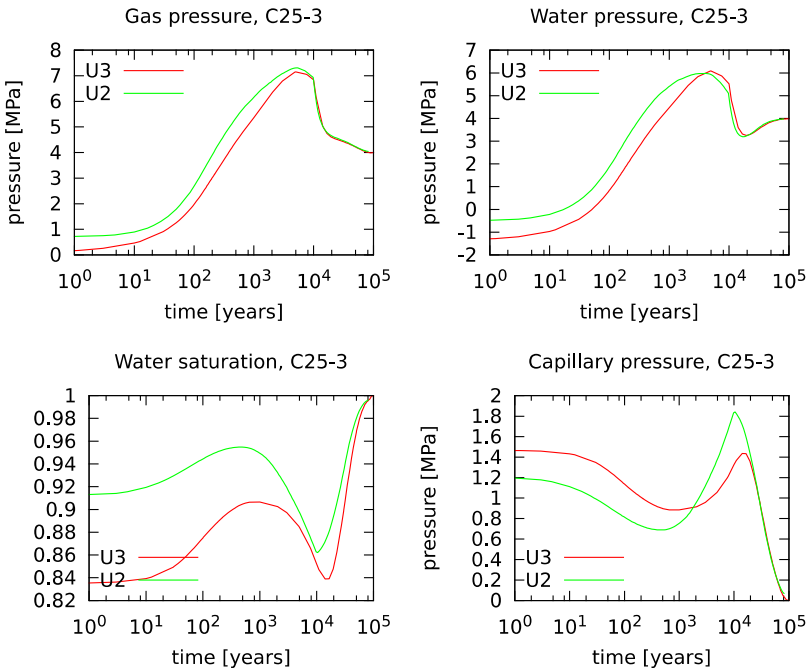

Figure 81 Solution in the point P-C25-3 for both U2 and U3 miscible simulations.

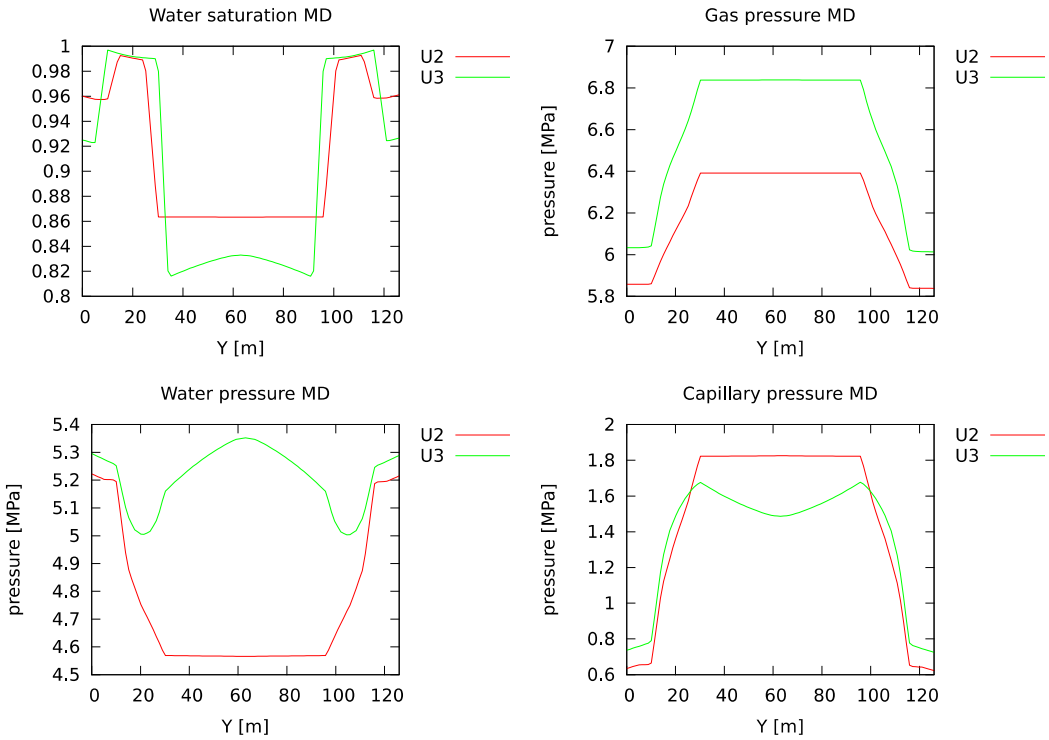

Figure 82 Solution in the Main drift at t=10000 years for both U2 and U3 miscible simulations.

3.5.4 Sensitivity Cases

For immiscible simulation a grid sensitivity analysis has been performed. We have compared the solution of U3 model on three different meshes that we call on the figures, coarse, intermediate and fine. The grid size for each grid is given in the following table.

Grid	Number of elements	Number of vertices
Coarse	27776	31885
Intermediate	100800	108779
Fine	162600	177072

Table 1 Size of grids used in grid sensitivity.

The comparison is presented for fluxes and solutions in the points. We have chosen to show the fluxes over section D1 (*Figure 83*) and the solutions in the point C-25-3 (Figure 84).

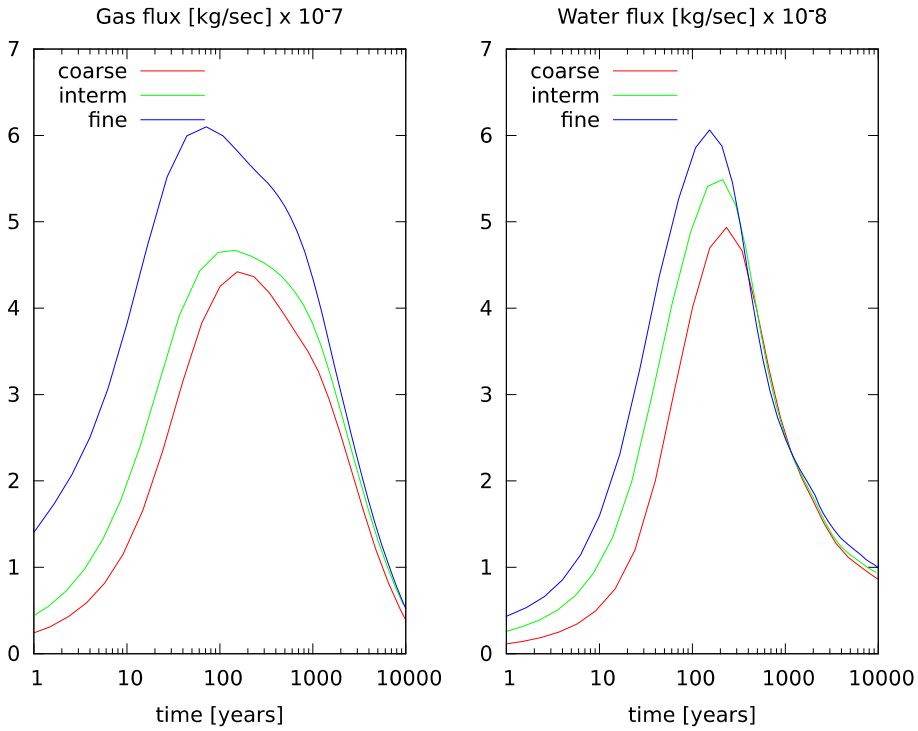

Figure 83 Flux comparison over section D1.

The red line represents coarse grid, the green one represents the intermediate grid and the blue one represents the fine grid. From these figures we see that the differences are largest in the fluxes which can be explained by two reasons.

First, in our numerical model the main unknowns are pressures, saturations and mass fractions. The fluxes are computed from these values as a post processing and are known to have one order of precision less than the primary variables.

The second reason is that the fluxes are calculated by integration over certain surfaces, which are represented differently in different grid. In the coarse grid this surface is represented by a small number of elements (4 in the drifts) but in finer grids the representation is better. This fact also contributes to differences in the precision of calculated fluxes.

Relying on comparison of the primary variables we conclude that the coarse grid still gives representative results and could be used for the whole repository simulation.

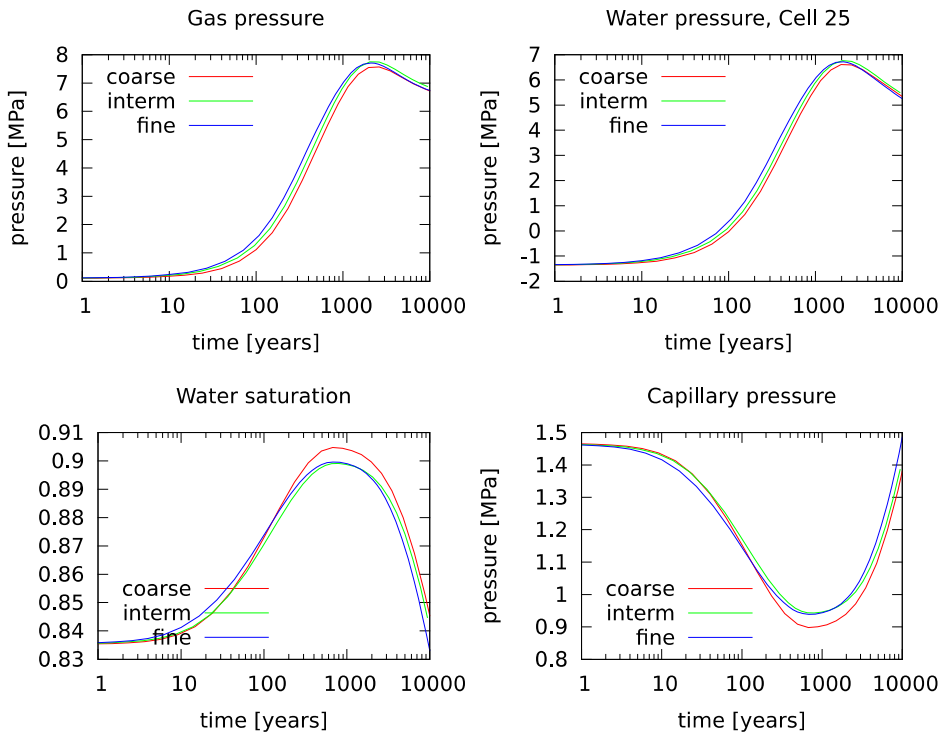

Figure 84 Comparison of the solutions in the point C25-3.

3.5.5 Discussion and Conclusions

We have presented results of numerical simulations of the module scale benchmark. Our approach to numerical modelling includes the use of the mathematical homogenization to reduce heterogeneity of the model, thus reducing its complexity. We have build tools and procedures to build several upscaled models, with different level of small scale details; three such models are built.

The numerical simulations have been performed for now only on the two most homogeneous models. We have performed immiscible and miscible simulations and given a brief comparison between the two simulations.

On immiscible simulation, which is faster than the immiscible, we have performed a grid sensitivity analysis which shows that smaller mesh used produces reliable results, and this mesh is used in the miscible simulation (full implementation of the simulation model).

Our simulations show that the maximum pressure in the module will be about 7 MPa, and that at the places where the fluxes were calculated the convection will be the main way of hydrogen transport. Transport of hydrogen dissolved in water is about two orders of magnitude less significant than the transport of gaseous hydrogen. However, the presence of dissolution/evaporation mechanism in the miscible model, compared to immiscible one, reduces the maximum gas pressure for approximatively 1 MPa.

3.5.6 References

[1] B. Amaziane, M. Jurak: FORGE Report WP 1.2: Contribution of CNRS/MoMaS, February 28, 2011.

[2] Dumux web-page: http://www.dumux.org.

[3] B. Flemisch, M. Darcis, K. Erbertseder, B. Faigle, A. Lauser, K. Mosthaf, S. Muthing, P. Nuske, A. Tatomir, M. Wol_, R. Helmig, DuMux: DUNE for Multi-{Phase, Component, Scale, Physics, ... } Flow and Transport in Porous Media. Advances in Water Resources 34(9), (2011) 1102-1112.

[4] FORGE WP 1.2 Benchmark specifications at a complete generic HLW repository scale.

[5] IAPWS: Guideline on the Henry's Constant and Vapor-Liquid Distribution Constant for Gases in H2O and D2O at High Temperatures, http://www.iapws.org/relguide/HenGuide.pdf

[6] E. Keilegavlen, J.M. Nordbotten, A.F. Stephansen, Tensor relative permeabilities: Origins, modeling and numerical discretization, International Journal of Numerical Analysis and Modeling, 9(3), (2012) 701-724.

[7] R. Reid: The Properties of Gases and Liquids, 5th edition, McGraw-Hill, 2001.

[8] F. Smaï : Développement d'outils mathématiques et numériques pour l'évaluation du concept de stockage gologique, PhD thesis, University Claude Bernard Lyon 1, 2009.

[9] W. Zijl, A. Trykozko: Numerical Homogenization of the Absolute Permeability Tensor Around a Well, SPE Journal 5 (2001), 399-408.

3.6 IRSN contribution

3.6.1 Introduction

This chapter presents the actual state of modelling work on the module scale carried out by IRSN within the Work Package 1.2 of FORGE project. It should be noted that IRSN uses a home-made code diphpom which is still under development. The code development and validation was the first goal within FORGE WP1.2 and application to the benchmark cases was the second objective. The code and its validation are presented in the FORGE Deliverable D1.6 "Final report on benchmark studies on repository-scale numerical simulations of gas migration. Part 1: cell scale benchmark".

3.6.2 Model Implementation

3.6.2.1 Code and Formulation

IRSN collaborated with University of Claude Bernard in Lyon to develop a 3D simulation tool for gas migration. It takes into account the convective and diffusive transport of N+1 components in 2 phases as well as mass exchanges between phases (dissolution and evaporation). The liquid phase and the solid matrix are assumed incompressible; the other phase follows the ideal gas law. The formulation is based on the classical mass conservation laws for both multi-component phases (g for gas and l for liquid) supplemented with generalized Darcy equations for each phase:

Equation 1

$$\frac{\partial}{\partial t}\left(\Phi \sum_{\alpha} \rho_\alpha X_\alpha^i S_\alpha\right) + div\left(\sum_{\alpha} \rho_\alpha X_\alpha^i \vec{q}_\alpha\right) - div\left(\Phi \sum_{\alpha} \rho_\alpha D_\alpha^i S_\alpha \vec{\nabla} X_\alpha^i\right) = Q_i$$
$$\vec{q}_\alpha = -\lambda_\alpha K\left(\vec{\nabla} P_\alpha - \rho_\alpha \vec{g}\right) \quad \alpha = \{l, g\} \quad i = \{0..N\}$$

where K is the absolute permeability tensor, g the gravity vector, Q_i the source term for the component i, and for each phase α: ρ_α is the density, $\lambda_\alpha = k_{r\alpha}/\mu_\alpha$ the mobility, $k_{r\alpha}$ the relative permeability, μ_α the dynamic viscosity, and we define capillary pressure $P_c = P_g - P_l$. Empirical laws are used for the capillary pressure and relative permeabilities (Brooks-Corey, Brusaert, Van Genuchten, Vauclin …).
These equations are completed by an appropriate set of closure equations related to the hypothesis of the existence of a local thermodynamical equilibrium (Henry law, Raoult-Kelvin law …).

In order to be able to handle material heterogeneities as well as the changes in the thermodynamical state of the system (one or two phases present), a special set of unknowns has been chosen, namely liquid pressure P_l and molar fraction of dissolved gas (for example hydrogen) X_l^i. They are naturally used to describe fully saturated conditions when only liquid phase is present. However, using thermodynamic equilibrium, it is possible to reconstruct all variables of a two phase system. Thus (P_l, X_l^{H2}) can be used as primary variables with standard physical meaning whenever the liquid phase is present. In the case of zero liquid saturation when only the gas phase is present it is possible to extend these variables using again the thermodynamic equilibrium.

The resulting system of quasi-linear equations has been treated with fully implicit Euler time discretization and with an exact Newton method to obtain a set of linear equations. The spatial discretization has been

done for triangles and tetrahedral elements with a finite element scheme within the Libmesh numerical library.

3.6.2.2 Benchmark Implementation

As a first step in modelling the repository at the module scale we decided to reduce the second FORGE benchmark and treat it on its horizontal symmetry plane. This allows us to stay within a 2D geometry. It is also an interesting test of possible simplification of the complex 3D repository scale modelling. We will thus seek to compare our results with the results of the complete 3D models of other teams. We stay as close as possible to the original specifications of the benchmark, even the source term will be kept unchanged with respect to cell scale simulations. Furthermore, it has been shown by other teams that the horizontal asymmetry in boundary conditions has only a limited effect on the simulation results. Thus we decided to mesh only half of the module (50 cells instead of 100). This decision will help us to keep the mesh as detailed as possible with 3 layers of elements in the 1cm interfaces all over all cells.

3.6.2.3 Grid

The 2D triangular mesh has been constructed with gmsh using both structured (for interfaces) and unstructured (elsewhere) algorithms. The interfaces where represented with 3 layers of elements, in order to be able to capture the permeability jump between the interfaces and the neighbouring materials (EDZ and bentonite). The mesh consisting of 149000 nodes was used for the calculations, see Figure 85.

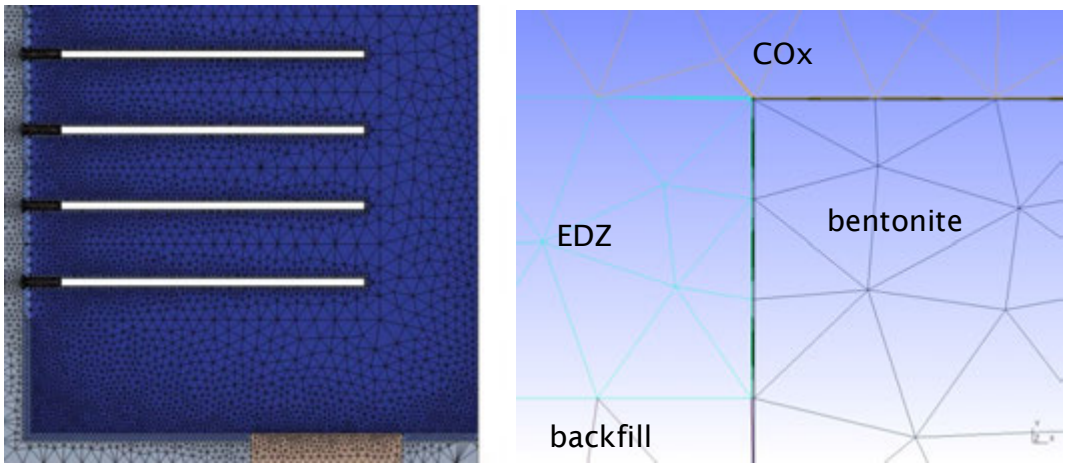

Figure 85 The mesh used for the module case: the part containing the main drift and a zoom at the interfaces around the plug in this drift.

The time stepping scheme was created on a basis of an initial time step $dt_0=10^{-8}$ years, and was incremented every 25 time steps by a factor of 1.1. In the case of failure of the Newton iterations, the last time step was divided by 2. After the end of the hydrogen injection at 10^4 years, the time step was to drop again to 10^{-8} years in order to resolve the very rapid water resaturation of the interfaces that follows the end of gas

injection. We have used a direct parallelizable solver (Mumps), which allows to split the inversion process over several calculation cores (we have tested the calculations on 4 and 8 cores).

3.6.2.4 Boundary Conditions and Sources

The boundary conditions imposed in the benchmark were expressed either as Dirichlet or Neumann ones. For the time varying boundary conditions imposed on the outlet of the drift, we have chosen to impose the conditions from the upstream side. We have used the BC version in terms of liquid pressure P_l and water saturation S_l from which the other variables (P_g, X_l^h) can be deduced. From the saturations it is possible to calculate the values of liquid molar fraction of hydrogen X_l^h as long as the water saturation is not equal to one. In this later case X_l^h becomes ambiguous. Such a problem appeared for late times of this time dependent BC in the drift and also on the "outer" boundary conditions, where the gas pressure and the liquid pressure were equal to 5MPa, and thus the water saturation was supposed to be 1. The values of X_l^h corresponding to the fully saturated state were chosen in a different way in both cases. For the drift BC it was chosen to be equal to the solubility limit corresponding to the gas phase pressure of 5MPa, and at the "outer" boundary it was set to a lower value in order to represent a sink boundary and to be compatible with the initial conditions, see Table 1. The obtained boundary conditions in terms of dissolved hydrogen molar fraction are presented in Figure 86.

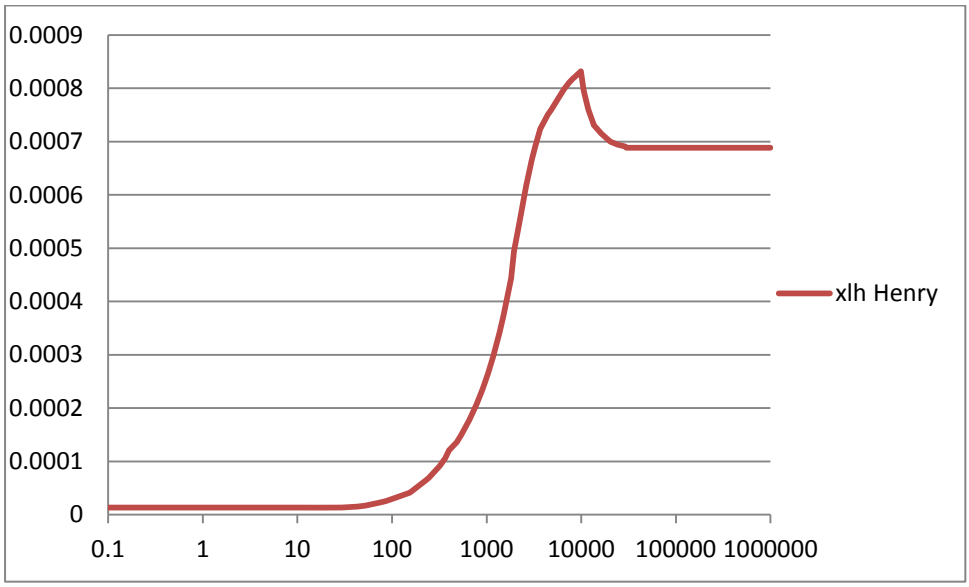

Figure 86 Boundary conditions for the drift in terms of X_l^h.

Finally the value of the source term to be applied on the surface of the waste canisters (excluded from the simulation domain) had to be adapted. We use the same value from surface density of production as in the case of the cell scale benchmark:

- for $0 < t \leq 10000$ years, Q^h_{2D}=322.4mol/year/cell = 1.6 g/m²/year
- for $t > 10000$ years, Q^h_{2D}=0

As in the original case the source term is localised on all over the waste canisters external surfaces.

3.6.2.5 Initial Conditions

The initial conditions were specified in the benchmark in terms of gas pressure and water saturation in the materials that were initially partially saturated (backfill in the drift, bentonite plug, interfaces). For these materials, as in the cell-scale benchmark, it was possible to calculate directly the corresponding water pressure and liquid molar fraction of hydrogen. The obtained values are given in Table 1. However this is not the case for fully saturated materials (EDZ and COx) where the liquid pressure of 5MPa was prescribed. In such a case X_l^h can take any value lower than the one obtained from the equilibrium relations. As the X_l^h initial values in desaturated zones are much lower than these limits and very close to each other, we chose to use the same X_l^h value for saturated materials. In this way we avoid discontinuities in initial variables and we ensure that the "top" boundary condition corresponds to an infinite reservoir condition (dissolved hydrogen has a sink at this boundary).

	-21.3MPa	1,33E-05	
	-2.98MPa	1,32E-05	
	72 kPa	1,32E-05	
	5MPa	1,32E-05	*6.9E-4*
	5MPa	1,32E-05	*6.9E-4*

Table 1 The Initial conditions imposed for the base cell case. The limit values are obtained in the case of saturated materials for the hypothetic (atmospheric) gas pressure of 1e+4Pa.

3.6.2.6 Deviations from the specification

The most important modifications with respect to the specifications come from the geometry change from the prescribed 3D to the plane 2D. Only one half of the module with 50 cells is being modelled. The change of geometry imposed to adapt the source term, see 3.6.2.4. After the analysis of the specifications it has been seen by several teams that the interfaces running along the backfill zone were unnecessary. On one side their presence in this place is not so well justified (or physically meaningfull) as between the bentonite plug and the EDZ. The interface and backfill zones are both much more permeable that the COX and the EDZ thus fulfilling the same role in the system. Taking account all this we decided to melt the interfaces with the backfill.

The other modifications are inherited from the cell scale calculations and they are recalled in the rest of this section.

Absolute permeability

In order to be coherent with the simulations made on the cell scale we have replaced the absolute permeabilities of the annex (§ 5) by the following values : for the host rock $K=10^{-21}m^2$, and for the EDZ and the interface facing plug $K=10^{-17}m^2$.

Liquid relative permeability in interfaces

The original definition of the benchmark defined the liquid relative permeability by a standard Van Genuchten function:

$$k_{r,l} = \sqrt{S_{le}}\left[1-\left(1-S_{le}^{1/m}\right)^{m}\right]^{2}$$

with the exponent m=0.75. However this function goes very rapidly to zero when S_{le} approaches 0. It has been noticed that the resolution of Equation 1 becomes awesome when $k_{r,l}$ goes to zero quicker that the inverse of the capillary function P_c^{-1} (which appears in front of the evolution term). For the van Genuchten capillary pressure function this limit is:

$$\lim_{S_{le}\to 0} P_c^{-1} = S_{le}^{1/m}$$

This is especially true in the case of the interfaces, where the convection is a dominant transport mode, and which tend to de- or resaturate very quickly. We have sought thus to regularize the relative liquid permeability in the interfaces by replacing the van Genuchten function near S_{le}=0 by a simple power law:

$$k_{r,l}^{interface} = \begin{cases} S_{le}^{1/2}\left(1-(1-S_{le}^{1/m})^{m}\right)^{2} & S_{le} > 0.38 \\ cst\, S_{le}^{1/m} & S_{le} \leq 0.38 \end{cases}$$

The value of cst is chosen in the way to insure the continuity of the $k_{r,l}$.

Residual water saturation

Another numerical problem was related to the possible complete desaturation of the interfaces which are very permeable and desaturate very easy. In such a case the simulation domain would be divided into two parts which evolve almost separately since the dry interface establish a capillary barrier between them. In this case the numerical resolution becomes tedious and the Newton procedure often converges to an unphysical solution. In order to avoid this problem a small residual water saturation is being imposed in the interfaces (S_{lr}=0.005).

Specific storage

The proposed model of implementation of specific storage was based on the liquid pressure dependency in the liquid density, see the annex (§ 5). However the concept of the specific storage was introduced in order to account for the compressibility of the rock and that of the liquid, and thus we consider that we should rather change the porosity than the liquid density, which, if applied as is, would perturb the mass balance calculations. We keep the same functional form and the specific storage coefficients as proposed in the benchmark, but the relation now reads:

$$\Phi_i(P_l) = \Phi_i^0 e^{S_S(P_l-P_0)}$$

where the reference conditions are denoted by an underscript 0 and correspond to the initial conditions.

3.6.3 Base Case Results

We present here the results obtained for the first 25 years. For the moment the calculations over longer periods are difficult to run (Newton method does not converge leading to a decrease of the time step down to very low values 10^{-12} years). In the following figures we present the results obtained so far. If the point series of pressures are considered, it can be noticed that the overall behaviour of the three disposal cells (1^{rst}, 25th and 50th) is similar, with some rapid evolution during a couple of first years, see Figure 5. The saturation of gas in the interfaces rapidly grows up to the maximal allowed value and the gas pressure decreases slightly up to 5 years and then starts to go up. The evolution of the 1rst cell (the closest to the main drift) is however slightly slower than for the other ones, for which the evolution curves are almost identical. We note also that the gas pressure increases within the access drift while the gas saturation decreases slightly in this region. The evolution of the points situated in the hostrock is very slow. The most spectacular variation during this initial period is the gas saturation curve in the interface of the main drift plug. In the middle point p-pu-1 the gas phase disappears completely after 22 years. Since the numerical problems appear at about that time, we suspect that this rapid resaturation is related to the small time steps size required at that time (calculation artefact).

In the following figures, Figure 88 and Figure 89, we show the values of field variables along prescribed lines. It is remarkable that the strong discontinuities in gas saturation are very well resolved. During this initial period three cells show a very similar behaviour, with the cell number 1 being again slightly different, see Figure 89. But the most interesting feature can be seen in Figure 88 in the main plug interface. We notice that the rapid water resaturation of the interface (from about S_w=0.2 at 1 year to S_w=0.67 at 10 years) is very inhomogeneous with large oscillations, which tend to slow down with the time however. The gas pressure is a reconstructed value, so it is important to analyse the primary variables in order to check the origin of the oscillations. It shows up that the liquid molar fraction of hydrogen is being smoothly resolved and that the oscillations are due to the liquid pressure. In this interface the liquid pressure is of about $9e^{+4}$ Pa, while in other parts it is rather of about 10^{+6}Pa. Thus one can suspect that the oscillations are due to the lack of precision of the non-linear solver.

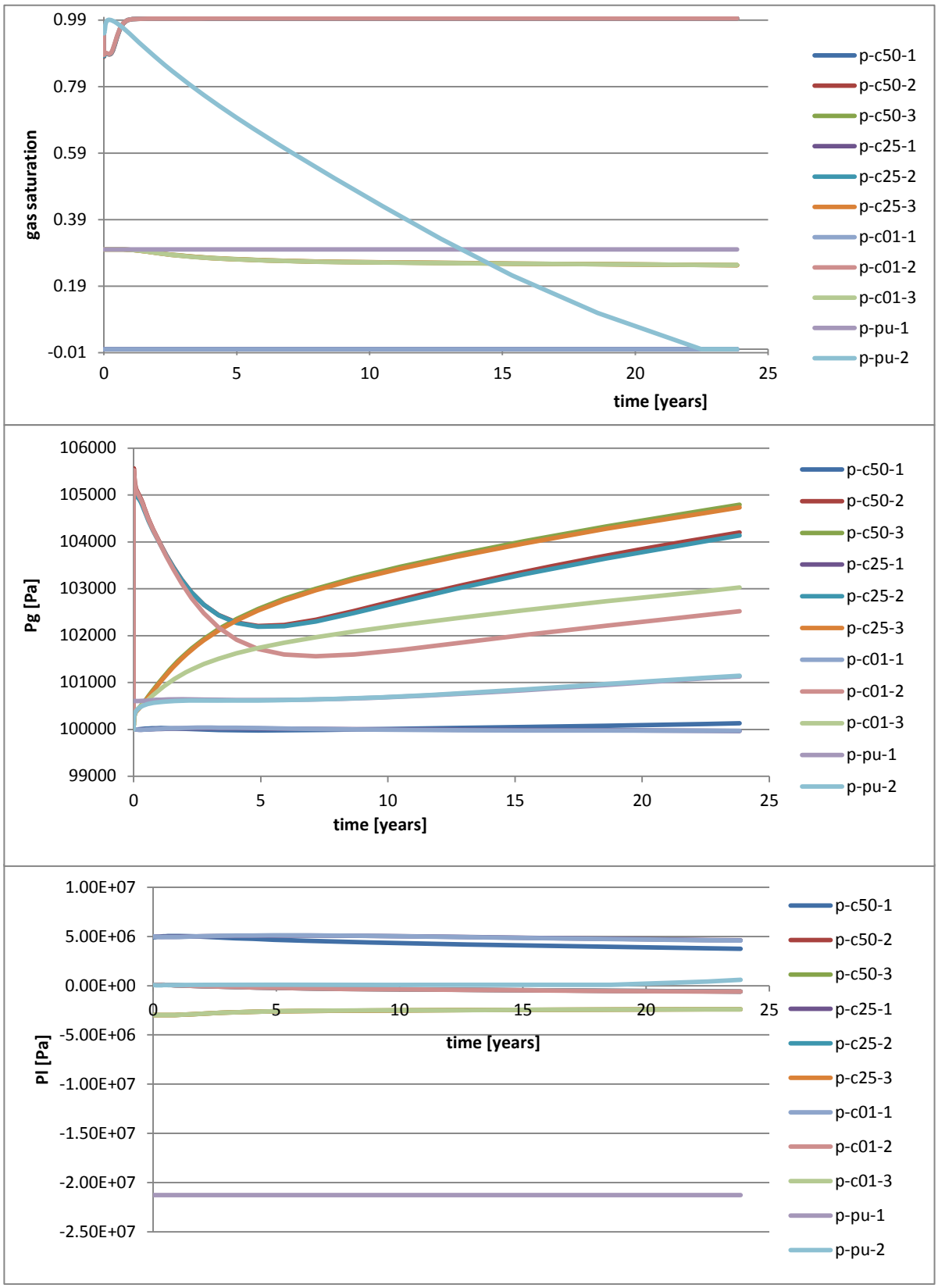

Figure 87 Time series of Pl, Pg and Sg in prescribed output points for the 2D module case.

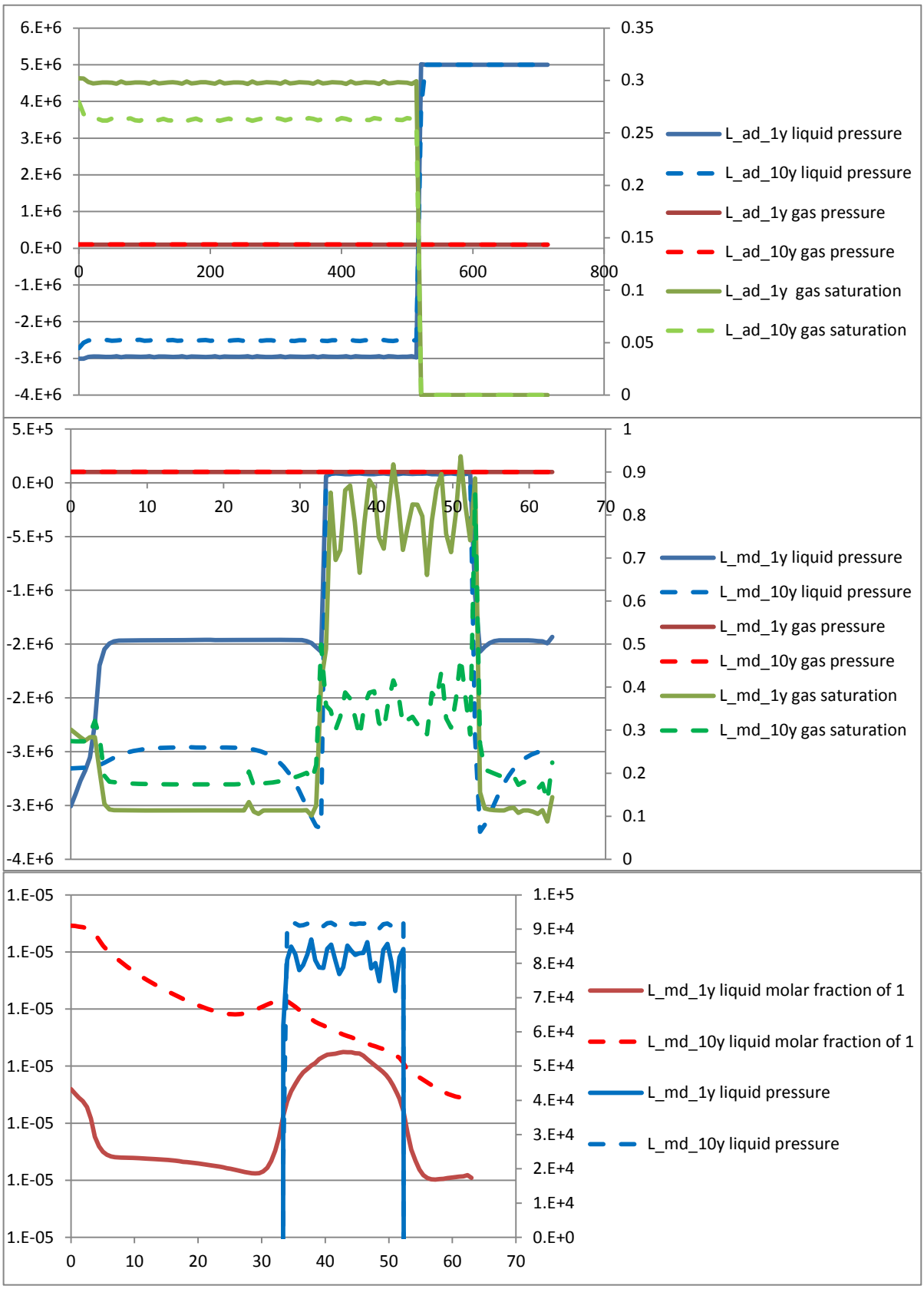

Figure 88 Base case results at 1y and 10y for prescribed lines L-AD and L-MD and a zoom on primary variables in the main plug interface along the L-MD.

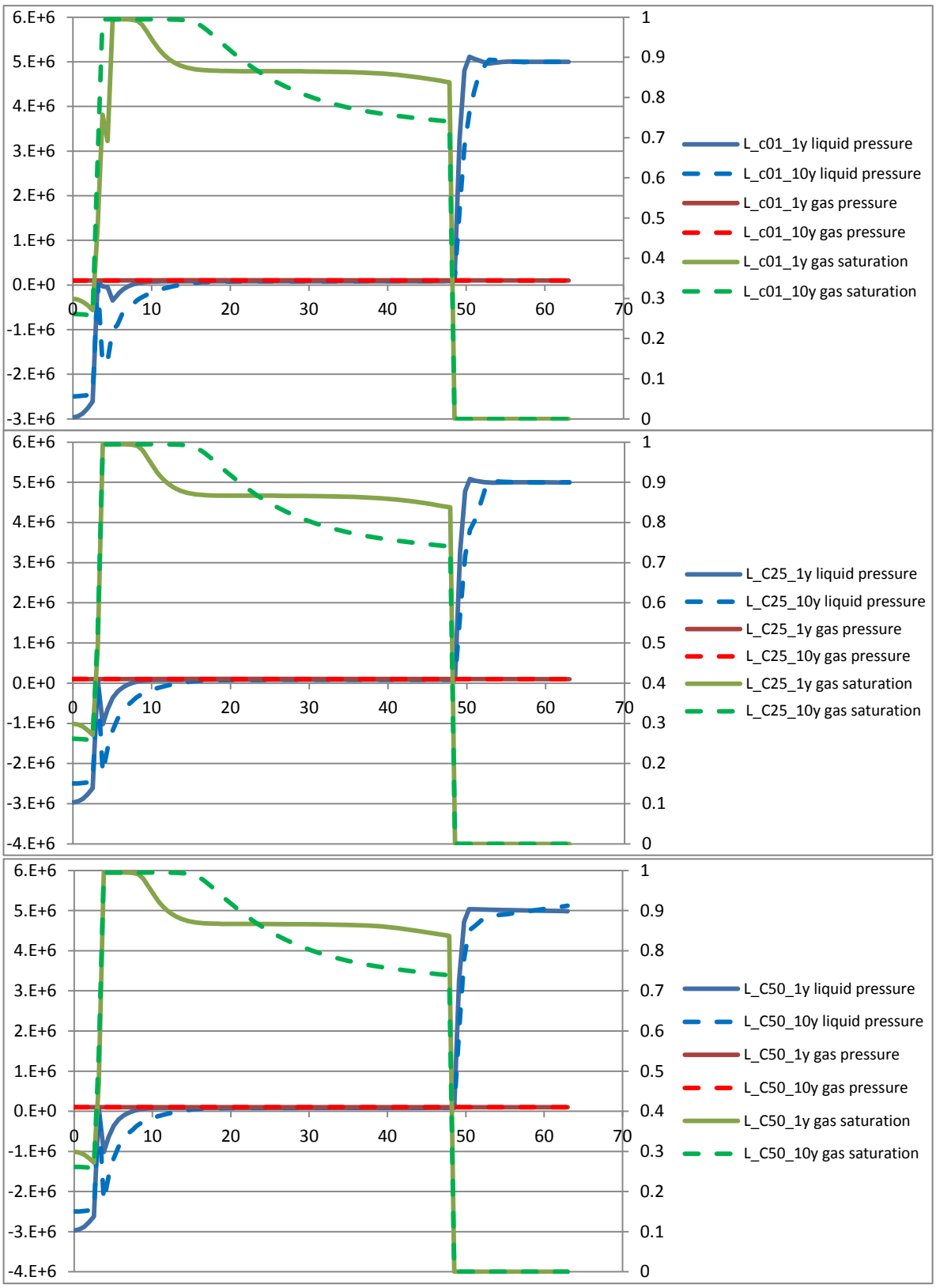

Figure 89 Base case results at 1y and 10y for prescribed lines along three cells (1, 25 and 50) in terms of phase pressures (left axis [Pa]) and saturation (right axis).

3.6.4 Sensitivity Cases

None.

3.6.5 Discussion and Conclusions

We have presented here the first step of the work done on the module scale benchmark. For the moment we have constructed a 2D triangular mesh and were able to represent the half of the module (50 cells) with the same amount of details as in the cell scale case. The resulting mesh consisted of 150 000 of nodes. The results over first 24 years are presented showing a very similar behaviour of cells, the cell number 1 (the closest to the main drift) evolving slightly slower. In the first years the cell interfaces become gas saturated, while the saturation of the access drift vary little from the initial level of 30% during the whole 25 year period of simulation. The interafce of the main drift plug becomes water saturated at 23 years. During first 25 years there is no desaturation of the EDZ and the hostrock. After first 5 years, gas pressure raises everywhere. Further calculations with the current model require very small time steps, which we suspect to be related to the very quick resaturation of the main drift interfaces leading to oscillations in calculated liquid pressure. Thus further work will be concentrated on limiting these oscillations to be able to progress with the simulation. Two possible ways will be explored, namely decreasing the stopping criterion for the Newton iterations and/or implementing a more efficient time stepping scheme.

3.6.6 Lessons Learnt

This second benchmark exercise was the first occasion for us to apply our home developed code diphpom to a supracellular scale. The simple change of space dimensions from 60m to 600m required new tools in order to be able to generate meshes and make the pre-processing - assignment of boundary conditions, material characteristics. The approach needs to be further improved and will be conducted outside of FORGE.

Issues for further consideration

Besides the obvious need to finish 2D simulations on the reference case as presented in this repport, our aim is to seek for parameters combination (source term, host rock porosity and permeability) that would allows us to replace/reproduce 3D calculations of the original benchmark (to be done as well). Due to the prevailing plane symmetry of the module it is very tempting to provide the possibility to replace 3D calculations by 2D ones which would ease the simulations on larger scales (eg. of a repository). We may also apply newly developed Discontinuous Galerkin scheme to this benchmark in order to test the efficiency of this method versus standard finite elements for complex applications.

3.6.7 References

Atkins P.W., Physical Chemistry, W.H. Freeman & Company, 6th edition, 1997
Bourgeat A., Jurak M., Smaï F., Two-phase, partially miscible flow and transport modelling in porous media; application to gas migration in a nuclear waste repository, Computational Geosciences, 13, 29-42, 2009
Couplex-gaz, momas.univ-lyon1.fr/cas_test/Cas_test_couplex_gaz_1.pdf
Emmerich W., Thermodynamics of Nonelectrolyte Solubility, in Developments and Applications in Solubility, ed. Trevor M. Letcher, Royal Society of Chemistry, 2007

Gray C.G., Gubbins K.E., Joslin C.G., Theory of Molecular Fluids: Volume 2: Applications, Oxford University Press, 2011

Helmig R, Multiphase Flow and Transport Processes in the Subsurface, Springer-Verlag, 1997

Horseman, S.T., Higgo, J.J.W., Alexander, J., Harrington, J.F., Water, gas and solute movement through argillaceous media, NEA Report CC-96/1, Paris, OECD, 1996

O. Ippisch, H.-J. Vogel, P. Bastian, 2006, Validity limits for the van Genuchten–Mualem model and implications for parameter estimation and numerical simulation, Advances in Water Resources, Volume 29, Issue 12, December 2006, Pages 1780-1789

Kiran E., Levelt Sengers J.M.H., eds., Supercritical Fluids: Fundamentals for Application, Kluwer Academics, 1994

Krichevsky I. R., Kasarnovsky J. S., Thermodynamical Calculations of Solubilities of Nitrogen and Hydrogen in Water at High Pressures, J. Am. Chem. Soc. 57, 2168-2171, 1935

Lassin, A., Dymitrowska, M., and Azaroual, M., Hydrogen solubility in pore water of partially saturated argillites: Application to Callovo-Oxfordian clayrock in the context of a nuclear waste geological disposal, Physics and Chemistry of the Earth, Parts A/B/C 36, 1721-1728, 2011

MoMaS Research group, Mathematical Modelling and Numerical Simulation for Nuclear Waste Management Problems, http://www.gdrmomas.org/pres-en.html

MoMaS test cases: http://sources.univ-lyon1.fr/cas_test.html

Oladyshkin S., Panfilov M., Hydrogen penetration in water though porous medium: application to a radioactive waste storage site, SRC SimTech, Preprint Series, Issue No. 2011-1, 2011

Smaï F., Développement des outils mathématiques et numériques pour l'évaluation du concept de stockage géologique, Ph.D. thesis of University of Claude Bernard of Lyon, 2009

Wu Y.S., Forsyth P.A., On the selection of primary variables in numerical formulation for modelling multiphase flow in porous media, J. Contam. Hydrol., 48(3-4):277-304. 2001

3.7 LEI contribution

3.7.1 Introduction

In this chapter the work done by Lithuanian Energy Institute (LEI) in the second benchmark exercise within the work package WP1.2 of FP7 project FORGE is presented.

This document is describing the modelling tool, model setup and deviation from the benchmark specification [1]. Also the modelling results of reference case is presented and analyzed.

3.7.2 Model Implementation

Gas transport modelling in the second exercise was performed with original and massively parallel (MP) version of TOUGH2 code [2] using PETRASIM [3] as the pre- and post-processor.

3.7.2.1 Code and Formulation

TOUGH2 is a numerical simulator for nonisothermal flows of multicomponent, multiphase fluids in one, two and three-dimensional porous and fractured media. The EOS5 fluid property module was selected for the description of the thermodynamics of hydrogen gas in this exercise. TOUGH2-MP [4] is designed to perform parallel simulation on multi-CPU computational platforms. More about code and formulation could be found in LEI contribution at cell scale.

3.7.2.2 Benchmark Implementation

The simulation was performed using a physical model (multiphase Darcy's law, with interaction between each phase: dissolution/evaporation and diffusion) as it prescribed in technical specification [1]. The objective of second exercise was to simulate gas production in the cell and understand how gas is moving from a cell toward the drift and finally toward the drift plugs. One of the major problems representing gas transfer in part of repository for radioactive waste is to model simultaneously all gas sources (located in the disposal cells) and the transfer pathways constituted by the network of interfaces, plugs and underground drifts.

3.7.2.3 Grid

According to the benchmark specification, the task of the second exercise consist of an "upstream" and "downstream" half of the module with 50 cells on each side of the access drift. As time varying boundary conditions (gas pressure and saturation) specified on the upstream and downstream ends of the main drift are very similar, thus only an upstream half of the module was taken into account in LEI model due to mirror boundary along the centre of access drift (Figure 90):

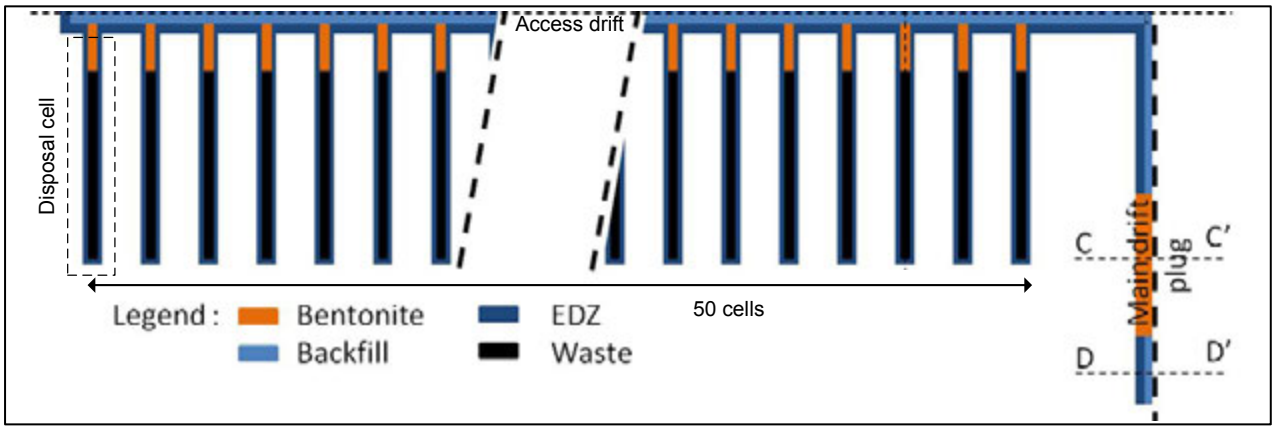

Figure 90 Modelling domain simulated by LEI team

The modelling domain is 3D. The materials in this simulation are argillite (natural host rock), EDZ (Excavation Damaged Zone), EDZ-material interface (material could be waste canisters, bentonite plug or

backfill depending on the position), bentonite plug (cells or main drift) and backfill of the drift. The waste canisters itself are supposed to be impermeable to gas and water and is not explicitly represented in the model. All interfaces considered as centimetre-thick regions and are represented with one layer of grid elements.

Currently PETRASIM offers only rectangular grid elements for mesh building. Therefore, the zones defined as circular sections were represented by rectangular elements with equivalent cross-sectional areas to the benchmark circular cell definition. The complete grid has ~90.000 rectangular elements (Figure 91):

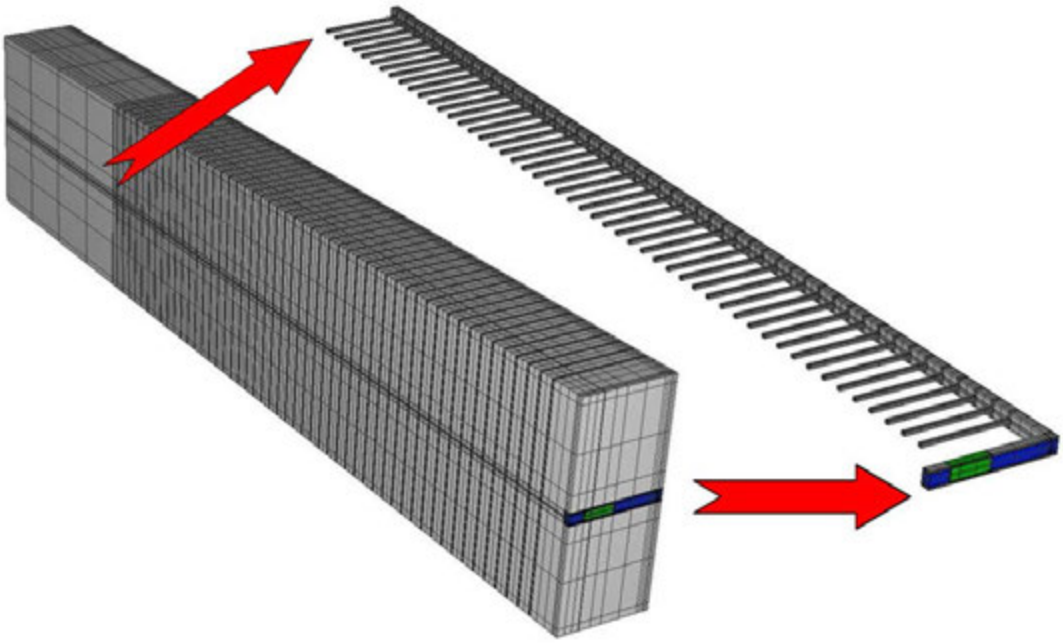

Figure 91 *Grid of LEI model coloured by material type: full model (left) and model pattern without considered host rock (right)*

In order to minimize grid discretization and computation time, plug interface in the main drift was shifted and has the same profile as the interface between backfill and the EDZ (Figure 92). In fact, it is deviation from benchmark specification, because plug interface is between two bentonite blocks instead of interface between bentonite plug and the EDZ.

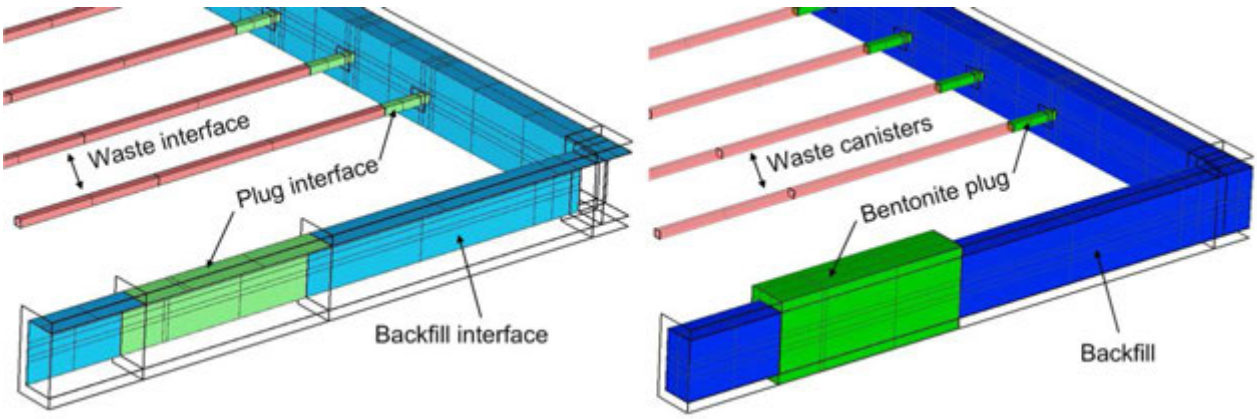

Figure 92 *Visualisation of interfaces (left) and engineered materials (right) in LEI model*

3.7.2.4 Boundary Conditions and Sources

Boundary conditions in LEI model were implemented as prescribed in technical specification. Time varying boundary conditions were implemented precisely using the same approach as in first exercise at cell scale. A gas-source term (100 mol/year/disposal cell) was represented by a simple step function lasting 10.000 years. In the numerical model it was assumed that hydrogen is injected direct into the interface between the canisters and EDZ.

3.7.2.5 Initial Conditions

According to the benchmark specification, gas saturation is 30 % in the bentonite plugs (cell and main drift) and drifts (main and access). 95 % of gas saturation is in all types of interfaces. Disturbed and undisturbed geological medium are fully water saturated and initial groundwater pressure varies linearly from 6 MPa at the bottom to 4 MPa at the top of the model (according to a continuous formulation, the gas and water pressures are the same if only dissolved gas appears). In parts of the model which initially were not fully water saturated, gas pressure is set to be 0.1 MPa. Then water pressure is in capillary equilibrium with the gas pressure and is deduced from the gas pressure and the saturation by applying van Genuchten model associated with each material.

3.7.2.6 Deviations from the specification

Geometry

Only the upstream half of the domain was modelled, assuming symmetry with the downstream half. Also interface in the main drift was shifted and has the same profile as the interface between backfill and the EDZ.

Solubility of hydrogen in water

In the benchmark specification Henry constant is defined to be $7.6 \cdot 10^{-6}$ mol·Pa^{-1}·m^{-3}. In LEI model original value of TOUGH2 Henry constant at 20 °C temperature ($8 \cdot 10^{-6}$ mol·Pa^{-1}·m^{-3}) was used.

Relative permeability of gas phase

Based on the benchmark specification, relative permeability functions for water and gas are expressed by integrating the Mualem prediction model in Van Genuchten capillarity model. The expression for water relative permeability is identical in benchmark specification and original version of TOUGH2. But expressions of gas phase relative permeability are different:

- In benchmark specification $$k_{rg} = \sqrt{1 - S_{we}} \cdot \left[1 - S_{we}^{\frac{1}{m}} \right]^{2m}$$
- In original TOUGH2 (if residual gas saturation S_{gr}=0) $$k_{rg} = 1 - k_{rl}$$
- In original TOUGH2 (if residual gas saturation S_{gr}>0) $$k_{rg} = (1 - S_{we})^2 \cdot (1 - S_{we}^2)$$

The third expression for gas relative permeability function was used in LEI model. Hence non-zero (10^{-6}) residual gas saturation (instead of zero as in benchmark specification) for all materials was assigned. Additional non-zero (10^{-5}) residual water saturation (instead of zero as in specification) for all type of interfaces was assigned too. LEI experiences using TOUGH2 showed that assigning of very low residual gas/water saturations to different materials help to avoid convergence problems in numerical models and accelerate the computations.

Tortuosity model

In benchmark specification tortuosity model is specified as:

$$\tau_0 \tau_\beta = \frac{S_\beta}{\tau_0^2}$$

Original version of TOUGH2 offers three alternative tortuosity models:

- Relative permeability (RP): $\tau_0 \tau_\beta = \tau_0 k_{r,\beta}(S_\beta)$
- Millington – Quirk (MQ): $\tau_0 \tau_\beta = \phi^{\frac{1}{3}} S_\beta^{\frac{10}{3}}$
- Constant diffusivity (CD): $\tau_0 \tau_\beta = S_\beta$

LEI analyses at cell scale showed that Millington-Quirk model determines the highest values of effective diffusion coefficients (especially in high saturation zones) among suggested TOUGH2 models. Higher diffusivity influence on decreased pressure in analyzed system and increased amount of dissolved hydrogen. As some other teams in benchmark studies use Millington-Quirk model for tortuosity, LEI team decided to use this model as well.

Simulation period

According to the technical specification, simulation period is 100.000 years. LEI team submit results for first 10.000 years, while only these results were post-processed due to very long computation time.

3.7.3 Base Case Results

At specific points

The locations of results points are shown in Figure 93:

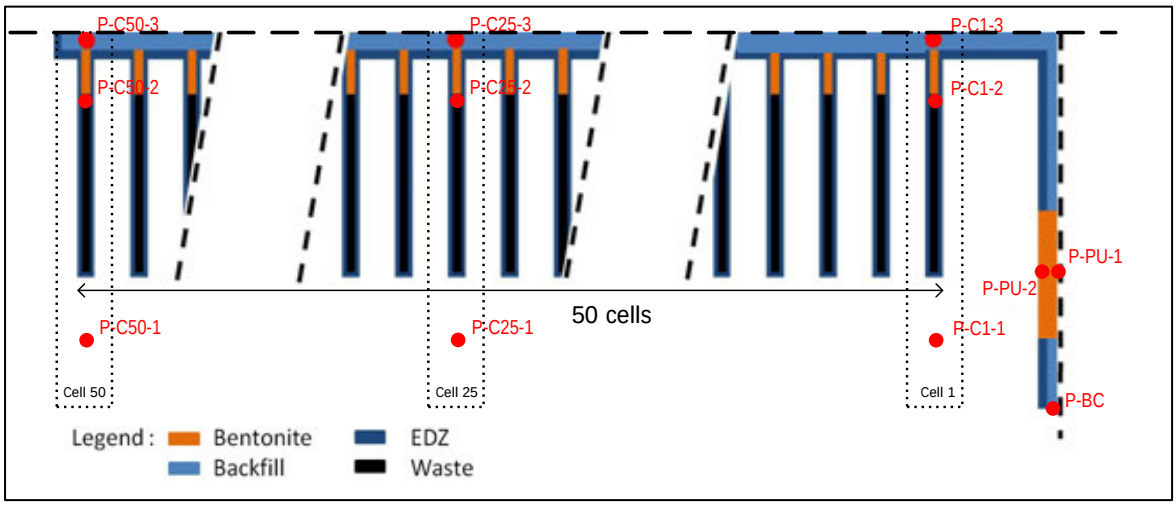

F

interface; P-BC in the end of main drift backfill (time varying boundary condition)

Significant level of gas saturation (Figure 94) is reached in the interfaces during gas generation period, but the evolution with time depends on interface type and the distance from the main drift. Initially all interfaces are almost fully (95 %) saturated with gas. The interface near waste canisters (points P-Cxx-2) is resaturated up to ~30 % within first 10 years. Full desaturation time for waste interface is different and varies between 400 and 1.100 years. Desaturation time is longer for the cells, which are further away from the main drift. Evolution of gas saturation in backfill interface is very similar in all analysed points (P-Cxx-3).

This interface becomes fully gas saturated within first 200 years and keeps such till the end of gas generation. Full desaturation time for plug interface (P-PU-2) is the same as well, but resaturation level is ~50 %, while in backfill interface is ~75 % during gas generation period. Evolution of gas saturation in the main drift plug (P-PU-1) is closely related to implemented time dependent boundary conditions in the end of main drift backfill (P-BC). No free gas was observed in the undisturbed host rock, 5 m away from the end of the cell (P-Cxx-1).

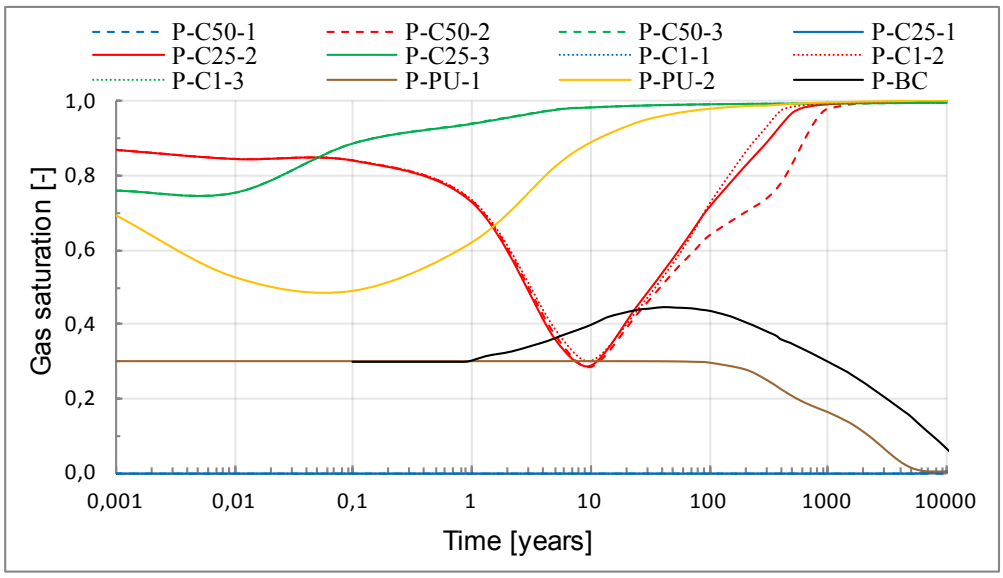

Figure 94 *Gas saturation evolution with time*

As it could be seen in Figure 95, peak pressure of 7.8 MPa was observed in waste and backfill interfaces (P-Cxx-2 and P-Cxx-3) by the end of gas generation period. Such pressure is higher in comparison to first benchmark exercise since observed peak pressure there was 5.7 MPa. The main reason for higher pressure is relative impermeable bentonite plug at the end of main drift, therefore time dependent boundary conditions gives small impact on the modelling results. However mechanical effects on repository and rock structures caused by the pressure build-up that may follow from gas generation are not presumable at module scale as well.

Evolution with time of gas pressure in main drift plug (P-PU-1) and in plug interface (P-PU-1) is very similar and closely linked to prescribed time varying boundary condition at the end of main drift (P-BC). As free gas do not appears in undisturbed host rock (P-Cxx-1), only water pressure profiles are given. As it could be seen, reduction of water pressure in time period between 10 and 5.000 is determined due to initial low pressures in engineered structures.

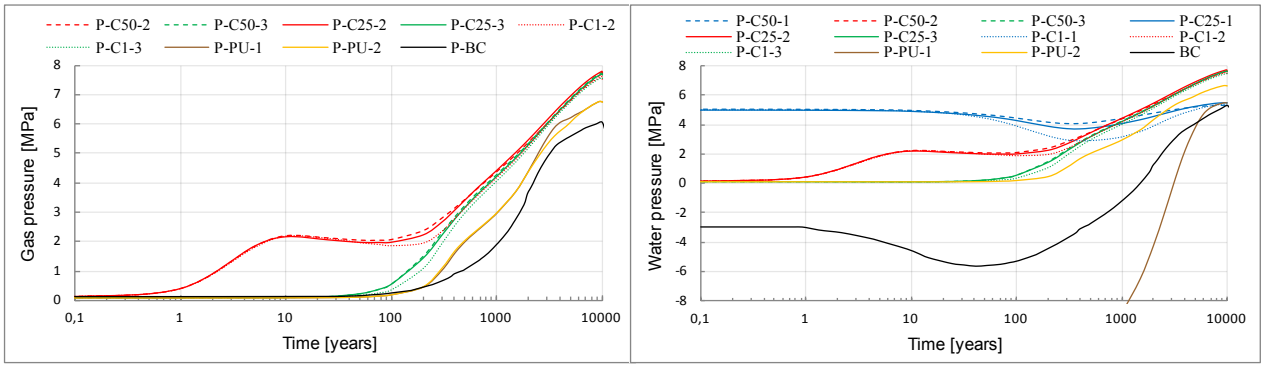

Figure 95 *Gas pressure (left) and liquid pressure (right) evolution with time for specific fluxes*

The locations of surfaces through which fluxes are calculated are shown in Figure 96:

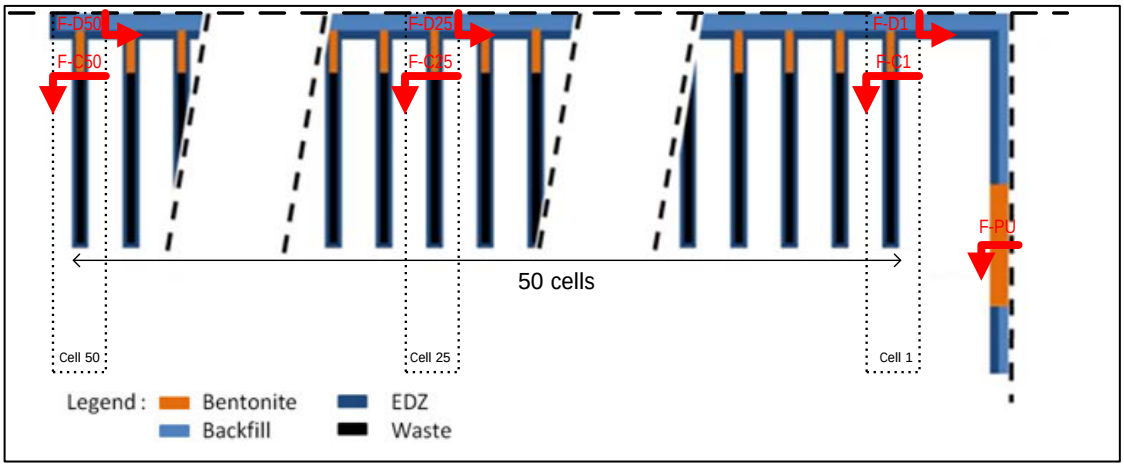

Figure 96 *Schematic representation of flux surfaces and directions of positive flow: F-Dxx through access drift backfill, interface and EDZ toward the main drift; F-Cxx through waste interface and EDZ toward the cell; F-PU through main drift plug and interface toward the end of main drift*

Flow rate of gaseous hydrogen through different surfaces is presented in Figure 97. Total flow rate of gas generated in the module and gas generated in single disposal cell are showed in this figure as well.

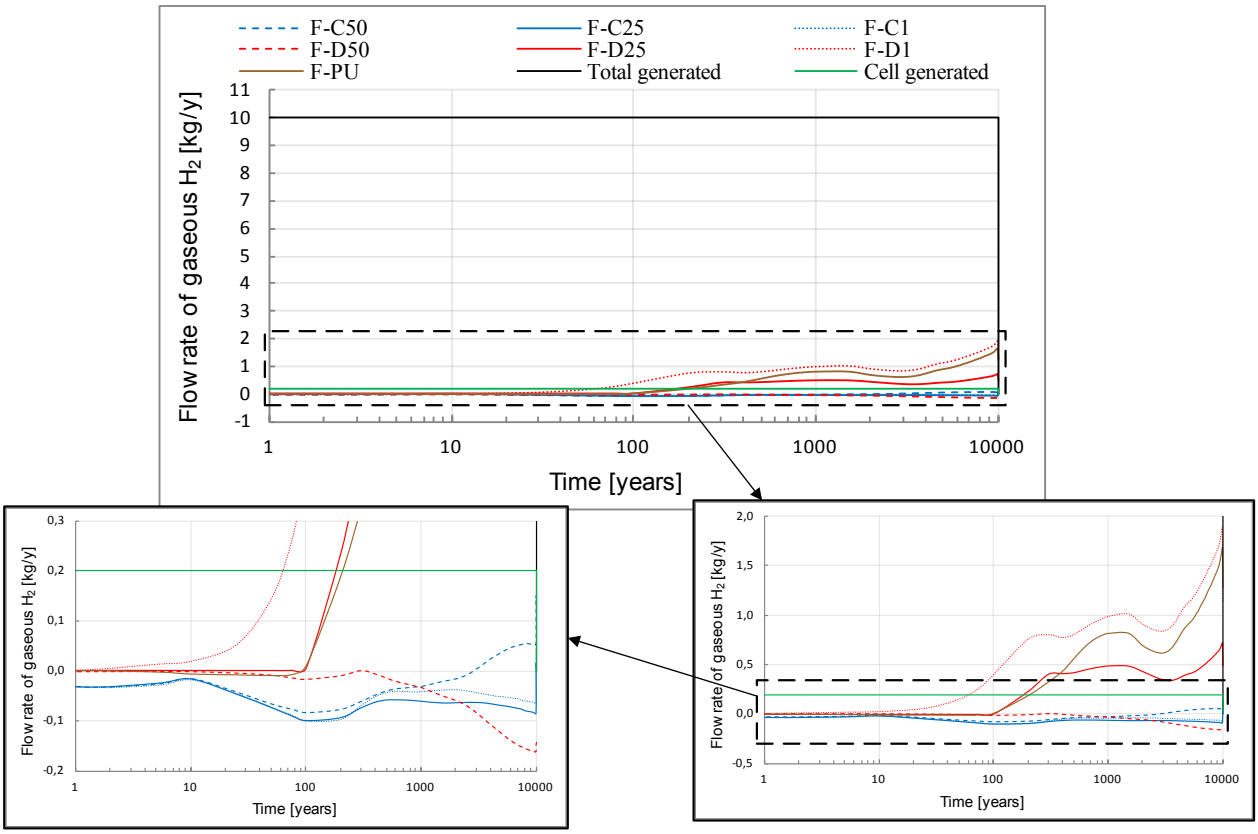

Figure 97 *Flow rate of gaseous hydrogen through different surfaces*

Total mass of gaseous hydrogen transported through analysed surfaces is presented in Table 2.

Table 2 : Total mass of gaseous hydrogen transported through different surfaces

Type of flux	Total transported mass, kg						
	F-C1	F-C25	F-C50	F-D1	F-D25	F-D50	F-PU
Gaseous hydrogen	-394	-652	301	8113	2914	-1214	5991

As could be seen in Figure 97, gas generated in the disposal cells is transported toward the access drift (surfaces F-Cxx) within first 3.000 years. But flux of gaseous hydrogen is reversed in the cell furthest away from the main drift (surface F-C1) beyond this time due to pressurisation in the module. Gas moves from the access drift toward the disposal cell in this case. Table 2 shows, that ~20 % (394 kg out of 2.000 kg) of generated gas in cell 1 is transported by advective flow toward the access drift, while remaining part dissolves and diffuse toward the host rock. In the centre of the module (cell 25) total transported mass of gaseous hydrogen toward the drift is higher: ~ 33 % (652 kg out of 2.000 kg).

Concerning gaseous hydrogen flux in different parts of access drift, the results are consistent with fluxes toward the cells. The flux is negative through surface F-D50 (gas moves toward the cell 50), while rest of fluxes are positive (gas moves toward the main drift) and progressively growing. For comparison, ~3 % (2.914 kg out of 100.000 kg) of generated gas is transported through F-D25, while ~8 % (8.113 kg out of 100.000 kg) is transported through F-D1. As gas reaches relative impermeable plug of the main drift, only ~6 % (5.991 kg out of 100.000 kg) of generated gas leaves the module in gaseous form. For safety aspect it is important that gaseous hydrogen passes the plug of main drift after ~100 years past repository closure.

Flow rate of dissolved hydrogen out of the module and comparison to gas generation rate are presented in Figure 98. It was observed that flow rate of dissolved hydrogen out of the module is very similar for both boundaries (upper and lower). Also it could be seen, that peak flow rate of dissolved H_2 is much lower in comparison to total gas generation rate, but higher than gaseous H_2 flux out of bentonite plug in the main drift. However total amount of dissolved hydrogen transported out of the module over upper and lower boundaries is 32.767 kg (~35 % of generated gas) during gas generation period. Dissolved hydrogen passes the outer boundaries after ~1.000 years past repository closure.

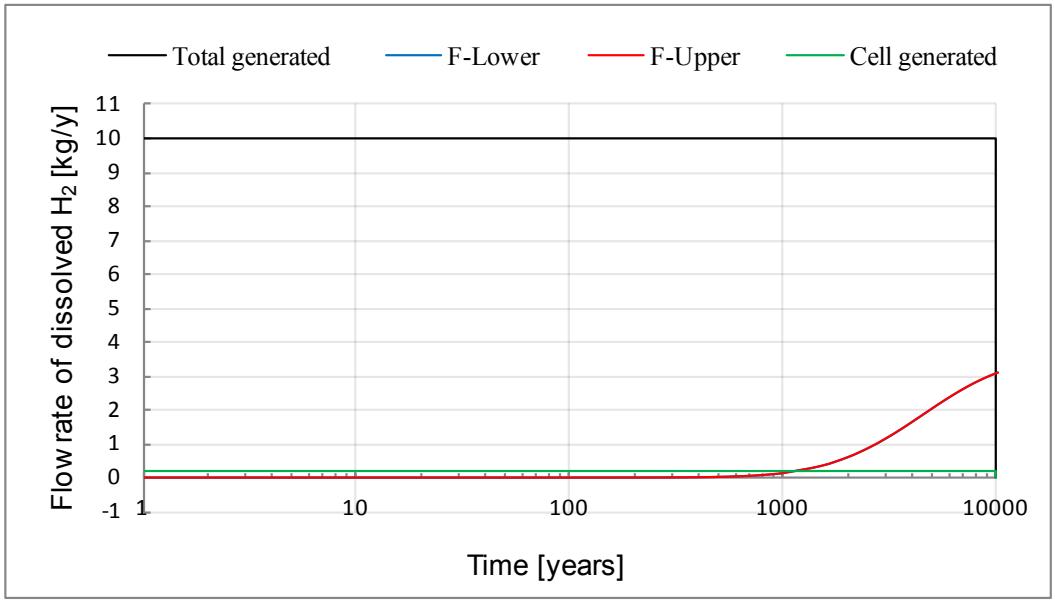

Figure 98 Flow rate of dissolved hydrogen out of the module

About 41 % of generated gas leaves the module during gas generation period. Major part (35 %) diffuses in dissolved form over the top and the bottom of the module, while remaining part moves in gaseous form out of the bentonite plug in the main drift.

3.7.4 Conclusions

The second benchmark exercise has been performed with original version of TOUGH2-MP code using PETRASIM as the graphical interface. Since modification of TOUGH2 source code were not possible due to application of PETRASIM, some deviations from technical specification, related to the estimation of gas phase relative permeability and tortuosity model could not be avoided in LEI model. Due to complex task, complicated geometry and long computation time, only upstream half of the model domain is modelled and results only for gas generation period is presented.

The main results of the base case could be summarised as follows:

- Peak pressure (7.8 MPa) was observed in waste and backfill interfaces by the end of gas generation (10.000 years);
- Significant level of gas saturation is reached in all types of interfaces, backfill, bentonite plug and engineered disturbed zone (EDZ). Minor amount of gas concentrates in some parts of undisturbed geological media;
- Gas moves along cells to access drift and main drift by advective flow, as well as out into host rock by diffusion;
- About ~41 % of generated gas leaves the module during gas generation period. Major part (35 %) diffuses in dissolved form over the top and the bottom of the module, while remaining part moves in gaseous form out of the bentonite plug in the main drift.

3.7.5 References

1. FORGE (2010). FORGE WP1.2: Benchmark specifications at a sub set of a repository containing several tens of HLW cells (module scale).
2. K. Prues, C. Oldenburg, G. Moridis. TOUGH2 Users's guide, Version 2.0. Lawrence Berkeley National Laboratory, LBNL-43134, 1999,198 p.
3. PetraSim user manual, Version 5.0, Thunderhead engineering, 2010.
4. K. Zhang, Y. Wu, K. Prues. 2008. User's Guide for TOUGH2-MP - A Massively Parallel Version of the TOUGH2 Code. LBNL-315E. 108 p.

3.8 ENSI/IFSN contribution

3.8.1 Introduction

Hydrogen gas is formed by anaerobic corrosion of metal components in a deep geological repository. FORGE aims to investigate the importance in relation to nuclear safety of the processes caused by gases in the near and far field of a deep geological repository. This includes the gas generation and the gas transport. The project lasts 4 years from 2009 to 2013 and is divided into five work packages. ENSI participates in the first work package WP1 (Treatment of gas in performance assessment). This work package is divided into two parts WP1.1 and WP1.2. The objective of WP1.1 is to review the state of the art of gas generation and transport in a geological repository for nuclear waste. Based on research coming from inside and outside of FORGE a compilation of technical and scientific knowledge has been made regarding gas aspects in a deep geological repository. WP1.2 aims to define and perform comparative safety-relevant calculations regarding gas transport in a stepwise approach from a cell scale, module scale until the repository scale. In this report the results of ENSI concerning the second benchmarks will be presented. The model for the module scale and the repository scale are represented in the Figure 99 and Figure 100. In this stepwise approach each model is included in the next one as it can be seen in these figures.

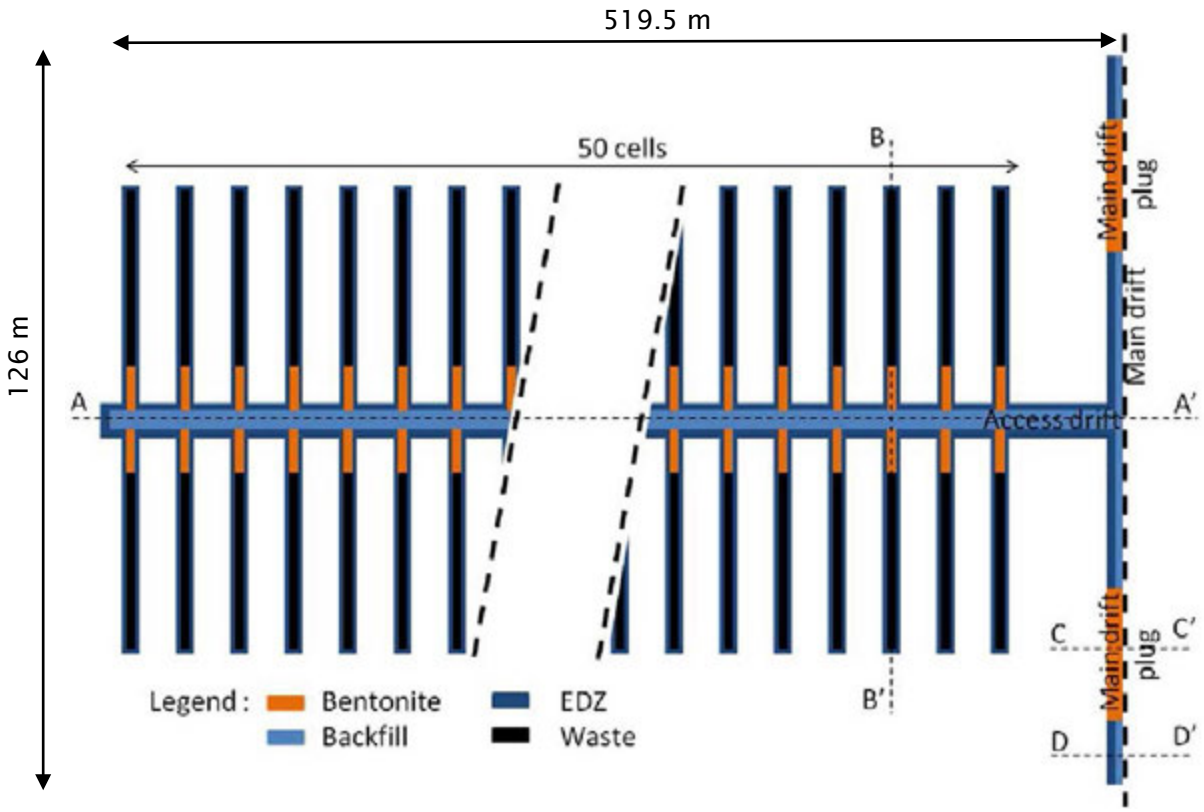

Figure 99 *Domain of the model proposed for the second benchmark exercise (module scale) [1].*

The module scale model implied, because of its geometric complexity, the acquisition and development of new software tools to be able to pre-process models with between 100'000 and one million nodes. For the second and third stage of the sectoral plan ENSI will have to evaluate full scale models of repositories. The second benchmark was thus a good exercise for the preparation of gas transport calculations in repository scale models.

The third benchmark exercise represents another scale in the modelling, in which an upscaling approach is practically unavoidable. Even for the second benchmarks exercise there were some teams like ENSI that in some parts use some upscaling approaches to obtain the results. From the point of view of computing programs in this field is the size of the model for the third benchmark exercise beyond the limit of what most of the current computing programs are able to pre-process. It is then when the upscaling approaches

are very appropriate. It is in this regard important to mention that not only the first benchmark but also the second and third contain small interfaces close to the waste canisters and bentonite plugs and also surrounding the access and main drifts. These interfaces compromise not only the convergence as it was explained in the ENSI contribution to the cell scale benchmark report but also increases the necessary number of mesh elements that need to be implemented, without using an upscaling approach, in order to represent accurately these tiny elements.

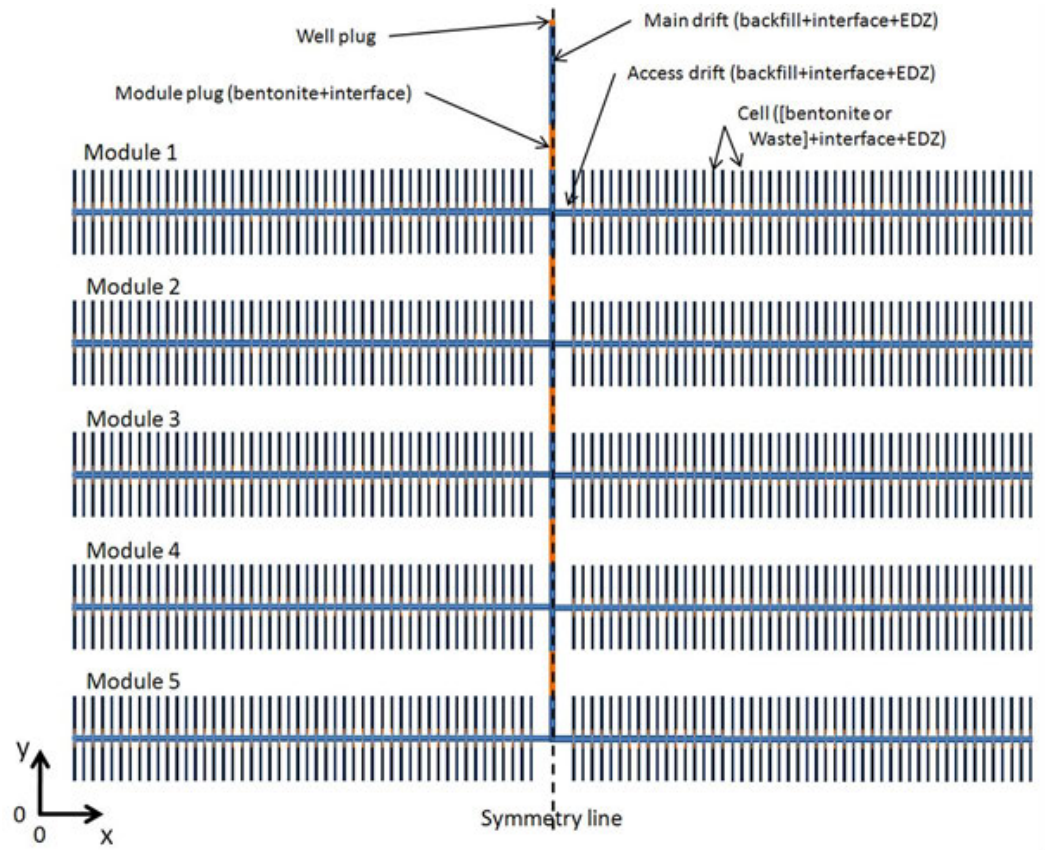

Figure 100 Domain of the model proposed for the third benchmark exercise (repository scale) [2].

The second benchmark required of ENSI some preparations and developments of the software tools to be able to create an adequate discretization for such a big model. That is why the first results of the second benchmark were obtained in the first quarter of 2013. Due to this preparation and development work no results could be obtained for the third benchmark within the project schedule. ENSI realized after the conclusion of the second benchmark that for the realization of the third benchmark a correct choice of the upscaling approach is necessary. The software tools to solve the exercise would no differ much of the ones used in the second benchmark. This third benchmark can be used by ENSI to check upscaling approaches. The results obtained by some groups for this benchmark can be used by ENSI in the future as reference results within another benchmark about upscaling outside the FORGE project.

It was clearly established from the beginning of the project by the team members that these benchmarks do not represent the reality of a particular disposal concept of a country but they represent a numerical exercise to compare results of different teams. The preparation and the realization of the benchmark were made in view of future reviews of similar calculation by ENSI during the sectoral plan. In this respect the priority was set on the preparation of the technical tools to perform this kind of calculations instead of trying to analyze the correct models and parameters. It is in this sense that the results presented here by ENSI have to be understood and not as the definitive results about the complete behaviour of the gas in a deep geological repository. They have to be seen as results of a numerical exercise performed by several teams and ENSI with currently available software tools. These numerical calculations allow us the acquisition and preparation of the necessary software tools and its implementation by comparing with the results of

other teams, in particular to determine the order of magnitude of the results and of their course of variation. There are some statistical errors related to the programs and also to the simplifications used by the different teams. Moreover, the results of the calculations were not compared to measurements coming from laboratory or field experiments what reinforces the thesis of the no interpretation of the results as the definitive behaviour of the gas in a geological repository but as reference for the order of magnitude of what in principle the measurements should provide. ENSI would like to remark here the importance of the combination of numerical results with measurements in order to understand correctly the processes occurring in the underground.

The benchmark exercises were from the numerically point of view very challenging and therefore all teams have to use different, sometimes code depending, kind of simplifications and approximations to obtain results. This explains together with the use of different codes the differences in some of the results. Despite these simplifications the results show concerning their range and their course of variation a good agreement. A lot of effort was put by ENSI into the correct implementation of the exercises avoiding as much as possible the use of simplifications. That was possible in the first exercise but in the second exercise some simplifications had to be made in order to avoid convergence problems. These convergence problems have to be understood more as a decrease of the speedup of the calculation rather than convergence problems causing a breakdown of the calculations, what sometimes but rarely happened.

The results obtained by ENSI of the second benchmark (module benchmark) exercises within the work package WP1.2 of FORGE will be described in this report. This chapter is divided into seven parts. In the next two chapters 3.8.2 and 3.8.3 a general description of the codes used and of the mathematical models will be presented. The third part 3.8.4 will deal with the implementation of the specifications of the benchmark. The fourth part 3.8.5 will show a selection of some results of the first benchmark exercise. The fifth 3.8.6 part will show the conclusions. In this benchmark no sensitivy analysis was prescribed.

3.8.2 Codes Used for the Calculation

The code chosen to perform the numerical simulations is TOUGH2 (Transport of unsaturated groundwater and heat), a general purpose numerical simulation program for multi-dimensional fluid and heat of flows of multiphase, multicomponent fluid mixtures in porous and fractured media [3]. It is applicable in geothermal reservoir engineering, nuclear waste isolation, environmental assessment and remediation and flow and transport in variably saturated media and aquifers. It is specially the two-phase flow capabilities, which are of concern in the calculations envisaged in this report. The program is developed and provided by the Lawrence Berkeley National Laboratory.

The first simulations for the FORGE project were conducted with TOUGH2 but after some difficulties such as the time-dependent boundary conditions or the long computational times it was decided to use the recently acquired program TOUGH2-MP to perform the numerical simulations for this exercise. TOUGH2-MP is a parallel version of the TOUGH2 code developed also by the Lawrence Berkeley National Laboratory [4].

ENSI acquired the program TOUGH2-MP in November 2009 and in January 2010 was decided to use TOUGH2-MP to implement the time-dependent boundary conditions and to increase the speedup of the calculations. The compilation and installation of the code took longer than expected. Our computer cluster consists of an IBM AIX machine with 4 nodes and each with 32 processors. This system was not included among the systems in which the program was tested. Therefore the compiling options had to be adapted to our system and additional features had to be installed in our system. The code needs also the external libraries AZTEC and METIS. The compilation of these libraries was also system-dependent and besides no compiling option was specified for our system.

After the installation of TOUGH2-MP some tests were performed successfully with inputs included in the distribution. The input for FORGE was implemented and adapted to the code TOUGH2-MP; in fact there are some slight differences between the inputs for the two codes TOUGH2 and TOUGH2-MP. Unfortunately many problems were found, related to the installation of the code and also related to the input file and our simulations could not be run with the program TOUGH2-MP. The input file was refined and the installation and compilation options were optimize but there were still problems. The input file was checked by the authors of the code in LBNL and no problem was found except that it run a little slow. In the meantime the input was tested again but with the module EOS3 (TOUGH2 module in which the gas phase consists of air instead of hydrogen like in the EOS5 module) and the code worked with this input. After some months of extensively checking of the code, a bug related to our computer architecture was found in the code, after the correction of this bug the input worked perfectly. In comparison with other gas transport simulations performed by ENSI, we soon realized that the input run relatively well at the beginning but after more or

less 100 years the code starts slowing down. The reason of that was that ENSI used in the first simulations two layers of mesh elements for the interface. Due to the small dimensions of the node elements of the grid especially in the interface the code run very slowly. To increase the size of the elements the two layers of interface were reduced to one layer and the computational time of the simulations was then improved.

3.8.3 Numerical Formulation

The basic mass- and energy balance equations solved by TOUGH2 can be written in the general form [3]:

$$\frac{d}{dt}\int_{V_n} M^k dV_n = \int_{\Gamma_n} F^k \cdot n d\Gamma_n + \int q^k dV_n \qquad (1)$$

The integration is over an arbitrary subdomain V_n of the flow system under study, which is bounded by the closed surface Γ_n. The quantity M appearing in the accumulation term (left hand side) represents mass or energy per volume, with κ = 1… NK labeling the mass components (water, air, H_2, solutes, etc.), and κ = NK + 1 the heat "component." F denotes mass or heat flux and q denotes sinks and sources. A normal vector n is defined on surface element $d\Gamma_n$, pointing inward into V_n.

The continuum equations (1) are discretized in space using the integral finite difference method (IFD; [5, 6]). Introducing appropriate volume averages, we have:

$$\frac{dM_n^k}{dt} = \frac{1}{V_n}\sum_m A_{nm} F_{nm}^k + q_n^k \qquad (2)$$

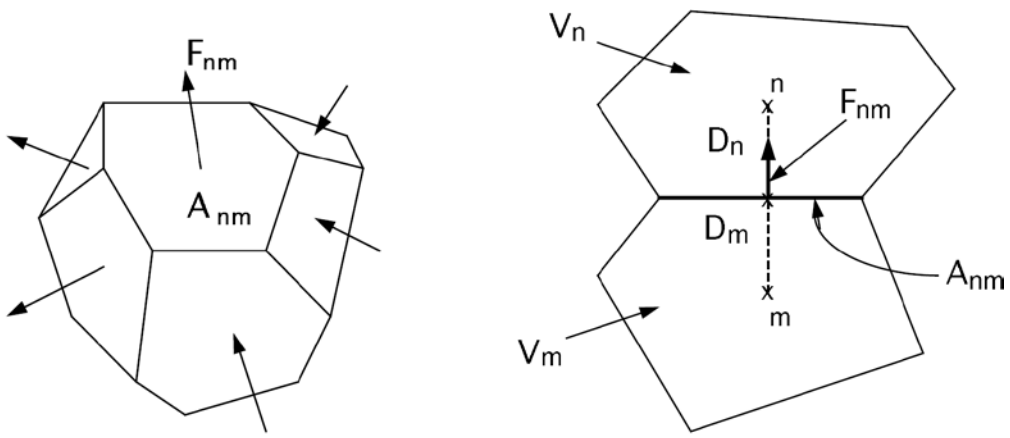

Figure 101 Space discretization in the integral finite difference method [3].

Time is discretized as a first-order finite difference. The flux and sink and source terms on the right-hand side of Eq. (2) are evaluated at the new time level, $t_{k+l} = t_k + \Delta t$, to obtain the numerical stability needed for an efficient calculation of multiphase flow. There are NEL nodes for which Eq. (2) has to be solved and NK+1 equations. Accordingly there are NEL x NK+1 independent primary variables $\{x_i;\ i = 1\ldots \text{NEL x NK+1}\}$ which completely define the state of the flow system at time level t_{k+l}. The time discretization results in the following set of coupled non-linear, algebraic equations:

$$R_{n,t+1}^k = M_{n,t+1}^k - M_{n,t}^k - \frac{\Delta t}{V_n}\left\{\sum_m A_{nm} F_{nm,t+1}^k + q_{n,t+1}^k\right\} = 0 \qquad (3)$$

These equations are solved by Newton/Raphson iteration, which is implemented as follows. An iteration index p is introduced and the residuals $R^k_{n,t+1}$ in Eq. (3) are expanded at iteration step p + 1 in a Taylor series in terms of those at index p. Retaining only terms up to first order, for each volume element (grid block) V_n, there are NEQ equations (κ = 1, 2, ..., NEQ; usually, NEQ = NK + 1), so that for a flow system with NEL grid blocks Eq. (4) represents a total of NEL x NEQ coupled non-linear equations for the increments $(x_{i,p+1} - x_{i,p})$:

$$-\left.\frac{\partial R^k_{n,t+1}}{\partial x_i}\right|_p (x_{i,p+1} - x_{i,p}) = R^k_{n,t+1}(x_{i,p}) \qquad (4)$$

3.8.4 Benchmark Implementation

In the last quarter of 2010 a second benchmark exercise in a module scale was defined [1]. The model for a module in the second benchmark is shown in Figure 99. The repository is divided into 10 modules and each module contains 100 waste tunnels, 50 at each side of the access drift. The module contains an access drift in the middle that connects all the waste tunnels of the module. The access drift ends in the main drift which connects all the modules. In comparison with the cell scale benchmark are the dimensions of the module scale much larger and the number of elements of the mesh increases by about a factor 100. In order to implement such big models ENSI undertook a program to acquire a meshing program and to build a conversion into Tough2. This is still an ongoing work, of which this benchmark constitutes a first test and a paper related to this work is going to be published in the next months.

The model for the second benchmark is shown in Figure 102. The waste and bentonite plugs have all the same circular sections. The section of the access drift and main drift are squared and identical. The cells are positioned at mid height of the access drift and at mid height of the whole calculation argillite layer that has a thickness of 150 m.

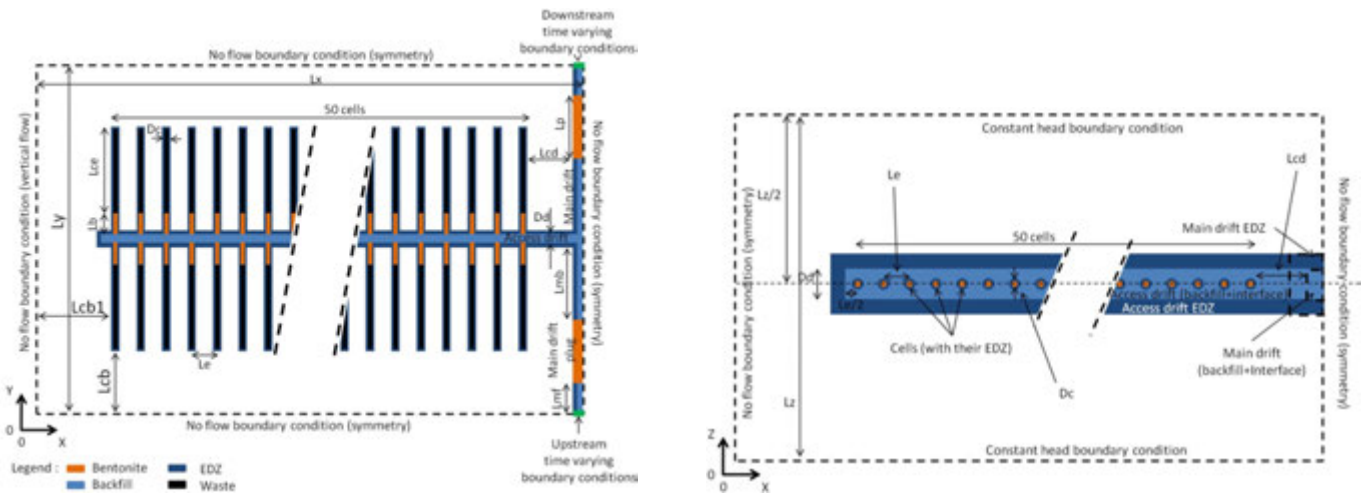

Figure 102 *Horizontal and vertical dimensions as well as boundary conditions for the model of the second benchmark [1].*

The values of the parameters represented in Figure 102 are listed in the Table 3.

Table 3 : List of all parameters about the dimensions of the model for the second benchmark [1].

Parameter description	Name	Value
X total extension of the simulation domain	Lx	714 m
Y total extension of the simulation domain	Ly	126 m
Z total extension of the simulation domain	Lz	150 m
Distance between cell end (with interface, without EDZ) and the boundary in the Y direction	Lcb	15 m
Distance between outer wall of the last cell (#50 - with interface, without EDZ) and the boundary in the X direction	Lcb1	200 m
Length of the bentonite plug in the cell (without interface)	Lb	5 m
Length of "waste zone" in the cell (with interface)	Lce	40 m
Distance between axes of two adjacent cells	Le	10 m
Cell diameter (with interface, without EDZ)	Dc	1 m
Access and main drifts side length (with interface, without EDZ)	Dd	6 m
Length of the bentonite plug in the main drift (without interface)	Lp	20 m
Distance between outer wall of the access drift (with interface, without EDZ) and end (without interface) of the main drift plug	Lmb	30 m
Distance between end without interface) of the main drift plug and external boundary	Lmf	10 m
Distance between outer wall of the main drift (with interdface, without EDZ) and outer wall of the first cell (with interface, without EDZ)	Lcd	20 m
Extension of interface (between waste-argillite, backfill-argillite and bentonite-argillite). Not mentioned in the figures	wi	1 cm
Extension of cell EDZ. Not mentioned in the figures	Cedz	0,5 m
Extension of access drift and main drift EDZ. Not mentioned in the figures	Dedz	1 m

The material parameters for the second benchmark are very similar to the parameter used in the first benchmark and listed in the ENSI contribution to the first benchmark report. A detailed description of the model and of the specifications can be seen in the document [1]. In this report the focus is on the implementation of the specifications by ENSI.
At the beginning a mesh with about 1'200'000 elements was created containing the definition of the interfaces of 1 cm thickness with one layer of mesh elements. It was soon realized that the calculations did not converge soon enough with time steps of about 1.0×10^5 seconds. As next step another mesh of about 863'772 nodes without an explicit interface was built and this was the mesh used to obtain the results presented in this report. With this simplification the time steps increase by a factor between 100 and 1'000 and so the calculations time decreases considerably. The calculations were performed until 60'000 years when the main variables of the system are stationary.

Figure 103 shows a transversal cut (perpendicular to the waste tunnels) of the mesh used for the calculations. The waste tunnels were represented as cylindrical elements as prescribed in the exercise. Along the waste tunnel an EDZ ring surrounds first the waste cell an then the bentonite plug. There is an interface between the EDZ and the cell as well as between the EDZ and the bentonite plug. This interface was originally included in the mesh but due to the increase of the calculation time it was decided to use an upscaling simplification and to include the interface in the EDZ by defining part of the EDZ with intermediate properties between the interface and the EDZ.

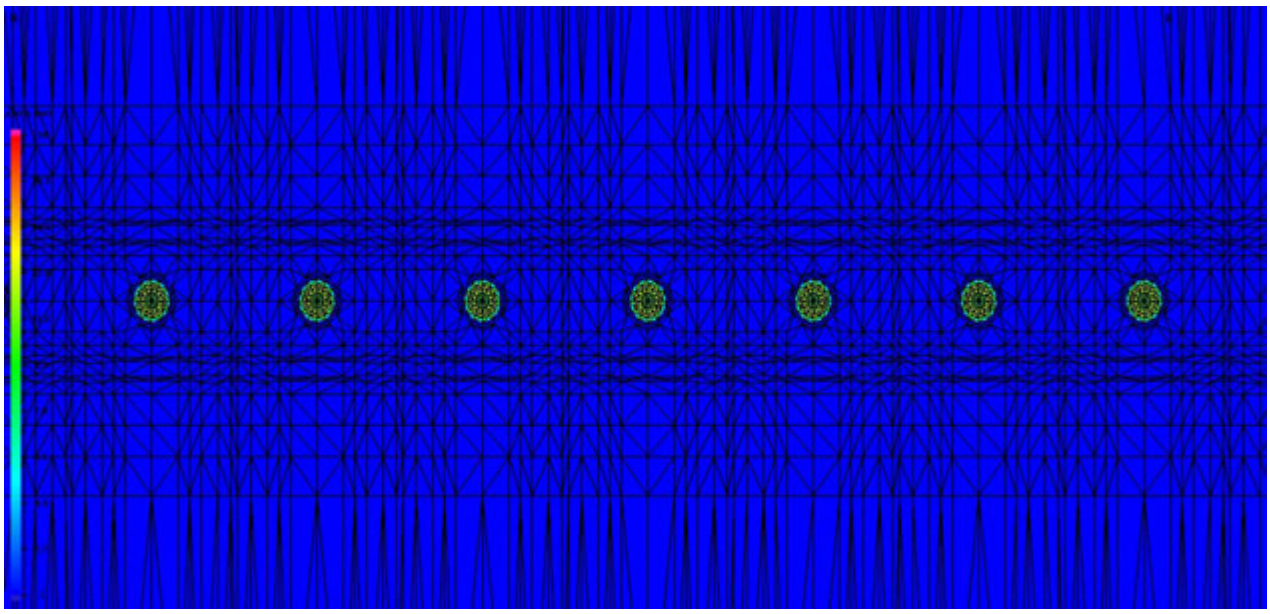

Figure 103 Detail of the mesh: Transversal cut of the cylindrical waste tunnels.

Figure 104 shows a longitudinal cut of the mesh for the module close to the main drift. The access drift as well as the main drift have a rectangular cross section as specified in the exercise. The access drift contains a backfill and it is surrounded by an EDZ. Between the EDZ and the backfill there is also an interface. Like before to simplify the model the interface was integrated in the EDZ and backfill. The main drift contains two bentonite plugs and the rest consists as for the acess drift of backfill and of a surrounding EDZ. In between there is also an interface that was integrated in the EDZ and in the backfill.

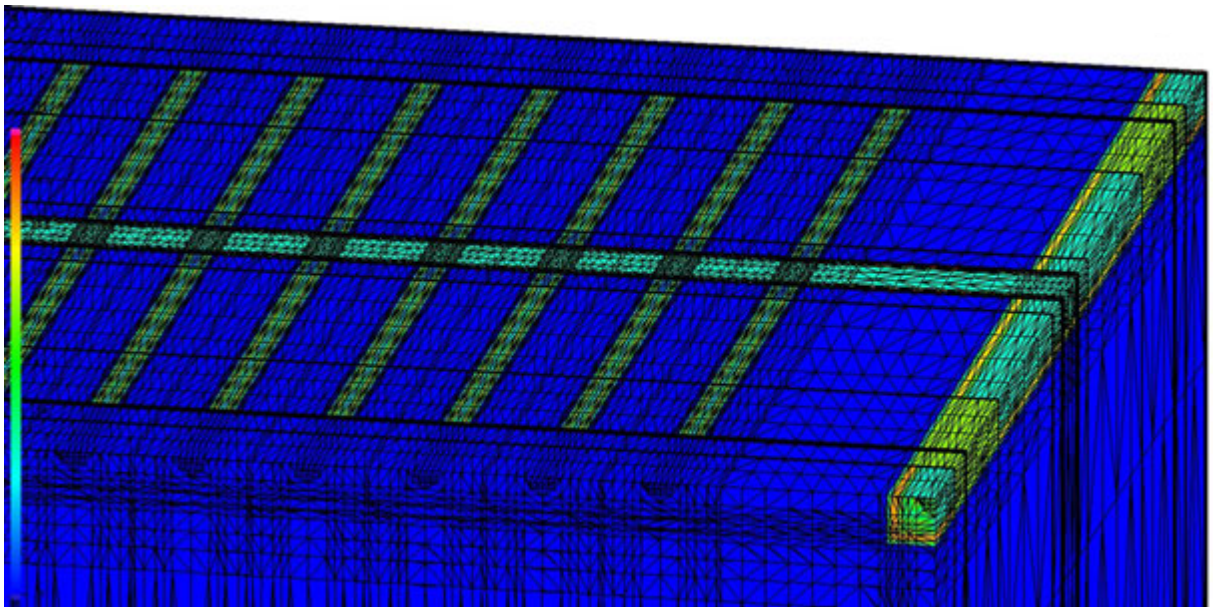

Figure 104 Detail of the mesh: Longitudinal cut of the module close to the main drift.

3.8.4.1 Models for the Gas Relative Permeability and Diffusion

The models for the relative permeability and for the diffusion prescribed in the exercise could not be implemented exactly as prescribed in [2]. The reason is that the code runs much slower with the prescribed

relative permeability models than with the default options of TOUGH2. Based on the big number of node elements at which the transport equation has to be solved, it was decided to use the default options for the relative permeability. In comparison with the first benchmark were the calculations of the second benchmark much more sensible to changes in models and parameters. These changes result in larger calculation times.

According to the prescriptions in the second exercise, the relative permeability for water is expressed by the Van Genuchten model:

$$k_r^w = \sqrt{S_{we}}\left[1-\left(1-S_{we}^{1/m}\right)^m\right]^2 \qquad (5)$$

k^w_r : relative permeability for water (-)

This expression is the same as the one for the Van Genuchten-Mualem model in the TOUGH2 code.

The relative permeability for gas is expressed similarly in the exercise as:

$$k_r^g = \sqrt{1-S_{we}}\left[1-S_{we}^{1/m}\right]^{2m} \qquad (6)$$

k^g_r : relative permeability for gas (-)

The expression (14) is not available in TOUGH2 therefore the code was changed in order to be able to use this expression. The calculations of the second benchmark run much slower with (14) and it was therefore decided to use the usual option of the TOUGH2 code, namely:

$$k_r^g = (1-S_{we})^2\left[1-S_{we}^2\right] \qquad (7)$$

In the first benchmark the prescribed formula (14) and also (15) were used and there were no differences between the results of the two calculations but solely in the calculation times.

The diffusion coefficient of dissolved H2 in the binary H2/water-vapour mixture of the porous medium is specified in the second benchmark as:

$$D^g_{H_2/vap} = (1-S_w)\left(\frac{\phi}{\tau^2}\right)D_0\left(\frac{P_0}{P}\right)\left(\frac{T}{T_0}\right)^{1.75} \qquad (8)$$

The diffusion coefficient of dissolved H2 in the water of the porous medium is specified in the exercise as:

$$D^w_{H_2} = S_w\left(\frac{\phi}{\tau^2}\right)\times 1.5710^{-14}\frac{T}{\mu_{water}(T)} \qquad (9)$$

In TOUGH2 the corresponding values are defined as:

$$D^g_{H_2/vap} = \phi\tau_0\tau_\beta\left(\frac{1}{\tau^2}\right)D_0\left(\frac{P_0}{P}\right)\left(\frac{T}{T_0}\right)^{1.75} \qquad (10)$$

and

$$D_{H_2}^{w} = \phi \tau_0 \tau_\beta \left(\frac{1}{\tau^2} \right) \times 1.5710^{-14} \frac{T}{\mu_{water}(T)} \qquad (11)$$

In this case the use of the prescribed expression caused a lack of convergence of the calculations and therefore the default expressions of TOUGH2 were used for the calculations. The first exercise was calculated with the prescribed models (16) and (17) because the difference in the calculation times was not so important.

The proposed expression for the Henry's law in FORGE has some differences with the respect to the used in the TOUGH2 code. Namely the expression in FORGE contains the concentration of hydrogen in mol/m3 und the expression in TOUGH2 uses the mole fraction of hydrogen. A conversion factor was implemented in the TOUGH2 code to use the suggested expression in FORGE.

3.8.4.2 Initial and Boundary Conditions

The calculation times were like in the first benchmark very sensitive to the variation in the initial conditions. The prescribed initial conditions consist of a water saturation of 100% for the host rock and for the EDZ. 70% water saturation for the bentonite and for the backfill and finally 5% for the interfaces. The pressure of the water saturated materials was linearly distributed between values at upper and lower boundaries and in the partially saturated materials the gas pressure is about 1 atm.

At the top of the domain with coordinate z=150 m a water pressure of 4x106 Pa and of 6x106 Pa at z=0 m were prescribed. In all other boundaries a non flow condition was prescribe except for the ends of the main drift which represent the connections with the other modules. On these surfaces a time dependent boundary condition representing the influence of the other modules was prescribed and it is represented in Figure 105.

The initial and boundary conditions were implemented as prescribed for this benchmark.

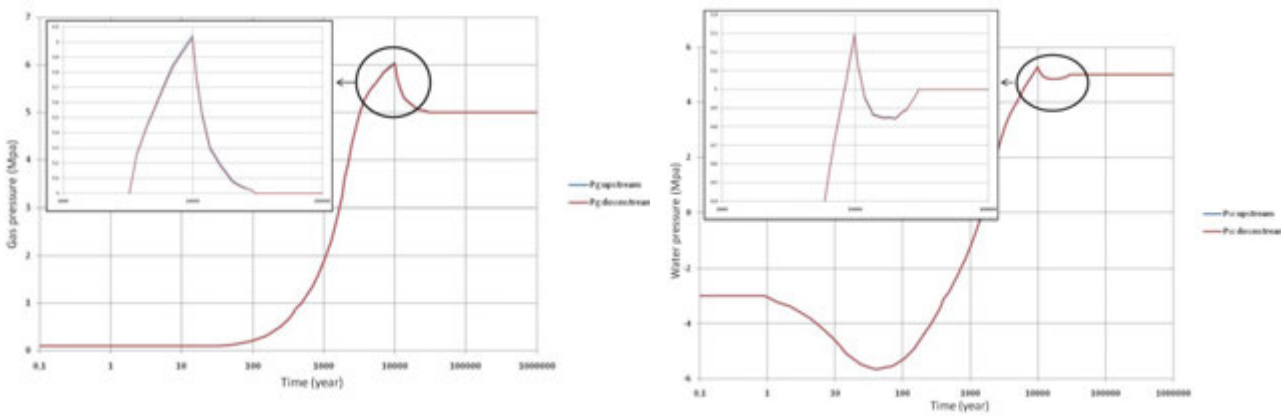

Figure 105 *Gas pressure (left) and water pressure (right) time varying boundary conditions on the backfill*

In the next sections results at some points, for some lines along the model and mass flows through some surfaces will be shown. In this report only a selection of some results will be provided. The complete list of results was delivered to the work package leader.

3.8.4.3 Deviations from the specification

The simplifications carried out by ENSI in this second benchmark had the objective of increasing the speed of the simulations. There were no problems of crashing of the code but sometimes with some model characteristics or parameters the calculations were too slow.

The main simplification as explained before was the integration of all interfaces of a thickness of 1 cm in the materials surrounding it. The following interfaces elements were prescribed in the benchmark:

- An interface between the waste material and the EDZ in the waste tunnel
- An interface between the bentonite plug and the EDZ in the waste tunnel
- An interface between the backfill and the EDZ in the access drift
- An interface between the backfill and the EDZ in the main drift
- An interface between the bentonite plug and the EDZ in the main drift

In a first set of calculations the interface was integrated explicitly in the model and the model contained about 1'200'000 mesh elements. The calculations with TOUGH2-MP in an IBM AIX UNIX system with the use of 32 processors were too slow with time steps of about 1.0×10^5 seconds. It was therefore decided to integrate the properties of the interfaces in the surrounding material by means of an averaging process.
Another deviation from the specification is the expression for the gas relative permeability and also for the gas diffusion coefficient as explained in the subchapter 3.8.4.1.

3.8.5 Base Case Results

In this chapter a selection of results will be shown. The results are classified by the kind of geometrical elements at which the results are provided. In the next subchapter 3.8.5.1 the results in the different prescribed points will be shown. In subchapter 3.8.5.2 the results along some lines in the model will be shown and finally in 3.8.5.3 the results of the mass flow rates across some prescribed surfaces will be shown.

3.8.5.1 Results at Specific Points

It was taken the convention that in case of one phase flow the gas pressure and water pressure are equal in order to avoid discontinuities in the representation. This was the convention used by most of the teams in the first benchmark. The other possible convention (used by ENSI for the first benchmark) is to take the phase pressure as zero whenever the gas phase disappears. The change from one convention to the other is trivial. In Figure 106 the points of the model for which results were required are shown.

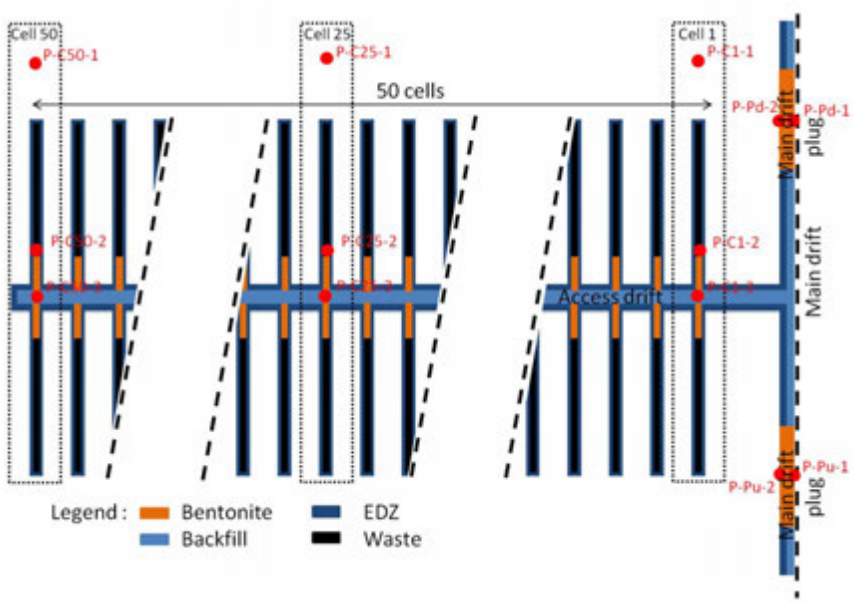

Figure 106 Points of the model for which results were required.

The evolution of the gas saturation is represented in Figure 107. The points at the intersection between the bentonite plugs and the waste tunnels maintain a small residual saturation until 10'000 years when the gas injection is zero. The gas saturation of these bentonite plugs, points P-C1-2, P-C25-2 and P-C50-2 decreases in 10 years to less than 0.2%. The saturation of the points P-Pu and P-Pd in the main drift decreases to zero after 1'000 years. As expected it was observed in the results a symmetry between the upper and lower part

of the main drift and for example the points P-Pu-1 and P-Pd-1 or the points P-Pu-2 and P-Pd-2 show similar values for the main variables. Between points in the same part of the main drift but at different x coordinates (see Figure 102) the values differ a little but not much. Points P-Pd-2 and P-Pu-2 are in the interface between bentonite and EDZ and the points P-Pd-1 and P-Pu-1 are in the bentonite plug. The saturation is faster in the points close to the clay rock. That can be seen by comparing the red and green curves of the Figure 107.

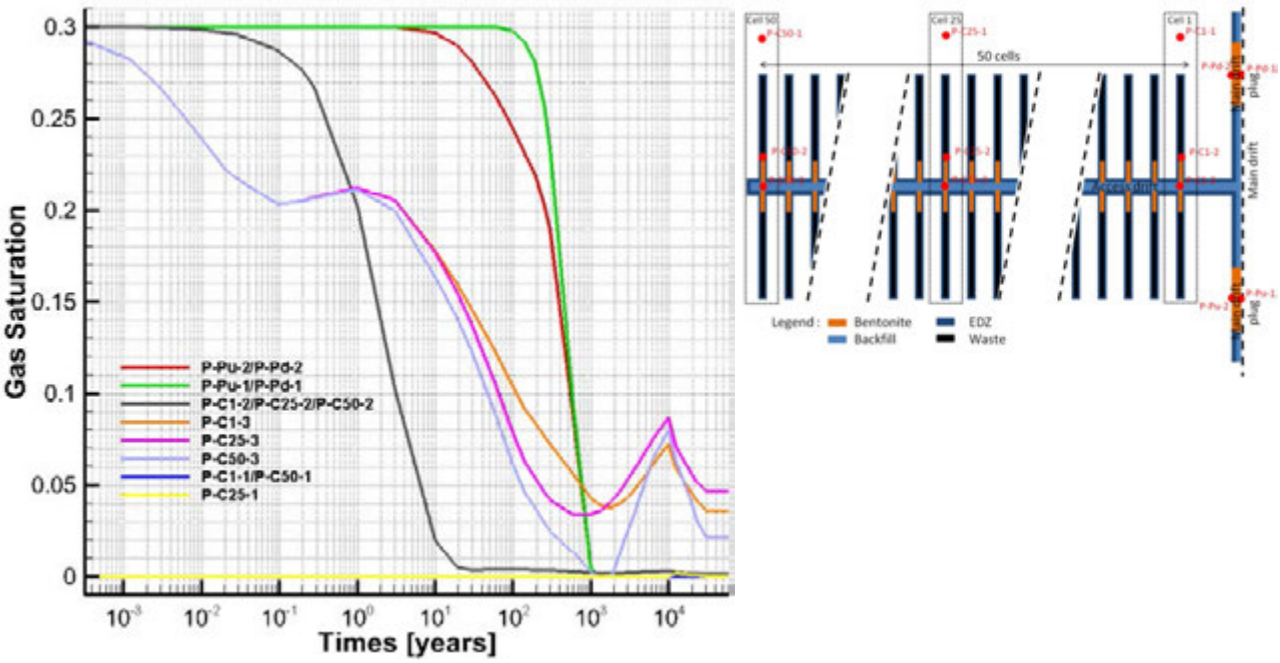

Figure 107 *Variation of the gas saturation with the time at the points shown in Figure 106.*

The points P-C1-1, P-C25-1 and P-C50-1 are not much affected by the gas injection. The saturation change very little but a variation of the gas and water pressure after 100 years can be detected in the Figure 108 and Figure 109 respectively. The water pressure decreases after 100 years from 5 MPa (initial water pressure at the clay rock at this depth) until between 1 MPa and 3 MPa depending on the waste tunnel. Afterwards the pressure increases and tends to take the initial values.

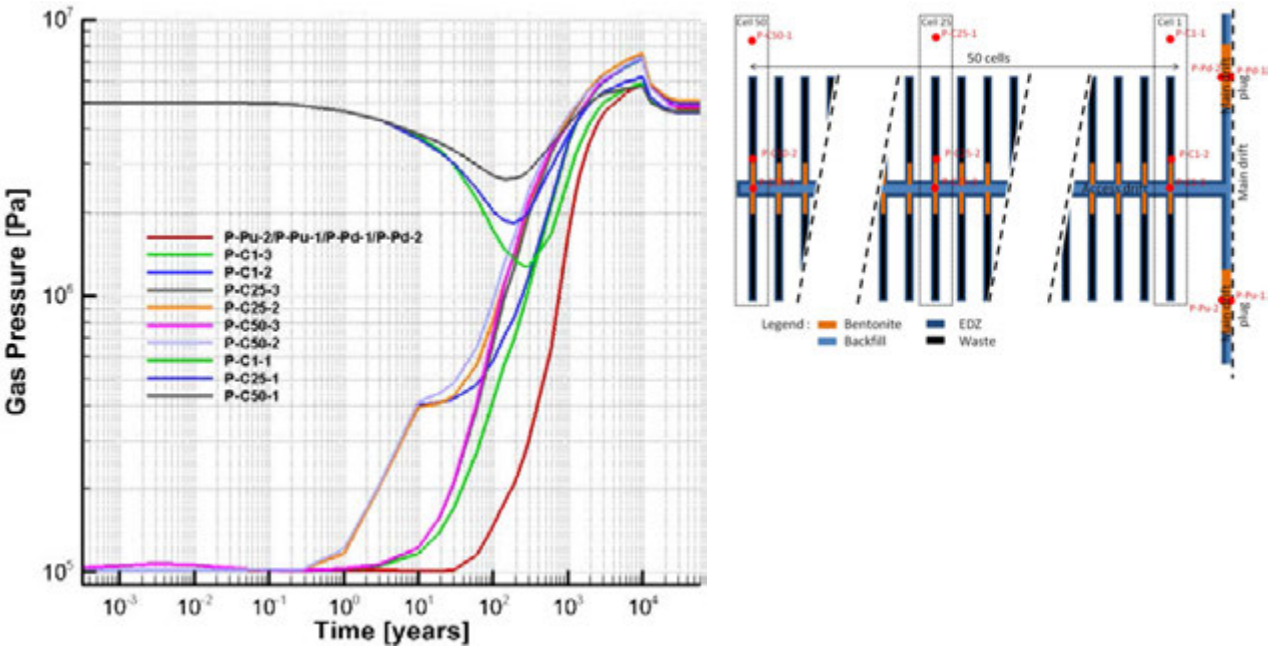

Figure 108 *Variation of the gas pressure with the time at the points shown in Figure 106.*

A suction pressure is observed in Figure 109 initially at the points P-C1-2, P-C1-3, P-C25-2, P-C25-3 P-C50-2, and P-C50-3 what causes an increase of the water saturation in these points as it can be seen in Figure 107.

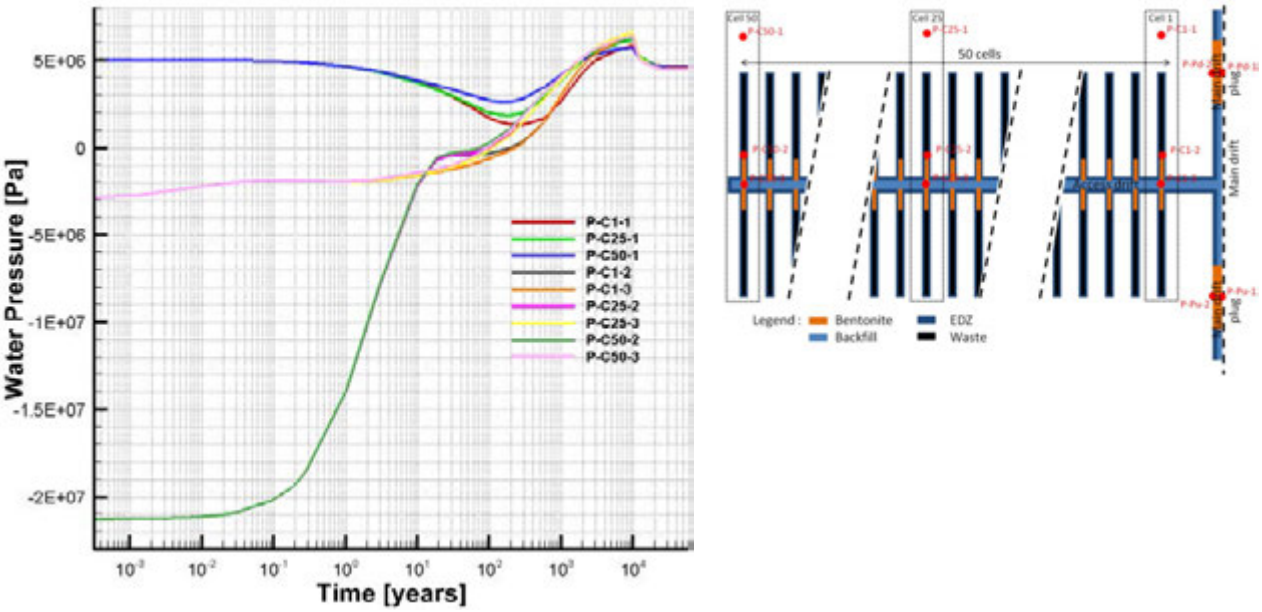

Figure 109 *Variation of the water pressure with the time at the points shown in Figure 106.*

3.8.5.2 Results along Lines of the Domain

In order to follow the evolution of different variables in the geometry, lines were defined along which results are provided for different times. There are three lines along the central waste tunnel and along the

first and last waste tunnel. A line goes along the access drift and another one along the main drift. These lines are shown in Figure 110.

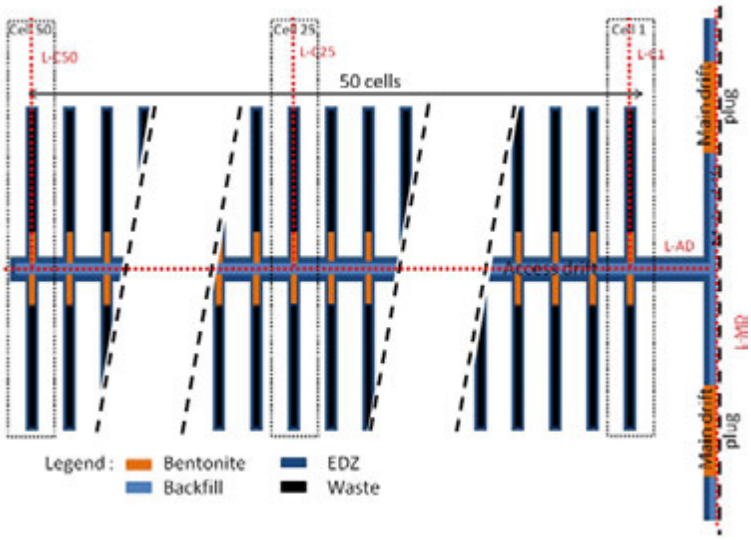

Figure 110 *Lines of the model along which results are provided.*

For the representation of the variation of the water saturation and of the gas pressure the times 1 year, 10 years, 100 years, 1'000 years, 10'000 years and 30'000 years were chosen. 30'000 years is the time at which variables like the saturation and pressure reach a plateau and from this time on no changes in the variables are detected as it can be seen in Figure 107, Figure 108 and Figure 109.

Line L-AD along the access drift

This is the longest line and spans from the beginning of the access drift at x coordinate 195 m until the end of the access drift at x coordinate 710 m. At 1 year the water saturation at the beginning of the line coincides with the initial water saturation of the clay rock. Along the line the initial saturation of the backfill of 70% has increased about 3% (Figure 111).

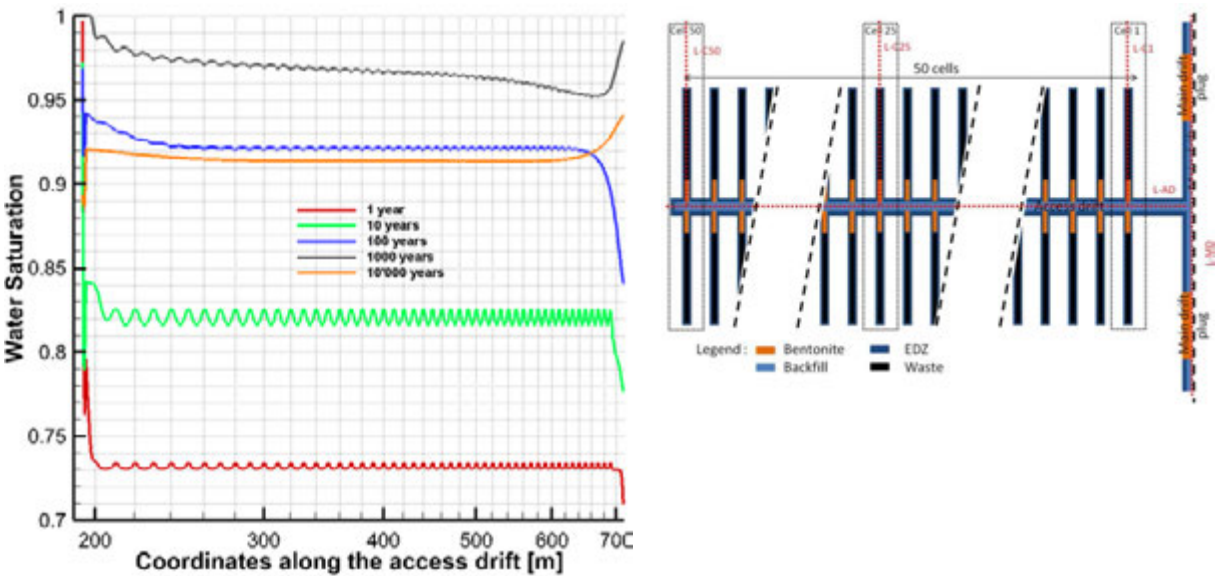

Figure 111 *Variation of the water saturation along the access drif; line L-AD in Figure 110.*

The water saturation increases rapidly in the backfill, namely about 83% after 10 years, 93% after 100 years and 97% after 1'000 years. It is observed in the Figure 111 that there is an oscillation of less that 1% of the water saturation specially the first 10 years afterwards the oscillations decrease. These oscillations are probably due to the non-stationary nature of the model at that time and also to the fine resolution of the x coordinate along the access drift. At 10'000 years the gas injection can counteract the water saturation and the water saturation decreases. Because of the influence of the main drift and that there are no more waste tunnels in the last part of the access drift the water saturation decreases here less quickly. The water saturation is in the end part of the access drift initially lower than in the other parts. That changes at a time between 100 and 1000 years at which the main drift saturated of water starts saturating the end part of the access drift. That is the reason why the curves of water saturation close to the main drift in Figure 111 show initially a decrease but an increase in the same position after 100 years.

The above mentioned increase of the gas pressure can be seen in the Figure 112. The gas pressure reaches maximal values of about 7.5 MPa and this pressure remains more or less constant along the access drift at 10'000 years.

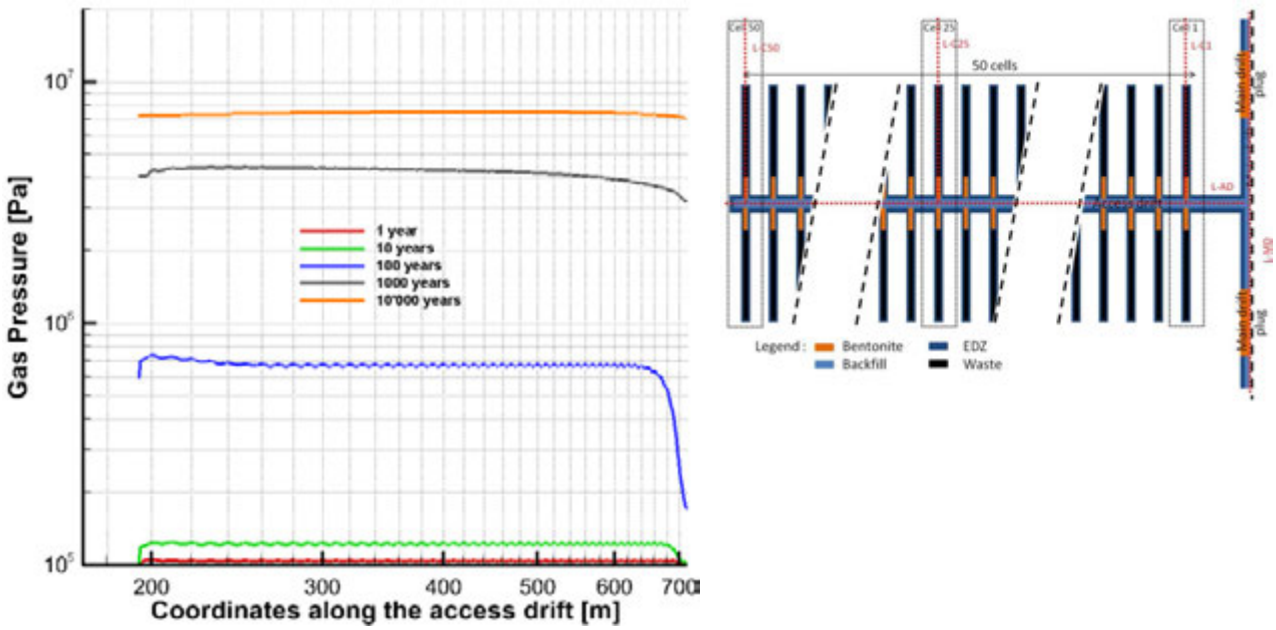

Figure 112 *Variation of the gas pressure along the access drift; line L-AD in Figure 110.*

Line L-C25 along the central waste tunnel

This line is parallel to the axis of the cell and spans from the beginning of the bentonite plug in the waste tunnel at a y coordinate of 66 m until the end of the simulation domain in the y direction at 126 m. The waste tunnel ends at a y coordinate of 111.5 m. The line contains a first part associated with the bentonite and the EDZ surrounding it and a second part associated with the EDZ surrounding the waste. The waste is not represented as a material in these calculations and only a tiny volume at the outer surface of the waste and surrounded by the EDZ is used to represent the injection of gas into the model.

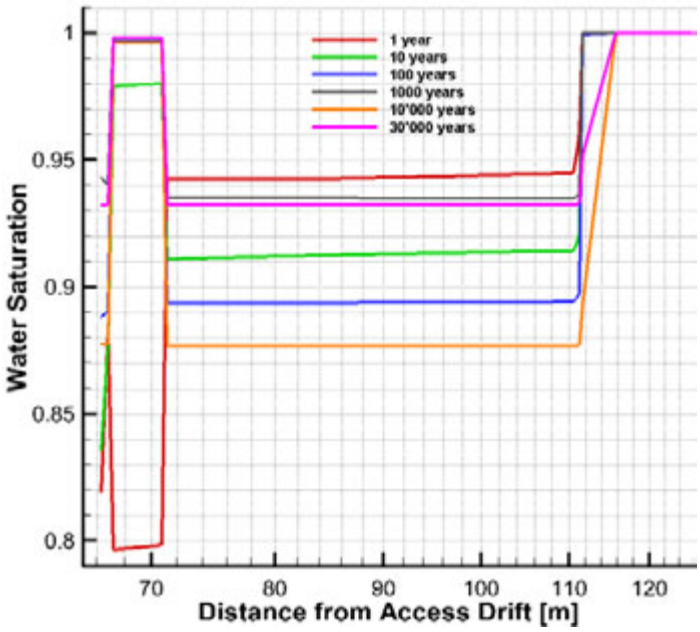

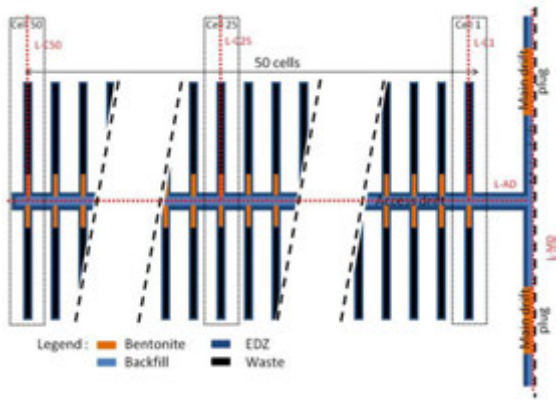

Figure 113 *Variation of the water saturation perpendicular to the access drift; line L-C25 in Figure 110.*

The variation of the water saturation is represented in Figure 113 and is characterized by a quick variation of the saturation close to the bentonite where the saturation changes from about 70% to 80% after 1 year and from 80% to 98% after 10 years. In the EDZ the saturation decreases to about 94% after one year and 92% after 10 years. In this way the gas opens a pathway for its transport along the repository.

It is interesting to observe the variation of the water saturation of the EDZ surrounding the cell represented in the central part of Figure 112. In this section there is a balance between the water tending to saturate the repository at about 1'000 years and the continuing increase of the gas injection until 10'000 years. The water saturation decreases initially due to the gas injection but it decreases until about 1'000 when the water pressure starts saturating the repository. At 10'000 it decreases again due to the amount of gas been injected exactly along this line and after stopping the injection the water saturation increases again.

At about 10'000 years a desaturation can be observed in the host rock close to the waste tunnels. The water saturation in this area reaches minimal values of about 90% but this part resaturates again after 10'000 when the gas injection disappears and reach a minimal value of about 95% at 30'000 years.

The variation of the gas pressure is represented in Figure 114 and as expected it is seen that the pressure increases systematically until 10'000 years when the injection of gas is interrupted and the gas pressure decreases at 30'000 years.

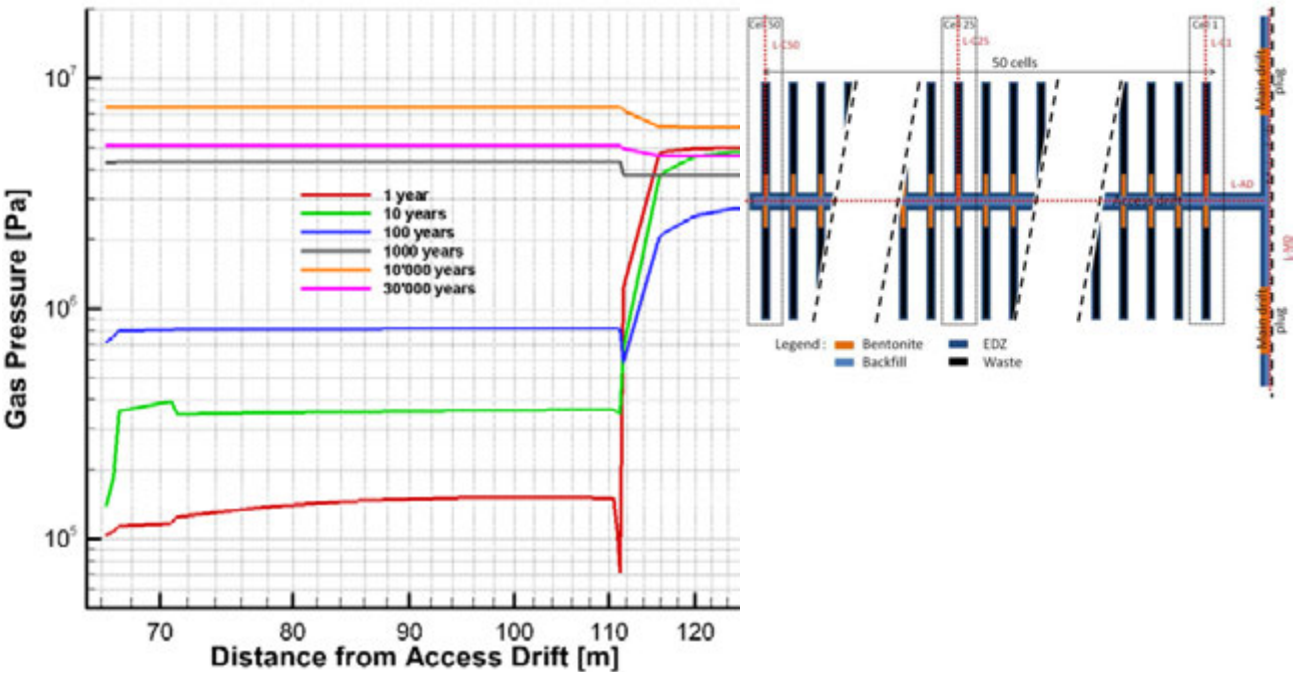

Figure 114 *Variation of the gas pressure perpendicular to the access drift; line L-C-25 in Figure 110.*

Line L-C1 along the lateral waste tunnel

The evolution of the water saturation and gas pressure along the lines L-C1 and L-C50 situated at the end and beginning of the access drift is very similar to the ones of the line L-C25. Here only the evolution of the water saturation is represented in Figure 115. The interpretation of the results of this graphic is similar to the one of Figure 113 for the line L-C25.

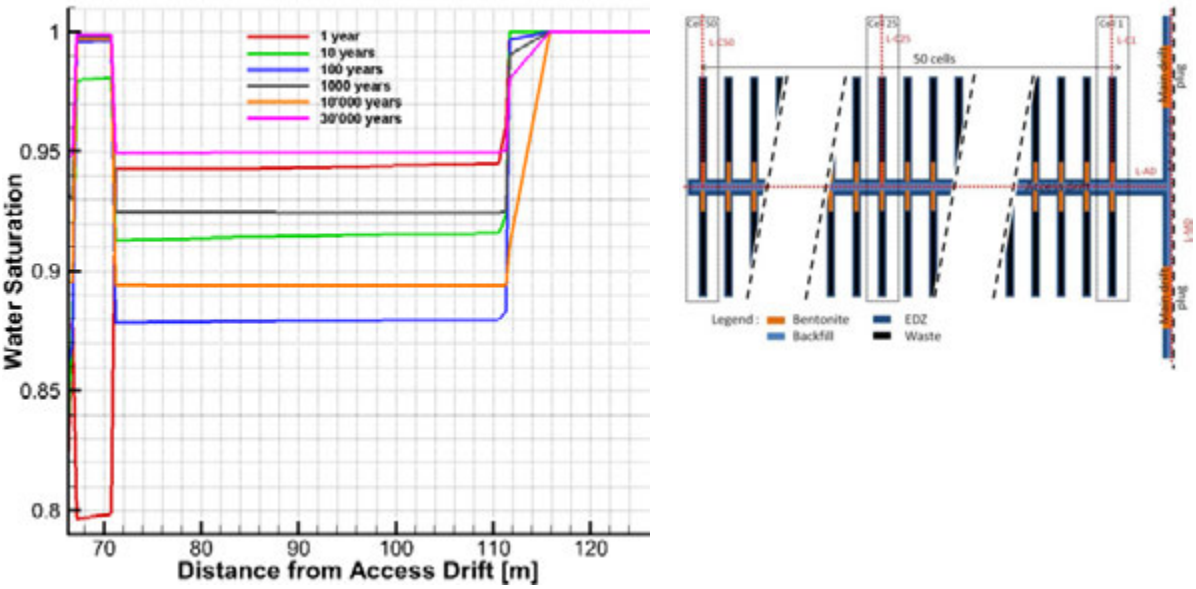

Figure 115 *Variation of the water saturation perpendicular to the access drift; line L-C-25 in Figure 110.*

Line L-MD along the main drift

The evolution of the water saturation along the line L-MD is shown in Figure 116. The first bentonite plug extends approximately from the y coordinate 10 m until 30 m and the second one from 96 m until 116 m. The line has fixed x and z coordinates of 714 m and 75 m. The z coordinate of 75 m corresponds to the middle of the host rock formation and of the simulation domain. The influence of the interface in the bentonite plug can be seen clearly after 100 years, even sooner there are some differences in the water saturation close to the bentonite. In the backfill of the main drift the water saturation increases faster than in the backfill of the access drift and it changes from 70% to 77% after one year.

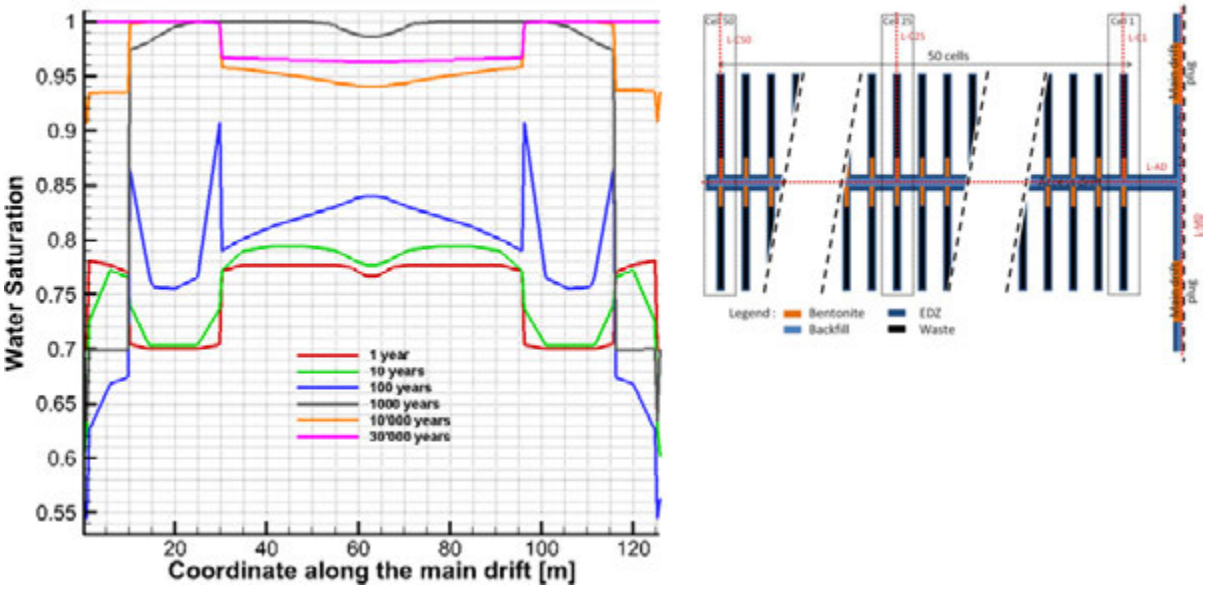

Figure 116 *Variation of the water saturation along the main drift; line L-MD in Figure 110.*

At 1'000 years the backfill is saturated but the bentonite is not yet fully saturated. The saturation of the bentonite is reached after 10'000 years. The saturation of the initial and end part of the main drift is only reached after 30'000. That is due to the imposed time depending boundary conditions at these end parts.

The variation of the gas pressure is represented in Figure 117. The gas pressure remains after a time between 10 and 100 years at atmospheric conditions (initial conditions) and afterwards the gas pressure increases initially in the middle of the main drift due to the arrival of the gas from the access drift. At 100 years the gas distributes along the central part of the main drift but not along the bentonite that saturates slowly. At 10'000 years the gas pressure is more of less uniform along the main drift and reached a maximal value of about 7 MPa. In the bentonite at that time the gas pressure is about 5.8 MPa.

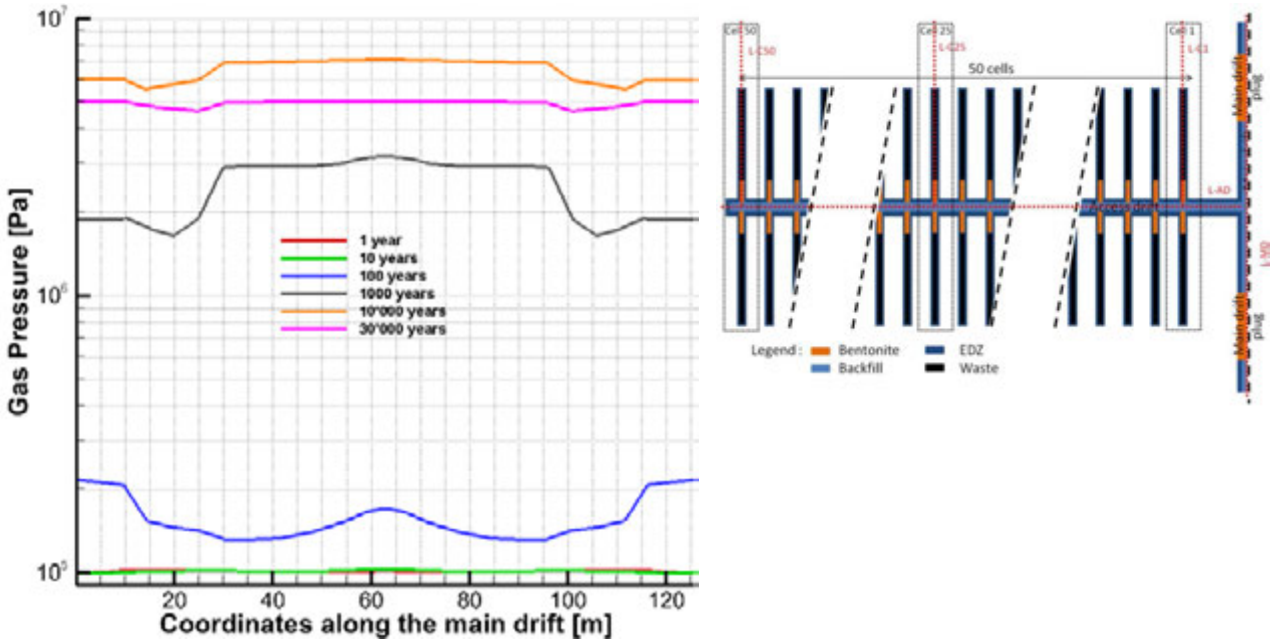

Figure 117 *Variation of the gas pressure along the main drift; line L-MD in Figure 110.*

At 10'000 years the gas pressure decreases and reaches a uniform value of 5 MPa which corresponds to water pressure in the middle of the simulation domain. Because of the approximately linear distribution of water pressure between the fixed boundary conditions at the top and at the bottom level of the formation of 4 MPa and 6 MPa.

3.8.5.3 Results for the Mass Flow Rates

In this section the evolution of the mass flow will be shown for different surfaces as represented in Figure 118. There are 8 different surfaces situated along the repository. F-Pd and F-Pu are in the middle of the bentonite plug and perpendicular to the main drift. It is expected because of symmetry that the mass flows through these two surfaces are similar. The results of the simulations confirm this symmetry. The surfaces F-C1, F-C25 and F-C50 are situated at the end of the bentonite plugs perpendicular to the first, to the middle and to the last waste tunnels respectively. Finally the surfaces F-D1, F-D25 and F-D50 are situated perpendicular to the access drift and always in the middle between two waste tunnels as it can be seen in Figure 118.

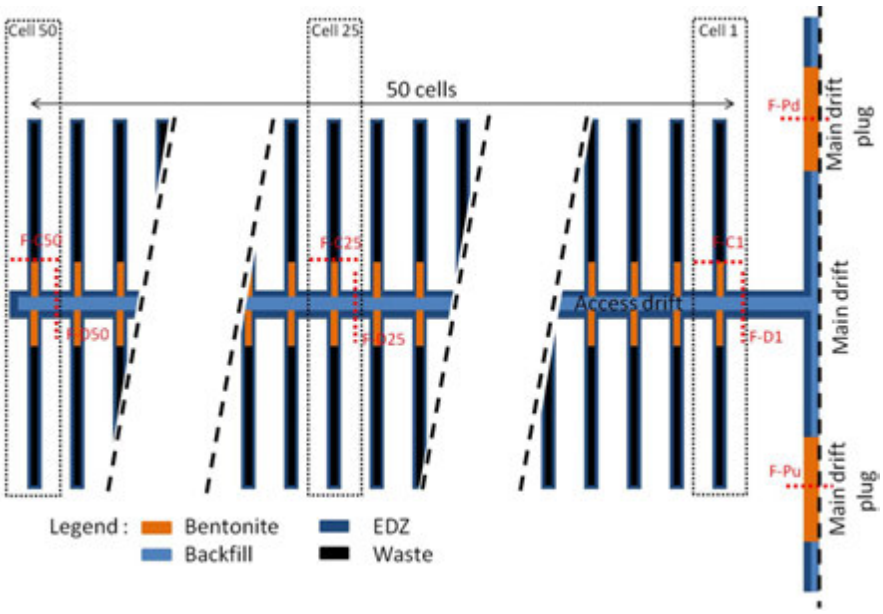

Figure 118 *Position of the surfaces used for the calculation of the mass flow rates.*

The mass flow of water is represented in Figure 119 and it is observed that after an initial suction of water in the waste tunnel the mass flow of water increases very quickly at the beginning in the surfaces perpendicular to the waste tunnels and reaches a maximum at a time of about 1 year afterwards the water flow decreases gradually.

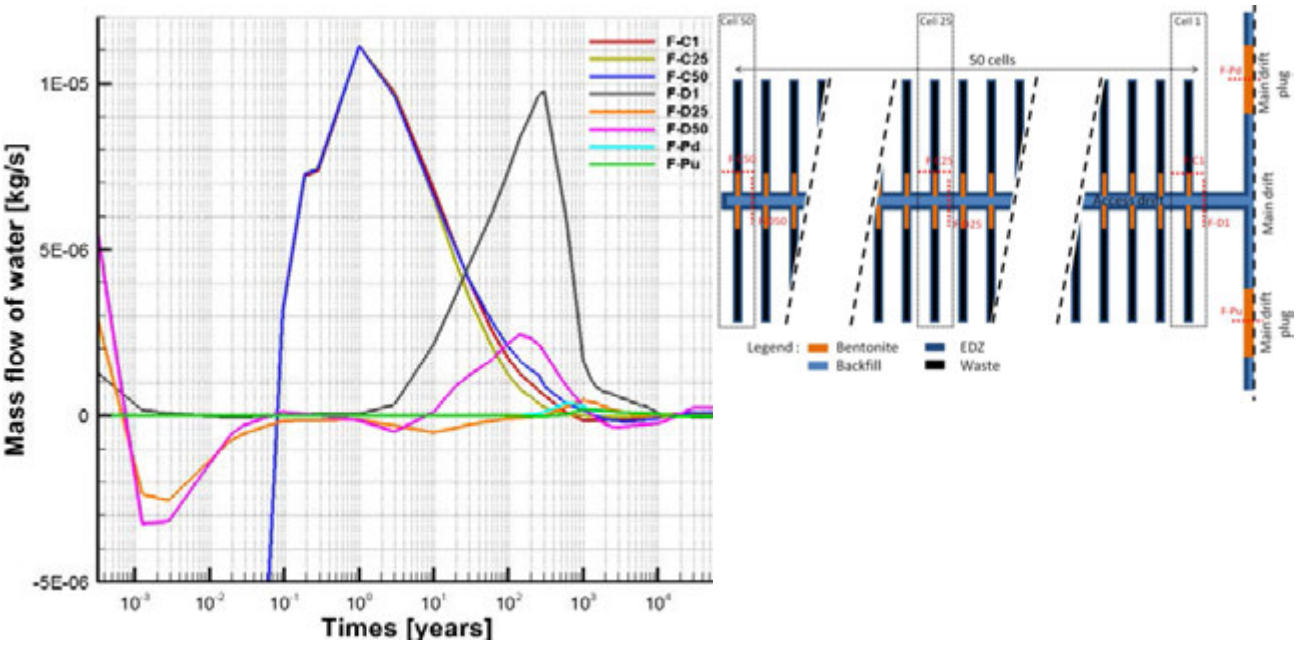

Figure 119 *Results for the mass flow rates of water through the different surfaces.*

In Figure 120 the mass flow of gas is represented. In the phase of negative pressures of water the gas can be expelled from the waste tunnels but the gas does not have space to flow. Therefore it reaches a minimum at 1 year when the water flow is maximal. Afterwards with the increasing gas injection the gas opens pathways for its flow and the mass flow of gas through the waste tunnels increases again. The mass flow increases in particular through the surface connecting the access drift to the main drift where the mass flow of gas reaches values of about 7×10^{-9} kg/s.

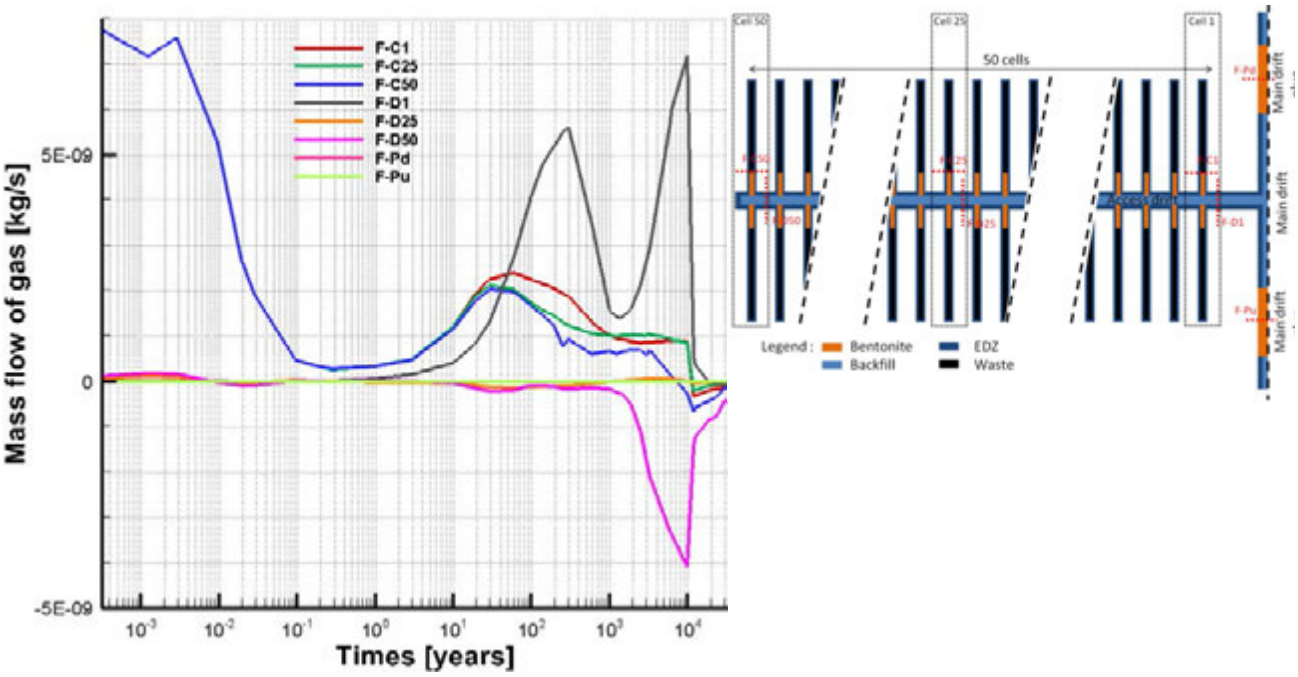

Figure 120 *Results for the mass flow rates of gas through the different surfaces.*

The mass flow of dissolved H_2 is represented in Figure 121 and the maximal values are reached in the surface connecting the access drift to the main drift where the mass flow of dissolved H_2 reaches values of about 1.8×10^{-10} kg/s much lower than the values of the gas flow.

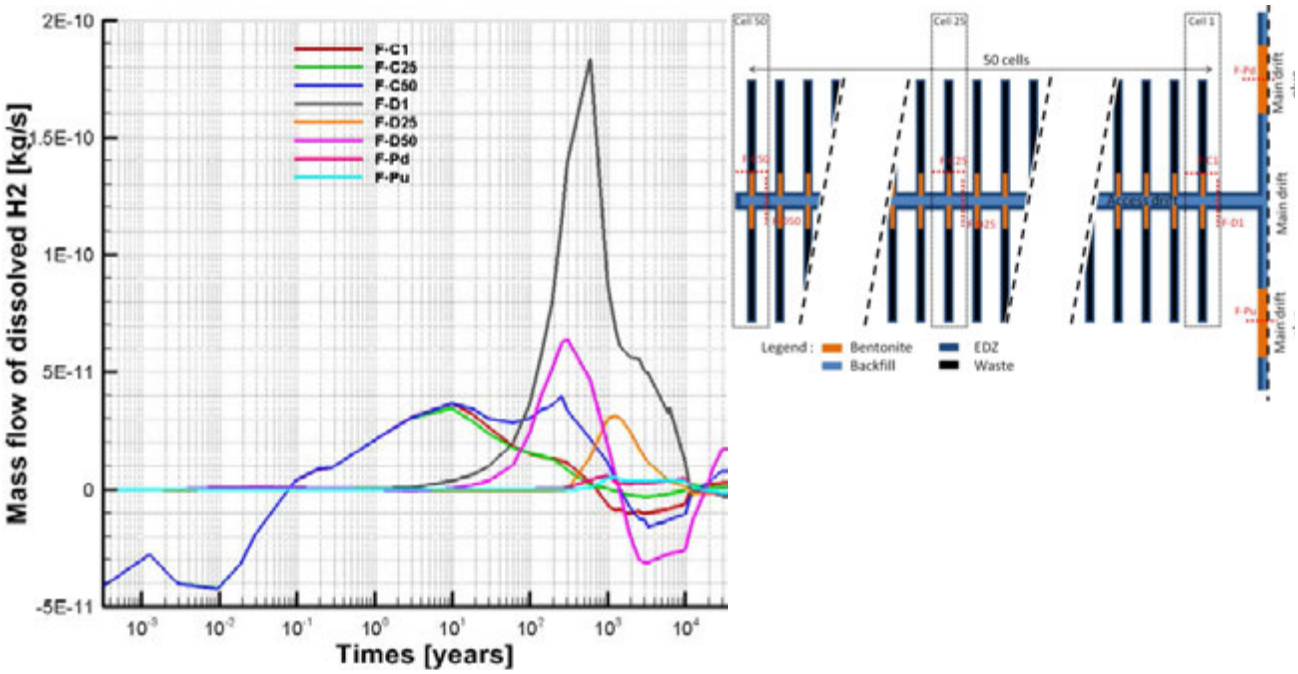

Figure 121 *Results for the mass flow rates of dissolved H2 through the different surfaces.*

3.8.6 Conclusions

The presence of the interfaces close to the EDZ is a challenging modelling element in the repository scale simulations. The results and the numerical convergence of the simulations are affected by the presence of an interface. The implementation into the code of these tiny mesh elements in the interface has to be performed carefully; otherwise the results or its convergence can be affected. In this benchmark it was observed that the presence of the discretization of the interface increases by a factor 100 or 1'000 the computational time of the simulations. It was therefore decided to integrate the material properties of the interfaces in the surrounding materials. For the second exercise it was initially used a mesh with about 1'200'000 elements including the interface mesh elements and then it was simplified to about 800'000 elements. As expected the computational time increases with the refinement of the mesh and the obtained results are similar.

A lot of work of ENSI was dedicated to install and compile TOUGH2-MP, to the modification of the code, to the acquisition and adaptation of a mesh program, to the creation of the respective input and finally to the control of the instabilities of the simulation. An important part of the work was also dedicated to the post processing of the results. On the one hand there were many results to process specially for the second benchmark with outputs of size of about 20 GB and on the other hand many of the results could not be obtained directly from the output of the code but by means of scripts or modifications of the code.

From the results of the two benchmarks it can be concluded that the interface and the EDZ represent the main pathway for the migration of the hydrogen to the drift in these conceptual models. The hydrogen is transported mainly in gas form but also dissolved in water along the interface and EDZ to the drift.

The results of the different teams are in general in the same order of magnitude. In the second benchmark exercise the differences between the results of the teams are more pronounced than in the first exercise. That could be explained by the increasing complexity of the benchmarks. The differences in the values of the saturation and pressure could be explained also due to the various approaches and simplification taken in the model by the different teams. Less clear are the differences of about one order of magnitude in the values of the mass flow rates that could not be explained only by the use of different approaches and simplifications.

3.8.7 Issues for Further Consideration

This benchmark exercise (in particular the third benchmark) shows that the upscaling methods are very important to represent correctly big scale models of a repository. More effort should be applied on the understanding of the upscaling methods and their implementation in the numerical codes.

The results of the calculations were not compared to measurements coming from laboratory or field experiments and therefore the results cannot be seen as the definitive behaviour of the gas in a geological repository but as reference for the order of magnitude of what in principle the measurements should provide. ENSI would like to remark here the importance of the combination of numerical results with measurements in order to understand correctly the processes occurring in the underground.

Another important point in opinion of ENSI is the explanation of the differences obtained by the different teams in the values of the mass flow rates. More effort should be made in this aspect in order to be able to explain these differences.

3.8.8 References

1. Wendling, J., et al., FORGE WP1.2: Benchmark specifications at a sub set of a repository containing several tens of HLW cells (module scale). 2010, Euratom 7th Framework project: FORGE 2010.
2. Wendling, J., et al., FORGE WP1.2: Benchmark specifications at a complete generic HLW repository scale. 2010, Euratom 7th Framework project: FORGE 2010.
3. Pruess, K., C. Oldenburg, and G. Moridis, TOUGH2 USER'S GUIDE, VERSION 2.0. 1999, Lawrence Berkeley National Laboratory: Berkeley, California.
4. Zhang, K., Y. Wu, and K. Pruess, User's Guide for TOUGH2-MP, A massively Parallel Version of the TOUGH2 Code. 2008, Lawrence Berkeley National Laboratory.
5. Narasimhan, T.N. and P.A. Witherspoon, An integrated finite difference method for analyzing fluid flow in porous media, in Water Resources Research. 1976. p. 57-64.
6. Narasimhan, T.N., P.A. Witherspoon, and A.L. Edwards, Numerical model for saturated-unsaturated flow in deformable porous media, part 2: the algorithm, in Water Resources Research. 1978. p. 255-261.

3.9 NWMO contribution

3.9.1 Introduction

Geofirma Engineering Ltd. conducted the module-scale benchmark modelling on behalf of the Nuclear Waste Management Organization (NWMO) in Canada.

3.9.2 Model Implementation

3.9.2.1 Code and Formulation

T2GGM (Quintessa and Geofirma, 2011 [1]), a modified version of TOUGH2 v2.0 with optional gas generation model, was selected as the two-phase flow modelling code. The gas generation model (GGM) capabilities were turned off, and TOUGH2-MP was not used. TOUGH2 is a general-purpose numerical simulation program for multi-phase fluid and heat flow in porous and fractured media developed by Lawrence Berkeley National Laboratory (Pruess et al. 1999 [2]). The EOS3 equation of state module used in T2GGM simulates the transport of a single separate gas phase in water (note that T2GGM allows for specification of alternate gases to air, the EOS3 default). EOS3 also models the transport of dissolved gas in water by diffusion and advection. Dispersive processes are not modelled.

Two minor modifications were made to the T2GGM code to facilitate the benchmark modelling studies:

- Time-dependent Dirichlet boundary conditions were added based on the implementation within TOUGH2-MP. TOUGH2-MP only allows for time-dependent pressure changes (assuming saturation and temperature remain constant), while this new implementation allows both time-dependent pressure and saturation as required by the benchmark specification.
- A new time-stepping scheme, based on the scheme within TOUGH2-MP with minor modifications, was implemented. This time stepping scheme allows for smaller increases in time step (when the simulation converges within a specified number of iterations) and smaller decreases in time step (when the simulation does not reach convergence within the maximum number of iterations). The scheme also minimizes the occurrence of oscillations between time step increases and decreases (e.g. when a time step decrease results in a time step solving within the specified number of iterations, this causes a subsequent time step increase that cannot be solved, requiring the time step to be decreased etc.) by preventing time step increases for five time steps following a reduction in time step.

mView, developed by Geofirma Engineering, was used for pre- and post-processing.

3.9.2.2 Grid

A 3D grid was developed, representing the entire model domain. Figure 122 shows the model domain, with boundary conditions, cells and drifts.

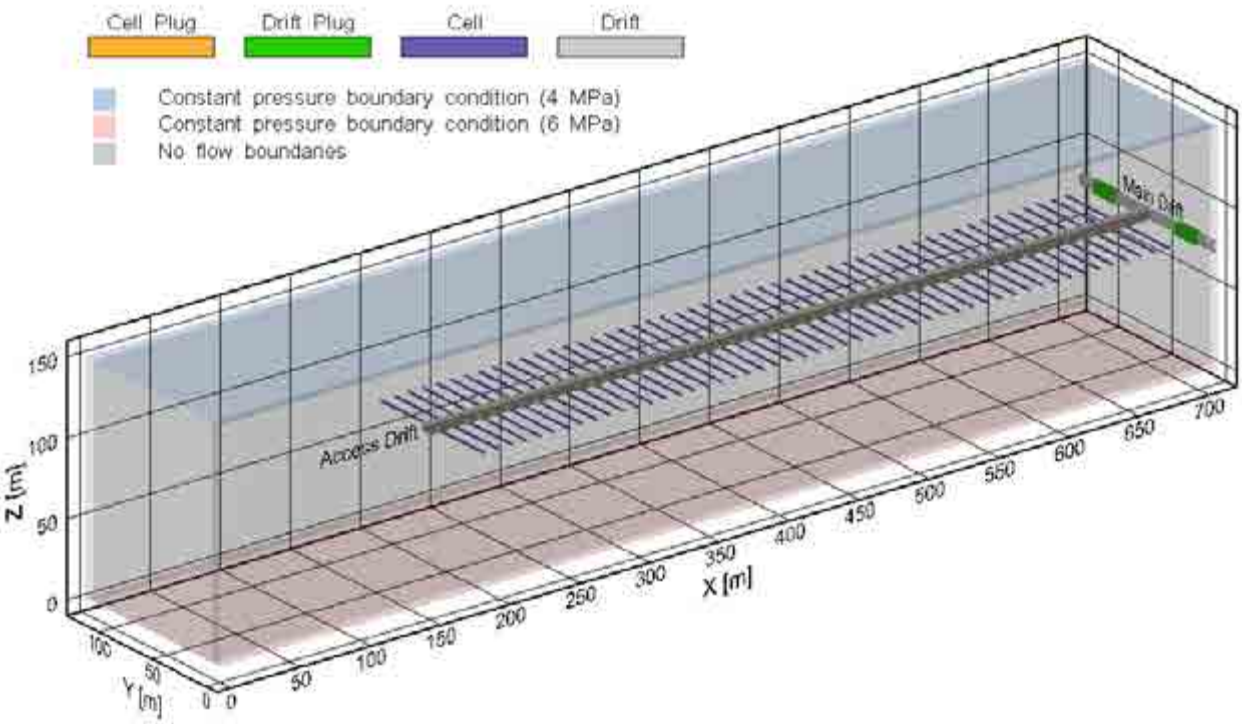

Figure 122 : 3D model domain with boundary conditions, cells and drifts. Note that variable pressure and saturation boundary conditions exist at the upstream (Y= 0) and downstream (Y= 126) ends of the main drift.

The greatest challenge in developing this grid was to obtain sufficient representation of the repository details, while maintaining a grid of tractable size. First attempts at gridding, which included some simplifications for the very thin interface, produced grids that were much too large for standard TOUGH2. While TOUGH-MP, which allows much larger grids than TOUGH2, was capable of simulating these large grids, the cumbersome size and complexity of these grids resulted in difficulties in isolating problems with the grid and model set-up and these MP simulations were abandoned. Major simplifications were required to develop a tractable grid, and after several iterations, the following simplifications were adopted:

(1) The cells were represented as rectangular in cross-section, with equivalent cross-sectional areas to the circular cells defined in the benchmark. Using rectangular-shaped cells allows for significantly fewer grid elements, producing an overall grid of tractable size. The impact of this grid simplification requires further examination, and is recommended for future analysis.

(2) Interface materials were combined with adjacent materials to provide tractable discretization. The impact of combining the interface with the EDZ was examined with the cell-scale model. However, the cell-scale model was not capable of judging the impact of upscaling the interface in the drifts or drift plug. The details of the interface combinations are as follows:

a) The interface between the cell containers and the EDZ was combined with the EDZ. The cell EDZ was divided into two components: (1) an inner EDZ which represents the combination of interface and EDZ, and (2) an outer EDZ which represents the EDZ alone. The inner EDZ of the cells was represented as a single element in the middle of the cell. Block volumes and areas were adjusted to represent the actual volumes and areas of the inner EDZ surrounding the waste. The benchmark specifies the waste containers as impermeable to gas and water. Figure 123 shows a detailed cross-section of the discretization of a cell.

b) The interface between the cell plug and the EDZ was combined with the EDZ, as above. Figure 124 shows a detailed cross-section of the discretization of the cell plug.

c) The interface between the drift backfill and the EDZ was combined with the backfill in a 0.5 m width block on the edges of the drift (both access and main drifts). Figure 125 shows a plan-view of the discretization of the access drift, and Figure 126shows a plan-view of the discretization of the main drift.

d) The interface between the main drift plug and the host rock was combined with the bentonite plug, also shown in Figure 126.

(3) EDZ and the interface at the end of the access drift are ignored (the far end from the main drift). This omission is expected to be inconsequential, as gas and water are expected to flow towards the main drift.

(4) The bentonite plugs in the main drift were shifted 5 m towards the access drift, to minimize discretization in the y direction. The length of the bentonite plugs remains unchanged at 20 m. The impact of this change is likely negligible.

The resulting grid has 121 847 nodes and 404 166 connections. This is still a very large grid for TOUGH2, and was terminated at 30 000 years after a run time of five weeks. It should be emphasized that sensitivity of the simulation to the above simplifications were not examined. Since a working model has been developed, TOUGH-MP can be revisited to consider larger grids, or simulate the current grid with shorter run times.

It should also be noted that the irregular grid of the final model does not strictly adhere to the TOUGH2 integral finite difference requirements; some nodal connections are not perpendicular to the connection area, resulting in shorter connection distances for these connections. The impact of these inaccuracies is expected to be small, and this has been confirmed at the cell-scale.

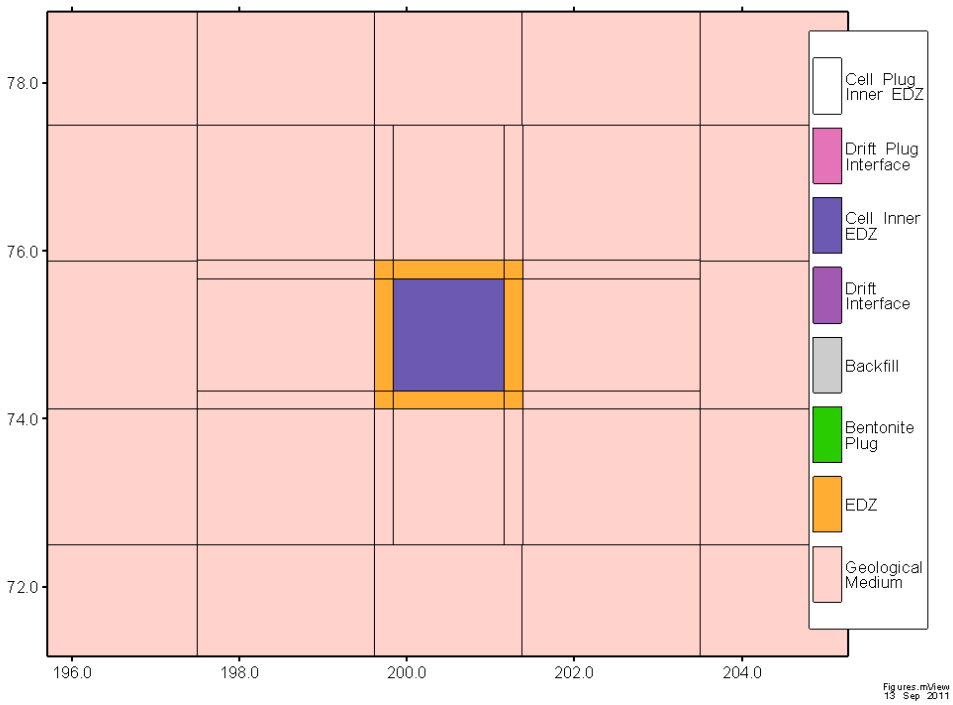

Figure 123: Grid discretization detail: cross-section of a cell. Note that cell areas and volumes for the inner cell EDZ have been corrected to remove the inactive waste containers, as described in the text.

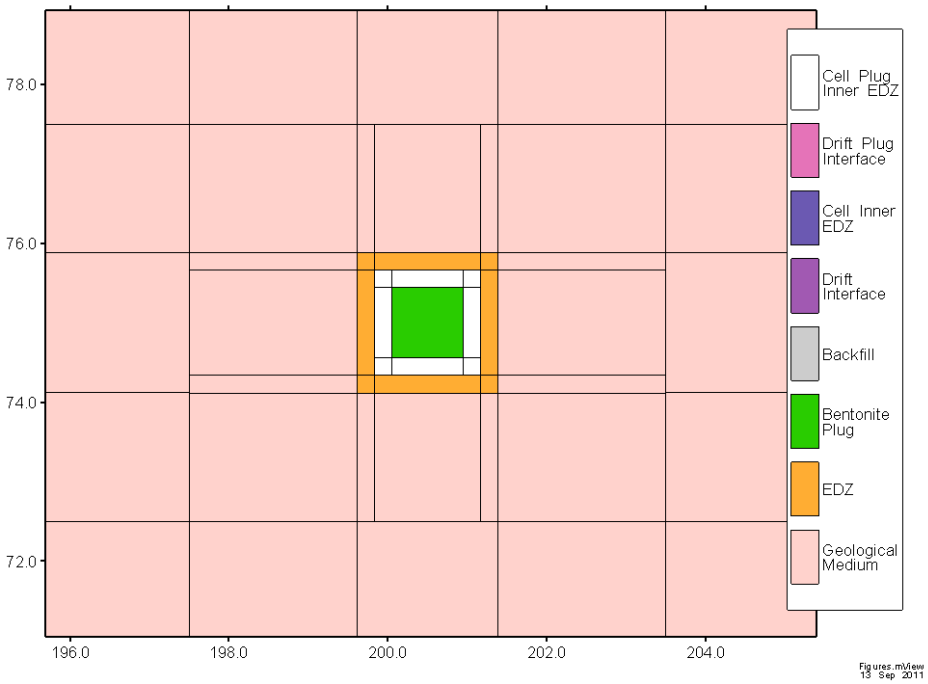

Figure 124: Grid discretization detail: cross-section of a cell plug.

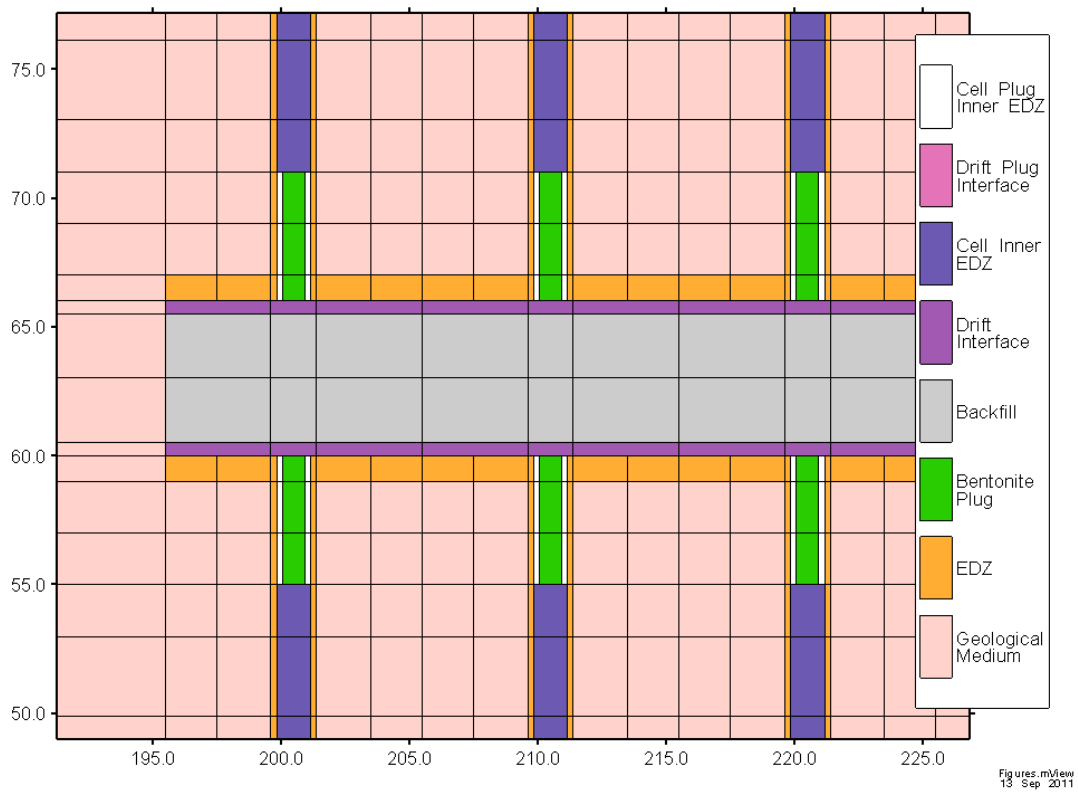

Figure 125: Grid discretization detail: plan view of the access drift.

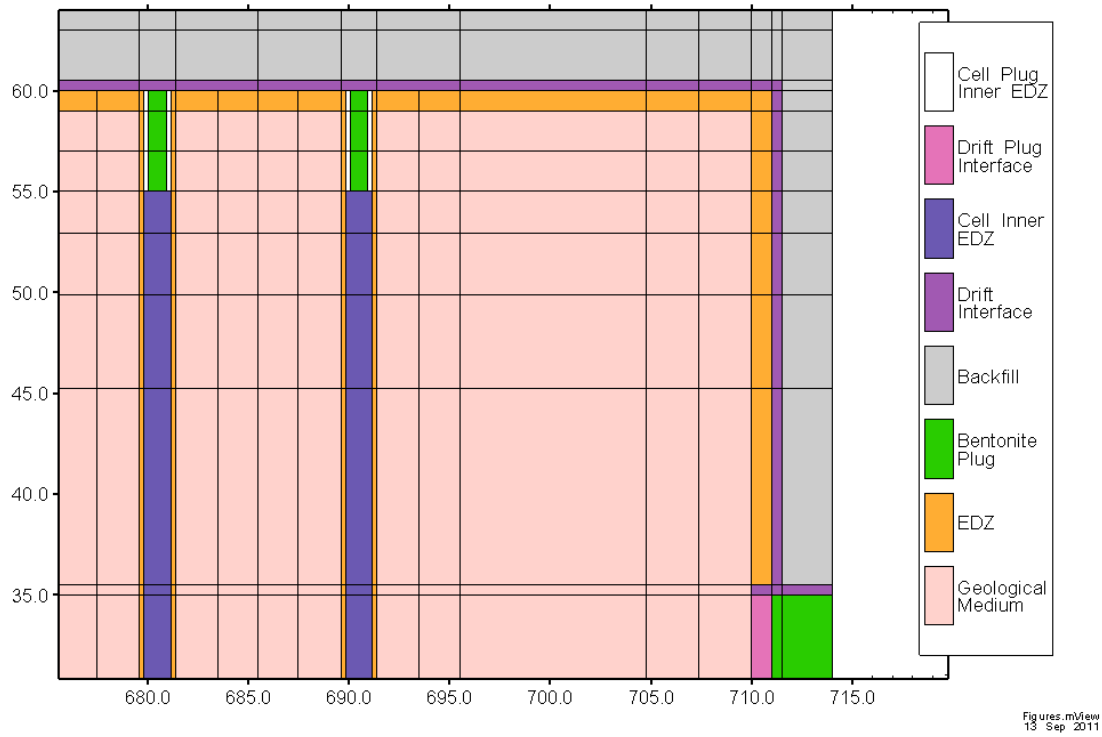

Figure 126: Grid discretization detail: plan view of the main drift.

3.9.2.3 Boundary Conditions and Sources

Constant pressure and zero gas saturation boundary conditions are specified on the top and the bottom of the model, at 4 MPa on the top boundary and 6 MPa on the bottom boundary. Variable saturation and pressure boundary conditions are specified at the upstream (Y=0 m) and downstream (Y=126 m) ends of the main drift. The boundary conditions at the upstream and downstream ends of the main drift are identical, with the exception of very slightly greater pressures at the upstream end between 400 and 30 000 years.

The benchmark specified H_2 gas to be generated at the surface of the waste containers, with the waste containers specified as a no-flow feature. Gas is generated at a rate of 100 mol/year/cell for the first 10 000 years, with no gas generation after 10 000 years. As the waste containers were not included in the model, gas generation was specified at all inner EDZ nodes of the cell (properties a combination of interface and EDZ). The generation term was proportioned between nodes according to block volume of the generation node.

3.9.2.4 Initial Conditions

Initial conditions in the host rock and EDZ are linearly interpolated pressures between the top and bottom boundaries, approximately 5 MPa at the repository horizon, and fully water saturated. In repository features, initial pressure is atmospheric and water saturation is 5% in the interfaces and 70% in the drift backfill and bentonite plugs.

3.9.2.5 Deviations from the specification

Several deviations from the specification are detailed in the gridding section. Upscaled parameters associated with the interface gridding simplifications were developed by weighting parameters by the relative volume of the contributing materials. For example, for the cell inner EDZ, with an interface 1 cm thick and an inner EDZ block 25 cm thick, the porosity (θ) is calculated as follows:

$$\theta_{inner\ edz} = \theta_{interface}\frac{0.01}{0.25} + \theta_{edz}\frac{0.24}{0.25}$$ *Equation 2*

Log weighting was used for the van Genuchten air-entry pressure parameter, as a simple linear average resulted in a curve with capillary pressures at very high liquid saturations slightly greater than capillary pressures in the EDZ or interface (see Figure 127). This effect is due to the linear weighting of the van Genuchten shape parameter, n, in addition to the air-entry pressure. Using log weighting for the air-entry pressure resolves the issue without much change to the overall shape of the curve, as shown in Figure 127. The van Genuchten capillary pressure function described by the benchmark and used in the modelling is provided below:

$$P_c = -\frac{1}{\alpha}\left[S^{*-1/m} - 1\right]^{1/n}$$ *Equation 3*

$$S^* = \frac{S_l - S_{lr}}{1 - S_{lr}}$$ *Equation 4*

where:

P_c	is the capillary pressure, Pa;
S*	is the effective saturation for the capillary pressure relationship (volume ratio);
S_l	is the liquid saturation (volume ratio);
S_{lr}	is the residual liquid saturation (volume ratio);
m	is a van Genuchten fitting parameter (unitless), equivalent to m = 1 – 1/n unless otherwise specified;
n	is a van Genuchten fitting parameter (unitless); and
α	is a van Genuchten fitting parameter, Pa-1. $1/\alpha$ is the air-entry pressure parameter.

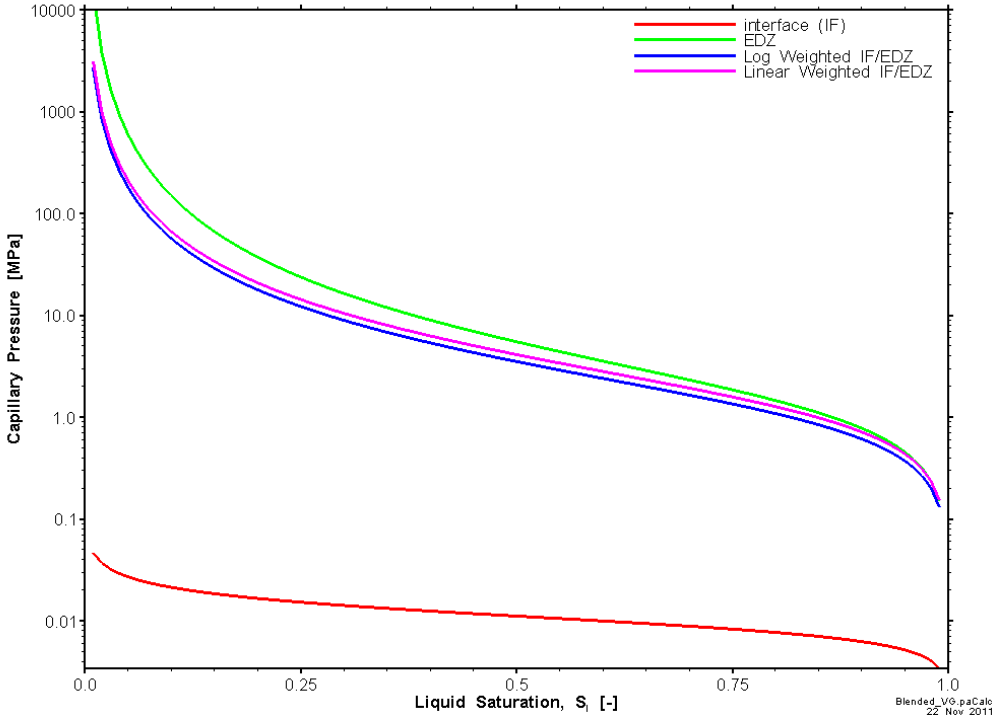

Figure 127: Capillary pressure curve for cell interface, EDZ and cell inner EDZ (combined interface and EDZ) at high liquid saturations

Table 4 provides the final parameters for upscaled interface materials. Table 4 also contains the initial conditions within the upscaled interface materials. These initial conditions are determined in the same manner as the parameters, weighted according to the relative volume of the contributing materials. Note that initial pressure conditions were not weighted: all materials with a partial saturation, including upscaled interface materials, were assigned a gas pressure of 0.1 MPa.

Table 4: Parameters and Initial Conditions for Upscaled Interface Materials

	K [m²]	Porosity [-]	Pore Compressibility [Pa⁻¹]	Tortuosity	S_{lr} [%]	S_{gr} [%]	n [-]	P_o [Pa]	Initial Water Saturation [%]
Inner cell EDZ	4.0E-14	0.18	1.06E-09	0.28	0	0	1.60	1.23E+06	96.2
Inner plug EDZ	5.0E-18	0.16	1.10E-09	0.28	0	0	1.60	1.23E+06	96.2
Main Drift Plug Interface	6.0E-20	0.35	8.24E-10	0.06	0	0	1.62	1.49E+07	69.35
Drift Interface	6.9E-17	0.40	2.06E-09	0.27	0	0	1.55	1.80E+06	68.7

Once the initial case (the base case) was working, an additional case was simulated with more conventional upscaled parameters. These improved parameters were upscaled as follows:

- scalar parameters, such as porosity, were calculated using a volumetric weighting approach, as described above.
- tensor parameters, such as permeability, used an arithmetic average when component materials were layered parallel to the direction of the tensor and a harmonic average when component materials were layered perpendicular to the direction of the tensor.

- van Genuchten shape parameter n was held constant (assumes relative permeability in the interface is the same as in the EDZ, backfill or bentonite), while the van Genuchten air entry pressure was calculated using the volumetric weighting approach of a scalar parameter.

The alternate case parameters are provided in Table 5, only for parameters that differ from the base case.

Table 5: Alternate Parameters for Upscaled Interface Materials

	Kx [m²]	Ky [m²]	Kz [m²]	n [-]	P_o [Pa]
Inner cell EDZ	5.2E-18	4.0E-14	5.2E-18	1.5	1.44E+06
Inner plug EDZ	5.0E-18	5.0E-18	5.0E-18	1.5	1.44E+06
Main Drift Plug Interface	1.0E-20	6.0E-20	1.0E-20	1.6	1.58E+07
Drift Interface	6.9E-17	6.9E-17	5.1E-17	1.5	1.96E+06

Another deviation from the benchmark is the relative gas permeability model. The benchmark defines the relative gas permeability using the Mualem model:

$$\boldsymbol{k_{rg} = (1 - S^{*})^{1/2}(1 - S^{1/m})^{2m}} \qquad \textit{Equation 5}$$

However, the modified van Genuchten model option in T2GGM, used in the models presented here, is the Luckner model, identical to the Mualem model except the 1/2 exponent is replaced by a 1/3 exponent:

$$\boldsymbol{k_{rg} = (1 - S^{*})^{1/3}(1 - S^{1/m})^{2m}} \qquad \textit{Equation 6}$$

A comparison between relative permeability curves is shown in Figure 128.

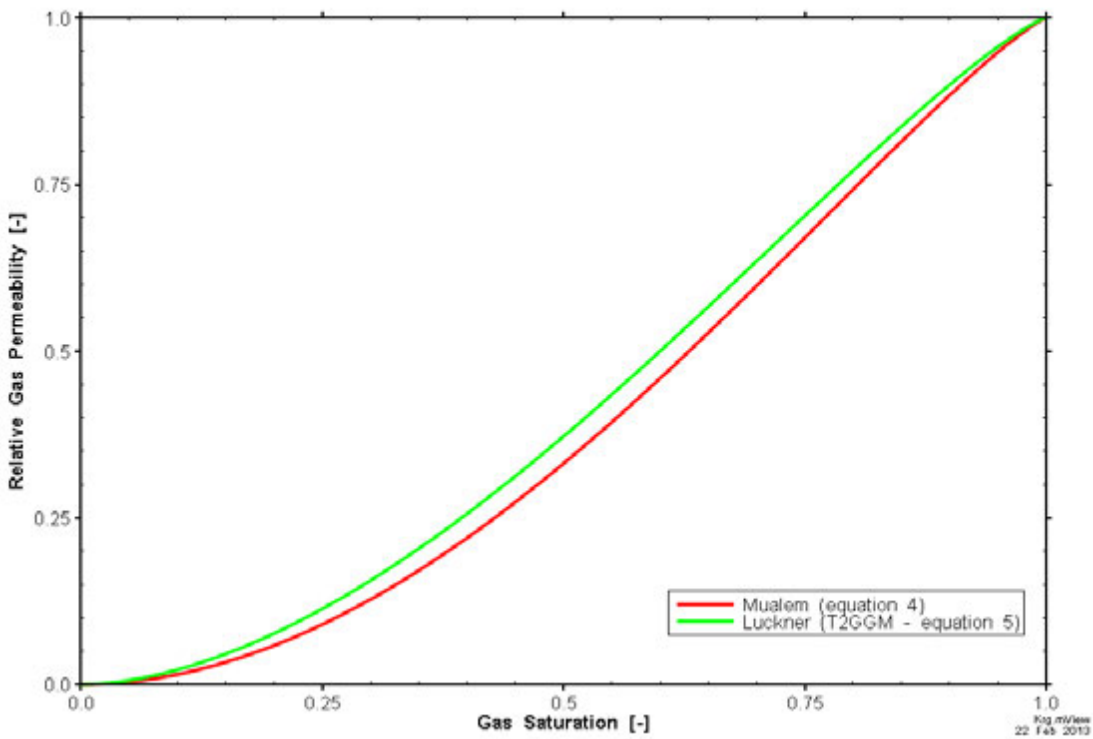

Figure 128: Relative gas permeability curves for the interface represented by the benchmark and T2GGM

3.9.3 Base Case Results

The module-scale model is only complete to about 30 000 years. The simulation time step became very small due to numeric instabilities associated with the very small gas saturations dissappearing from the system.

Output points and slices presented below correspond to those defined in the benchmark. Note that in the subsequent figures showing gas saturation, white space indicates areas where gas saturations are below the legend threshold of 1E-6, often at zero gas saturation. For figures showing gas pressure, white areas indicate areas where there is no gas, and therefore no gas pressure.

Immediately apparent at 1 year (see Figure 129) is the absence of gas in the cell interface and EDZ at 1 year, despite the generation of a gas phase in the cells. This is a result of the dissolution of the gas initially present in the interface (less than 5% initial gas) and the negative water pressures, i.e., suction, in the cells (as a result of the initial gas pressure equal to 0.1 MPa) causing the immediate dissolution of any gas phase generated. As the cell water pressures increase, the generated gas remains in the gas phase, and the gas saturation increases above zero. Gas is still present in the drifts at 1 year due to the greater amount of initial gas in the drifts (approximately 30% initial gas).

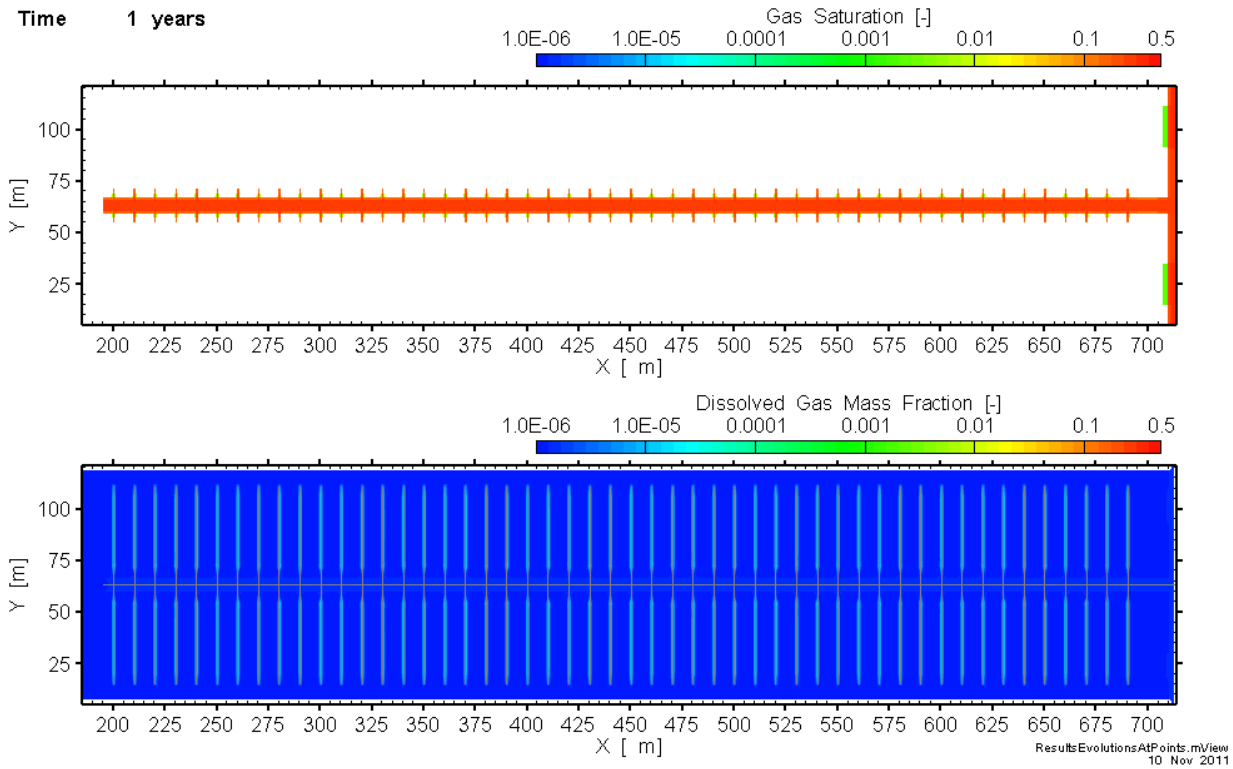

Figure 129: Gas saturation and dissolved gas mass fraction at 1 year, at a plan slice through the middle of the repository.

Over time, it is also apparent that the boundary conditions at the upper and lower ends of the main drift do not seem to correspond with conditions within the cells and access drift. Two processes are modelled by the main drift boundary condition (see gray line in Figure 130 and Figure 131 for the boundary condition):

(1) Between 1 and 1000 years, there is a drop in water saturation and water pressure, identical in both the upstream and downstream boundary conditions. Presumably, this is due to the bentonite plugs in the main drift, with their very high capillary pressures drawing water into the plugs during resaturation.

(2) Between 400 and 30 000 years, pressures upstream (Y=0) are slightly greater than downstream (Y=126). Note that the difference is so small, it is not apparent on the plot. Based on this

pressure difference and the location of the module within the repository, it would be expected for water and gas to flow along the main drift from the upstream to the downstream boundary.

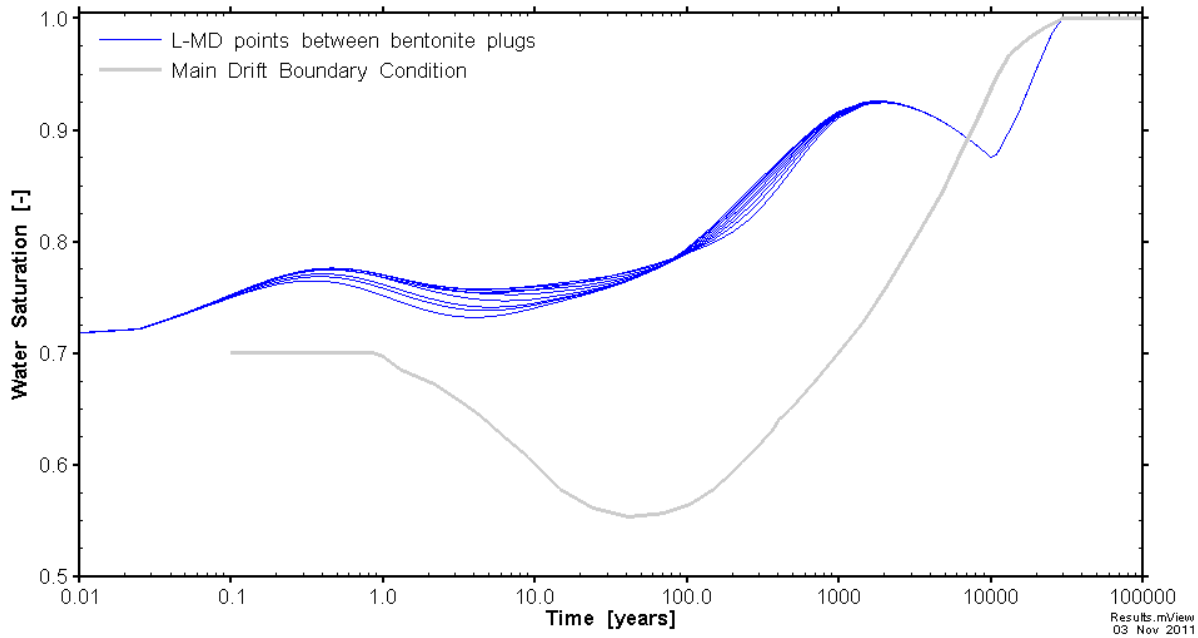

Figure 130: Water saturation with time at L-MD points between the bentonite plugs (Y= 35 to Y= 90), compared to the main drift boundary condition.

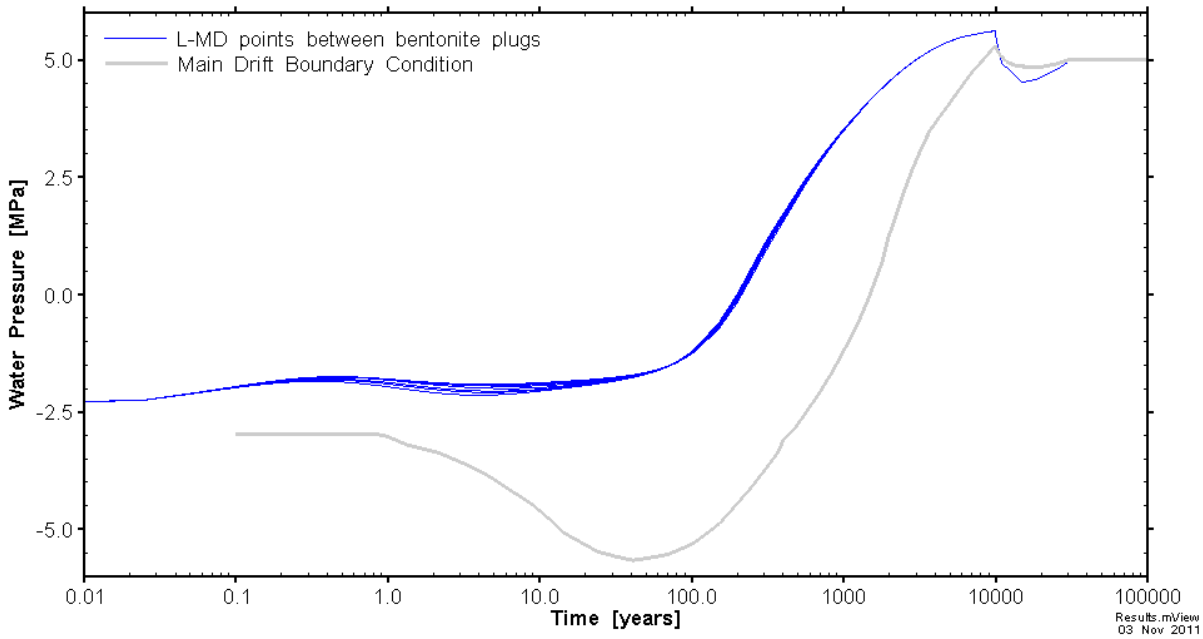

Figure 131: Water pressure with time at L-MD points between the bentonite plugs (Y= 35 to Y= 90), compared to the main drift boundary condition.

Water saturation and water pressure along the L-MD line (a line along the center of the main drift), shown in Figure 132, best illustrates the differences between the module main drift, defined as the main drift between the bentonite plugs (Y=35 to Y=90), and the main drift boundary conditions. Note that the low

initial capillary and water pressures between Y=15 to Y=35, and between Y=90 and Y=110 are due to the bentonite plugs in the main drift. Two additional figures, Figure 130 and Figure 131, show water saturation and water pressure with time at all the module main drift points in the L-MD line between the bentonite plugs compared to the main drift boundary condition. In the module main drift, water saturates the drifts up until approximately 0.5 years, when a small dip in water saturation of approximately 3% is observed, due to the bentonite drawing water as described above. Water saturations return to the same level as at 0.5 years by approximately 80 years. There is a small corresponding drop in water pressure of approximately 0.4 MPa. Generally, the model drift resaturates and water pressures equilibrate towards host rock pressures more rapidly than expressed by the boundary condition.

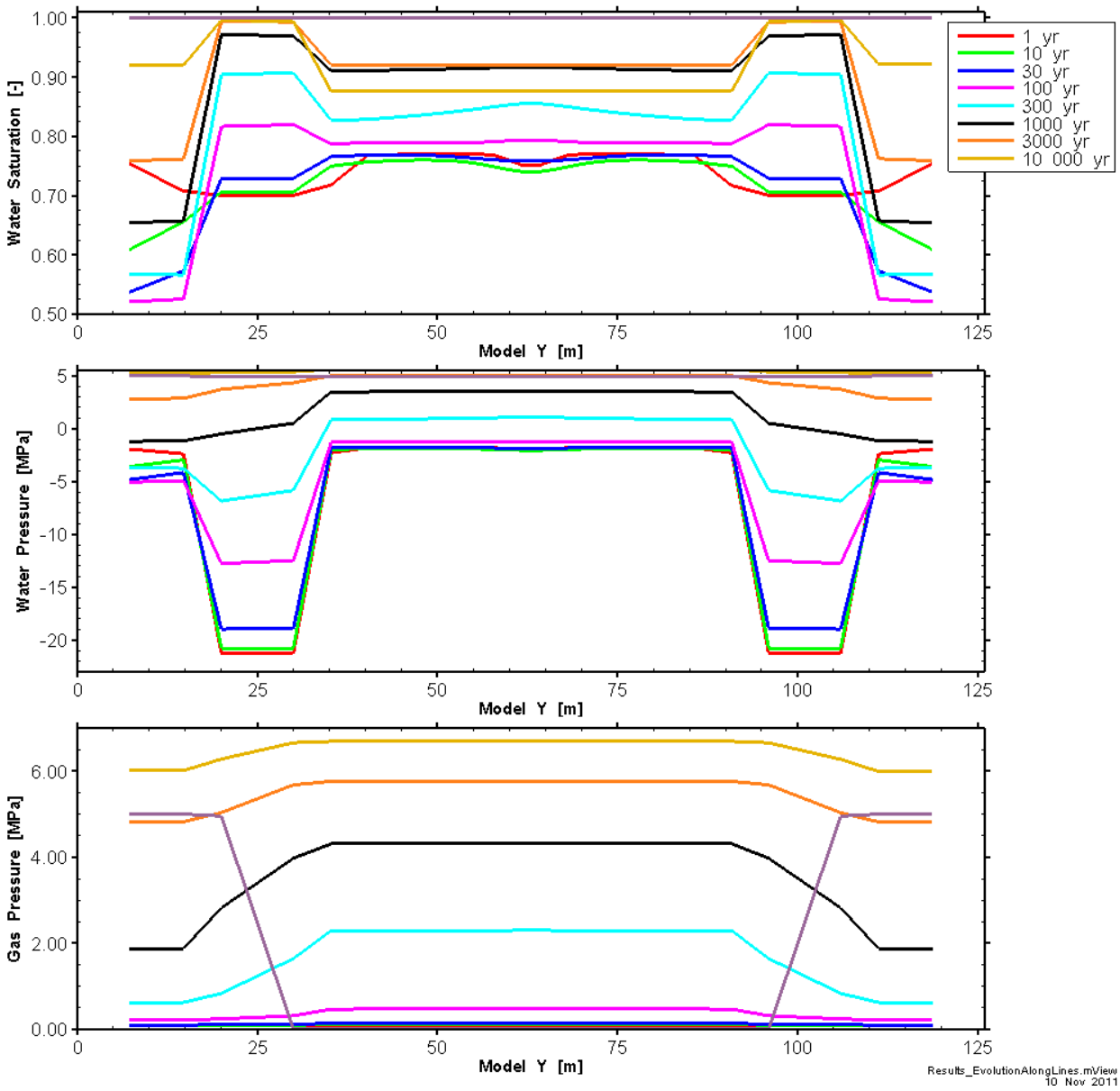

Figure 132: Evolution of water saturation, water pressure and gas pressure for various times along the L-MD line.

This incongruence in the boundary condition causes gas and water from the module to flow towards both the upstream and downstream boundary conditions for the first 10 000 years, as shown by the F-P flows in Figure 133. After 10 000 years when gas generation ceases, water begins to flow in from the boundary conditions. As well, since pressures at the boundary condition are, prior to 10 000 years, considerably lower than the module, a strong pressure gradient develops between the ends of cell 1 and adjacent cells

and the boundary condition, resulting in gas flow in these cells away from the access drift and towards the boundary condition (see gas saturations at 300 years in Figure 134). Once gas has penetrated the host rock, gas flows from the cells through the host rock towards the boundary condition.

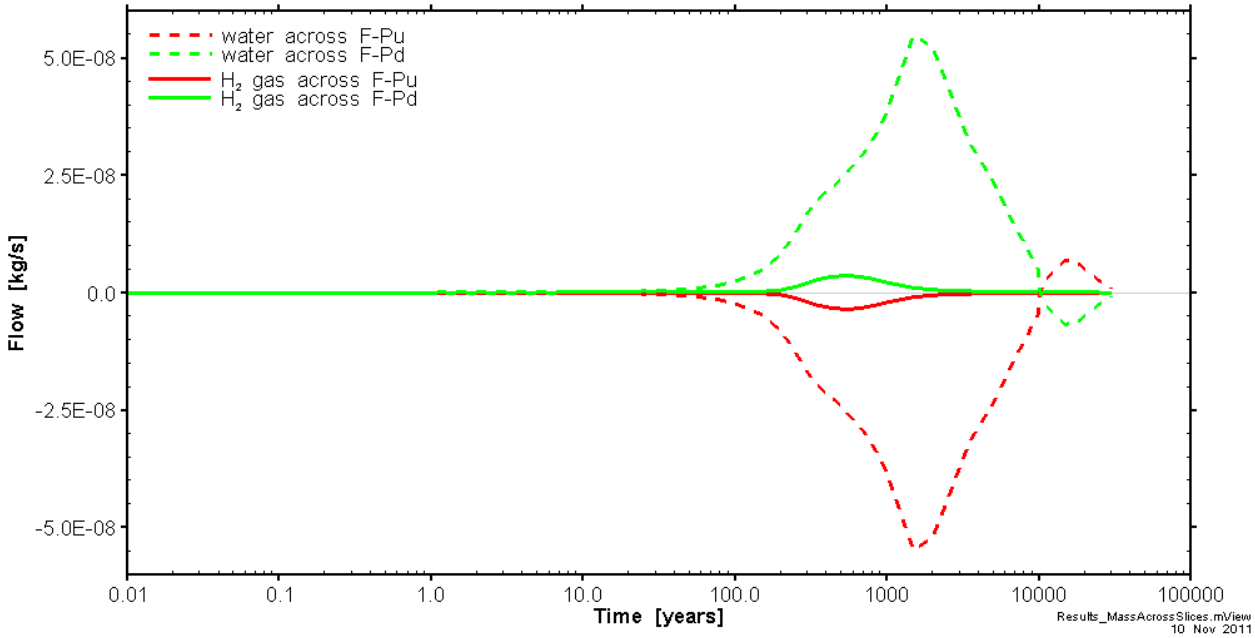

Figure 133: Evolution of water and H_2 gas with time across F-P surfaces.

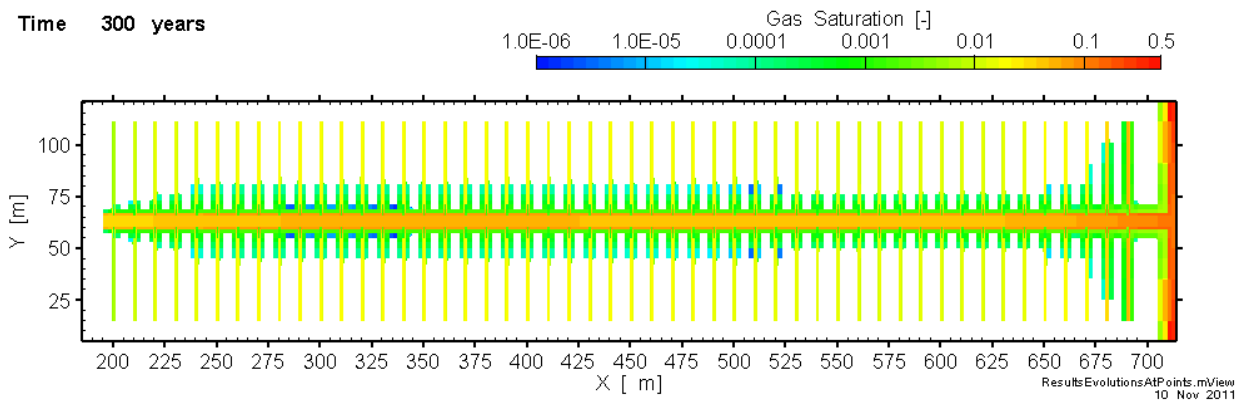

Figure 134: Plan view of gas saturations at 300 years, through the middle of the repository.

Note that after 1000 years, water saturations begin to drop in the module (see Figure 130) due to gas generated in the repository flowing out to the main drift but impeded from flowing out of the main drift (through the boundary conditions) by the bentonite blocks in the main drift. The decrease in module water saturation after 1000 years in Figure 130 is correctly not represented by the main drift boundary condition, due to the presence of the bentonite blocks preventing transmission of gas along the main drift.

For the first 1000 years, water and H_2 gas generated within the cells travel towards the access drift, along the access drift and to the main drift. Water and gas flow across slices in the cells, access drift and main drift are shown in Figure 135 through Figure 138. Note the exception at cell 1 (F-C1) in Figure 137, where at approximately 350 years the gas flow direction turns away from the access drift and towards the main drift boundary through the host rock. This is a consequence of the main drift boundary condition, as described above. Both water and gas flows divide in the main drift and flow towards both the upstream and downstream boundary conditions, as shown by F-Pu (upstream) and F-Pd (downstream) in Figure 136. This

is due to the difference between the boundary conditions and the equilibration of module water pressures (i.e., module pressures rise more rapidly than the prescribed boundary pressures in the main drift, due to equilibration of pressure in the module with the formation pressure, as explained above).

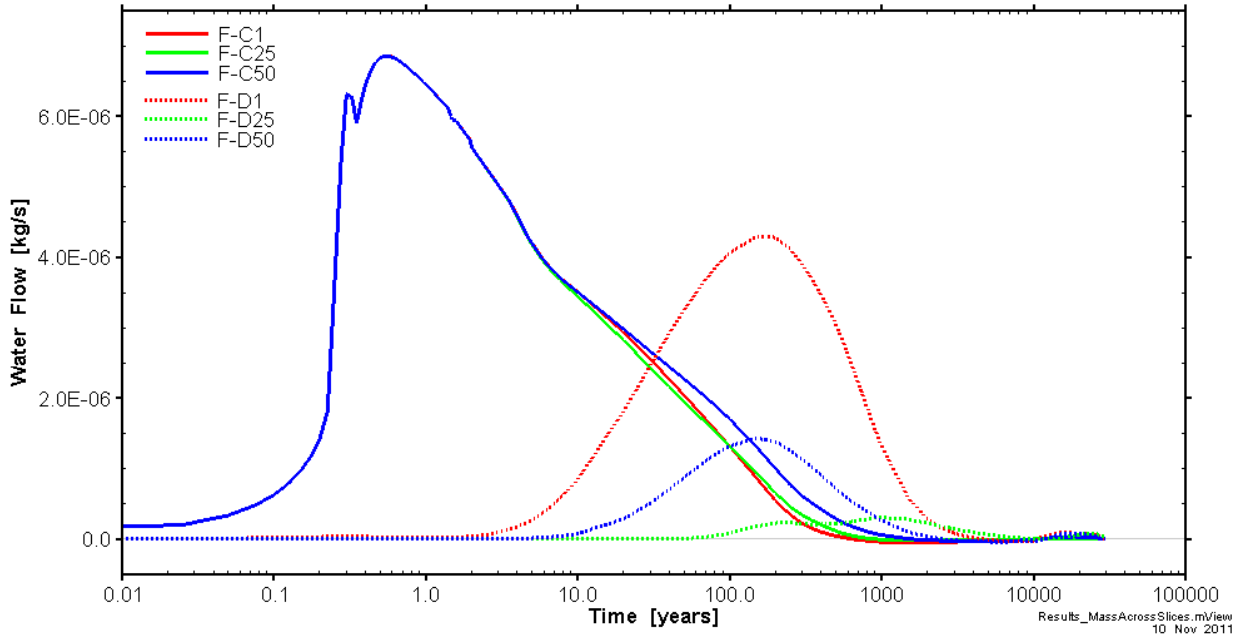

Figure 135: Evolution of liquid water with time across F-C (cell) and F-D (access drift) surfaces.

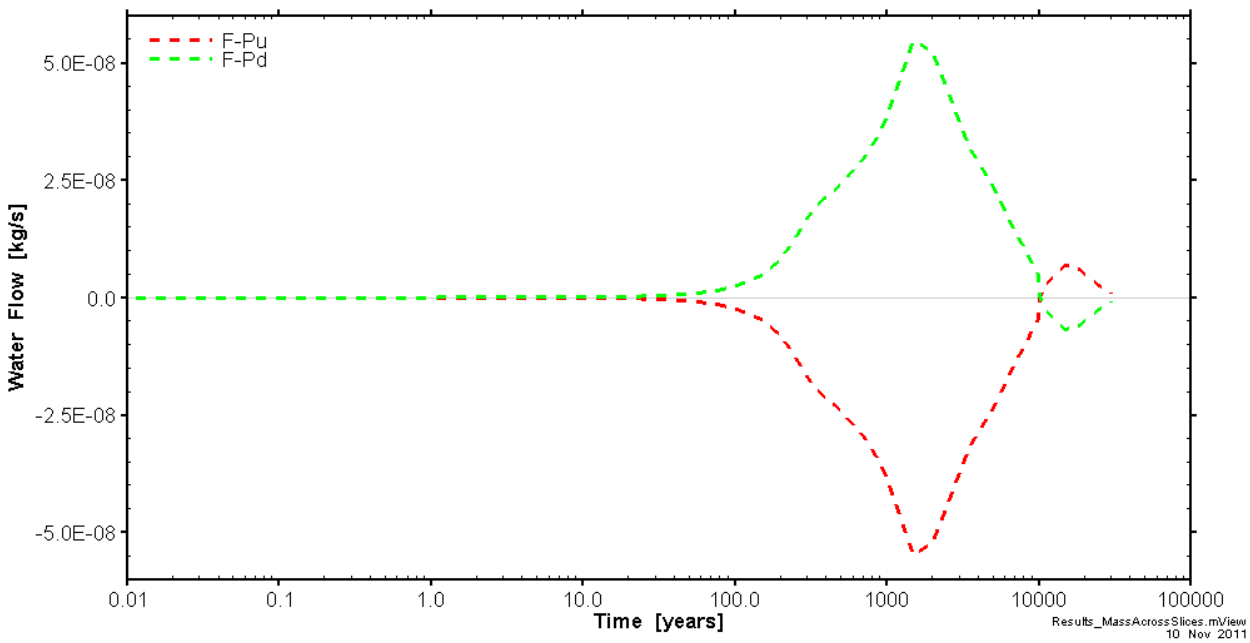

Figure 136: Evolution of liquid water with time across F-P (main drift) surfaces.

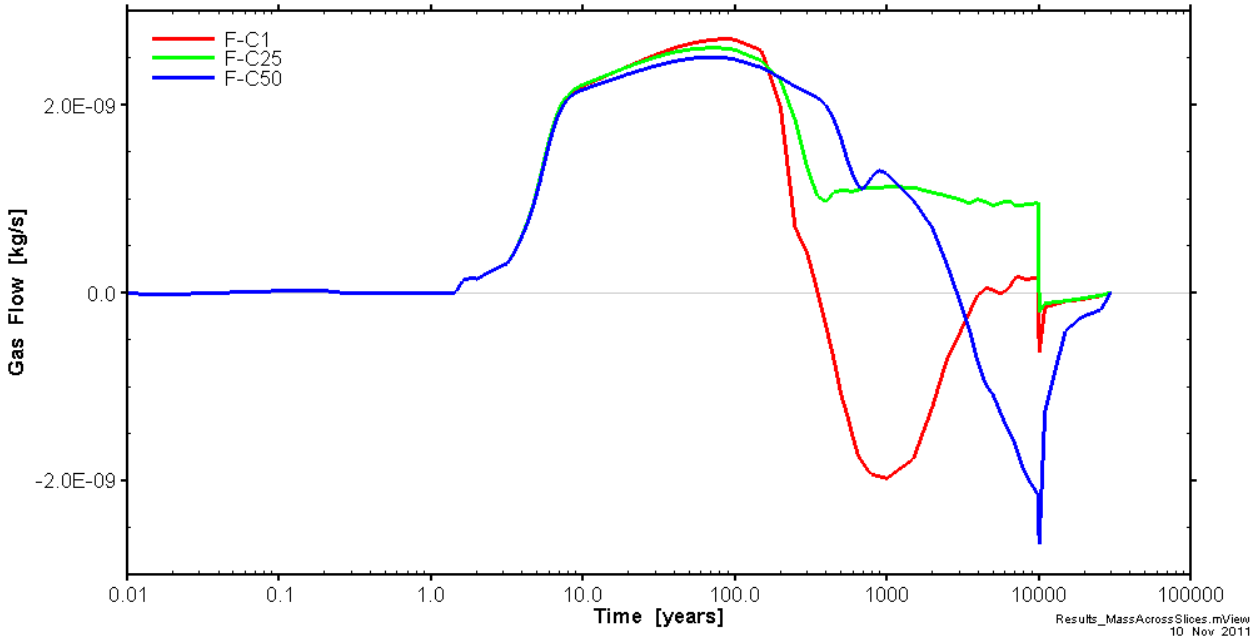

Figure 137: Evolution of H_2 gas with time across F-C (cell) surfaces.

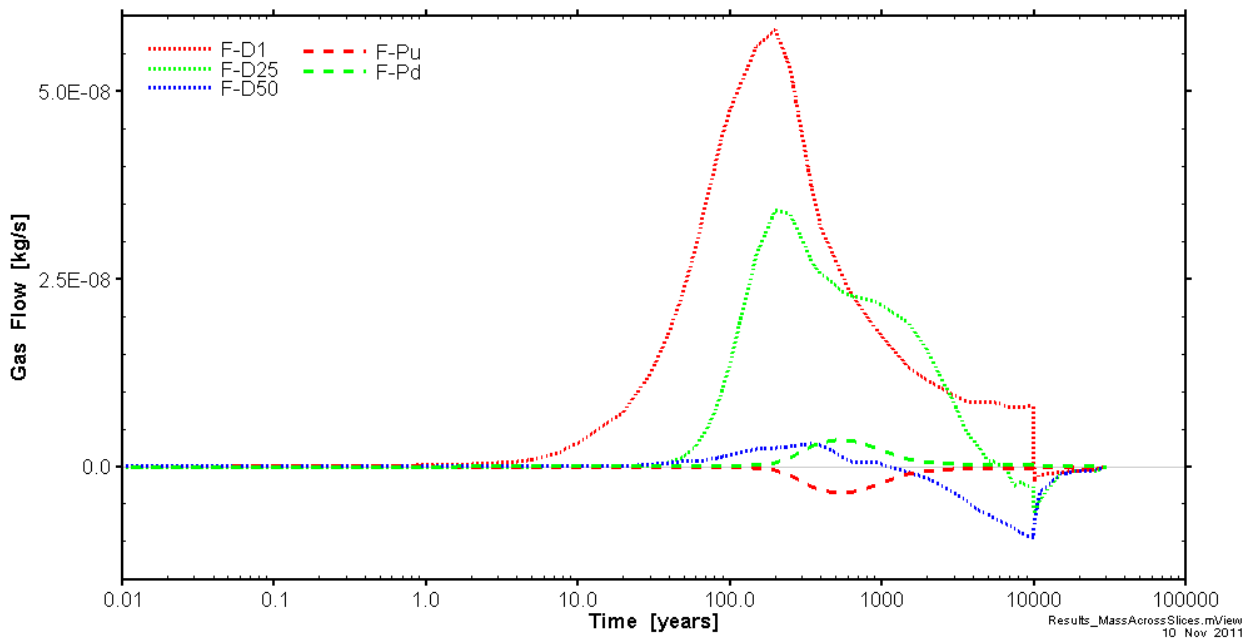

Figure 138: Evolution of H_2 gas with time across F-D (access drift) and F-P (main drift) surfaces.

Gas flow in the access drift is least near cell 50 (F-D50), farthest from the main drift, and greatest near cell 1 (F-D1), closest to the main drift, as F-D1 has collected the gas from all the cells along the drift (Figure 138). The same pattern is not repeated for the water flows, as water flows in the access drift near the middle cell (F-D25) are the smallest flows (Figure 135). This somewhat odd pattern of water flows is due to the water pressure gradients along the access drift. Water pressures at all points in the system are shown in Figure 139, with water pressures in the access drift described here represented by the dark blue lines. There is very little difference in water pressure within the access drift between cell 50 and 25 until approximately 50 years, when water flows begin to increase at cell 25. The water pressure difference

remains small, as does the water flow at cell 25, compared to the water pressure difference between with cell 1 and cell 25. Water pressures equilibrate more quickly in the middle of the module and farthest from the main drift (dashed red, green and blue lines in Figure 139), due to boundary condition effects close to the main drift, and results in low pressure gradients in the middle of the module. For cells farthest from the main drift, differences in water pressure between the module and the host rock along the whole length of cell 50 result in greater water gradients and therefore greater water flows at cell 50 (F-C1 after 20 years and F-D50).

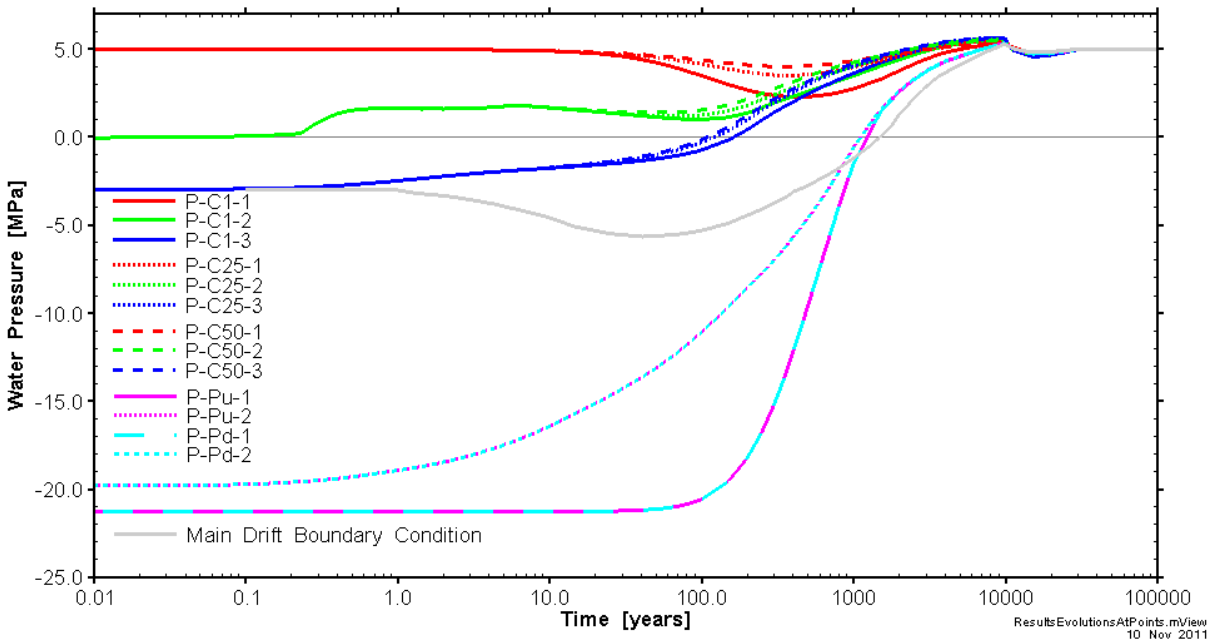

Figure 139: Water pressures at all output points.

Gas and water flow directions begin to change after 1000 years (Figure 135 to Figure 138), as gas and water pressures in the repository increase. Gas pressures increase due to gas generation and the impedance of gas transport out of the module by the bentonite seals in the main drift. Water pressures increase due to equilibration with the surrounding host rock. Water pressures at all output points are shown in Figure 139, and gas pressures in Figure 140. Around the time gas and water pressures at the cells reach adjacent host rock pressures of approximately 5 MPa, water and gas flows begin to reverse direction, and flow away from the access drift and away from the main drift, and into the host rock. This is evident in the gas flows at cell 50 (F-C50 in Figure 137 and F-D50 in Figure 138) and cell 25 (F-D25 in Figure 138). Water flows in all cells and the access drift at cell 1 and cell 50 are also slightly negative after 1000 years, although it is difficult to observe in Figure 135. Water flows in the access drift continue to flow into the main drift. Note that pressures in the middle of the module, near cell 25, are less variable than at the edge of the module at cell 50 as previously described. Consequently, flow changes occur earlier at cell 50 than at cell 25, and for gas flow out of the cells and water flow in the access drift, the flow direction does not change at all at cell 25 (F-C25 in Figure 137).

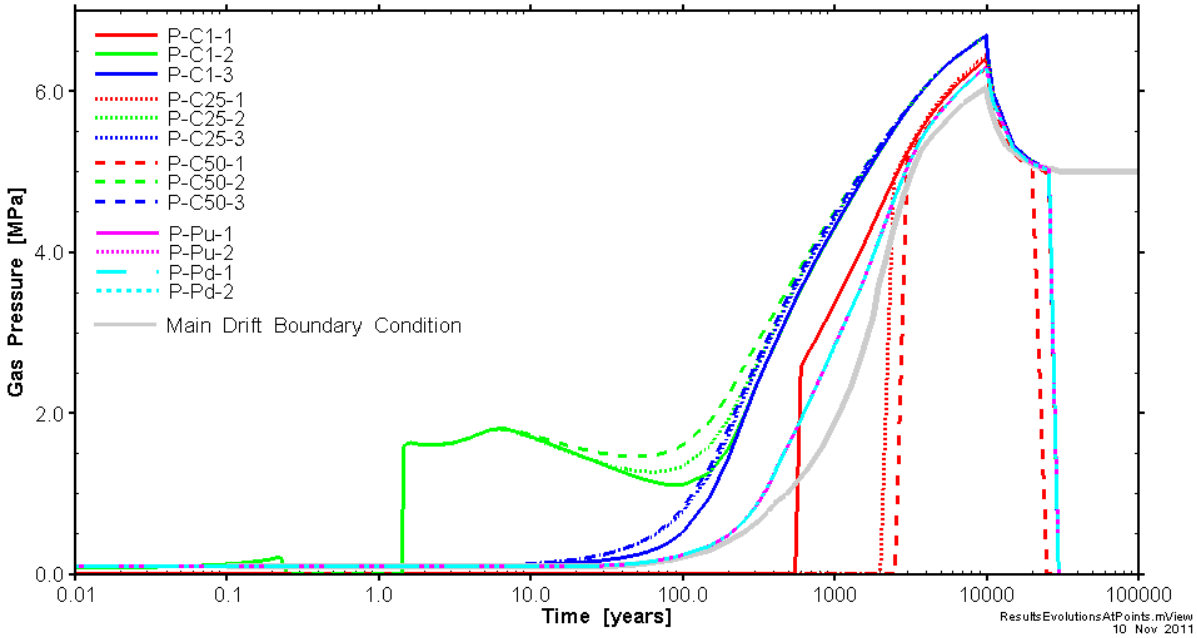

Figure 140: Gas pressure at all output points.

Note certain features of gas pressures in the cells (green lines for P-C1-2, P-C25-2 and P-C50-2 in Figure 140): the zero gas pressure around 1 year is due to zero gas saturations in the cells at that time; the relatively high gas pressure in the cells once the gas phase resumes in the cells at 1.5 years is due to the greater water pressures in the cells resulting from equilibration with the host rock while the cells were fully water saturated; the drop in gas pressure after 10 years is a result of the bentonite plugs at the end of each cell drawing water due to their high capillary pressures, with a corresponding drop in the gas pressure; and the delay in the drop in gas pressure is due to bentonite plugs preferentially sucking water from the adjacent host rock, until pressures in the host rock adjacent to the bentonite plugs decrease below pressures in the cells.

While the main direction of gas flow before 1000 years had been towards the main drift, some gas was also travelling outwards from the cells and drifts into the host rock. Starting close to the access drift, gas began to migrate into the host rock by 100 years (see Figure 141). At 300 years (see Figure 142), gas migration out into the host rock expanded along the cell away from the access drift, and at 1000 years (see Figure 143), gas had penetrated all the host rock between cells for all cells except those cells farthest from the main drift. Near cell 1 (closest to the main drift), boundary condition effects increased migration of gas into the host rock. For the remainder of cells, gas migration into the host rock occurred over a greater length of the cell (closest to the access drift) at cells near the middle and farthest from the main drift (i.e. cells between approximately X = 200 m to X = 525 m). This can be explained by the water pressures in the module: water pressures equilibrated more quickly in the middle of the module and farthest from the main drift as previously described, resulting in less water flowing into the cells, thus allowing gas to migrate outwards more easily. For cells farthest from the main drift, differences in water pressure between the module and the host rock along the whole length of cell 50 resulted in sufficient water flow to delay gas flow into the host rock until approximately 3000 years (see Figure 144).

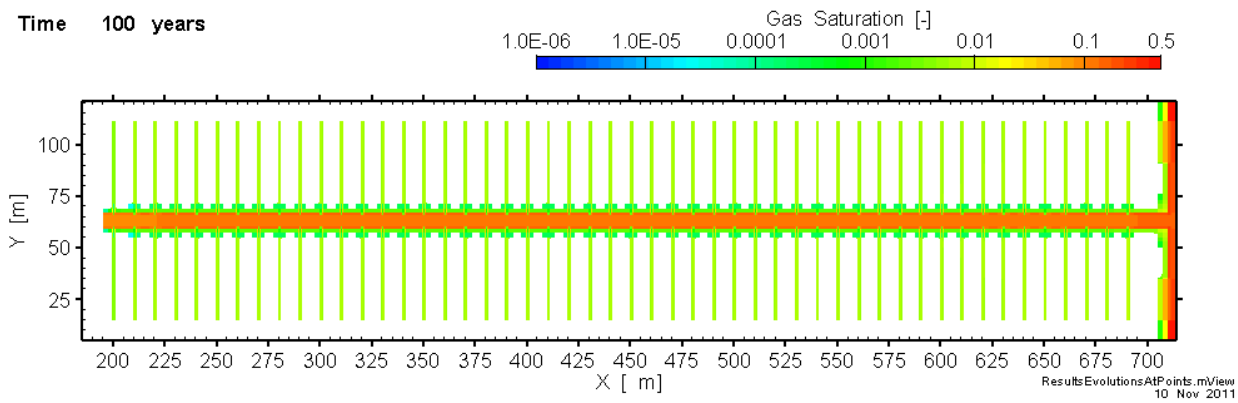

Figure 141: Gas saturation and at 100 years, at a plan slice through the middle of the repository.

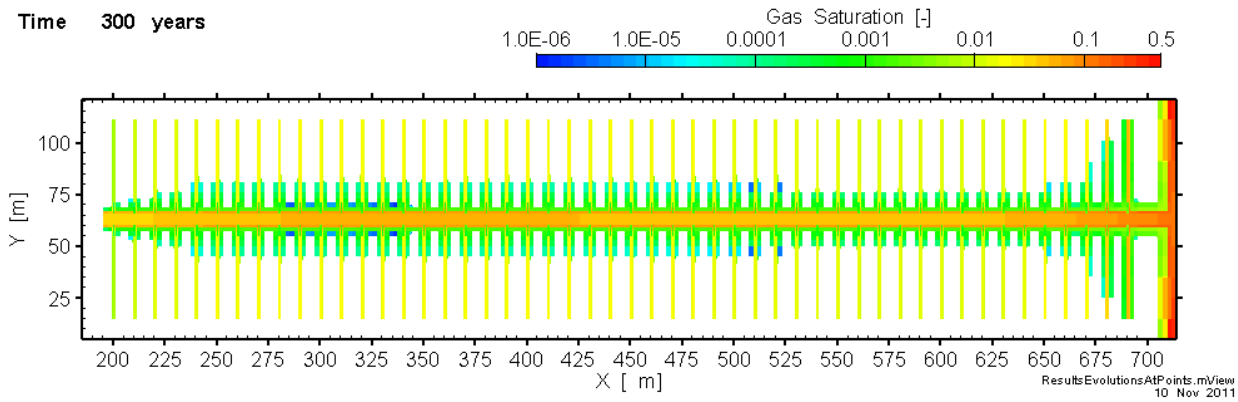

Figure 142: Gas saturation and at 300 years, at a plan slice through the middle of the repository.

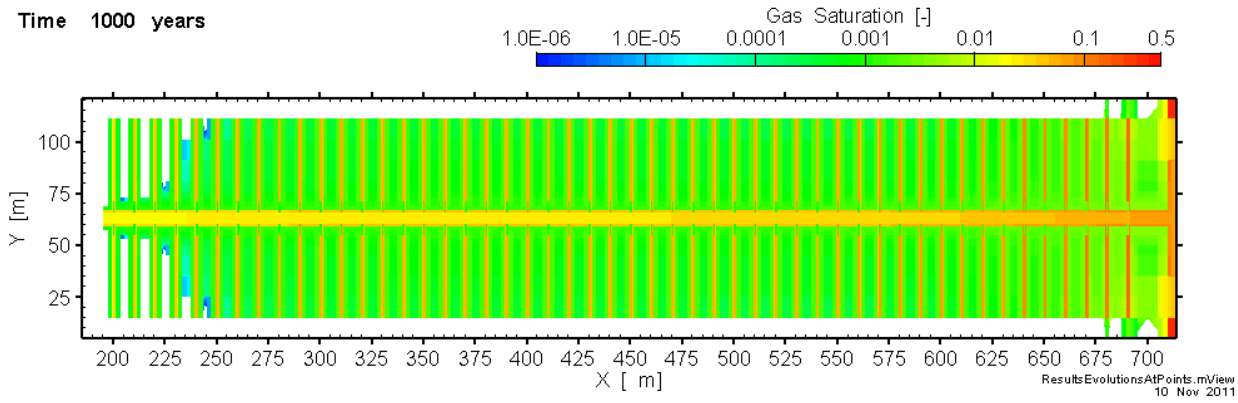

Figure 143: Gas saturation and at 1000 years, at a plan slice through the middle of the repository.

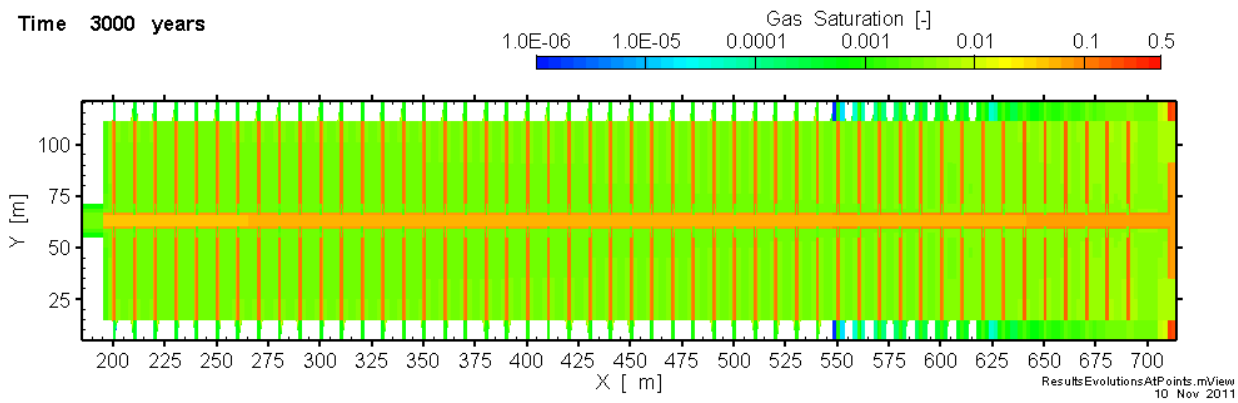

Figure 144: Gas saturation and at 3000 years, at a plan slice through the middle of the repository.

At 10 000 years, gas generation has ceased. Peak gas pressures of 6.7 MPa are observed within the cells and drifts at this time (see Figure 140). Gas saturations at this time are shown in Figure 145 in plan view, and Figure 146 at a vertical slice through a cell. Gas saturations have reached the Y boundary, and have migrated as far as 30 m out into the host rock away from the main drift in the X direction. Dissolved gas mass fraction has migrated approximately 30 m farther than the gas phase, although this dissolved gas is at very low concentrations. In the vertical direction, gas saturations have migrated upwards approximately 50 m and downwards approximately 25 m. Dissolved gas has migrated within 15 m of the top and bottom boundaries.

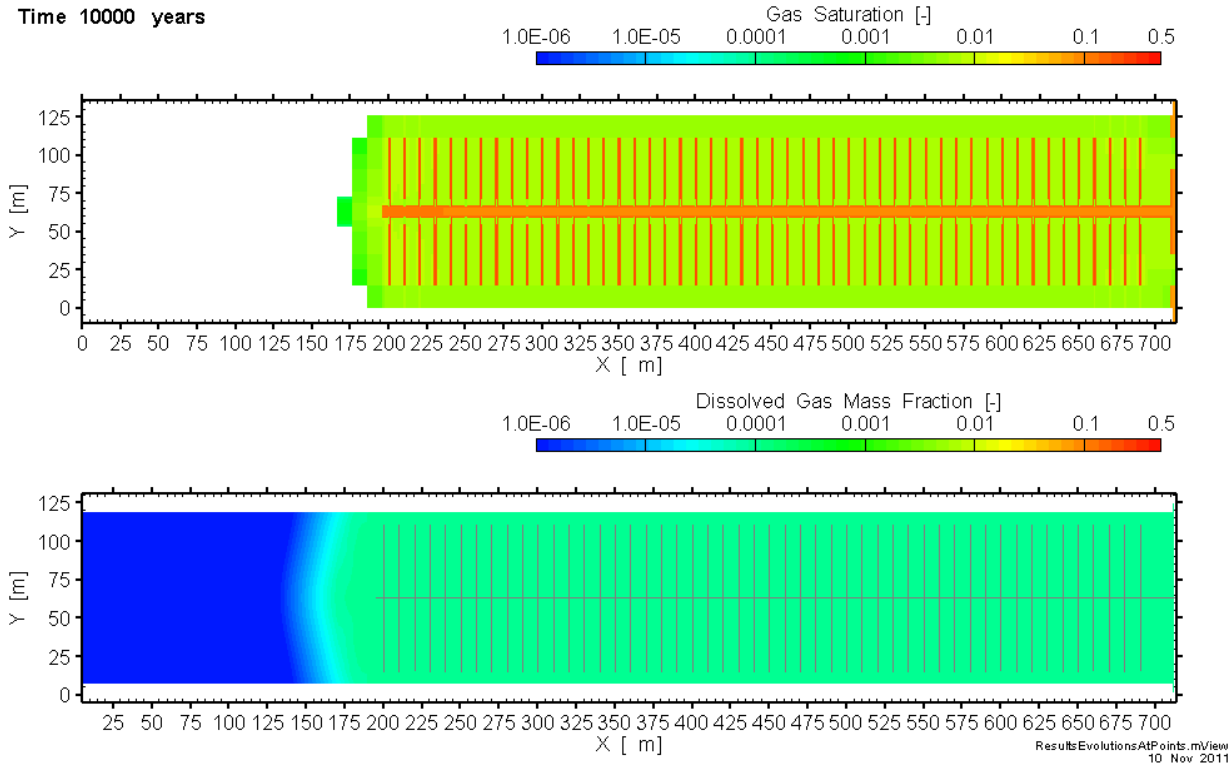

Figure 145: Gas saturation and dissolved gas mass fraction at 10 000 years, at a plan slice through the middle of the repository.

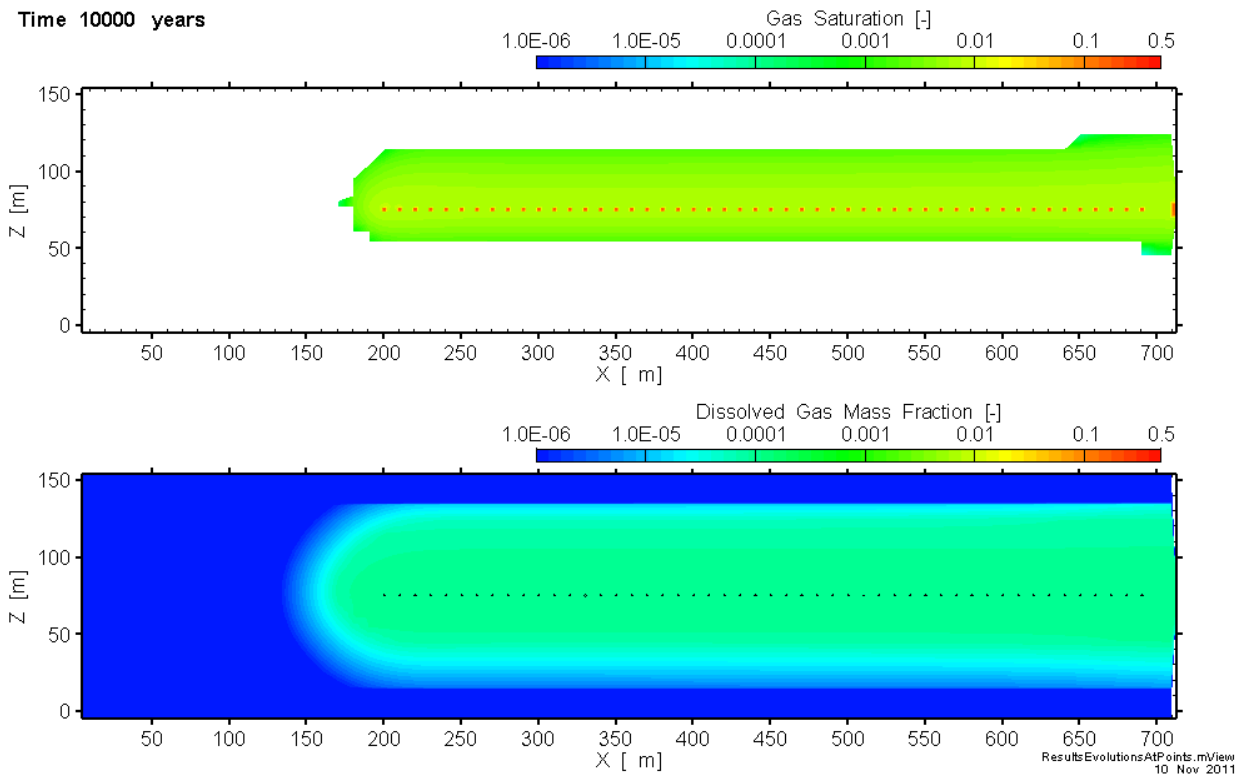

Figure 146: Gas saturation and dissolved gas mass fraction at 10 000 years, for a vertical XZ slice at Y = 72 (just above the bentonite plugs in the cells). Note that locations of cells are shown as black circles for clarity with dissolved gas mass fraction.

After 10 000 years, gas phase present in the system dissolves, and only a small amount of gas just above the repository remains by 30 000 years (see Figure 147). The module has approximately 13 kg of initial mass and approximately 100 800 kg of mass is generated in the module. At the end of 30 000 years, only 0.001 kg remains in the gas phase, and 100 675 kg is present as dissolved gas. The difference exits the system from the main drift boundaries, both upstream and downstream (155 kg and 164 kg, respectively), primarily as free phase gas (99%). A negligible amount of dissolved gas exits the system from the top and bottom boundaries. A mass balance error of 0.2% was calculated, and it should be noted that this error includes error associated with the calculation of mass leaving across the main drift boundary conditions (which is limited by the time step output resolution).

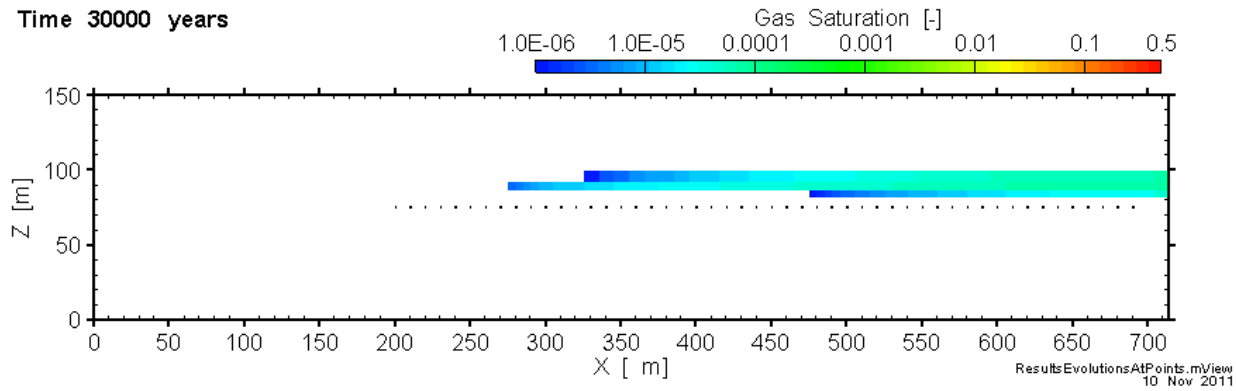

Figure 147: Gas saturation at 30 000 years, for a vertical XZ slice at Y = 72 (just above the bentonite plugs in the cells). Note that locations of cells are shown as black circles for clarity.

In examining gas saturations in the different repository materials, it is not clear by 300 years which component of the repository system allows the most gas transport, although bentonite is obviously a barrier to gas transport (see Figure 148). In examining H_2 gas flows by material across F-C slices, as shown in Figure 149, approximately half the total flow, a little more with time, is represented by the inner EDZ (upscaled interface material). The apparent minimal importance of the interface in the cells is likely due to the low permeability of the inner EDZ of the cell plugs, as the transmissivity of the inner EDZ of the plugs is equal to the transmissivity of the EDZ around the plug (1.2E-11 m^2/s). The transmissivity of the cell inner EDZ is greater than the EDZ (9.8E-8 m^2/s), but this is clearly limited by the transmissivity of the plug inner EDZ. This suggests that for the cells (including the plug), the interface plays a small role. The cell-scale model also concluded that the cell interface was of minimal importance; however, this included the plug interface (i.e. removal of both cell and plug interfaces had minimal impact on flows out of the system). An interesting sensitivity case would be removal of the cell and plug interfaces at the module-scale.

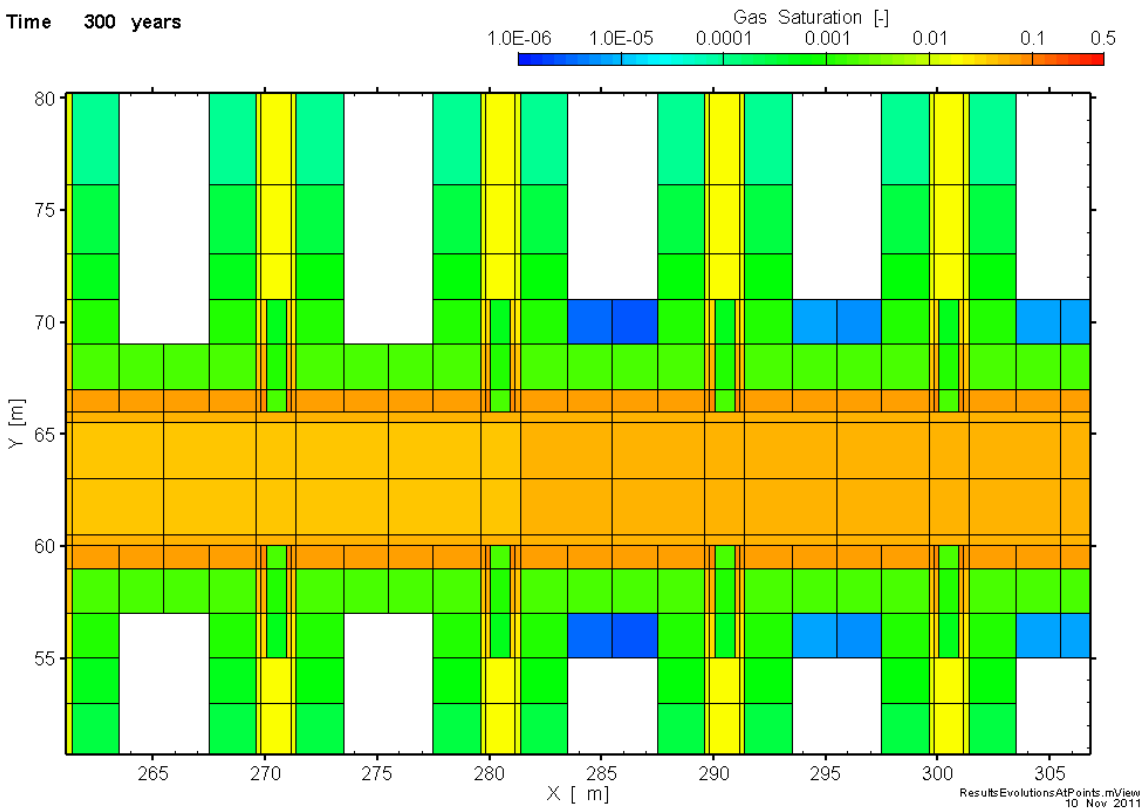

Figure 148: Gas saturation at 300 years, at a detail of a plan slice through the middle of the repository. Green blocks are either bentonite plugs at the end of cells, or host rock. White areas are areas with gas saturation less than 1E-6. Reminder that cell centers of upscaled interface and EDZ have modified block volumes similar to the adjacent EDZ blocks.

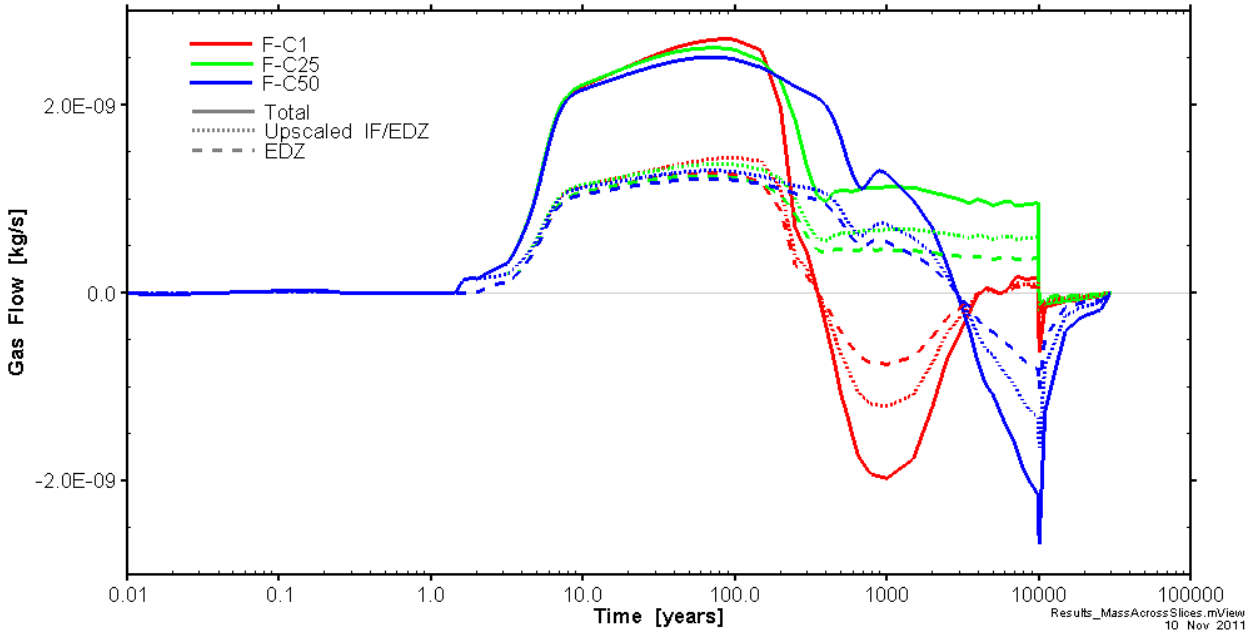

Figure 149: H2 gas flow across F-C slices, shown for material components in the slice, upscaled interface (IF)/EDZ and EDZ.

Across F-D slices, shown in Figure 150, the backfill has the greatest transmissivity of 2.5E-9 m^2/s, followed by the upscaled interface with a transmissivity of 3.4E-10 m^2/s and the EDZ with a transmissivity of 4.9E-11 m^2/s. While the backfill transmits the greatest portion of flow, the upscaled interface provides a significant contribution, with 36% of total peak flow at 350 years, while only representing 9% of the total cross-section area of the access drift (including EDZ).

In the F-P slices through the main drift plugs, shown in Figure 151, approximately three-quarters of gas flow occurs through the upscaled interface (combined with bentonite) with a transmissivity of 5.9E-13 m^2/s, and the remainder flows through the bentonite plug with a transmissivity of 2.9E-13 m^2/s.

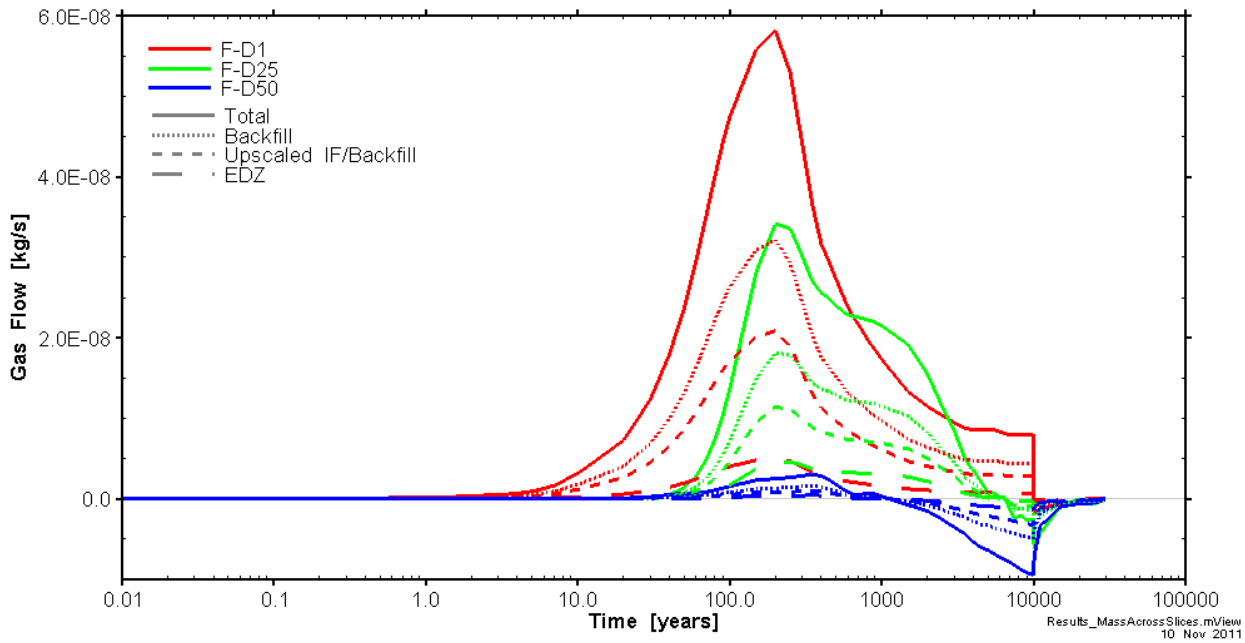

Figure 150: H_2 gas flow across F-D slices, shown for material components in the slice, backfill, upscaled interface (IF)/backfill and EDZ.

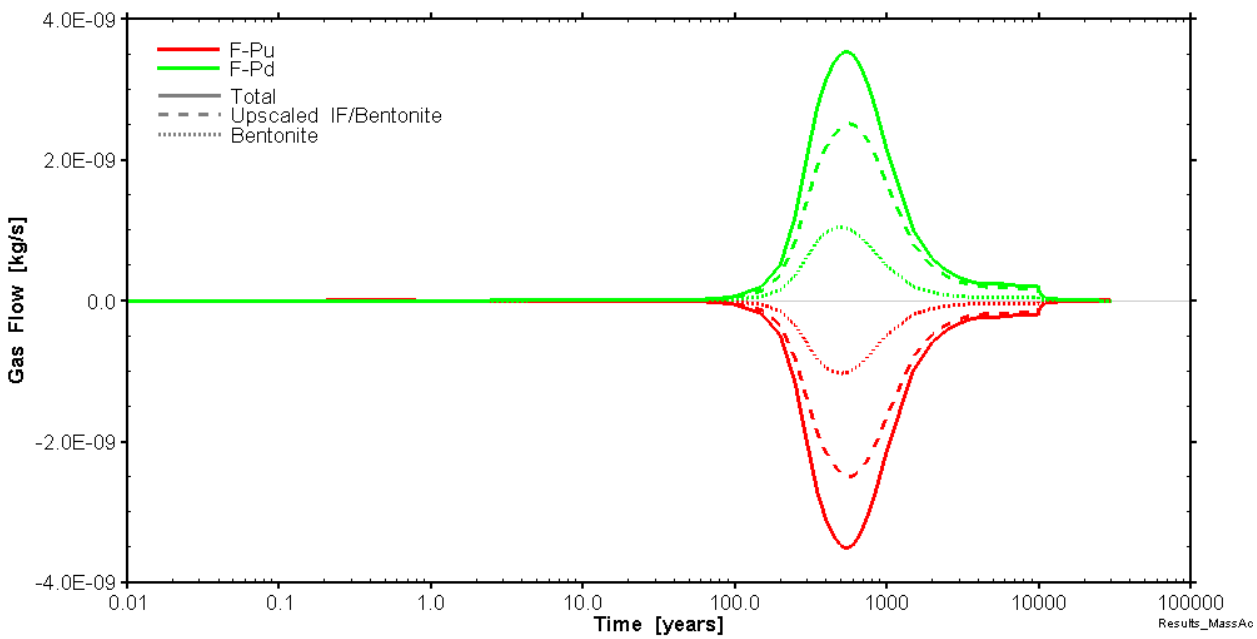

Figure 151: H_2 gas flow across F-P slices, shown for material components in the slice, upscaled interface (IF)/bentonite and bentonite.

3.9.4 Sensitivity Cases

A single sensitivity case with alternate upscaled parameters was simulated, as described in Section 3.9.2.5. This simulation is only complete to approximately 7000 years.

The alternate parameter case has slightly different parameters for the upscaled interface elements (Table 5). These upscaled interface elements have slightly anisotropic permeabilities due to the method used for upscaling permeability (average permeability for flows parallel to the interface and harmonic weighting for flows perpendicular to the interface); relative permeabilities equivalent to the material combined with the interface (EDZ, backfill or bentonite); and van Genuchten air entry pressures weighted by volume of the contributing material.

The change in parameters had little impact on the results, as shown by the water and gas flows in Figure 152 through Figure 155; the water saturations in Figure 156; and the water and gas pressures in Figure 157 and Figure 158. The greatest differences occur with water saturations within the cell (P-C1-2, P-C25-2, P-C50-2), with the alternate parameter set having greater water saturations after approximately 200 years, with a maximum difference of approximately 5% at the current end of the simulation. This difference in cell water saturation does not seem to affect saturations, pressures or flows in the access drift.

The minimal differences between these two cases suggest that the first modelling attempt (the reference case) is a sufficiently suitable representation of an upscaled interface.

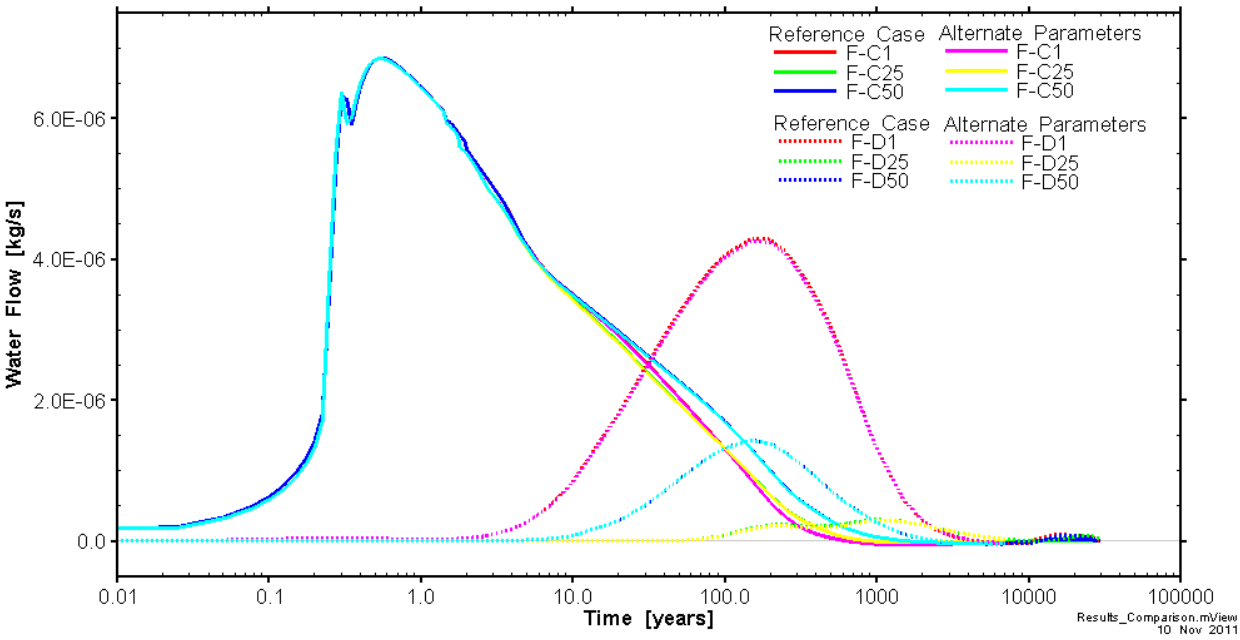

Figure 152: Comparison of alternate parameters to reference case: evolution of liquid water with time across F-C (cell) and F-D (access drift) surfaces.

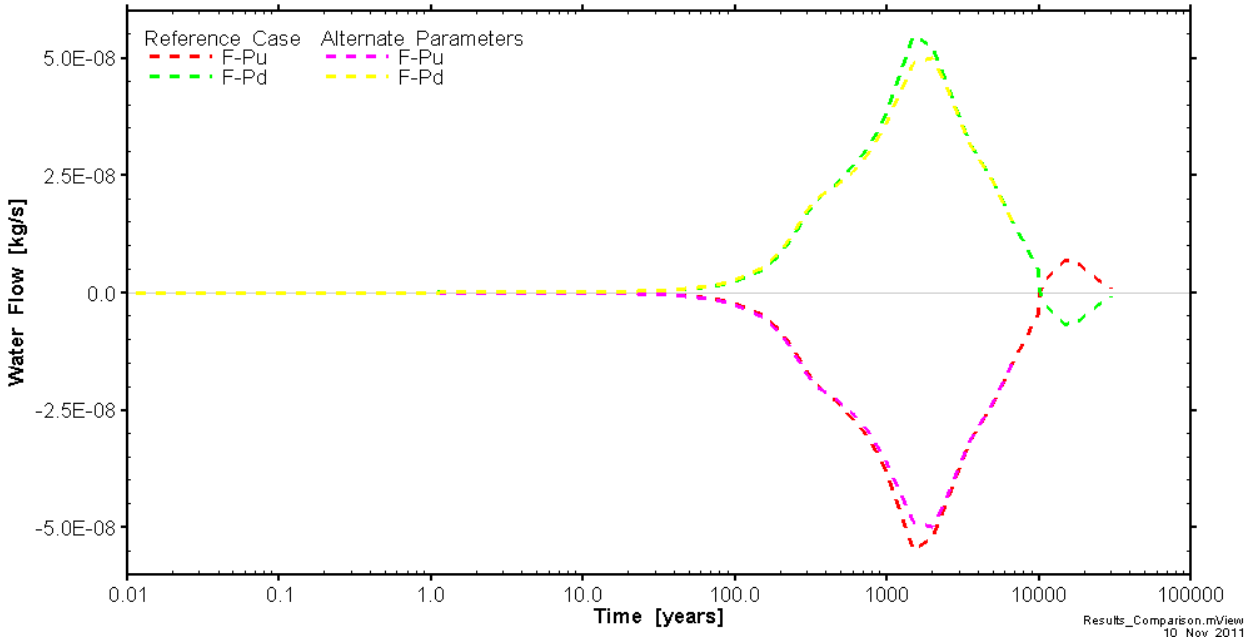

Figure 153: Comparison of alternate parameters to reference case: evolution of liquid water with time across F-P (main drift) surfaces.

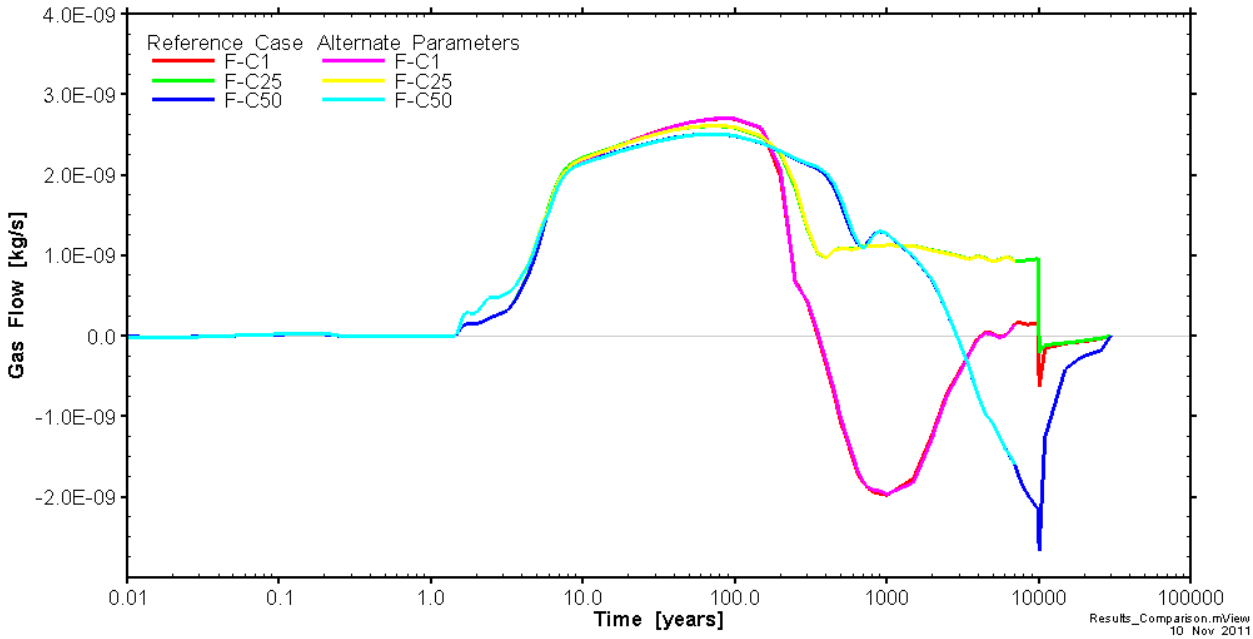

Figure 154: Comparison of alternate parameters to reference case: evolution of H_2 gas with time across F-C (cell) surfaces.

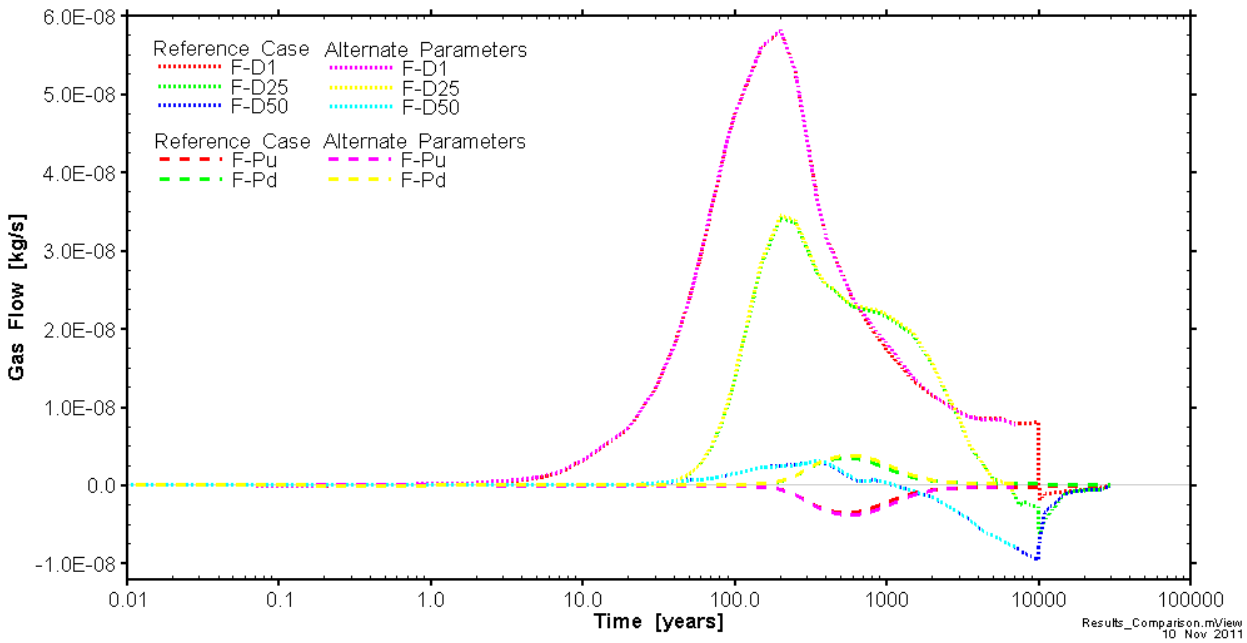

Figure 155: Comparison of alternate parameters to reference case: evolution of H_2 gas with time across F-D (access drift) and F-P (main drift) surfaces.

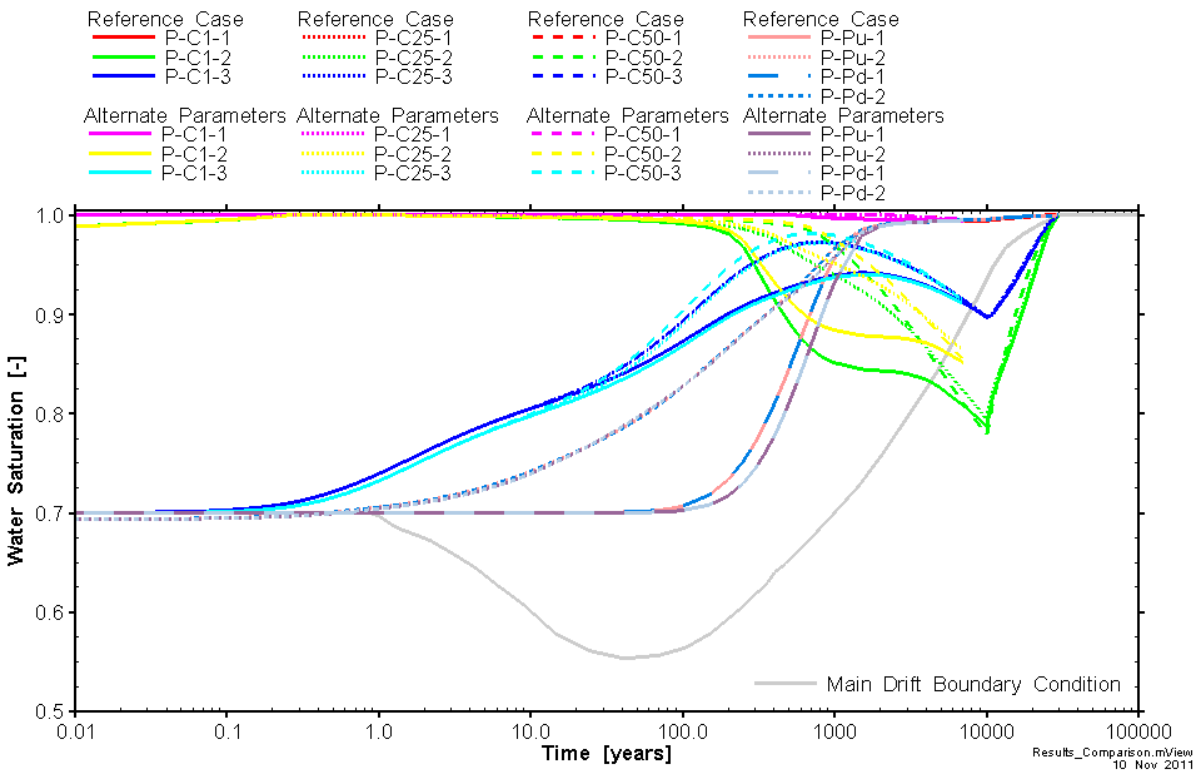

Figure 156: Comparison of alternate parameters to reference case: water saturation at all output points.

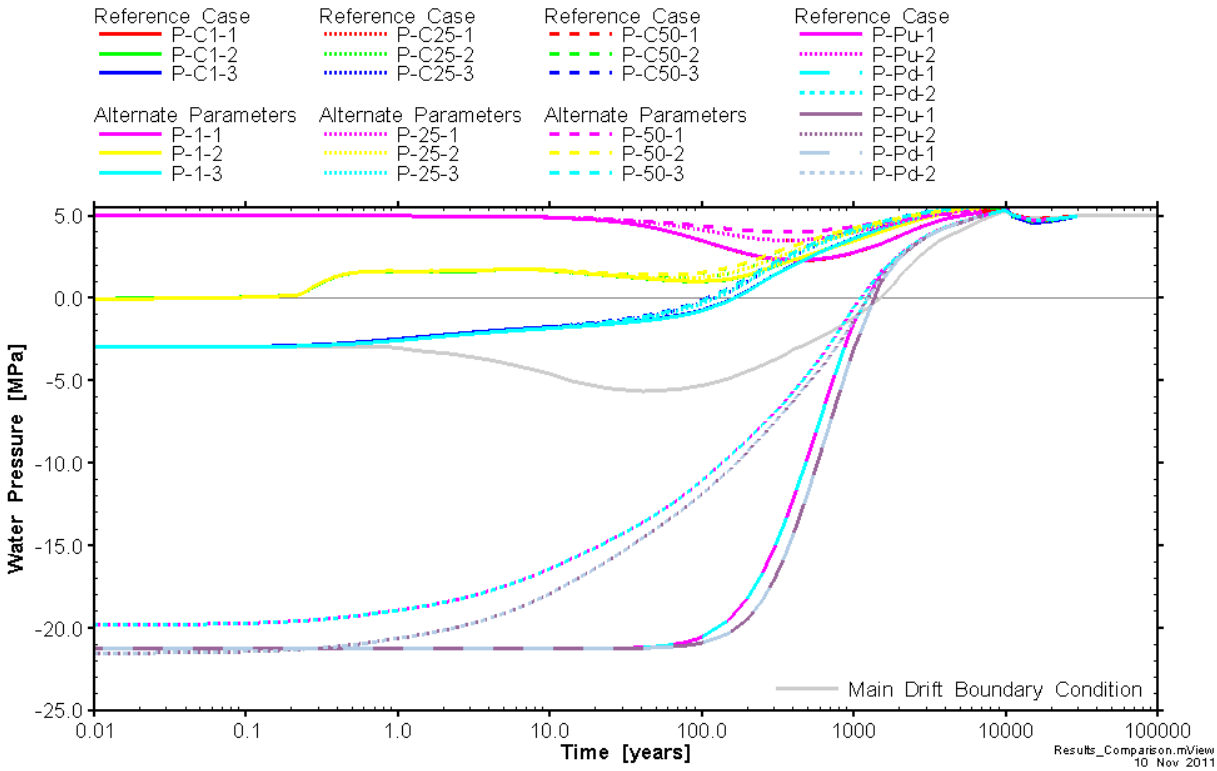

Figure 157: Comparison of alternate parameters to reference case: water pressure at all output points.

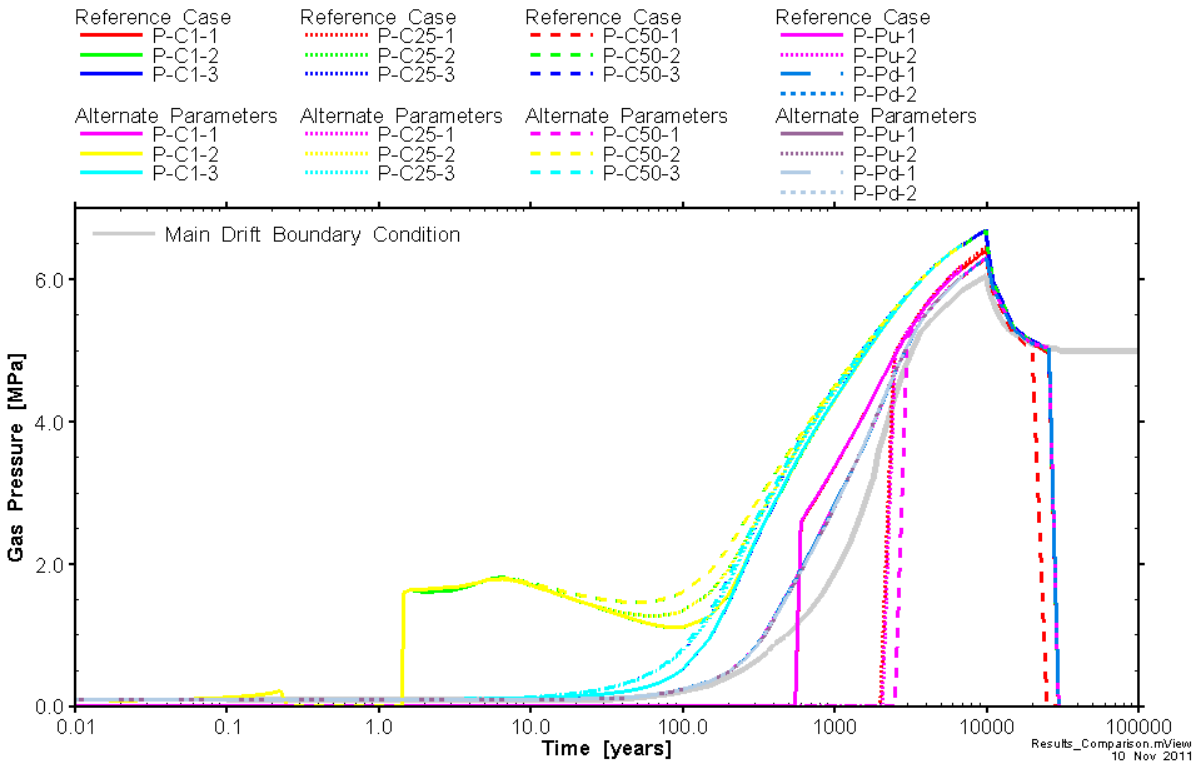

Figure 158: Comparison of alternate parameters to reference case: gas pressure at all output points.

3.9.5 Discussion and Conclusions

A 3D model of the module-scale benchmark was developed for WP1.2-2. The challenge in developing the module scale model was developing a grid discretization that adequately represented the module, while maintaining a tractable grid size. In order to obtain a working model, the interfaces were upscaled and several other simplifications were implemented, such as shifting the main drift bentonite plugs. The simulation is only complete to 30 000 years.

Module behavior and the applied boundary conditions in the main drift are not aligned. Water saturations and pressures in the module equilibrate with host rock pressures more quickly than specified in the boundary condition, and as a result, gas and water flows from the cells and access drift in the module to both the upstream and downstream main drift boundary conditions. As seen in the cell-scale results, the specified pressure and saturation boundary condition at the drift is pivotal to model performance, and determines the magnitude and direction of gas flows. Despite the inconsistent boundary conditions, insights can be gained from this model.

Initially, gas migrates along the cells towards the access drift, and along the access drift towards the main drift. In addition to flowing through the access and main drift, gas also migrates into the host rock. Once pressures in the module begin to equilibrate with the host rock, changes in water and gas flow direction are seen in the cells and the access drift. Pressures in the middle of the module are less variable than at the edges, and consequently, water flows are smaller, water flow direction in the access drift and gas flow direction within the cell do not reverse as at the edges of the repository. Maximum gas pressures of 6.7 MPa are observed throughout the module cells and access drift at 10 000 years, the time at which gas generation stops. By 30 000 years, there is only a very small amount of H_2 gas left in the system (0.001 kg), with the majority of generated gas present in a dissolved form (100 675 kg). A relatively small amount of H_2 exits at both the upstream and downstream main drift boundary conditions (155 kg and 164 kg, respectively), primarily in the gas phase (99%).

Cell-scale modelling identified that the EDZ is an important feature along cells, with the interface playing a relatively small role in terms of transporting gas, likely due in large part to the low conductivity of the cell bentonite plug interface. In the module scale modelling and along the access drifts, the EDZ plays a less important role for gas transport, due the relatively high permeability of the backfill (5.0E-17 m^2) compared to the EDZ (5.0E-18 m^2). Along the bentonite plugs in the main drift, the interface (combined with bentonite at the outer edge of the plug) is important (no EDZ is present), with three-quarters of all gas flow occurring through the interface.

3.9.6 Issues for further consideration

Further modelling would improve confidence in the existing model, particularly to examine the effect of discretization (notably the effect of rectangular cells and coarse discretization) and interface upscaling. A no-interface case would also be of interest, to pursue the cell-scale conclusion that the interfaces are of small importance.

3.9.7 References

[1] Quintessa and Geofirma. 2011. T2GGM Version 2: Gas Generation and Transport Code. Quintessa Ltd. and Geofirma Engineering Ltd. report for the Nuclear Waste Management Organization NWMO DGR-TR-2011-33 R000. Toronto, Canada.

[2] Pruess, K., C. Oldenburg and G. Moridis. 1999. TOUGH2 User's Guide, Version 2.0. Lawrence Berkeley National Laboratory LBNL-43134. Berkeley, USA.

4. Global synthesis of the benchmark at module scale

This synthesis is mainly focused on the module scale benchmark. All global statement developed at the cell scale are valid but will not be reproduced here (model and code development, meshing problems, time step management problems …). Please refer to the cell scale benchmark document for further details.

Among the 9 teams implied initially in FORGE WP1.2 benchmark exercise, results of only 6 of them are presented here for direct comparison as:

- SCK/CEN has not participated to this module scale benchmark;
- CEA model is an horizontal 2D plane (whereas most of the teams have a full 3D model) and is not including interfaces between materials nor EDZ
- IRSN model is a 2D horizontal plane (whereas most of the teams have a full 3D model) and for numerical problem reasons only 25 years of simulation are available.

After a global description of the main phenomenological results at module scale this synthesis will focus on upscaling techniques used by the different teams and finally some discussion on the representativity of the evaluation will be developed.

N.B. *: there are two other document linked to this one, on cell scale (report FORGE D1.6-R part 1: cell scale benchmark) and repository scale (report FORGE D1.6 –R part 3: repository scale benchmark) benchmark. The repository scale benchmark has a final conclusion synthethising all the conclusions of the global benchmark work*

4.1 Comparison of the available results at module scale and main phenomenological understandings

Concerning the gas pressure evaluation from the different teams, a comparison is made at cell 25, in the middle of the module to be as far as possible from all boundary condition and reduce as much as possible its effect on the calculation (see chapter 4.2). One can see on Figure 159 that the global evolution of the gas pressure just upstream the cell plug is coherent between all the available results.

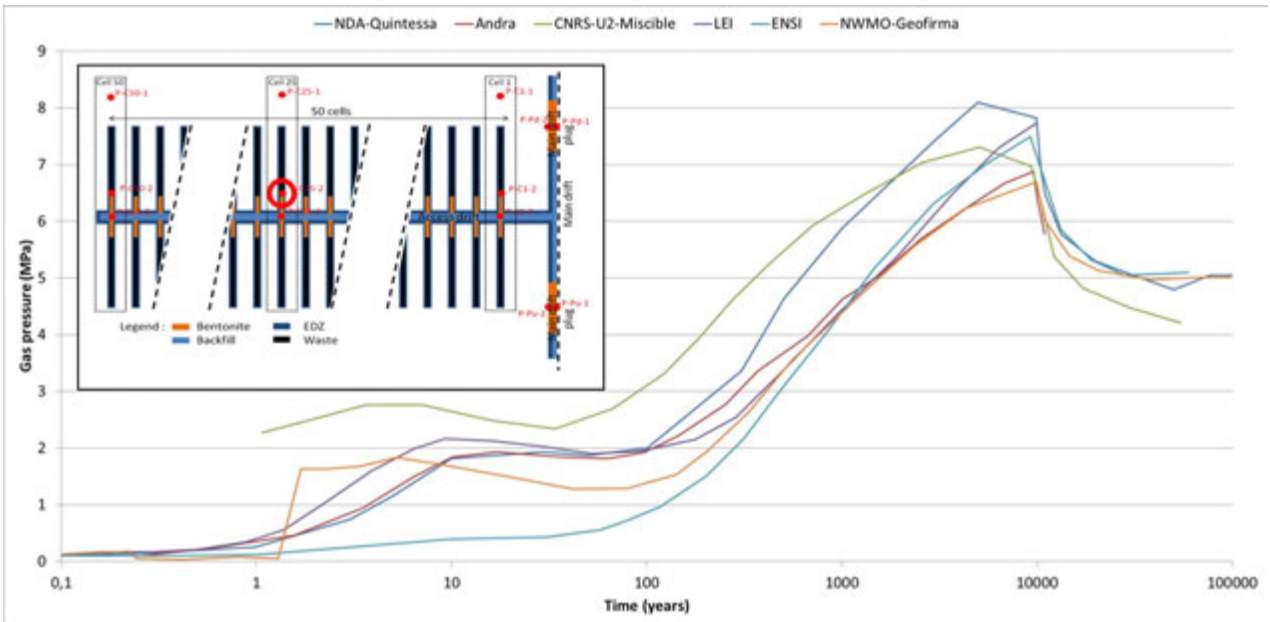

Figure 159 : comparison of gas pressure at point P_C25-2 for all teams

The gas pressure initially equal to the atmospheric pressure is gradually increasing to reach a maximum of around 7-8 MPa at 10 000 years approximately, this time correspond to the end of the gas source term. Based on Figure 159, the numerical and "teams dependent" uncertainty on the maximum gas pressure can be estimated to be around 1 MPa.

As stated by several teams, although in this module scale exercise boundary conditions are further away compared to the cell benchmark, its influence on the results can be significant once near the boundary and especially the main drift. Nevertheless, as these boundary conditions are prescribed in terms of pressures, it is worth comparing the simulated fluxes at this boundary. Figure 160 represent the free gas fluxes calculated by each team in the downstream part of the simulated domain in the main drift. Results are more scattered than for pressures and uncertainty on the maximum value is more than one order of magnitude. But for all teams this flux is significantly lower than the gas production term (around 20 Kg/y for the whole module and constant during the first 10 000 years) meaning that dissolution (and diffusion in the host rock water under dissolved form) is the main process at module scale. This conclusion was already drawn at cell scale but due to boundary conditions will have to be assessed at repository scale as well to be confirmed.

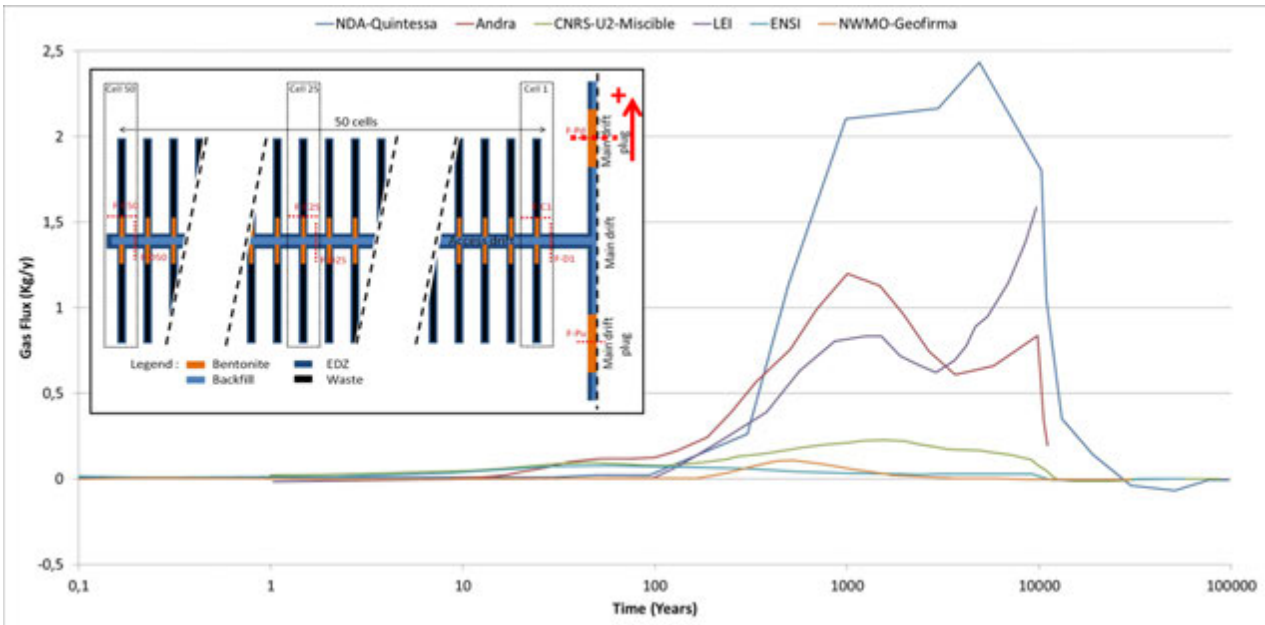

Figure 160 : Comparison of gas fluxes across the main drift for all teams

Even if uncertainties on gas fluxes are high, complex behavior of gas movement were assessed by all teams. For instance, Figure 161shows that plug permeability is low enough to force part of the free gas to move toward the end of the module and to dissolve in the last cells before moving under dissolved form in the argillites water: even if during the first hundred years, gas fluxes are directed toward the main drift (positive flux values), after several thousands of years they are directed toward the end of the module (negative values).

Except for this last behavior, the main phenomenological understandings evaluated at cell scale are confirmed at module scale:

- Gas pressure in never reaching values more than several MPa over the water pressure, thus the argilites desaturation is only of several percent at the most and only in the very vivinity of the cell;
- Most of the generated gas is dissolving immediately and only a small part is flowing under free form toward the access drift and even a smaller part toward the main drift;

- After the end of the gas source term, free gas pressure is rapidly decreasing and the gas phase disappears.

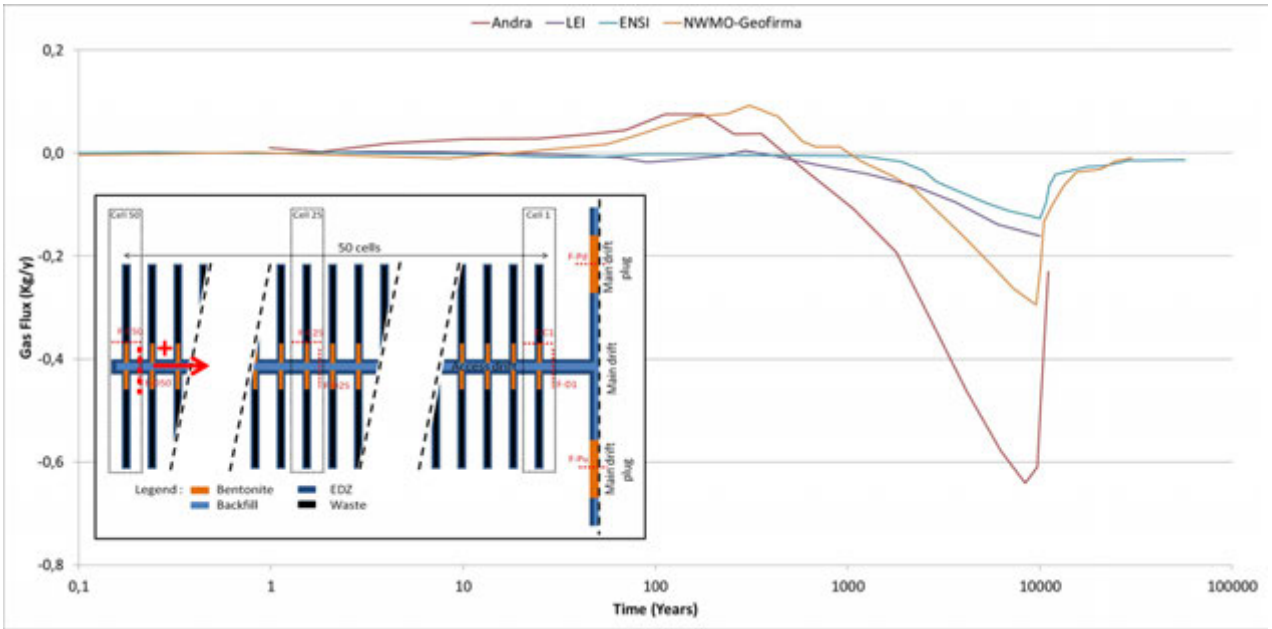

Figure 161 : comparison of gas fluxes across section F_D50 (for teams showing this result in their contribution)

4.1 Numerical and upscaling techniques used in the frame work of this module scale benchmark

Most of the teams have used high performance computing on massively parallel computers, using up to (around) 100 cores to achieve the simulations. Most of the codes used have the capability to use multicore computers with a friendly user interface. However, Quintessa using an homemade code was unable to perform parallel computing but was nethertheless able to compute this benchmark showing that computer power (and code optimization) allows nowadays to do complex calculations with single core computers.

The CNRS (and Geofirma on a lesser extent) has chosen to develop an upscaling technic based on mathematical formulations allowing determination of upscaled hydraulic retention curves and permeability curves for homogenized material (see § 3.5 for more details). The results for pressure are comparable with results from other teams using full geometrical discretization of the modelled domain. For gas fluxes as results are more scattered, comparison is more subjective but CNRS results are in the swarm of other results.

Such a technic could be applied by teams having no numerical cluster to complete PA/SA programs, but is quite demanding in terms of computational effort to implement the mathematical scheme in their one code. Nevertheless mathematical upscaling technics are efficient enough to continue development.

Rem: For repository scale benchmark numerical upscaling technics will be used by all teams to complete the simulation as the modelled domain is too big to achieve results in a reasonable computing time without this technic.

4.2 Representativity of the evaluation

The mathematical model used for numerical simulations at module scale is the same as the one used for the first cell cell benchmark. So remarks made for the cell results phenomenological representativity are still valid, and especially the fact that there is no mechanical coupling (i.e. no implementation of pathway dilation for bentonite).

Concerning numerical issues, as the boundary conditions are pushed away from the central cells, the results concerning these ones are more representative. Nevertheless, for cells near the main drift, and for results concerning the drifts themselves, boundary conditions are still constraining significantly the results. This is one of the reasons why a repository scale benchmark is needed, including only phenomenological boundary conditions derived from natural hydrogeological behavior (i.e. upper and lower aquifer hydraulic behavior).

Even with the boundary constraint, this benchmark has globally confirmed the phenomenological behavior at cell level compared with the results issued from the cell scale, and especially that dissolution and migration under dissolved form in the argillites water is the major process concerning gas migration in terms of mass transported. But free gas phase is present over the whole module during a period of time comparable of the duration of the gas source term. Some specific behavior of the module scale were even produced, i.e. the fact that some of the free gas produced is moving toward the end of the module instead of migration toward the main drift showing the efficiency of the main drift plug in terms of gas migration. However, this conclusion is to be confirmed at repository scale as if may be linked, at least partially, to the boundary conditions imposed.

On a general point of view, this benchmark confirms the idea that numerical simulation is a powerful tool (if not the only one) to give a trend, a tendency, a general evolution but has to address uncertainty of the gas modeling to help bounding the results, only way to enable a representative phenomenological analysis.

5. ANNEX: Full description of the benchmark at module scale

5.1 Context and Objectives

From WP1 participants point of view, the aim of the benchmark should less be a comparison of numerical codes then an exercise trying to answer some precise questions in a PA logic (for example, which could be the relative role of the EDZ, interfaces, backfill in the migration of gas at storage scale?). This clearly includes numerical considerations, but they are a mean and not an objective.

One of the difficulties is to find a common playground for all participants, which allows bringing some add-on for each one. After discussion, a general agreement was that the reference exercise will be as generic as possible (without targeting precisely on national concepts) and to propose sensitivity analyses making it possible to cover national specificities. What is aimed is more to feel how the systems react and why they can react differently rather than an inter-comparison of codes.

A second agreement was that, although the final aim of the benchmark studies is to represent repository-scale simulations, the first exercise should be rather simple and at cell scale. This first step was done during 2009 and first part of 2010. Results are showing a significant role of interfaces between plug and argillite and a transfer dominated at this scale by convection toward the drifts, radial diffusion being of secondary order.

Representing the transfer of gas at a larger scale including drifts and several tens of cells is then worthwhile. In this context, one of the major problems in representing gas transfers in a repository for radioactive waste is to model simultaneously all gas sources (generally located in the disposal cells) and the transfer pathways constituted by the network of interfaces, plugs and undergrounds drifts.

This document contains the specifications for such an exercise.

5.2 Benchmark General specification at module scale

One of the major difficulties in the representation of gas transfer in a repository is to take into account simultaneously all the sources terms (generally located inside the storage cells) and to represent at the same time the transfer network constituted by the different drifts and cells.

For this exercise we assume a repository having a simple architecture (see Figure 162). This architecture is more or less representative of some general concepts for HLW repository zones but without any national specificity. The main features are:

- Subdivision of the all repository into several modules linked by a main drift;
- All the modules are equal and contains an access drift serving 50 cells on each side;
- All modules are separated from their neighbors by a drift seal.

This test case is limited to a portion of such a repository containing an access drift serving a number of cells (see Figure 162). This portion is called a module (a drift serving two rows of vitrified HLW cells containing each 50 cells, see Figure 163).

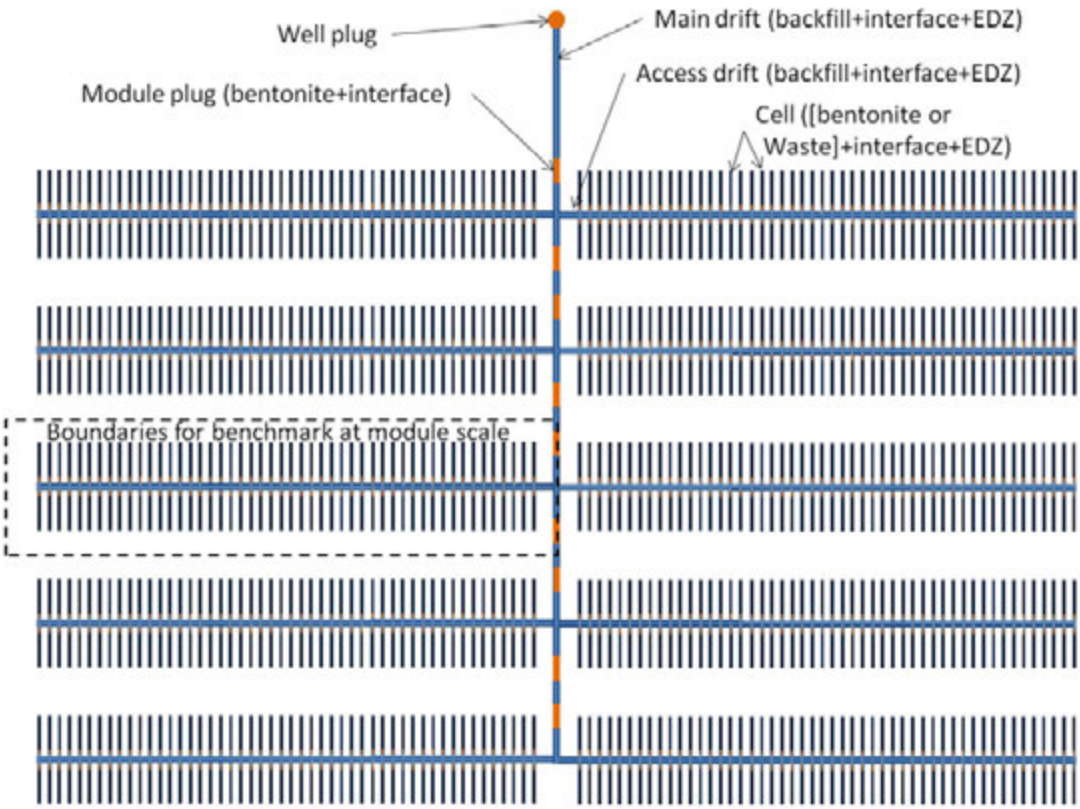

Figure 162 *Schematic representation of a repository for HLW*

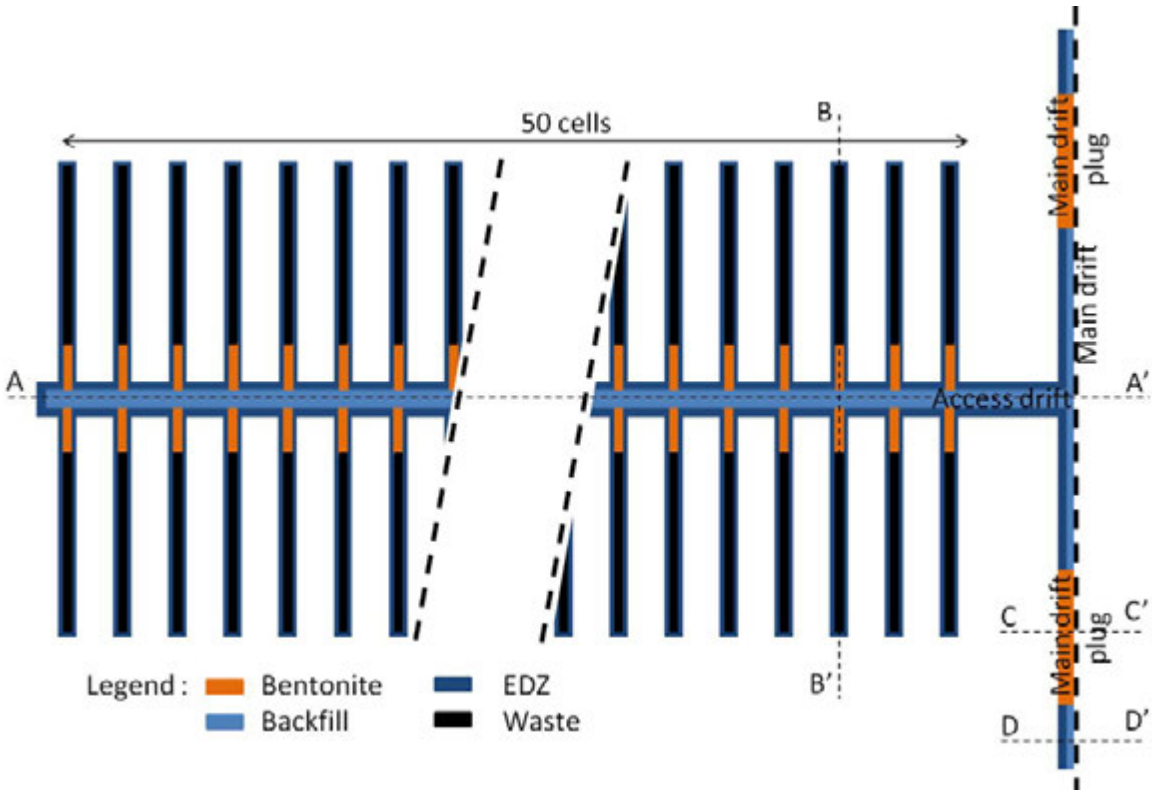

Figure 163 *Schematic representation of the module to be simulated. Definition of the A-A', B-B', C-C' and D-D' cross sections*

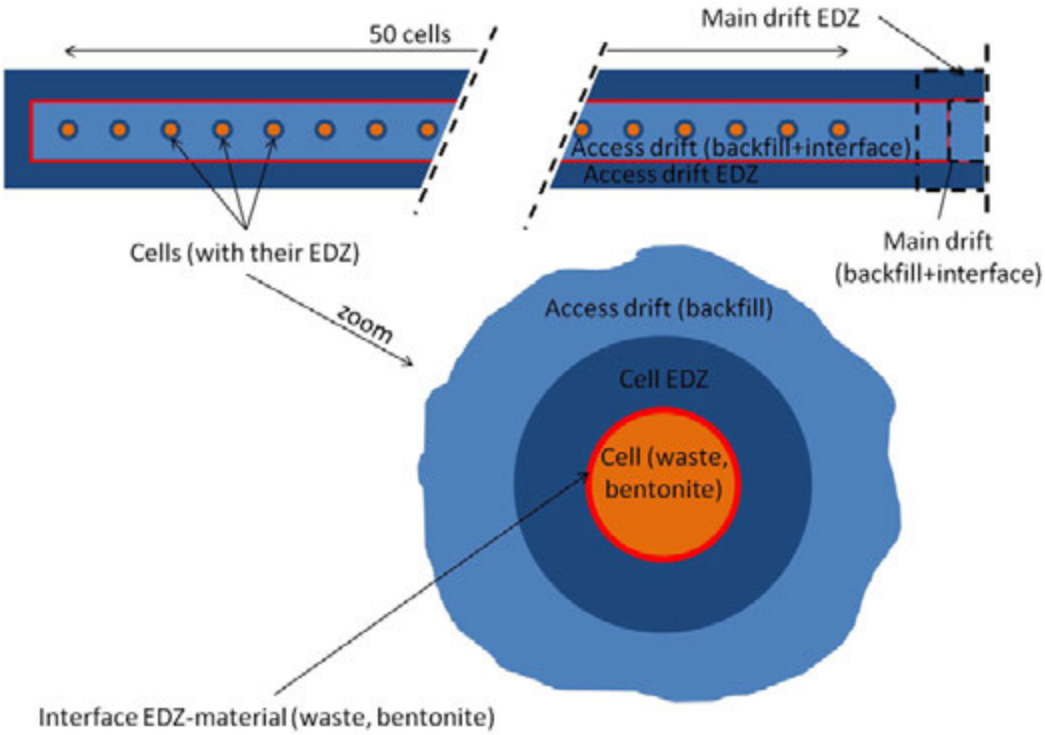

Figure 164 *Schematic representation of the A-A' vertical cross section (see figure 2 for definition)*

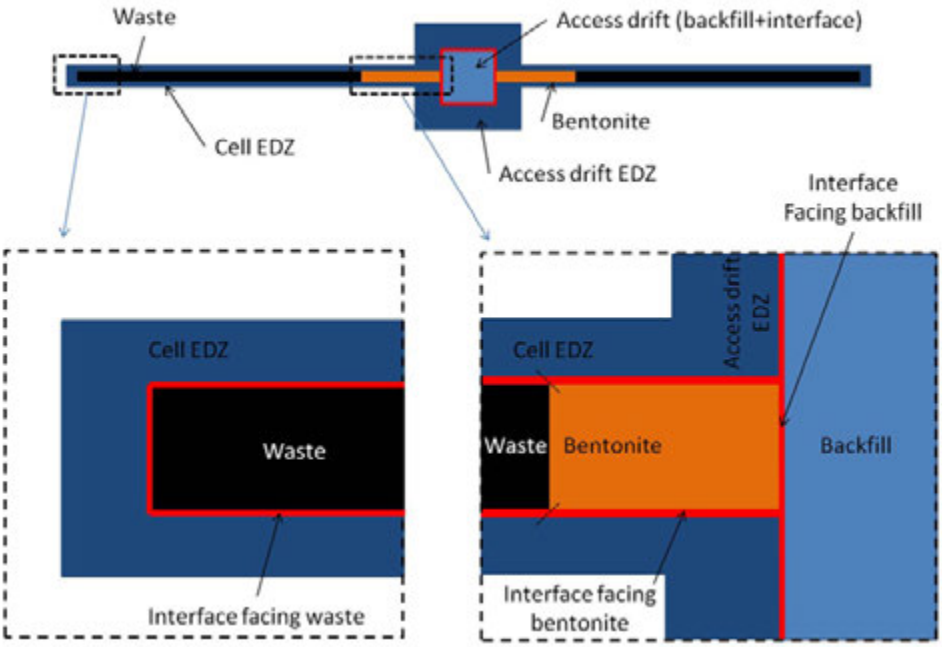

Figure 165 *Schematic representation of the B-B' vertical cross section (see figure 2 for definition)*

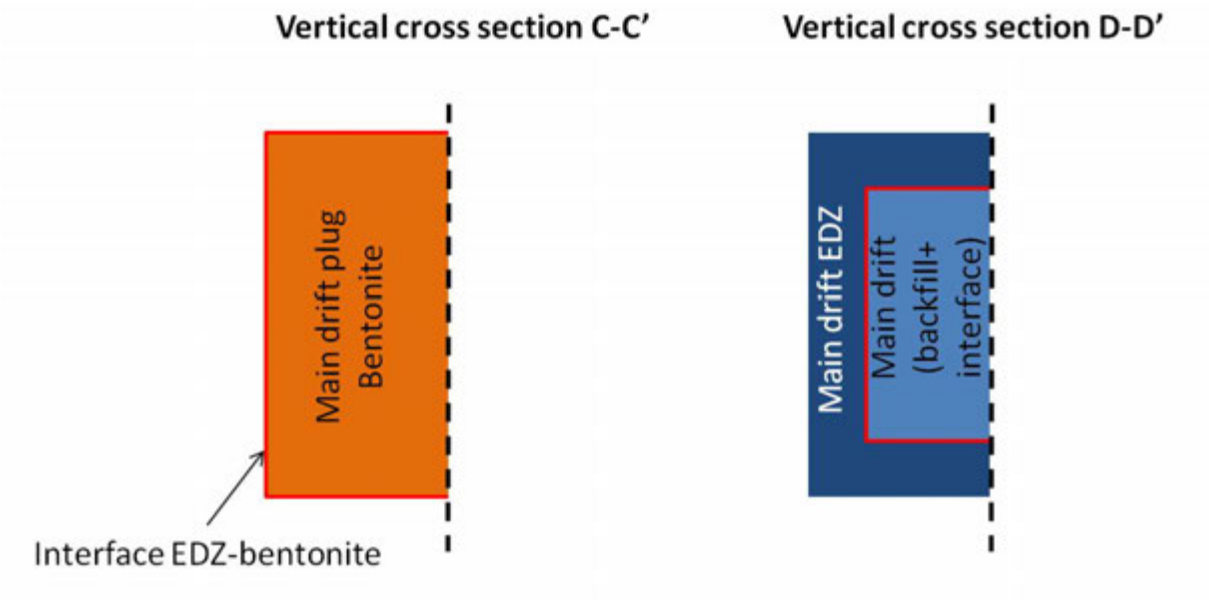

Figure 166 *Schematic representation of vertical cross section C-C' and D-D' (see figure 2 for definitions)*

More details on the domain to be simulated are given in Figure 163, Figure 164, Figure 165 and Figure 167.

The calculation domain is 3D and includes the full extension of the argillite layer (150 m). In the horizontal plane, the extension is determined by the axial distance between each cell and their length. A common gas production term is given for each cell.

It is imposed on the external cylinder representing schematically the cell. The materials to take into account in this simulation are argillite (natural medium), EDZ (Excavation Damaged Zone), EDZ-material

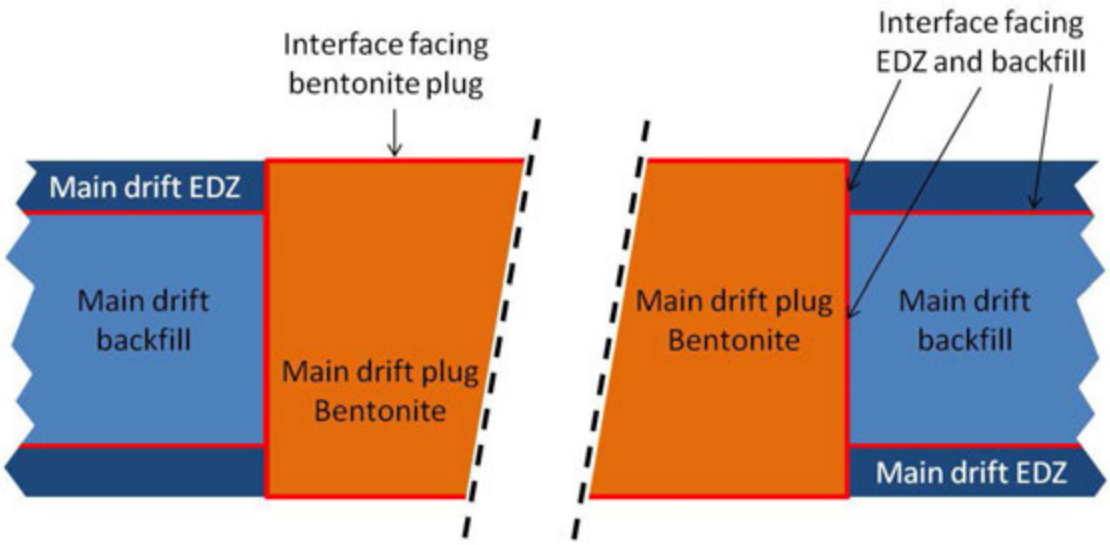

interface (material can be bentonite or backfill depending on the position), bentonite (cells and drift plug) and backfill of the drift. The waste itself is supposed to be impermeable to gas and water and is not explicitly represented.

Figure 167 *Schematic representation of the main drift plugs and backfills interfaces*

In the cell the EDZ is not overcut at bentonite plug emplacement (see Figure 164), but in the drift it is (see Figure 166). The bentonite-argillite interface is present around all types of plugs. The interface is in fact present around all "drift/cell filling material" and can have different physical characteristics depending on the material (waste, backfill, and bentonite) (see Table 7).

The main objective of this simulation is to understand how gas is moving from a cell toward a drift and finally toward a drift plugs (is convection still the main process at this scale, which part of the gas generated inside the cells is moving across the drift plugs, what is the characteristic time for this transfer, what pressure can be achieved, …).

However, a secondary objective is to study the different methods (homogenization, domain decomposition, high performance calculation, …) used by the different teams to achieve this simulation taking into account all the physics described below and restraining the computation time and/or the mesh size to something manageable.

Note that all characteristics already defined in the first exercise at cell scale are the same for this exercise at module scale.

5.3 Detailed description of the test case

5.3.1 Geometry

For the cells, waste and bentonite plugs have the same circular sections. Sections of the access drift and main drift are squared and identical. Cells are positioned at mid height of the access drift and at mid height of the whole calculation domain (argillite layer). There are 50 cells on each side of the access drift.

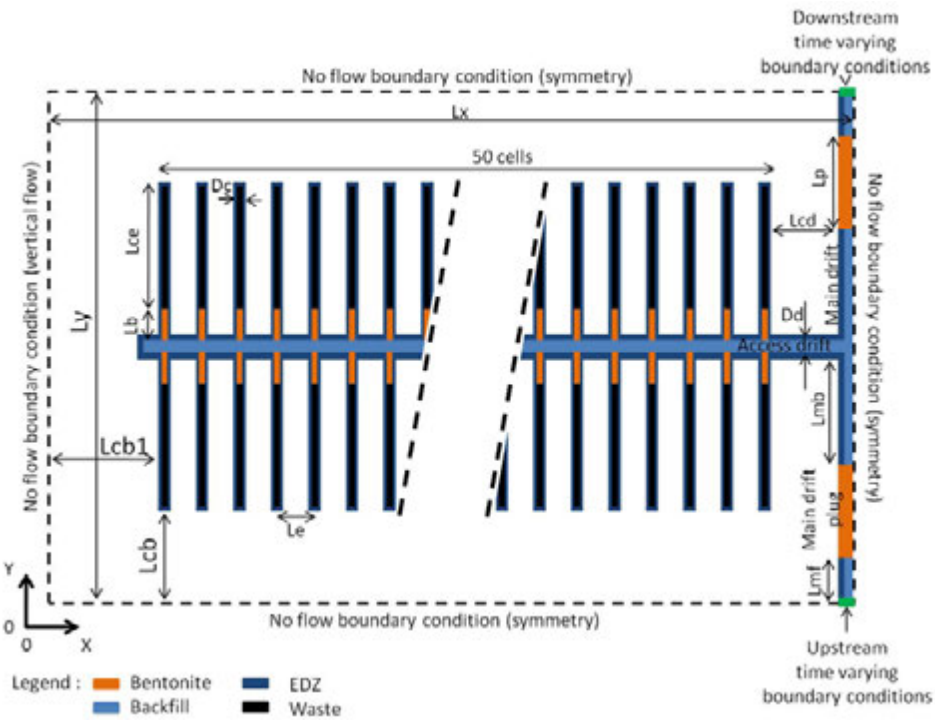

Figure 168 Horizontal dimensions and boundary conditions

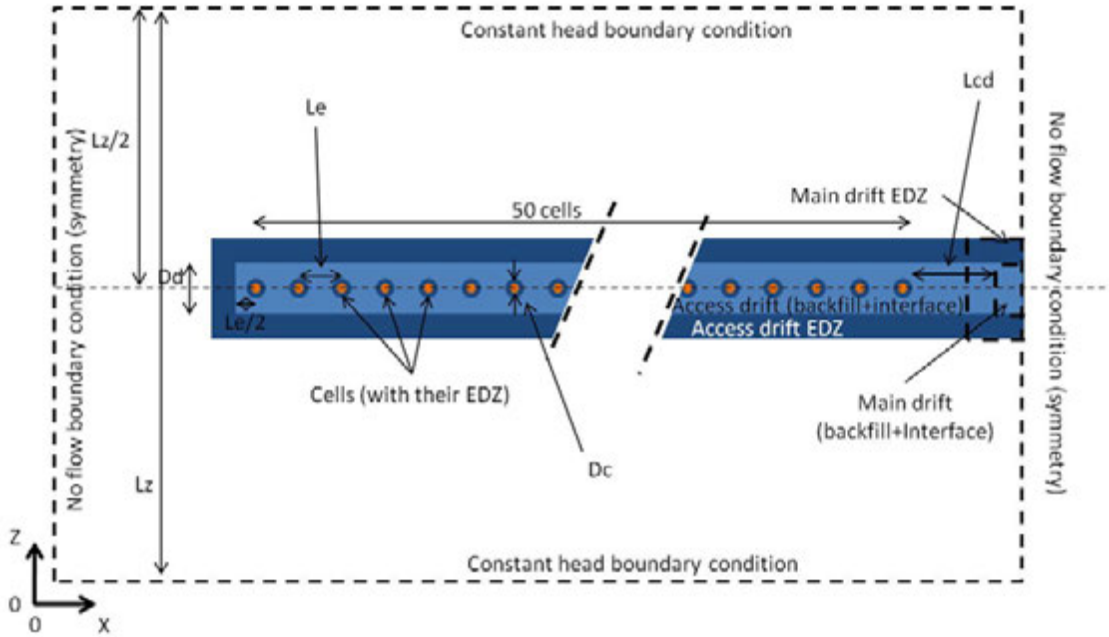

Figure 169 Vertical dimensions and boundary conditions on cross section A-A'

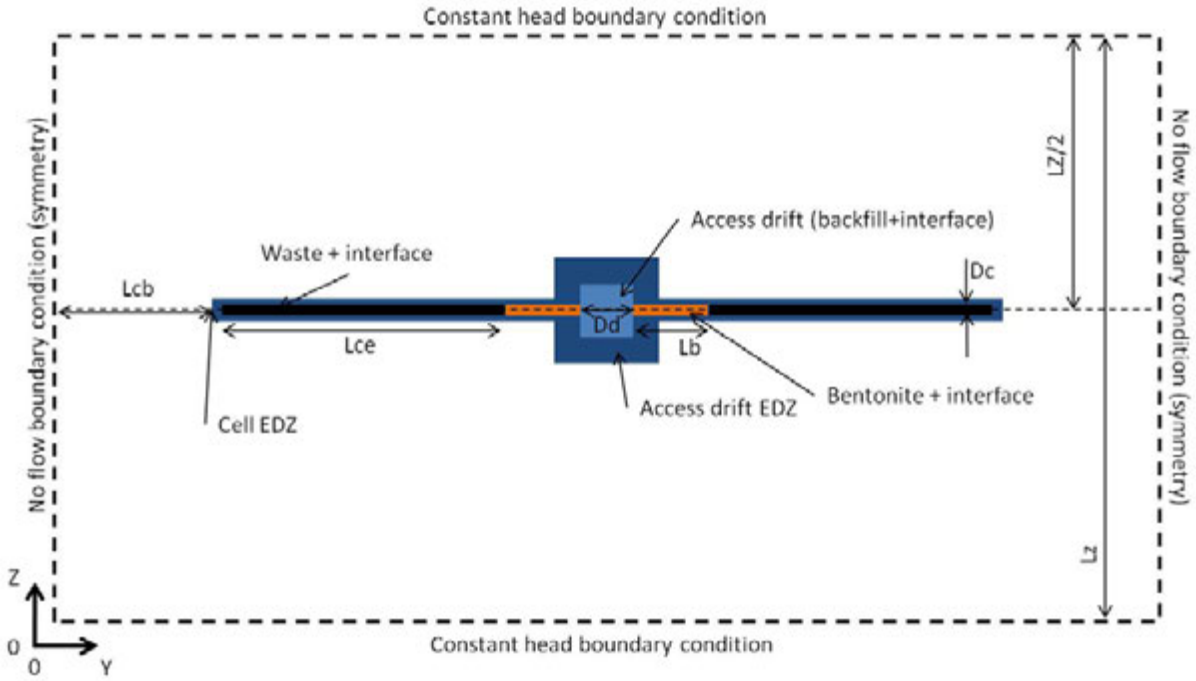

Figure 170 Vertical dimensions and boundary conditions on cross section B-B'

Table 6 Dimensions relative to the simulated domain

Parameter description	Name	Value
X total extension of the simulation domain	Lx	714 m
Y total extension of the simulation domain	Ly	126 m
Z total extension of the simulation domain	Lz	150 m
Distance between cell end (with interface, without EDZ) and the boundary in the Y direction	Lcb	15 m
Distance between outer wall of the last cell (#50 - with interface, without EDZ) and the boundary in the X direction	Lcb1	200 m
Length of the bentonite plug in the cell (without interface)	Lb	5 m
Length of "waste zone" in the cell (with interface)	Lce	40 m
Distance between axes of two adjacent cells	Le	10 m
Cell diameter (with interface, without EDZ)	Dc	1 m
Access and main drifts side length (with interface, without EDZ)	Dd	6 m
Length of the bentonite plug in the main drift (without interface)	Lp	20 m
Distance between outer wall of the access drift (with interface, without EDZ) and end (without interface) of the main drift plug	Lmb	30 m
Distance between end without interface) of the main drift plug and external boundary	Lmf	10 m
Distance between outer wall of the main drift (with interface, without EDZ) and outer wall of the first cell (with interface, without EDZ)	Lcd	20 m
Extension of interface (between waste-argillite, backfill-argillite and bentonite-argillite). Not mentioned in the figures	wi	1 cm
Extension of cell EDZ. Not mentioned in the figures	Cedz	0,5 m
Extension of access drift and main drift EDZ. Not mentioned in the figures	Dedz	1 m

5.3.2 Boundary Conditions

See also

Figure 168 to Figure 170

$x \in [0, x_{\max}], y \in [0, y_{\max}], z \in [0, z_{\max}], t \in [0, t_{end}]$

With $x_{\max}$ =714 m, $y_{\max}$ =126 m, $z_{\max}$ =150 m, t_{end} =100000 years

o Conditions on the top and bottom of the simulation domain:

$$P_w(x, y, z = z\min, t) = 6\,10^6\,Pa \quad S_w(x, y, z = z\min, t) = 1 \quad X_{H_2}^w = 0$$

$$P_w(x, y, z = z\max, t) = 4\,10^6\,Pa \quad S_w(x, y, z = z\max, t) = 1 \quad X_{H_2}^w = 0$$

When gaseous phase is not present, the gas pressure corresponds also to a concentration via Henry's law (see mathematical model for details).

o Conditions on the vertical sides of the simulation domain:

$$Flux_w(x = 0, y, z, t) = 0 \quad Flux_g(x = 0, y, z, t) = 0$$

$$Flux_w(x = x_{\max}, y, z, t) = 0 \quad Flux_g(x = x_{\max}, y, z, t) = 0$$

$$for \quad y \in [0, y_{\max}], z \in [0, z_{\max}], t \in [0, t_{end}]$$

$$Flux_w(x, y = 0, z, t) = 0 \quad Flux_g(x, y = 0, z, t) = 0$$
$$Flux_w(x, y = y_{\max}, z, t) = 0 \quad Flux_g(x, y = y_{\max}, z, t) = 0$$
$$for \quad x \in \left[0, x_{\max} - \frac{Dd}{2}\right], \quad z \in [0, z_{\max}], \quad t \in [0, t_{end}]$$

$$Flux_w(x, y = 0, z, t) = 0 \quad Flux_g(x, y = 0, z, t) = 0$$
$$Flux_w(x, y = y_{\max}, z, t) = 0 \quad Flux_g(x, y = y_{\max}, z, t) = 0$$
$$for \quad x \in \left[x_{\max} - \frac{Dd}{2}, x_{\max}\right], \quad z \in \left[\frac{z_{\max} + Dd}{2}, z_{\max}\right], \quad t \in [0, t_{end}]$$
$$and \quad x \in \left[x_{\max} - \frac{Dd}{2}, x_{\max}\right], \quad z \in \left[0, \frac{z_{\max} - Dd}{2}\right], \quad t \in [0, t_{end}]$$
$$and \quad x \in \left[0, x_{\max} - \frac{Dd}{2}\right], \quad z \in [0, z_{\max}], \quad t \in [0, t_{end}]$$

At intersection between main drift and outer limits of the model:

y=0 or y= $y_{\max}$ and

$$x \in \left[x_{\max} - \frac{Dd}{2}, x_{\max}\right], \quad z \in \left[\frac{z_{\max} - Dd}{2}, \frac{z_{\max} + Dd}{2}\right]$$

The boundary conditions are time varying, on both sides of the model: there is a small amount of gas flowing from one side of the model to the other one inside the main drift. A graphical representation of the time varying water pressure and gas pressure is presented in Figure 171 and Figure 172.

These boundary conditions have been determined using a simulation at the global repository scale and modified to cope with this benchmark definition. For example the gas source term applied in the whole storage simulation is not the same as the one used up to now in the FORGE WP1.2 benchmark and boundary conditions have been modified so that the gas peak occurs at the end of the source term. This is also why on the boundary of the simulation domain there is a part of backfill: the data available was on backfill pressures and saturation, not on bentonite.

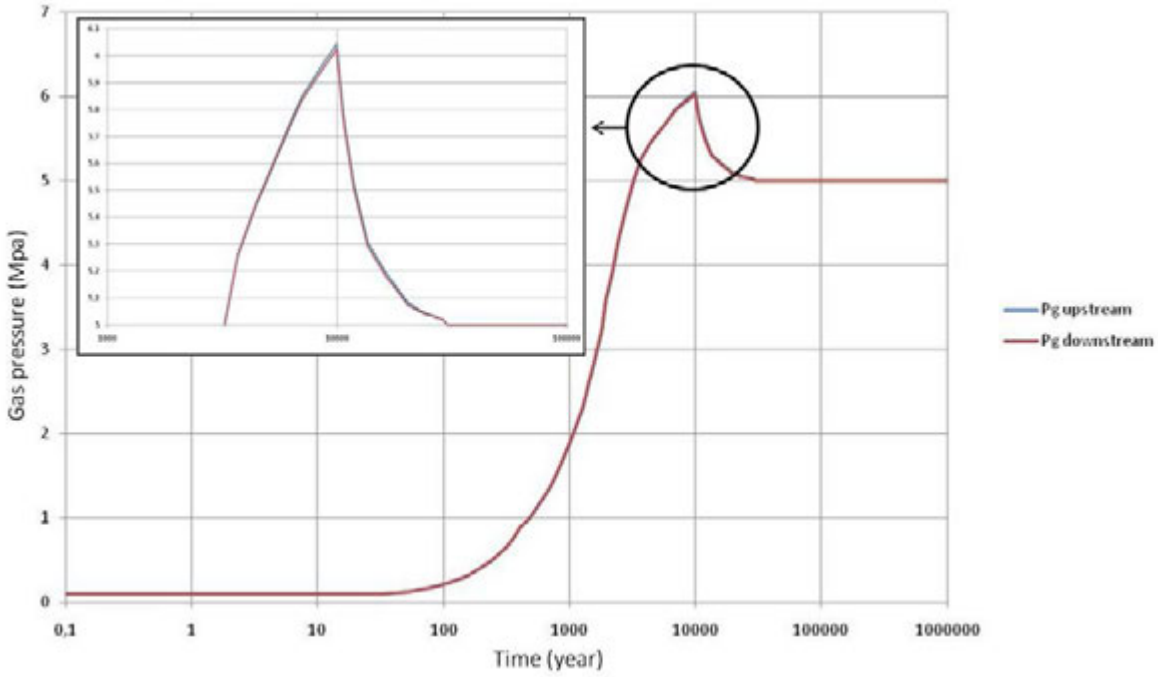

Figure 171 *Gas pressure time varying boundary conditions on the backfill of the main drift*

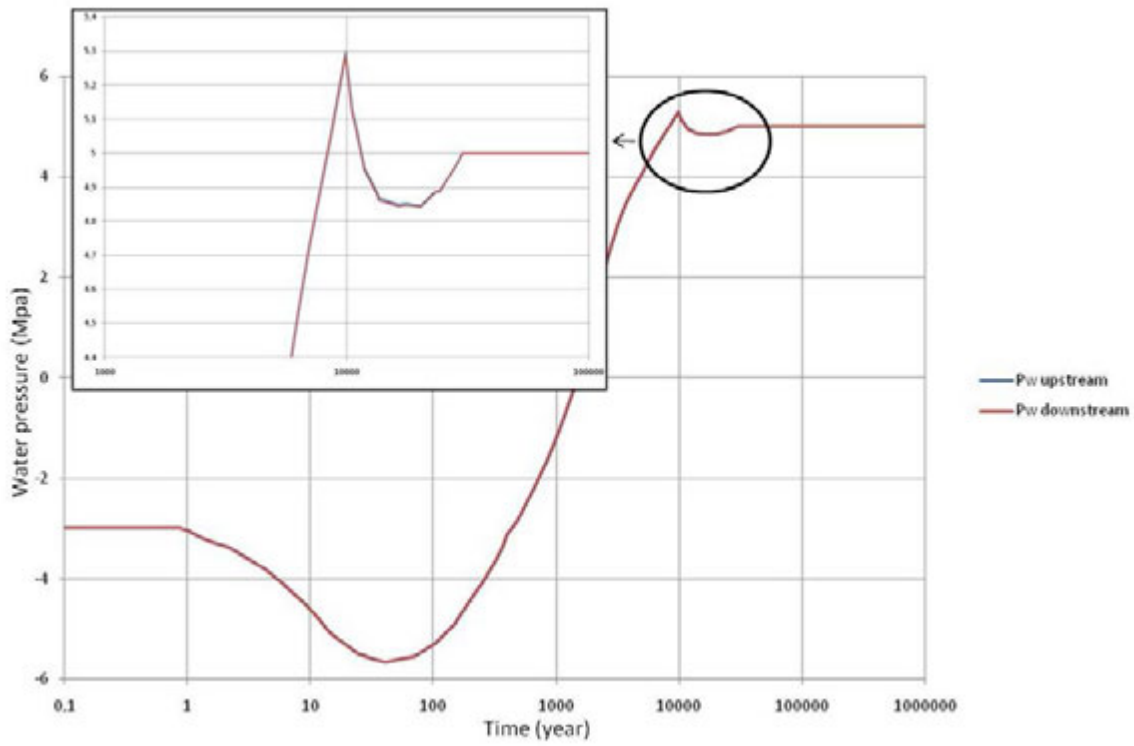

Figure 172 *Water pressure time varying boundary condition*

As fluxes of water and or gas are very small from upstream part to downstream part of the simulation domain, the differences in terms of gas and water pressure for the time varying boundary conditions are quite small (only several meters of water at the peak).

5.3.3 Physical Parameters

The values of the different physical parameters needed for this simulation are given in the following table. The simulation is supposed to be isothermal at 20°C (293°K) during all the calculation.

Note: The gravity is taken into account for this 3D simulation.

Table 7 Values for physical parameters

Parameter (at 20°C)	Materials		
	Interface facing plug (cf.*)	Interface facing waste	Interface facing backfill and edz
K [m²]	$5.0\ 10^{-18}$	$1.0\ 10^{-12}$	$1.0\ 10^{-15}$
Porosity [%]	30	100	40
Specific storage coefficient [m⁻¹]	$4.6\ 10^{-06}$	$4.6\ 10^{-06}$	$4.6\ 10^{-06}$
Two-phase flow parameters			
S_{gr} [%]	0	0	0
S_{wr} [%]	0	0	0
Van Genuchten parameters			
n [-]	4	4	4
P_r [Pa]	10^4	10^4	10^4
τ (Tortuosity)	1	1	1

Parameter (at 20°C)	Materials			
	Backfills	Bentonite plugs	EDZ	Geological medium
K [m²]	$5.0\ 10^{-17}$	$1.0\ 10^{-20}$	$5.0\ 10^{-18}$	$1.0\ 10^{-20}$
Porosity [%]	40	35	15	15
Specific storage coefficient [m⁻¹]	$1.0\ 10^{-05}$	$4.4\ 10^{-06}$	$2.3\ 10^{-06}$	$2.3\ 10^{-06}$
Two-phase flow parameters				
S_{gr} [%]	0	0	0	0
S_{wr} [%]	0	0	0	0
Van Genuchten parameters				
n [-]	1.5	1.6	1.5	1.5
P_r [Pa]	$2\ 10^6$	$1.6\ 10^7$	$1.5\ 10^6$	$1.5\ 10^7$
τ (Tortuosity)	2	4.5	2	2

* For all the bentonite plugs (cells and main drift): interface facing plug: only in the radial (perpendicular to the axis) direction (not in the longitudinal direction)

(See figure 4 and figure 6)

- ***Viscosity of the gas mixture:***

The viscosity of the gas mixture (water vapour + hydrogen) can be estimated by a classical Wilke approximation or by a simplified formula as follows:

$$\mu_g = \frac{1}{\frac{X^g_{H_2}}{\mu^g_{H_2}} + \frac{X^g_{wvap}}{\mu^g_{wvap}}} \quad \text{With} \quad \mu^g_{H_2}(T=293K) = 9\,10^{-6}\,Pa.s \quad \mu^g_{wvap}(T=293K) = 10^{-5}\,Pa.s$$

- ***Diffusion coefficient of dissolved H_2 in water:***

$$D_{H_2/water} = 1.57\ 10^{-14}\frac{T}{\mu_{water}(T)} \quad (m^2/s)$$

- ***Diffusion coefficient of gaseous H_2 in water vapour:***
  (T_0=293 K and at P_0=1.0·10^5 Pa: D_0=9.5·10^{-5} m^2/s)

$$D^g_{H_2-H_2O} = D_0\left(\frac{P_0}{P}\right)\left(\frac{T}{T_0}\right)^{1.75} \quad (m^2/s)$$

- ***Diffusion coefficient of dissolved H_2 in the water of the porous medium:***

$$D^w_{H_2} = S_w\left(\frac{\omega}{\tau^2}\right)D_{H_2/eau}$$

- ***Diffusion coefficient of dissolved H_2 in the binary H_2/water-vapour mixture of the porous medium:***

$$D^g_{H_2/vap} = (1-S_w)\left(\frac{\omega}{\tau^2}\right)D^g_{H_2-H_2O}$$

- ***Solubility of hydrogen in water:*** $H_{H_2}(T=293K) = 7.610^{-6}\ mol.Pa^{-1}.m^{-3}$

Note: Temperature in diffusion models is expressed in Kelvin.

5.3.4 Initial conditions

Water saturation:

- in the geological medium is equal to 100%;
- in the cells and drifts EDZ is equal to 100%
- in the bentonite plugs is equal to 70%;
- in the backfill of the main drift and of the access drift is equal to 70%
- in the interfaces is equal to 5% ;

Pressure:

- in the fully initially water-saturated materials, the water pressure is linearly distributed between values at upper and lower boundary (see Boundary limits);
- In partially-saturated materials at initial time, the gas pressure is equal to 0.1 MPa (~1 atmosphere). The water pressure is deduced from the gas pressure and the saturation by applying Van Genuchten models associated with each material.

5.3.5 Production term for Hydrogen

The hydrogen-production term is to be distributed over the whole external surface (radial and lateral) of all the wastes, as follows:

- for 0 < t ≤ 10000 years, $Q^{g}_{H_2} = 100\ mol/year/cell$ $Q^{w}_{H_2} = 0$
- for t > 10000 years $Q^{g}_{H_2} = 0\ mol/year/cell$ $Q^{w}_{H_2} = 0$

5.3.6 Simulation period

The simulation will be performed between $t_0=0$ and t_{end} =100.000 years.

5.4 Output results

For all output results, times will be expressed in years, pressures will be expressed in MPa, and mass flows will be expressed in kg/s.

5.4.1 Evolution with time of mass flows across surfaces

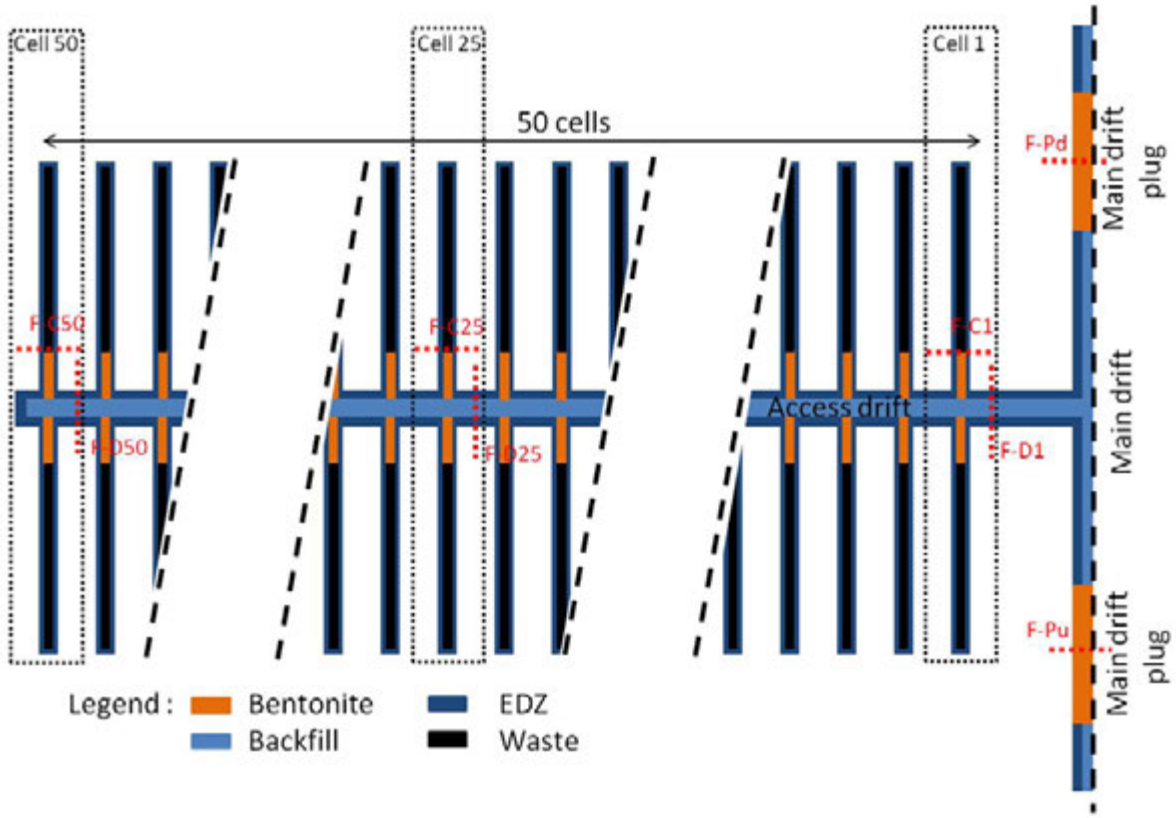

Figure 173 Schematic representation of the surfaces across which flows will be calculated

Type of mass flows: total flows, diffusive flows and advective flows for the following components/phases:

- Liquid water
- Water vapor
- Gaseous H2
- Dissolved H2

Type of surfaces:

- For each of cells 50, 25 and 1 (see Figure 11 for their locations), flows in the cell interface and the cell EDZ, across the following surface: vertical plane passing through the end (close to the wastes) of the cell bentonite plug. Corresponding to surfaces F-C50, F-C25 and F-C1 on Figure 173

  Mathematical description of the surfaces: y=71 m; 0.49 m < radius from the cells axis < 1 m;

- For each of cells 50, 25 and 1, flows in the access drift backfill, access drift interface and access drift EDZ, across the following surface: vertical plane 5 m away – downstream - from the cell axis. Corresponding to surfaces F-D50, F-D25 and F-D1 on Figure 173;

  Mathematical description of the surfaces: 59 m < y < 67 m; 146 m < z < 154 m;

  x=695.5 m for cell 1; x=445.5 m for cell 25, x=205.5 m for cell 50;

- Flows in the main drift plugs and main drift interfaces (as shown in Figure 5, cross section C-C') across the following surface: vertical planes passing through the middle of the plug; flows are computed separately for upstream and downstream main drift plugs. Corresponding to surfaces F-Pu and F-Pd on Figure 173

  Mathematical description of the surfaces: y=20 m or y=106 m; 711 m < x < 714 m;

  72 m < z < 78 m;

- Global water flow across the upper and lower boundaries of the whole simulation domain (not presented on Figure 173). Flows are computed separately for upper and lower boundaries;
- Global hydrogen flow across the upper and lower boundaries of the whole simulation domain (not presented on Figure 173). Flows are computed separately for upper and lower boundaries.

5.4.2 Evolution along lines at different times

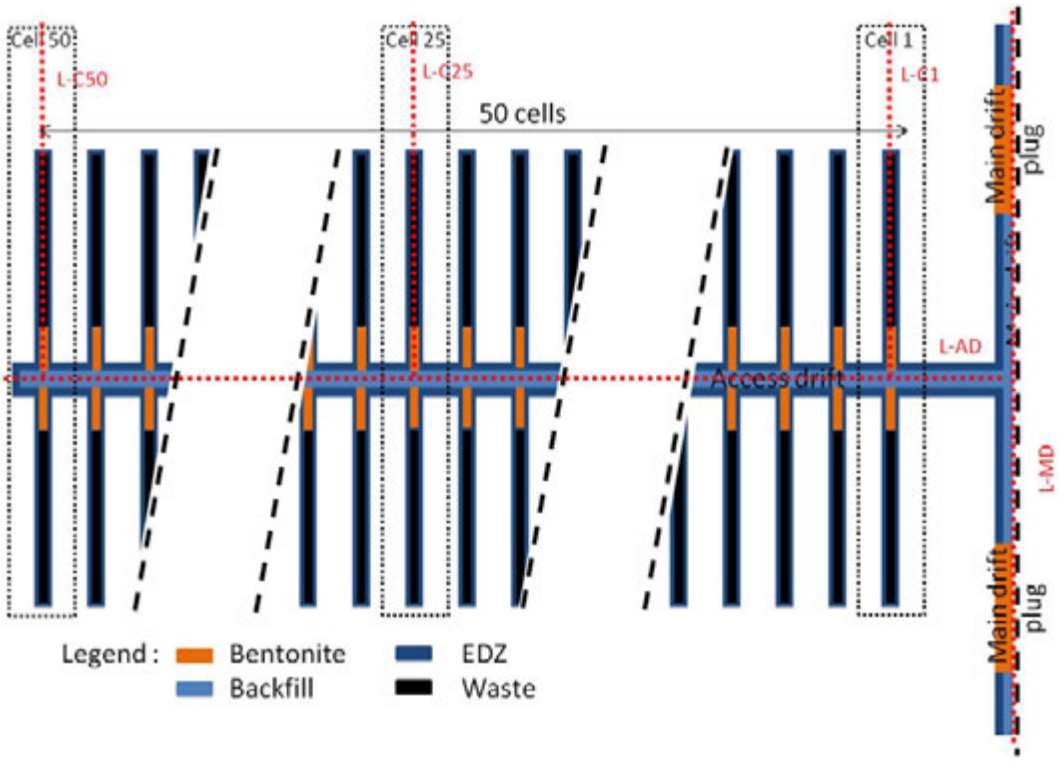

Figure 174 Schematic representation of the lines on which results should be given

Evolution along lines of:

- Water saturation
- Water pressure
- Gas pressure (in the gas phase when it exists)
- Dissolved H2 pseudo-pressure (see Henry's law, equations (18) and (18'), in § 5.5 for details)
- Capillary pressure

Times to be used (years):

1, 3, 10, 30, 100, 300, 1 000, 3 000, 10 000, 30 000, 100 000

Types of lines:

- For cells 50, 25 and 1 (respectively line L-C50, L-C25 and L-C1 on Figure 174): lines parallel to the axis of the cell, in the interface – upper part - between waste (or bentonite) and EDZ, and going from the outer boundary to the EDZ of the access drift

  Mathematical description of the lines: 66 m < y < 126 m; z=75.495 m;

  x=690.5 m for cell 1; x=440.5 m for cell 25, x=200.5 m for cell 50;

- Line parallel to the axis of the access drift, in the interface – upper part - between backfill and EDZ of the access drift, and going from the end of the access drift to the EDZ of the main drift (L-AD on Figure 174)

Mathematical description of the line: 194 m < x < 711 m; y=63 m; z=77.995 m;

- Line parallel to the axis of the main drift, in the interface – upper part - between backfill (or bentonite) and EDZ of the main drift, and going from the upstream boundary to the downstream boundary (crossing the whole simulation domain (L-MD on Figure 174)

  Mathematical description of the line: x=714 m; 0 < y <126 m; z=77.995 m

5.4.3 Evolution with time at given points

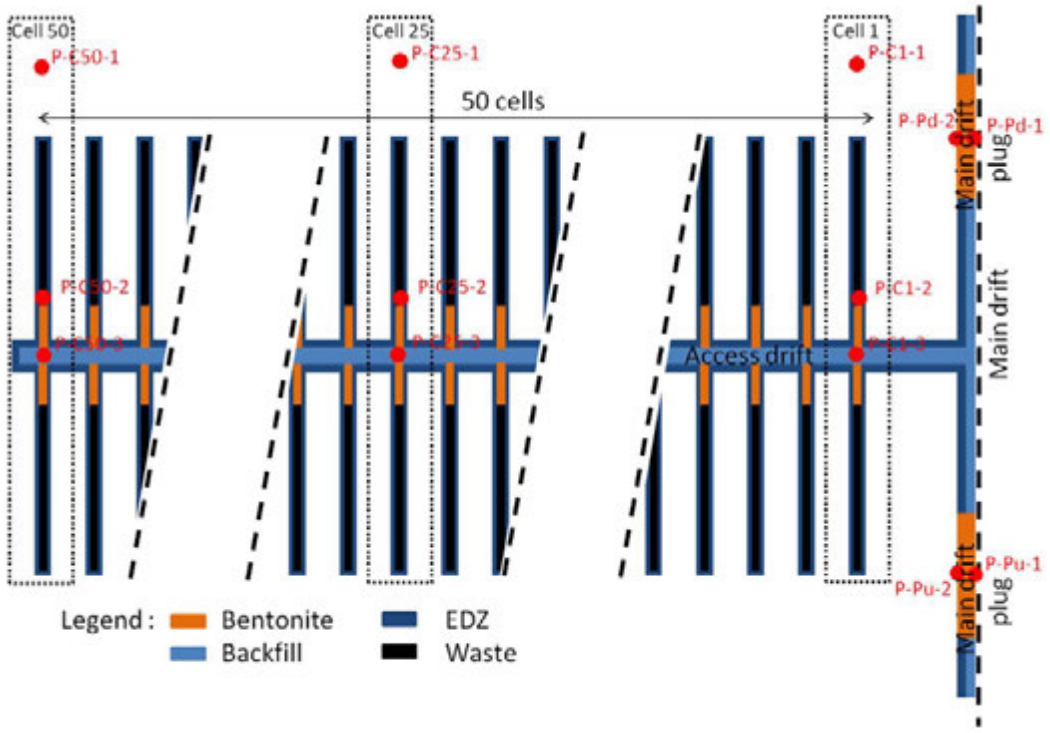

Figure 175 Schematic representation of the points where results should be given

Evolution with time of:

- Water saturation
- Water pressure
- Gas pressure (in the gas phase when it exists)
- Dissolved H2 pseudo-pressure (see Henry's law, equations (18) and (18'), in § 5.5 for details)
- Capillary pressure

Type of points:

- For cell 50 (see Figure 175):
    - Point P-C50-1: point whose horizontal coordinates are along the axis of the cell, 5 m away from the end of the cell (with interface, without EDZ) ;

      coordinates: x=200.5 m; y=116 m; z=75.495 m (this point is along line L-C50)
    - Point P-C50-2: point situated in the interface between waste and EDZ (upper part) as close as possible to the bentonite plug;

      coordinates: x=200.5 m; y=71.005 m; z=75.495 m (this point is along line L-C50)
    - Point P-C50-3: point situated in the interface between access drift and EDZ (upper part) ; horizontal coordinates are those of the intersection axes of cell 50 and access drift;

      coordinates: x=200.5 m; y=63 m; z=77.995 m (this point is along line L-AD)
    - Same types of point as for cell 50 but for cell 25 (points P-C25-1, P-C25-2, P-C25-3) and cell 1 (points (P-C1-1, P-C1-2, P-C1-3), see Figure 175;

      P-C25-1: coordinates: x=440.5 m; y=116 m; z=75.495 m (point along line L-C25);

      P-C25-2: coordinates: x=440.5 m ; y=71.005 m ; z=75.495 m

      (point along line L-C25);

      P-C25-3: coordinates: x=440.5 m; y=63 m; z=77.995 m; (point along line L-AD)

      P-C1-1: coordinates: x=690.5 m; y=116 m; z=75.495 m (point along line L-C1);

      P-C1-2: coordinates: x=690.5 m; y=71.005 m; z=75.495 m (point along line L-C1);

      P-C1-3: coordinates: x=690.5 m; y=63 m; z=77.995 m; (point along line L-AD);

- For upstream plug (see Figure 175):
    - Point P-Pu1: situated at the middle of the length and on the axis of the plug (in the middle of the bentonite); horizontal coordinates: x=714 m; y=20 m ; z=75 m
    - Point P-Pu-2: situated at the middle of the length of the plug and in the interface between bentonite and EDZ; horizontal coordinates: x=711.005 m; y=20 m ; a=75 m
    - Same points as for upstream plug, but in the downstream plug (points P-Pd-1 and P-Pd-2, see Figure 175).

      P-Pd-1: horizontal coordinates: x=714 m; y=106 m; z=75 m;

      P-Pd2: horizontal coordinates: x=711.005 m; y=106 m; z=75 m

5.5 Mathematical model proposed for the exercise

Remark: *This model is the same as the one proposed in the first part of the benchmark at cell scale.*

The capillary pressure is defined as the difference between gas pressure and water pressure:

$$P_C = P_g - P_w \qquad (1)$$

- *Pc*: capillary pressure (Pa)
- *Pg*: total pressure of the gas phase(Pa)
- *Pw*: water pressure (Pa)

The dependence between water and gas saturation in each porous medium is expressed by:

$$S_g + S_W = 1 \quad \text{With} \quad S_g = \frac{V_g}{V_p} \text{ and } S_w = \frac{V_w}{V_p}$$

- Sg: gas saturation (-)
- Sw: water saturation (-)
- Vg: gas volume (m3)
- Vw: water volume (m3)
- Vp: pore volume (m3)

Van Genuchten model is used to express capillary pressure function of the effective saturation in a given porous medium:

$$S_{we} = \frac{S_w - S_{wr}}{1 - S_{wr} - S_{gr}} \qquad (2)$$

$$S_{we} = \frac{1}{\left[1 + \left(\frac{P_c}{P_r}\right)^n\right]^m} \qquad (3)$$

- Swe: Effective water saturation (-)
- Swr = residual water saturation (-)
- Pr: reference pressure for Van Genuchten law (Pa). Generally the value for this coefficient is higher than the gas entry pressure for a given porous medium
- n, m: coefficients for Van Genuchten law. We have $m = 1 - \frac{1}{n}$

The relative permeability for water is expressed by integrating the Mualem prediction model in the Van Genuchten capillarity model:

$$k_r^w = \sqrt{S_{we}}\left[1 - \left(1 - S_{we}^{1/m}\right)^m\right]^2 \qquad (4)$$

- k_r^w : relative permeability for water (-)

The relative permeability for gas is expressed similarly:

$$k_r^g = \sqrt{1 - S_{we}}\left[1 - S_{we}^{1/m}\right]^{2m} \qquad (5)$$

- k_r^g : relative permeability for gas (-)

The water and gas movement in a porous medium is represented by the mass conservation law and the energy conservation law (reduced to the generalized Darcy law):

$$U_w = -\frac{kk_r^w(S_w)}{\mu_w}(\nabla P_w + \rho_w g \nabla z) \quad (6)$$

$$U_g = -\frac{kk_r^g(S_g)}{\mu_g}(\nabla P_g + \rho_g g \nabla z) \quad (7)$$

- K: intrinsic permeability of the porous medium (m2)
- μg: viscosity of the total gas phase (kg.s-1.m-1)
- μw: viscosity of water (kg.s-1.m-1)
- ρ: volumetric mass of the total gas phase (kg.m-3)
- ρw: volumetric mass of water (kg.m-3)

$$\rho_w(P_w) = \rho_{atm} \exp[S_s(P_w - P_{atm})] \quad (8)$$

  ρatm: volumetric mass of water at atmospheric pressure (kg.m-3)
  Patm: atmospheric pressure (Pa)
  Ss: specific storage (Pa-1)
- g: gravity (m.s-2)
- z: altitude (m)
- Ug: Darcy velocity for the gas phase (m.s-1)
- Uw: Darcy velocity for water (m.s-1)

Equation of conservation for water:

$$\frac{\partial(\rho_w \omega S_w)}{\partial t} + \nabla(\rho_w U_w) = Q^w \quad (9)$$

- ω: porosity (-)
- Qw: consumption/production of water (kg.m-3.s-1)

Equation of conservation for the total gas phase:

$$\frac{\partial(\rho_g \omega S_g)}{\partial t} + \nabla(\rho_g U_g) = Q^g \quad (10)$$

- Qg: consumption/production for the total gas phase (kg.m-3.s-1)

The mass fraction of gaseous hydrogen is expressed as:

$$X_{H_2}^g = \frac{\rho_{H_2}^g}{\rho_g} \quad (11)$$

With $\rho_{H_2}^g = \frac{m_{H_2}^g}{V_g}$ and $\rho_g = \frac{m^g}{V_g}$

- $X_{H_2}^g$ is the mass fraction of hydrogen in the total gas phase (-)
- $m_{H_2}^g$ is the hydrogen mass in the gas phase (kg)
- m^g is the total mass of the gas phase (kg)

- $\rho_{H_2}^{g}$ is the volumetric mass of gaseous hydrogen in the gas phase (kg.m-3)

Mass conservation law for gaseous hydrogen:

$$\frac{\partial}{\partial t}(\omega S_g \rho_g X_{H_2}^{g}) + \nabla(\rho_g X_{H_2}^{g} U_g - J_{H_2}^{g}) + \Omega_{H_2}^{g/l} = Q_{H_2}^{g} \qquad (12)$$

- $\Omega_{H_2}^{g/l}$ is the exchange term from the gaseous phase to the liquid phase for H2 (kg.m-3.s-1)
- $Q_{H_2}^{g}$ is the consumption/production term for gaseous hydrogen (kg.m-3.s-1)
- $J_{H_2}^{g}$ is the diffusive term for gaseous hydrogen (kg.m-2.s-1)

Diffusive flux for a binary mixture of gas (H2 and water vapor) can be expressed by Fick's law:

$$J_{H_2}^{g} = \rho_g D_{H_2 vap}^{g} \nabla X_{H_2}^{g} \qquad (13)$$

- $D_{H_2 vap}^{g}$ is the diffusion coefficient for gaseous hydrogen in water vapor (m2.s-1)

The mass fraction of dissolved hydrogen is expressed as:

$$X_{H_2}^{w} = \frac{\rho_{H_2}^{w}}{\rho_w} \qquad (14)$$

With $\rho_{H_2}^{w} = \frac{m_{H_2}^{w}}{V_w}$ and $\rho_w = \frac{m^w}{V_w}$

- $X_{H_2}^{w}$ is the mass fraction of dissolved hydrogen (-)
- $m_{H_2}^{w}$ is the dissolved hydrogen mass (kg)
- m^w is the total mass of the liquid phase (kg)
- $\rho_{H_2}^{w}$ is the volumetric mass of dissolved hydrogen in the liquid phase (kg.m-3)

Mass conservation law for dissolved hydrogen is expressed as:

$$\frac{\partial}{\partial t}(\omega S_w \rho_w X_{H_2}^{w}) + \nabla(\rho_w X_{H_2}^{w} U_w - J_{H_2}^{w}) + \Omega_{H_2}^{l/g} = Q_{H_2}^{w} \qquad (15)$$

- $\Omega_{H_2}^{l/g}$ is the exchange term from the liquid phase to the gas phase for H2 (kg.m-3.s-1)
- $Q_{H_2}^{w}$ is the consumption/production term for dissolved hydrogen (kg.m-3.s-1)
- $J_{H_2}^{w}$ is the diffusive term for dissolved hydrogen (kg.m-2.s-1)

The exchange terms from between liquid and gaseous phase are linked by the following relation:

$$\Omega_{H_2}^{l/g} = -\Omega_{H_2}^{g/l} \qquad (16)$$

Diffusive flux for dissolved hydrogen can be expressed by Fick's law:

$$J^{w}_{H_2} = \rho_w D^{w}_{H_2 vap} \nabla X^{w}_{H_2} \quad (17)$$

- $D^{w}_{H_2 vap}$ is the diffusion coefficient for dissolved hydrogen in water vapor (m2.s-1)

Part of the gas will be dissolved in the pore water. The solubility limit for the gas depends mainly on thermodynamic conditions and can be expressed by Henry's law:

$$C^{w}_{H_2} = H_{H_2}(T) P^{g}_{H_2} \quad (18)$$

Where $C^{w}_{H_2} = \dfrac{X^{w}_{H_2} \rho_w}{M_{H_2}}$

- $C^{w}_{H_2}$ is the maximum concentration of hydrogen in water (mol.m-3)
- H_{H_2} is the constant of Henry's law for hydrogen (mol.m-3.Pa-1)
- $P^{g}_{H_2}$ is the partial pressure of hydrogen in the total gaseous phase (Pa)
- M_{H_2} is the molar mass for hydrogen (kg.mol-1)

***Remark**: given the actual hydrogen concentration in water, $C'^{w}_{H_2}$, it is possible to define a "pseudo pressure" of the dissolved hydrogen, $P'^{g}_{H_2}$, by inversion of Henry's law:*

$$P'^{g}_{H_2} = \frac{C'^{w}_{H_2}}{H_{H_2}(T)} \quad (18')$$

The relation between partial pressure of each gas present in the total gas phase and total gas pressure is given by Dalton law that writes for a binary mixture (H2 and water vapor):

$$P_g = P^{g}_{H_2} + P^{g}_{wvap} \quad (19)$$

- P^{g}_{wvap} is the partial pressure of water vapor in the total gas phase (Pa)

Each of the gases is supposed perfect:

$$P^{g}_{H_2} = \frac{\rho^{g}_{H_2}}{M_{H_2}} RT \text{ and } P^{g}_{wvap} = \frac{\rho^{g}_{wvap}}{M_{wvap}} RT \quad (20, 21)$$

For the gas mixture this writes:

$$P_g = \frac{\rho_g}{M_g} RT \quad (22)$$

- Mg: molar mass for the total gaseous phase (H2 + water vapor) (kg.mol-1)
- R: constant of the perfect gas (J.mol-1.K-1): R = 8.314 J.mol-1.K-1
- T: temperature (°K)

Saturation pressure for water vapor is only depending on temperature and can by expressed by:

$$\log_{10}(P_{sat}) = 2.786 + 0.031514T_c - 1.2373x10^{-4}T_c^{\ 2} + 4.2267x10^{-7}T_c^{\ 3} - 8.1308x10^{-10}T_c^{\ 4} \quad (23)$$

- Psat: saturation pressure for water vapor (Pa)
- Tc: Temperature (°C)

Kelvin's law is giving a relation between saturation pressure for water vapor, effective pressure for water vapor and capillary pressure:

$$P_{wvap}^{g}(T, S_w) = \exp\left(\frac{M_w P_c(S_{w)}}{\rho_w RT}\right) P_{sat}(T) \quad (24)$$

FORGE

Fate Of Repository Gases

European Commission FP7

Final report on benchmark studies on repository-scale numerical simulations of gas migration Part 3: repository scale benchmark

FORGE Reports D1.4R and D1.6-R pt 3

Keywords.

Benchmark, repository scale, numerical simulation, repository

Bibliographical reference

WENDLING, J (COMPILER). 2013. Final report on benchmark studies on repository-scale numerical simulations of gas migration Part 3: repository scale benchmark .

FORGE Reports D1.4R and D1.6-R pt 3. 102pp.

Euratom 7th Framework Programme Project: FORGE

EURATOM

FORGE Deliverable D1.6-R

Final report on benchmark studies on repository-scale numerical simulations of gas migration Part 3: repository scale benchmark[1]

September 2013

Authored by:

France	Eloi Treille & Jacques Wendling (ANDRA)
United Kingdom	Simon Norris (NDA RWMD)
	Kate Thatcher & Alex Bond (Quintessa)
Canada	Helen Leung (NWMO)
	Nicola J. Calder (Geofirma)

Compiled by:	Jacques Wendling	Date: September 2013
Checked by:	Simon Norris	Date: 28th March 2014
Approved by:	Richard Shaw	Date: 30th April 2014

[1] J. Wendling, L. Yu, E. Treille, S. Norris, K. Thatcher, A. Bond, H, Leung, N.J. Calder, *Final report on benchmark studies on repository-scale numerical simulations of gas migration, Part 3 repository scale benchmark*, European Commission FORGE Deliverable D1.6-R, 2013.

Fate **O**f **R**epository **G**as**E**s (FORGE)

The multiple barrier disposal concept is the cornerstone of all proposed schemes for geological disposal of radioactive wastes. The concept is based on a series of passive complementary barriers, both engineered and natural, that act to achieve the required level of safety for radioactive waste disposed in a geological repository.

Demonstrating an appropriate understanding of gas generation and migration is a key component in a safety case for a geological repository for radioactive waste. On the basis of work to date, the overall behaviour of waste-derived gas and its influences on repository system performance require improved understanding. Key issues to be further examined relating to an enhanced understanding of gas-related processes include: dilational versus visco-capillary flow mechanisms; long-term integrity of seals, in particular gas flow along contacts; role of the EDZ as a conduit for preferential flow; and laboratory to field up-scaling. Such issues are the focus of the integrated, multi-disciplinary European Commission FORGE project.

The FORGE project links international radioactive waste management organisations, regulators and academia, and is specifically designed to tackle the key research issues associated with the generation and movement of repository gases associated with waste disposed in a geological repository. Of particular importance are the long-term performance of bentonite buffers, plastic clays, indurated mudrocks and crystalline formations. Further experimental data are required to reduce uncertainty relating to the quantitative treatment of gas in performance assessment.

FORGE will address these issues through a series of laboratory and field-scale experiments, including the development of new methods for up-scaling allowing the optimisation of concepts through detailed scenario analysis. The FORGE partners are committed to training and CPD through a broad portfolio of training opportunities and initiatives which form a significant part of the project.

Further details on the FORGE project and its outcomes can be accessed at www.FORGEproject.org.

Contact details:

EC FORGE Work Package 1 Leader:

Dr Simon Norris

Nuclear Decommissioning Authority – Radioactive Waste Management Directorate

Tel +44 1925 802891

Fax +44 1925 802948

Email simon.norris@nda.gov.uk

Web address: www.nda.gov.uk

Address NDA Harwell
Building 587
Curie Avenue
Harwell Science and Innovation Campus
Didcot
Oxon OX11 0RH
United Kingdom

Table of content

1. Context and introduction 1

2. Definition of the benchmark 2

3. Summary of the work done by the different teams 4

3.1 NDA RWMD contribution 4

3.1.1 Introduction 4
3.1.2 Model Implementation 4
3.1.3 Base Case Results 10
3.1.4 Sensitivity Cases 20
3.1.5 Evaluating the three benchmark studies 27
3.1.6 Discussion and Conclusions 31
3.1.7 References 32

3.2 SCK-CEN contribution 33

3.3 Andra contribution 34

3.3.1 Introduction 34
3.3.2 Model Implementation 34
3.3.3 Base Case Results 38
3.3.4 Discussion and Conclusions 42

3.4 CEA contribution 44

3.5 CNRS contribution 45

3.6 IRSN contribution 46

3.7 LEI contribution 47

3.8 ENSI/IFSN contribution 48

3.9 NWMO contribution 49

3.9.1 Introduction 49
3.9.2 Model Implementation 50
3.9.3 Base Case Results 55
3.9.4 Sensitivity Cases 70
3.9.5 Discussion and Conclusions 73
3.9.6 Issues for further consideration 74
3.9.7 References 74

4. Global synthesis of the benchmark at repository scale 75

4.1 Comparison of the available results at repository scale and main phenomenological understandings 75

4.2 Numerical and upscaling techniques used in this repository scale benchmark 78

4.3 How representative are the models? 78

5. Global synthesis of the whole benchmark exercise 79

ANNEX : full description of the benchmark at repository scale

6. Context and objectives 81

6.1 Benchmark general specification at repository scale 81

6.2 Detailed description of the test case 87
6.2.1 Geometry 87
6.2.2 Boundary conditions 90
6.2.3 Physical parameters 91
6.2.4 Initial conditions 93
6.2.5 Production term for hydrogen 94
6.2.6 SIMULATION PERIOD 94
6.3 Output results 94
6.3.1 Evolution with time of mass flows across surfaces at module scale 94
6.3.2 Evolution with time at given points at module scale 95
6.3.3 Evolution with time of mass flux over surfaces and of pressures/saturation at given points at repository scale 96
6.4 Mathematical model proposed for the exercise 98

List of figures

Definition of benchmark

Figure 1 Schematic representation of a repository for HLW 2

NDA contribution

Figure 2 QPAC geometry definition. 4
Figure 3 Whole repository model showing five modules connected to a main drift. 6
Figure 4 Cylindrical grid used for sub-models with distorted outer cells to fit into the Cartesian whole repository grid. 7
Figure 5 Model grid showing the network of tunnels and plugs. Tunnel backfill is shown in yellow, with the EDZ in green and plugs in red. HA cells are not shown. 7
Figure 6 Arrangement of sub-models in the whole repository model. Six subsystems are used to represent all the HA cells. Access tunnels are shown in yellow and reside in the whole repository model. 8
Figure 7 Schematic diagram of the method for connecting sub-models into the main model grid. Two compartments (WRM1 and WRM2) within the whole repository grid have N HA cells connected to them in the plans. In the model, these N HA cells are removed and replaced by a single HA sub-model. The diagram illustrates how fluxes between the sub-model and the whole repository model are calculated and scaled between the plug-end of the sub-model and the access tunnel. 9
Figure 8 The cumulative source term for free gas production by 500 HA cells within the whole repository model compared to the total amount of free and dissolved in the whole model. The amount of free and dissolved gas is calculated by subtracting the initial amount of gas in the model (see Section 3.1.2.1) from the amount of gas at the given time step. 11
Figure 9 The total amount of free and dissolved gas in sub-model 6. These are calculated by subtracting the initial amount of gas in the model from the amount at each time step. The inset shows the same curves alongside the source term for sub-model 6. Note that the sub-model represents half of an HA cell. 12
Figure 10 The change in gas pressure through time for the whole repository at the depth of the HA cells. Note that gas pressure is equal to water pressure when there is no gas present (see Section 3.1.2.1). The sub-models are not represented in this diagram so pressures shown in the sub-model locations are for the host rock beneath the sub-model. 13
Figure 11 The change in water saturation through time for the whole repository at the depth of the HA cells. The sub-models are not represented in this diagram so saturation shown in the sub-model locations is for the host rock beneath the sub-model. 14
Figure 12 The change in gas pressure through time for sub-model 6, which represents the majority of HA cells with surrounding host rock. Note that gas pressure is equal to water pressure when there is no gas present (see Section 3.1.2.1). 15
Figure 13 The change in water saturation through time for sub-model 6, which represents the majority of HA cells with surrounding host rock. 15
Figure 14 The change in dissolved gas concentration (kg/kg) through time for the whole repository at the depth of the HA cells. The sub-models are not represented in this diagram so concentration shown in the sub-model locations is for the host rock beneath the sub-model. 16
Figure 15 The change in dissolved gas concentration (kg/kg) through time for sub-model 6, which represents the majority of HA cells with surrounding host rock. 16

Figure 16 Gas pressures in module 3 for locations shown in the inset. Note that gas pressure is equal to water pressure when there is no gas present (see Section 3.1.2.1). 17
Figure 17 Gas pressures in the shaft and aquifer for locations shown in the inset. Note that gas pressure is equal to water pressure when there is no gas present (see Section 3.1.2.1). 18
Figure 18 Flux of free gas through the plug EDZ for each sub-model, compared with the gas source in a single submodel. These values have been multiplied by 2 to give the flux for a whole HA cell, rather than the half model. 18
Figure 19 Flux of free gas in the access drift for module 1, 3 and 5 (-m1,-m3 and –m5). D1 is close to the main shaft, D25 is in the middle of the module and D50 is 10 m from the end of the drift. 19
Figure 20 Flux of free gas through the main drift plugs (F-md and F-w) and through the top and bottom of the model. Note that all but the Plug 1 and Top argillite fluxes are too small to be seen on the graph. 19
Figure 21 Flux of dissolved gas through to top and bottom of the clay (argillite) and the shaft. 20
Figure 22 Layout of sub-models for two alternative cases, with 16 and 30 sub-models. 21
Figure 23 Comparison of gas pressures for upscaled (dotted lines) and sub-model (solid lines) runs. The locations of the output are shown in Figure 15. 22
Figure 24 Peak pressures in the HA cells for the upscaled model (left) and the 30 sub-model case (right). Colours are only for display, maximum pressures are labelled. Note that the maximum pressure in the upscaled module compartments is a different quantity to the maximum pressure observed in a sub-model, but for the purposes of the discussion here, the comparison is informative. 23
Figure 25 Peak pressures in the HA cells for the 16 sub-model case. Colours are only for display, maximum pressures are written on. 23
Figure 26 Fluxes out of modules 1, 3 and 3 for the base case, 16 sub-model run and 30 sub-model run. 24
Figure 27 Water saturation of the tunnel network including plugs and interfaces through time. 26
Figure 28 Fluxes of gas through the bentonite and though the interface at plug 1 and the shaft plug. The flux through plug 1 from the base case is included for comparison. 27
Figure 29 Comparison of the water and gas pressure boundary conditions supplied for the cell scale model (solid lines) with pressures in the access drift from the whole repository model (WRM, dotted lines). 28
Figure 30 Comparison of the water saturation boundary condition supplied for the cell scale model (solid line) and the saturation in the access drift supplied from the whole repository model (dotted line). 28
Figure 31 Comparison of the water and gas pressure boundary conditions supplied for the module scale model and the equivalent pressures in the main drift taken from the whole repository model. Plug1 represents pressures in the main drift backfill on the shaft side of plug 1 and Plug2 represents pressures in the main drift backfill on the shaft side of plug 2. 29
Figure 32 Comparison of the water saturation boundary conditions in the main drift supplied for the module scale model and the equivalent water saturations taken from the whole repository model. Plug1 represents saturations in the main drift backfill on the shaft side of plug 1 and Plug2 represents saturations in the main drift backfill on the shaft side of plug 2. 30

Andra contribution

Figure 33: Extension of the model, emplacement and extension of the macro-components used in the mesh 36
Figure 33 : gas pressures at different points in the modules of the repository 39
Figure 34 : gas pressures near the access drift and in the upper aquifer 40
Figure 35 : Hydrogen mass flow out of the central cell for each module 40
Figure 36 : hydrogen mass flow in the module drift 41
Figure 37 : hydrogen mass flux across module plugs (positive values toward the access) 42

NWMO contribution

Figure 38: 3D model domain with boundary conditions, cells and drifts for Half-Domain model. 49
Figure 39: 3D model domain with boundary conditions, cells and drifts for Main-Drift model. Note white spaces represent location of modules. 50
Figure 40: Grid discretization detail: cross-section of a cell. Note that cell areas and volumes for the inner cell EDZ have been corrected to remove the inactive waste containers, as described in the text. 52
Figure 41: Grid discretization detail: cross-section of a cell plug. 52
Figure 42: Grid discretization detail: plan view of the access and main drift. 53
Figure 43: Water saturation in modules 1, 3 and 5. 56
Figure 44: Water pressure in modules 1, 3 and 5. 57
Figure 45: Hydrogen gas flows in modules 1, 3 and 5. 57
Figure 46: Dissolved hydrogen gas flows in modules 1, 3 and 5. Note that F-C flows are plotted against the left axes, and F-D flows are plotted against the right axes. 58
Figure 47: Repository and shaft water saturation evolution. Note that P-w-2 and P-w-3 are identical. 59
Figure 48: Repository and shaft water pressure evolution. 60
Figure 49: Repository and shaft gas pressure evolution. 60
Figure 50: H_2 gas flow through the main drift and well 61
Figure 51 : Hydrogen and dissolved hydrogen flows through bentonite seal in the shaft. Negative flows indicate downward flow. 62
Figure 52: Vertical slice of gas and water flow in the shaft at 650 years 63
Figure 53: Gas and dissolved gas in a vertical slice near the shaft at 1000 years. 63
Figure 54: Gas and dissolved gas in a vertical slice near the shaft at 10 000 years. 64
Figure 55: 3D gas saturations in the repository at various times. The transparent blue plane delineates the bottom of the aquifer. 64
Figure 56: Gas flow comparison between main-drift model input and half-domain model flows out of each module. 65
Figure 57: Water flow comparison between main-drift model input and half-domain repository flows out of each module. 66
Figure 58: Water saturation comparison between the main-drift and half-domain models. Note that P-w-2 and P-w-3 overlap one another, and therefore P-w-2 is hidden. 67
Figure 59: Water pressure comparison between the main-drift and half-domain models 67
Figure 60: Gas pressure comparison between the main-drift and half-domain models 68
Figure 61: Comparison of H_2 gas flow along main drift and shaft between main-drift and half-domain models 69
Figure 62: Comparison of dissolved H_2 gas flow along main drift and shaft between main-drift and half-domain models 69
Figure 63: Water saturation comparison of half-domain model with and without interfaces. 70
Figure 64: Gas pressure comparison of half-domain model with and without interfaces. 71

Figure 65: Gas flows at F-C, F-D, F-MD and F-w slices for both the reference (base) and no-interface cases. Note that F-D flows are plotted against the right axis and all other flows are plotted against the left axis. 71
Figure 66: Dissolved gas flows at F-C, F-D, F-MD and F-w slices for both the reference (base) and no-interface cases. Note that F-C and F-D flows are plotted against the left axis and F-MD and F-w flows are plotted against the right axis. 72
Figure 67: Mass of dissolved gas in the aquifer over the course of the simulation, for both the reference (base) and no-interface cases. 73
Figure 68: Gas pressure in the central part of the access drift of the central module (module 3) 75
Figure 69 : Gas flux in the access drift of module 3 just beside and toward the main drift 76
Figure 70 : Gas pressure in the main drift just downstream the last horizontal plug and near the well 77
Figure 71 : Gas flux through the most downstream horizontal plug in the main drift 77

Full benchmark description at repository scale

Figure 72: schematic of a repository for HLW 82
Figure 73: schematic of a module. Definition of the A-A', B-B', C-C' and D-D' cross sections 83
Figure 74: schematic of the A-A' vertical cross section (see figure 2 for definition) 83
Figure 75: schematic of the B-B' vertical cross section (see figure 2 for definition) 84
Figure 76: schematic of vertical cross section C-C' and D-D' (see figure 2 for definitions) 84
Figure 77: schematic of the main drift plugs and backfill interfaces 85
Figure 78 : Schematic of the shaft and the upper aquifer 86
Figure 79: horizontal dimensions 87
Figure 80: horizontal and vertical dimensions on cross section A-A' 87
Figure 81: horizontal and vertical dimensions on cross section B-B' 88
Figure 82: dimensions linked to the shaft and the upper aquifer and boundary conditions 88
Figure 83: other dimensions at repository scale and vertical boundary conditions for argillites and upper aquifer 90
Figure 84: schematic of the surfaces across which flows will be calculated 94
Figure 85: schematic of the points where results should be given 95
Figure 86: locations of the surfaces to compute fluxes at repository scale. 97
Figure 87: schematic of the locations of control surfaces and points in the vicinity of the shaft and in the upper aquifer 98

List of tables

NWMO contribution

Table 1 : Parameters and initial conditions for upscaled interface materials 55

Full description of the benchmark at repository scale

Table 2: Dimensions relative to the simulated domain 89
Table 3: values for physical parameters 92

1. Context and introduction

This document is the third part (out of three) of the final report on the work done for FORGE WP1.2 in the context of a benchmark simulation concerning gas generation and migration at repository depth (many hundreds of metres below ground level) and repository scale.

The work presented is linked to the third benchmark proposed in the FORGE WP1.2 context. The first one was realised at cell scale, the second one at module scale (several tens of cells) and the present one is to be made at a repository scale (ten modules).

One of the main problems in dealing with different teams from different countries, who have different disposal concepts, is to find a common representation as a basis for the benchmark. This implies simplifications are necessary to real concepts, in order that they be represented at a basic level that has some degree of consistency to all participants. Another point is to find a common benchmark definition that can satisfy any team, so something quite simple is needed at the outset, so that teams can have a first trial and, in comparing the respective results thus obtained, verify that basics are well understood by each team.

At the start of WP1.2 activities, after discussion, there was a general agreement that the reference exercise will be as generic as possible (without targeting precisely on national concepts), with sensitivity analyses making it possible to cover national specificities. The aim here is more to understand the behaviour of the modeled system as understood by each participant, rather than to undertake an inter-comparison of codes.

To give some added value to this first exercise, a feature not yet well represented in usual gas simulations was introduced: the explicit representation of the interface between canisters and cell walls.

After a brief description of the benchmark definition (see Section 2), Section 3 of this report collates the results of each WP1.2 participant. To conclude, some conclusions are drawn.

N.B. *: there are two other document linked to this one, on cell scale (report FORGE D1.6-R part 1: cell scale benchmark) and module scale (report FORGE D1.6 –R part 2: module scale benchmark) benchmark.*

2. Definition of the benchmark

N.B. *: The complete definition of the benchmark can be found in the Annex*

N.B. 2 *: This benchmark is the third proposed in the context of FORGE WP1.2. The first one was defined at cell level. The type of cell considered is a somehow generic high level waste cell in a clay host rock. The results can be found in the reports FORGE D1-6-R part 1: "cell scale benchmark". The second one was defined at module scale (several tens of cells) and results can be found in the reports FORGE D1-6-R part 2: "module scale benchmark".*

One of the major difficulties in the representation of gas transfer in a repository is to take into account simultaneously all the sources terms (generally located inside the storage cells) and to represent at the same time the transfer network constituted by the different drifts and cells.

For this third exercice of FORGE WP1.2 we assume a repository having a simple architecture (see Figure 1). This architecture is the same as the one used to define a module in the second benchmark and is more or less representative of some general concepts for HLW repository zones but without any national specificity. The main features are:

- Subdivision of the all repository into several modules linked by a main drift;
- All the modules are equal and contains an access drift serving 50 cells on each side;
- All modules are separated from their neighbors by a drift seal.

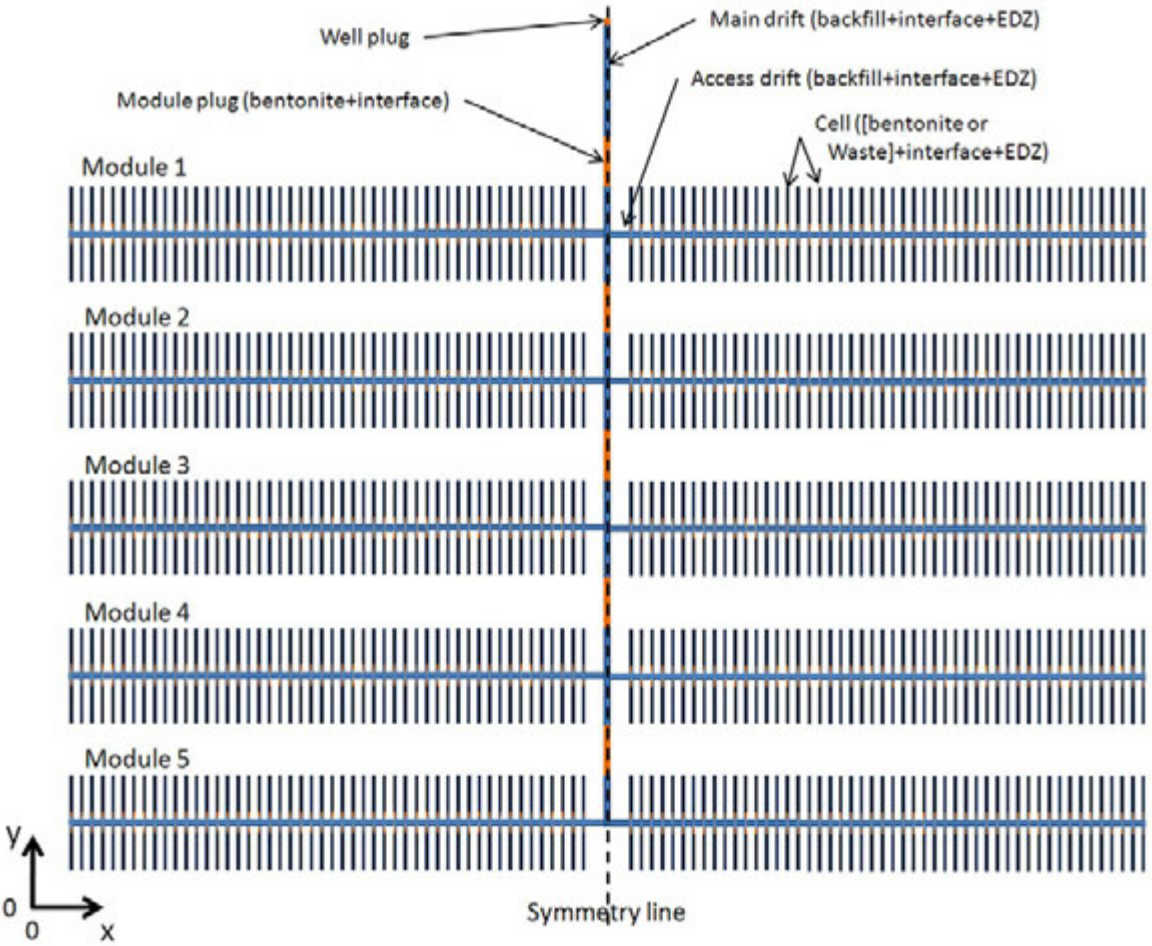

Figure 1 Schematic representation of a repository for HLW

To stay as generic as possible, the gas flux rate in this benchmark is represented by a simple step function lasting 10,000 years; the simulation time is limited to 100,000 years. To understand the distinct role of each phenomenon, the reference case is not considering any coupling. This will be done further on in the sensitivity analysis.

More details and the complete benchmark definition can be found in the Annex.

3. Summary of the work done by the different teams

3.1 NDA RWMD contribution

3.1.1 Introduction

This document presents the model setup, results, sensitivity cases and key learning points from the third benchmark (see Annex) produced by the UK Nuclear Decommissioning Authority (NDA) and Quintessa team. It also draws together the conclusions for the three benchmark studies.

3.1.2 Model Implementation

3.1.2.1 Code and Formulation

QPAC is a general purpose modeling tool designed for flexibility and robustness. The 'model as input' approach for the input syntax allows the user to adjust all aspects of the model formulation and to create couplings in internal parameters so that, within certain limitations, any one input parameter can be a function of any other, and such couplings can be expressed naturally through the input language. Problems are solved monolithically and using a time-implicit method supported by automatic time-stepping. Collections of user-input can be compiled to create 'modules'. Such modules (e.g. thermal transport, reactive transport, simple Darcy flow, Multi-Phase-Flow etc.) can be tested and quality assured much like a conventional code and then used in a modular fashion in new models. The Multi-Phase-Flow module used in this exercise is one example of such a module.

QPAC does not impose a numerical method on the user, but rather provides a rather generic concept of compartments (volumes) and interfaces (faces between volumes) on which variables (unknowns for the calculation) and properties can be defined (Figure 2). Regions where different process models (sub-systems) are represented are connected via 'joiners'. Most QPAC models and modules use a Finite Volume formulation, however Mixed Element and Finite Difference schemes can also be adopted. The Multi-Phase-Flow module uses a conventional Finite Volume formulation.

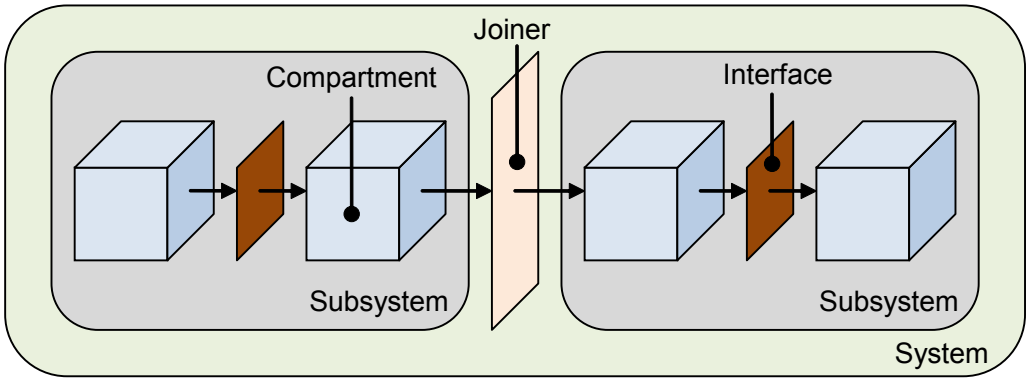

Figure 2 QPAC geometry definition.

Grids of compartments and interfaces can be created using the standard QPAC input language on both axi-symmetric (cylindrical) and Cartesian grids. Also abstract geometries of arbitrary or abstract compartment and interface structures can be created, and attached to the more conventional gridded structures.

The benchmark was implemented in the Quintessa multi-physics code "QPAC" using the benchmark specification (see Annex) as the only source of input. The standard QPAC Multi-Phase-Flow (MPF) module includes all the process model functionality required by this case [1], and hence the process and geometry could be implemented exactly as described in the specification, i.e. multiphase flow of water with a gas phase (hydrogen) together with consideration of dissolved hydrogen and water vapour diffusion.

Consistent with the specification there is no distinction between the initially present gas (air) and hydrogen generated during the model run. QPAC uses a control volume approach for spatial discretisation.

The MPF module uses a continuous formulation for water and gas; this means that for numerical reasons, when fully water saturated, small amounts of immobile gas are assumed to be present and that this gas is in pressure equilibrium with the water (i.e. capillary pressure is zero).

Dissolution is considered to proceed according to Henry's law:

$$p = k_H . c$$

where

p is the pressure of the gas phase (this is equal to the total pressure of the gas phase when only a single gas is present, or the partial pressure when a mixture of gases are present) (Pa)

c is the concentration of the gas in the solution (mol m^{-3})

k_H is Henry's constant for the gas (Pa m^3 mol^{-1})

In a two-phase (or multi-phase) system, comprising gas and water, as the amount of free gas becomes increasingly small the gas pressure tends to the water pressure. When only very small amounts of free gas are present the gas pressure is equal to the water pressure, but there may not be sufficient gas to satisfy the equilibrium dissolved gas concentration calculated using the equation above. This implies that all the gas will dissolve, there will be no free gas, and the system will transition to a single phase system (water partially saturated with dissolved gas).

Two mathematical approaches are available to model this phase transition:

- Apply different mathematical models for multi-phase and single phase conditions, with discontinuous change between models according to defined criteria.
- Apply a single mathematical model, so there is no discontinuity, but appropriately modify the mathematical model when single phase conditions are implied.

In the QPAC code the latter approach is taken. The amount of gas that can be dissolved is given by:

$$Amount\ dissolved\ gas = \min\left(\frac{p}{k_H} V_w m_g,\ Hf\ A_g\right)$$

Where

V_w is the volume of water (m^3)

m_g is the molar weight of gas (g mol^{-1})

A_g is the total amount of gas either as free gas or dissolved gas (in the given model compartment) (kg)

Hf is the Henry's law scaling factor which defaults to 0.99 (-)

Since QPAC primarily solves for the amount of gas present in any compartment, the above equation is simple to evaluate and restricts the amount of dissolved gas when there is very little gas in a given compartment. When there is a very small amount of gas, 1% (by default) of the total gas is always free gas to maintain the continuous formulation. Under these conditions, QPAC calculates a gas pressure that is equal to the water pressure. The Hf parameter can be adjusted to increase or decrease the strength of this effect, and the user will ensure that the parameterisation of the residual gas phase is effectively immobile once the water becomes under-saturated with respect to dissolved gas.

This approach is similar to some other multi-phase codes (e.g. Eclipse) and is consistent with other physic-chemical mathematical models, for example it is possible to calculate a vapour pressure for a single phase (liquid only) system. It also has a conceptual basis: dissolved gas molecules will have a range of energies, and some molecules will have sufficient energy to effectively be disassociated from water, even if the number of such molecules is too small for a distinct free gas phase to form.

3.1.2.2 Grid

The whole repository geometry consists of 10 modules, each with 100 HA cells, 50 on either side of an access drift. The 10 modules are arranged 5 on each side of the main repository drift, and there is a line of symmetry down the centre of the main drift (Figure 2). The repository is hosted in a clay layer, overlain by an aquifer and a shaft connects the main drift to the top of the model through the clay and the aquifer. Only the left had side of the repository has been modelled in QPAC, with a no flow boundary representing the line of symmetry down the main drift.

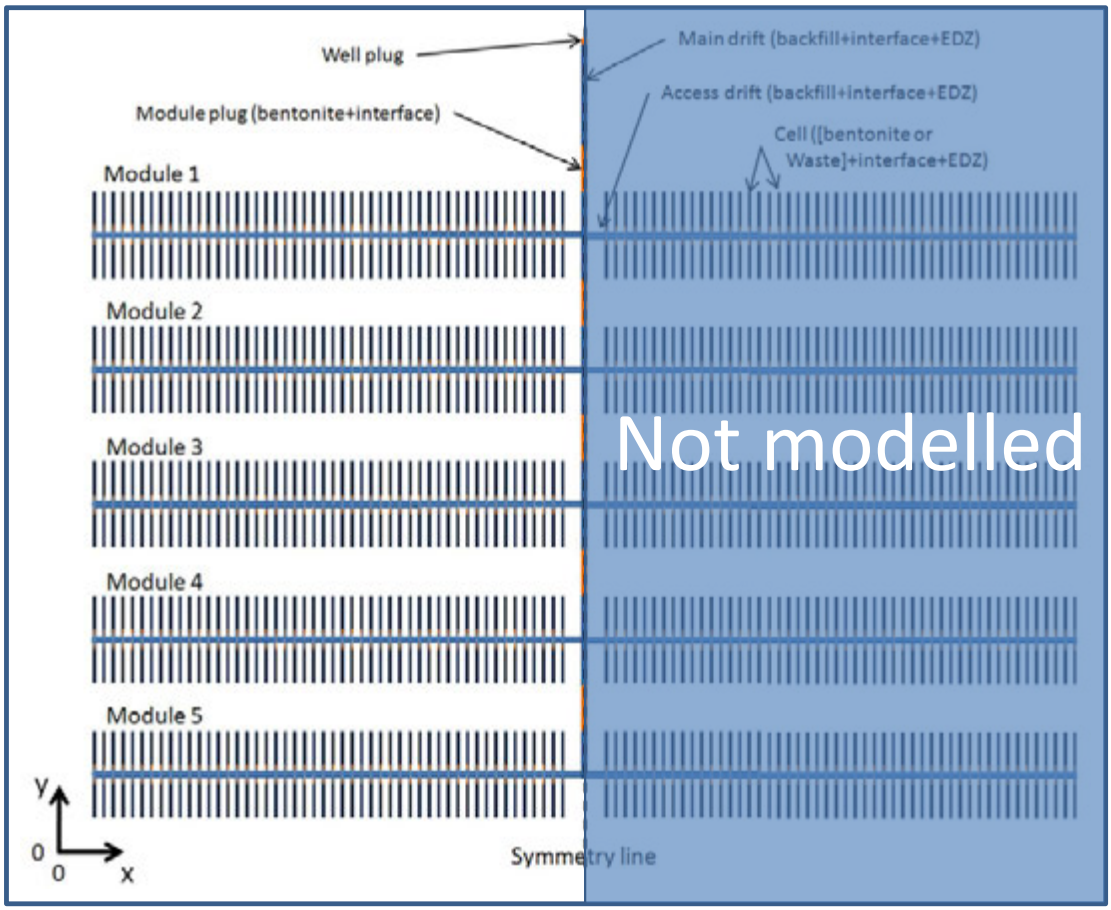

Figure 3 Whole repository model showing five modules connected to a main drift.

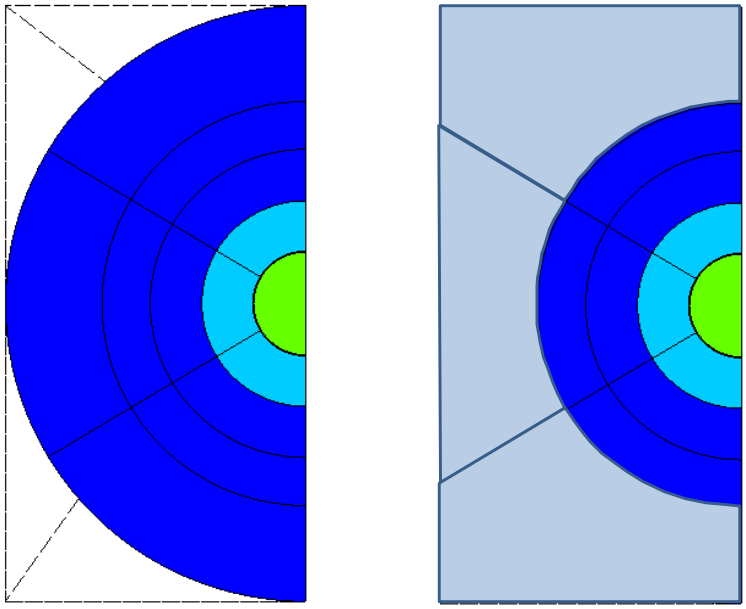

Figure 4 *Cylindrical grid used for sub-models with distorted outer cells to fit into the Cartesian whole repository grid.*

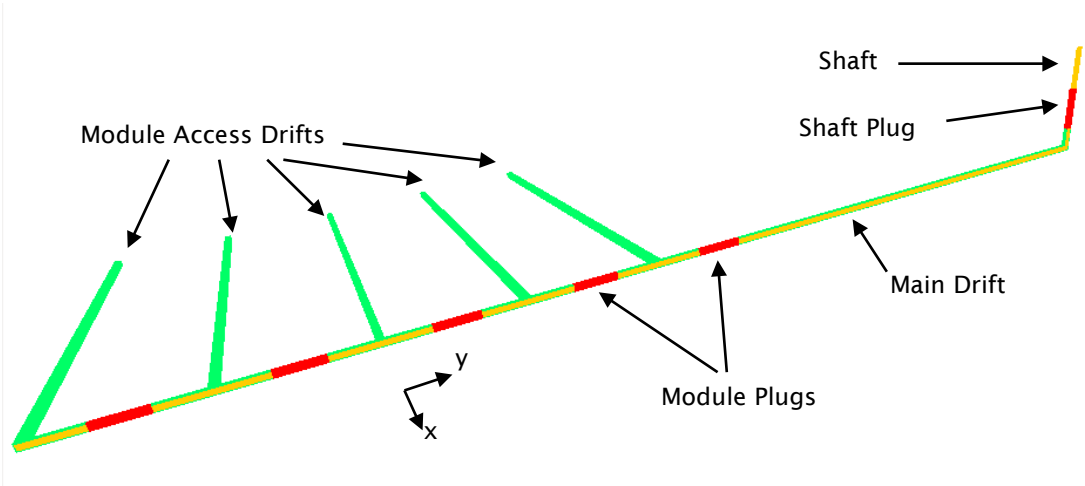

Figure 5 *Model grid showing the network of tunnels and plugs. Tunnel backfill is shown in yellow, with the EDZ in green and plugs in red. HA cells are not shown.*

Bentonite plugs in the main drift separate each module and the drift leading to the shaft (Figure 4). There is also a bentonite plug in the shaft, just below the aquifer layer. An EDZ surrounds the drifts and waste cells, but not the plugs and interfaces are present between the EDZ and tunnel backfill or waste, as well as around the plugs. The interfaces are not present at the base of the structures as gravity would close any gaps here.

The model geometry is constructed using a Cartesian grid for the main part of the model and cylindrical grids for the individual HA cells. The outer compartments in the cylindrical model have adjusted volumes so that the cylindrical grid fits inside the Cartesian grid (Figure 3, and Annex). The HA cell grids are constructed as sub-models that are fully coupled to the main part of the grid. Each sub-model contains one fully discretised representation of an HA cell.

The work at the module scale (see Annex) showed that the majority of HA cells in the whole repository module will see a very similar local environment to each other. Most of the HA cells are adjacent to two other HA cells and are connected to a tunnel at one end with HA cells from another module at the non-tunnel end (HA cells labelled 6 in Figure 6). For the reference model, the assumption is that all these HA cells can be represented by a single HA cell. HA cells at the edges and corners of the repository will have different influences at their boundaries, so a total of six HA sub-models have been used to represent the behaviour of all the HA cells in the model. The location of HA cells represented by the six HA sub-models are shown in Figure 6. This was judged to be the sensible maximum averaging that could be adopted while retaining the general behaviour shown at the module scale. HA sub-model 1 represents only 2 HA cells in the whole model, compared to HA sub-model 6 which represents 384 HA cells. This approach to upscaling reduces the overhead of representing each feature explicitly, without the need to upscale the material properties through conventional homogenisation techniques.

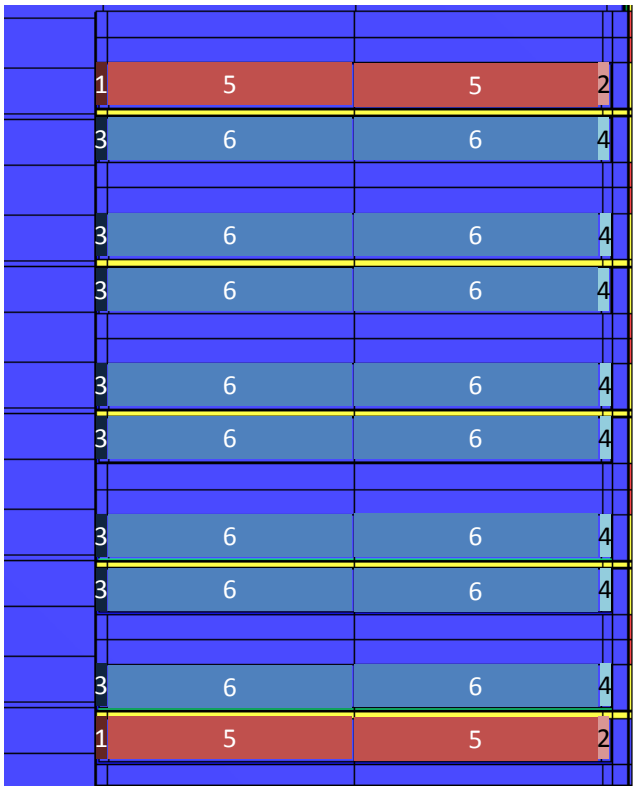

Figure 6 *Arrangement of sub-models in the whole repository model. Six subsystems are used to represent all the HA cells. Access tunnels are shown in yellow and reside in the whole repository model.*

The HA sub-models are fully coupled to the model grid, using scaled fluxes to allow a single HA sub-model to represent an average behaviour of multiple HA cells at multiple locations. The whole repository grid is set up such that volumes of rock containing sets of HA cells with the same expected behaviour are represented by large compartments. All compartments representing volumes which contain HA cells are then discarded but the boundary interfaces between the discarded compartments and the rest of the model remain. The sub-models are then used in place of the discarded volumes with appropriate scaling of fluxes. This flux scaling requires that mass fluxes on a single interface applied to the sub-model and the whole-repository are different to give overall mass conservation. The plug of the HA cell in the sub-model connects directly to the tunnel EDZ in the whole repository model with the other sides of the sub-model connecting to the host rock. We assumed no flow symmetry boundaries between HA cells in the whole repository model, so sub-models are not connected to each other directly.

The reference mass fluxes between the sub-model and the wider repository are first calculated based on the pressure and concentration gradients between the sub-model compartment and the whole repository

compartments, using the compartment face areas associated with the sub-model (Figure 5). These reference mass fluxes are then scaled. For fluxes applied on the sub-model, the volume weighted arithmetic mean of reference fluxes across all connections between a given interface in the sub-model and the whole repository model is used. The net fluxes applied to the sub-model represent the average behaviour of the connections to the whole repository model when the sub-model is used multiple times. The mass flux applied to the whole repository model side of each interface is the reference flux multiplied by the number of sub-models being represented in the discarded volume; the flux is simply scaled to reflect the number of HA cells that the sub-model represents.

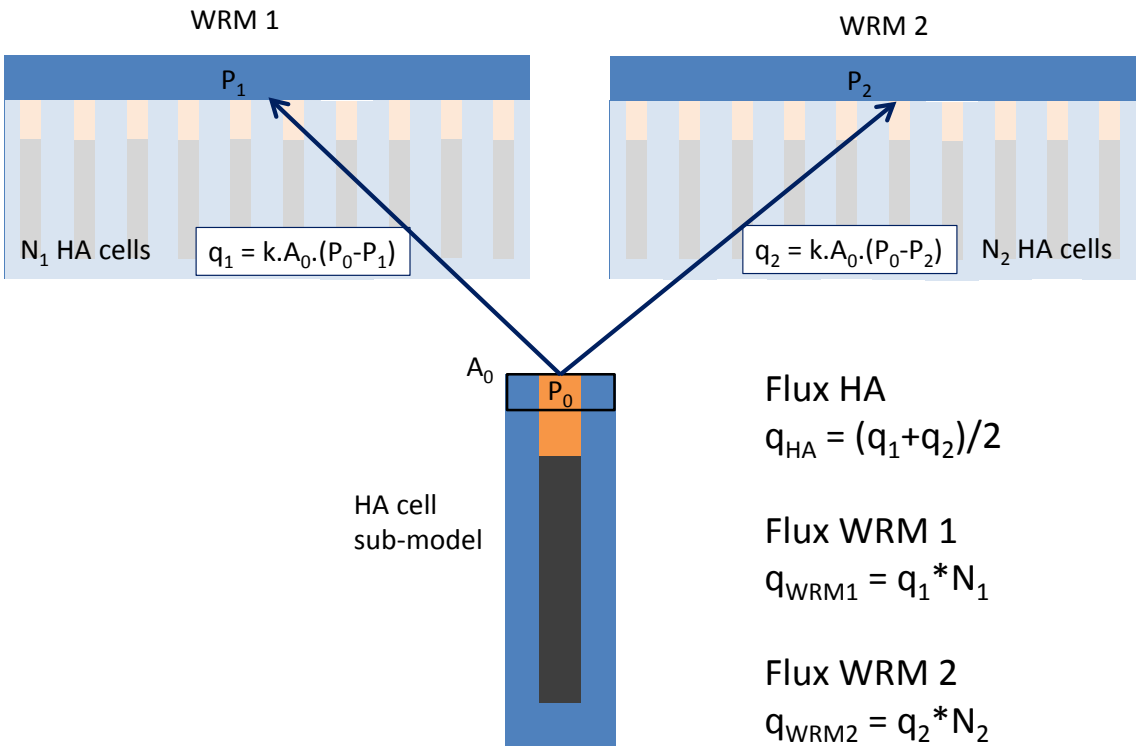

Figure 7 *Schematic diagram of the method for connecting sub-models into the main model grid. Two compartments (WRM1 and WRM2) within the whole repository grid have N HA cells connected to them in the plans. In the model, these N HA cells are removed and replaced by a single HA sub-model. The diagram illustrates how fluxes between the sub-model and the whole repository model are calculated and scaled between the plug-end of the sub-model and the access tunnel.*

3.1.2.3 Boundary Conditions and Sources

The boundary conditions are set up to be consistent with the specification, with no flow across the top boundary and a constant pressure of 6 MPa on the bottom boundary of the model. There is a lateral head gradient across the aquifer layer in the y-direction, with a pressure at z = 0 of 4.5 MPa at the shaft end and 4.0 MPa at the other end. The lateral boundaries in the clay layer are all noflow.

Within a sub-model, the compartments representing the waste are discarded and the source of the H_2 gas is applied on the interface of the compartments that would have been touching the waste. H_2 gas is generated at the rate of 100 mol/year/cell over the first 10000 years of the model run, consistent with the specification.

<u>Initial Conditions</u>

Initial saturations are as specified, with water saturations of 70 % in the bentonite plugs and the backfill and 5 % in the upper part of the interfaces. The remainder of the model is fully water saturated, but because of

the continuous formulation, it is numerically convenient to prevent zero phase saturations, hence the starting saturation of air in the model is 1e-6 in all fully saturated water compartments.

The initial pressures in the model were calculated by running the model without any engineered features for 10,000 years to reach a steady state pressure regime consistent with the boundary conditions. The pressures obtained at the end of this run are used for the initial condition in the fully saturated parts of the model. Where significant gas is initially present, the gas pressure is set to atmospheric.

Deviations from the specification

The base case presented here is for a model with no interfaces, as this ran much faster and is more sensible a conceptualisation, enabling more investigation in the sensitivities of the model. Results from models with interfaces are presented as a sensitivity case.

3.1.2.4 Implementation Issues and Model Stability

The single biggest difficulty in the whole repository model was the same as for previous benchmarks: representing the interfaces. Because of the low capillary pressures in the interfaces they act as a capillary barrier between the porous media they sit between. As a consequence large sections of the model only have a weak hydraulic communication. This tends to make the solution matrices highly compartmentalised and pushed towards singularity. As such, significant care was required in order set the solver parameters such that stable solutions could be obtained while retaining timestep progress and stability.

3.1.3 **Base Case Results**

Corrosion of the HA canisters produced H_2 gas at a rate of 100 mol/year/canister, which results in a total source of approximately 100 kg/year for the 500 canisters represented in the model (~20 kg/year per module). For the first few hundred years, the majority of this gas is free gas, but after around 750 years, the greater proportion of H_2 in the model is dissolved (Figure 7). About 70% by weight of the H_2 is dissolved and 30% is free gas until 10,000 years when the amount of free gas decreases; by 55,000 years, there is no free gas in the model and only 20% of the gas generated in the HA cells is still within the model domain at the end of the simulation. These calculations ignore the air that was initially present in the model as the amount of air as gas is around 2000 kg which is small in comparison to the amount of H_2.

Gas leaves the model domain between 10 kyrs and 100 kyrs as dissolved gas, through the bottom boundary of the model and through the downstream boundary of the aquifer (all other boundary conditions in the model, other than the upstream aquifer boundary, are no flow). The amount of free gas leaving the model domain is less than 0.1% of the total amount of H_2 leaving the model.

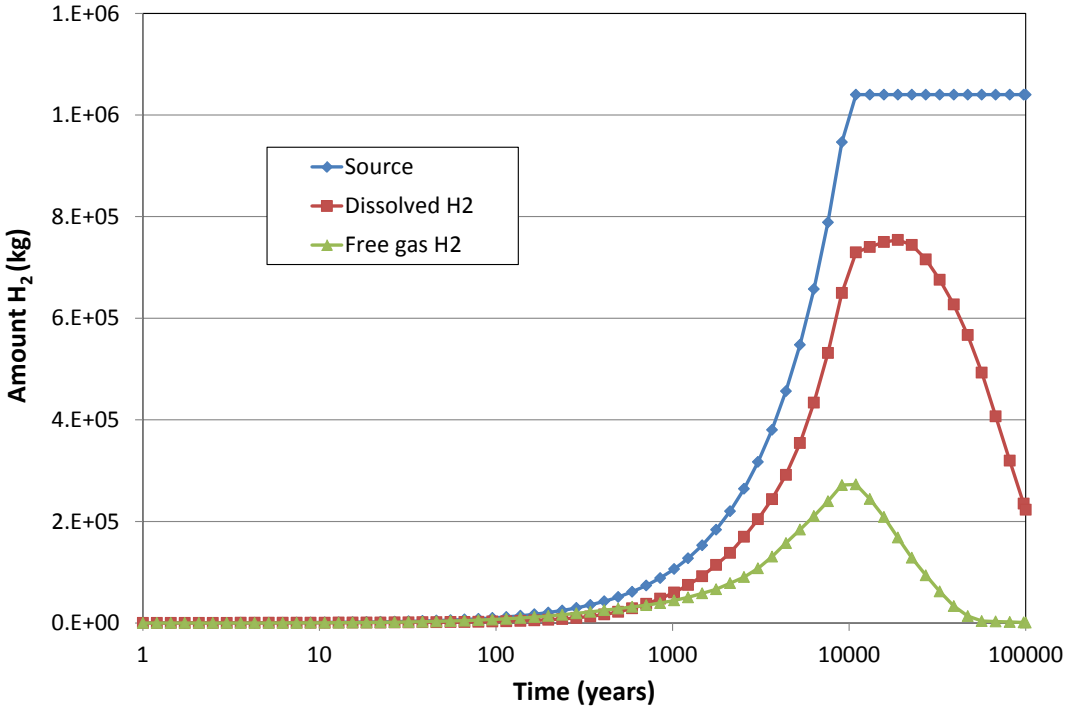

Figure 8 *The cumulative source term for free gas production by 500 HA cells within the whole repository model compared to the total amount of free and dissolved in the whole model. The amount of free and dissolved gas is calculated by subtracting the initial amount of gas in the model (see Section 3.1.2.1) from the amount of gas at the given time step.*

The sub-model represents a half space with the canister and plug, an EDZ and some host rock. At early time (< 10 years) the gas produced around the cell dissolves into the local pore fluid. From 100 to 1000 years, less than 20% of the generated gas remains in the sub-model and from 5,000 to 15,000 years, the gas within the sub-model is mostly free gas, but more than 90% of the generated gas has left the sub-model (Figure 8). There is no free gas left in the sub-model after 55,000 years and the total amount of dissolved gas is around 1% of the total amount of gas generated by the HA cell. In total, 40% of the generated gas leaves the sub-model as free gas, flowing through the plug EDZ, whilst the remaining 60% moves into the host rock mainly as free gas between 1000 to 10,000 years.

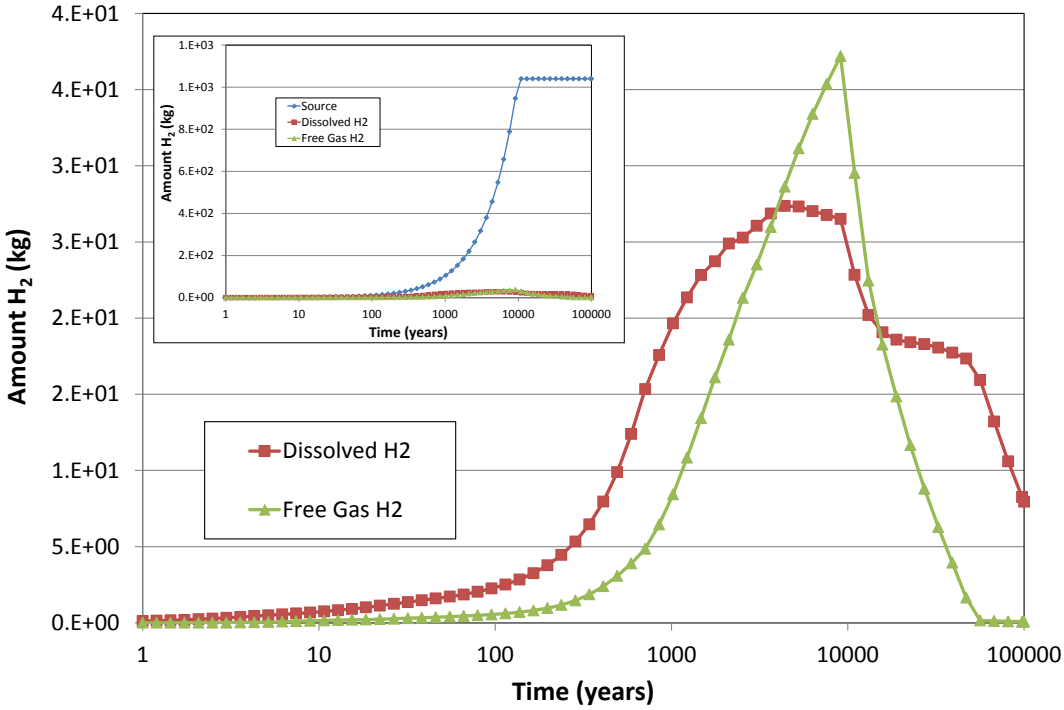

Figure 9 *The total amount of free and dissolved gas in sub-model 6. These are calculated by subtracting the initial amount of gas in the model from the amount at each time step. The inset shows the same curves alongside the source term for sub-model 6. Note that the sub-model represents half of an HA cell.*

At closure of the repository (t = 0 years), the air pressure in the plugs and backfill is at atmospheric pressure (Figure 9 and Figure 11) and these materials have 70% water saturation (Figure 10 and Figure 12). The backfill and cell plugs start resaturating immediately, reducing the water saturation in the EDZs which have permeability 500 times higher than the clay host rock. The cell plugs reach a saturation of 0.995 within 20 years of closure. The module plugs are not surrounded by an EDZ and therefore only start to resaturate after 100 years (Figure 10). The gas pressure in the host rock around the tunnels and HA cells drops as water moves towards the backfill and plugs (eg Figure 15, P-C1-1), but the host rock remains dominantly saturated.

The effects of the gas generation are dominant in most of the model by 1000 years. Gas pressure in the tunnels, plugs and surrounding host rock is above hydrostatic pressure and is highest in the drifts and close to the canister. The main drift connected to the shaft is isolated from the pressure increase by the module 1 plug (Figure 9) and continues to resaturate becoming fully saturated at hydrostatic pressure by 3000 years (Figure 10).

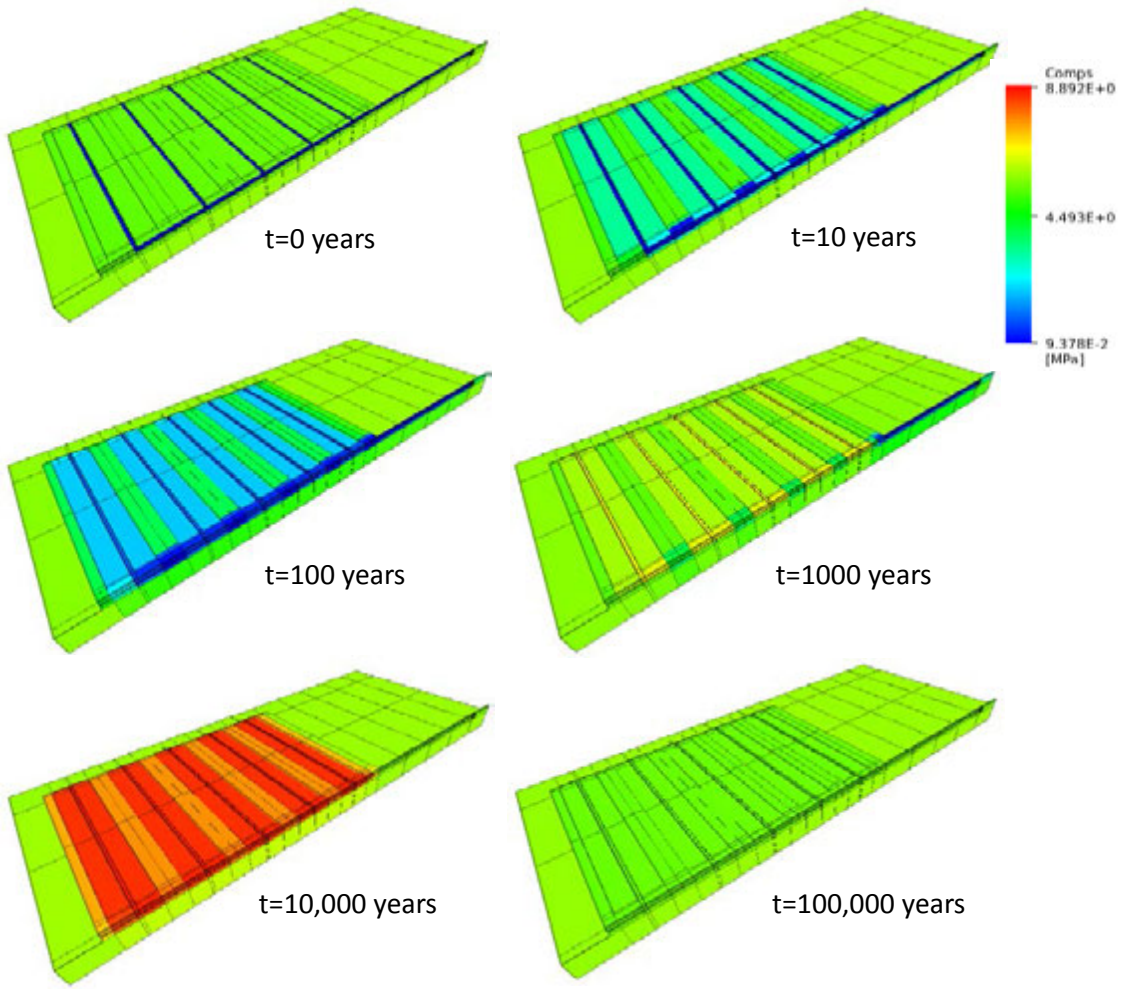

Figure 10 *The change in gas pressure through time for the whole repository at the depth of the HA cells. Note that gas pressure is equal to water pressure when there is no gas present (see Section 3.1.2.1). The sub-models are not represented in this diagram so pressures shown in the sub-model locations are for the host rock beneath the sub-model.*

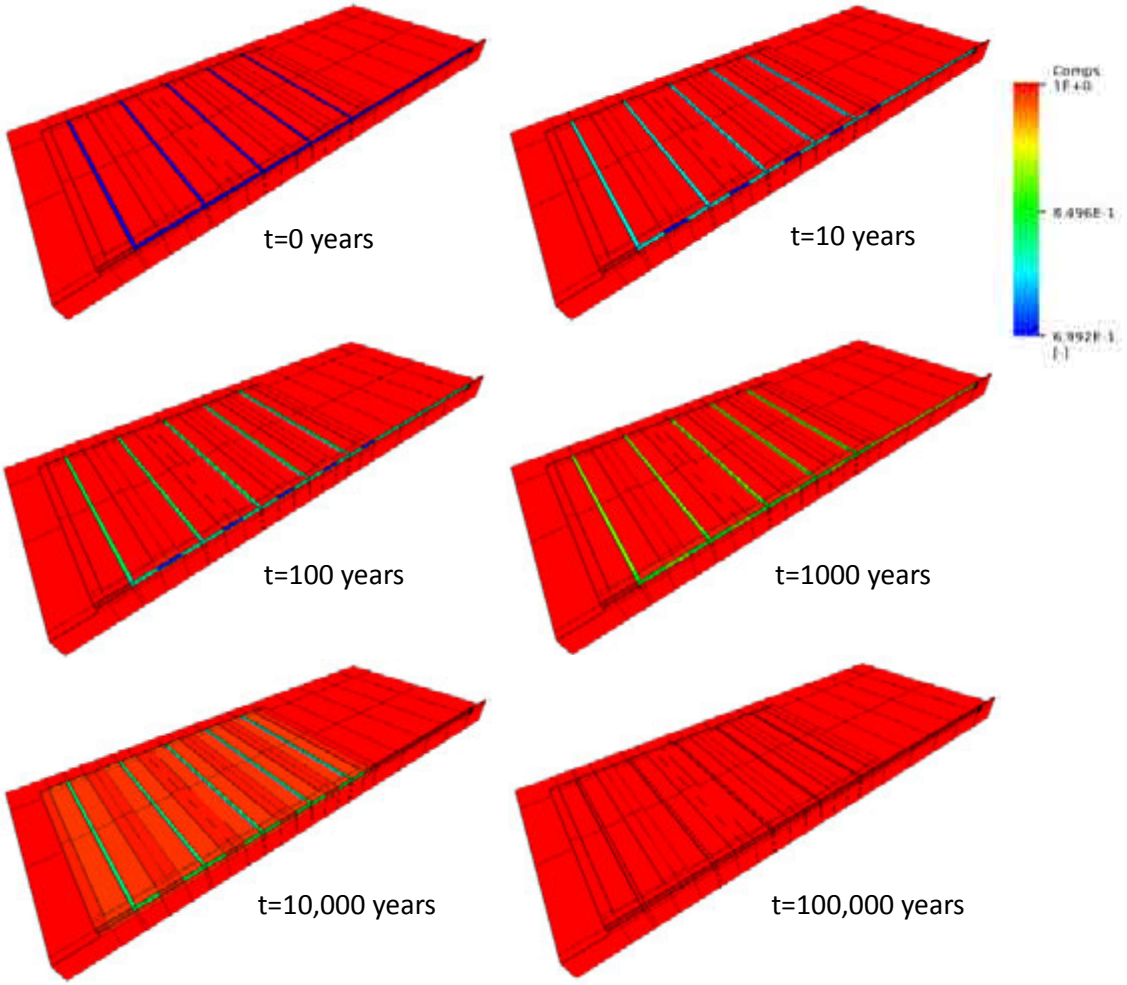

Figure 11 *The change in water saturation through time for the whole repository at the depth of the HA cells. The sub-models are not represented in this diagram so saturation shown in the sub-model locations is for the host rock beneath the sub-model.*

Pressures close to the engineered parts of the system reach a peak at around 5000 years and then remain high until the end of gas production at 10,000 years (Figure 15, P-md-1). The pressure stops rising because free gas migrates further into the previously water-saturated host rock (e.g. between the modules). The host rock around the canisters has a very small saturation of free gas (Figure 10 and Figure 12) which, due to large numbers of cells, in fact represents a significant amount of gas. The maximum pressure in the model is 8.93 MPa, which is 3.6 MPa above hydrostatic pressure and occurs in the EDZ next to the canister. Pressures in the host rock beneath the sub-model reach 8.68 MPa, an increase of 3.32 MPa. Despite the high gas pressure, the plugs in the main drifts remain 99% water saturated, only fully resaturating after gas production has ceased. As parameterised, the plugs are extremely effective in not transmitting the pressure to the shaft, where the model results show resaturation followed by a steady pressure consistent with the boundary conditions (Figure 16).

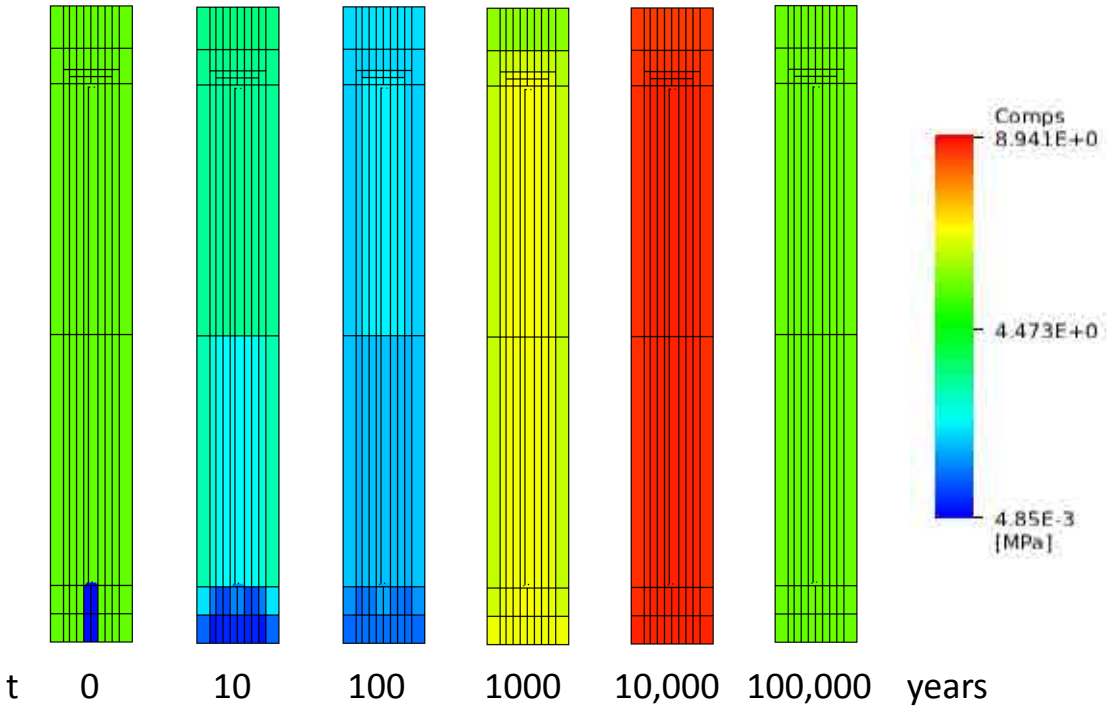

Figure 12 *The change in gas pressure through time for sub-model 6, which represents the majority of HA cells with surrounding host rock. Note that gas pressure is equal to water pressure when there is no gas present (see Section 3.1.2.1).*

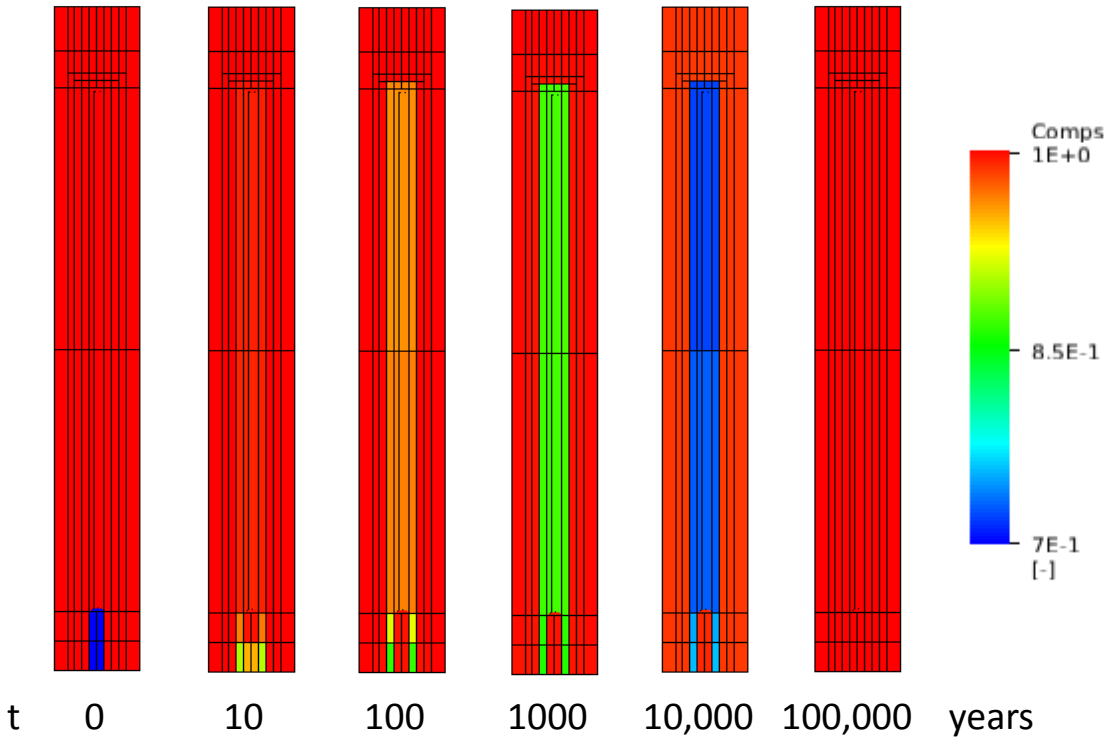

Figure 13 *The change in water saturation through time for sub-model 6, which represents the majority of HA cells with surrounding host rock.*

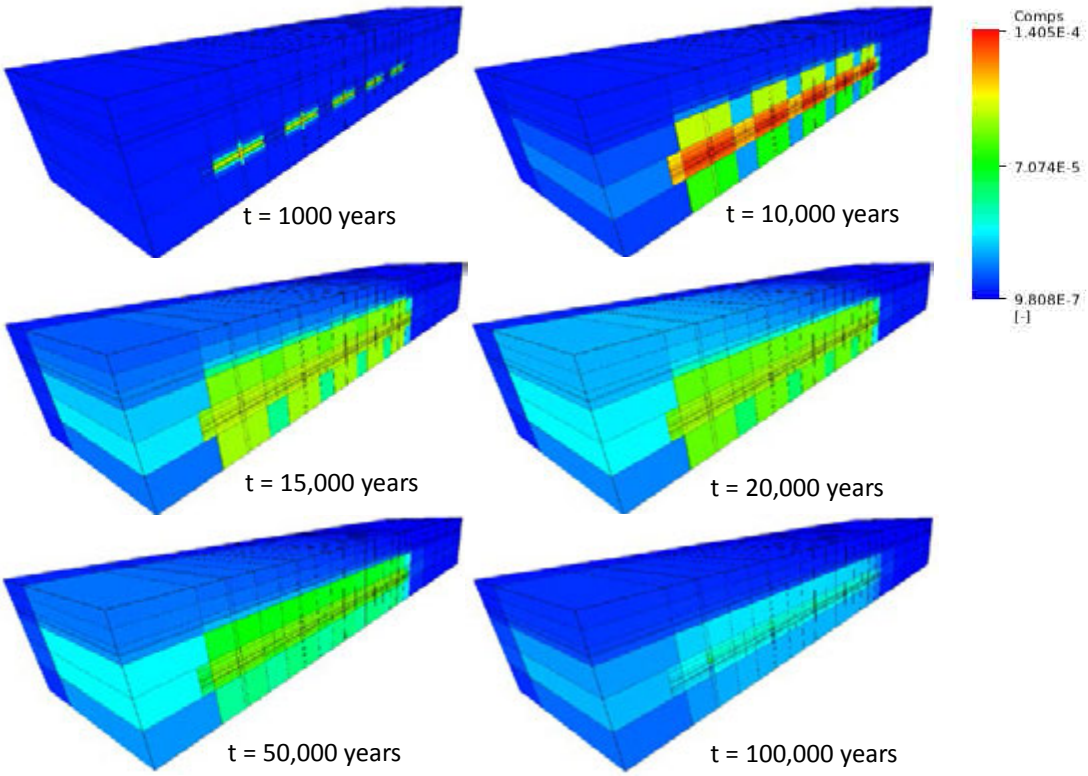

Figure 14 *The change in dissolved gas concentration (kg/kg) through time for the whole repository at the depth of the HA cells. The sub-models are not represented in this diagram so concentration shown in the sub-model locations is for the host rock beneath the sub-model.*

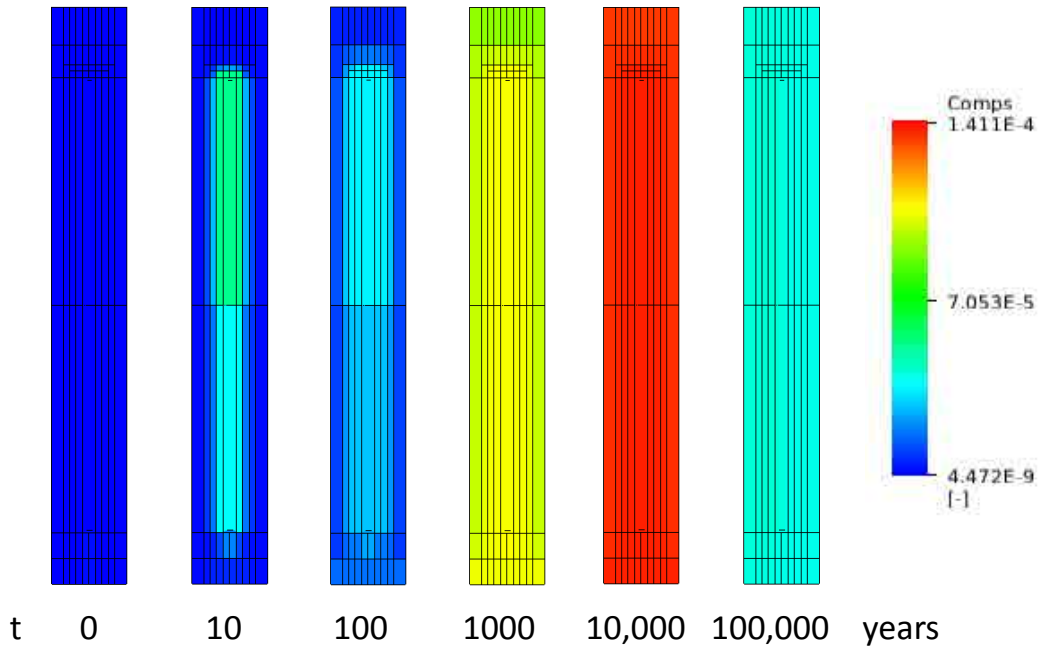

Figure 15 *The change in dissolved gas concentration (kg/kg) through time for sub-model 6, which represents the majority of HA cells with surrounding host rock.*

After the end of gas production at 10,000 years, pressures return to hydrostatic and all free gas dissolves.

The dissolved gas spreads out from the canister and tunnels into the host rock (Figure 13 and Figure 14) in a broadly radial pattern. The dissolved H_2 reaching the aquifer is diluted by the relatively high flow of fresh water which helps to maintain an upward diffusive gradient. A plume of dissolved gas moves through the aquifer from around 15,000 to 50,000 years, but the concentration of H_2 is significantly lower than the concentrations around the waste canisters.

Over half of the gas produced migrates directly into the host rock from the canister EDZ, initially as free gas which then dissolves. The remaining free gas migrates out of the sub-model through the cell plug EDZ. This flux is similar for all sub-models until 1000 years (Figure 17) but at later times, gas starts to move into the sub-models at the far end of the access drifts due to the relatively large volume of host rock into which dissolution and diffusion can occur and hence lower gas pressures. The peak free gas flux from each HA-cell is around 0.17 kg/year (Figure 17) and there are 100 HA-cells in each module. The peak free gas flux out of modules 1 and 3 is ~3 kg/year (noting that 20 kg/year is generated per module, or ~0.2 kg/year per HA-cell) indicating the scale of the dissolution that occurs within the access drifts (Figure 18). The fluxes through the module plugs are extremely small because high pressure builds up on both sides of the plug so there is little pressure gradient. There is a pressure gradient across plug 1, and the flux through this plug is 2 orders of magnitude smaller than the flux at the end of the modules (Figure 19). The dissolved flux into the aquifer is 200 times greater than the free gas flux (Figure 19 and Figure 20) which illustrates the overall dominance of diffusive transport over advective transport in low permeability rocks with very efficient seals.

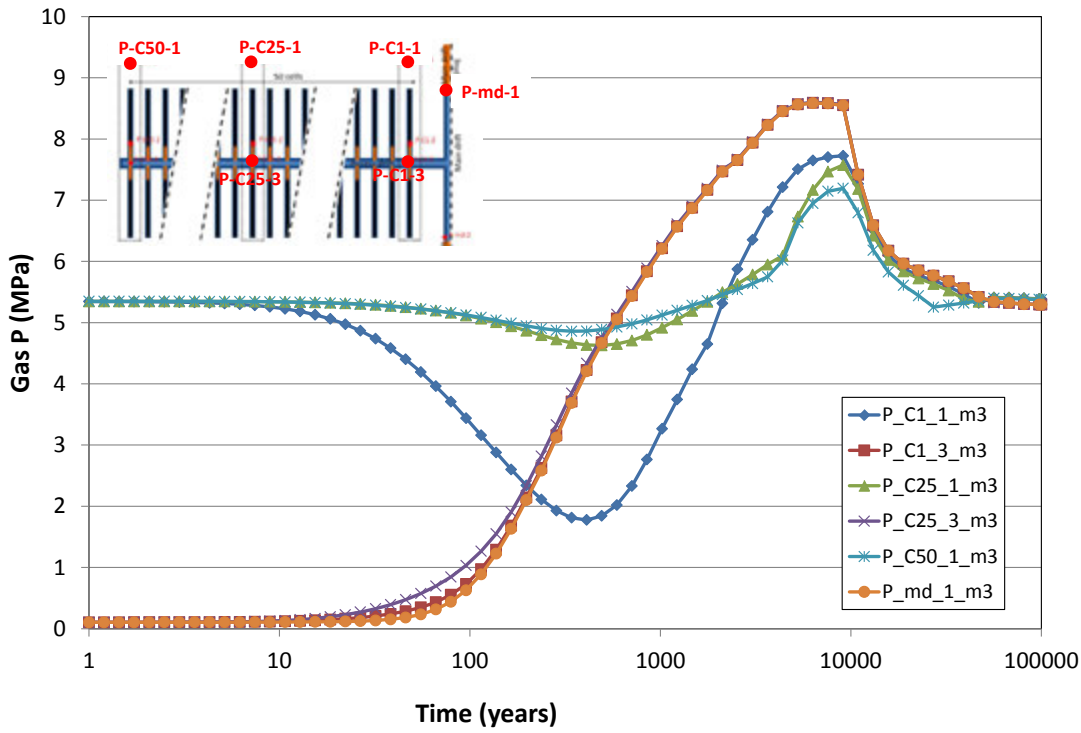

Figure 16 *Gas pressures in module 3 for locations shown in the inset. Note that gas pressure is equal to water pressure when there is no gas present (see Section 3.1.2.1).*

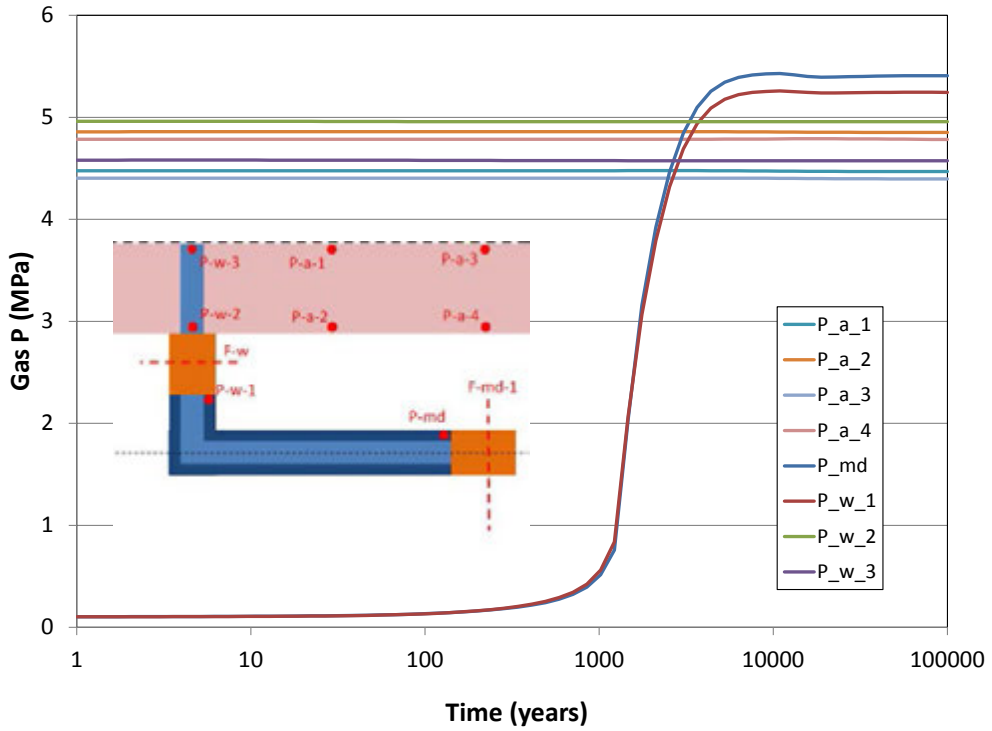

Figure 17 *Gas pressures in the shaft and aquifer for locations shown in the inset. Note that gas pressure is equal to water pressure when there is no gas present (see Section 3.1.2.1).*

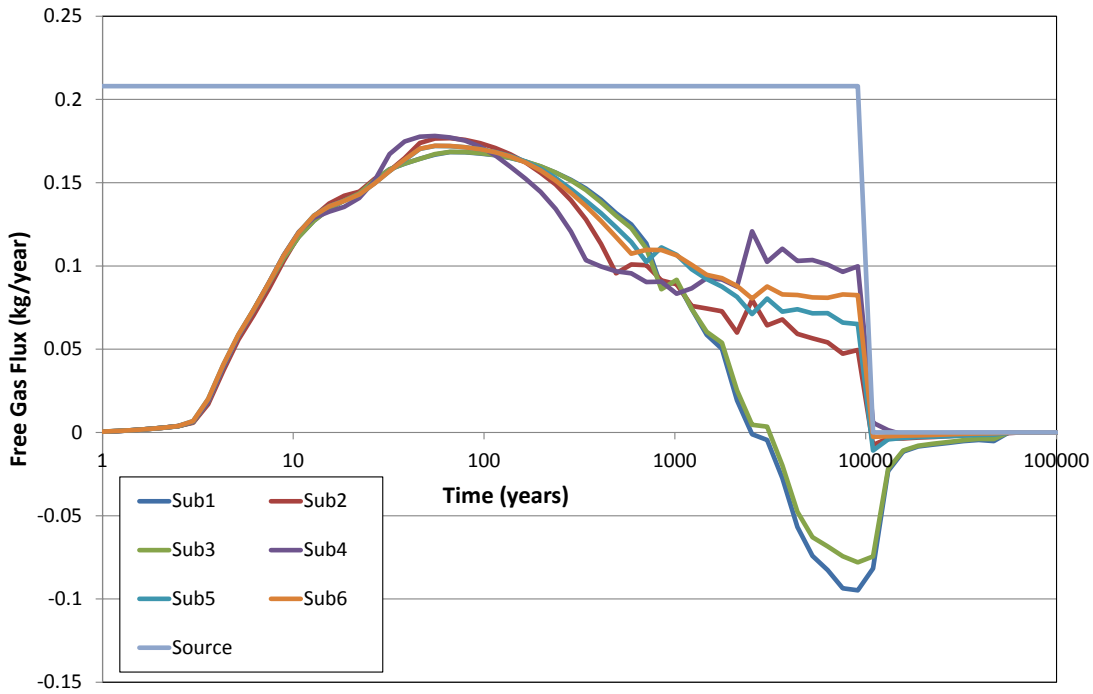

Figure 18 *Flux of free gas through the plug EDZ for each sub-model, compared with the gas source in a single submodel. These values have been multiplied by 2 to give the flux for a whole HA cell, rather than the half model.*

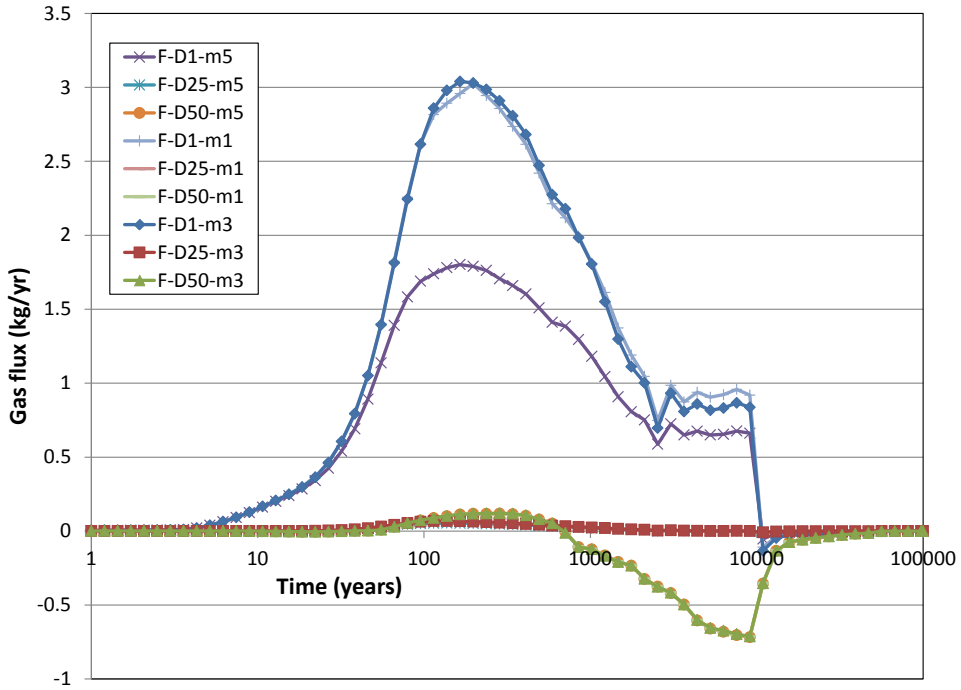

Figure 19 *Flux of free gas in the access drift for module 1, 3 and 5 (-m1,-m3 and -m5). D1 is close to the main shaft, D25 is in the middle of the module and D50 is 10 m from the end of the drift.*

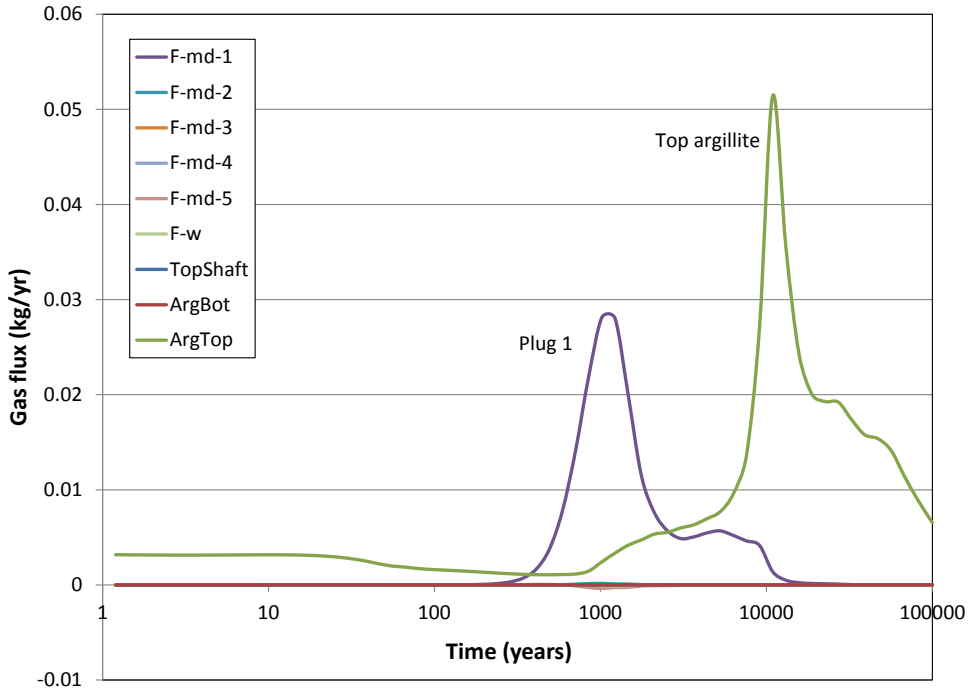

Figure 20 *Flux of free gas through the main drift plugs (F-md and F-w) and through the top and bottom of the model. Note that all but the Plug 1 and Top argillite fluxes are too small to be seen on the graph.*

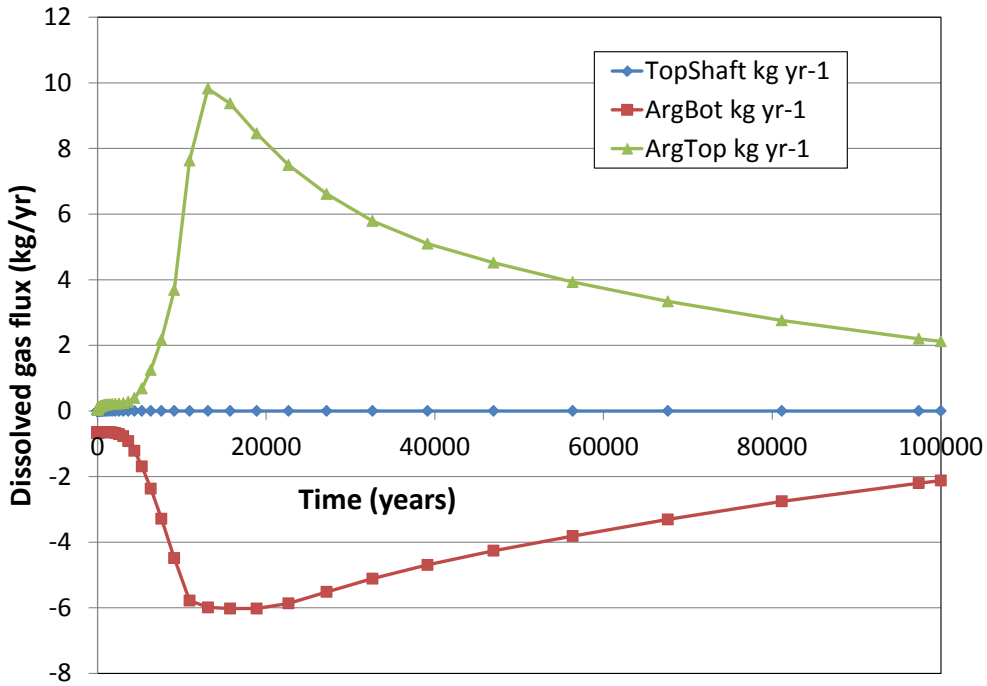

Figure 21 *Flux of dissolved gas through to top and bottom of the clay (argillite) and the shaft.*

3.1.4 Sensitivity Cases

3.1.4.1 Case descriptions

Case 1 : Upscaled modules

In order to give insight into the benefits of representing more detailed structures via sub-models, a model was run in which the HA cells and their surrounding rock were represented by homogeneous, upscaled material properties rather than using the sub-modelling approach. Simple, conventional volume weighting for scalars and arithmetic or harmonic weighting for vectors were used to create effective porosity and permeability values for the upscaled volume. This run was used to give a rough baseline model performance, such that we could test that addition of sub-models and easily pick out non-physical behaviour.

Case 2 : Number of sub-models

Two sensitivity cases were run to assess the implications of the averaging implicit in the sub-model method. A run with 16 sub-models looked at whether significant gradients exist in the x-direction and a run with 30 sub-models looked at averaging in the y-direction (Figure 21). Addition of the extra sub-models and extra model discretisation required for the 16 sub-model run slowed the model runs.

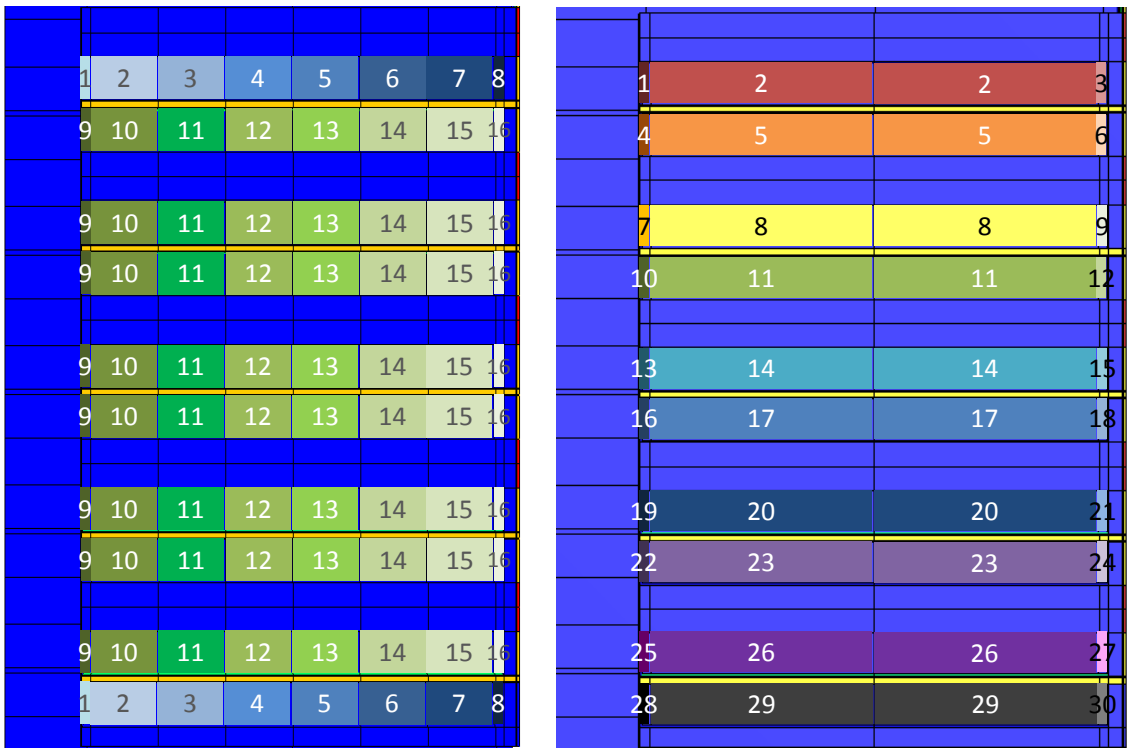

Figure 22 *Layout of sub-models for two alternative cases, with 16 and 30 sub-models.*

Case 3 : Varying EDZ properties

The base case assumes that the tunnels, HA cell plugs and canisters are surrounded by EDZs; there are no EDZs around the module plugs. In the base case, the module plugs are extremely good seals, effectively confining the free gas produced in one module to that module and not transmitting differences in fluid pressures. It is conceivable that an EDZ could be present around the main drift plugs even if the original EDZ created by excavation of the tunnel is removed. Excavating the original EDZ could cause a second EDZ albeit of smaller dimensions, which could allow water and gas to travel past the plugs. The potential consequences of the presence of EDZs around the main drift plugs have been investigated as one sensitivity case.

Although the rock is likely to be damaged during excavation, over long timescales, the backfill will swell, exerting a pressure on the host rock and the host rock will creep. Both of these processes could close any open pathways in the EDZ, reducing permeability and making the EDZ a less effective host rock. An additional sensitivity run in which all EDZ zones have been replaced by host rock was also performed.

Case 4 : No head gradient in aquifier

There was some discussion amongst the teams as to how the proposed boundary conditions in the aquifer should be implemented. To test the sensitivity of the model to the conditions in the top boundary, a model run with a hydrostatic head gradient and no lateral flow in the aquifer was performed.

Case 5 : Interfaces

In the specification, interfaces are shown between the backfill and host rock, around plugs and around the waste canister, but are not present beneath the engineered materials. Interfaces were not included in the base case model because they significantly increase run times and it is not clear how realistic they are over long time scales. However, to complement the work done at the module-scale (see Annex), a case with the interfaces present was implemented.

3.1.4.2 Sensitivity case results

Case 1 : Upscaled modules

There are some small differences between the pressures in the modules depending on whether sub-models or an upscaled representation is used, but the overall behaviour is the very similar (Figure 22). The reduction in gas pressure in the host rock during resaturation is smaller and later when using sub-models compared to the upscaled approach which is consistent with the increased discretisation and more accurate material representation in the sub-models. Pressures in the drift increase more rapidly with the sub-models as the pathway for gas transport from the canister to the drift is explicitly represented and maintained.

The model with upscaled material properties for the HA cells and surrounding host rock captures the main features observed in the base case model. There are some small differences between the models but when considered alongside the uncertainties in the model parameterisation, the upscaled model represents the whole repository well.

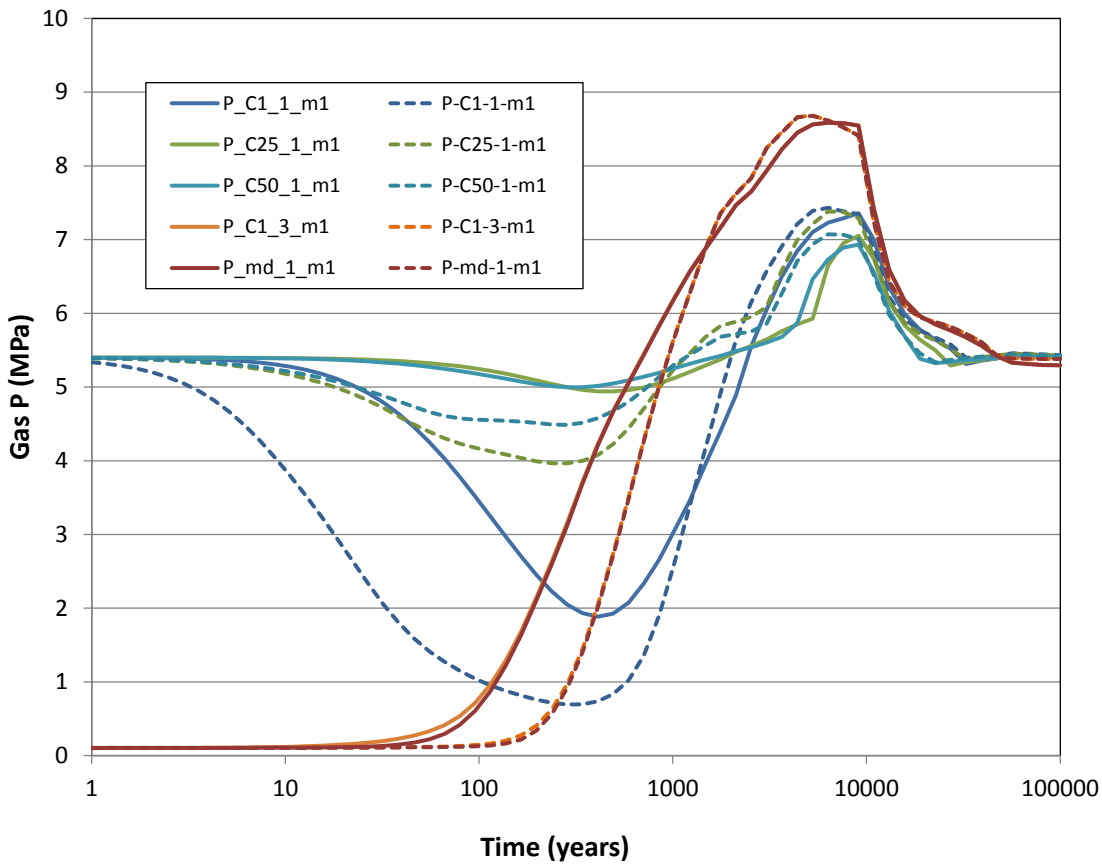

Figure 23 *Comparison of gas pressures for upscaled (dotted lines) and sub-model (solid lines) runs. The locations of the output are shown in Figure 15.*

Case 2 : Number of sub-models

The two runs with additional sub-models indicate that the averaging used in the base case captures the main variability in the system. The 30 model run, shows that modules 2, 3 and 4 all have similar pressure behaviour as each other, with lower peak pressures in modules 1 and 5 (Figure 23). This is slightly different to the behaviour in the base case in that it was assumed that only the outer halves of modules 1 and 5 would see the effects of the adjacent host rock. The upscaled model (Figure 23) shows different pressures in the two halves of module 1 and 5, illustrating that the module pressures are more strongly coupled to the drifts when sub-models are used that when upscaled properties are used.

The 16 sub-model run showed that there are no significant gradients along the module (Figure 24).

Fluxes from the module into the main drift are slightly higher in the base case than in the cases with extra sub-models, but the overall behaviour of the system has not changed (Figure 25).

This sensitivity test shows that there are no significant gradients along a module and that modules 2, 3 and 4 show similar behaviour. This supports the initial assumption that a large number of the HA cells will see very similar conditions in the repository and that the averaging used to represent these cells is appropriate. Given that the fluxes only change by a small amount over the three different models, it is unlikely that the assumptions used in the averaging are having a significant effect on the results.

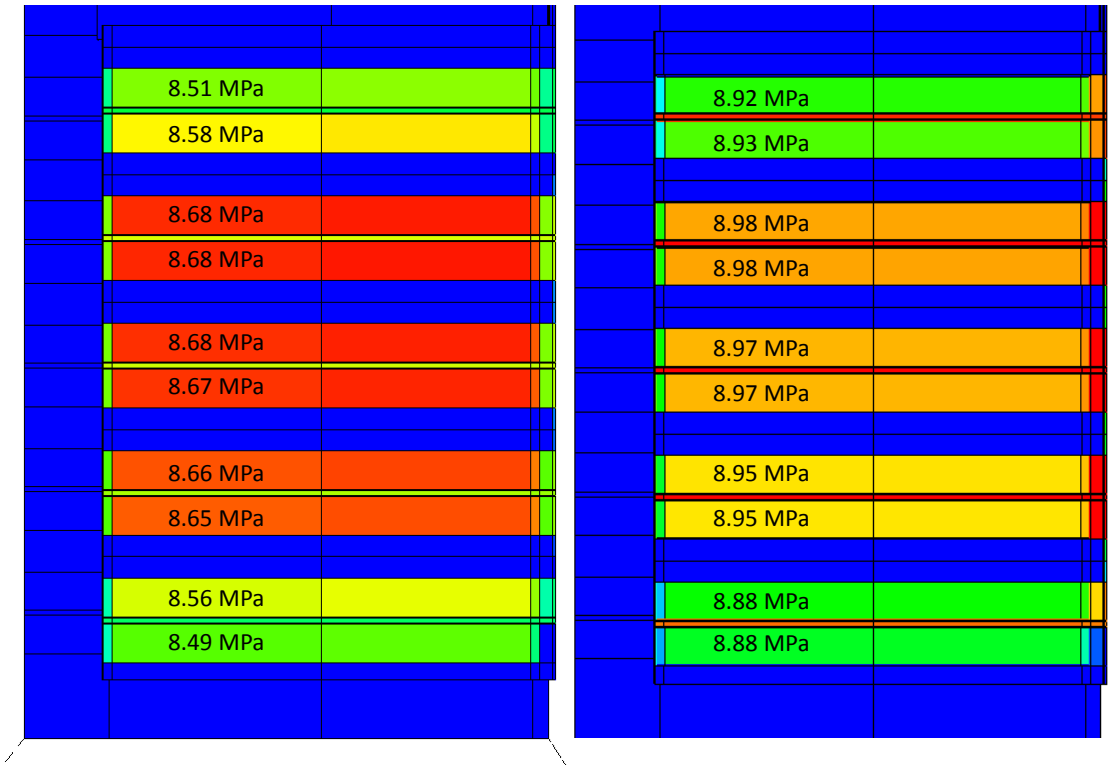

Figure 24 *Peak pressures in the HA cells for the upscaled model (left) and the 30 sub-model case (right). Colours are only for display, maximum pressures are labelled. Note that the maximum pressure in the upscaled module compartments is a different quantity to the maximum pressure observed in a sub-model, but for the purposes of the discussion here, the comparison is informative.*

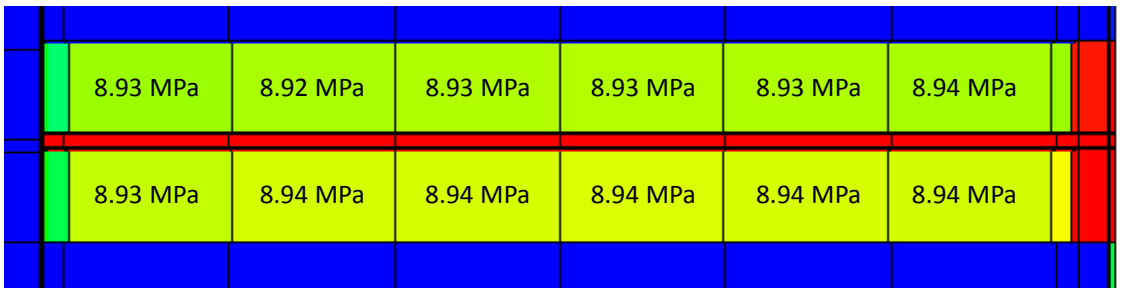

Figure 25 *Peak pressures in the HA cells for the 16 sub-model case. Colours are only for display, maximum pressures are written on.*

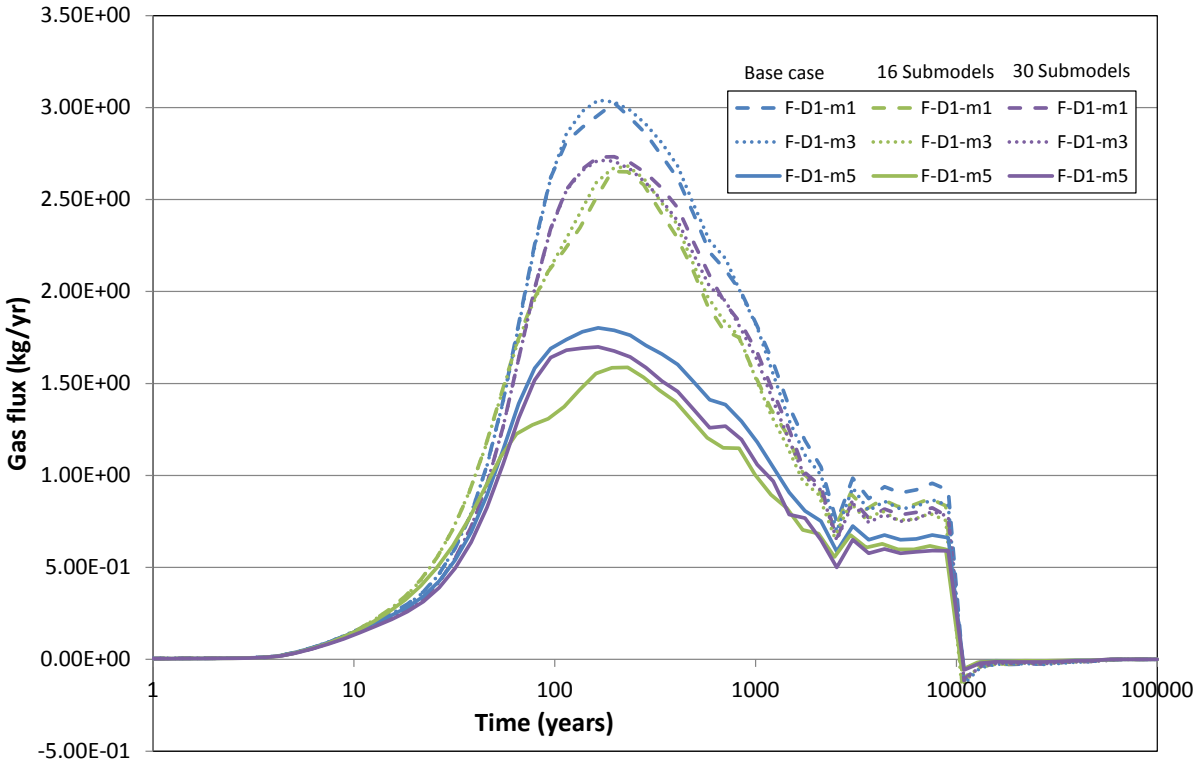

Figure 26 *Fluxes out of modules 1, 3 and 3 for the base case, 16 sub-model run and 30 sub-model run.*

Case 3 : Varying EDZ properties

The model results show that the presence of an EDZ around the main plugs has little impact on pressures and saturations in the model. The main difference between the base case run and the run with EDZs around the main drift plugs is the flux of free gas around the plugs. In the base case, the free gas flux through plug 1 reached a peak of 0.03 kg/year (Figure 19) compared to 5 kg/year if there is an EDZ around this plug. A flux of up to 3 kg/year is also present across the shaft seal when EDZs are present around the plugs. The presence of the EDZ around the plug significantly reduces the sealing performance of the plug.

When EDZs are removed from the model, the resaturation of the backfill and plugs is slower as the water must come from the host rock instead of the higher permeability EDZ. This results in a more significant pressure drop in the host rock and the host rock becomes partially saturated with respect to water earlier. The total amount of free gas within the model is indistinguishable from the base gas, but the fluxes across the cell plugs are three orders of magnitude lower and the flux across plug 1 is an order of magnitude lower.

The model is sensitive to the presence and parameterisation of the EDZ. This is one of the biggest uncertainties in the model and it can significantly change that flux of gas through the shaft seal.

Case 4 : No head gradient in aquifier

The conditions in the aquifer have little effect on the pressures and saturation at the depth of the repository. The fluxes from the argillite into the aquifer do change, with the total diffusive flux into the aquifer dropping off more rapidly with no-flow in the upper aquifer because the concentration gradient is not maintained by inflow of fresh water. There is also an increase in the gaseous flux to the aquifer at around 20,000 years with fluxes reaching 0.55 kg/year at around 70,000 years and remaining at this value until the end of the model run. Whilst the behaviour is different from the base case, these fluxes are very small in comparison to gas generation rates (100 kg/year) and are spread over a wide area.

The conditions in the aquifer above the repository are important for understanding the eventual fate of some of the dissolved gas, but do not affect the performance of the repository in this case.

Case 5 : Interfaces

Including interfaces in the model does not significantly change the overall behaviour of the system. Pressures are slightly higher when interfaces are included (peak pressure is about 0.2 MPa higher) but the change in pressure through time is the same as for the base case. The resaturation of the plugs and tunnel backfill is also similar to the base case although slower as water is only available from the EDZ beneath the tunnel. The very low capillary pressure of the interfaces in the model causes the interfaces to remain dry for over 50,000 years (Figure 26). The wetting of the interfaces causes significant numerical difficulties. To overcome these difficulties and enable water to enter the interface compartments, the capillary pressure was increased by an order of magnitude when the run reached 46,000 years. In a repository, it is likely that the backfill will have expanded to fill the initial gaps close to the tunnel wall, so interfaces are unlikely to exist several tens of thousands of years after backfilling. Increasing the capillary pressure of the interfaces is therefore likely to make the model behaviour closer to reality. When the interfaces do become saturated the water moves from the shaft end of the interfaces through the network.

The presence of an open interface may allow gas to flow from the HA cells to the shaft. The model results show that at least 10 times as much free gas moves past plug 1 in the case with interfaces compared to the base case, but that at the shaft plug, the free gas flows remain negligible (Figure 27). This showns that interfaces could enhance transport of gas out of the repository, but the fluxes are so small that this kimited bypass of plug 1 only changes the location in the system where the gas dissolves. Compared to the 100 kg/year of gas generated by each HA cell, a flux of up to 0.25 kg/yr through plug 1 is relatively small.

The presence of interfaces in the model presents significant numerical challenges but it is not clear that the interfaces, as currently parameterised, are an important feature within the repository. The bentonite backfill is likely to expand upon resaturation and the clay host rock will creep, so it seems unlikely that gas filled gaps will be present after a few years. The impact of the interfaces on the modelling is small and whilst they do act as conduits for gas, the vast majority of gas dissolves in the groundwater before reaching the shaft seal.

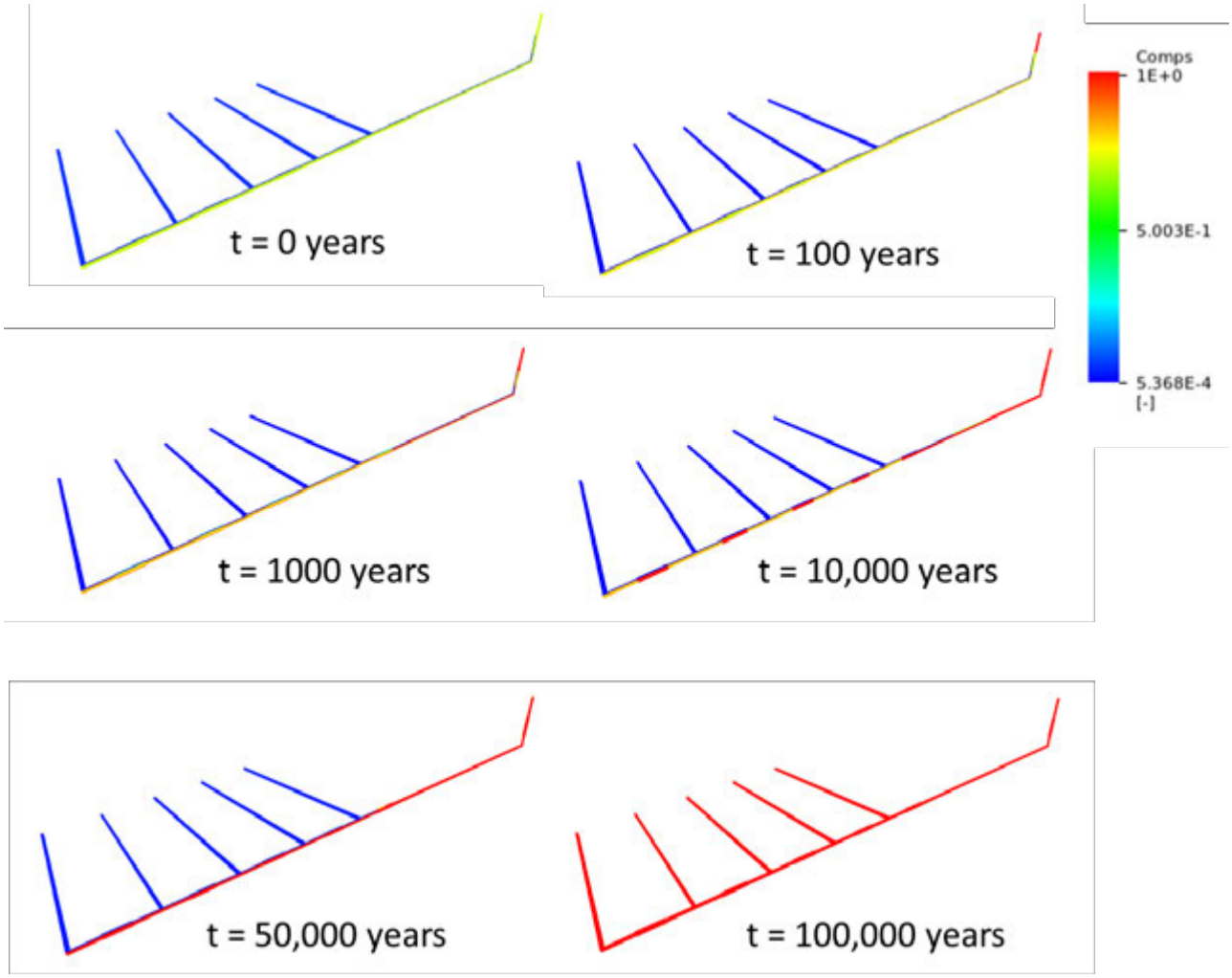

Figure 27 *Water saturation of the tunnel network including plugs and interfaces through time.*

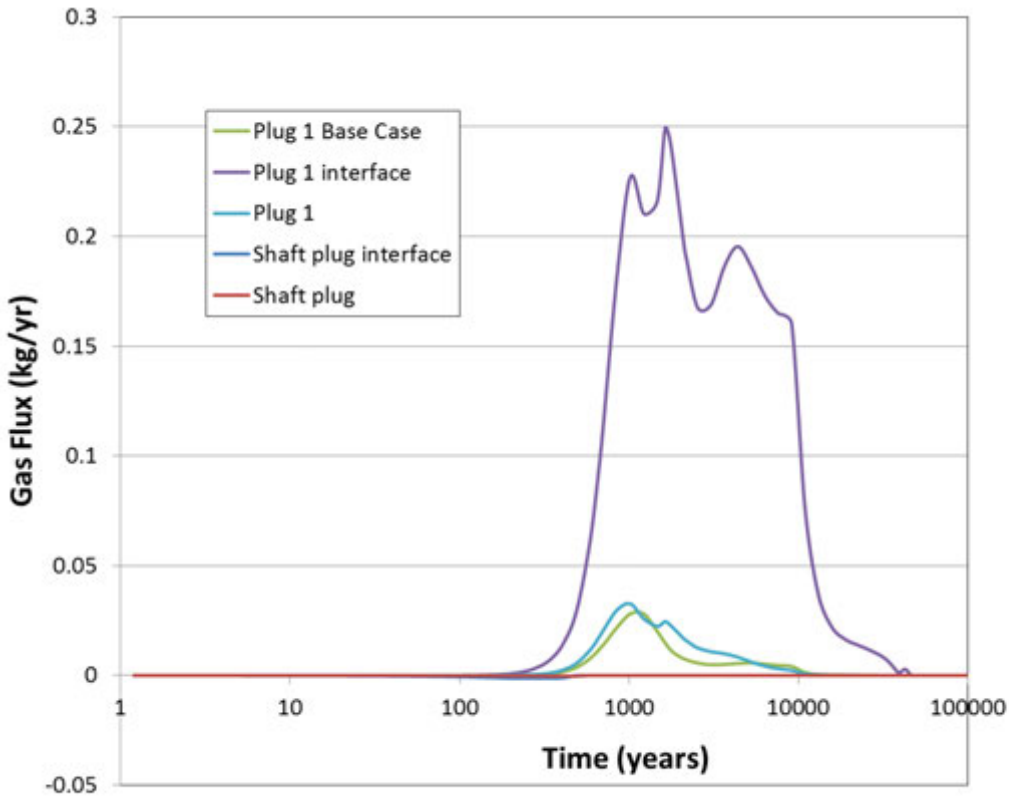

Figure 28 *Fluxes of gas through the bentonite and though the interface at plug 1 and the shaft plug. The flux through plug 1 from the base case is included for comparison.*

3.1.5 Evaluating the three benchmark studies

The benchmark studies were conducted in increasing size order, starting with a single HA cell, moving on to a single module with 100 cells connected to an access drift and ending with the whole repository model described in this report [2,3]. In order to construct the smaller models, assumptions had to be made about the effect of the remainder of the repository through implementation of boundary conditions. In this section, we compare the assumed boundary conditions to the equivalent pressures and saturations observed in the whole repository model.

3.1.5.1 BM1: Single HA cell

In the single HA cell model, the boundary conditions were supplied in terms of pressures and water saturation in the access drift close to the HA cell plug (see Annex).

The boundary conditions used for both gas and water pressure underestimate the pressures that have been calculated in the whole repository model by up to a factor of 2 (Figure 28). This will have led to pressures in the HA cell being too low resulting in lower gas dissolution.

The boundary conditions for water saturation are also significantly different from the conditions in the access drift in the whole repository model. The boundary conditions show an early decrease in saturation followed by a steady increase, whereas the model shows that resaturation of the backfill is faster at the start but then stops and reverses due to the gas production (Figure 29).

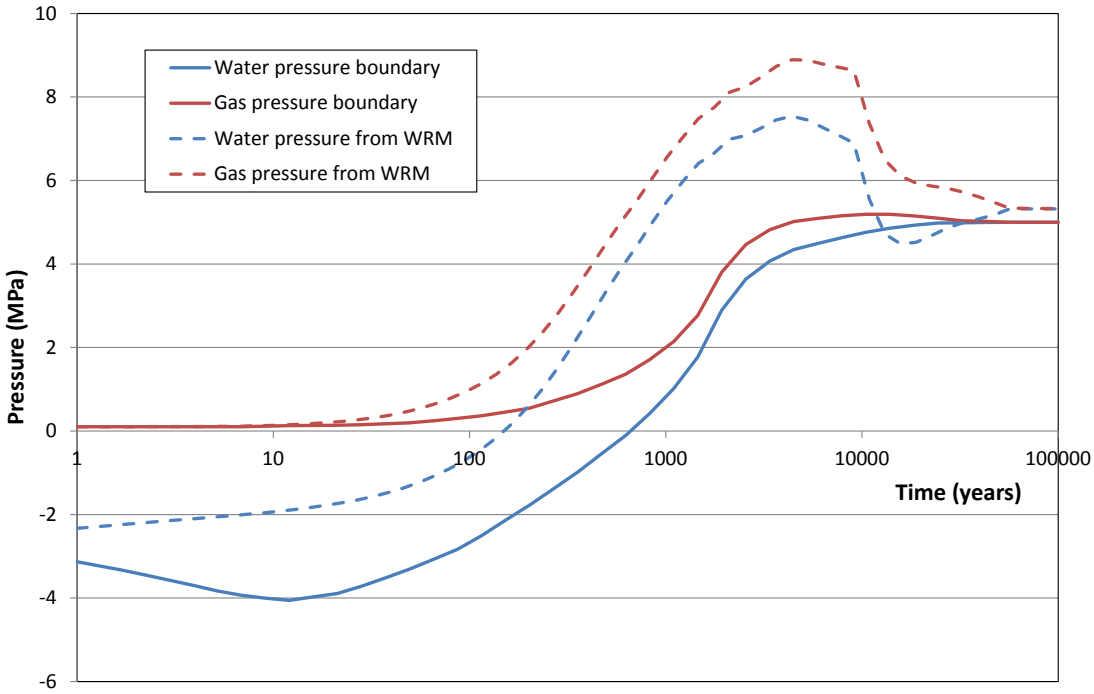

Figure 29 *Comparison of the water and gas pressure boundary conditions supplied for the cell scale model (solid lines) with pressures in the access drift from the whole repository model (WRM, dotted lines).*

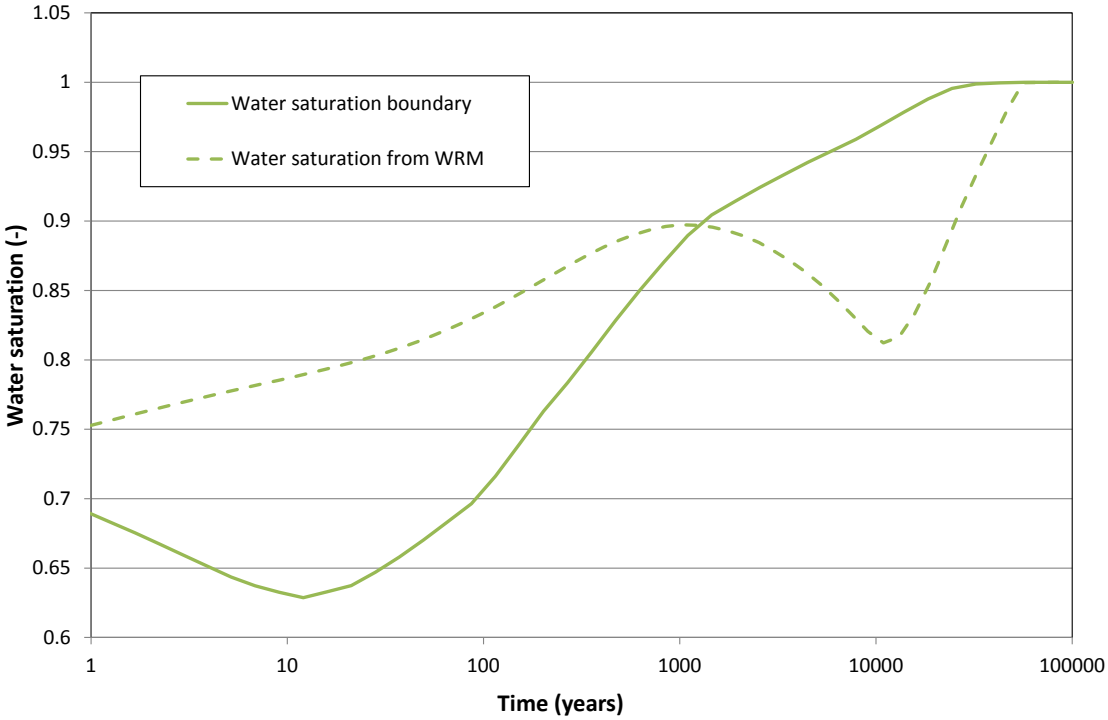

Figure 30 *Comparison of the water saturation boundary condition supplied for the cell scale model (solid line) and the saturation in the access drift supplied from the whole repository model (dotted line).*

3.1.5.2 BM2: Single module

For the single module benchmark (see Annex), the boundary conditions supplied were pressures and water saturation on the outside of the module plug (ie not inside the module). Two comparisons are made with the whole repository model, assuming that the single module modelled represents module 1 or module 2.

The gas and water pressure boundary conditions are a reasonable approximation of the pressures at Plug1 in the whole repository model (Figure 30). These pressures are significantly lower than those observed at plug 2. The difference is because the plug 1 pressures are in the main drift leading to the shaft and don't see much effect from the gas generation. The water saturations are a less good fit (Figure 31).

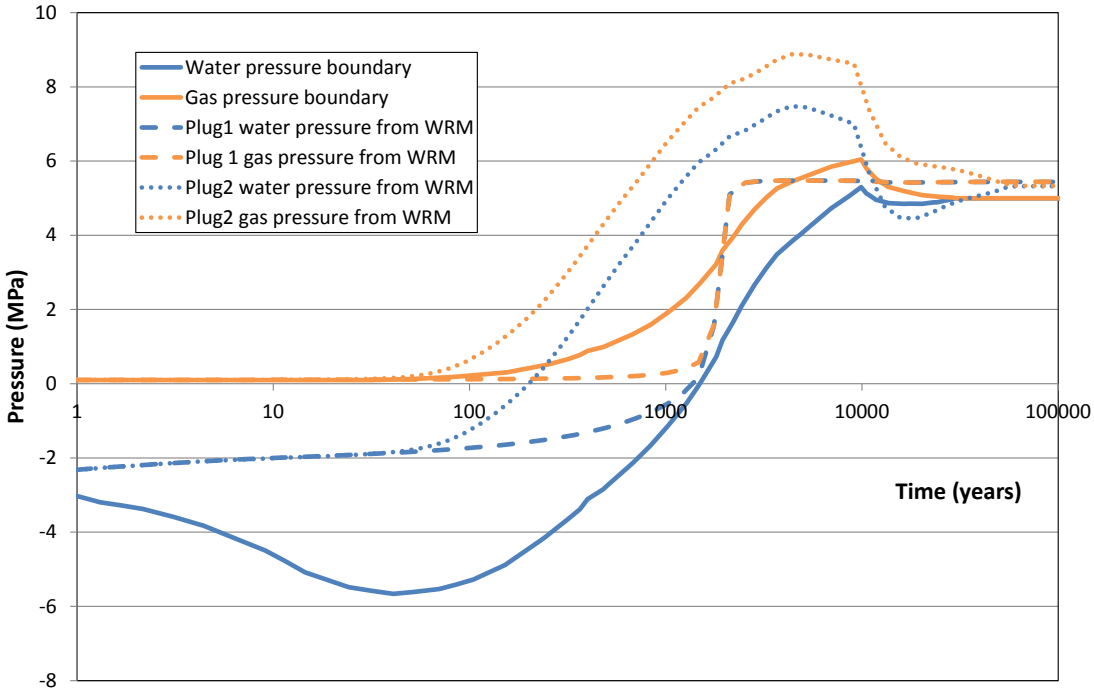

Figure 31 *Comparison of the water and gas pressure boundary conditions supplied for the module scale model and the equivalent pressures in the main drift taken from the whole repository model. Plug1 represents pressures in the main drift backfill on the shaft side of plug 1 and Plug2 represents pressures in the main drift backfill on the shaft side of plug 2.*

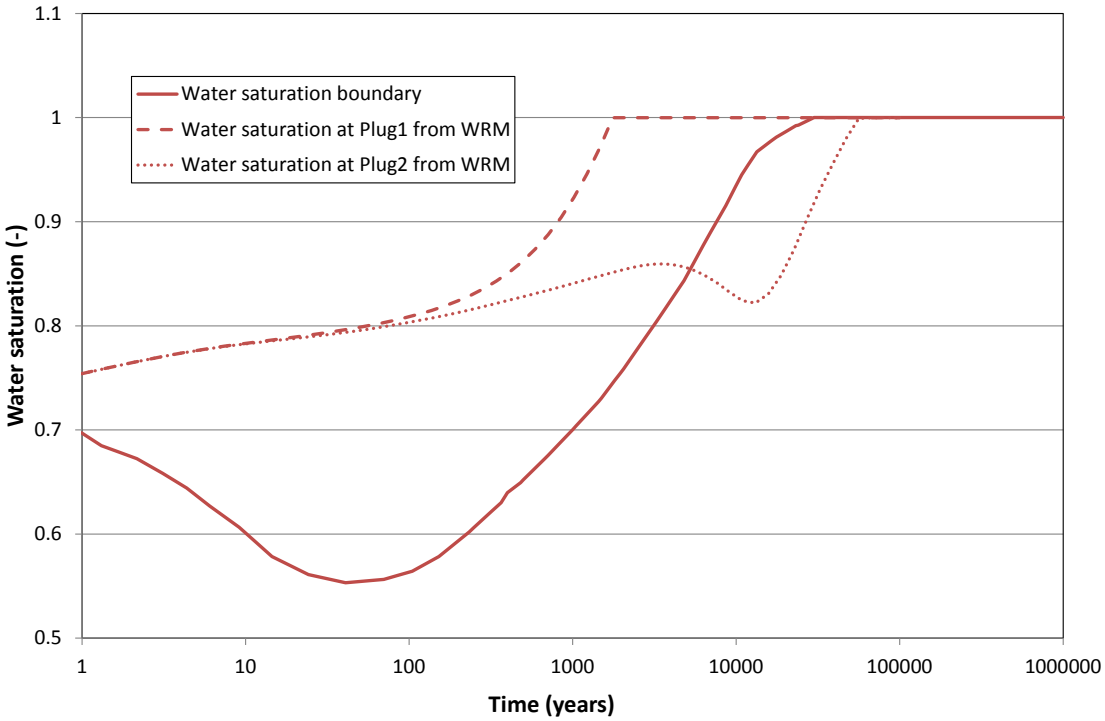

Figure 32 *Comparison of the water saturation boundary conditions in the main drift supplied for the module scale model and the equivalent water saturations taken from the whole repository model. Plug1 represents saturations in the main drift backfill on the shaft side of plug 1 and Plug2 represents saturations in the main drift backfill on the shaft side of plug 2.*

3.1.5.3 Comparison of three benchmark studies

All three benchmark studies gave results that were consistent with the process models, parameterisation and boundary conditions used. However, the boundary conditions were not consistent across the scales, which highlights the importance of representing the whole system to understand the behaviour at the smaller scale even in such a low permeability system.

For the single HA cell, the boundary conditions had a strong control on the results of the model, yet the boundaries underestimated the water pressure increase in the access drift and use a very different water saturation profile relative to the larger scale cases. The results from the HA cell model are therefore not consistent with the whole repository results because of the discrepancy in the boundary conditions compared with the modelled conditions.

The boundary conditions for the single module benchmark had much less a control on the results of this model as the highly efficient plugs dominate the behaviour of the system. Although the boundary conditions used are not consistent with the results from the whole repository model, the results from the two models are reasonably similar.

3.1.6 Discussion and Conclusions

3.1.6.1 Lessons Learnt

- Using QPAC, it is possible to construct stable and realistic modes at the whole repository scale whilst, at the same time, including details of the system at the millimetre scale. This was achieved by exploiting the flexibility of the code, allowing adaptations specific to the problem and through a pragmatic approach to capturing the key features of the model, alongside rigourous testing of the process model and grid stability.

- The two most important features of the model which enabled such a representation of the system were non-conformant grids, in which the grid becomes coarser with distance from detailed parts of the model, and averaging over features that are repeated many times in the repository, in this case, the HA cells. Both of these features considerably reduce the number of compartments required to represent the repository and hence reduce the computational overhead in running the model.

- The work illustrates, for this disposal system, the importance of modelling the system as a whole rather than as discrete units in separate models. The difference in results across scales is due to the boundary conditions imposed on the smaller scale models, which are derived from another model. Ensuring consistency between the conceptual model and parameterisation across scales is necessary to draw accurate conclusions at any given spatial scale.

- The models have been designed to represent ANDRA's disposal concept in which the seals are intended to prevent free gas migration to the shaft (which may provide a less robust barrier than the natural host rock and hence permit more rapid transport of radioactive gas to the surface), and ensure the dominant transport of gas away from the repository is as a dissolved phase in the host rock. We have demonstrated that, for the model parameterisation used, very nearly all of the gas generated within the repository dissolves in water in the host rock with very little advection of free gas outside the main disposal area. The main drift plugs are very effective in sealing the system, but if they were to fail or work less effectively, there would be significantly more advection of gas towards the shaft. The results of the models are also sensitive to the presence or absence of interfaces and whether the plugs are surrounded by an EDZ which can act as a transport pathway.

3.1.6.2 Issues for further consideration

- Experimentally, interfaces between clay and another material have been shown to be preferential pathways for gas migration [5]. Whilst interfaces have been included in a number of the benchmark models, they have been represented as voids initially filled with air and with very low suctions. In reality, the interfaces will initially be open voids but will close with time as clays swell into the void. The time dependent behaviour of the voids needs to be better characterised for a more accurate depiction in the model. Once the voids are closed, gas migration along the interface is likely to be via dilatant flow.

- Experimental work in the FORGE programme [6] has demonstrated that gas flow through bentonite and clay host rock is likely to occur by dilatant flow rather than two-phase flow – such a dilatant flow mechanism is not specified in the benchmark definition. From the perspective of the safety performance of such a facility it may be necessary to determine whether dilatant flow could compromise the safety functions required of the bentonite seals, and hence impact the potential performance of a facility as a whole.

- While the general phenomonology of dilatant flow mechanisms are reasonably well-understood, there is considerable uncertainty in the detailed process models for the hydro-mechanical properties of bentonite and natural argillites required for making predictions. Providing an high level of confidence in these non-linear flow mechanisms, such that they can be readily included in modelling studies, is likely to require substantial specialist experimental and supporting work at a variety of spatial scales.

- Representing the physics of dilatant flow is likely to require full hydro-mechanical coupling, which at the scale of a whole repository model is probably impractical. However, using the general understanding of dilatant flow processes, abstracted physical models could be developed to represent dilatant flow in a large model in a simplified sense. Such an approach could provide an initial assessment of whether dilatant flow is a process that needs to be considered more thoroughly, or whether current models capture the major characteristics of gas flow in a repository sufficiently well. Such a simplified process model was considered in the first benchmark [2], but was not taken forward due to a lack of supporting data.

- Therefore, in the short term, it may be appropriate to investigate the likely consquences of such process uncertainty, in order to understand the importance of explict representation of such processes. Given the flexibility of the benchmarking models developed in this work package, these existing models could be readily adapted to support such an investigation.The outcomes from such an investigation could then be used to inform future experimental work.

- As specified for the benchmark, gas generation in the whole repository model is a function of time and is independent of the condiitons in the repository. Coupling gas generation to saturation and temperatures in the repository could provide a more realistic source term for gas migration, as was demonstrated by other whole-repository modelling conducted by NDA for FORGE [4], also using QPAC.

- The modelling has shown the importance of the multi-scale approach, however including small scale features in large models is computationally expensive and especially challenging when using a single-threaded code such as QPAC. The work presented here has demonstrated that such model can be practical when run on a single core using a desktop PC. Extending the QPAC code to include parallel processing would enable more detailed models both in terms of discretisation and non-linear processes, and is a realistic prospect for future development.

3.1.7 References

1 Bond AE. and Benbow SJ. (2009). QPAC Multi-Phase Flow Module Functional Specification and Architectural Design. Quintessa Report QRS-3000C-4 v1.0.

2 FORGE (2013). Deliverable D1.6 Final report on benchmark studies on repository-scale numerical simulations of gas migration. Part 1 : cell scale benchmark

3 FORGE (2013). Deliverable D1.6 Final report on benchmark studies on repository-scale numerical simulations of gas migration. Part 2 : module scale benchmark

4 Towler GHT and AE Bond. (2011) Investigation of Gas generation and Resaturation Issues: Input to EC FORGE Project. QRS-1378ZC-R2 Version 2.0. NDA Report.

5 Jacops E, Maes N, Maes T, Volckaert G and Weetjens E. (2013) Results and interpretation of gas-driven radionuclide transport in undisturbed and disturbed Boom Clay. FORGE Report. D4.17 – SCK – CEN ER-222.

6 Cuss RJ, Harrington JF, Noy DJ, Wikman, A and Sellin P. (2010) Large scale gas injection test (LASGIT) : Results from two gas injection tests. Clays in natural and engineered barriers for radioactive waste confinement. 4th International Meeting, March 2010, Nantes, France.

3.2 SCK-CEN contribution

No contribution

3.3 Andra contribution

3.3.1 Introduction

This report gives a view of the work done by Andra in the framework of the "repository scale" benchmark of package WP1.2 of the FORGE project. The work done covers only the reference case with two different conceptual models.

This report first describes the code used and the slight deviations from the benchmark specifications, then the main results of the reference calculation are presented and commented.

3.3.2 Model Implementation

3.3.2.1 Code and Formulation

Numerical simulations rely on TOUGH2, a general-purpose numerical simulation program for multi-phase fluid and heat flow in porous and fractured media. Tough2 was developed at the Earth Sciences Division of Lawrence Berkeley National Laboratory (LBNL).

Simulations have been performed using Tough2-MP, a massively parallel (MP) version of the Tough2 code, designed for computationally efficient parallel simulation of isothermal and non-isothermal flows of multi-component, multiphase fluids in one, two, and three-dimensional porous and fractured media.

Tough2-MP features several fluid property modules [EOS (Equation Of State) modules].

In the framework of this benchmark, numerical simulations are performed using EOS5 module (water, hydrogen).

TOUGH2(-MP) solves mass and energy balance equations that describe fluid and heat flow in general multiphase, multicomponent systems. Fluid advection is described with a multiphase extension of Darcy's law; in addition there is diffusive mass transport in all phases.

The description of thermodynamic conditions is based on the assumption of local equilibrium for all phases. Fluid and material/formation parameters can be arbitrary nonlinear functions of the primary thermodynamic variables.

One of the specificities of TOUGH2(-MP) code is that the mathematical formulation is changing from saturated state to unsaturated state, mainly, the primary variables are not the same in the two formulations. For EOS5 module (water, hydrogen), primary variables are as follows:

- single-phase conditions: pressure, air mass fraction, temperature
- two-phase conditions: gas phase pressure, gas saturation, temperature

For numerical simulation the continuous space and time variables must be discretized. InTOUGH2, space discretization is made directly from the integral form of the basic conservation equations, without converting them into partial differential equations. This "integral finite difference" method (IFDM) avoids any reference to a global system of coordinates, and thus offers the advantage of being applicable to regular or irregular discretizations in one, two, and three dimensions.

Time is discretized fully implicitly as a first-order backward finite difference. This together with 100 % upstream weighting of flux terms at interfaces is necessary to avoid impractical time step limitations in flow problems involving phase (dis-)appearances.

The discretization results in a set of strongly coupled nonlinear algebraic equations, with the time-dependent primary thermodynamic variables of all grid blocks as unknowns. These equations are cast in residual form, i.e., {residual} ≡ {left-hand side} - {right-hand side} = 0, and are solved simultaneously, using

Newton-Raphson iteration. Time steps can be automatically adjusted (increased or reduced) during a simulation run, depending on the convergence rate of the iteration process. Automatic time step adjustment is essential for an efficient solution of multiphase flow problems, where intrinsic time scales for significant changes in the flow system may vary by many orders of magnitude during a simulation run. Different methods are available to solve the linear equations arising at each iteration step, including preconditioned conjugate gradient solvers, as well as sparse direct matrix methods. While direct methods are more predictable and less problem-dependent in their performance, it is only through the application of iterative conjugate gradient methods that solutions for large grid systems (10,000 blocks or more) and three-dimensional problems can be accomplished.

Further description and more details about Tough2/Tough2-MP codes are available from the Tough2 Homepage on the web, at http://esd.lbl.gov/TOUGH2, and from the Tough2-MP Homepage on the web at http://tough2.com.

3.3.2.2 Benchmark Implementation

The mathematical model is the same as described in the benchmark specifications, except for the following processes:

Diffusion terms:

In Tough2/Tough2-MP, diffusive flux of component κ (water or hydrogen for EOS5 module) in fluid phase β (liquid or gas) is expressed as follows: $f_\beta^\kappa = -\phi\tau_0\tau_\beta\rho_\beta d_\beta^\kappa \nabla X_\beta^\kappa$.

where ϕ is porosity, $\tau_0\tau_\beta$ is the tortuosity which includes a porous medium dependent factor, τ_0 and a coefficient that depends on phase saturation S_β, $\tau_\beta = \tau_\beta(S_\beta)$, ρ_β is density, d_β^κ is the diffusion coefficient of component κ in bulk fluid phase β, and X_β^κ is the mass fraction of component κ in phase β.

Tortuosity effects have a porous medium-dependent part τ_0 and a saturation-dependent part $\tau_\beta(S_\beta)$, with S_β as the fluid phase β saturation. The following three alternative formulations are available in Tough2 / Tough2-MP:

- Relative permeability model: tortuosity will be taken as $\tau_0\tau_\beta = \tau_0 k_{r\beta}(S_\beta)$.
- Saturation model: s $\tau_0\tau_\beta = \tau_0 S_\beta$ will be used.
- Millington-Quirk model: $\tau_0\tau_\beta = \phi^{1/3} S_\beta^{10/3}$, with ϕ as the porosity. This model is used for the benchmark simulations.

Solubility of Hydrogen in water:

In Tough2/Tough2-MP, the solubility of hydrogen in liquid water is represented by Henry's law. Henry's coefficient Kh (expressed in Pa^{-1}) for hydrogen dissolution in water, is the ratio between dissolved hydrogen mass fraction and gaseous hydrogen partial pressure.

It is a linear function of temperature, varying from 1,697 10^{-10} Pa^{-1} at 0 °C to 1,379 10^{-10} Pa^{-1} at 25 °C.

For the 20°C temperature used in the numerical simulations, Kh is equal to 1,443 10^{-10} Pa^{-1}. This value is equivalent to a Henry's constant of 8,0 10^{-6} expressed in $mol.Pa^{-1}.m^{-3}$ (different from the 7.6 10^{-6} $mol.Pa^{-1}.m^{-3}$ mentioned in the benchmark description).

Specific storage coefficient:

Tough2/Tough2-MP codes do not use specific storage coefficient S_S as an input parameter, but pore compressibility. Relation between pore compressibility C, expressed in Pa^{-1}, and specific storage coefficient S_S expressed in m^{-1} as follows:

$$C = \frac{S_S}{\rho_w g \phi} - \beta_w$$

With: ρ_w liquid water density (kg/m³)

g magnitude of the gravitational acceleration vector (m/s²)

ϕ porosity (-)

β_w liquid water compressibility (Pa⁻¹)

3.3.2.3 Grid

For symmetry reasons, only the left part of the repository scale is meshed (Figure 2).

The main drift and its environment (EDZ, interfaces, plugs), the vertical shaft and the upper aquifer are explicitly represented.

The cells, the drifts, the shaft and their environment (interfaces, EDZ) are represented with square cross sections

This allows using a regular, structured mesh

For each module of the repository scale geometric domain (see Figure 2):

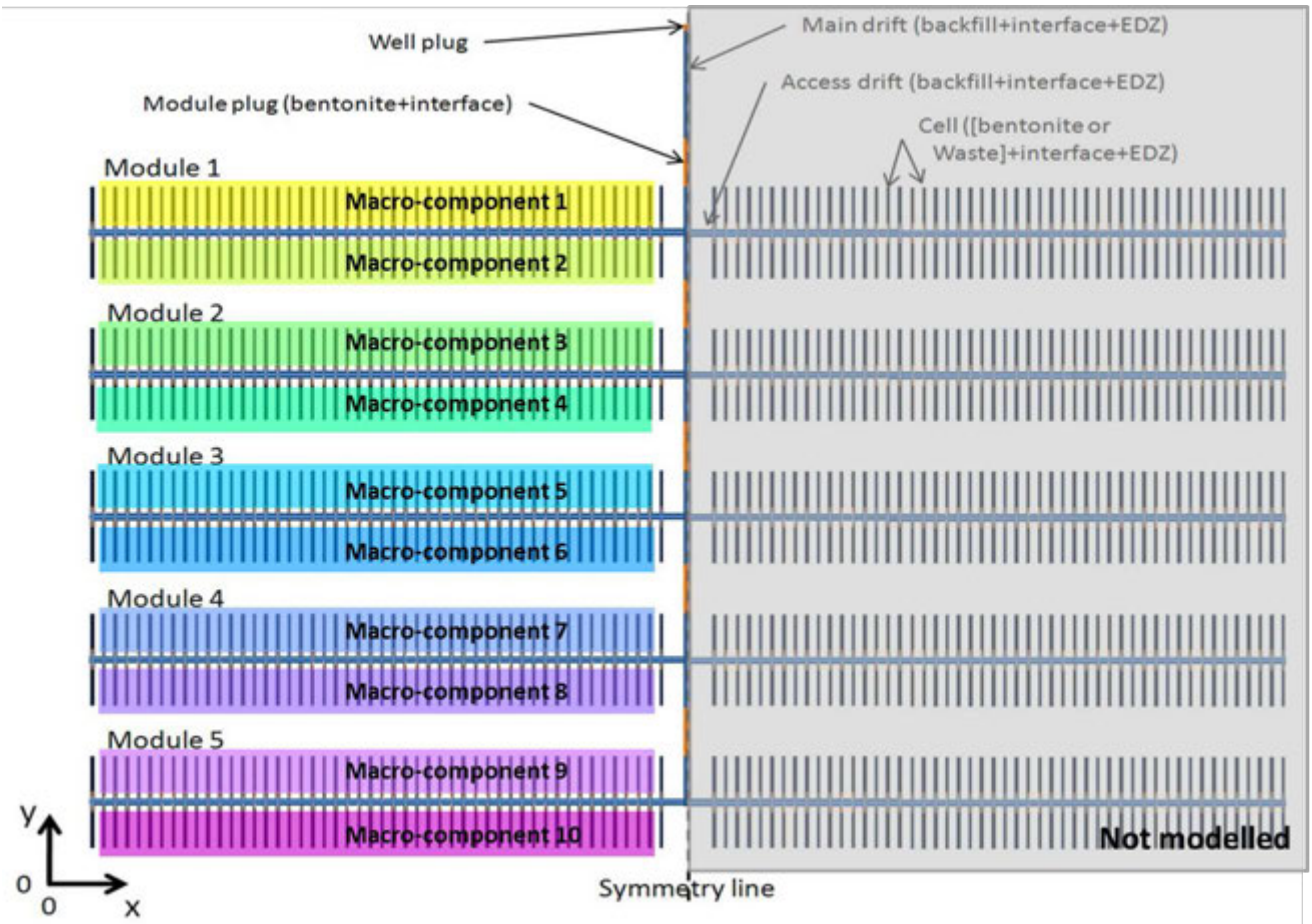

Figure 33: Extension of the model, emplacement and extension of the macro-components used in the mesh

- the access drift is explicitly represented, with all heads of the {N=50} cells. on both upstream and downstream sides of the access drift:
- On each side of the access drift, the first and the last cells (which are the closest and the farthest to the main drift) and their environment are explicitly represented;
- On each side of the access drift, the other (inner) {N-2} cells and their environment are merged to a single macro-component. In this macrocomponent, every material (waste package, interface, plug, EDZ) remains explicitly represented (no merging of materials). In this macrocomponent, the following quantities (geometric and input data) are multiplied by {N-2}: volumes of elements, areas of connections between elements, gas production rate defined for one cell. This macrocomponent is connected to every {N-2} head part of the cell along the access drift.

This upscaling technique leads to a corresponding geometrical mesh of 1,300,000 cells

3.3.2.4 Boundary Conditions and Sources

Boundary conditions can be of two basic types.

Dirichlet conditions prescribe thermodynamic conditions, such as pressure, saturation, temperature, on the boundary. Dirichlet conditions can be implemented by assigning very large volumes (e.g., $V = 10^{50}$ m^3) to grid blocks adjacent to the boundary, so that their thermodynamic conditions do not change at all from fluid or heat exchange with finite-size blocks in the flow domain. In addition, a small value (such as $D = 10^{-9}$ m) should be specified for the nodal distance of such blocks, so that boundary conditions are in fact maintained in close proximity to the surface where they are desired, and not at some distance from it.

In the original version of Tough2-MP 2.0, only time dependent pressure boundary conditions are available. Numerical developments have been performed in the Fortran source code of Tough2-MP to provide additional capabilities for a time-dependent gas saturation boundary conditions (gas saturation is one of the primary variables for EO55 module).

Attention must be paid to assume, at every time, coherence between boundary gas saturation, boundary water pressure, capillary pressure in access drift material, and realistic gas pressure.

Neumann conditions prescribe fluxes of mass or heat crossing boundary surfaces. A special case of Neumann boundary conditions is “no flux,” which in the integral finite difference framework is handled with simplicity itself, namely, by not specifying any flow connections across the boundary. More general flux conditions are prescribed by introducing sinks or sources of appropriate strength into the elements adjacent to the boundary. Using this technique, time-dependent hydrogen production term is then applied directly in the interface volumes which are besides the external surfaces of the different waste packages

3.3.2.5 Initial Conditions

Flow systems are initialized by assigning a complete set of primary thermodynamic variables to all grid blocks into which the flow domain is discretized. During the initialization of a TOUGH2-MP run, all grid blocks are first assigned to default thermodynamic conditions. The defaults can then be overwritten for selected domains by assigning domain-specific conditions in specific data blocks.
The primary variables used depend on the fluid phase composition. During phase change primary variables will be automatically switched from one set to another. In multiphase flow systems, therefore, different grid blocks will in general have different sets of primary variables, and must be initialized accordingly.

3.3.2.6 Deviations from the specification

The different conceptual and physical processes and assumptions are in accordance with the benchmark specifications, and/or the original version of Tough2-MP, except for the following aspects:

Physical parameters:

Some physical parameters and fluid properties are internally computed and/or tabulated in Tough2/Tough2-MP Fortran source code. They have not been replaced by the mathematical expressions presented in the benchmark description.

Water vapor pressure:

In standard EOS5 module of Tough2-MP, vapor pressure is equal to saturated vapor pressure of water. It is not expressed by Kelvin's equation. At a 20°C temperature, this vapor pressure is 2337 Pa.

Viscosity of the gas mixture:

Dynamic viscosity of hydrogen is both pressure and temperature dependent in Tough2/Tough2-MP. For the 20°C temperature used in the numerical simulations, values expressed in Pa.s are:

8,8 10^{-6} Pa.s when pressure is lower than 0,1 MPa

8,95 10^{-6} Pa.s at 10,0 MPa and 9,22 10^{-6} Pa.s at 200,0 MPa

Values at intermediate pressures are linearly interpolated.

The dynamic viscosity of hydrogen-vapor mixture is approximated as dynamic viscosity of hydrogen.

Outputs:

In the original version of Tough2-MP 2.0, mass flow rates from diffusion are not printed in the standard output file.

Developments have been performed in the Fortran source code of Tough2-MP to print the diffusive fluxes of each component (water, hydrogen) in both liquid and gas phase. These fluxes are necessary for computing, after the end of the simulation, the total rate of flow for each component

3.3.3 Base Case Results

This benchmark implies no artificial boundary conditions; the boundaries of the model are natural ones and the conditions imposed as well. Therefore, results are more realistic than for the previous benchmarks at smaller scales (cell scale and module scale).

- **Gas pressure**

Wherever in the repository, gas pressure is never higher than 8 Mpa, which is coherent with results of the module scale benchmark.

Something really important to notice is that gas pressure evolution is quite the same in each module (Figure 2), and that at cell scale the evolution is also quite similar. This derives from the fact that the main drift plugs are efficient concerning gas migration. More precisely, the plugs in between two adjacent modules limits drastically the gas flow in-between these modules, and the plug downstream module 1 is limiting the gas flow toward the well.

More than this, time for maximum gas pressure is also very similar all around the module and in each cell. The main drift plugs are efficient enough to impose an homogenized gas pressure inside all modules. The maximum of this value is somehow linked to the plugs « gas entry pressure ».

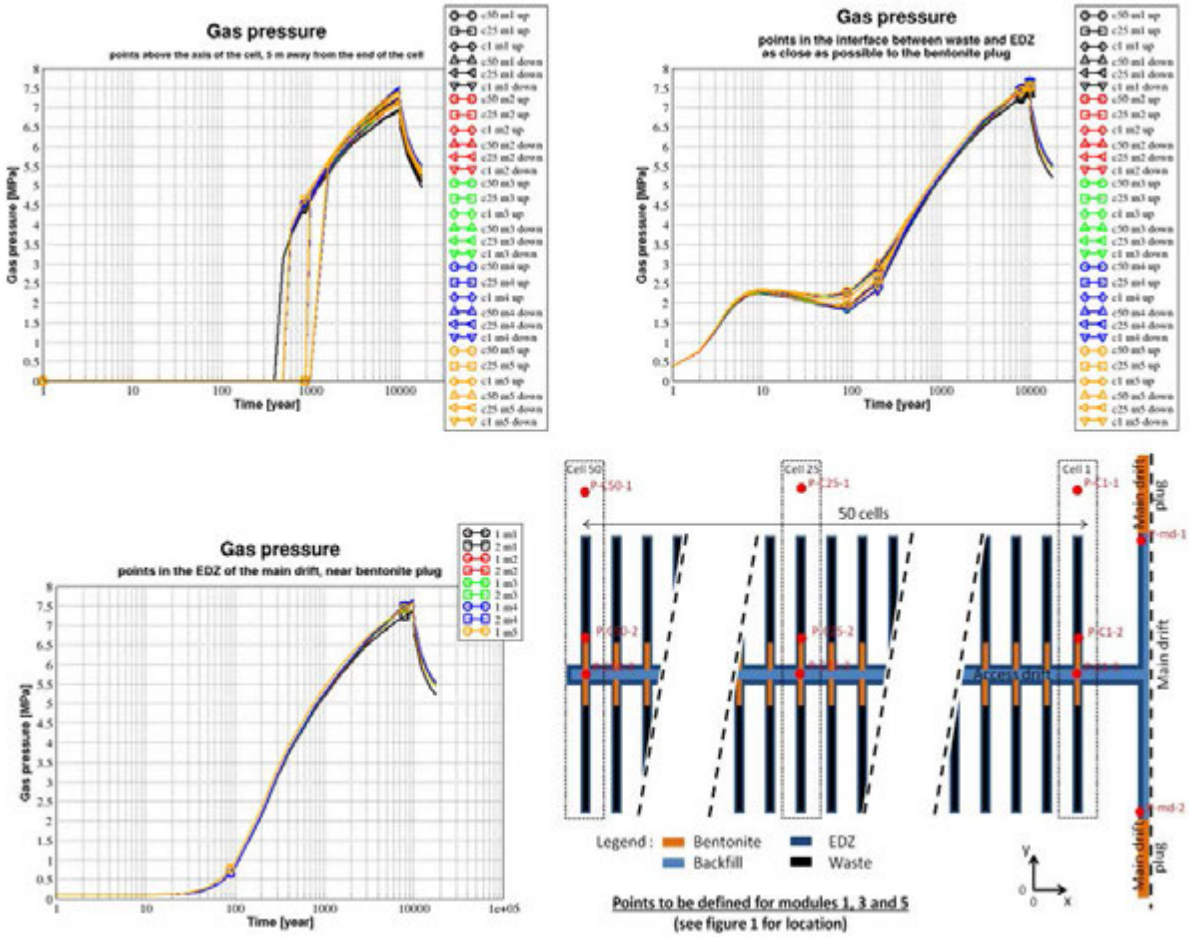

Figure 34 : gas pressures at different points in the modules of the repository

Once in the main drift downward module 1, there is no more gas production term and the free gas is dissolving rapidly during its way toward the access drift (Figure 3). Just downward the last module plug the gas pressure maximum is are und 5 MPA but arriving at the well the maximum pressure is lower than 1 Mpa.

As gas pressure is equal to zero at all times, this means that no free gas phase is passing through the well plug and arriving in the upper aquifer (Figure 3). The access drift plug, in coordination with the ones separating each module, is efficient enough to avoid gas flow toward the upper aquifer.

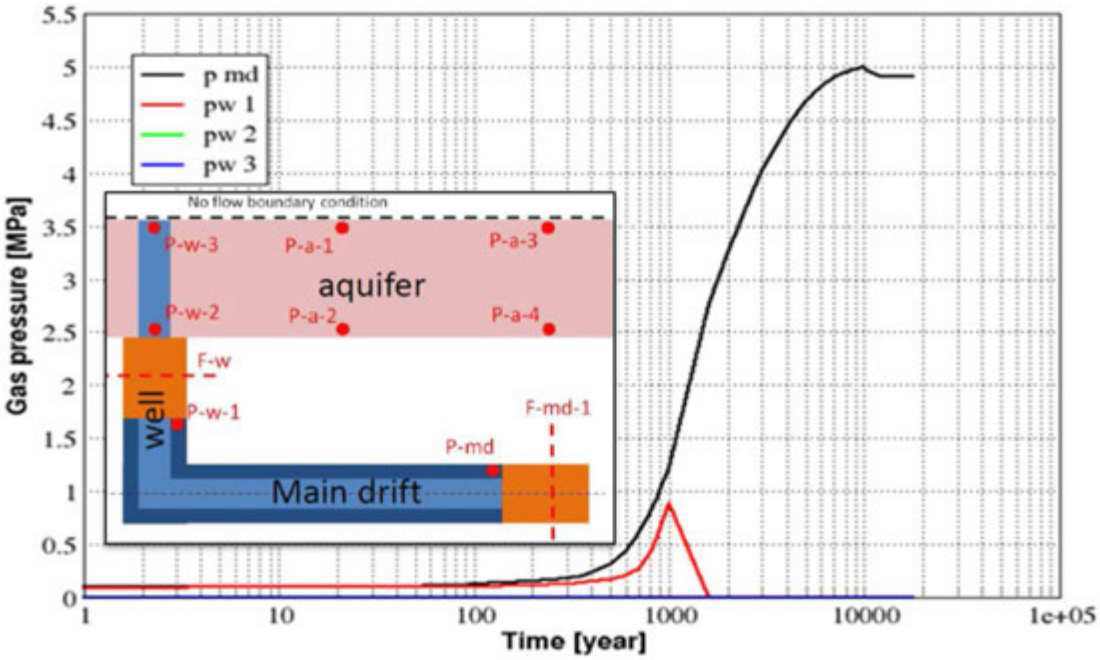

Figure 35 : gas pressures near the access drift and in the upper aquifer

- **Hydrogène mass flow**
  - **In the celles**

Hydrogen mass flow out of a representative cell (cell in the middle of the module) is quite similar for each module, except for module 5, the farthest from the shaft (Figure 4).

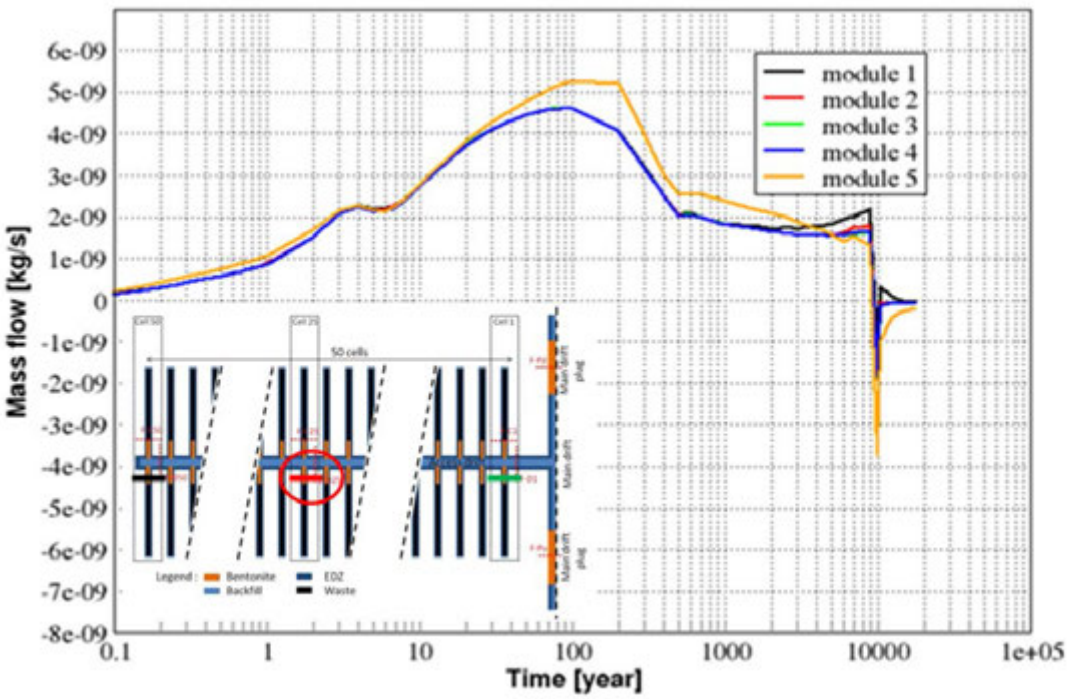

Figure 36 : Hydrogen mass flow out of the central cell for each module

This, once again, shows that the main drift plugs are quite efficient and that all modules are reacting more or less the same.

- **In the Access drift**

In the drift of a module, the hydrogen flows are also more or less the same in each module (Figure 36). Especially the behavior at the end of each module is similar and corresponds to the one already described for the module scale benchmark: part of the free gas flow is moving toward the end of the module (negative mass flux) to dissolve in the argillites rock instead of moving toward the main drift. This is representative of a high level of efficiency of the module plug that is unable to let all the free gas passes through it.

Never the less, near the main drift, the behavior is significantly different depending of the position of the module in the repository: module 5 (far away from the access) has the lowest free gas flow rate, the 3 modules in the "center" of the repository behaves the same way, and module 1 (the nearest from the access) shows a higher free gas mass flux.

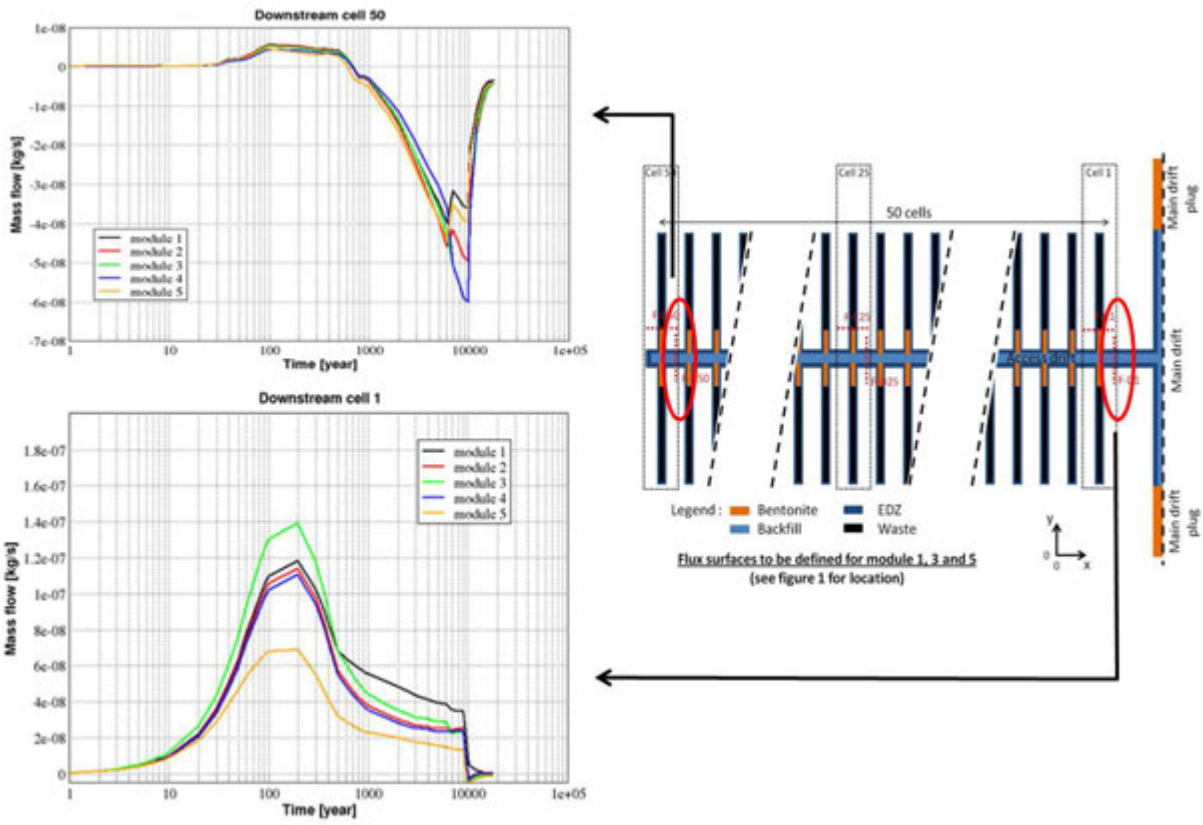

Figure 37 : hydrogen mass flow in the module drift

- **In the module plugs**

Hydrogen mass flow in-between modules are quite small due to the fact that (i) each module has the same geometry and (ii) the gas source term is the same in each module cell. Each module is producing the same amount of hydrogen at the same time, so the gas pressure is equilibrate in-between modules. This is not true for module 1 which has no downstream counterpart: gas flux across module 1 plug is one order of magnitude higher than across any other module plugs. In the detail, this influence is already visible for module 2 plug but in a very less extent. For module plug 5, the same type of behavior as for the end of the module is visible: a negative flux showing that part of the free gas moving out of module 4 (at least) is directed toward the argilites and not toward the access.

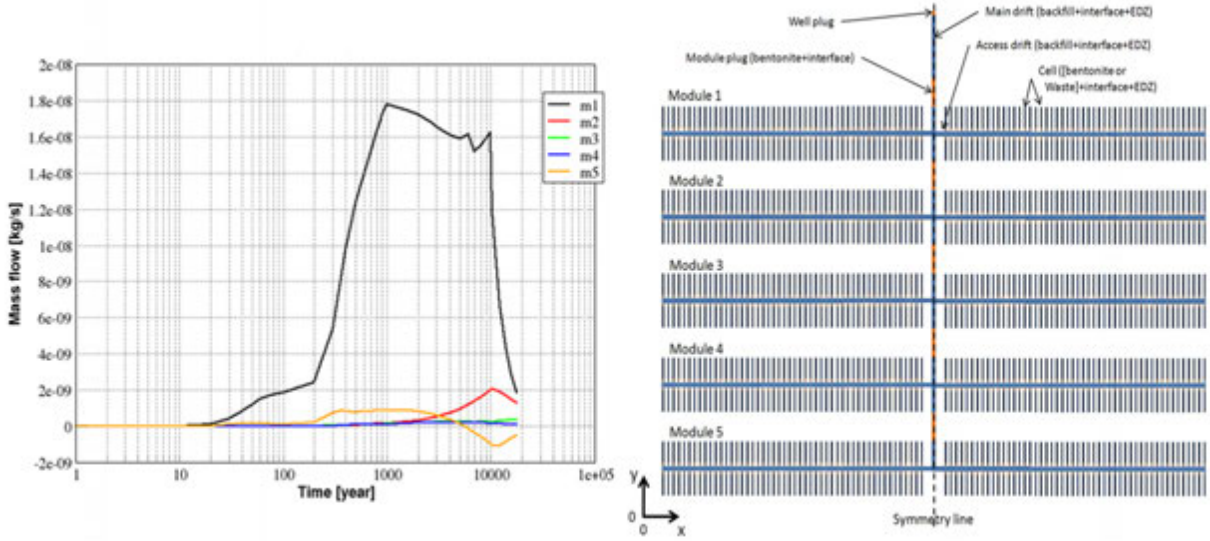

Figure 38 : hydrogen mass flux across module plugs (positive values toward the access)

3.3.4 Discussion and Conclusions

This benchmark at a representative repository scale is showing that numerical simulation is feasible at this scale, having a good representation o at cell scale as well as at the repository scale.

However, to achieve this result application of an upscaling technique consisting in merging several similar components at different locations in a single macro-component was needed. This technic proves to be very efficient and somehow easy to apply when repetitive geometric schemes are involved in a global pattern.

More than this, to achieve results over several hundreds of thousands of years, in a reasonable time, high performance computing using massively parallel clusters was needed. About 100 cores were used for this simulation at the repository scale. As clusters of several 1 000 of cores are now available, hydraulic-gas transient in even more complex structure (more realistic, complying with real repository constraints) could be simulated.

Coming to the results, in terms of gas pressure and hydrogen flows, they are in a general way similar for each module and similar to the results obtained at the module scale.

The main results to retain are that:

- There is very little gas transfer in the shaft environment: most of the hydrogen produced in the modules is staying inside the module and dissolves in the host rock. Dissolution and diffusion as dissolved species is the main transfer process for gas;
- Upper aquifer layer remains in saturated conditions: no free gas phase is passing the access drift plug;
- Gas pressure is never reaching values more than several Mpa over the natural hydrostatic pressure. In our simulations, this is mainly linked to the EDZ and interfaces gas entry pressure which is quite low and enables part of the gas to move along the plugs.
- Nether the less, the bentonite core of the plugs is efficient enough to reduce very significantly (in conjunction with the dissolution/diffusion processes) the free gas flow rate out of the modules and toward the access.

- Gaz pressure staying relatively low compared to retention curves in the argilites and the bentonites, the water desaturation in these two materials stays very low during the entire hydraulic transient. Most of the gas moving in these materials is present under dissolved form in the available water.

3.4 CEA contribution

No contribution

3.5 CNRS contribution

No contribution

3.6 IRSN contribution

No contribution

3.7 LEI contribution

No contribution

3.8 ENSI/IFSN contribution

No contribution

3.9 NWMO contribution

3.9.1 Introduction

Geofirma Engineering Ltd. conducted the repository-scale benchmark modelling on behalf of the Nuclear Waste Management Organization (NWMO) in Canada.

The repository scale domain is large and detailed. Consequently, the challenges of the model are incorporating small-scale details, such as the very thin interface between the cells or drifts and the host rock, in a model of a tractable size. Two modelling approaches were taken:

(1) Half-Domain Model: A 3D grid was developed, representing one-half of the model domain, assuming symmetry along the main drift and shaft. The grid was based on the grid developed for the module-scale. Figure 2 shows the model domain, with boundary conditions, cells and drifts.

(2) Main-Drift: A 3D grid representing the main drift and shaft (Figure 3). Input to the main drift from the modules was based on output from the module-scale model. This modelling approach has some circularity as the main drift boundary conditions in the module-scale model are dependent on the repository-scale model results, while the module source input in the repository-scale model are dependent on the results of the module-scale model. The circularity can be addressed by ensuring that the discrepancy between pressures used as module-scale boundary conditions and those pressures calculated using main-drift repository-scale model is minimized. The advantage of this approach is quick run times.

Note that the benchmark specification refers to the repository shaft as a well. Since the term shaft is more appropriate for a repository, shaft is used throughout this section.

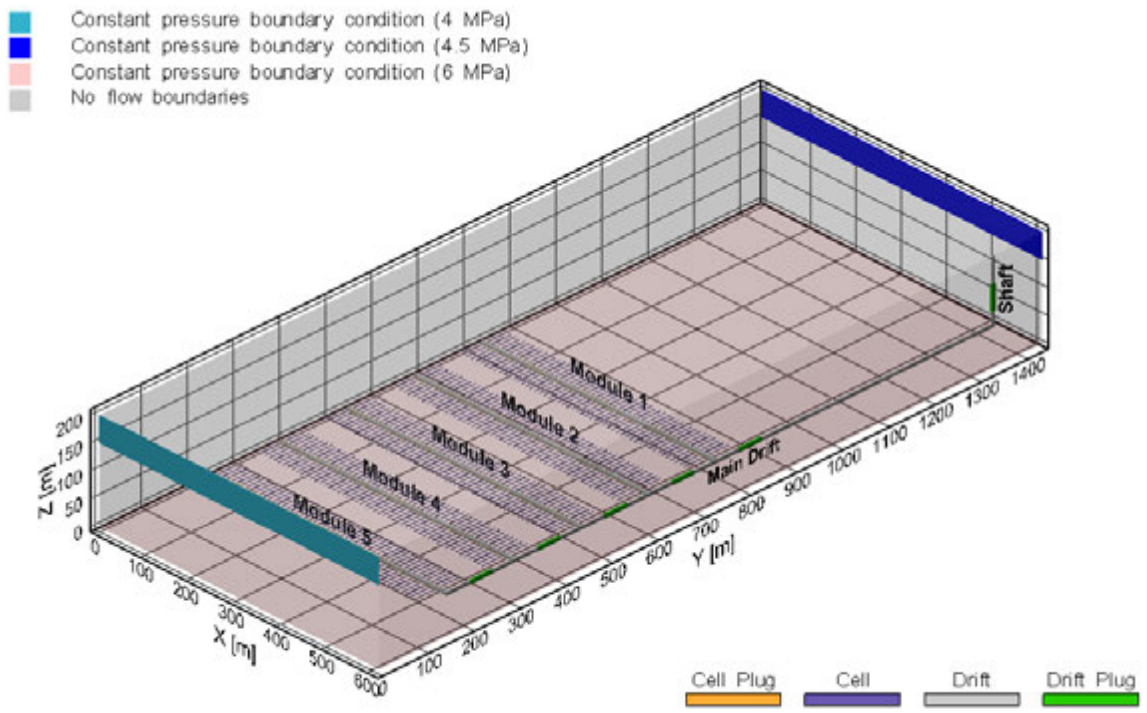

Figure 39: 3D model domain with boundary conditions, cells and drifts for Half-Domain model.

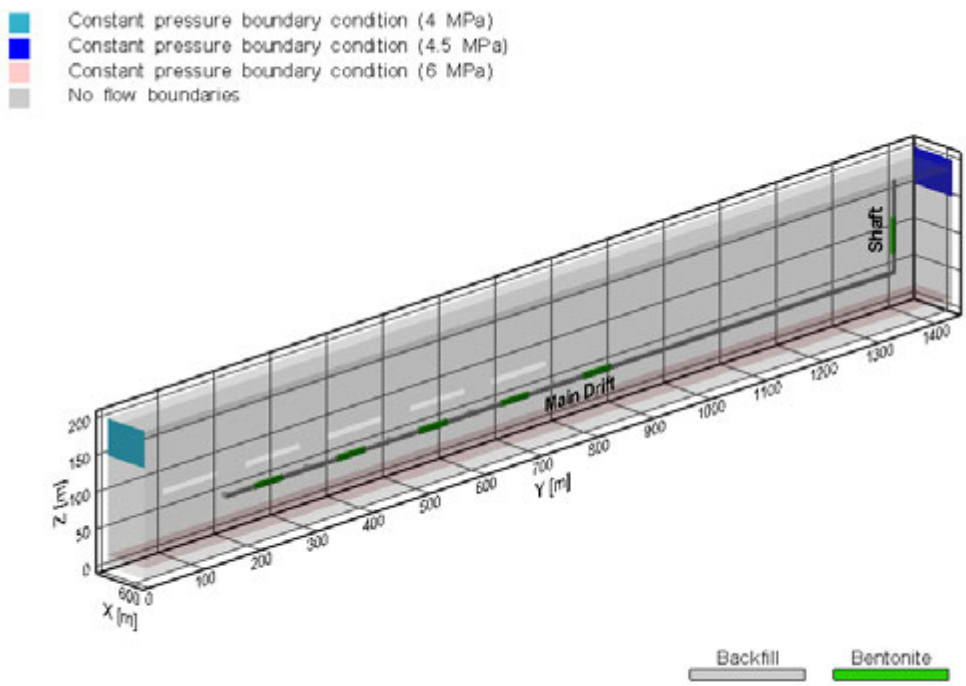

Figure 40: 3D model domain with boundary conditions, cells and drifts for Main-Drift model. Note white spaces represent location of modules.

3.9.2 Model Implementation

3.9.2.1 Code and Formulation

T2GGM version 3.1 (Suckling, 2012 [1]), a modified version of TOUGH2 v2.0 with optional gas generation model, was selected as the two-phase flow modelling code. The gas generation model (GGM) capabilities were turned off, and TOUGH2-MP was used for the half-domain model. TOUGH2 is a general-purpose numerical simulation program for multi-phase fluid and heat flow in porous and fractured media developed by Lawrence Berkeley National Laboratory (Pruess et al. 1999 [2]). The EOS3 equation of state module used in T2GGM simulates the transport of a single separate gas phase in water (note that T2GGM allows for specification of alternate gases to air, the EOS3 default). EOS3 also models the transport of dissolved gas in water by diffusion and advection. Dispersive processes are not modelled.

One minor modification was made to the T2GGM code to facilitate the repository-scale benchmark modelling studies: the option to use the Mualem relative gas permeability equation as defined in the benchmark. Previous cell-scale and module-scale modelling used the Luckner model, which is very similar to the Mualem model.

mView, developed by Geofirma Engineering, was used for pre- and post-processing.

3.9.2.2 Grid

<u>Half-Domain Model</u>

The greatest challenge in developing this grid was to obtain sufficient representation of the repository details, while maintaining a grid of tractable size. Similar problems were encountered in the module-scale model, which has a smaller domain with a similar level of detail. The repository-scale modelling builds on the work of the module-scale modelling:

(1) The code was switched to T2GGM-MP. Module-scale modelling used standard T2GGM.

(2) The module-scale discretization was coarsened, and then expanded to include the full repository domain.

Consequently, the grid uses the same simplifications employed in the module-scale models as discussed below:

(1) The cells were represented as rectangular in cross-section, with equivalent cross-sectional areas to the circular cells defined in the benchmark. Using rectangular-shaped cells allows for significantly fewer grid elements, producing an overall grid of tractable size.

(2) Interface materials were combined with adjacent materials to provide tractable discretization. The details of the interface combinations are as follows:

a) The interface between the cell containers and the EDZ was combined with the EDZ. The cell EDZ was divided into two components: (1) an inner EDZ which represents the combination of interface and EDZ, and (2) an outer EDZ which represents the EDZ alone. The inner EDZ of the cells was represented as a single element in the middle of the cell. Block volumes and areas were adjusted to represent the actual volumes and areas of the inner EDZ surrounding the waste. The benchmark specifies the waste containers as impermeable to gas and water. Figure 4 shows a detailed cross-section of the discretization of a cell.

b) The interface between the cell plug and the EDZ was combined with the EDZ, creating and inner and outer EDZ as above. Figure 5 shows a detailed cross-section of the discretization of the cell plug.

c) The interface between the drift backfill and the EDZ was combined with the backfill in a 0.5 m width block on the edges of the drift (both access and main drifts). Figure 6 shows a plan-view of the discretization of the access and main drifts.

d) The interface between the main drift plug and the host rock was combined with the bentonite plug, also shown in Figure 6.

(3) EDZ and the interface at the end of the access drift are ignored (the far end from the main drift). This omission is expected to be inconsequential, as gas and water are expected to flow towards the main drift.

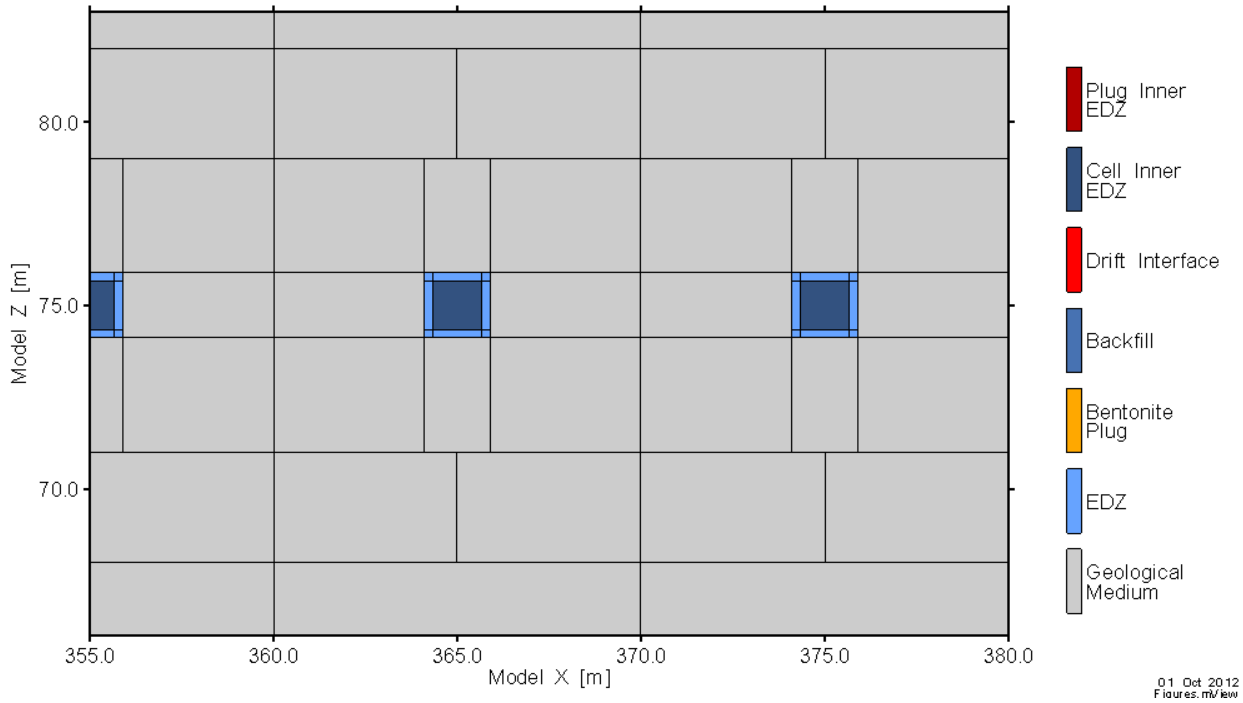

Figure 41: Grid discretization detail: cross-section of a cell. Note that cell areas and volumes for the inner cell EDZ have been corrected to remove the inactive waste containers, as described in the text.

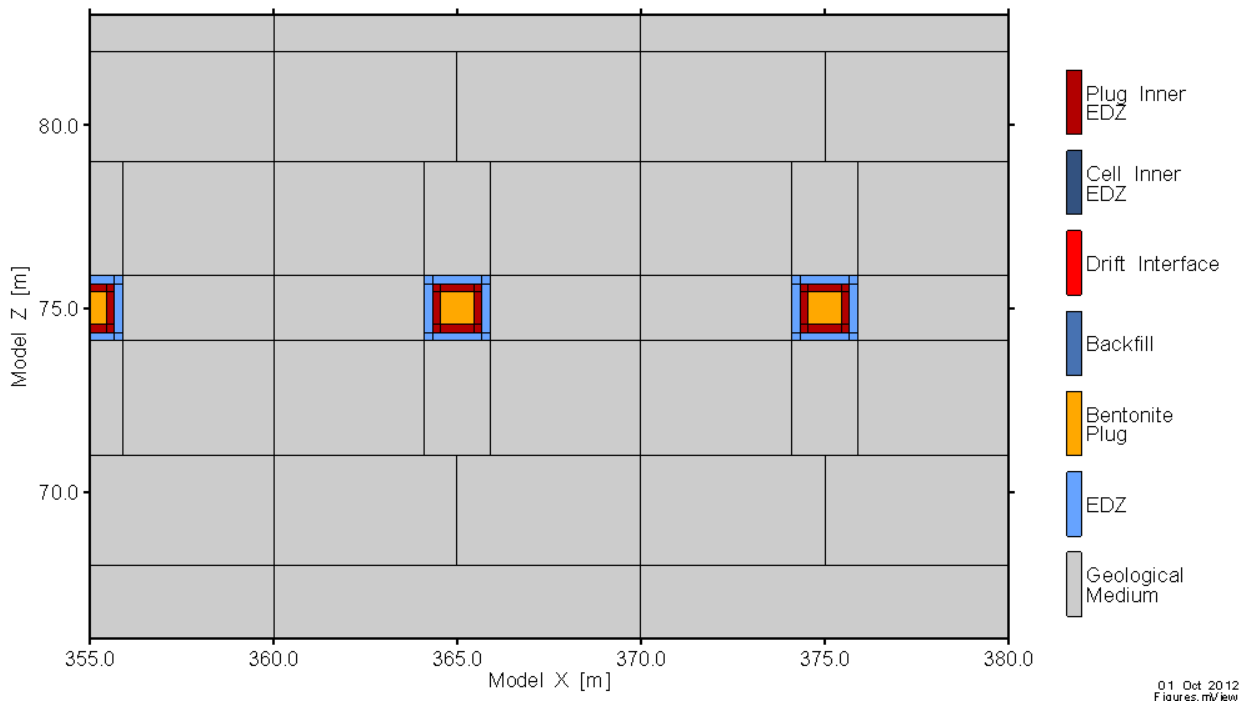

Figure 42: Grid discretization detail: cross-section of a cell plug.

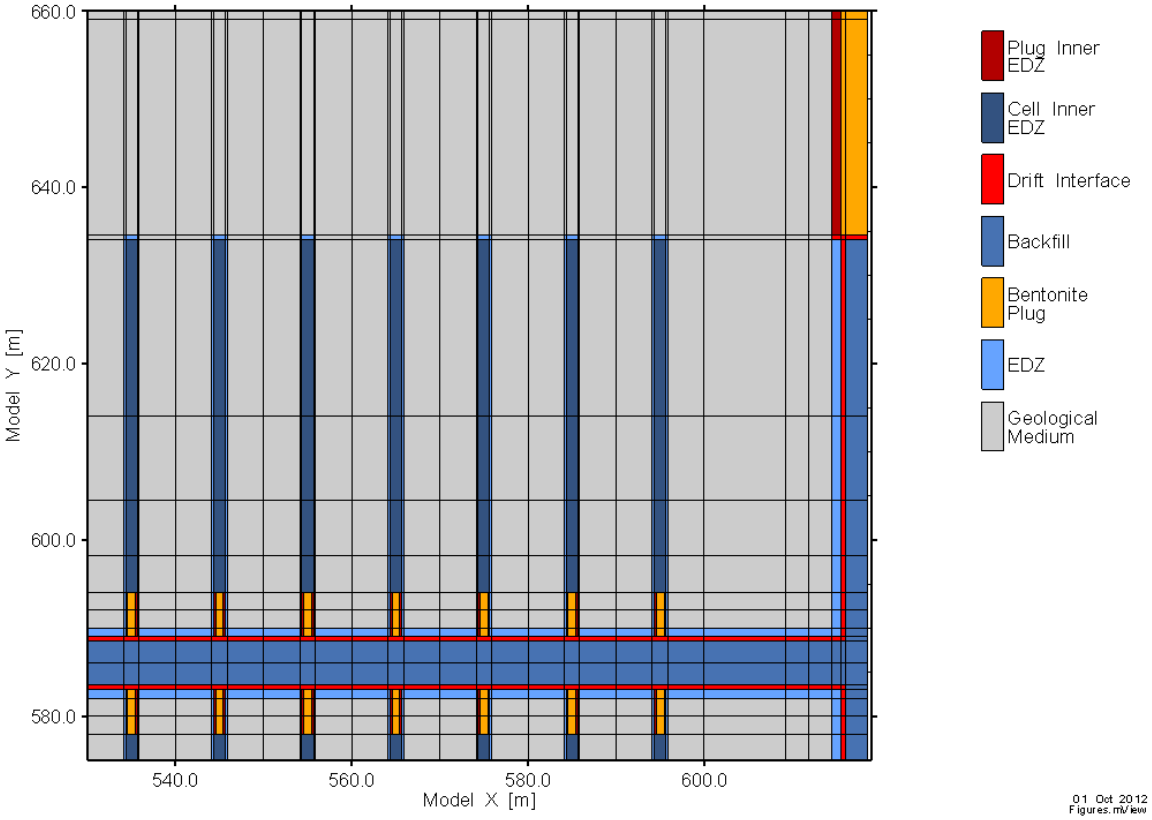

Figure 43: Grid discretization detail: plan view of the access and main drift.

The resulting grid had 212 400 nodes and 706 549 connections. This is still a very large grid for T2GGM-MP, with run times of approximately one week to reach 30 000 years, using 8 processors.

It should also be noted that the irregular grid of the final model does not strictly adhere to the TOUGH2 integral finite difference requirements; some nodal connections are not perpendicular to the connection area, resulting in shorter connection distances for these connections. The impact of these inaccuracies is expected to be small, and this has been confirmed at the cell-scale.

<u>Main Drift Model</u>

As the half-domain approach took some time to develop, debug and simulate, this simpler approach was developed. As an extension of the module-scale model, it contains the same simplification for interface upscaling as described for the half-domain model above. The cells are not explicitly modelled, with blocks within the module (at the edge of the model) removed from calculations. Gas and water input into the main drift (from the modules) is extracted from the module-scale model, with the assumption that the flow of gas into the main drift is the same for each module. As well, only positive flow (from the panel to the main drift) is considered. Small negative water flows (from the main drift to the panel) occur after 3000 years, and small negative gas flows occur after 10 000 years; these are ignored (i.e., gas or water input is set to zero). As these negative flows are very small relative to peak flow rates, the impact of their exclusion is expected to be minimal. The module-scale model was rerun once, with boundary conditions extracted from the first repository-scale simulation.

The final grid had 2442 nodes and 6733 connections. Run times were less than 10 minutes.

3.9.2.3 Boundary Conditions, Initial Conditions and Sources

For both the half-domain and main drift models, boundary and initial conditions are identical. A constant pressure and zero gas saturation boundary condition is specified on the bottom of the model (Z= 0 m), at

6 MPa. The top 50 m of the model (Z= 150 to 200 m) is an aquifer, with constant pressure and zero gas saturation boundary conditions specified at 4.5 MP at Y = 1437 m (the edge of the model closest to the shaft) and 4.0 MPa at Y = 0 m. Initial conditions in the host rock and EDZ are based on steady-state pressures for a fully water saturated simulation with no repository, resulting in pressures of approximately 5 MPa at the repository horizon, and fully water saturated. In repository features, initial pressure is atmospheric and water saturation is 5% in the interfaces and 70% in the drift backfill and bentonite plugs.

Since the aquifer boundary condition is applied over a depth of 50 m, the aquifer boundary condition includes hydrostatic pressures assuming that the bottom of the aquifer has the pressure values of 4.0 (at Y = 0 m) and 4.5 MPa (at Y = 1437 m) defined in the benchmark. Initially, the aquifer boundary condition of 4 and 4.5 MPa was defined at the top of the aquifer. This difference resulted in a different direction of geosphere flows: when the boundary condition is defined at the bottom of the aquifer, geosphere flows are upwards, where as when the boundary condition is at the top of the aquifer, geosphere flows are downwards. It was presumed, based on the pressure boundary conditions defined and a conservative flow field, that geosphere flows were intended to be upwards. Note that the difference has a very marginal effect on results: peak hydrogen and dissolved hydrogen flows within the repository were less than 10% greater with downwards geosphere flows compared to the upwards geosphere flows of the model presented here.

The benchmark specified H_2 gas to be generated at the surface of the waste containers, with the waste containers specified as a no-flow feature. Gas is generated at a rate of 100 mol/year/cell for the first 10 000 years, with no gas generation after 10 000 years. As the waste containers were not included in the half-domain model, gas generation was specified at all inner EDZ nodes of the cell (properties a combination of interface and EDZ, as described below). The generation term was proportioned between nodes according to block volume of the generation node. The source term for the main drift model is derived from output at the module-scale model.

3.9.2.4 Deviations from the specification

Upscaling of parameters for the inner EDZ and other interface combinations are as follows:

- Scalar parameters, such as porosity, were calculated using a volumetric weighting approach. For example, for the cell inner EDZ, with an interface 1 cm thick and an inner EDZ block 25 cm thick, the porosity (θ) is calculated as follows:

$$\theta_{inner\ edz} = \theta_{interface}\frac{0.01}{0.25} + \theta_{edz}\frac{0.24}{0.25} \qquad \textit{Equation 1}$$

- Tensor parameters, such as permeability, used an arithmetic average when component materials were layered parallel to the direction of the tensor and a harmonic average when component materials were layered perpendicular to the direction of the tensor.

- Van Genuchten shape parameter n was held constant (assumes relative permeability in the interface is the same as in the EDZ, backfill or bentonite), while the van Genuchten air entry pressure was calculated using the volumetric weighting approach of a scalar parameter.

Table 1 provides the final parameters for upscaled interface materials. Table 1 also contains the initial conditions within the upscaled interface materials. These initial conditions are determined in the same manner as a scalar parameter, weighted according to the relative volume of the contributing materials, and ignoring the benchmark specification where the interface at the bottom of a cell or drift is fully water saturated. Note that initial pressure conditions were not weighted: all materials with a partial saturation, including upscaled interface materials, were assigned a gas pressure of 0.1 MPa as defined by the benchmark for partially saturated materials.

Table 1 : Parameters and initial conditions for upscaled interface materials

	$K_{parallel}$ [m²]	$K_{perpendicular}$ [m²]	Porosity [-]	Pore Compressibility [Pa⁻¹]	Tortuosity	S_{lr} [%]	S_{gr} [%]	n [-]	P_o [Pa]	Initial Water Saturation [%]
Inner cell EDZ	4.0E-14	5.2E-18	0.18	1.06E-09	0.28	0	0	1.5	1.44E+06	96.2
Inner cell plug EDZ	5.0E-18	5.0E-18	0.16	1.10E-09	0.28	0	0	1.5	1.44E+06	96.2
Main Drift Plug Interface	6.0E-20	1.0E-20	0.35	8.24E-10	0.06	0	0	1.6	1.58E+07	69.4
Drift Interface	5.1E-17	6.9E-17	0.40	2.06E-09	0.27	0	0	1.5	1.96E+06	68.7

3.9.3 Base Case Results

Model results for the half-domain model are presented, followed by results for the main-drift model, and how it compares to the half-domain model.

Output points and slices presented below correspond to those defined in the benchmark (locations shown in Figure 44, Figure 45, Figure 46, and Figure 47). Note that in the subsequent figures showing gas saturation, white space indicates areas where gas saturations are below the legend threshold of 1E-6, often at zero gas saturation. For figures showing gas pressure, white areas indicate areas where there is no gas, and therefore no gas pressure.

3.9.3.1 Half-Domain Model

Only a single module will be shown for the figures in most of this section, for visual simplification of these figures. To justify this simplified reprensentation, the first set of figures show results at three modules (1, 3 and 5, locations of modules shown in Figure 1 and Figure 2) to demonstrate the similarity between modules. Figure 7 shows the water saturation evolution in the modules. Results are similar for each module (note only module 1, 3 and 5 are shown). This similarity between module results extends to pressure results, as shown in Figure 8. Hydrogen and dissolved hydrogen gas flows in the modules, shown in Figure 9 and Figure 10, are also very similar between modules with some differences seen at module 5, close to the main drift. Due to the similarity between modules, the subsequent description of repository evolution will only show results for Module 3.

Gas flows in the module itself is as expected, with gas flowing along cells and drifts towards the shaft, as demonstrated by the greatest gas flows at F-D1 (closest to the main drift), which is the accumulation of all the gas flows in the module (Figure 9). After 1000 years, the behaviour is more complex, with little difference in gas flows between F-D25 and F-D1, due in part to the general reduction of gas flow out of the modules resulting from partial saturation of bentonite seals in the main drift. Dissolved gas flows exhibit more complex behavious from the start of the simulation, due to more complex water gradients in the module (Figure 10). High water pressure gradients between the host rock and the module near cell 50 (farthest from main drift) result in greater dissolved gas flows at cell 50 than at cell 25 (middle of repository). High capillary pressures in the cell plugs results in in high water (and therefore dissolved H_2) flows at all F-C slices.

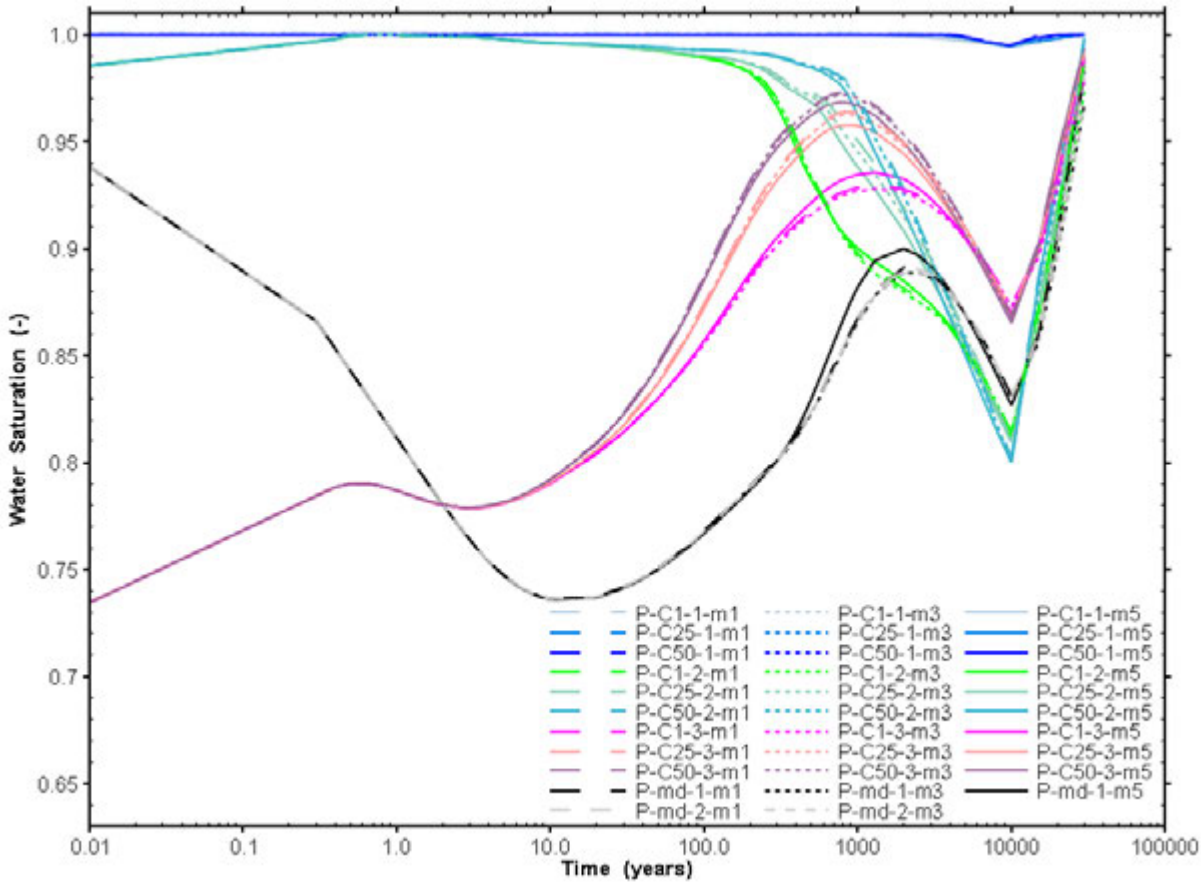

Figure 44: Water saturation in modules 1, 3 and 5.

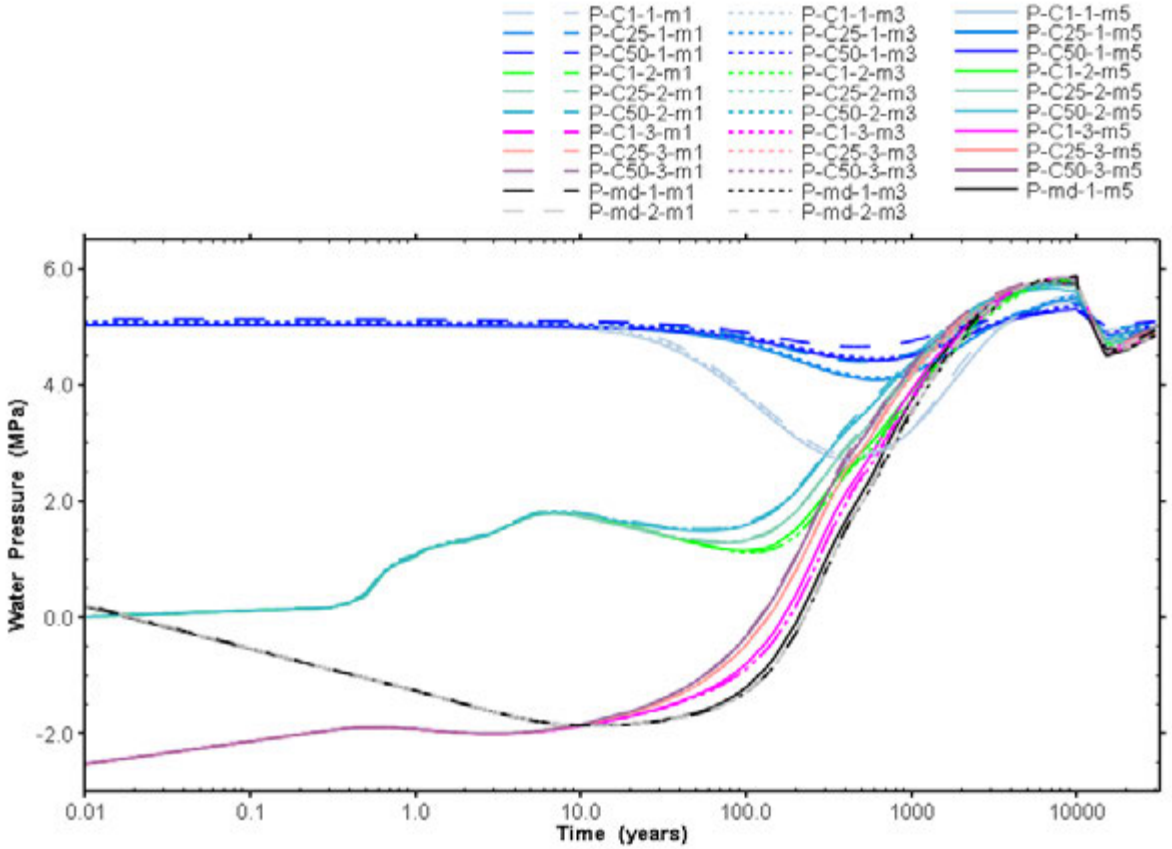

Figure 45: Water pressure in modules 1, 3 and 5.

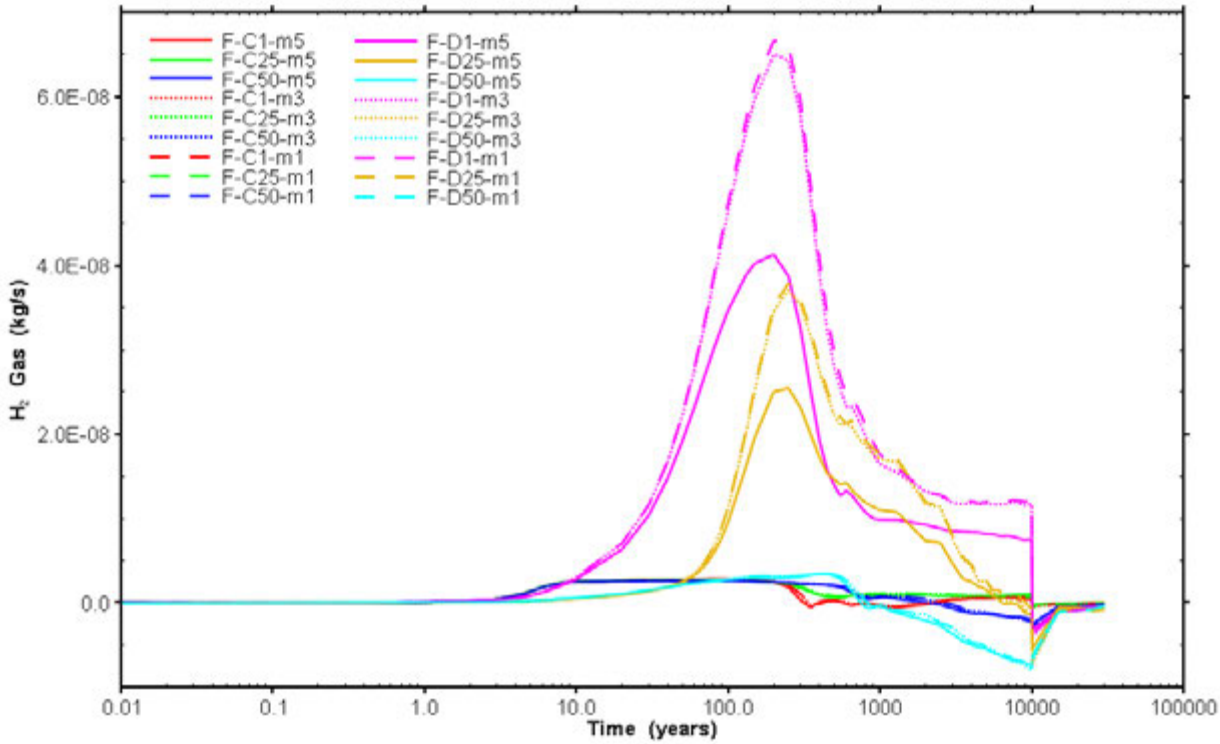

Figure 46: Hydrogen gas flows in modules 1, 3 and 5.

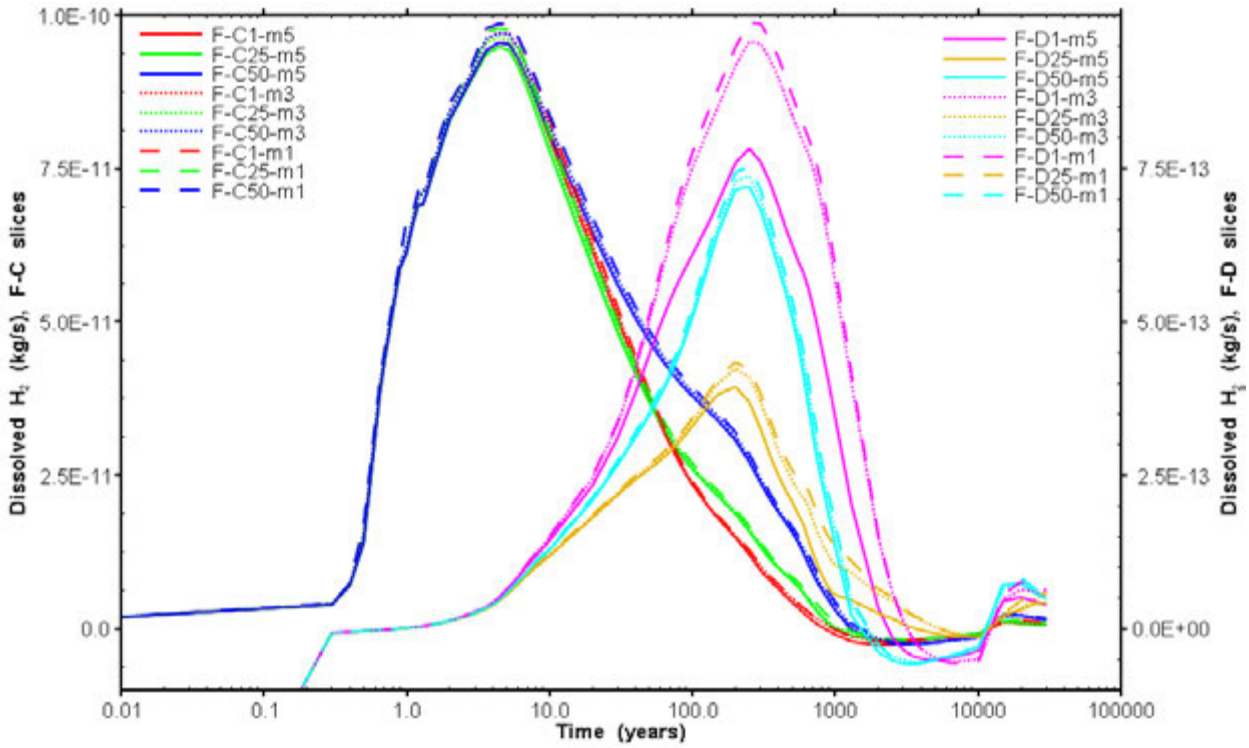

Figure 47: Dissolved hydrogen gas flows in modules 1, 3 and 5. Note that F-C flows are plotted against the left axes, and F-D flows are plotted against the right axes.

The water saturation, water pressure and gas pressure evolution in the repository and shaft is shown in Figure 11, Figure 12 and Figure 13 respectively. Additional points to those described above were added within the cell seal near P-C25-2-m3 (module 3, cell 25), as well as the main drift seal (note that seal results on either side of module 3 were indistinguishable). P-md1-m3, P-md and P-w-1 are located in the EDZ, which is initially fully water saturated. Locations are shown in Figure 45, Figure 46, and Figure 47.

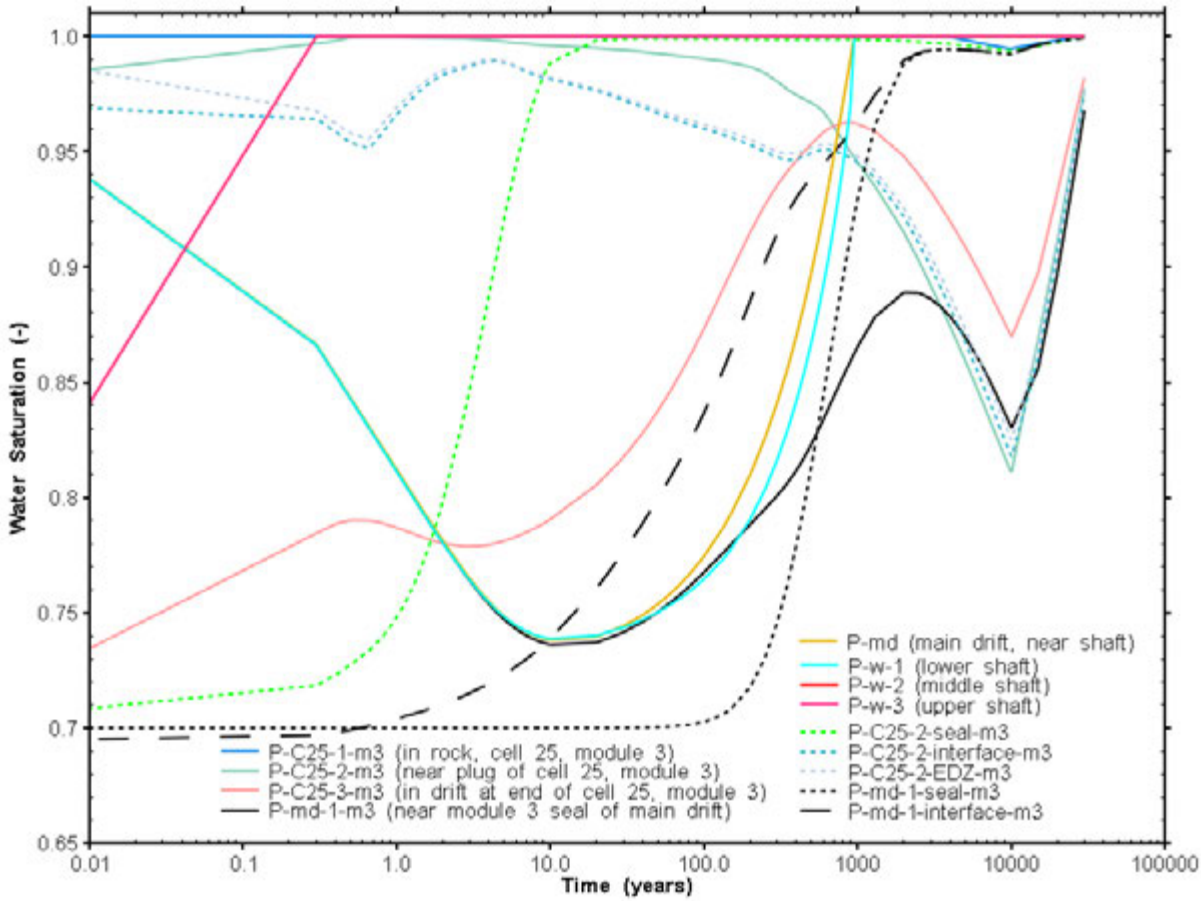

Figure 48: Repository and shaft water saturation evolution. Note that P-w-2 and P-w-3 are identical.

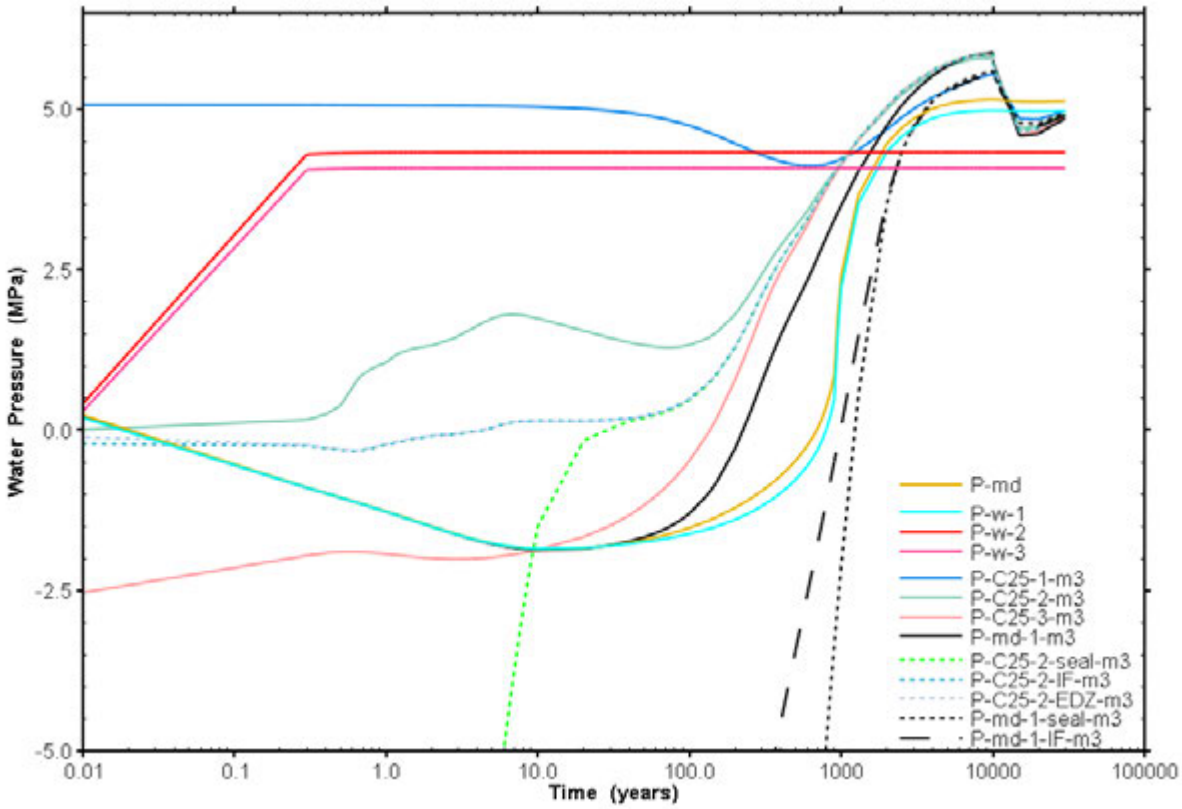

Figure 49: Repository and shaft water pressure evolution.

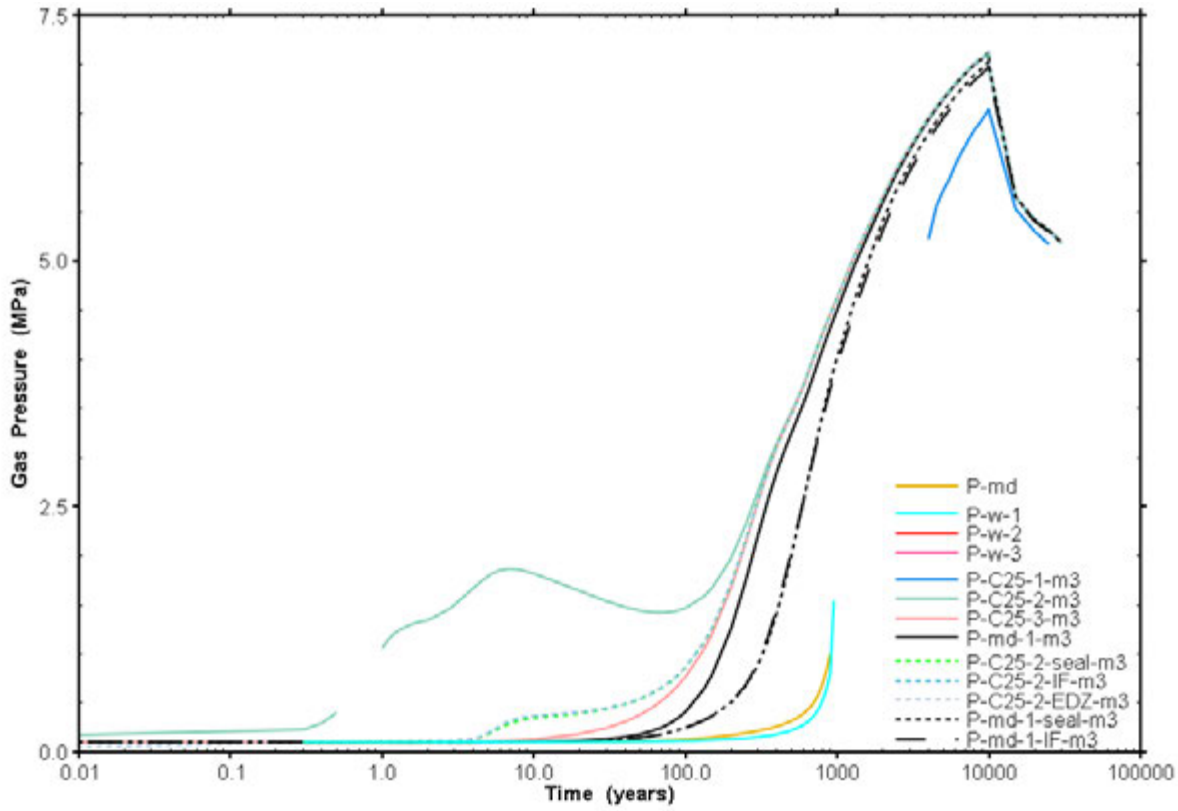

Figure 50: Repository and shaft gas pressure evolution.

The cells go through a short period of full water saturation around 1 year (P-C25-2-m3, solid green line), as water inflow due to large pressure gradients (between host rock and initial atmospheric gas pressure in the repository) dissolves all generated gas. Prior to 10 years, the cells and access drifts saturate with water as initial pressures equilibrate, and the main drift and shaft near bentonite seals desaturate as the bentonite seals draw water due to high capillary pressures in bentonite. At P-C25-3-m3 (solid pink line) in the access drift, there is a small drop in water saturation and water pressure just before one year, attributed to the increase in water saturation at that point in the cell bentonite seal (P-C25-2-seal, dashed green line) resulting from high capillary pressures in bentonite.

By 20 years, the seal at the end of cell 25 (P-C25-seal-m3, dashed green line) is almost fully water saturated. The interface and EDZ surrounding the seal (P-C25-2-IF-m3, dashed blue line, and P-C25-2-EDZ-m2, dashed grey line) remains partially saturated, allowing gas to escape through to the access drift. The main drift seals (P-md-1-seal-m3, black short dashed line) and their interfaces (P-md-1-IF-m3, black long dashed line) become mostly water saturated around 2000 years, with a small amount of gas present representing a small leakage of gas through the seal. This small leakage of gas is quantified by the gas flows through the bentonite seals in the main drift, shown in Figure 14. The flow of gas through the main drift bentonite seals is greatest at module 5 and module 1, due to greater pressure gradients at the ends of the repository.

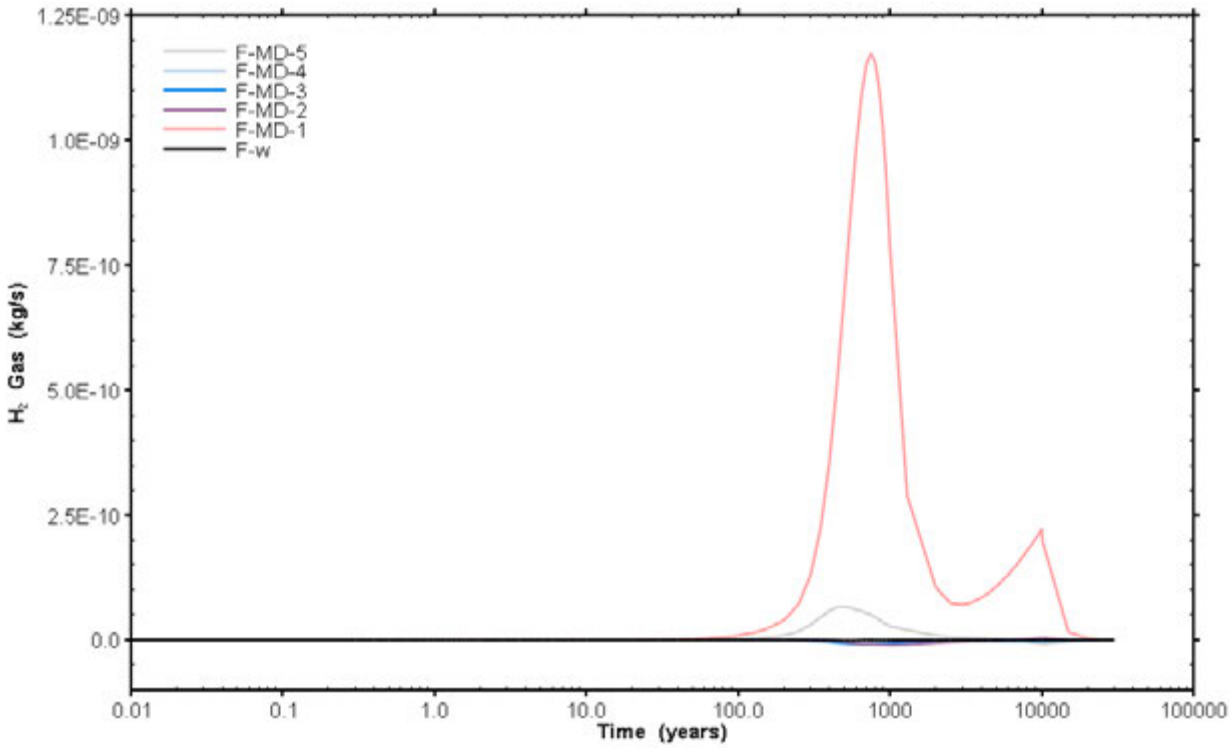

Figure 51: H_2 gas flow through the main drift and well

Between 1000 and 2000 years, as less gas escapes the system from the partially saturated seals and water pressures approach hydrostatic (5 MPa), gas production begins to steadily increase gas pressure and reduce water saturations in the cells, access drifts and main drift (e.g., bump in the water saturation curve in the access drift P-25-3-m3 (solid pink line) and main drift P-md-1-interface-m3 (solid black line)). Gas migrates into the host rock, with small reductions in water saturation apparent at P-C-25-1 (solid dark blue line) at about 5000 years (Figure 11). At 10 000 years, when gas generation ceases, peak gas pressures of 7.1 MPa are reached in the cells and drifts. Water saturation begins to increase throughout the repository until the repository is mostly water saturated at 30 000 years.

At the top of the shaft (above the seal, P-w-2 and P-w-3), initial gas saturations are very quickly dissolved and the shaft remains fully water saturated for the remainder of the simulation. Below the shaft seal (P-w-1, cyan line), and along the main drift until the first repository seal (P-md, gold line), the shaft and drift

becomes fully saturated with water at approximately 1000 years. Water pressures in the lower shaft and drift do not increase above hydrostatic pressure, reaching hydrostatic pressure at approximately 10 000 years.

Figure 15 shows hydrogen gas flows through the bentonite seal in the shaft, also indicating no flow of gas up the shaft. The small downward flow of gas prior to the saturation of the seal at 1000 years, shown at 650 years in Figure 16, is due to pressure gradients in the seal, with greater gas pressures at the top of the seal and the shaft above the seal already water saturated (note that this gas flow is due to initial gases only). Also prior to saturation of the shaft at 1000 years, water flows in the shaft are primarily towards the bentonite seal as the seal saturates (high capillary pressures in the bentonite draws water in from surrounding rock and shaft), as shown in Figure 16, and are therefore downwards for the particular slice through the bentonite seal shown in Figure 15. Dissolved gases flowing away from the shaft along the aquifer (Z= 150 to 200 m), as shown in Figure 17, are initial shaft gases. After saturation of the bentonite seal at 1000 years, gas flows cease and the flow of dissolved gas through the shaft is diminished, although this gas and dissolved gas flow is primarily still downwards i.e., the gas and dissolved gases are representative of initial shaft gases migrating towards the repository. There is a relatively very small amount of dissolved gas migrating upwards through the shaft starting at 7000 years, not discernible in Figure 15.

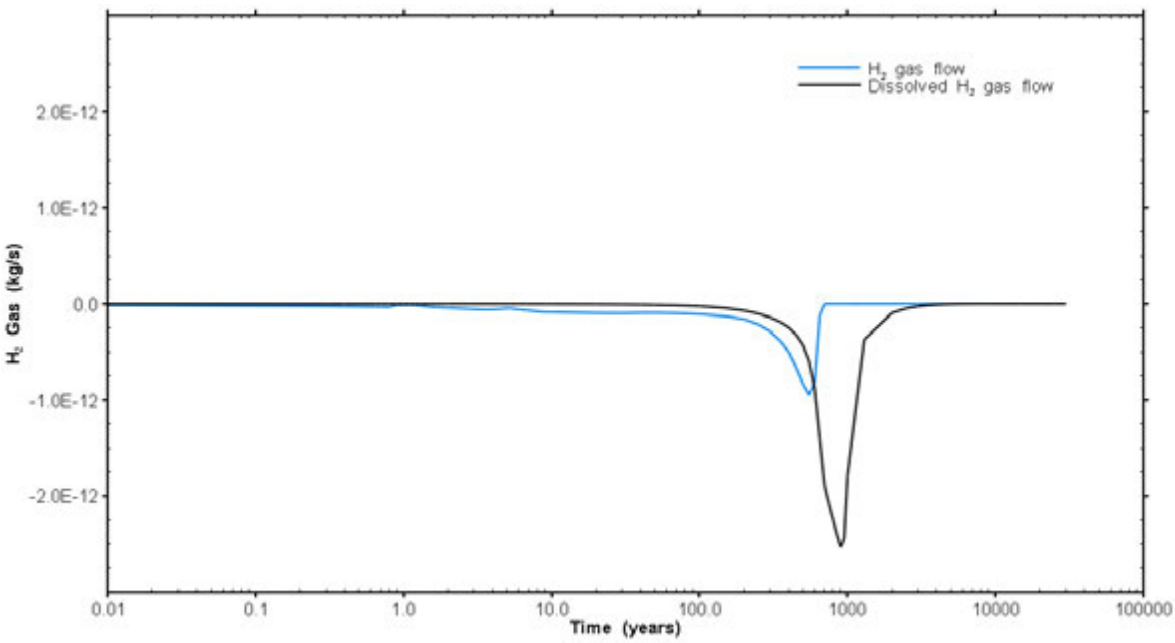

Figure 52 : Hydrogen and dissolved hydrogen flows through bentonite seal in the shaft. Negative flows indicate downward flow.

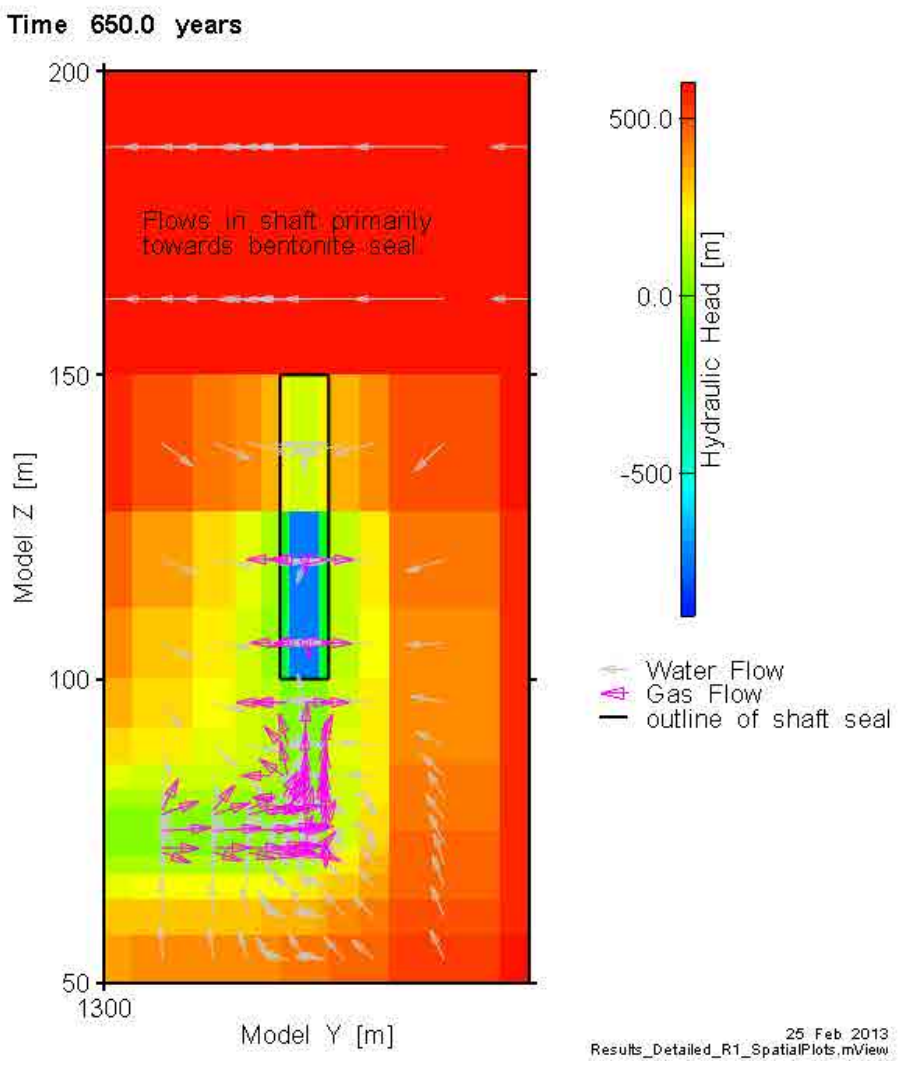

Figure 53: Vertical slice of gas and water flow in the shaft at 650 years

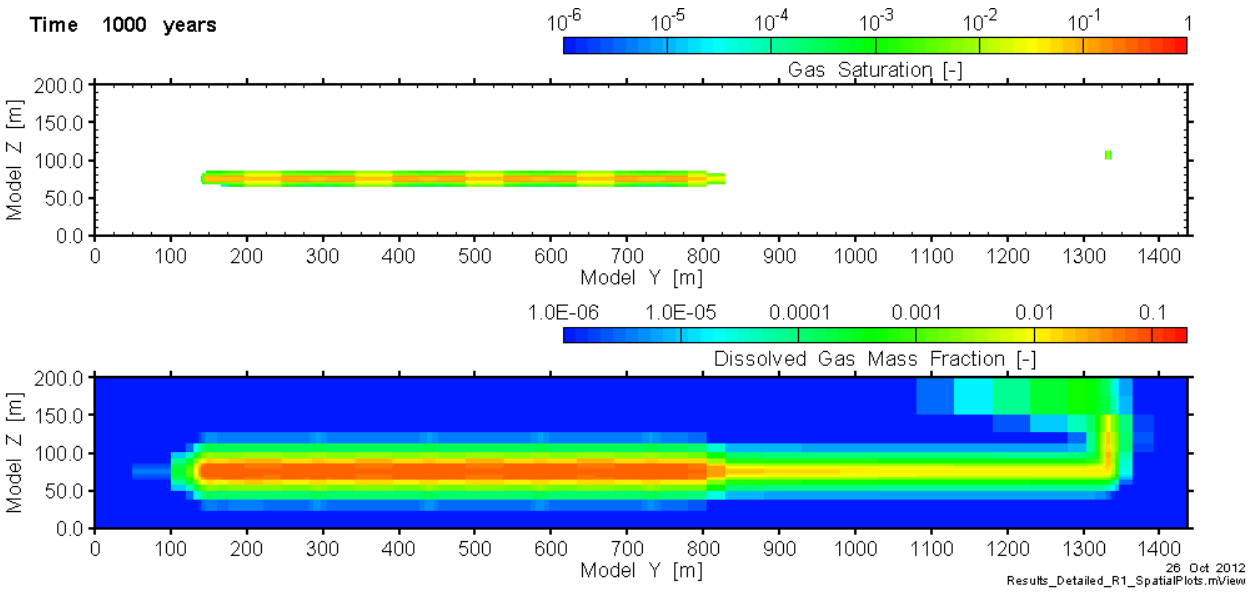

Figure 54: Gas and dissolved gas in a vertical slice near the shaft at 1000 years.

While gas does not migrate upwards through the shaft, it also does not migrate up through the host rock into the aquifer. Gas phase that migrates into the host rock dissolves in the water over time. Figure 18 shows gas saturations at 10 000 years along the main drift, and Figure 19 shows 3D gas saturations at various times, illustrating that the gas phase does not extend beyond approximately 35 m above the repository in the host rock. The primary pathway for generated gases to reach surface is through dissolution and migration of the dissolved gas upwards in the host rock.

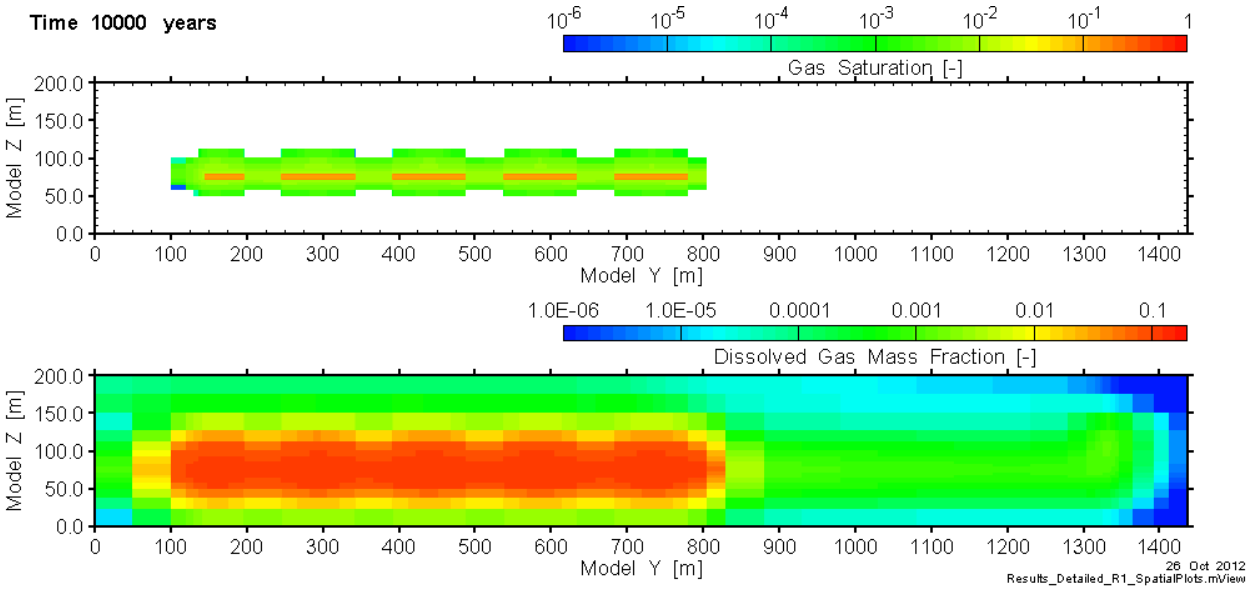

Figure 55: Gas and dissolved gas in a vertical slice near the shaft at 10 000 years.

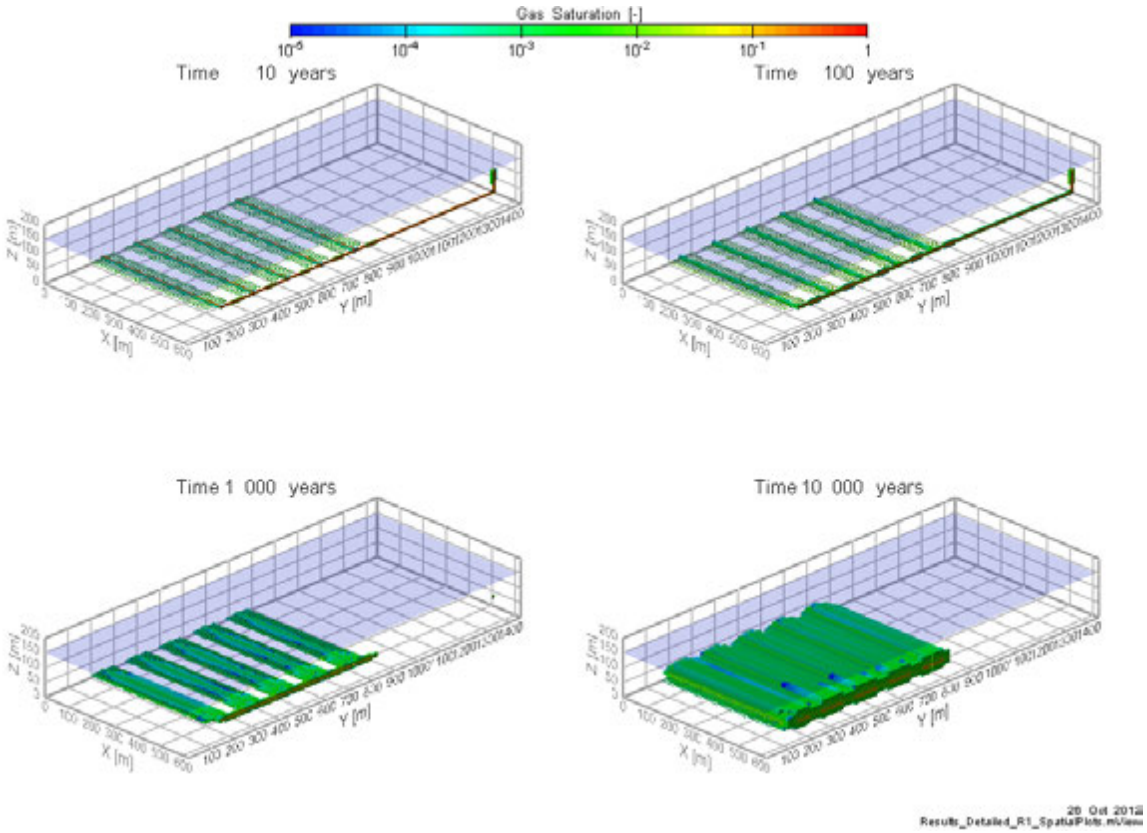

Figure 56: 3D gas saturations in the repository at various times. The transparent blue plane delineates the bottom of the aquifer.

3.9.3.2 Main Drift Model

The main drift model was created as a quick assessment of the repository scale. As such, it used the previous module-scale model to develop the inputs (note that boundary conditions were updated based on initial results of the main-drift model), which are the same for each module of the repository. While the output from the half-domain model could also be used, this model assesses the effectiveness of using a series of detailed small-scale models (such as the module-scale and main drift models) to represent the full-scale system. Figure 20 and Figure 21 compares the gas and water flow input into the main drift model (as output from the module-scale model) to the gas and water flows at the each module within the half-domain model. Generally, the shape of the curves is similar, with the main drift model inputs underestimating the peak gas flow, and overestimating the peak water flow, relative to the half-domain model. The exception is the half-domain gas flows for module 5, which are less than the main drift model inputs. The main drift model input uses the same input for all modules, and consequently does not adequately represent gas flows at this end of the repository, farthest from the shaft.

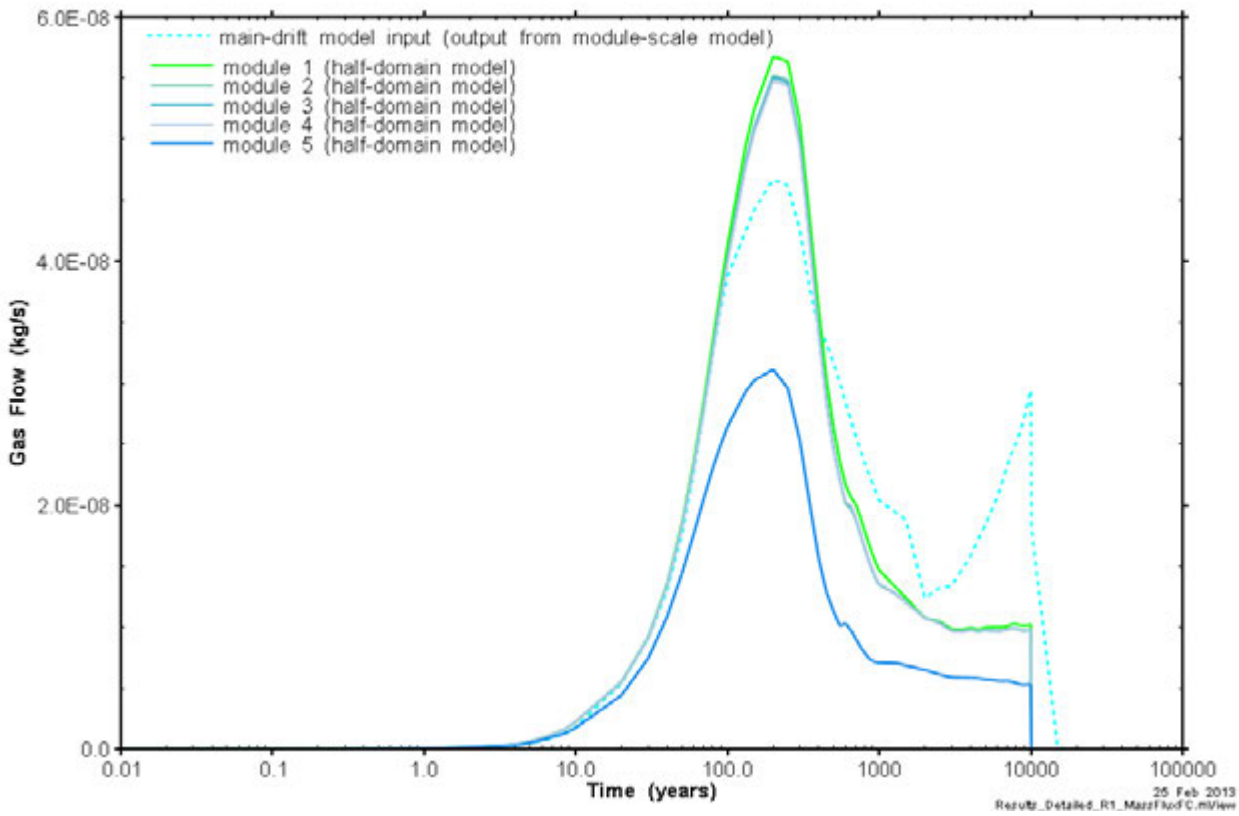

Figure 57: Gas flow comparison between main-drift model input and half-domain model flows out of each module.

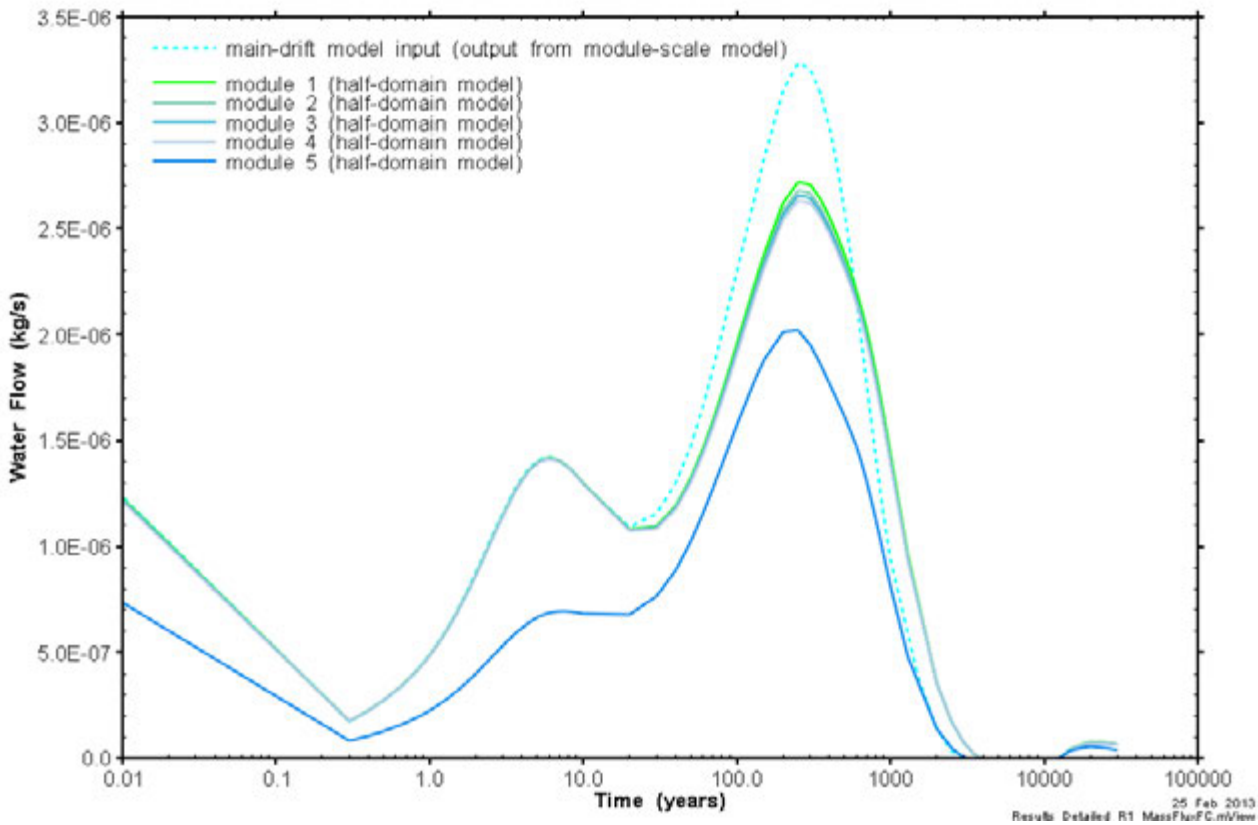

Figure 58: Water flow comparison between main-drift model input and half-domain repository flows out of each module.

Despite these small differences in peak water and gas flow exiting the panels, the water saturation, water pressure and gas pressure evolution in the main drift and shaft are similar, as shown in Figure 22 through Figure 24. There are small differences in the peaks and timing of the saturation and pressure curves, although the trends of the curves are the same. Peak gas pressures are similar (in main drift near module 3), at 6.9 MPa for the main-drift model and 7.1 MPa for the half-domain model, and the drifts are fully water saturated before 30 000 years.

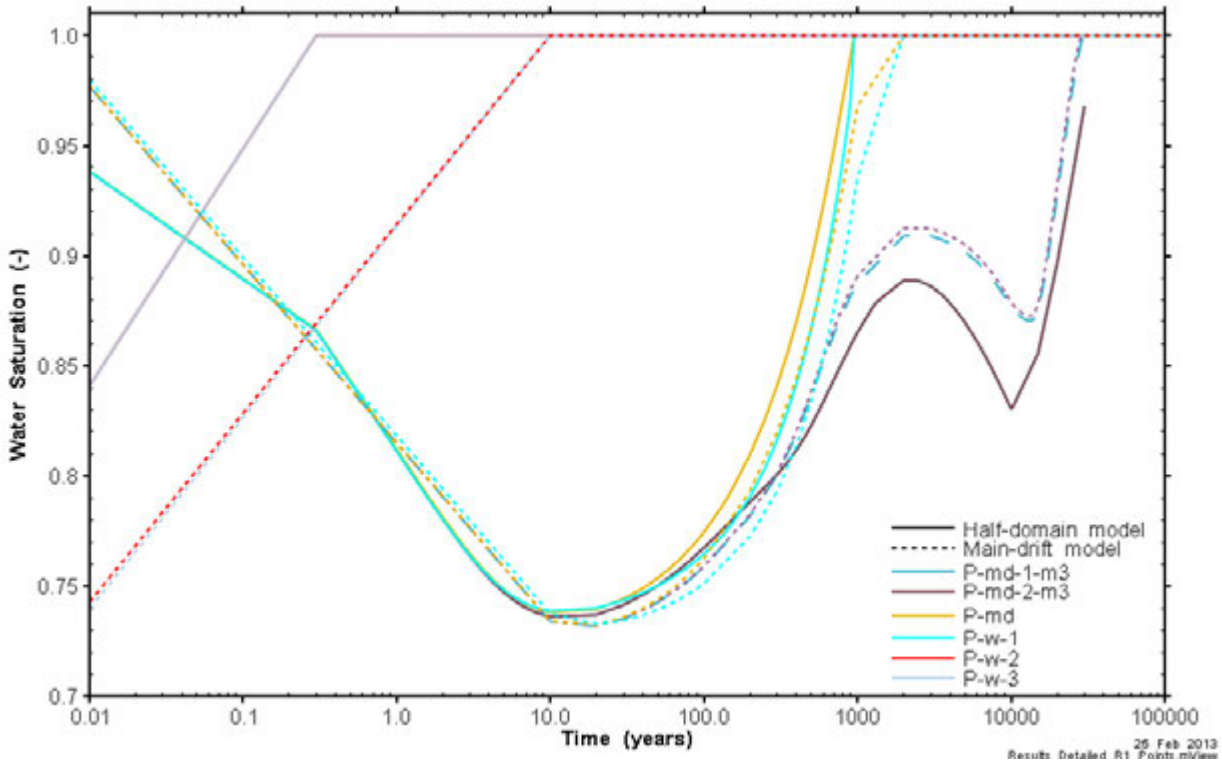

Figure 59: Water saturation comparison between the main-drift and half-domain models. Note that P-w-2 and P-w-3 overlap one another, and therefore P-w-2 is hidden.

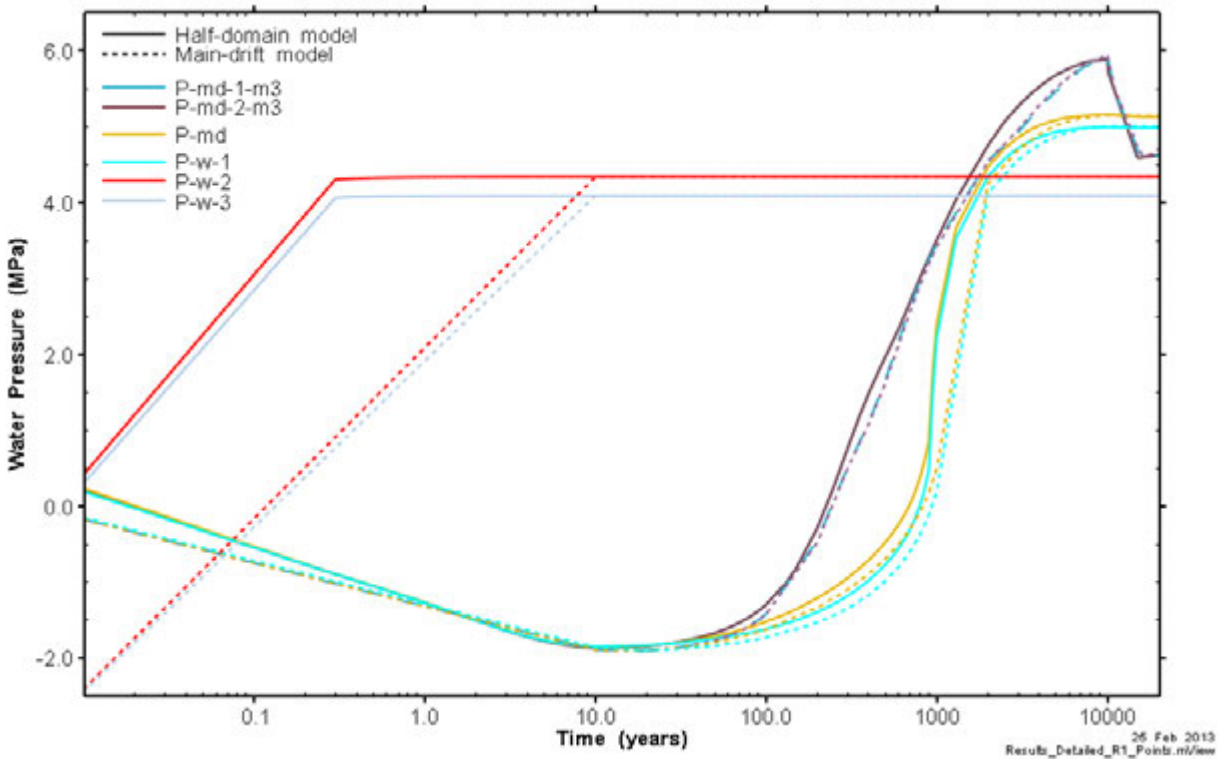

Figure 60: Water pressure comparison between the main-drift and half-domain models

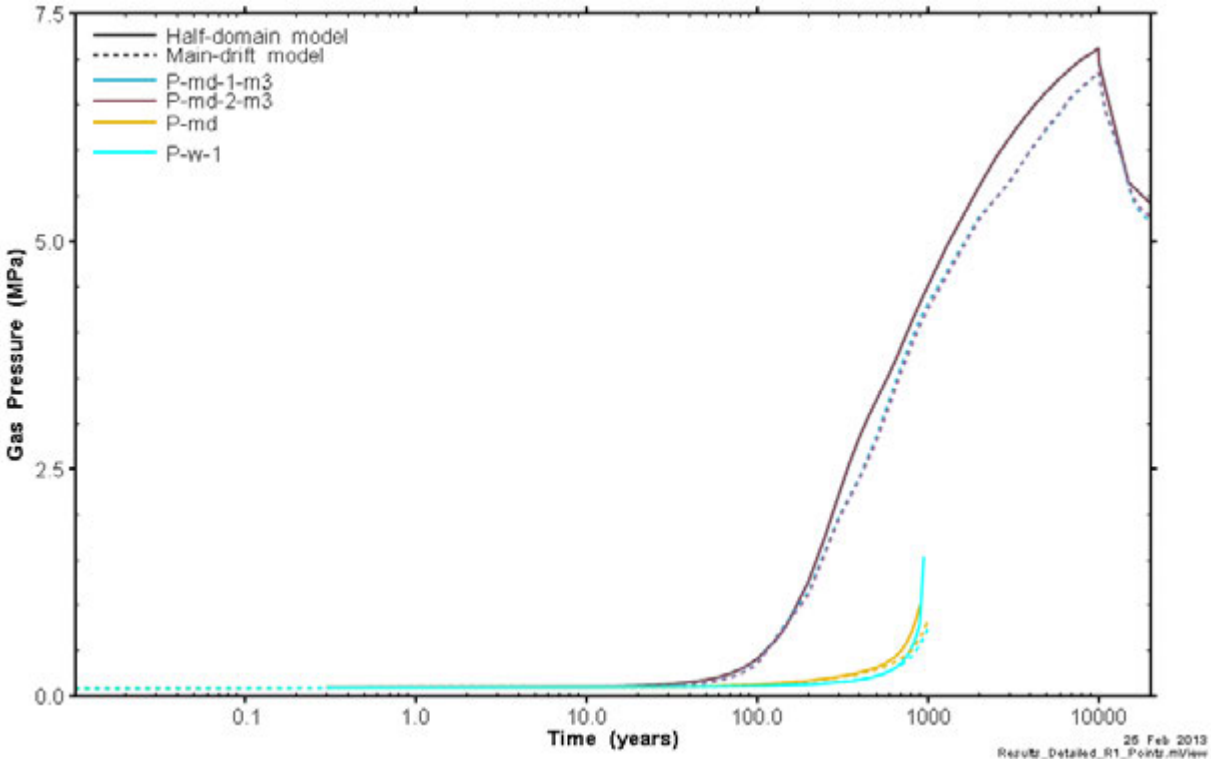

Figure 61: Gas pressure comparison between the main-drift and half-domain models

Figure 25 and Figure 26 compare H_2 gas and dissolved H_2 gas flows along the main drift, between the main-drift and half-domain models. The gas flows in the main drift model generally overestimates gas flows and underestimates dissolved gas flows, which is in opposition to the discrepancies between the module-scale inputs to the main drift module and the half-domain model (Figure 20 and Figure 21). There are also greater discrepancies at module 5, which is not surprising given that this module differed from the other modules in the half-domain model, yet was treated to be similar to other modules in the main-drift model.

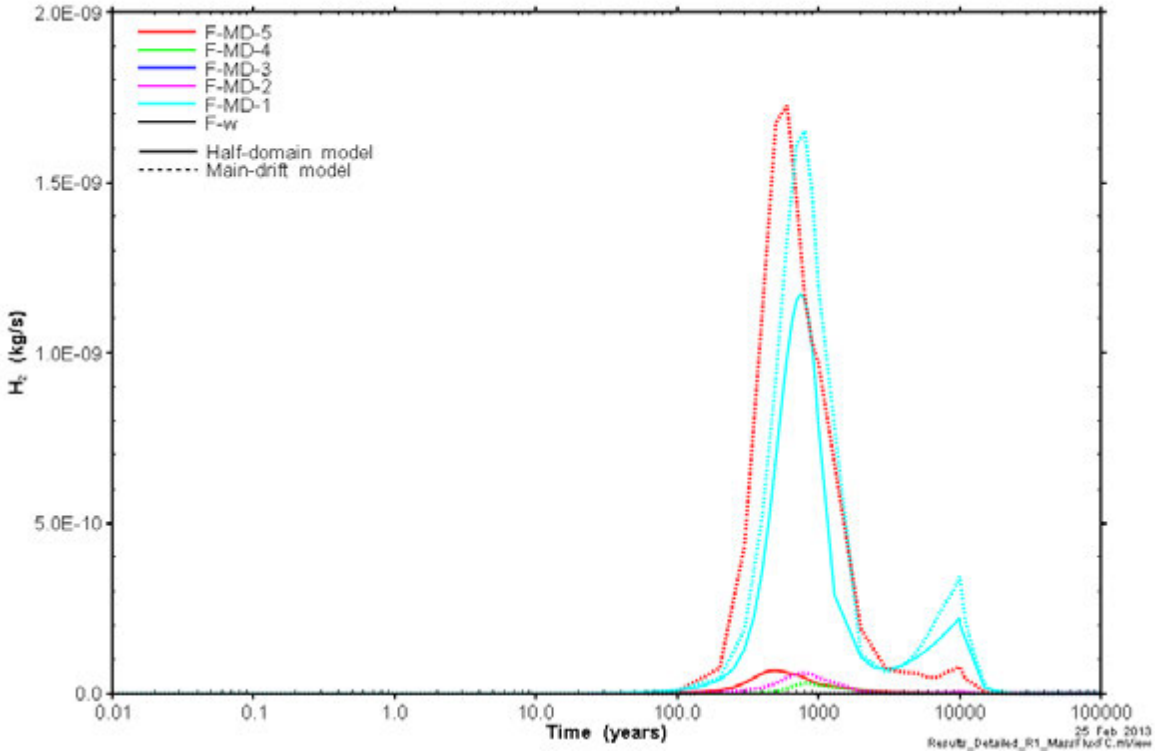

Figure 62: Comparison of H_2 gas flow along main drift and shaft between main-drift and half-domain models

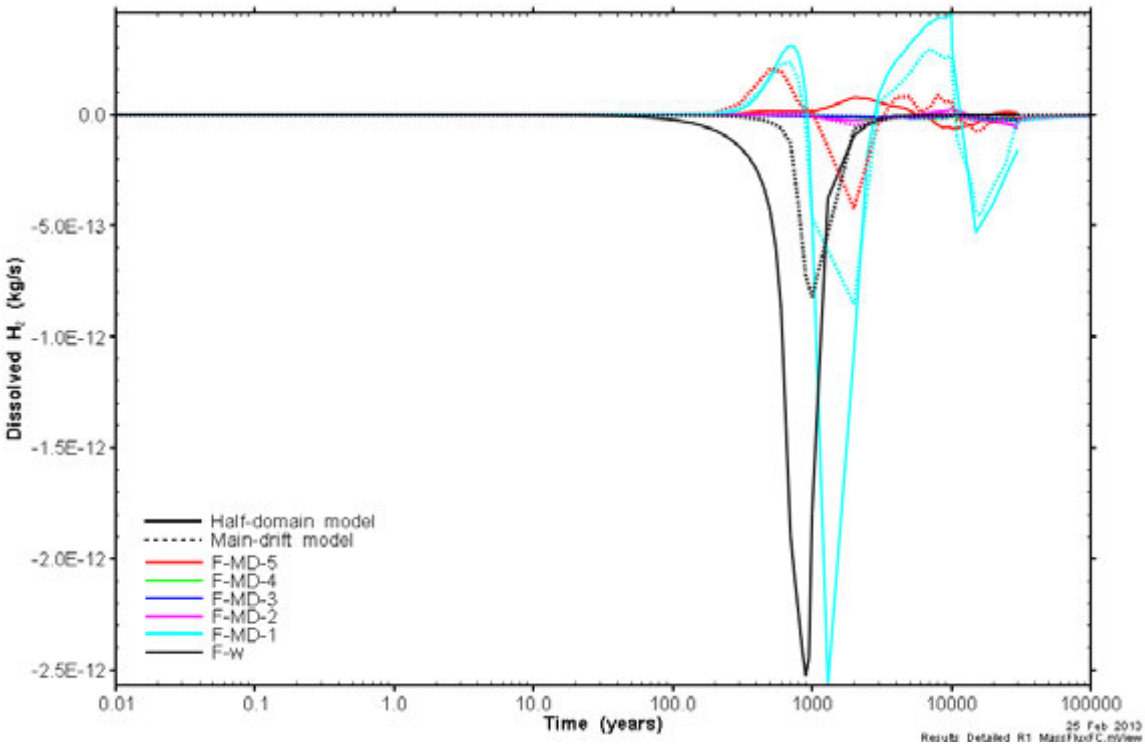

Figure 63: Comparison of dissolved H_2 gas flow along main drift and shaft between main-drift and half-domain models

3.9.4 Sensitivity Cases

A single sensitivity case was simulated with the half-domain model to illustrate the effects of the interface. Properties for all elements which contained a combination of interface and an adjacent material were replaced with the properties for the adjacent material (e.g., EDZ). In the base case, the interface provides a permeable pathway with low capillary pressures. The exception is at the cell seal interface, where permeability is the same as the EDZ, but the interface has much lower capillary pressures (two orders of magnitude) and greater porosities. Compared to the base case, this simulation was numerically more stable and was able to use coarser convergence criteria. The resulting run time of 4.5 days is shorter than the one week run time of the base case, and improved run times may also be seen with coarser discretization (refined discretization was required in some cases to capture the upscaled interface elements).

From a repository water saturation and pressure perspective, the interfaces had minimal impact. Figure 27 and Figure 28 shows the water saturation and gas pressure for the no interface case, compared to the reference half-domain model (with interface).

Gas and dissolved gas flows in the cells, access and main drifts were reduced in the no-interface case. Figure 29 shows gas flows, and Figure 30 shows dissolved gas flows. Flow in the shaft (F-w) is unchanged in that gas and dissolved gas flows are downwards, as shown for dissolved gas flows in Figure 30. Note that flows in the access drift are greater than flows out of the cells, due to the accumulation of flow out of all the cells. Flows in the main drift are much reduced, due to the seals in the main drift (which is the location of these flow observations).

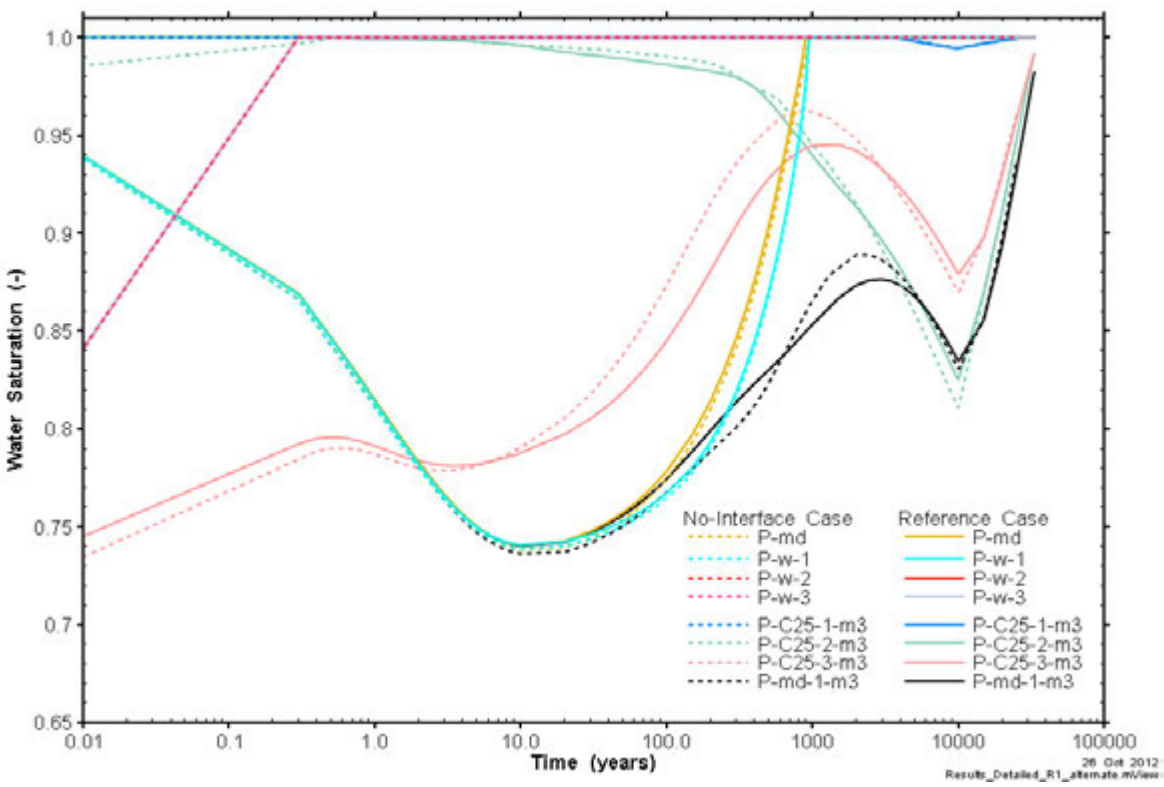

Figure 64: Water saturation comparison of half-domain model with and without interfaces.

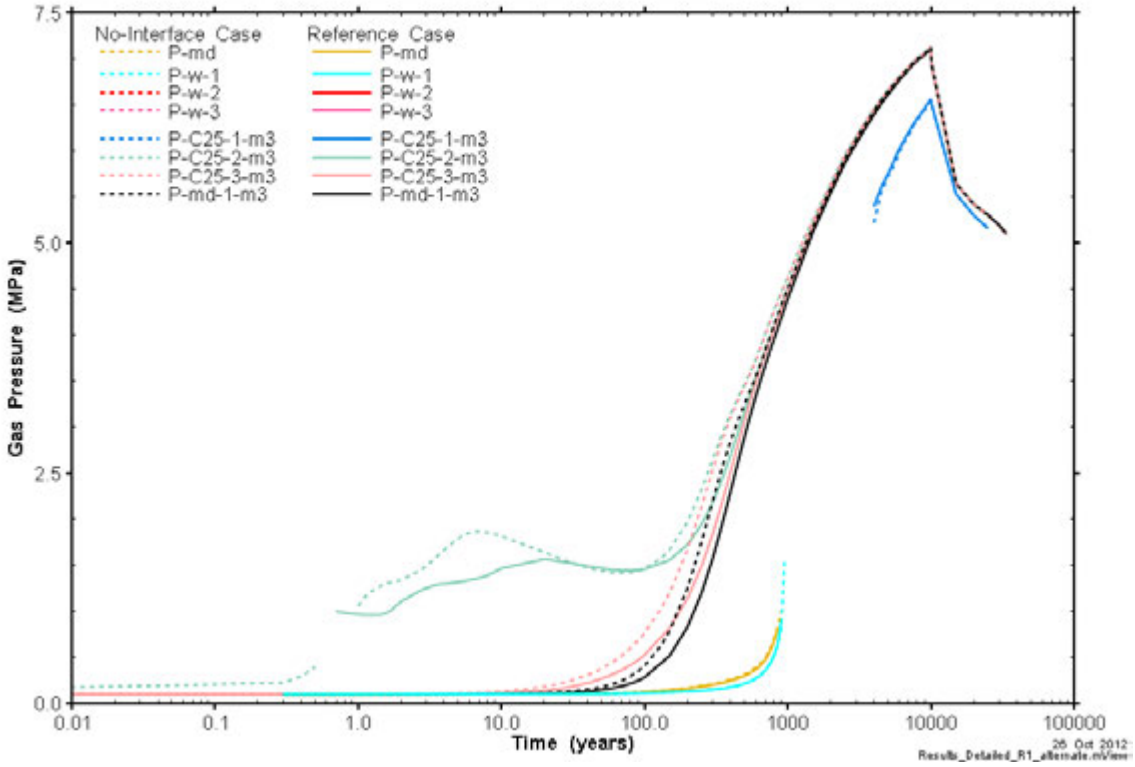

Figure 65: Gas pressure comparison of half-domain model with and without interfaces.

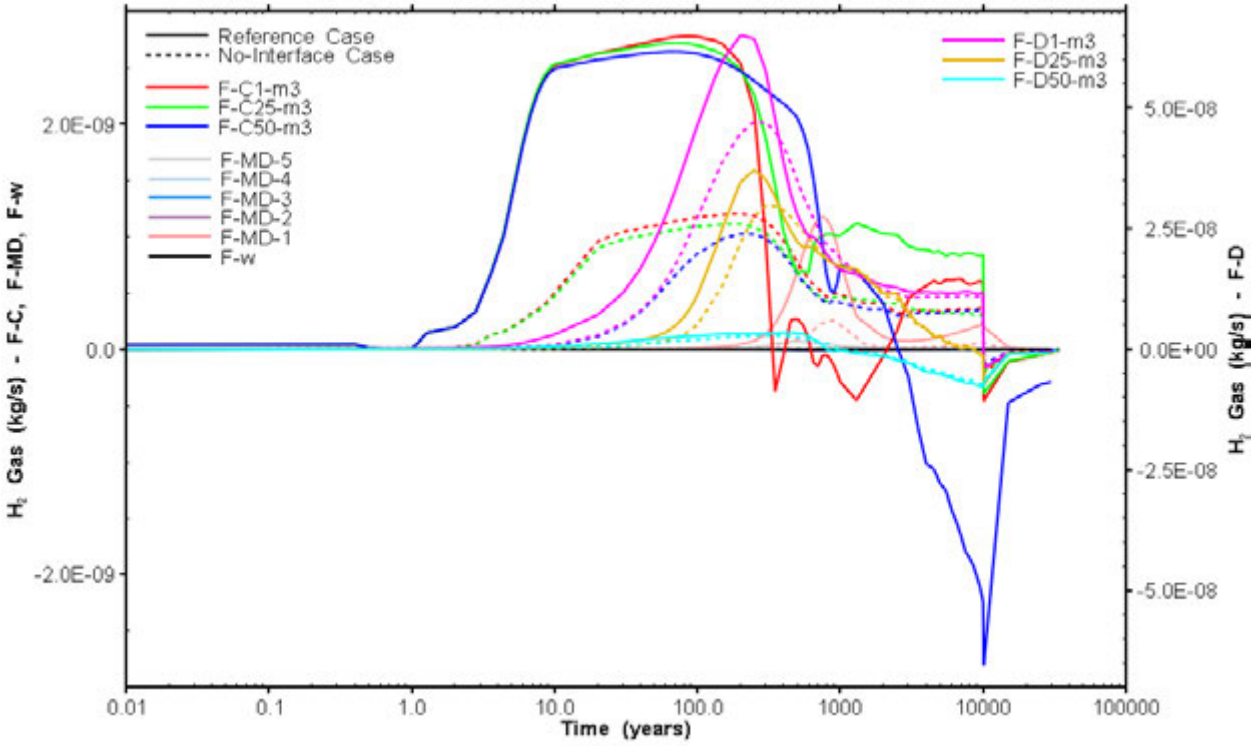

Figure 66: Gas flows at F-C, F-D, F-MD and F-w slices for both the reference (base) and no-interface cases. Note that F-D flows are plotted against the right axis and all other flows are plotted against the left axis.

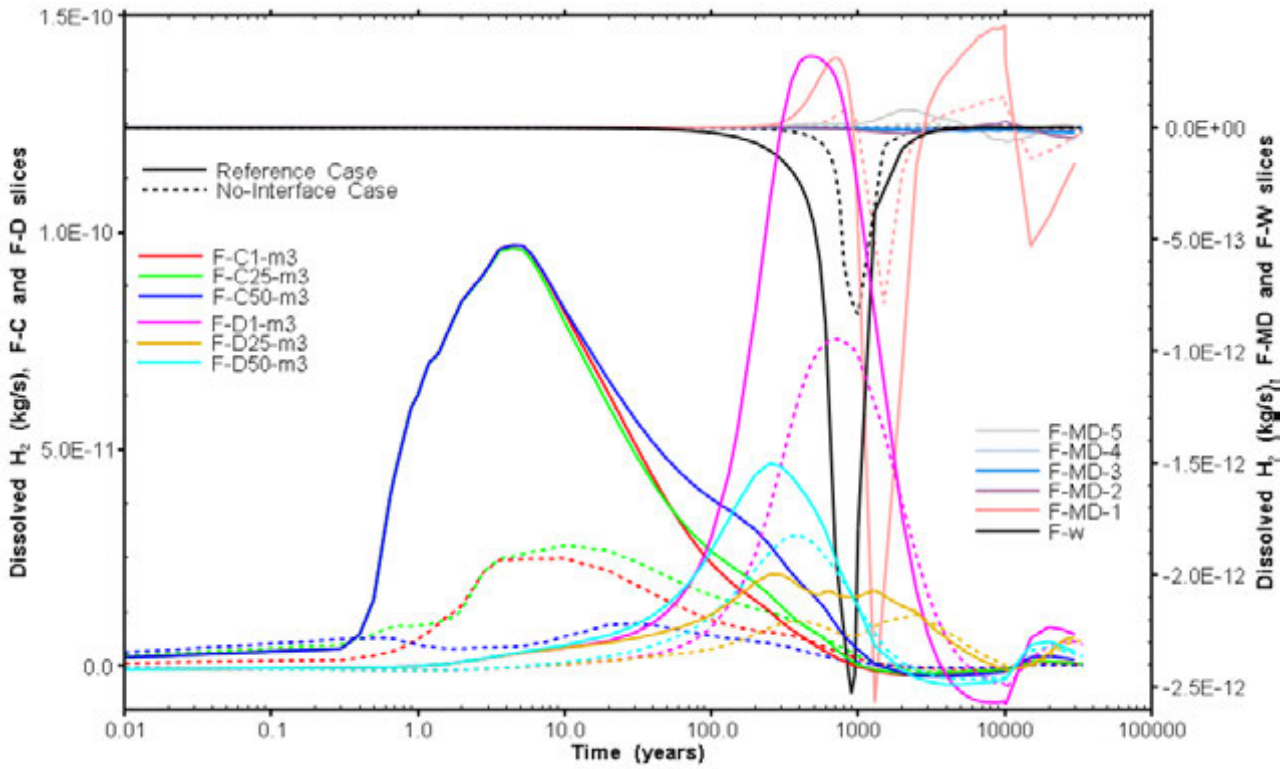

Figure 67: Dissolved gas flows at F-C, F-D, F-MD and F-w slices for both the reference (base) and no-interface cases. Note that F-C and F-D flows are plotted against the left axis and F-MD and F-w flows are plotted against the right axis.

In the absence of gas or dissolved gas reaching surface through the shaft, the no-interface case provides a good representation of the saturation and pressures in the system, as well as the amount of dissolved gas reaching surface. Figure 31 shows the amount of dissolved gas in the aquifer over time, for both the base and no-interface cases, showing that the amount of dissolved gas reaching surface in each case is almost identical. This is perhaps not surprising since dissolved gas in the aquifer is a result of gas dissolving and diffusing into the host rock, rather than being transported along the repository cells and drifts containing the interfaces. In an alternate repository scenario where the shaft is an important pathway to surface, the no-interface case would likely provide a non-conservative estimate of gas and dissolved gas to surface.

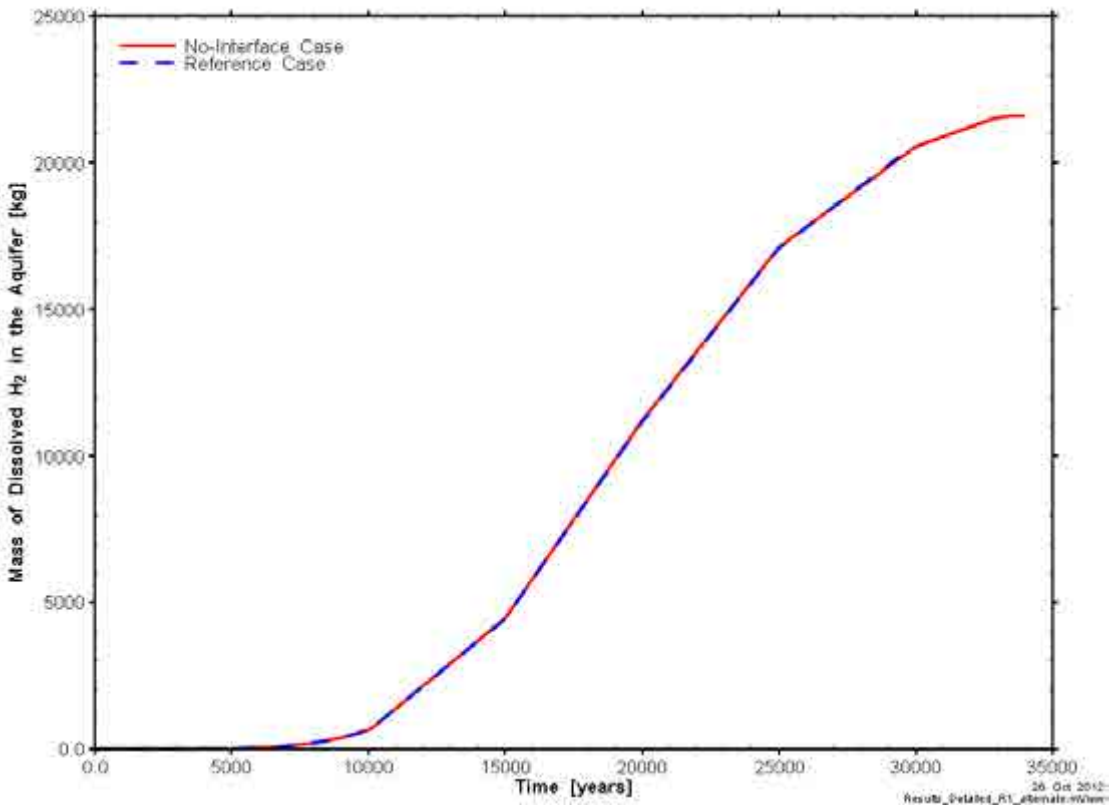

Figure 68: Mass of dissolved gas in the aquifer over the course of the simulation, for both the reference (base) and no-interface cases.

3.9.5 Discussion and Conclusions

The challenge in developing the repository scale model was developing a grid discretization that adequately represented the repository, while maintaining a tractable grid size. Two models were developed (1) a half-domain model, and (2) a main drift model, using output from the module-scale model as input into the main drift. For both models, interfaces were upscaled. The half-domain model took approximately 1 week to complete to 30 000 years, and the main drift model completes to 100 000 years in under 10 minutes.

The maximum gas pressure in the repository develops once the seals in the main drift have mostly saturated, limiting flow of gas out of the system. Characterization of the seals, their capacity for resaturation (capillary pressure curves, particularly at the saturated end of the curve) and the presence of an interface or EDZ surrounding these seals will significantly affect the maximum pressure in the repository. The presence of interfaces, albeit uspcaled interfaces, had minimal impact on repository pressures and saturations, as seen in the sensitivity case with no-interfaces.

Gas transport occurs along the main drift and shaft, and into the host rock. No free gas enters the aquifer or passes the bentonite seal in the shaft over the course of the simulation. Dissolved gas does reach the aquifer, by means of the host rock. No dissolved gas is transported up the shaft. Characterization of diffusion in the host rock is clearly important to determine the amount of gas reaching the aquifer at surface.

The main drift model provided a very quick assessment of the performance of the main drift and shaft. In this particular repository, this model provides a reasonable estimate of repository saturations and pressures. However, there is a discrepancy between model inputs and outputs, in that while the main-drift model inputs underestimates gas flows and overestimates water flows into the main drift, it overestimates gas flows and underestimates water flows along the main drift. The current main drift model is an

incomplete assessment of this upscaling approach, using a somewhat cumbersome module-scale model. A more comprehensive development of a set of scaled models (cell through repository, with linked boundary conditions) may provide sufficient assessment of a full-scale repository, with less difference between flow results. While a half-domain model may be desired to ensure validity of the set of connected models, the quick run times of the main-drift model approach would allow for greater analysis of sensitivities.

In addition to the half-domain and main drift models, a no-interface sensitivity case was simulated. The no-interface case provides an excellent representation of the repository evolution, including saturations, pressures and dissolved gas at surface, with some improvement in numeric stability. With a different repository system, which had some transport up the shaft, a no-interface case would be expected to underestimate gas and dissolved gas flows up the shaft. The limited impact of interfaces may in part be due to the low permeabilities of the interface at the seals, particularly the cell seal which has the same permeability as the EDZ (but lower air-entry pressures and higher porosities).

3.9.6 Issues for further consideration

Two model uncertainties were not examined by this set of models: the impact of an explicit interface, and the effect of coarse discretization. Previous cell-scale modelling found that the interface had minimal impact on results, unless the EDZ permeability was low. The no-interface case supports these results; however, it should be noted that the no-interface case suggests that flows along the drifts and shaft are underestimated, which would be important in a scenario where the shaft was an important pathway for gas and dissolved gas. Different discretizations have not been examined directly, and would be best examined using a small-scale model such as the main-drift model.

Several issues related to the benchmark definition also require further consideration. The benchmark defines only interfaces (no EDZ) surrounding the bentonite plugs in the main drift. This is likely conservative for gas pressures, as gas pressures increase once the bentonite plugs become water-saturated and prevent flow along the drift. However, it is likely non-conservative from the perspective of gas and dissolved gas migrating along the main drift and up the shaft. As well, only two-phase flow is considered. It is generally acknowledged that other gas migration processes, such as dilation, may occur in saturated bentonite materials at sufficiently high pressures. Gas flow by dilation mechanisms will likely occur along interfaces to the bentonite seals and may result in higher permeability of these interfaces.

3.9.7 References

[1] Suckling, P., J. Avis, N. Calder, P. Humphreys, F. King and R. Walsh. 2012. T2GGM Version 3.1: Gas Generation and Transport Code. Quintessa Ltd. and Geofirma Engineering Ltd. report for the Nuclear Waste Management Organization NWMO TR-2012-23 R000. Toronto, Canada.

[2] Pruess, K., C. Oldenburg and G. Moridis. 1999. TOUGH2 User's Guide, Version 2.0. Lawrence Berkeley National Laboratory LBNL-43134. Berkeley, USA.

4. Global synthesis of the benchmark at repository scale

This synthesis is mainly focused on the repository scale benchmark. All global statement developed at the cell scale and module scale are valid but will not be reproduced here (model and code development, meshing problems, time step management problems …). Please refer to the cell scale benchmark and the module scale benchmark document for further details.

Of the 9 teams who initially participated in the FORGE WP1.2 benchmark exercise, only 3 have presented results at the global repository scale.

After a global description of the main phenomenological results at module scale this synthesis will focus on upscaling techniquess used by the different teams and finally some discussion on how representative the results are.

N.B. *: There are two other document linked to this one, on cell scale (report FORGE D1.6-R part 1: cell scale benchmark) and module scale (report FORGE D1.6 –R part 2: module scale benchmark) benchmark.*

4.1 Comparison of the available results at repository scale and main phenomenological understandings

In general, results from the different models are similar at all scales. The global hydraulic transient behavior already described at module scale is here confirmed.

In particular, for gas pressure the three models produced similar maximum pressures (around 7-8 Mpa) at the same time, which corresponds to the end of the gas production period (just before 10 000 years). This maximum value is not affected by the boundary conditions, as was the case in the cell scale and module scale simulations, and is more representative of what could really happened in a such a repository. This result shows that to estimate the hydraulic transient it is necessary to represent the whole repository in the simulations as boundary conditions can have a very significant effect on gas pressures.

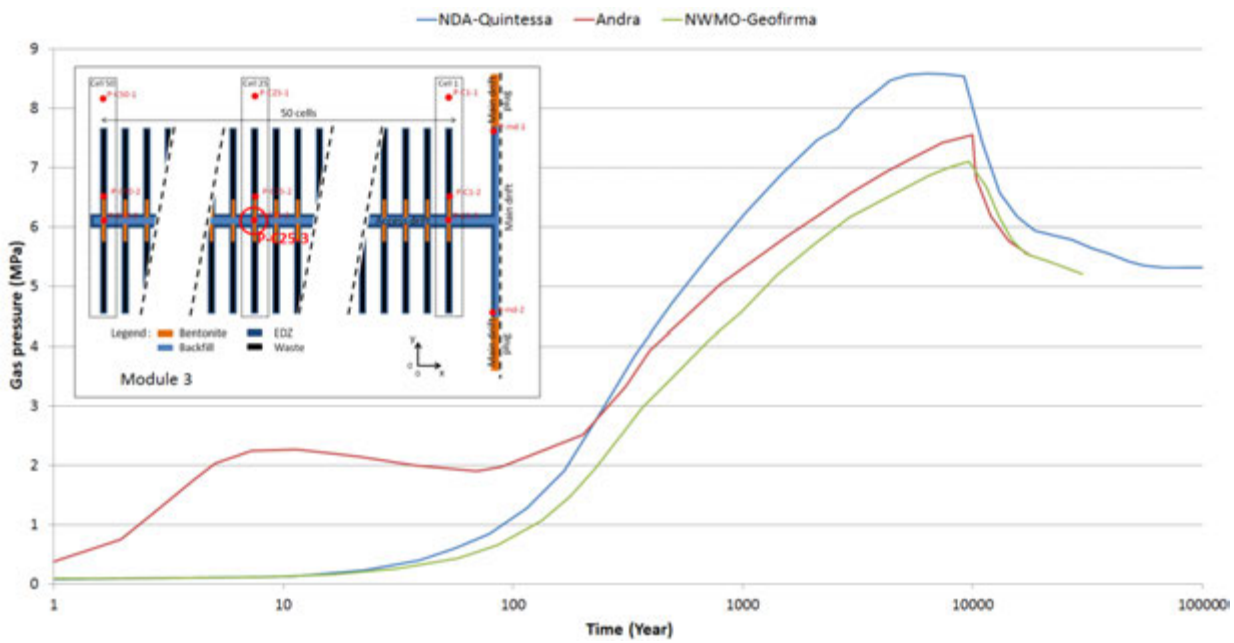

Figure 69: Gas pressure in the central part of the access drift of the central module (module 3)

Knowing that the retention curve of the host rock is quite high, gas pressures lower than 8 Mpa imply that the water desaturation in the host rock is quite small. Only a few percent of the porosity is desaturated by the gas phase and only in the vicinity of the cells and the drift over a few meters at most. More deeply in the host rock, radially to the excavations, the water saturation always stays at 100%.

Concerning the free gas flux out of the module, the general behaviour is similar, with some variance in the magnitude of results between the different teams The ratio between the highest and the lowest peak flux value is around 2, so the order of magnitude is well captured by the different simulations at several kg/y at about 200 years. The cumulative free gas flux out of the module is significantly lower than the gas generation source term (20 kg/y over 10 000 years) in coherence with previous results at module scale showing that dissolution and migration under dissolved form in the host rock water is by far the main transfer process at the module scale.

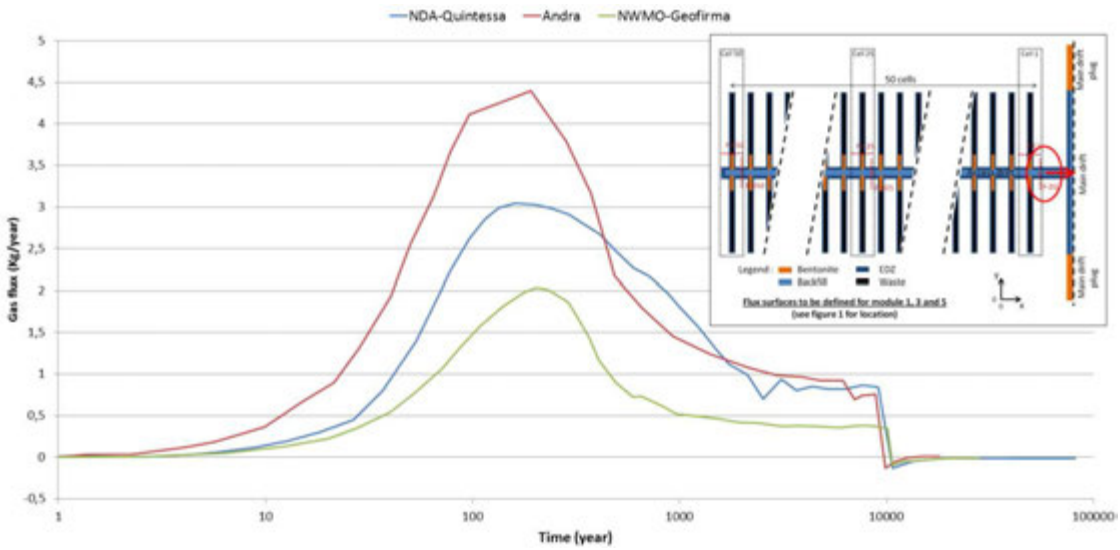

Figure 70 : Gas flux in the access drift of module 3 just beside and toward the main drift

Results from the three models close to the well show larger differences, both in gap pressure and in gas flux.

When it comes to gas pressure Figure 70 shows that depending on the team, the expected evolution is quite different. Just downstream the last main drift plug (point P-md in Figure 70), two teams out of three found that the gas pressure could increase up to a value just above the hydrostatic water pressure. For the last team gas pressure never goes higher than 1.5 Mpa and the gas phase disappears at about one thousand years. For the gas pressure just upstream the well, two teams out of three found that it never increases higher than 1 Mpa to 1.5 Mpa and that gas phase no more exist after 1 000 years. For the other team this pressure can rise up to the hydrostatic pressure. However, this apparent discrepancy can be explained by the fact that Quintessa code (QPAC) is assuming a very small saturation of free gas even when water saturation is equal to one (so gas pressure is always calculated and equal to water pressure at saturation), whereas the code used by Geofirma and Andra assumes that below some critical free gas saturartion there is no free gas and gas pressure is zero.

For gas fluxes the results are also significantly different (see Figure 71). For one team this flux is one order of magnitude higher than for the two others.

Nevertheless, even if different, these results at repository scale show a similar global behavior:

- Gas pressure near the well is never significantly higher than hydrostatic water pressure and this pressure decreases from the last plug toward the well. This decrease shows that during the transfer

from last plug toward the well part of the free gas dissolves in the water, and the low pressure values shows that the flux through the well is very low if not nil.

- Gas flux through the last module plug is very low, less than 1 Kg/y in all models. This is very small compared to the total amount of gas produced in the total repository (200 Kg/y), showing once again that the vast majority of the gas produced in the repository dissolves in water, either in the modules or during the transfer toward the well.

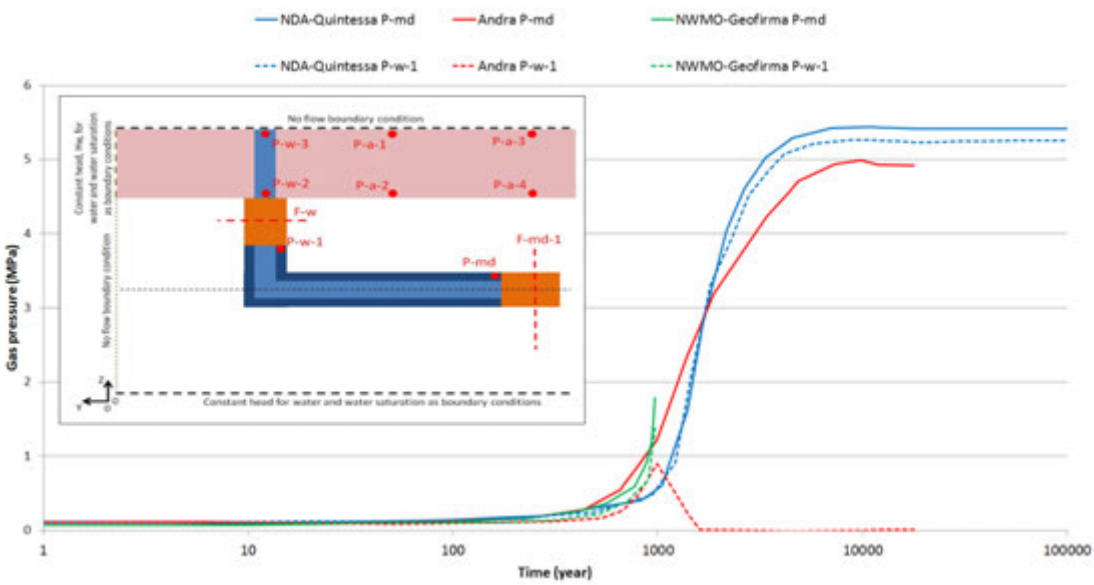

Figure 71 : Gas pressure in the main drift just downstream the last horizontal plug and near the well

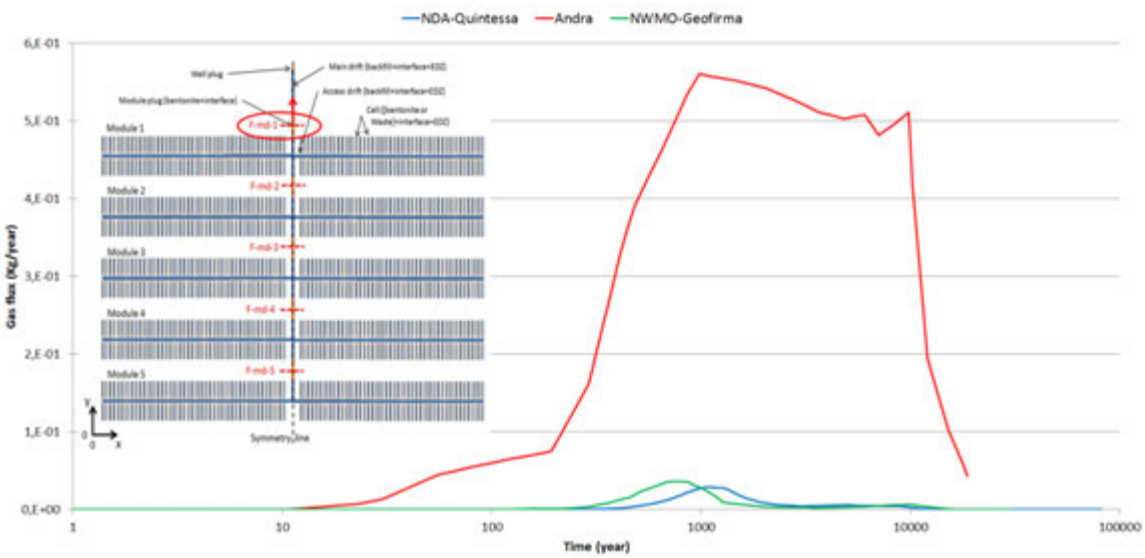

Figure 72 : Gas flux through the most downstream horizontal plug in the main drift

4.2 Numerical and upscaling techniques used in this repository scale benchmark

All teams who participated in the repository benchmark had to use upscaling techniques as the modelled domain is too big to achieve results in a reasonable computing time without. The techniques adopted by the 3 teams are similar and based on the fact that for finite volume discretization scheme it is possible to globalize several identical features in a "macro-component" to reduce significantly the mesh. The drawback is that all the features implemented in a "macro-component" are reacting exactly the same way, but in the repository case several sensitivity analysis have shown that this is phenomenologically representative.

More than this, most of the teams have used high performance computing on massively parallel computers, using up to (around) 100 cores to achieve the simulations. Most of the codes used have the capability to use multicore computers with a friendly user interface. However, Quintessa using an internally developed code did not perform parallel computing but was never-the-less able to compute this benchmark showing that computer power (and code optimization) allows such complex calculations to be performed with single cores.

4.3 How representative are the models?

The mathematical model used for numerical simulations at repository scale is the same as the one used for the first cell and module benchmarks. So remarks made for the cell and module results phenomenological representativity are still valid, and especially the fact that there is no mechanical coupling (i.e. no implementation of pathway dilation for bentonite).

Concerning numerical issues, as the boundary conditions in this repository scale benchmark are pushed away to reach natural ones, the results are more representative compared to the one obtained at cell and module scales.

Nevertheless, this benchmark has globally confirmed the phenomenological behavior at cell level and module level, and especially that dissolution (and migration under dissolved form in the argillites water) is the major process concerning gas migration. But free gas phase is present over all the modules during a period of time comparable of the duration of the gas source term. Some specific behavior at the module scale was also confirmed, i.e. the fact that some of the free gas produced is moving toward the end of the module instead of migrating toward the main drift showing the efficiency of the main drift plug in terms of preventing gas migration.

In general, this benchmark confirms the idea that numerical simulation is a powerful tool (if not the only one) to give a trend or a general evolution but one has to keep in mind that uncertainty of the gas modeling are quite significant and that the values estimated (pressures, fluxes, characteristic time scales, …) are to be considered only as orders of magnitude.

5. Global synthesis of the whole benchmark exercise

The benchmark excercice produced in FORGE is subdivided in three sub-exercices at different geometrical scales, which are the cell scale, the module scale and the repository scale. Each exercice is summarized in a document:

- D1.6-R part 1: cell scale benchmark
- D1.6-R part 2: module scale benchmark
- D1.6-R part 3: repository scale benchmark (this document)

Although each benchmark has its own specific features, on the overall the phenomenological results are coherent and can be summarized as follows: benchmark studies undertaken in the FORGE framework are based on clay stone host rock repositories. In this context, free gas is mainly flowing along the partially desaturated material present in (and directly around) the galleries, using backfill, EDZ and interfaces between EDZ and bentonite plug to migrate from source term production zones (mainly the waste cells themselves) toward the access. Gas migration through these materials is slow, impeded by their small area and the lack of gas transport through less permeable EBS components, such as the bentonite plugs. During its migration, free gas is always in contact with water (present in the partially desaturated pores) and dissolution can take place. Thus, only a very small part of the total generated gas volume (if any) can reach the access in the gaseous phase. During this process, the host rock doesn't significantly desaturate due to gas pressurization and, on the whole, most of the gas is migrating (mainly by diffusion) under dissolved form toward the under and over laying geological layers through the host rock.

On a more mathematical and/or numerical point of view, some general conclusions can also be proposed:

- It is possible to model a whole repository taking into account both the large and very small scale features. To achieve such a numerical simulation some simplifications have however to be considered (among which no complex mechanical coupling) and upscaling techniques have to be addressed ('numerical' and/or 'mathematical'). On the overall, these simulations give good estimations of gas pressures variations but less accurate estimations of gas fluxes.
- Simulations done in the benchmarks are globally based on generalized Darcy formulation for advection, Fick's law for diffusion and Henry's law for phase changes. Some attempts were made to introduce a simple 'proof of principle' mechanical coupling (in order to roughly take into account 'pathway dilation' processes), however, there is currently insufficient information to properly parameterize such a model.
- Actual high performance calculation protocols are quite efficient for parallel computing using from several tens to several hundreds of core. As nowadays easily available numerical clusters contain typically this same range of cores, no specific work was done on this subject. However it was shown that some codes could successfully represent the benchmarks using only a single computational core and with similar run times to the parallelized codes.
- Upscaling technics are powerful tools to integrate small scale information into km scale models. In the framework of FORGE, two main types of technics were developed or used. A very efficient so called 'numerical' upscaling based on heavily use of non-conform grids enabling, with finite volume formulation, to embed small scale detailed sub-models in large scale coarser grids. The so called 'mathematical' upscaling (homogenization of all parameters over a given volume based on some energy conservation law) is also very powerful but can lead to homogenized relative permeability and retention curves with very particular and somehow 'non-physical' shapes that needs to be addressed.

ANNEX

Full description of the benchmark at repository scale

6. Context and objectives

From WP1 participants point of view, the aim of the benchmark should less be a comparison of numerical codes than an exercise trying to answer some precise questions in a PA (Performance Assessment) logic (for example, what could be the relative role of the EDZ, interfaces, backfill in the gas stransfer at repository scale?). This clearly includes numerical considerations, but they are a mean and not an objective.

One of the difficulties is to find a common playground for all participants, which allows bringing some add-on for each one. After discussion, a general agreement was that the reference exercise will be as generic as possible (without targeting precisely on national concepts) and to propose sensitivity analyses making it possible to cover national specificities. What is aimed is more to feel how the systems react and why they can react differently rather than an inter-comparison of codes.

A second agreement was that, although the final aim of the benchmark studies is to represent repository-scale simulations, the first exercise should be rather simple and at cell scale. This first step was done during 2009 and first part of 2010. Results are showing a significant role of interfaces between plug and argillite and a transfer dominated at this scale by convection towards the drifts, radial diffusion being of secondary order.

Representing the transfer of gas at a larger scale including drifts and several tens of cells is then worthwhile. In this context, one of the major problems in representing gas transfer in a repository for radioactive waste is to model simultaneously all gas sources (generally located in the disposal cells) and the transfer pathways constituted by the network of interfaces, plugs and underground drifts. The second benchmark at module scale (several tens of cells, see Figure 1 for schematic representation) shows once more that interface plays an important role in the transient hydraulic-gas evolution as well as significant differences with the cell results such as the important role of dissolution/diffusion process along the pathways in the drifts. Although at this scale some teams had important numerical problems, especially concerning the establishment of the mesh, none of them used explicit upscaling techniques.

The simulation of a complete generic repository including ten modules (see Figure 1) will force the teams to introduce a certain amount of upscaling in their simulations. More than this, having a complete repository will permit to validate the results at smaller scales (cell and module) and to give evaluation of the impact of gasin the shafts.

This document contains the specifications for such an exercise.

6.1 Benchmark general specification at repository scale

One of the main difficulties in the representation of gas transfer in a repository is to take into account simultaneously all the source terms (generally located inside the storage cells) and to represent at the same time the transfer network constituted by the different drifts and cells.

For this exercise we assume a repository having a simple architecture (see Figure 1). This architecture is more or less representative of some general concepts for HLW repository zones but without any national specificity. The main features are:

- Subdivision of the whole repository into several modules linked by a main drift;
- All the modules are identical and contains an access drift serving 50 cells on each side;
- Two opposite modules are not separated by a seal;
- In the main drift, seals are located between all module connections.

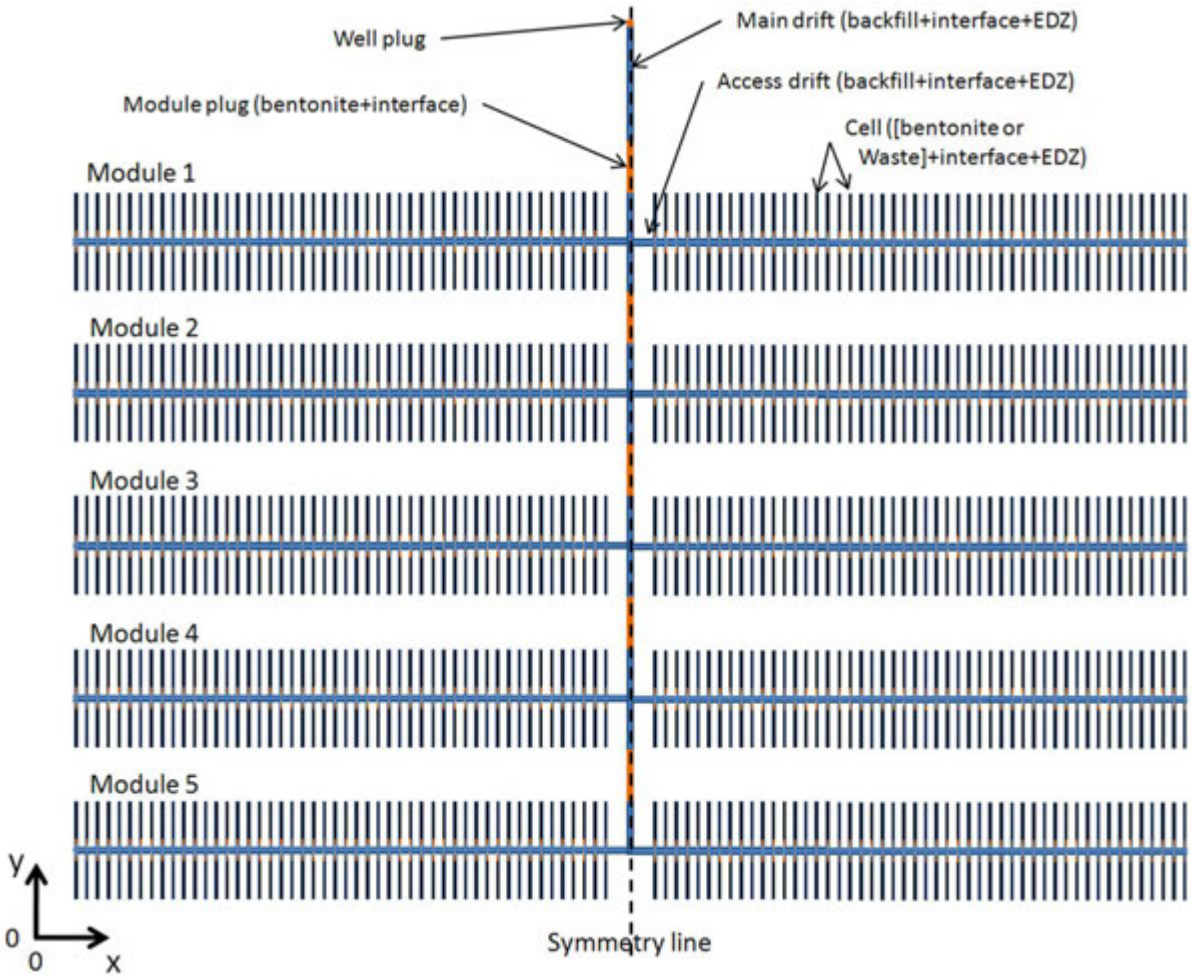

Figure 73: schematic of a repository for HLW

More details on the domain to be represented are given in Figure 2 to Figure 7

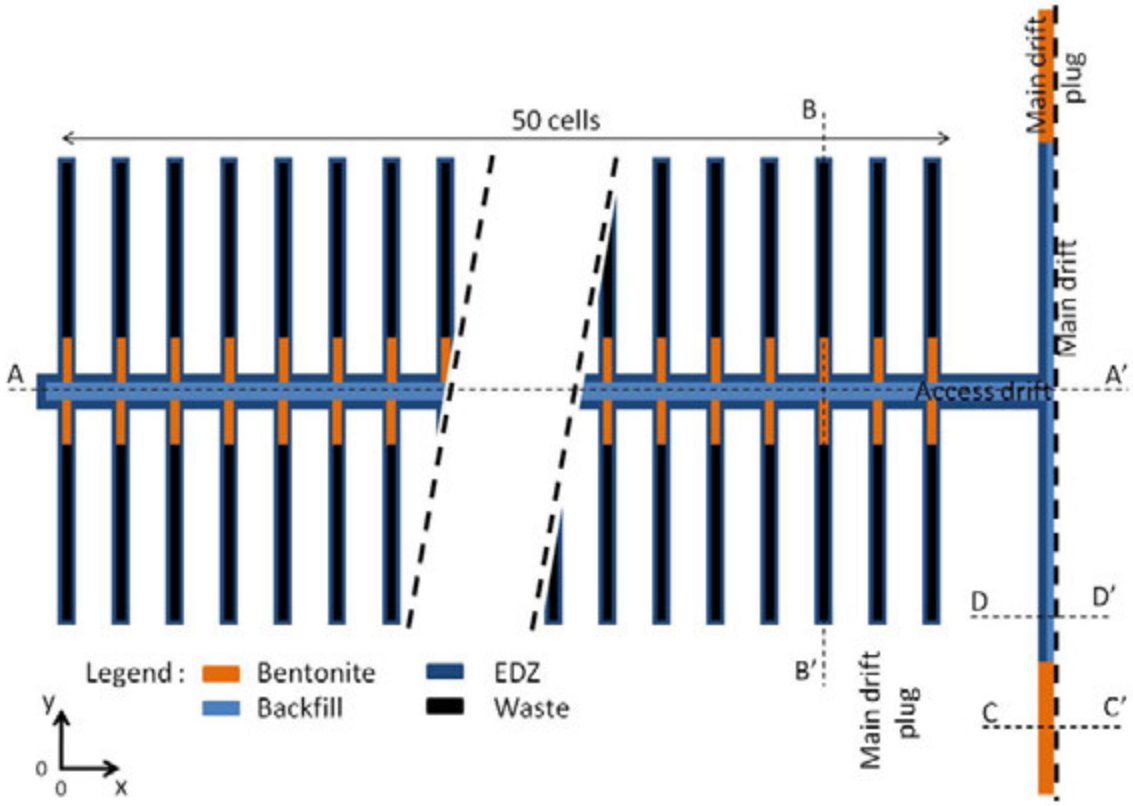

Figure 74: schematic of a module. Definition of the A-A', B-B', C-C' and D-D' cross sections

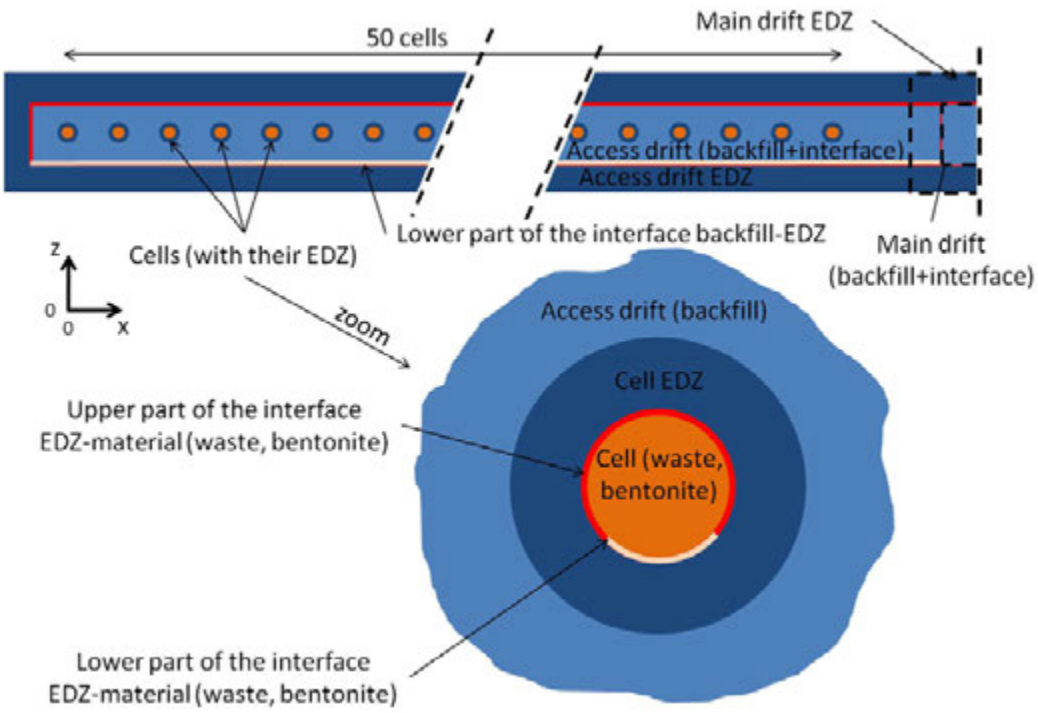

Figure 75: schematic of the A-A' vertical cross section (see figure 2 for definition)

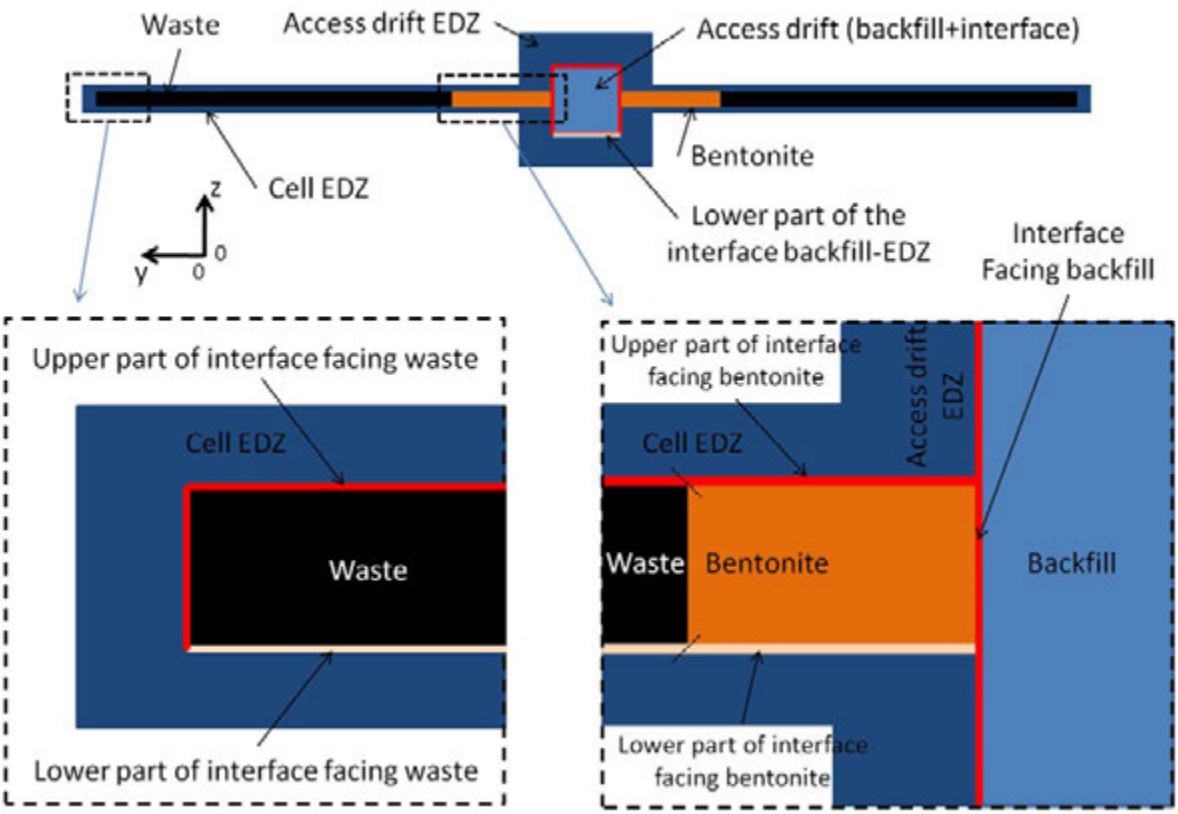

Figure 76: schematic of the B-B' vertical cross section (see figure 2 for definition)

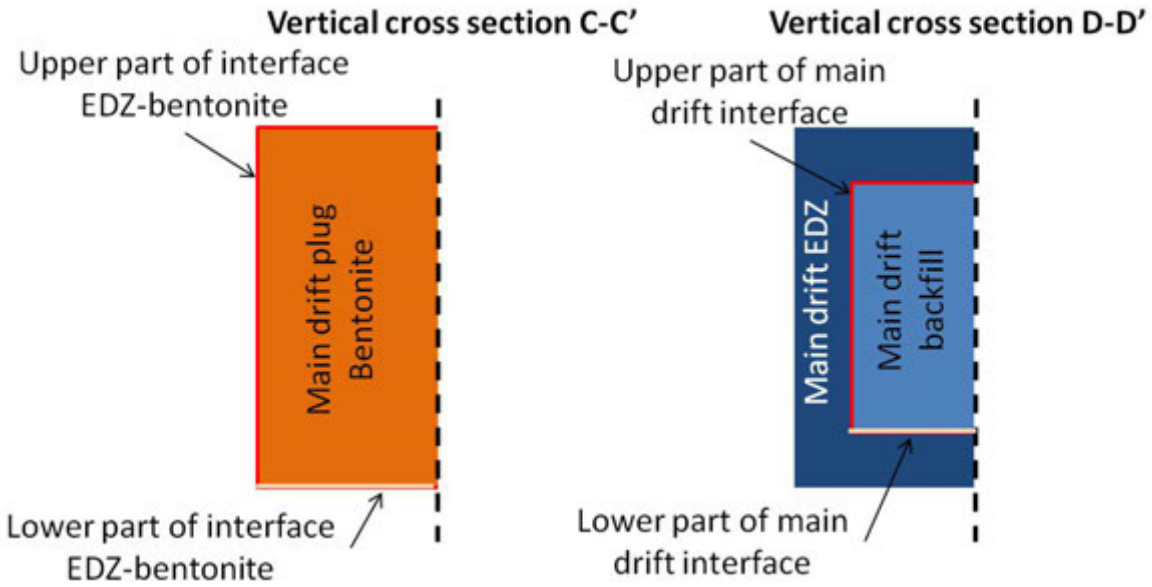

Figure 77: schematic of vertical cross section C-C' and D-D' (see figure 2 for definitions)

The calculation domain is 3D and includes the whole vertical extension of the argillite layer (150 m) and its upper aquifer (see Figure 7) . The horizontal extension is determined by the distance between each cell axis, their length and the total number of modules in place in the global repository. A common gas production term is given for each cell. It is imposed on the outer wall of the cell (the waste cell itself is supposed to be gas-tight and water-tight and is not explicitly represented) The materials to take into account in this simulation are argillite (natural medium), EDZ (Excavation Damaged Zone), EDZ-material interface (material can be bentonite or backfill depending on the position), bentonite (cells and drift plugs), backfill of the drifts and shaft and upper aquifer geological medium.

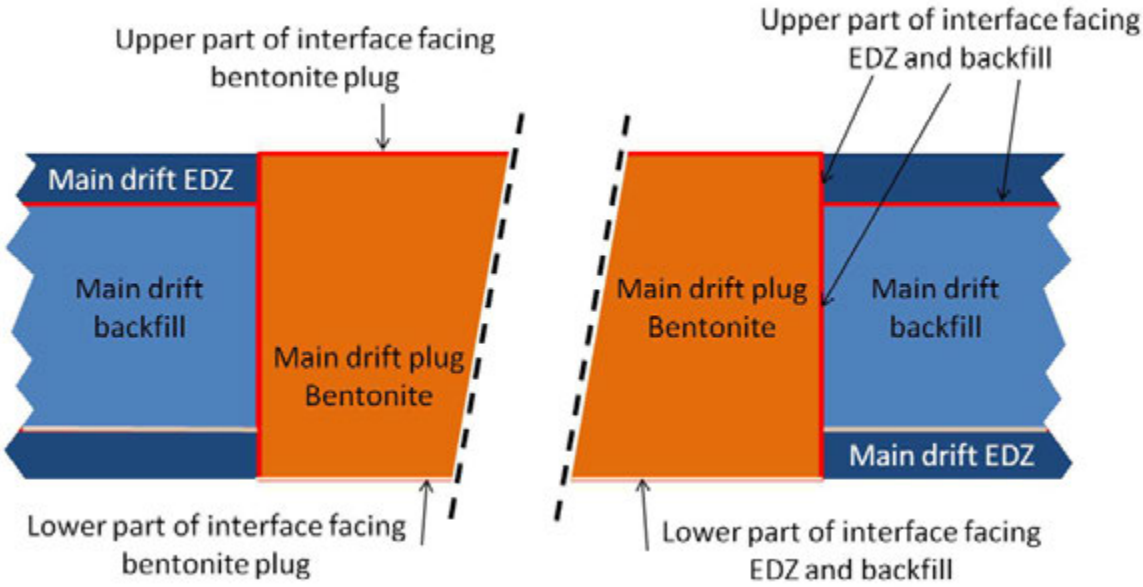

Figure 78: schematic of the main drift plugs and backfill interfaces

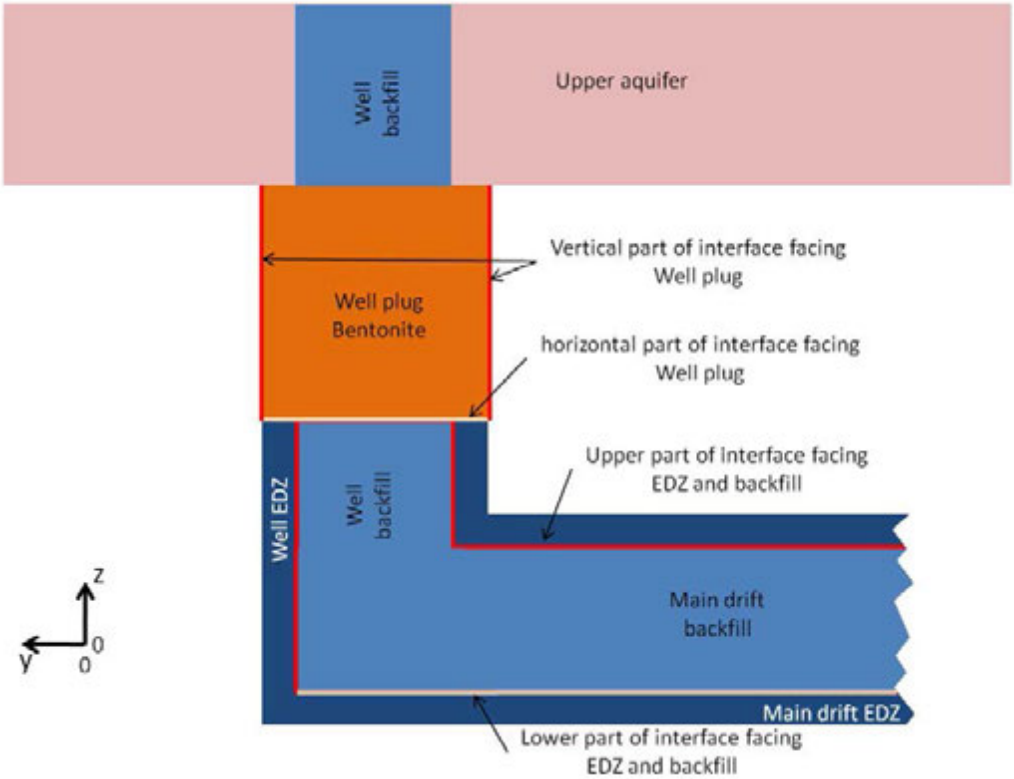

Figure 79 : Schematic of the shaft and the upper aquifer

In the cell the EDZ is not overcut at bentonite plug emplacement (seeFigure 4, lower right picture, but in the drift it is (seeFigure 6. The bentonite-argillite interface is present around all types of plugs. The interface is in fact present around all "drift/cell filling materials" and can have different physical properties depending on the material (waste, backfill, bentonite) they are facing (see Table 2). Especially, the lower part of this interface has different hydraulic properties to represent the impact of the gravity effects and interface width is reduced (even to zero) due to the weight of the filling materials (waste, bentonite or backfill). In case the drifts are represented by squares, the lower side is to be represented differently from the 3 other "upper" sides. In case of a circular representation, the lower quarter of the perimeter is supposed to represent the lower part of the interface.

The main objective of this simulation is to understand how gas is moving from a cell towards a drift and finally towards the shaft and possibly the upper aquifer (is diffusion the main process at the repository scale, which proportion of the gas generated inside the cells is moving across the shaft plugs, what is the characteristic time for this transfer, which pressure can be achieved, …).

However, a secondary objective is to study the different methods (homogenization, domain decomposition, high performance computing …) used by the different teams to perform this simulation taking into account all the physics described in the following sectionsbelow and restraining the computation time and/or the mesh size to something which is not prohibitive.

Note that all geometrical and physical properties already defined either in the first exercise at cell scale or in the second at module scale are the same for this exercise at repository scale.

6.2 Detailed description of the test case

Note that in the following sections the figures are mainly presenting the dimensions to take into account in the simulations. Some elements, mainly the interfaces, are not always explicitly represented.

6.2.1 Geometry

For the cells, waste and bentonite plugs have the same circular sections. Sections of the access drift and main drift are squared and identical. Cells are positioned at mid height of the access drift and at mid height of host rock (argillite layer). Section of the shaft is squared. There are two opposite sets of 50 cells (on each side of the access drift) in a module. There are 10 modules in the global repository (see Figure 1).

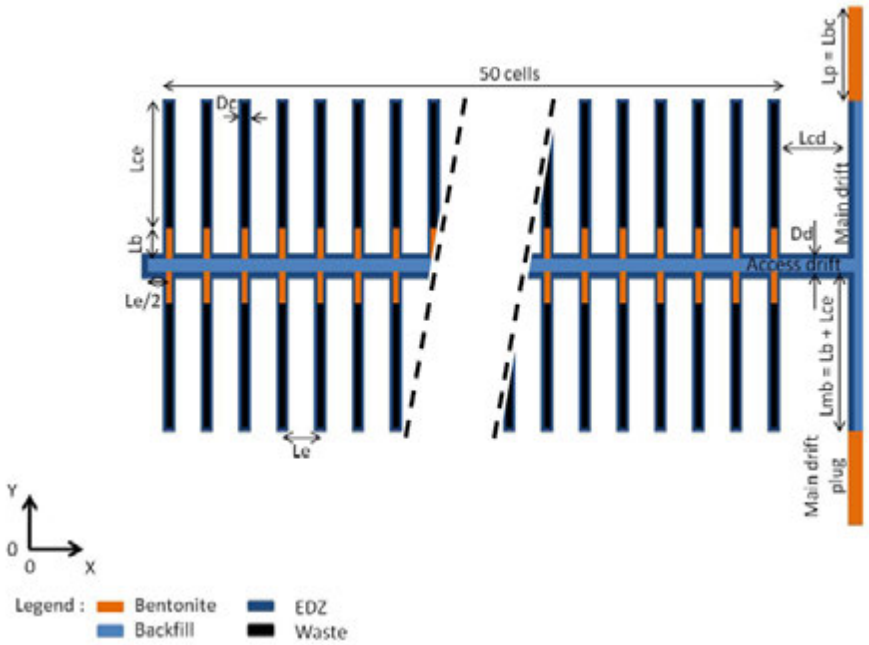

Figure 80: horizontal dimensions

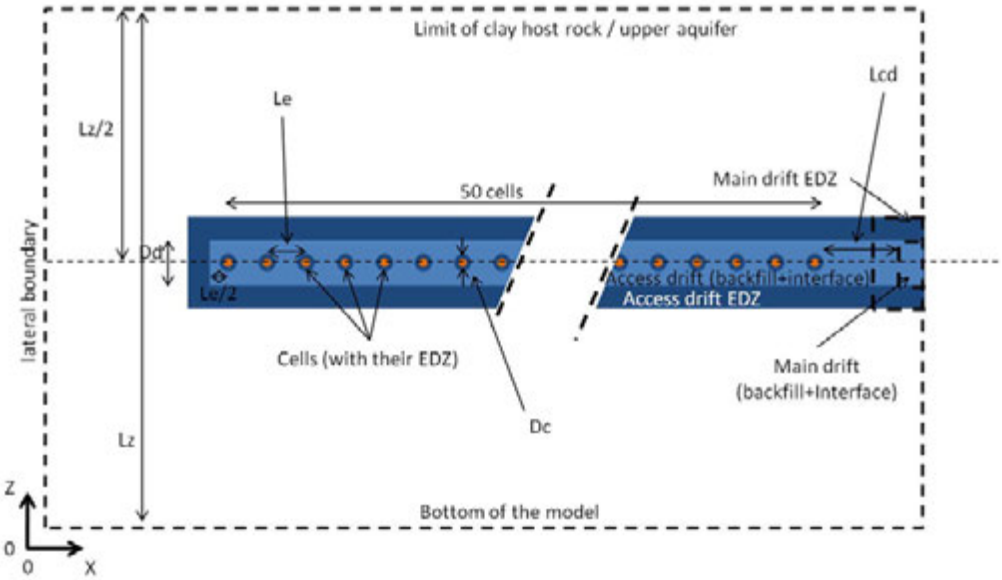

Figure 81: horizontal and vertical dimensions on cross section A-A'

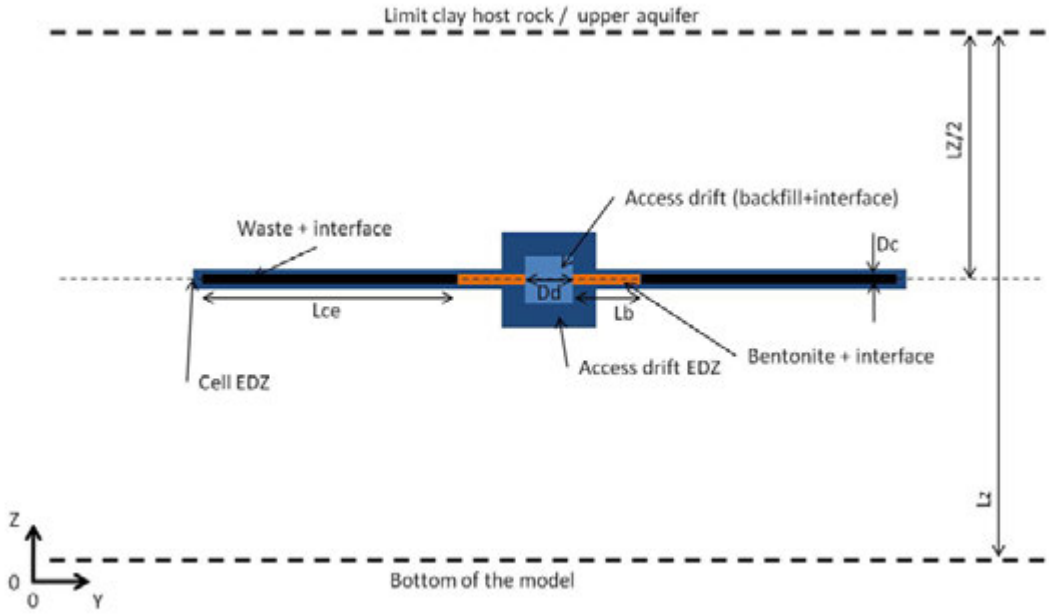

Figure 82: horizontal and vertical dimensions on cross section B-B'

At repository scale, there is a symmetry axis represented by the middle of the main drift (see Figure 1). To get rid as much as possible of the boundary conditions, the upper aquifer is represented. It is assumed that the geological layer over is quite tight, and that the shaft contains a seal inside this layer so that no representation over the top of the upper aquifer is needed.

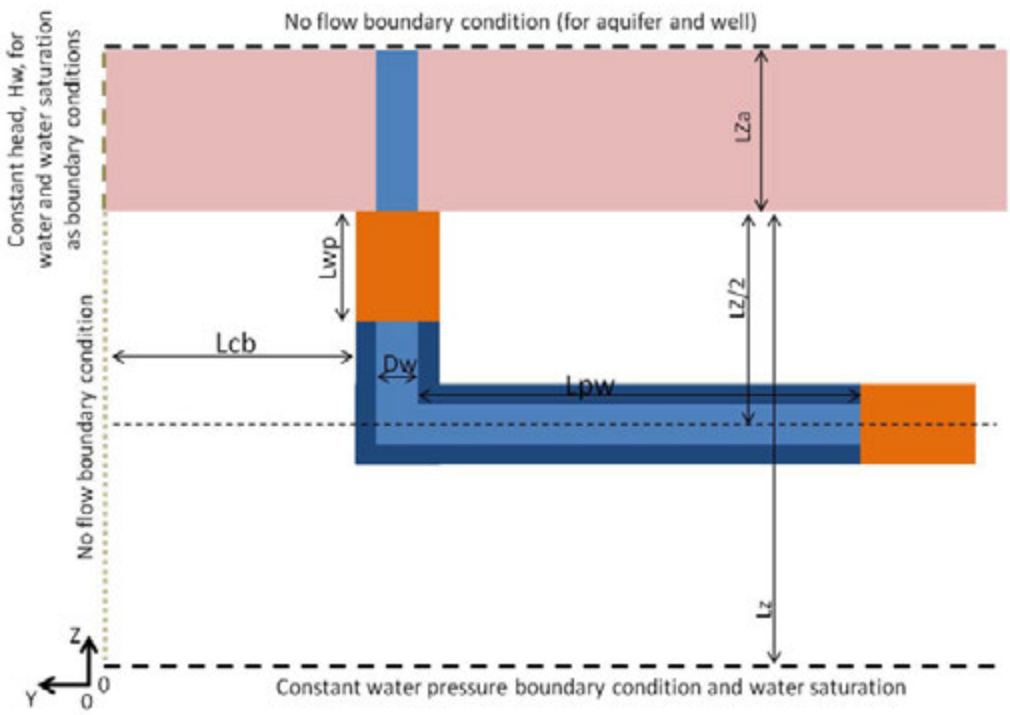

Figure 83: dimensions linked to the shaft and the upper aquifer and boundary conditions

Table 2: Dimensions relative to the simulated domain

Parameter description	Name	Value
X total extension of the simulation domain	Lx	1238 m
Y total extension of the simulation domain	Ly	1437 m
Z total extension of the simulation domain	Lz+lza	200 m
Vertical extension of the argillite layer	Lz	150 m
Vertical extension of the upper aquifer layer	Lza	50 m
Distance from the repository to the vertical boundaries	Lcb	100 m
Length of the bentonite plug in the cell (without interface)	Lb	5 m
Length of "waste zone" in the cell (with interface)	Lce	40 m
Distance between axes of two adjacent cells	Le	10 m
Cell diameter (with interface, without EDZ)	Dc	1 m
Length of main drift between outer wall cell (with interface, without EDZ) and first drift seal	Lpw	500 m
Side of the well	Dw=Dd	6 m
Length of the well seal (without interface)	Lwp	50 m
Access and main drifts side length (with interface, without EDZ)	Dd	6 m
Length of the bentonite plug in the main drift (without interface) distance between two cells end between two adjacent modules	Lp=Lbc	50 m
Distance between outer wall of the access drift (with interface, without EDZ) and end (without interface) of the main drift plug	Lmb=Lb+Lce	45 m
Distance between outer wall of the main drift (with interface, without EDZ) and outer wall of the first cell (with interface, without EDZ)	Lcd	20 m
Extension of interface (between waste-argillite, backfill-argillite and bentonite-argillite). Not mentioned in the figures	wi	1 cm
Extension of cell EDZ. Not mentioned in the figures	Cedz	0,5 m
Extension of access drift, main drift and well EDZ. Not mentioned in the figures	Dedz	1 m

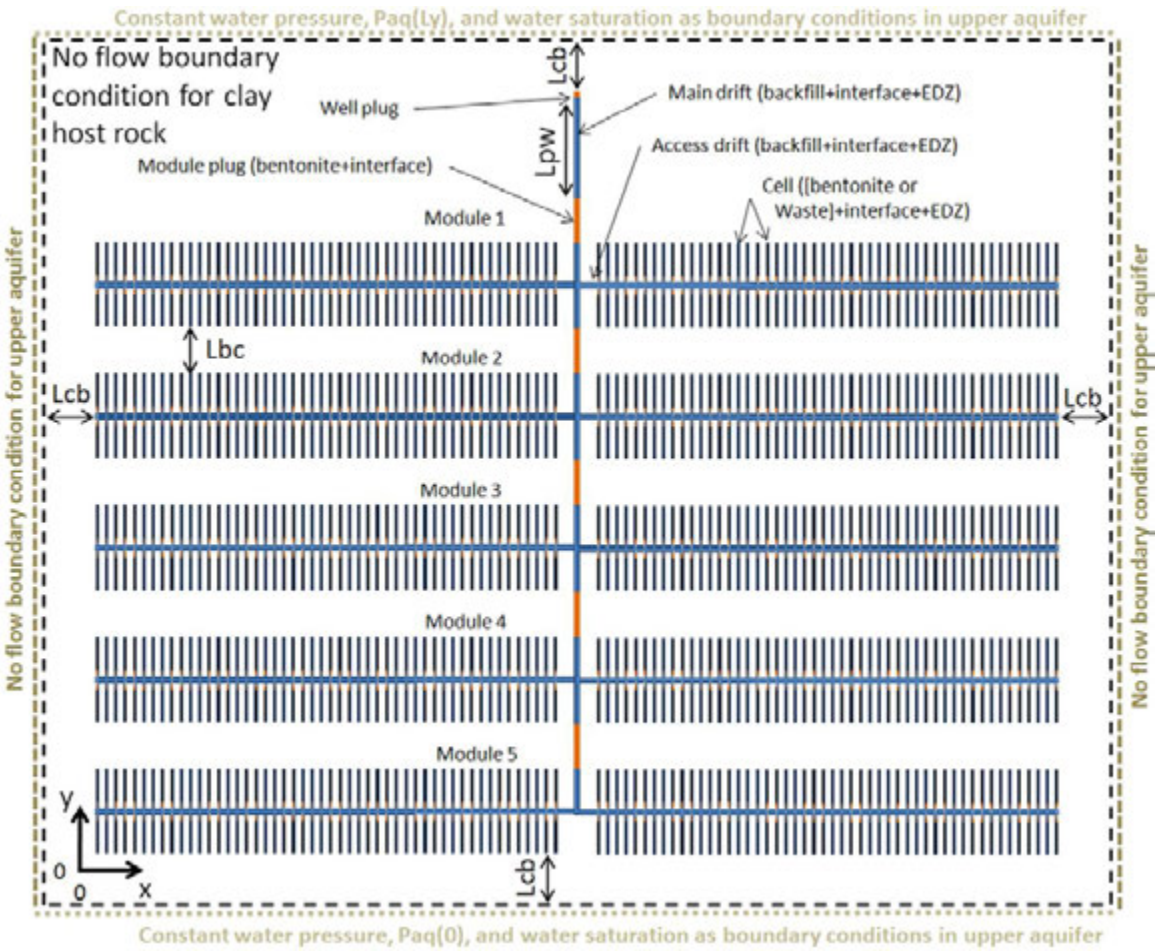

Figure 84: other dimensions at repository scale and vertical boundary conditions for argillites and upper aquifer

6.2.2 Boundary conditions

See also Figure 9, Figure 11 and Figure 12.

$$x \in [0, Lx], y \in [0, Ly], z \in [0, Lz + Lza], t \in [0, t_{end}]$$

with Lx=1438 m, Ly=1637 m, Lz+Lza=200 m (Lz=150 m, Lza = 50 m), t_{end} =100000 years

o Conditions on the top and bottom boundaries of the simulation domain:

$$P_w(x, y, z = 0, t) = 6\,10^6\,Pa \qquad S_w(x, y, z = 0, t) = 1 \qquad X^w_{H_2}(x, y, z = 0, t) = 0$$

It is assumed that the geological layer above the upper aquifer is water and gas tight, so that no flow boundary condition can be assumed on the top of the upper aquifer (top boundary of the simulation domain, z=Lz+Lza).

$$Flux_w(x, y, z = Lz + Lza, t) = 0 \quad Flux_g(x, y, z = Lz + Lza, t) = 0$$

When gaseous phase is not present, the pseudo-gas pressure corresponds also to a dissolved mass fraction or concentration via Henry's law (see mathematical model for details).

o Conditions on the lateral vertical boundaries of the argillite layer:

$$Flux_w(x=0,y,z,t)=0 \qquad Flux_g(x=0,y,z,t)=0$$
$$Flux_w(x=Lx,y,z,t)=0 \qquad Flux_g(x=Lx,y,z,t)=0$$
$$for \quad y\in[0,Ly], z\in[0,Lz], t\in[0,t_{end}]$$

$$Flux_w(x,y=0,z,t)=0 \qquad Flux_g(x,y=0,z,t)=0$$

$$Flux_w(x,y=Ly,z,t)=0 \qquad Flux_g(x,y=Ly,z,t)=0$$
$$for \quad x\in[0,Lx], \quad z\in[0,Lz], \quad t\in[0,t_{end}]$$

o Boundary conditions on the lateral vertical boundaries of the upper aquifer layer:

We suppose that in the upper aquifer layer the hydraulic gradient is parallel to the Y direction (no flow on the X boundaries), and directed from the well toward the repository

$$Flux_w(x=0,y,z,t)=0 \qquad Flux_g(x=0,y,z,t)=0$$
$$Flux_w(x=Lx,y,z,t)=0 \qquad Flux_g(x=Lx,y,z,t)=0$$
$$for \quad y\in[0,Ly], z\in[Lz,Lz+Lza], t\in[0,t_{end}]$$

$$P_w(x,y=0,z,t)=Paq(0)=4.0\,10^6\,Pa \qquad S_w(x,y=0,z,t)=1 \qquad X^w_{H_2}(x,y=0,z,t)=0$$
$$P_w(x,y=Ly,z,t)=Paq(Ly)=4.5\,10^6\,Pa \qquad S_w(x,y=y_{\max},z,t)=1$$
$$for \quad x\in[0,Lx], \quad z\in[Lz,Lz+Lza], \quad t\in[0,t_{end}]$$

6.2.3 Physical parameters

The simulation is supposed to be isothermal at 20°C (293 K) during all the calculation period.

The gravity is taken into account for this 3D simulation.

Table 3: values for physical parameters

Parameter (at 20°C)	Materials*		
	Interface (upper part) facing plug	Interface (upper part) facing waste (cf. *)	Interface (upper part) facing backfill and EDZ (cf. *)
K [m²]	$5.0\ 10^{-18}$	$1.0\ 10^{-12}$	$1.0\ 10^{-15}$
Porosity [%]	30	100	40
Specific storage coefficient [m⁻¹]	$4.6\ 10^{-06}$	$4.6\ 10^{-06}$	$4.6\ 10^{-06}$
Two-phase flow parameters			
S_{gr} [%]	0	0	0
S_{wr} [%]	0	0	0
Van Genuchten parameters			
n [-]	4	4	4
P_r [Pa]	10^4	10^4	10^4
τ (Tortuosity)	1	1	1

Parameter (at 20°C)	Materials			
	Backfills	Bentonite plugs	EDZ	Geological medium
K [m²]	$5.0\ 10^{-17}$	$1.0\ 10^{-20}$	$5.0\ 10^{-18}$	$1.0\ 10^{-20}$ (assumed isotropic)
Porosity [%]	40	35	15	15
Specific storage coefficient [m⁻¹]	$1.0\ 10^{-05}$	$4.4\ 10^{-06}$	$2.3\ 10^{-06}$	$2.3\ 10^{-06}$
Two-phase flow parameters				
S_{gr} [%]	0	0	0	0
S_{wr} [%]	0	0	0	0
Van Genuchten parameters				
n [-]	1.5	1.6	1.5	1.5
P_r [Pa]	$2\ 10^6$	$1.6\ 10^7$	$1.5\ 10^6$	$1.5\ 10^7$
τ (Tortuosity)	2	4.5	2	2

* for the lower part of all interfaces (see figures 3 through 7) the values are the same as those of the adjacent EDZ. If cells/drifts are represented by circles, this part is a quarter (90°) of the total circumference. In the case of a square representation, the lower edge is considered.
(see figure 4, figure 6 and figure 7).

- ***Viscosity of the gas mixture:***

The viscosity of the gas mixture (water vapour + hydrogen) can be estimated by a classical Wilke approximation or by a simplified formula as follows:

$$\mu_g = \frac{1}{\frac{X^g_{H_2}}{\mu^g_{H_2}} + \frac{X^g_{wvap}}{\mu^g_{wvap}}} \quad \text{with} \quad \mu^g_{H_2}(T = 293K) = 9\ 10^{-6}\ Pa.s \quad \mu^g_{wvap}(T = 293K) = 10^{-5}\ Pa.s$$

- ***Diffusion coefficient of dissolved H_2 in water:***

$$D_{H_2/water} = 1.57\ 10^{-14} \frac{T}{\mu_{water}(T)} \quad (m^2/s)$$

- ***Diffusion coefficient of gaseous H_2 in water vapour:***
  (T_0=293 K and at P_0=1.0□10^5 Pa: D_0=9.5□10^{-5} m^2/s)

$$D^g_{H_2-H_2O} = D_0 \left(\frac{P_0}{P}\right)\left(\frac{T}{T_0}\right)^{1.75} \quad (m^2/s)$$

- ***Diffusion coefficient of dissolved H_2 in the water of the porous medium:***

$$D^w_{H_2} = S_w \left(\frac{\omega}{\tau^2}\right) D_{H_2/water}$$

- ***Diffusion coefficient of dissolved H_2 in the binary H_2/water-vapour mixture of the porous medium:***

$$D^g_{H_2/vap} = (1 - S_w)\left(\frac{\omega}{\tau^2}\right) D^g_{H_2-H_2O}$$

- ***Solubility of hydrogen in water:*** $H_{H_2}(T = 293K) = 7.610^{-6}\ mol.Pa^{-1}.m^{-3}$

Note: Temperature in diffusion models is expressed in Kelvin.

6.2.4 Initial conditions

Water saturation:

- in the geological medium is equal to 100%;
- in the cells and drifts EDZ is equal to 100%
- in the bentonite plugs is equal to 70%;
- in the backfill of the main drift and of the access drift is equal to 70%
- in the upper part of the interfaces is equal to 5%, 100% in the lower part ;

Pressure:

- in the fully initially water-saturated materials (argilites, EDZ, upper aquifer), the water pressure is supposed to be hydrostatic and in line with all the boundary conditions (in the argilites layer and in the upper aquifer).
- in partially-saturated materials at initial time, the gas pressure is equal to 0.1 MPa (~1 atmosphere). The corresponding water pressure is deduced from the gas pressure and the saturation by applying Van Genuchten capillary pressure relationships relative to each material.

6.2.5 Production term for hydrogen

The hydrogen-production term is to be distributed over the whole radial and lateral outer surface of all the wastes, as follows:

- for 0 < t ≤ 10000 years, $Q^{g}_{H_2} = 100\ mol/year/cell$ $\quad Q^{w}_{H_2} = 0$
- for t > 10000 years $Q^{g}_{H_2} = 0\ mol/year/cell$ $\quad Q^{w}_{H_2} = 0$

6.2.6 SIMULATION PERIOD

The simulation will be performed between t_o=0 and t_{end} =100.000 years.

6.3 Output results

For all output results, times will be expressed in years, pressures will be expressed in MPa, mass flows will be expressed in kg/s.

6.3.1 Evolution with time of mass flows across surfaces at module scale

Note *: the exact position of the surfaces inside a specific module are given in the "module scale" benchmark specification*

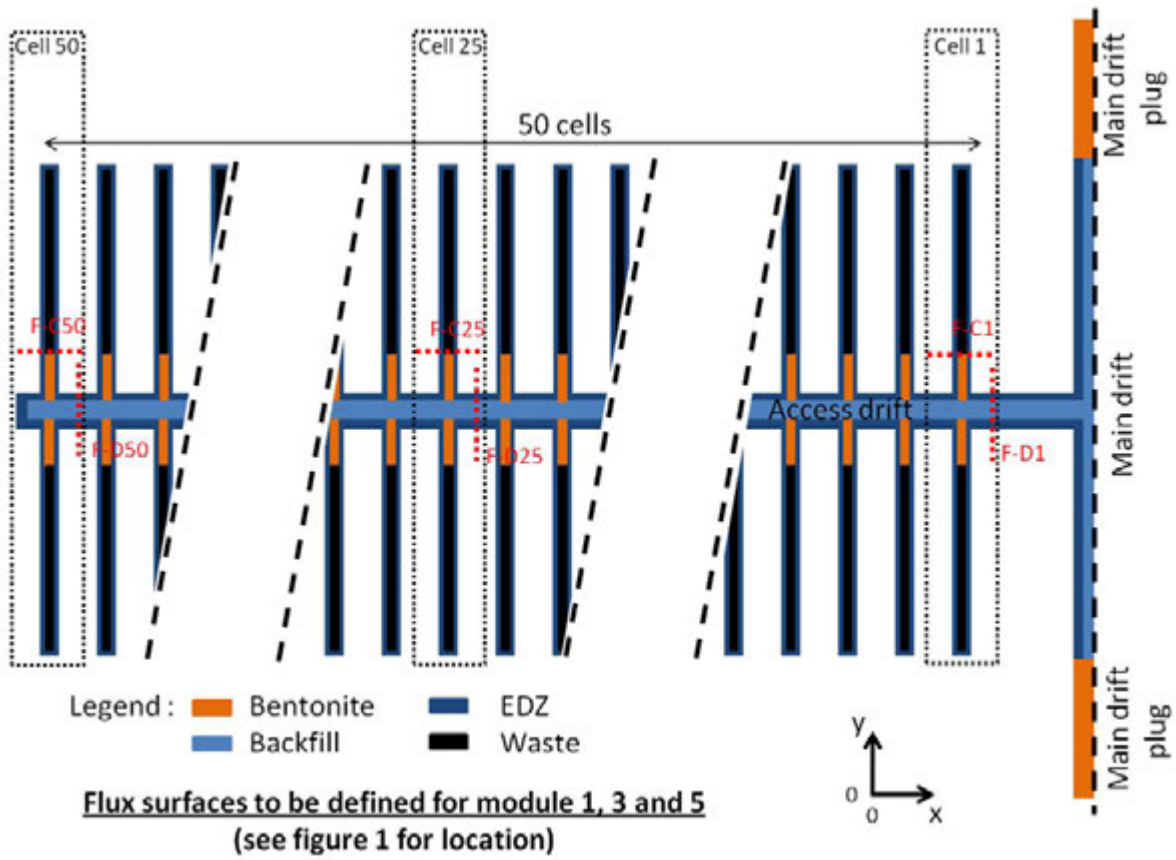

Figure 85: schematic of the surfaces across which flows will be calculated

Type of mass flows: total flows, diffusive flows and advective flows for the following components/phases:

- Liquid water

- Water vapour
- Gaseous hydrogen
- Dissolved hydrogen

For modules 1, 3 and 5 (see Figure 1 or Figure 12 for locations, add "-mx" at the end of the surface manes, "x"=1, 3 or 5 depending on the module). Type of surfaces:

- For each of cells 50, 25 and 1 (see Figure 13 for their locations), flows in the cell interface and the cell EDZ, across the following surface: vertical plane passing through the end (close to the wastes) of the cell bentonite plug. Corresponding to surfaces F-C50, F-C25 and F-C1
- For each of cells 50, 25 and 1, flows in the access drift backfill, access drift interface and access drift EDZ, across the following surface: vertical plane 5 m away – downstream - from the cell axis. Corresponding to surfaces F-D50, F-D25 and F-D1 on 3;
- Global hydrogen flow across the upper and lower boundaries of the argillites layer of the whole simulation domain (not presented on 3). Flows are computed separately for upper and lower boundaries. For upper argillites layer boundary, flows are computer separately for the well and for the argillites.

6.3.2 Evolution with time at given points at module scale

***Note**: the exact position of the points inside a specific module are given in the "module scale" benchmark specification*

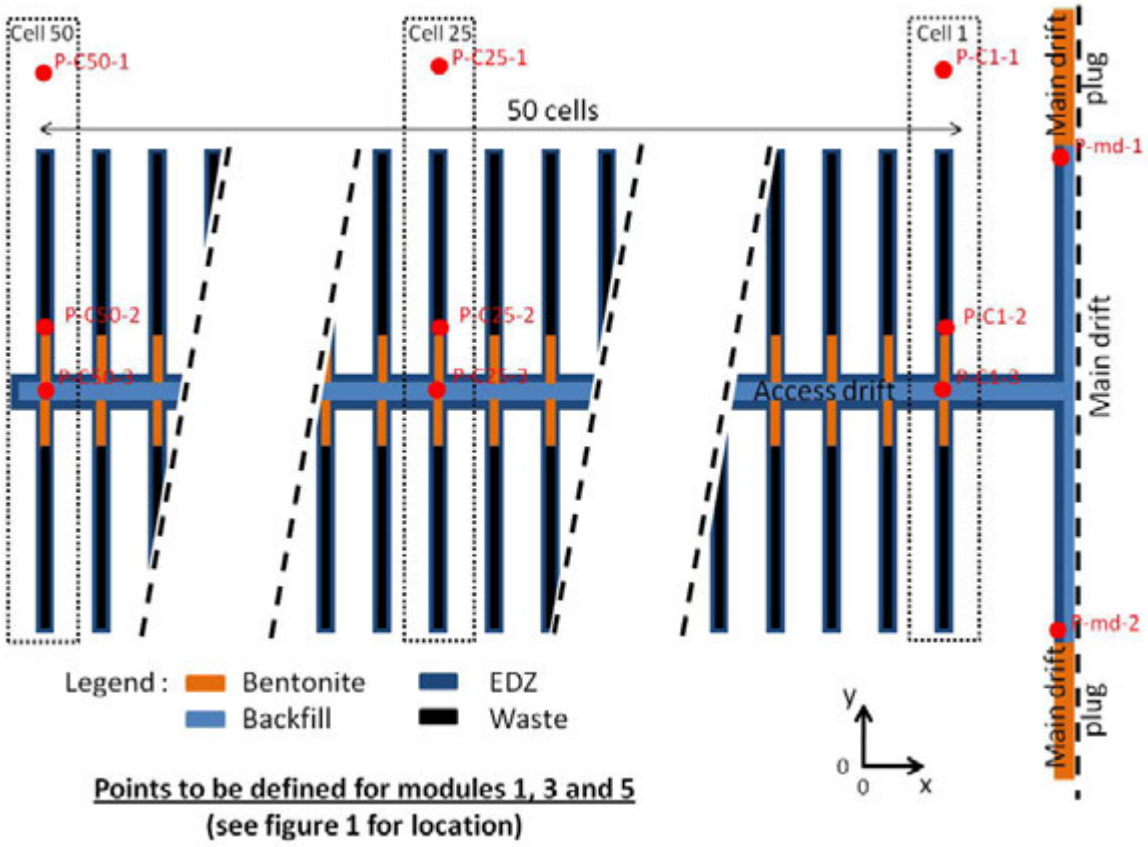

Figure 86: schematic of the points where results should be given

Evolution with time of:

- Water saturation

- Water pressure
- Gas pressure in the gas phase when it exists, zero otherwise
- Dissolved hydrogen pseudo-pressure (see Henry's law, equations (18) and (18'), in § 5 for details)
- Capillary pressure

For modules 1, 3 and 5 (see Figure 1 or Figure 12 for locations, add "-mx" at the end of the points manes, "x"=1, 3 or 5 depending on the module). Type of points:

- For cell 50 (see Figure 14):
    - Point P-C50-1: point whose horizontal coordinates are along the axis of the cell, 5 m away from the end of the cell (with interface, without EDZ) ;
    - Point P-C50-2: point situated in the interface between waste and EDZ (upper part) as close as possible to the bentonite plug;
    - Point P-C50-3: point situated in the interface between access drift and EDZ (upper part) ; horizontal coordinates are those of the intersection axes of cell 50 and access drift;
- Same types of point as for cell 50 but for cell 25 (points P-C25-1, P-C25-2, P-C25-3) and cell 1 (points (P-C1-1, P-C1-2, P-C1-3), see Figure 14;
- Points P-md-1 and P-md-2 near bentonite plug in the main drift: situated as close as possible from the plug, in the EDZ of the main drift.

6.3.3 Evolution with time of mass flux over surfaces and of pressures/saturation at given points at repository scale

At repository scale, some surfaces are defined to control fluxes, in the bentonite plugs, in the middle of each module seals (F-md-1, F-md-2, F-md-3, F-md-4, F-md-5, see figure 15) and as well for the well seal (F-w, see figure 16). The type of mass flows (total flows, diffusive flows and advective flows) are to be defined for the following components/phases:

- Liquid water
- Water vapour
- Gaseous hydrogen
- Dissolved hydrogen

Concerning more specifically the part between the last module plug, the top of the shaft and globally the upper aquifer, some points are defined for pressures and saturation control (see figure 16). For these points, evolution with time is needed for:

- Water saturation
- Water pressure
- Gas pressure in the gas phase when it exists, zero otherwise
- Dissolved hydrogen pseudo-pressure (see Henry's law, equations (18) and (18'), in § 5 for details)
- Capillary pressure

These points are positioned as followed:

- Points P-md and P-w-1 near bentonite plug in the main drift: situated as close as possible from the plug, in the EDZ of the main drift;

- Point P-w-2 in the center of the backfill of the well just above the well bentonite plug. P-w-3 in the center of the well backfill just under the upper limit of the aquifer;
- Point P-a-4 in the upper aquifer just above its lower limit, same X value as the main drift axis, same Y value as F-md-1 surface. For P-a-3, same X and Y position as P-a-4, but on the top of the aquifer layer;

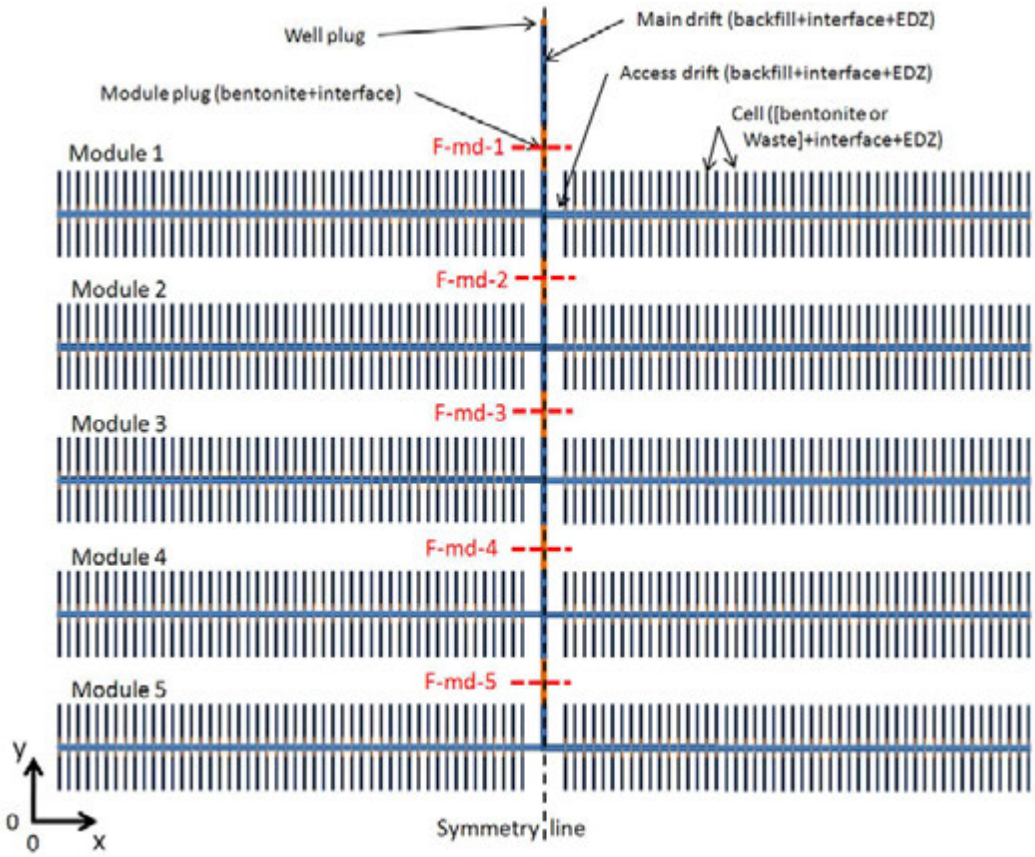

- Point P-a-1 at the center of [P-w-3,P-a-3] segment. Point P-a-2 at the center of [P-w-2,P-a-4] segment.

Figure 87: locations of the surfaces to compute fluxes at repository scale.

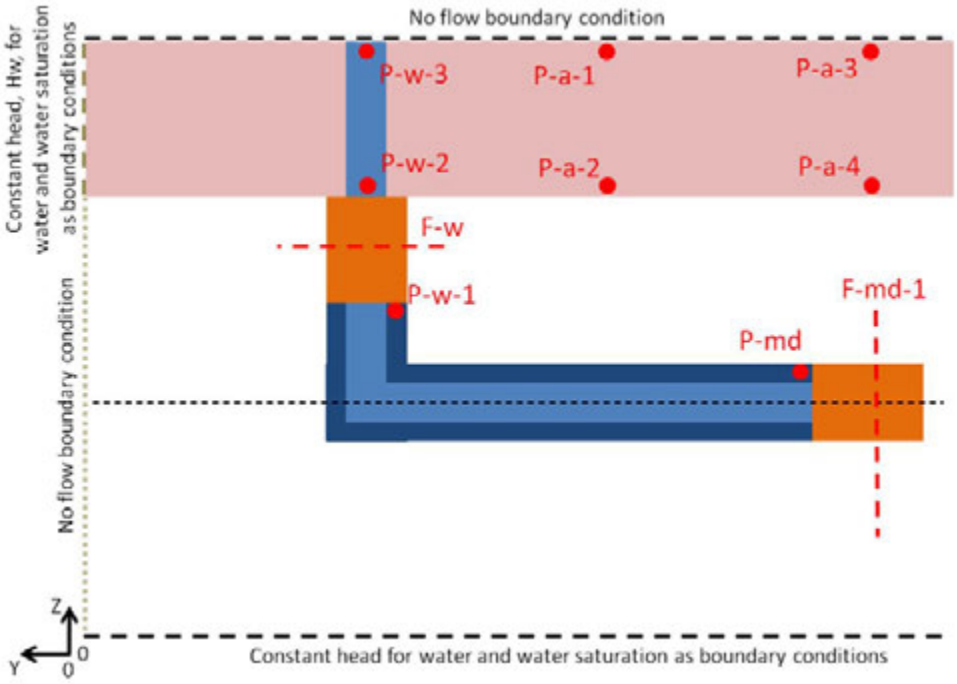

Figure 88: schematic of the locations of control surfaces and points in the vicinity of the shaft and in the upper aquifer

6.4 Mathematical model proposed for the exercise

Remark: *This model is the same as the one proposed in the first part of the benchmark at cell scale.*

The capillary pressure is defined as the difference between total gas pressure and water pressure:

$$P_C = P_g - P_w \qquad (1)$$

- *Pc*: capillary pressure (Pa)
- *Pg*: total pressure of the gas phase(Pa)
- *Pw*: water pressure (Pa)

The dependence between water and gas saturation in each porous medium is expressed by:

$$S_g + S_W = 1 \quad \text{with} \quad S_g = \frac{V_g}{V_p} \text{ and } S_w = \frac{V_w}{V_p}$$

- Sg: gas saturation (-)
- Sw: water saturation (-)
- Vg: gas volume (m3)
- Vw: water volume (m3)
- Vp: pore volume (m3)

Van Genuchten relationships are used to express capillary pressure P_c as a function of the effective saturation S_{we} in a given porous medium:

$$S_{we} = \frac{S_w - S_{wr}}{1 - S_{wr} - S_{gr}} \qquad (2)$$

$$S_{we} = \frac{1}{\left[1+\left(\frac{P_c}{P_r}\right)^n\right]^m} \quad (3)$$

- Swe: effective water saturation (-)
- Swr = residual water saturation (-)
- Pr: reference pressure for Van genuchten law (Pa). In general the value for this coefficient is higher than the gas entry pressure for a given porous medium
- n, m: coefficients for Van Genuchten relationship. $m = 1 - \frac{1}{n}$

The relative permeability for liquid phase k_r^w is expressed by integrating the Mualem prediction model in the Van Genuchten capillarity model:

$$k_r^w = \sqrt{S_{we}}\left[1-\left(1-S_{we}^{1/m}\right)^m\right]^2 \quad (4)$$

- k_r^w : relative permeability for liquid phase (-)

The relative permeability for gas phase k_r^g : is expressed in a similar way:

$$k_r^g = \sqrt{1-S_{we}}\left[1-S_{we}^{1/m}\right]^{2m} \quad (5)$$

- k_r^g : relative permeability for gas phase (-)

The water and gas movement in a porous medium is represented by the mass conservation law and the energy conservation law (reduced to the generalized Darcy law):

$$U_w = -\frac{kk_r^w(S_w)}{\mu_w}(\nabla P_w + \rho_w g \nabla z) \quad (6)$$

$$U_g = -\frac{kk_r^g(S_g)}{\mu_g}(\nabla P_g + \rho_g g \nabla z) \quad (7)$$

- K: intrinsic permeability of the porous medium (m2)
- μg: viscosity of the total gas phase (kg.s-1.m-1)
- μw: viscosity of water (kg.s-1.m-1)
- ρ: volumetric mass of the total gas phase (kg.m-3)
- ρw: volumetric mass of water (kg.m-3)

$$\rho_w(P_w) = \rho_{atm}\exp\left[S_s(P_w - P_{atm})\right] \quad (8)$$

  ρatm: volumetric mass of water at atmospheric pressure (kg.m-3)
  Patm: atmospheric pressure (Pa)
  Ss: specific storage (Pa-1)
- g: gravity (m.s-2)
- z: altitude (m)
- Ug: Darcy velocity for the gas phase (m.s-1)
- Uw: Darcy velocity for water (m.s-1)

Equation of conservation for water:

$$\frac{\partial(\rho_w \omega S_w)}{\partial t} + \nabla(\rho_w U_w) = Q^w \quad (9)$$

- ω: porosity (-)
- Qw: consumption/production of water (kg.m-3.s-1)

Equation of conservation for the total gas phase:

$$\frac{\partial(\rho_g \omega S_g)}{\partial t} + \nabla(\rho_g U_g) = Q^g \qquad (10)$$

- Qg: consumption/production for the total gas phase (kg.m-3.s-1)

The mass fraction of gaseous hydrogen is expressed as:

$$X_{H_2}^g = \frac{\rho_{H_2}^g}{\rho_g} \qquad (11)$$

With $\rho_{H_2}^g = \frac{m_{H_2}^g}{V_g}$ and $\rho_g = \frac{m^g}{V_g}$

- $X_{H_2}^g$ is the mass fraction of hydrogen in the total gas phase (-)
- $m_{H_2}^g$ is the hydrogen mass in the gas phase (kg)
- m^g is the total mass of the gas phase (kg)
- $\rho_{H_2}^g$ is the volumetric mass of gaseous hydrogen in the gas phase (kg.m-3)

Mass conservation law for gaseous hydrogen:

$$\frac{\partial}{\partial t}(\omega S_g \rho_g X_{H_2}^g) + \nabla(\rho_g X_{H_2}^g U_g - J_{H_2}^g) + \Omega_{H_2}^{g/l} = Q_{H_2}^g \qquad (12)$$

- $\Omega_{H_2}^{g/l}$ is the exchange term from the gaseous phase to the liquid phase for H2 (kg.m-3.s-1)
- $Q_{H_2}^g$ is the consumption/production term for gaseous hydrogen (kg.m-3.s-1)
- $J_{H_2}^g$ is the diffusive term for gaseous hydrogen (kg.m-2.s-1)

Diffusive flux for a binary mixture of gas (H2 and water vapor) can be expressed by Fick's law:

$$J_{H_2}^g = \rho_g D_{H_2 vap}^g \nabla X_{H_2}^g \qquad (13)$$

- $D_{H_2 vap}^g$ is the diffusion coefficient for gaseous hydrogen in water vapor (m2.s-1)

The mass fraction of dissolved hydrogen is expressed as:

$$X_{H_2}^w = \frac{\rho_{H_2}^w}{\rho_w} \qquad (14)$$

With $\rho_{H_2}^w = \frac{m_{H_2}^w}{V_w}$ and $\rho_w = \frac{m^w}{V_w}$

- $X_{H_2}^w$ is the mass fraction of dissolved hydrogen (-)
- $m_{H_2}^w$ is the dissolved hydrogen mass (kg)
- m^w is the total mass of the liquid phase (kg)
- $\rho_{H_2}^w$ is the volumetric mass of dissolved hydrogen in the liquid phase (kg.m-3)

Mass conservation law for dissolved hydrogen is expressed as:

$$\frac{\partial}{\partial t}(\omega S_w \rho_w X_{H_2}^w) + \nabla(\rho_w X_{H_2}^w U_w - J_{H_2}^w) + \Omega_{H_2}^{l/g} = Q_{H_2}^w \qquad (15)$$

- $\Omega_{H_2}^{l/g}$ is the exchange term from the liquid phase to the gas phase for H2 (kg.m-3.s-1)
- $Q_{H_2}^w$ is the consumption/production term for dissolved hydrogen (kg.m-3.s-1)
- $J_{H_2}^w$ is the diffusive term for dissolved hydrogen (kg.m-2.s-1)

The exchange terms from between liquid and gaseous phase are linked by the following relation:

$$\Omega_{H_2}^{l/g} = -\Omega_{H_2}^{g/l} \qquad (16)$$

Diffusive flux for dissolved hydrogen can be expressed by Fick's law:

$$J_{H_2}^w = \rho_w D_{H_2 vap}^w \nabla X_{H_2}^w \qquad (17)$$

- $D_{H_2 vap}^w$ is the diffusion coefficient for dissolved hydrogen in water vapor (m2.s-1)

Part of the gas will be dissolved in the pore water. The solubility limit for the gas depend mainly on thermodynamic conditions and can be expressed by Henry's law:

$$C_{H_2}^w = H_{H_2}(T) P_{H_2}^g \qquad (18)$$

Where $C_{H_2}^w = \dfrac{X_{H_2}^w \rho_w}{M_{H_2}}$

- $C_{H_2}^w$ is the maximum concentration of hydrogen in water (mol.m-3)
- H_{H_2} is the constant of Henry's law for hydrogen (mol.m-3.Pa-1)
- $P_{H_2}^g$ is the partial pressure of hydrogen in the total gaseous phase (Pa)
- M_{H_2} is the molar mass for hydrogen (kg.mol-1)

***Remark**: given the actual hydrogen concentration in water, $C'^w_{H_2}$, it is possible to define a "pseudo pressure" of the dissolved hydrogen, $P'^g_{H_2}$, by inversion of Henry's law:*

$$P'^g_{H_2} = \frac{C'^w_{H_2}}{H_{H_2}(T)} \qquad (18')$$

The relation between partial pressure of each gas present in the total gas phase and total gas pressure is given by Dalton law that writes for a binary mixture (H2 and water vapor):

$$P_g = P_{H_2}^g + P_{wvap}^g \qquad (19)$$

- P_{wvap}^g is the partial pressure of water vapor in the total gas phase (Pa)

Each of the gases is supposed perfect:

$$P_{H_2}^g = \frac{\rho_{H_2}^g}{M_{H_2}} RT \text{ and } P_{wvap}^g = \frac{\rho_{wvap}^g}{M_{wvap}} RT \qquad (20,21)$$

For the gas mixture this writes:

$$P_g = \frac{\rho_g}{M_g} RT \qquad (22)$$

- Mg: molar mass for the total gaseous phase (H2 + water vapor) (kg.mol-1)
- R: constant of the perfect gas (J.mol-1.K-1): R = 8.314 J.mol-1.K-1
- T: temperature (°K)

Saturation pressure for water vapor is only depending on temperature and can by expressed by:

$$\log_{10}(P_{sat}) = 2.786 + 0.031514T_c - 1.2373x10^{-4}T_c^{\ 2} + 4.2267x10^{-7}T_c^{\ 3} - 8.1308x10^{-10}T_c^{\ 4} \qquad (23)$$

- Psat: saturation pressure for water vapor (Pa)
- Tc: Temperature (°C)

Kelvin's law is giving a relation between saturation pressure for water vapor, effective pressure for water vapor and capillary pressure:

$$P_{wvap}^{g}(T, S_w) = \exp\left(\frac{M_w P_c(S_{w)}}{\rho_w RT}\right) P_{sat}(T) \qquad (24)$$